

BEST AVAILABLE COPY

SECOND DECLARATION OF PAUL POLAKIS, Ph.D.

I, Paul Polakis, Ph.D., declare and say as follows:

1. I am currently employed by Genentech, Inc. where my job title is Staff Scientist.
2. Since joining Genentech in 1999, one of my primary responsibilities has been leading Genentech's Tumor Antigen Project, which is a large research project with a primary focus on identifying tumor cell markers that find use as targets for both the diagnosis and treatment of cancer in humans.
3. As I stated in my previous Declaration dated May 7, 2004 (attached as Exhibit A), my laboratory has been employing a variety of techniques, including microarray analysis, to identify genes which are differentially expressed in human tumor tissue relative to normal human tissue. The primary purpose of this research is to identify proteins that are abundantly expressed on certain human tumor tissue(s) and that are either (i) not expressed, or (ii) expressed at detectably lower levels, on normal tissue(s).
4. In the course of our research using microarray analysis, we have identified approximately 200 gene transcripts that are present in human tumor tissue at significantly higher levels than in normal human tissue. To date, we have successfully generated antibodies that bind to 31 of the tumor antigen proteins expressed from these differentially expressed gene transcripts and have used these antibodies to quantitatively determine the level of production of these tumor antigen proteins in both human tumor tissue and normal tissue. We have then quantitatively compared the levels of mRNA and protein in both the tumor and normal tissues analyzed. The results of these analyses are attached herewith as Exhibit B. In Exhibit B, "+" means that the mRNA or protein was detectably overexpressed in the tumor tissue relative to normal tissue and "-" means that no detectable overexpression was observed in the tumor tissue relative to normal tissue.
5. As shown in Exhibit B, of the 31 genes identified as being detectably overexpressed in human tumor tissue as compared to normal human tissue at the mRNA level, 28 of them (i.e., greater than 90%) are also detectably overexpressed in human tumor tissue as compared to normal human tissue at the protein level. As such, in the cases where we have been able to quantitatively measure both (i) mRNA and (ii) protein levels in both (i) tumor tissue and (ii) normal tissue, we have observed that in the vast majority of cases, there is a very strong correlation between increases in mRNA expression and increases in the level of protein encoded by that mRNA.



6. Based upon my own experience accumulated in more than 20 years of research, including the data discussed in paragraphs 4-5 above and my knowledge of the relevant scientific literature, it is my considered scientific opinion that for human genes, an increased level of mRNA in a tumor tissue relative to a normal tissue more often than not correlates to a similar increase in abundance of the encoded protein in the tumor tissue relative to the normal tissue. In fact, it remains a generally accepted working assumption in molecular biology that increased mRNA levels are more often than not predictive of elevated levels of the encoded protein. In fact, an entire industry focusing on the research and development of therapeutic antibodies to treat a variety of human diseases, such as cancer, operates on this working assumption.
7. I hereby declare that all statements made herein of my own knowledge are true and that all statements made on information or belief are believed to be true, and further that these statements were made with the knowledge that willful false statements and the like so made are punishable by fine or imprisonment, or both, under Section 1001 of Title 18 of the United States Code and that such willful statements may jeopardize the validity of the application or any patent issued thereon.

Dated: 3-29-06

By: Paul Polakis

Paul Polakis, Ph.D.

DECLARATION OF PAUL POLAKIS, Ph.D.

I, Paul Polakis, Ph.D., declare and say as follows:

1. I was awarded a Ph.D. by the Department of Biochemistry of the Michigan State University in 1984. My scientific Curriculum Vitae is attached to and forms part of this Declaration (Exhibit A).
2. I am currently employed by Genentech, Inc. where my job title is Staff Scientist. Since joining Genentech in 1999, one of my primary responsibilities has been leading Genentech's Tumor Antigen Project, which is a large research project with a primary focus on identifying tumor cell markers that find use as targets for both the diagnosis and treatment of cancer in humans.
3. As part of the Tumor Antigen Project, my laboratory has been analyzing differential expression of various genes in tumor cells relative to normal cells. The purpose of this research is to identify proteins that are abundantly expressed on certain tumor cells and that are either (i) not expressed, or (ii) expressed at lower levels, on corresponding normal cells. We call such differentially expressed proteins "tumor antigen proteins". When such a tumor antigen protein is identified, one can produce an antibody that recognizes and binds to that protein. Such an antibody finds use in the diagnosis of human cancer and may ultimately serve as an effective therapeutic in the treatment of human cancer.
4. In the course of the research conducted by Genentech's Tumor Antigen Project, we have employed a variety of scientific techniques for detecting and studying differential gene expression in human tumor cells relative to normal cells, at genomic DNA, mRNA and protein levels. An important example of one such technique is the well known and widely used technique of microarray analysis which has proven to be extremely useful for the identification of mRNA molecules that are differentially expressed in one tissue or cell type relative to another. In the course of our research using microarray analysis, we have identified approximately 200 gene transcripts that are present in human tumor cells at significantly higher levels than in corresponding normal human cells. To date, we have generated antibodies that bind to about 30 of the tumor antigen proteins expressed from these differentially expressed gene transcripts and have used these antibodies to quantitatively determine the level of production of these tumor antigen proteins in both human cancer cells and corresponding normal cells. We have then compared the levels of mRNA and protein in both the tumor and normal cells analyzed.
5. From the mRNA and protein expression analyses described in paragraph 4 above, we have observed that there is a strong correlation between changes in the level of mRNA present in any particular cell type and the level of protein



expressed from that mRNA in that cell type. In approximately 80% of our observations we have found that increases in the level of a particular mRNA correlates with changes in the level of protein expressed from that mRNA when human tumor cells are compared with their corresponding normal cells.

6. Based upon my own experience accumulated in more than 20 years of research, including the data discussed in paragraphs 4 and 5 above and my knowledge of the relevant scientific literature, it is my considered scientific opinion that for human genes, an increased level of mRNA in a tumor cell relative to a normal cell typically correlates to a similar increase in abundance of the encoded protein in the tumor cell relative to the normal cell. In fact, it remains a central dogma in molecular biology that increased mRNA levels are predictive of corresponding increased levels of the encoded protein. While there have been published reports of genes for which such a correlation does not exist, it is my opinion that such reports are exceptions to the commonly understood general rule that increased mRNA levels are predictive of corresponding increased levels of the encoded protein.

7. I hereby declare that all statements made herein of my own knowledge are true and that all statements made on information or belief are believed to be true, and further that these statements were made with the knowledge that willful false statements and the like so made are punishable by fine or imprisonment, or both, under Section 1001 of Title 18 of the United States Code and that such willful statements may jeopardize the validity of the application or any patent issued thereon.

Dated: 5/07/04

By: Paul Polakis

Paul Polakis, Ph.D.

CURRICULUM VITAE

PAUL G. POLAKIS
Staff Scientist
Genentech, Inc
1 DNA Way, MS#40
S. San Francisco, CA 94080

EDUCATION:

Ph.D., Biochemistry, Department of Biochemistry,
Michigan State University (1984)

B.S., Biology. College of Natural Science, Michigan State University (1977)

PROFESSIONAL EXPERIENCE:

2002-present	Staff Scientist, Genentech, Inc S. San Francisco, CA
1999- 2002	Senior Scientist, Genentech, Inc., S. San Francisco, CA
1997 -1999	Research Director Onyx Pharmaceuticals, Richmond, CA
1992- 1996	Senior Scientist, Project Leader, Onyx Pharmaceuticals, Richmond, CA
1991-1992	Senior Scientist, Chiron Corporation, Emeryville, CA.
1989-1991	Scientist, Cetus Corporation, Emeryville CA.
1987-1989	Postdoctoral Research Associate, Genentech, Inc., South San Francisco, CA.
1985-1987	Postdoctoral Research Associate, Department of Medicine, Duke University Medical Center, Durham, NC

1984-1985

Assistant Professor, Department of Chemistry,
Oberlin College, Oberlin, Ohio

1980-1984

Graduate Research Assistant, Department of
Biochemistry, Michigan State University
East Lansing, Michigan

PUBLICATIONS:

1. Polakis, P. G. and Wilson, J. E. 1982 Purification of a Highly Bindable Rat Brain Hexokinase by High Performance Liquid Chromatography. **Biochem. Biophys. Res. Commun.** 107, 937-943.
2. Polakis, P. G. and Wilson, J. E. 1984 Proteolytic Dissection of Rat Brain Hexokinase: Determination of the Cleavage Pattern during Limited Digestion with Trypsin. **Arch. Biochem. Biophys.** 234, 341-352.
3. Polakis, P. G. and Wilson, J. E. 1985 An Intact Hydrophobic N-Terminal Sequence is Required for the Binding of Rat Brain Hexokinase to Mitochondria. **Arch. Biochem. Biophys.** 236, 328-337.
4. Uhing, R. J., Polakis, P. G. and Snyderman, R. 1987 Isolation of GTP-binding Proteins from Myeloid HL60 Cells. **J. Biol. Chem.** 262, 15575-15579.
5. Polakis, P. G., Uhing, R. J. and Snyderman, R. 1988 The Formylpeptide Chemoattractant Receptor Copurifies with a GTP-binding Protein Containing a Distinct 40 kDa Pertussis Toxin Substrate. **J. Biol. Chem.** 263, 4969-4979.
6. Uhing, R. J., Dillon, S., Polakis, P. G., Truett, A. P. and Snyderman, R. 1988 Chemoattractant Receptors and Signal Transduction Processes in Cellular and Molecular Aspects of Inflammation (Poste, G. and Crooke, S. T. eds.) pp 335-379.
7. Polakis, P. G., Evans, T. and Snyderman, R. 1989 Multiple Chromatographic Forms of the Formylpeptide Chemoattractant Receptor and their Relationship to GTP-binding Proteins. **Biochem. Biophys. Res. Commun.** 161, 276-283.
8. Polakis, P. G., Snyderman, R. and Evans, T. 1989 Characterization of G25K, a GTP-binding Protein Containing a Novel Putative Nucleotide Binding Domain. **Biochem. Biophys. Res. Commun.** 160, 25-32.
9. Polakis, P., Weber, R. F., Nevins, B., Didsbury, J., Evans, T. and Snyderman, R. 1989 Identification of the *ral* and *rac1* Gene Products, Low Molecular Mass GTP-binding Proteins from Human Platelets. **J. Biol. Chem.** 264, 16383-16389.
10. Snyderman, R., Perianin, A., Evans, T., Polakis, P. and Didsbury, J. 1989 G Proteins and Neutrophil Function. In *ADP-Ribosylating Toxins and G Proteins: Insights into Signal Transduction.* (J. Moss and M. Vaughn, eds.) Amer. Soc. Microbiol. pp. 295-323.

11. Hart, M.J., Polakis, P.G., Evans, T. and Cerrione, R.A. 1990 The Identification and Characterization of an Epidermal Growth Factor-Stimulated Phosphorylation of a Specific Low Molecular Mass GTP-binding Protein in a Reconstituted Phospholipid Vesicle System. *J. Biol. Chem.* 265, 5990-6001.
12. Yatani, A., Okabe, K., Polakis, P., Halenbeck, R., McCormick, F. and Brown, A. M. 1990 ras p21 and GAP Inhibit Coupling of Muscarinic Receptors to Atrial K⁺ Channels. *Cell*. 61, 769-776.
13. Munemitsu, S., Innis, M.A., Clark, R., McCormick, F., Ullrich, A. and Polakis, P.G. 1990 Molecular Cloning and Expression of a G25K cDNA, the Human Homolog of the Yeast Cell Cycle Gene CDC42. *Mol. Cell. Biol.* 10, 5977-5982.
14. Polakis, P.G., Rubinfeld, B., Evans, T. and McCormick, F. 1991 Purification of Plasma Membrane-Associated GTPase Activating Protein (GAP) Specific for rap-1/krev-1 from HL60 Cells. *Proc. Natl. Acad. Sci. USA* 88, 239-243.
15. Moran, M. F., Polakis, P., McCormick, F., Pawson, T. and Ellis, C. 1991 Protein Tyrosine Kinases Regulate the Phosphorylation, Protein Interactions, Subcellular Distribution, and Activity of p21ras GTPase Activating Protein. *Mol. Cell. Biol.* 11, 1804-1812.
16. Rubinfeld, B., Wong, G., Bekesi, E., Wood, A., McCormick, F. and Polakis, P. G. 1991 A Synthetic Peptide Corresponding to a Sequence in the GTPase Activating Protein Inhibits p21^{ras} Stimulation and Promotes Guanine Nucleotide Exchange. *Internatl. J. Peptide and Prot. Res.* 38, 47-53.
17. Rubinfeld, B., Munemitsu, S., Clark, R., Conroy, L., Watt, K., Crosier, W., McCormick, F., and Polakis, P. 1991 Molecular Cloning of a GTPase Activating Protein Specific for the Krev-1 Protein p21^{rap1}. *Cell* 65, 1033-1042.
18. Zhang, K., Papageorge, A., G., Martin, P., Vass, W. C., Olah, Z., Polakis, P., McCormick, F. and Lowy, D. R. 1991 Heterogenous Amino Acids in RAS and Rap1A Specifying Sensitivity to GAP Proteins. *Science* 254, 1630-1634.
19. Martin, G., Yatani, A., Clark, R., Polakis, P., Brown, A. M. and McCormick, F. 1992 GAP Domains Responsible for p21^{ras}-dependent Inhibition of Muscarinic Atrial K⁺ Channel Currents. *Science* 255, 192-194.
20. McCormick, F., Martin, G. A., Clark, R., Bollag, G. and Polakis, P. 1992 Regulation of p21ras by GTPase Activating Proteins. *Cold Spring Harbor Symposia on Quantitative Biology*. Vol. 56, 237-241.
21. Pronk, G. B., Polakis, P., Wong, G., deVries-Smits, A. M., Bos J. L. and McCormick, F. 1992 p60^{v-src} Can Associate with and Phosphorylate the p21^{ras} GTPase Activating Protein. *Oncogene* 7,389-394.
22. Polakis P. and McCormick, F. 1992 Interactions Between p21^{ras} Proteins and Their GTPase Activating Proteins. In Cancer Surveys (Franks, L. M., ed.) 12, 25-42.

23. Wong, G., Muller, O., Clark, R., Conroy, L., Moran, M., Polakis, P. and McCormick, F. 1992 Molecular cloning and nucleic acid binding properties of the GAP-associated tyrosine phosphoprotein p62. *Cell* 69, 551-558.
24. Polakis, P., Rubinfeld, B. and McCormick, F. 1992 Phosphorylation of rap1GAP in vivo and by cAMP-dependent Kinase and the Cell Cycle p34^{cdc2} Kinase in vitro. *J. Biol. Chem.* 267, 10780-10785.
25. McCabe, P.C., Haubrauck, H., Polakis, P., McCormick, F., and Innis, M. A. 1992 Functional Interactions Between p21^{rap1A} and Components of the Budding pathway of *Saccharomyces cerevisiae*. *Mol. Cell. Biol.* 12, 4084-4092.
26. Rubinfeld, B., Crosier, W.J., Albert, I., Conroy, L., Clark, R., McCormick, F. and Polakis, P. 1992 Localization of the rap1GAP Catalytic Domain and Sites of Phosphorylation by Mutational Analysis. *Mol. Cell. Biol.* 12, 4634-4642.
27. Ando, S., Kaibuchi, K., Sasaki, K., Hiraoka, T., Nishiyama, T., Mizuno, T., Asada, M., Nunoi, H., Matsuda, I., Matsuura, Y., Polakis, P., McCormick, F. and Takai, Y. 1992 Post-translational processing of rac p21s is important both for their interaction with the GDP/GTP exchange proteins and for their activation of NADPH oxidase. *J. Biol. Chem.* 267, 25709-25713.
28. Janoueix-Lerosey, I., Polakis, P., Tavitian, A. and deGunzburg, J. 1992 Regulation of the GTPase activity of the ras-related rap2 protein. *Biochem. Biophys. Res. Commun.* 189, 455-464.
29. Polakis, P. 1993 GAPs Specific for the rap1/Krev-1 Protein. in GTP-binding Proteins: the ras-superfamily. (J.C. LaCale and F. McCormick, eds.) 445-452.
30. Polakis, P. and McCormick, F. 1993 Structural requirements for the interaction of p21^{ras} with GAP, exchange factors, and its biological effector target. *J. Biol. Chem.* 268, 9157-9160.
31. Rubinfeld, B., Souza, B., Albert, I., Muller, O., Chamberlain, S., Masiarz, F., Munemitsu, S. and Polakis, P. 1993 Association of the APC gene product with beta-catenin. *Science* 262, 1731-1734.
32. Weiss, J., Rubinfeld, B., Polakis, P., McCormick, F., Cavenee, W. A. and Arden, K. 1993 The gene for human rap1-GTPase activating protein (rap1GAP) maps to chromosome 1p35-1p36.1. *Cytogenet. Cell Genet.* 66, 18-21.
33. Sato, K. Y., Polakis, P., Haubruck, H., Fasching, C. L., McCormick, F. and Stanbridge, E. J. 1994 Analysis of the tumor suppressor activity of the K-ras gene in human tumor cell lines. *Cancer Res.* 54, 552-559.
34. Janoueix-Lerosey, I., Fontenay, M., Tobelem, G., Tavitian, A., Polakis, P. and DeGunzburg, J. 1994 Phosphorylation of rap1GAP during the cell cycle. *Biochem. Biophys. Res. Commun.* 202, 967-975.
35. Munemitsu, S., Souza, B., Mueller, O., Albert, I., Rubinfeld, B., and Polakis, P. 1994 The APC gene product associates with microtubules in vivo and affects their assembly in vitro. *Cancer Res.* 54, 3676-3681.

36. Rubinfeld, B. and Polakis, P. 1995 Purification of baculovirus produced rap1GAP. **Methods Enz.** 255,31
37. Polakis, P. 1995 Mutations in the APC gene and their implications for protein structure and function. **Current Opinions in Genetics and Development** 5, 66-71
38. Rubinfeld, B., Souza, B., Albert, I., Munemitsu, S. and Polakis P. 1995 The APC protein and E-cadherin form similar but independent complexes with α -catenin, β -catenin and Plakoglobin. **J. Biol. Chem.** 270, 5549-5555
39. Munemitsu, S., Albert, I., Souza, B., Rubinfeld, B., and Polakis, P. 1995 Regulation of intracellular β -catenin levels by the APC tumor suppressor gene. **Proc. Natl. Acad. Sci.** 92, 3046-3050.
40. Lock, P., Fumagalli, S., Polakis, P. McCormick, F. and Courtneidge, S. A. 1996 The human p62 cDNA encodes Sam68 and not the rasGAP-associated p62 protein. **Cell** 84, 23-24.
41. Papkoff, J., Rubinfeld, B., Schryver, B. and Polakis, P. 1996 Wnt-1 regulates free pools of catenins and stabilizes APC-catenin complexes. **Mol. Cell. Biol.** 16, 2128-2134.
42. Rubinfeld, B., Albert, I., Porfiri, E., Fiol, C., Munemitsu, S. and Polakis, P. 1996 Binding of GSK3 β to the APC- β -catenin complex and regulation of complex assembly. **Science** 272, 1023-1026.
43. Munemitsu, S., Albert, I., Rubinfeld, B. and Polakis, P. 1996 Deletion of amino-terminal structure stabilizes β -catenin in vivo and promotes the hyperphosphorylation of the APC tumor suppressor protein. **Mol. Cell. Biol.** 16, 4088-4094.
44. Hart, M. J., Callow, M. G., Sousa, B. and Polakis P. 1996 IQGAP1, a calmodulin binding protein with a rasGAP related domain, is a potential effector for cdc42Hs. **EMBO J.** 15, 2997-3005.
45. Nathke, I. S., Adams, C. L., Polakis, P., Sellin, J. and Nelson, W. J. 1996 The adenomatous polyposis coli (APC) tumor suppressor protein is localized to plasma membrane sites involved in active epithelial cell migration. **J. Cell. Biol.** 134, 165-180.
46. Hart, M. J., Sharma, S., elMasry, N., Qui, R-G., McCabe, P., Polakis, P. and Bollag, G. 1996 Identification of a novel guanine nucleotide exchange factor for the rho GTPase. **J. Biol. Chem.** 271, 25452.
47. Thomas JE, Smith M, Rubinfeld B, Gutowski M, Beckmann RP, and Polakis P. 1996 Subcellular localization and analysis of apparent 180-kDa and 220-kDa proteins of the breast cancer susceptibility gene, BRCA1. **J. Biol. Chem.** 1996 271, 28630-28635
48. Hayashi, S., Rubinfeld, B., Souza, B., Polakis, P., Wieschaus, E., and Levine, A. 1997 A Drosophila homolog of the tumor suppressor adenomatous polyposis coli

down-regulates β -catenin but its zygotic expression is not essential for the regulation of armadillo. *Proc. Natl. Acad. Sci.* 94, 242-247.

49. Vleminckx, K., Rubinfeld, B., Polakis, P. and Gumbiner, B. 1997 The APC tumor suppressor protein induces a new axis in *Xenopus* embryos. *J. Cell. Biol.* 136, 411-420.

50. Rubinfeld, B., Robbins, P., El-Gamil, M., Albert, I., Porfiri, P. and Polakis, P. 1997 Stabilization of β -catenin by genetic defects in melanoma cell lines. *Science* 275, 1790-1792.

51. Polakis, P. The adenomatous polyposis coli (APC) tumor suppressor. 1997 *Biochem. Biophys. Acta*, 1332, F127-F147.

52. Rubinfeld, B., Albert, I., Porfiri, E., Munemitsu, S., and Polakis, P. 1997 Loss of β -catenin regulation by the APC tumor suppressor protein correlates with loss of structure due to common somatic mutations of the gene. *Cancer Res.* 57, 4624-4630.

53. Porfiri, E., Rubinfeld, B., Albert, I., Hovanes, K., Waterman, M., and Polakis, P. 1997 Induction of a β -catenin-LEF-1 complex by wnt-1 and transforming mutants of β -catenin. *Oncogene* 15, 2833-2839.

54. Thomas JE, Smith M, Tonkinson JL, Rubinfeld B, and Polakis P., 1997 Induction of phosphorylation on BRCA1 during the cell cycle and after DNA damage. *Cell Growth Differ.* 8, 801-809.

55. Hart, M., de los Santos, R., Albert, I., Rubinfeld, B., and Polakis P., 1998 Down regulation of β -catenin by human Axin and its association with the adenomatous polyposis coli (APC) tumor suppressor, β -catenin and glycogen synthase kinase 3 β . *Current Biology* 8, 573-581.

56. Polakis, P. 1998 The oncogenic activation of β -catenin. *Current Opinions in Genetics and Development* 9, 15-21

57. Matt Hart, Jean-Paul Concordet, Irina Lassot, Iris Albert, Rico del los Santos, Herve Durand, Christine Perret, Bonnee Rubinfeld, Florence Margottin, Richard Benarous and Paul Polakis. 1999 The F-box protein β -TrCP associates with phosphorylated β -catenin and regulates its activity in the cell. *Current Biology* 9, 207-10.

58. Howard C. Crawford, Barbara M. Fingleton, Bonnee Rubinfeld, Paul Polakis and Lynn M. Matrisian 1999 The metalloproteinase matrilysin is a target of β -catenin transactivation in intestinal tumours. *Oncogene* 18, 2883-91.

59. Meng J, Glick JL, Polakis P, Casey PJ. 1999 Functional interaction between Galpha(z) and Rap1GAP suggests a novel form of cellular cross-talk. *J Biol Chem.* 17, 36663-9

60. Vijayasurian Easwaran, Virginia Song, Paul Polakis and Steve Byers 1999 The ubiquitin-proteasome pathway and serine kinase activity modulate APC mediated regulation of β -catenin-LEF signaling. *J. Biol. Chem.* 274(23):16641-5.
61. Polakis P, Hart M and Rubinfeld B. 1999 Defects in the regulation of beta-catenin in colorectal cancer. *Adv Exp Med Biol.* 470, 23-32
62. Shen Z, Batzer A, Koehler JA, Polakis P, Schlessinger J, Lydon NB, Moran MF. 1999 Evidence for SH3 domain directed binding and phosphorylation of Sam68 by Src. *Oncogene.* 18, 4647-53
64. Thomas GM, Frame S, Goedert M, Nathke I, Polakis P, Cohen P. 1999 A GSK3- binding peptide from FRAT1 selectively inhibits the GSK3-catalysed phosphorylation of axin and beta-catenin. *FEBS Lett.* 458, 247-51.
65. Peifer M, Polakis P. 2000 Wnt signaling in oncogenesis and embryogenesis—a look outside the nucleus. *Science* 287,1606-9.
66. Polakis P. 2000 Wnt signaling and cancer. *Genes Dev*;14, 1837-1851.
67. Spink KE, Polakis P, Weis WI 2000 Structural basis of the Axin-adenomatous polyposis coli interaction. *EMBO J* 19, 2270-2279.
68. Szeto, W., Jiang, W., Tice, D.A., Rubinfeld, B., Hollingshead, P.G., Fong, S.E., Dugger, D.L., Pham, T., Yansura, D.E., Wong, T.A., Grimaldi, J.C., Corpuz, R.T., Singh J.S., Frantz, G.D., Devaux, B., Crowley, C.W., Schwall, R.H., Eberhard, D.A., Rastelli, L., Polakis, P. and Pennica, D. 2001 Overexpression of the Retinoic Acid-Responsive Gene Stra6 in Human Cancers and its Synergistic Induction by Wnt-1 and Retinoic Acid. *Cancer Res* 61, 4197-4204.
69. Rubinfeld B, Tice DA, Polakis P. 2001 Axin dependent phosphorylation of the adenomatous polyposis coli protein mediated by casein kinase 1 epsilon. *J Biol Chem* 276, 39037-39045.
70. Polakis P. 2001 More than one way to skin a catenin. *Cell* 2001 105, 563-566.
71. Tice DA, Soloviev I, Polakis P. 2002 Activation of the Wnt Pathway Interferes with Serum Response Element-driven Transcription of Immediate Early Genes. *J Biol. Chem.* 277, 6118-6123.
72. Tice DA, Szeto W, Soloviev I, Rubinfeld B, Fong SE, Dugger DL, Winer J,

- Williams PM, Wieand D, Smith V, Schwall RH, Pennica D, Polakis P. 2002 Synergistic activation of tumor antigens by wnt-1 signaling and retinoic acid revealed by gene expression profiling. *J Biol Chem.* 277,14329-14335.
73. Polakis, P. 2002 Casein kinase I: A wnt'er of disconnect. *Curr. Biol.* 12, R499.
74. Mao, W., Luis, E., Ross, S., Silva, J., Tan, C., Crowley, C., Chui, C., Franz, G., Senter, P., Koeppen, H., Polakis, P. 2004 EphB2 as a therapeutic antibody drug target for the treatment of colorectal cancer. *Cancer Res.* 64, 781-788.
75. Shibamoto, S., Winer, J., Williams, M., Polakis, P. 2003 A Blockade in Wnt signaling is activated following the differentiation of F9 teratocarcinoma cells. *Exp. Cell Res.* 29211-20.
76. Zhang Y, Eberhard DA, Frantz GD, Dowd P, Wu TD, Zhou Y, Watanabe C, Luoh SM, Polakis P, Hillan KJ, Wood WI, Zhang Z. 2004 GEPIS—quantitative gene expression profiling in normal and cancer tissues. *Bioinformatics*, April 8

EXHIBIT B

	tumor mRNA	tumor IHC
UNQ2525	+	+
UNQ2378	+	+
UNQ972	+	-
UNQ97671	+	+
UNQ2964	+	+
UNQ323	+	+
UNQ1655	+	+
UNQ2333	+	+
UNQ9638	+	+
UNQ8209	+	+
UNQ6507	+	+
UNQ8196	+	+
UNQ9109	+	+
UNQ100	+	+
UNQ178	+	+
UNQ1477	+	+
UNQ1839	+	+
UNQ2079	+	+
UNQ8782	+	+
UNQ9646	+	-
UNQ111	+	+
UNQ3079	+	+
UNQ8175	+	+
UNQ9509	+	+
UNQ10978	+	-
UNQ2103	+	+
UNQ1563	+	+
UNQ16188	+	+
UNQ13589	+	+
UNQ1078	+	+
UNQ879	+	+

Gene-expression profiles predict survival of patients with lung adenocarcinoma

DAVID G. BEER¹, SHARON L.R. KARDIA², CHIANG-CHING HUANG³, THOMAS J. GIORDANO⁴, ALBERT M. LEVIN², DAVID E. MISEK⁵, LIN LIN¹, GUOAN CHEN¹, TAREK G. GHARIB¹, DAFYDD G. THOMAS⁴, MICHELLE L. LIZYNESS⁴, RORK KUICK⁵, SATORU HAYASAKA³, JEREMY M.G. TAYLOR³, MARK D. IANNETTONI¹, MARK B. ORRINGER¹ & SAMIR HANASH⁵

¹Departments of ¹Surgery, ²Epidemiology, ³Biostatistics, ⁴Pathology and ⁵Pediatrics, University of Michigan, Ann Arbor, Michigan, USA
Correspondence should be addressed to D.G.B.; email: dgbeer@umich.edu.

Published online: 15 July 2002, doi:10.1038/nm733

Histopathology is insufficient to predict disease progression and clinical outcome in lung adenocarcinoma. Here we show that gene-expression profiles based on microarray analysis can be used to predict patient survival in early-stage lung adenocarcinomas. Genes most related to survival were identified with univariate Cox analysis. Using either two equivalent but independent training and testing sets, or 'leave-one-out' cross-validation analysis with all tumors, a risk index based on the top 50 genes identified low-risk and high-risk stage I lung adenocarcinomas, which differed significantly with respect to survival. This risk index was then validated using an independent sample of lung adenocarcinomas that predicted high- and low-risk groups. This index included genes not previously associated with survival. The identification of a set of genes that predict survival in early-stage lung adenocarcinoma allows delineation of a high-risk group that may benefit from adjuvant therapy.

Lung cancer remains the leading cause of cancer death in industrialized countries. Most patients with non-small cell lung cancer (NSCLC) present with advanced disease, and despite recent advances in multi-modality therapy, the overall 10-year survival rate remains a dismal 8–10%. However, a significant minority of patients (~25–30%) with NSCLC have stage I disease and receive surgical intervention alone. Although 35–50% of patients with stage I disease will relapse within 5 years^{2,4}, it is not currently possible to identify specific high-risk patients.

Adenocarcinoma is currently the predominant histological subtype of NSCLC (refs. 1,5,6). Although morphological assessment of lung carcinomas can roughly stratify patients, there is a need to identify patients at high risk for recurrent or metastatic disease. Preoperative variables that affect survival of patients with NSCLC have been identified^{7–10}. Tumor size, vascular invasion, poor differentiation, high tumor-proliferative index and several genetic alterations, including K-ras (refs. 11,12) and p53 (refs. 10,13) mutations, have prognostic significance. Multiple independently assessed genes or gene products have also been investigated to better predict patient prognosis in lung cancer^{14–16}. Technologies that simultaneously analyze the expression of thousands of genes¹⁷ can be used to correlate gene-expression patterns with numerous clinical parameters—including patient outcome—to better predict tumor behavior in individual patients¹⁸. Analyses of lung cancers using array technologies have identified subgroups of tumors that differ according to tumor type and histological subclasses and, to a lesser extent, survival among adenocarcinoma patients^{21,22}. Here we correlated gene-expression profiles with clinical outcome in a cohort of patients with lung adenocarcinoma and identified specific genes that

predict survival among patients with stage I disease. For further validation, we also show that the risk index predicted survival in an independent cohort of stage I lung adenocarcinomas.

Hierarchical profile clustering yields three tumor subsets

Using oligonucleotide arrays, we generated gene-expression profiles for 86 primary lung adenocarcinomas, including 67 stage I and 19 stage III tumors, as well as 10 non-neoplastic lung samples. Selected sample replicates showed high correlation among coefficients and reliable reproducibility. We determined transcript abundance using a custom algorithm and the data set was trimmed of genes expressed at extremely low levels, that is, genes were excluded if the measure of their 75th percentile value was less than 100. Although potentially resulting in the loss of some information, trimming in this manner decreased the possibility that the clustering algorithm would be strongly influenced by genes with little or no expression in these samples. Hierarchical clustering with the resulting 4,966 genes yielded 3 clusters of tumors (Fig. 1). All 10 non-neoplastic samples clustered tightly together within Cluster 1 (data not shown). We examined the relationships between cluster and patient and tumor characteristics (Fig. 1 and Supplementary Figure A online). There were associations between cluster and stage ($P = 0.030$) and between cluster and differentiation ($P = 0.01$). Cluster 1 contained the greatest percentage (42.8%) of well differentiated tumors, followed by Cluster 2 (27%) and Cluster 3 (4.7%). Cluster 3 contained the highest percentage of both poorly differentiated (47.6%) and stage III tumors (42.8%), yet contained 3 (14.3%) moderately differentiated and 1 (5%) well differentiated stage I tumor. Notably, 11 stage I tumors were present in Cluster 3, sug-



gesting a common gene-expression profile for this subset of stage I and stage III tumors.

For patients with stage I and stage III tumors, the average ages were 68.1 and 64.5 years and the percentage of smokers was 88.9% and 89.5%, respectively. Marginally significant associations between cluster and smoking history were observed ($P = 0.06$). A significant relationship between histopathological classification and cluster was only discernable for bronchioloalveolar adenocarcinomas (BAs), which were only present in Clusters 1 and 2 ($P = 0.0055$) and comprised 35.7% and 12.3% of tumors for Clusters 1 and 2, respectively.

We examined the heterogeneity in gene-expression profiles based on the trimmed data set among normal lung samples and stage I and stage III adenocarcinomas by calculating correlation coefficients between all pairs of samples. In contrast to normal lung samples that displayed highly similar gene-expression profiles (median correlation, 0.9), both stage I and III lung tumors demonstrated much greater heterogeneity in their expression profiles with lower correlation coefficients (median values, 0.82 and 0.79, respectively).

Northern-blot and immunohistochemistry analyses

Of the 4,966 genes examined, 967 differed significantly between stage I and III adenocarcinomas, a number in excess of that expected by chance alone (248 at alpha level (α) = 0.05). Three genes were arbitrarily selected to verify the microarray expression data. The mRNA from 20 of the normal lung and tumor samples was examined by northern-blot hybridization with probes for insulin-like growth factor-binding protein 3 (IGFBP3), cystatin C

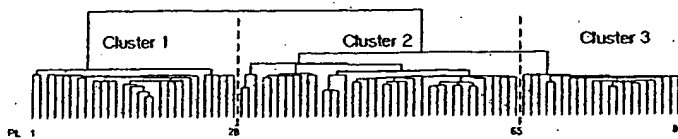


Fig. 1 Unsupervised classification analysis of lung adenocarcinomas. 3 classes of tumors identified by agglomerative hierarchical clustering of gene-expression profiles using the 4,966 expressed genes. Patient and histopathological information for each lung adenocarcinoma case by cluster designation and methods for K-ras 12/13th-codon mutational status and nuclear p53 protein accumulation are provided (Supplementary Figure A online). TN classification denotes information regarding patient tumor size and nodal involvement. Associations between cluster membership and patient or histopathological variables are indicated at significance level ($P \leq 0.05$).

and lactate dehydrogenase A (LDH-A) (Fig. 2a). Two gene probes not represented on the microarrays were used as controls, including histone H4, a potential index of overall cell proliferation, and 28S ribosomal RNA, a control for sample loading and transfer. The relative amounts of IGFBP3, cystatin C and LDH-A mRNA strongly correlated with microarray-based measurements (Fig. 2b). In both assays, IGFBP3 and LDH-A mRNA levels increased from stage I to stage III adenocarcinomas and were higher than those in normal lung. Cystatin C mRNA levels were more variable but relatively greater in normal lung than tumors. These results suggest that the oligonucleotide microarrays provided reliable measures of gene expression. The tumors showed slightly greater histone H4 expression than the normal lung, likely reflecting increased proliferation of tumor cells.

Immunohistochemistry was performed for IGFBP3, cystatin C and HSP-70 to determine whether mRNA overexpression was reflected by an increase of their corresponding proteins in tumors.

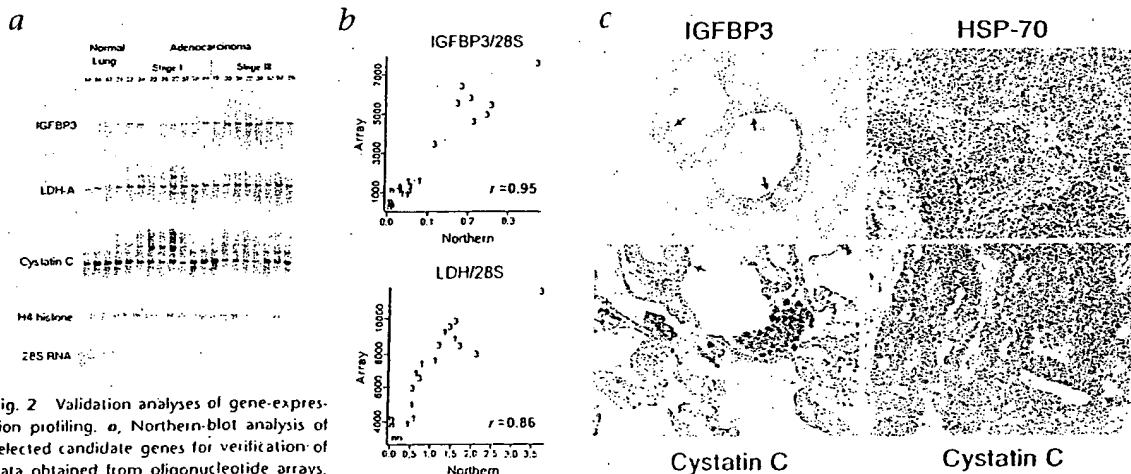


Fig. 2 Validation analyses of gene-expression profiling. a, Northern-blot analysis of selected candidate genes for verification of data obtained from oligonucleotide arrays. The same sample RNA for the 4 uninvolved lung, 8 stage I and 8 stage III tumors was used for the northern-blot and oligonucleotide array analyses. b, Correlation analysis of quantitative data obtained from oligonucleotide arrays and northern blots measured by integrated phosphorimager-based signals for the IGFBP3 and LDH-A genes. The ratio of IGFBP3, cystatin C and LDH-A mRNA to 28S rRNA was determined. The relative values for each gene from each sample are shown. n, non-neoplastic normal lung; 1, stage I tumors; 3, stage III tumors. c, Immunohistochemical analysis of IGFBP3, HSP-70 and cystatin C in lung and lung adenocarcinomas. Cytoplasmic IGFBP3 immunoreactivity in a neoplastic gland (tumor L27)

with prominent apical staining (blue reactant staining, arrow, upper left). Diffuse cytoplasmic HSP-70 immunoreactivity (tumor L27), yet stromal elements show no reactivity (upper right). Normal lung parenchyma (lower left) shows cytoplasmic cystatin C immunoreactivity in alveolar pneumocytes (arrow) and intra-alveolar macrophages but tumor (L90) shows diffuse cytoplasmic cystatin C immunoreactivity with prominent apical staining (lower right). Magnification, $\times 200$

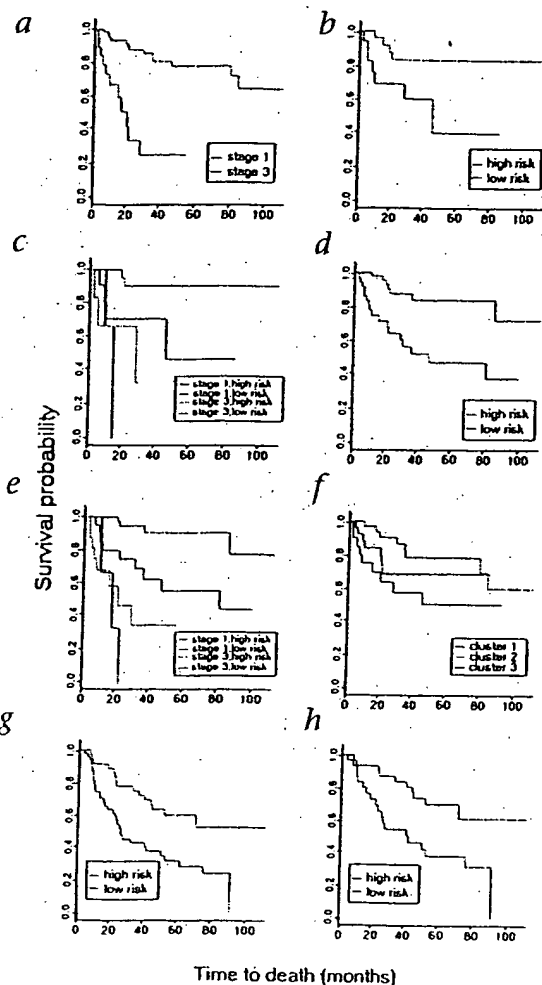


Fig. 3 Gene-expression profiles and patient survival. **a**, Relationship between tumor stage and patient survival (stage 1 and stage 3 differ significantly, $P < 0.0001$). **b**, Relationship between the survival in the 43 test samples and their risk assignments based on the 50-gene risk index estimated in the 43 training samples. The high- and low-risk groups differ significantly ($P = 0.024$). **c**, Relationship between patient survival and the risk assignments in test samples (in **b**) conditional for tumor stage. The high- and low-risk stage I groups differ significantly ($P = 0.028$), whereas stage III low- and high-risk groups did not ($P = 0.634$). **d**, Relationship between survival in the test cases and their risk assignments based on the 86 'leave-one-out' cross-validation of the 50-gene risk index. The high- and low-risk groups differ significantly ($P = 0.0006$). **e**, Relationship between test case's risk assignment and survival (in **d**) conditional on tumor stage. The high- and low-risk stage I lung adenocarcinoma groups differ significantly from each other ($P = 0.003$), whereas low- and high-risk stage III tumors do not. **f**, Relationship between tumor class identified by hierarchical clustering and patient survival. Survival for patients in Cluster 3 differed relative to the tumors in Cluster 2 ($P = 0.037$) and approached significance for Cluster 1 and 2 combined ($P = 0.06$). **g**, Analysis of the Michigan-based risk index using top cross-validated survival genes identify a low- and high-risk group in an independent cohort of 84 Massachusetts-based lung adenocarcinomas that are significantly different ($P = 0.003$). **h**, Among the 62 stage I lung adenocarcinomas in the Massachusetts sample, the high- and low-risk groups differed significantly ($P = 0.006$).

After conservatively choosing the 60th percentile cutoff point from the training set, we then applied this risk index and cutoff point to the testing set. The risk index of the top 50 genes correctly identified low- and high-risk individuals within the independent testing set ($P = 0.024$) (Fig. 3b and Supplementary Methods online). Notably, 11 stage I tumors were included in the high-risk subgroup. When this risk assignment was then conditionally examined for stage progression (Fig. 3c), low- and high-risk groups among stage I tumors were found to differ ($P = 0.028$) in their survival.

Identification of a robust set of survival genes

Although predictive of patient survival, a single training-testing set may not provide the most robust set of genes due to random sampling issues. Therefore, a 'leave-one-out' cross-validation approach was used to identify genes associated with survival from all 86-tumor samples. We first developed a 50-gene risk index in each training set, and then applied the risk index to the test case held out from the full set of tumors and assigned the held out tumor to the high- or low-risk groups (Fig. 3d). The high and low-risk subgroups determined in the test cases differed significantly in their overall survival ($P = 0.0006$). Among the larger group of stage I lung adenocarcinomas, the low-risk ($n = 46$) and high-risk ($n = 21$) groups had markedly different survival ($P = 0.003$) (Fig. 3e). Table 1 lists selected examples of the cumulative top 100 genes derived from this cross-validation procedure (complete list in Supplementary Table A online).

It was also noted that many of the stage I patients in the high-risk subgroup (Fig. 3e) were present in Cluster 3 (Fig. 1). Kaplan-Meier analysis (Fig. 3f) demonstrated a significantly worse survival ($P = 0.037$) for patients in Cluster 3 relative to patients in Cluster 2 and approaching significance for Cluster 1 and 2 combined ($P = 0.06$). This further indicates the important relationship between gene-expression profiles and patient survival, independent of disease stage.

Consistent with previous analyses of lung adenocarcinomas²³, 40% of stage I and 57.8% of stage III tumors had 12th or 13th codon K-ras gene mutations. Those patients with tumors containing K-ras mutations showed a trend of poorer survival, but

Immunoreactivity for both IGFBP-3 and HSP-70 (Fig. 2c) was detected in the cytoplasm of the adenocarcinomas, with little detectable reactivity in the stromal or inflammatory cells. Cystatin C was detected in alveolar pneumocytes and intra-alveolar macrophages in non-neoplastic lung parenchyma and also consistently in the cytoplasm of neoplastic cells.

Gene-expression profiles predict survival

As expected, Kaplan-Meier survival curves (Fig. 3a) and log-rank tests indicated poorer survival among stage III compared with stage I adenocarcinomas ($P = < 0.0001$). Two statistical approaches were used to determine whether gene-expression profiles could predict survival using the data set of 4,966 genes. In one approach, equal numbers of randomly assigned stage I and stage III tumors constituted training ($n = 43$) and testing ($n = 43$) sets. In the training set, the top 10, 20, 50 or 75 genes were used to create risk indices that were evaluated for their association with survival using the 50th, 60th or 70th percentile cutoff points to categorize patients into high or low groups. The results were similar across cutoff points but the 50-gene risk index had the best overall association with survival in the training set.

Table 1 Selected examples of the top 100 genes from cross-validation

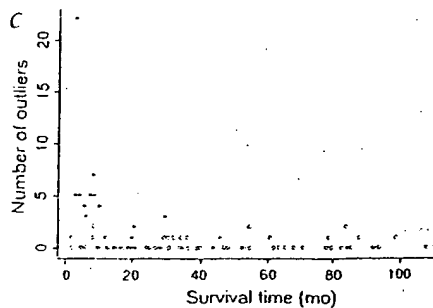
Gene name	P (normal versus tumor t-test)	% Change in tumor	P (stage I versus stage III t-test)	% Change in stage III	Coefficient β	Unigene comment
CASP4	0.56	-6%	0.02	57%	0.0022	Apoptosis-related Caspase 4, apoptosis- related cysteine protease
P63	9.73E-04	37%	0.03	43%	0.0010	Transmembrane protein (63 kD), endoplasmic reticulum/ Golgi intermediate compartment
KRT7	8.02E-08	126%	0.11	55%	0.0003	Cell adhesion and structure Keratin 7
LAMB1	0.14	-20%	0.01	60%	0.0027	Laminin, β 1
BMP2	0.54	-21%	0.27	47%	0.0044	Cell cycle and growth regulators Bone morphogenetic protein 2
CDC6	1.31E-05	1070%	0.05	148%	0.0124	CDC6 (cell division cycle 6, <i>Saccharomyces cerevisiae</i> homolog)
S100P	2.10E-08	1572%	0.19	77%	0.0001	S100 calcium-binding protein P
SERPINE1	2.89E-03	72%	0.25	30%	0.0008	Serine (or cysteine) proteinase inhibitor, clade E (nexin)
STX1A	8.65E-08	54%	0.07	26%	0.0031	Syntaxin 1A (brain)
ADM	0.05	39%	0.04	117%	0.0016	Cell signaling adrenomedullin
AKAP 12	8.53E-03	-47%	0.05	214%	0.0010	A kinase (PRKA) anchor protein (gravin) 12
ARHE	0.06	-39%	0.05	87%	0.0092	ras homolog gene family, member E
GRB7	2.02E-03	38%	0.63	15%	0.0030	Growth factor receptor-bound protein 7
VEGF	6.50E-08	174%	0.02	85%	0.0013	Vascular endothelial growth factor
WNT10B	0.05	31%	0.48	20%	0.0022	Wingless-type MMTV integration site family, member 10B
HSPA8	0.36	8%	9.01E-04	51%	0.0008	Chaperones Heat-shock 70 kD protein 8
ERBB2	0.04	92%	0.37	120%	0.0013	Receptors v-erb-b2 avian erythroblastic leukemia viral oncogene homolog 2
FXD3	0.10	111%	0.31	73%	0.0046	FXD domain-containing ion transport regulator 3
SLC20A1	1.34E-03	58%	0.02	66%	0.0021	Solute carrier family 20 (phosphate transporter), member 1
CSTB	1.57E-04	50%	0.15	34%	0.0001	Enzymes, cellular metabolism Cystatin B (stelin B)
CTSL	0.48	-10%	0.03	67%	0.0007	Cathepsin L
CYP24	3.16E-06	N/A	0.97	2%	0.0008	Cytochrome P450, subfamily XXIV (vitamin D 24-hydroxylase)
FUT3	1.07E-07	114%	0.97	-1%	0.0033	Fucosyltransferase 3 (galactoside 3(4)-L- fucosyltransferase, Lewis blood group included)
MLN64	0.20	32%	0.42	80%	0.0007	Steroidogenic acute regulatory protein related
PDE7A	0.12	33%	0.01	-35%	-0.0187	Phosphodiesterase 7A
PLGL	0.04	-68%	0.35	-170%	-0.0011	Plasminogen-like
SLC1A6	0.07	-32%	0.12	86%	0.0069	Solute carrier family 1 (high-affinity aspartate/ glutamate transporter), member 6
COPEB	0.10	-33%	0.26	25%	0.0016	Transcription and translation Core promoter element binding protein
CRK	0.10	32%	0.03	48%	0.0098	v-crk avian sarcoma virus CT10 oncogene homolog
RELA	0.26	-7%	0.01	20%	0.0034	v-rel avian reticuloendotheliosis viral oncogene homolog A
KIAA0005	2.21E-04	40%	0.02	45%	0.0010	Unknown function KIAA0005 gene product
MCB1	0.27	125%	0.33	459%	0.0018	Mammaglobin 1

Bolded genes were also significant for survival in 43 tumor training set (Fig. 3b).

Table 1 Selected examples of the cumulative top 100 genes identified using training-testing, cross-validation of all 86 lung tumor samples. The percent change, as well as the direction, for the average values of the 10 non-neoplastic lung to all tumors, and for the 67 stage I to the 19 stage III tumors are shown. A positive coefficient β value is indicative of a relationship of gene expression to a

poorer patient outcome. The genes are listed in potential functional categories. Genes that were also present in the top 50 survival genes using the 43-tumor training set (Fig. 3b) are indicated in bold type. Complete listing of the gene probe sets and annotated gene and unigene identifiers can be found in the Supplementary Methods.





820

this difference did not reach statistical significance among all patients ($P = 0.25$), between patients within tumor clusters ($P = 0.41$) or when analyzed separately among stage I ($P = 0.22$) and stage III ($P = 0.53$) patients. Nuclear accumulation of p53 was detected in 17.9% stage I and in 22.2% stage III tumors. No significant relationship was observed for p53 staining and patient survival, cluster or tumor stage.

Confirmation using an independent set of adenocarcinomas
The robustness of our 50-gene risk index in predicting survival in lung adenocarcinomas was tested using oligonucleotide gene-expression data obtained from a completely independent (Massachusetts-based) sample of 84 lung adenocarcinomas (62 stage I, 14 stage II and 8 stage III; ref. 21, and dataset A at www.genome.wi.mit.edu/MPPR/lung). To ensure equivalent power for testing and comparability of samples, the criteria for including tumors in the analysis were 40% or greater tumor cellularity, no mixed histology (that is, adenosquamous) and patient survival information. To obtain comparative gene-expression measures between the two data sets, gene sequences present on the U95A and HuGeneFL array were examined, and expression data for our top 50 cross-validation genes for all 84 Massachusetts samples were obtained and processed²⁴ (see also Supplementary Methods online). When we examined the risk assignment of these 84 samples, employing the identical cutoff point used for the 86 Michigan-based lung samples, we observed low- and high-risk groups (Fig. 3g; $P = 0.003$). Notably, among the 62 stage I tumors, high- and low-risk groups were observed that differed significantly ($P = 0.006$) in their survival (Fig. 3h).

Survival genes had graded and outlier expression patterns
A statistical and graphical analysis of the 100 survival-related

genes (Table 1) clustered against all 86 tumors revealed individual tumors with substantially elevated expression in both a limited and larger number of genes (Fig. 4a). Among these genes, we observed two distinct patterns of expression related to patient survival. One pattern, designated 'outlier', included genes showing substantially elevated expression (greater than five times the interquartile range among all samples), whereas the other pattern, designated 'graded', was characterized by continuously distributed expression with patient survival (Fig. 4b). The *erbB2* and *Reg1A* genes are examples of outlier expression patterns and *S100P* and *crk* genes of graded patterns. The number of outliers per person in the top 100 genes was identified and plotted according to survival times and events (Fig. 4c). Both stage I and stage III lung adenocarcinomas showed outlier gene patterns and 10 tumors contained 3 or more outlier genes.

Because gene amplification may result in increased gene expression, the nine genes with outlier expression patterns (*erbB2*, *SLC1A6*, *Wnt 1*, *MGB1*, *Reg1A*, *AKAP12*, *PACE*, *CYP24*, *KYNU*) and one gene with a graded expression pattern (*KRT18*) were examined using quantitative genomic PCR to evaluate genomic copy number (Fig. 5a). Gene amplification of *erbB2* (17q12) was detected in tumor L94, which had the highest *erbB2* mRNA expression (Fig. 4a). Gene amplification was not detected for any of the other seven tested genes in tumor L94, as well as in other tumors. The two genes most frequently demonstrating the outlier pattern in these lung adenocarcinomas were *KYNU* and *CYP24*, and were present in 10 and 9 tumors, respectively. *CYP24* has been described as a gene amplified and overexpressed in breast cancer²⁵, and these results indicate elevated expression in lung adenocarcinoma.

To determine whether the graded or outlier gene-expression patterns also occur at the protein-expression level, 10 of the 100

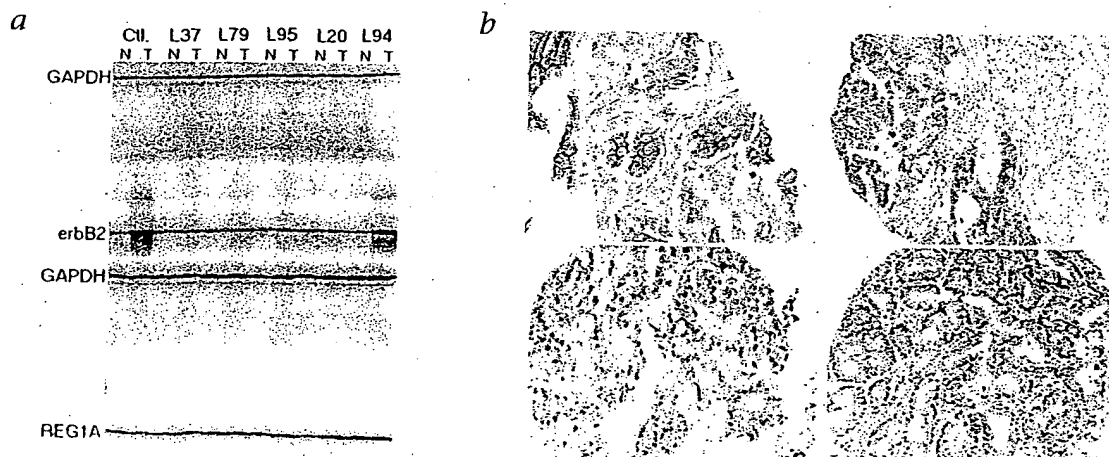


Fig. 5 Gene amplification and protein expression of survival-related genes. **a**, Analysis of potential gene amplification for 9 genes showing outlier expression patterns in the lung tumors (*erbB2*, *SLC1A6*, *Wnt 1*, *MGB1*, *Reg1A*, *AKAP12*, *PACE*, *CYP24* and *KYNU*) and examined using quantitative genomic PCR. A gene showing graded expression pattern (*KRT18*), and one gene (*PACE4*) with a similar chromosome location as *PACE*, were used as controls. Only *erbB2* and *Reg1A* are shown. An esophageal adenocarcinoma with known high-level genomic amplification of *erbB2* was used as a positive control and normal esophagus DNA was used as a negative control (C11). PCR fragment sizes were 343 bp for *GAPDH*, 166 bp for *erbB2* and 126 bp for

Reg1A. DNA is from normal lung (N) and tumor (T) from each patient (for example L37). **b**, Immunohistochemical analysis of survival related genes with lung adenocarcinoma microarrays using the tumors from this study. The transmembrane *erbB2* protein (top left) expression is substantially increased in tumor L94 containing the amplified *erbB2* gene (Fig. 4a and b). Expression of VEGF (top right) and *S100P* (bottom left) was located within the neoplastic cells and the pattern of immunoreactivity was consistent with the graded expression pattern demonstrated by their mRNA profiles. Expression of the oncogene *crk* (bottom right) was abundantly expressed in neoplastic lung cells. Magnification, $\times 400$ (*erbB2*); $\times 200$ (VEGF, *S100P* and *crk*).

ARTICLES

top survival genes (Table 1) for which specific antibodies were available were chosen for immunohistochemical analysis using lung-tumor arrays from this study (Fig. 5b). Expression of membrane *erbB2* protein was substantially increased in the *erbB2*-amplified tumor L94 and very low levels of expression were present in other tumors, consistent with mRNA-expression measurements (Fig. 4a and b). CDC6 protein expression was also substantially higher in tumor L94, consistent with mRNA levels (data not shown). Expression of vascular endothelial growth factor (VEGF) and S100P (Fig. 5b), as well as cytokeratin 18 (KRT18), cytokeratin 7 (KRT7) and fas-associated death domain (FADD) protein (data not shown), was located within the lung tumor cells and consistent with the graded expression pattern of the mRNA profiles. The oncogene *crk* showed both graded mRNA as well as a graded protein-expression pattern with survival, and was abundantly expressed in the tumor cells (Fig. 5b). These results indicate that many survival-associated genes are expressed at the protein level and demonstrate similar mRNA and protein-expression patterns.

Discussion

We used several approaches for the analysis of gene-expression data related to clinicopathological variables and patient survival. One approach, hierarchical clustering, was used to examine similarities among lung adenocarcinomas in their patterns of gene expression. Previous studies of lung tumors^{21,22} have also used this method to describe subclasses of lung tumors. Here, we found three clusters that showed significant differences with respect to tumor stage and tumor differentiation. This suggests, as expected, that tumors with similar histological features of differentiation demonstrate similarities in gene expression. This feature also partly underlies the observed statistical association of tumor stage and cluster, as many of the higher-stage tumors, often poorly differentiated and previously associated with a reduced survival^{9,10}, were located in Cluster 3. Although this cluster contained the highest percentage of stage III tumors, it also contained a nearly equal mixture of stage I and stage III tumors and not all tumors were poorly differentiated. This indicates that a subset of stage I lung adenocarcinomas share gene-expression profiles with higher-stage tumors. Notably, 10 of the 11 stage I tumors found in Cluster 3 were the high-risk stage I tumors identified using the risk index in the 'leave-one-out' cross-validation.

In contrast to previous analyses of lung adenocarcinomas^{21,22}, we validated the expression data from the arrays. The strong correlation of northern-blot analysis and oligonucleotide-array data for gene expression in the same samples (Fig. 2b) indicates that these studies provide robust gene-expression estimates. Immunohistochemistry using the same tumor samples in tissue arrays demonstrates protein expression within the lung tumor cells. Together, these studies indicate that many of the genes identified using gene-expression profiles are likely relevant to lung adenocarcinoma. For example, *IGFBP3* gene expression is increased in lung adenocarcinomas (Fig. 2c). *IGFBP3* protein modulates the autocrine or paracrine effects of insulin-like growth factors, elevated *IGFBP3* expression is observed in colon cancer²⁴, and increased serum *IGFBP3* is associated with progression in breast cancer²⁷. Heat-shock protein 70 (HSP-70) is increased in lung adenocarcinomas of smokers²⁸ and is associated with increased metastatic potential in breast cancer²⁹. Increased serum lactate dehydrogenase is correlated with tumor stage and tumor burden³⁰, and cystatin C, a cysteine protease inhibitor ex-

pressed in human lung cancers³¹, is prognostic in some cancers³². The decreased expression of this protease inhibitor may affect the invasive properties of the tumor cell.

The cross-validation analytical strategy we used is particularly informative for these types of gene-expression analyses for disease outcome^{33,34}, and identification of cross-validated genes with a larger tumor cohort may help refine this risk index for use in a clinical setting. The gene-expression data also provide opportunities to observe overarching patterns that advance our understanding of associations between genes and disease. For example, the top 100 survival genes include those involved in signaling, cell cycle and growth, transcription, translation and metabolism. Expression of many of these genes is likely a function of increased proliferation and metabolism in the more aggressive tumors. Some genes, such as *erbB2* and *Reg1A* (Fig. 4a and b), were highly overexpressed in a few patients having poor survival. In one tumor, the *erbB2* gene was amplified (Fig. 5a), demonstrating that genomic changes may underlie the overexpression of a subset of these outlier genes. Immunohistochemistry confirmed protein overexpression in this patient's tumor (Fig. 5b). Notably, seven of the eight outlier genes were not amplified, indicating that other mechanisms underlie the increased mRNA expression of these survival-related genes.

Most genes showed a graded relationship between expression and patient survival. Genes such as that encoding VEGF, known to be strongly associated with survival in lung cancer^{35,36} were identified as related to patient survival in our study. VEGF demonstrated a graded expression pattern, as did the S100P and *crk* oncogene (Fig. 5b). S100P is a calcium-regulated protein not previously reported in lung cancer. The *crk* gene, the cellular homolog of the *v-crak* oncogene, is a member of a family of adaptor proteins involved in signal transduction and interacts directly with c-jun N-terminal kinase 1 (JNK1)³⁷. Although *crk* has not been shown to have a role in lung cancer, its role in the MAP-kinase pathway, which leads to activation of matrix metalloproteinase secretion and cell invasion³⁸, indicates potential involvement in the tumor cell invasion or metastasis of some lung adenocarcinomas. Among the many genes identified in this study, like *crk*, that may be causally involved in lung cancer progression (Table 1), some were related to survival in many patients, and others in only smaller subsets of patients. This result is consistent with the complex molecular architecture of tumors in general, the heterogeneity of lung adenocarcinomas in particular and the multiple mechanisms underlying tumor-cell survival, invasion and metastasis³⁹.

Our results demonstrate that a gene-expression risk profile—based on the genes most associated with patient survival—can distinguish stage I lung adenocarcinomas and differentiate prognoses. The particular genes that define the clusters, or are associated with survival, likely reflect the characteristics of the particular tumors included in the analysis. Current therapy for patients with stage I disease usually consists of surgical resection without adjuvant treatment^{2,3}. Clearly, the identification of a high-risk group among patients with stage I disease would lead to consideration of additional therapeutic intervention for this group, possibly leading to improved survival of these patients.

Methods

Patient population. Sequential patients seen at the University of Michigan Hospital between May 1994 and July 2000 for stage I or stage III lung adenocarcinoma were evaluated for this study. Consent was received and the project was approved by the local Institutional Review Board. Primary tumors and adjacent non-neoplastic lung tissue were obtained at the time of

surgery. Peripheral portions of resected lung carcinomas were sectioned, evaluated by a study pathologist and compared with routine H&E sections of the same tumors, and utilized for mRNA isolation. Regions chosen for analysis contained a tumor cellularity greater than 70%, no mixed histology, potential metastatic origin, extensive lymphocytic infiltration or fibrosis. Tumors were histopathologically divided into two categories based on their growth pattern: bronchial-derived, if they exhibited invasive features with architectural destruction, and bronchioloalveolar, if they exhibited preservation of the lung architecture. All stage I patients received only surgical resection with intra-thoracic nodal sampling and no other treatments. Stage III patients received surgical resection plus chemotherapy and radiotherapy.

Gene-expression profiling and K-ras mutation analysis. RNA isolation, cRNA synthesis and gene-expression profiling were performed as described²⁴. Details of gene annotation and K-ras mutation analysis are provided in supplementary information.

Northern-blot analysis. Total cellular RNA (10 µg) was separated in 1.2% agarose-formaldehyde gels and vacuum-transferred to Gene Screen Plus (NEN Life Science Products, Boston, Massachusetts). Hybridization conditions and probe labeling were as described²⁵. Individual sequence-validated cDNA image clones for human *IGFBP3* (clone 1407750), *LDH-A* (clone 2420241), *cystatin C* (CTS3; clone 949938) were from Research Genetics (Huntsville, Alabama). The human histone H4 cDNA and the 28S ribosomal RNA 26-mer oligonucleotide probe were prepared and labeled as described²⁶.

Gene-amplification analysis. 11 genes were selected for the analysis of genomic alterations. Primers were designed using PrimerSelect 4.05 Windows 32 software (DNASTAR, Madison, Wisconsin), avoiding pseudogenes or potential homologous regions. Forward and reverse primers for the genes are provided (Supplementary Methods online). Quantitative genomic-PCR was then applied and analyzed as described²⁷.

Immunohistochemical staining. The H&E-stained slides of all primary lung tumors were used to identify the most representative regions of each tumor and a tissue microarray (TMA) block was constructed as described²⁸. Immunohistochemistry (IHC) was performed using both routine and sections from the TMA block as described²⁹. Detailed methods and the concentrations used for all antibodies are provided in the Supplementary Methods.

Statistical methods. *t*-tests were used to identify differences in mean gene-expression levels between comparison groups. Agglomerative hierarchical clustering³⁰ was applied using the average linkage method to investigate whether there was evidence for natural groupings of tumor samples based on correlations between gene-expression profiles. To investigate the robustness of the clustering inference, gene-expression values were perturbed by adding random Gaussian error of magnitude obtained from a duplicate sample to each data point and then reclustered to determine concordance in the tumor's class membership. Pearson, χ^2 and Fisher's exact tests were used to assess whether cluster membership was associated with physical and genetic characteristics of the tumors.

To determine whether gene-expression profiles were associated with variability in survival times, 2 separate but complementary approaches were used. In the first approach, the 86 tumors were randomly assigned to equivalent training and testing sets consisting of equal numbers of stage I and III tumors in order to validate a novel risk-index function that captured the effect of many genes at once. In the second approach, cross-validation³¹ was used to more robustly identify the genes associated with survival. Briefly, a 'leave-one-out' cross-validation procedure in which 85 of the 86 tumors (the training set) was used to identify genes that were univariately associated with survival. The risk index was defined as a linear combination of the gene-expression values for the top genes identified by univariate Cox proportional-hazard regression modeling³², weighted by their estimated regression coefficients. Kaplan-Meier survival plots and log-rank tests were then used to assess whether the risk-index assignment to high/low categories was validated in the test set. A more detailed description is provided (Supplementary Methods online).

Note: Supplementary information is available on the Nature Medicine website.

Acknowledgments

We thank D. Sanders for technical assistance; D. Sing for assistance with the figures; and G. Omenn for critical reading of this manuscript. This work was supported by National Cancer Institute grant: U19 CA-85953 and the Tissue Core of the University of Michigan Comprehensive Cancer Center (NIH CA-46952).

Competing interests statement

The authors declare that they have no competing financial interests.

RECEIVED 5 APRIL; ACCEPTED 14 JUNE 2002

1. Fry, W.A., Phillips, J.L. & Menck, H.R. Ten-year survey of lung cancer treatments and survival in hospitals in the United States. *Cancer* 66, 1867–1876 (1999).
2. Williams, D.E. et al. Survival of patients surgically treated for stage I lung cancer. *J. Thorac. Cardiovasc. Surg.* 82, 70–76 (1981).
3. Paoletto, P.C. et al. Postsurgical stage I bronchogenic carcinoma: Morbid implications of recurrent disease. *Ann. Thorac. Surg.* 38, 331–338 (1984).
4. Naruke, T. et al. Prognosis and survival in resected carcinoma based on the new international staging system. *J. Thorac. Cardiovasc. Surg.* 96, 440–447 (1988).
5. Kaisermann, M.C. et al. Evolving features of lung adenocarcinoma in Rio de Janeiro, Brazil. *Oncol. Rep.* 8, 189–192 (2001).
6. Roggli, V.L. et al. Lung cancer heterogeneity: A blinded and randomized study of 100 consecutive cases. *Hum. Pathol.* 16, 569–579 (1985).
7. Gail, M.H. et al. Prognostic factors in patients with resected stage I non-small cell lung cancer: A report from the Lung Cancer Study Group. *Cancer* 54, 1802–1813 (1984).
8. Takise, A. et al. Histopathologic prognostic factors in adenocarcinomas of the peripheral lung less than 2 cm in diameter. *Cancer* 61, 2083–2088 (1988).
9. Ichinose, Y. et al. Is T factor of the TMN staging system a predominant prognostic factor in pathologic stage I non-small cell lung cancer. *J. Thorac. Cardiovasc. Surg.* 106, 90–94 (1993).
10. Harpole, D.H. et al. A prognostic model of recurrence and death in stage I non-small cell lung cancer utilizing presentation, histopathology, and oncoprotein expression. *Cancer Res.* 55, 51–56 (1995).
11. Rodenhuis, S. et al. Mutational activation of the K-ras oncogene: A possible pathogenic factor in adenocarcinoma of the lung. *N. Engl. J. Med.* 317, 929–935 (1987).
12. Slebos, R.J.C. et al. K-ras oncogene activation as a prognostic marker in adenocarcinoma of the lung. *N. Engl. J. Med.* 323, 561–565 (1990).
13. Horió, Y. et al. Prognostic significance of p53 mutations and 3p deletions in primary resected non-small cell lung cancer. *Cancer Res.* 53, 1–4 (1993).
14. Kern, J.A. et al. C-erbB-2 expression and codon 12 K-ras mutations both predict shortened survival for patients with pulmonary adenocarcinomas. *J. Clin. Invest.* 93, 516–520 (1994).
15. Ebina, M. et al. Relationship of p53 overexpression and up-regulation of proliferating cell nuclear antigen with the clinical course of non-small cell lung cancer. *Cancer Res.* 54, 2496–2503 (1994).
16. Mehdi, S.A. et al. Prognostic markers in resected stage I and II non-small cell lung cancer: an analysis of 260 patients with 5 year follow-up. *Clin. Lung Cancer* 1, 59–67 (1997).
17. Schneider, P.M. et al. Multiple molecular marker testing (p53, c-Ki-ras, c-erbB-2) improves estimation of prognosis in potentially curative resected non-small cell lung cancer. *Br. J. Cancer* 83, 473–479 (2000).
18. Herbst, R.S. et al. Differential expression of E-cadherin and type IV collagenase genes predicts outcome in patients with stage I non-small cell lung carcinoma. *Clin. Oncol.* 6, 790–797 (2000).
19. Liotta, L. & Petricion, E. Molecular profiling of human cancer. *Nature Rev. Genet.* 1, 48–56 (2000).
20. Golub, T.R. Editorial: Genome-wide views of cancer. *N. Engl. J. Med.* 344, 601–602 (2001).
21. Bhattacharjee, A. et al. Classification of human lung carcinomas by mRNA expression profiling reveals distinct adenocarcinoma subclasses. *Proc. Natl. Acad. Sci. USA* 98, 13790–13795 (2001).
22. Garber, M.E. et al. Diversity of gene expression in adenocarcinoma of the lung. *Proc. Natl. Acad. Sci. USA* 98, 13784–13789 (2001).
23. Mills, N.E. et al. Increased prevalence of K-ras oncogene mutations in lung adenocarcinoma. *Cancer Res.* 55, 1444–1447 (1995).
24. Giordano, T.J. et al. Organ-specific molecular classification of lung, colon and ovarian adenocarcinomas using gene expression profiles. *Am. J. Pathol.* 159, 1231–1238 (2001).
25. Albertson, D.G. et al. Quantitative mapping of amplicon structure by array CGH identifies CYP24 as a candidate oncogene. *Nature Genet.* 25, 144–146 (2000).
26. Kansra, S. et al. IGFBP-3 mediates TGF β 1 proliferative response in colon cancer cells. *Int. J. Cancer* 87, 373–378 (2000).
27. Vadgama, J.V. et al. Plasma insulin-like growth factor-I and serum IGF-binding protein 3 can be associated with the progression of breast cancer, and predict the risk of recurrence and the probability of survival in African-American and Hispanic



ARTICLES

- women. *Oncology* 57, 330-340 (1999).
28. Volm, M., Mattern, J. & Stammers, G. Up-regulation of heat shock protein 70 in adenocarcinoma of the lung in smokers. *Anticancer Res.* 15, 2607-2609 (1995).
29. Ciocca, D.R. et al. Heat shock protein hsp70 in patients with axillary lymph node-positive breast cancer: prognostic implications. *J. Natl. Cancer Inst.* 85, 570-574 (1993).
30. Rotenberg, Z. et al. Total lactate dehydrogenase and its isoenzymes in serum of patients with non-small cell lung cancer. *Clin. Chem.* 34, 668-670 (1988).
31. Krepeta, E. et al. Cysteine proteases and cysteine protease inhibitors in non-small cell lung cancer. *Neoplasia* 45, 318-331 (1998).
32. Kos, J. et al. Cysteine proteinases and their inhibitors in extracellular fluids: Markers for diagnosis and prognosis in cancer. *Int. J. Biol. Markers* 15, 84-89 (2000).
33. Golub, T.R. et al. Molecular classification of cancer: Class discovery and class prediction by gene expression monitoring. *Science* 286, 531-537 (1999).
34. Hedenfalk, I. et al. Gene-expression profiles in hereditary breast cancer. *N. Engl. J. Med.* 344, 539-548 (2001).
35. Ohta, Y. et al. Vascular endothelial growth factor and lymph node metastasis in primary lung cancer. *Br. J. Cancer* 76, 1041-1045 (1997).
36. Shibusa, T., Shijubo, N. & Abe, S. Tumor angiogenesis and vascular endothelial growth factor expression in stage I lung adenocarcinoma. *Clin. Cancer Res.* 4, 1483-1487 (1998).
37. Girardin, S.E. & Yaniv, M. A direct interaction between JNK1 and Cdk1 is critical for Rac1-induced JNK activation. *EMBO J.* 20, 3437-3446 (2001).
38. Liu, E. et al. The Ras-mitogen-activated protein kinase pathway is critical for the activation of matrix metalloproteinase secretion and the invasiveness in v-erbB-transformed 3Y1. *Cancer Res.* 60, 2361-64 (2000).
39. Hanahan, D. & Weinberg, R.A. The hallmarks of cancer. *Cell* 100, 57-70 (2000).
40. Hanson, L.A. et al. Expression of the glucocorticoid receptor and K-ras genes in urethan-induced mouse lung tumors and transformed cell lines. *Exp. Lung Res.* 17, 371-387 (1991).
41. Lin, L. et al. A minimal critical region of the 8p22-23 amplicon in esophageal adenocarcinomas defined using STS-amplification mapping and quantitative PCR includes the GATA-4 gene. *Cancer Res.* 60, 1341-1347 (2000).
42. Kononen, J. et al. Tissue microarrays for high throughput molecular profiling of tumor specimens. *Nature Med.* 4, 844-847 (1998).
43. Johnson, R. & Wichern, D.W. *Applied Multivariate Statistical Analysis*. 543-578 (Prentice Hall, New Jersey, 1988).
44. Stone, M. Asymptotics for and against cross-validation. *Biometrika* 64, 29-38 (1977).
45. Cox, D.R. Regression models and life tables. *J.R. Stat. Soc.* 34, 187-220 (1972).





Analysis of mRNA expression and protein abundance data: an approach for the comparison of the enrichment of features in the cellular population of proteins and transcripts

Dov Greenbaum^{3,†}, Ronald Jansen^{1,†} and Mark Gerstein^{1,2,*}

¹Departments of Molecular Biophysics & Biochemistry, ²Computer Science and
³Genetics, 266 Whitney Avenue, Yale University, PO Box 208114, New Haven,
CT 06520, USA

Received on July 2, 2001; revised on October 5, 2001; accepted on October 22, 2001

ABSTRACT

Motivation: Protein abundance is related to mRNA expression through many different cellular processes. Up to now, there have been conflicting results on how correlated the levels of these two quantities are. Given that expression and abundance data are significantly more complex and noisy than the underlying genomic sequence information, it is reasonable to simplify and average them in terms of broad proteomic categories and features (e.g. functions or secondary structures), for understanding their relationship. Furthermore, it will be essential to integrate, within a common framework, the results of many varied experiments by different investigators. This will allow one to survey the characteristics of highly expressed genes and proteins.

Results: To this end, we outline a formalism for merging and scaling many different gene expression and protein abundance data sets into a comprehensive reference set, and we develop an approach for analyzing this in terms of broad categories, such as composition, function, structure and localization. As the various experiments are not always done using the same set of genes, sampling bias becomes a central issue, and our formalism is designed to explicitly show this and correct for it. We apply our formalism to the currently available gene expression and protein abundance data for yeast. Overall, we found substantial agreement between gene expression and protein abundance, in terms of the enrichment of structural and functional categories. This agreement, which was considerably greater than the simple correlation between these quantities for individual genes, reflects the way broad categories collect many individual measurements into simple, robust averages. In particular, we found

that in comparison to the population of genes in the yeast genome, the cellular populations of transcripts and proteins (weighted by their respective abundances, the transcriptome and what we dub the translome) were both enriched in: (i) the small amino acids Val, Gly, and Ala; (ii) low molecular weight proteins; (iii) helices and sheets relative to coils; (iv) cytoplasmic proteins relative to nuclear ones; and (v) proteins involved in 'protein synthesis', 'cell structure', and 'energy production'.

Supplementary information: <http://genecensus.org/expression/translatome>

Contact: mark.gerstein@yale.edu

INTRODUCTION

High throughput experimentation, measuring mRNA (Schena *et al.*, 1995; Eisen and Brown, 1999; Ferea and Brown, 1999; Lipshutz *et al.*, 1999) and protein expression (Anderson and Seilhamer, 1997; Futcher *et al.*, 1999; Gygi *et al.*, 1999a; Ross-Macdonald *et al.*, 1999; Lopez, 2000; MacBeath and Schreiber, 2000; Nelson *et al.*, 2000; Zhu *et al.*, 2000) are currently the single richest source of genomic information. However, how to best interpret this data is still an open question (Bassett *et al.*, 1996; Wittes and Friedman, 1999; Zhang, 1999; Gerstein and Jansen, 2000; Searls, 2000; Sherlock, 2000; Claverie, 1999; Einarson and Golemis, 2000; Epstein and Butow, 2000; Shapiro and Harris, 2000). Understanding how protein abundance is related to mRNA transcript levels is essential for interpreting gene expression, protein interactions, structures and functions in a cellular system (Hatzimanikatis *et al.*, 1999). Moreover, as protein concentration is the more relevant variable with respect to enzyme activity, it connects genomics to the physical chemistry of the cell (Kidd *et al.*, 2001). Protein abundance may also be invaluable for diagnostics and for determining drug targets (Corthals *et al.*, 2000).

*To whom correspondence should be addressed.
†These authors contributed equally to this work.

Previously, we surveyed the population of protein features—such as folds, amino acid composition, and functions—in yeast, and other recently sequenced genomes (Gerstein, 1997, 1998a,b; Gerstein and Hegyi, 1998; Hegyi and Gerstein, 1999; Das and Gerstein, 2000; Lin and Gerstein, 2000), and we extended this concept to compare the population of features in the yeast transcriptome to that in the genome (Drawid *et al.*, 2000; Jansen and Gerstein, 2000). Others have also done related work (Frishman and Mewes, 1997; Tatusov *et al.*, 1997; Jones, 1998; Wallin and von Heijne, 1998; Frishman and Mewes, 1999; Wolf *et al.*, 1999). Here, we present a new methodology to compare the features of the mRNA expression population with the protein abundance population.

Precise terminology is essential for this comparison. Unfortunately, 'proteome' is used inconsistently. Proteome can logically be used to describe all the distinct proteins in the genome (Qi *et al.*, 1996; Cavalcoli *et al.*, 1997; Fey *et al.*, 1997; Garrels *et al.*, 1997; Gaasterland, 1999; Jones, 1999; Sali, 1999; Tekala *et al.*, 1999; Bairoch, 2000; Cambillau and Claverie, 2000; Doolittle, 2000; Pandey and Mann, 2000; Rubin *et al.*, 2000) and, in this context, it is equivalent to what others may refer to as the coding part of the genome. However, in papers on two-dimensional (2D) electrophoresis, it is often used to describe the sum total of proteins in a cell, taking into account the different levels of protein abundance (Shevchenko *et al.*, 1996; Gygi *et al.*, 2000a; Lopez, 2000; Washburn and Yates, 2000). In an effort to be clear, we propose the term 'translatome' for this second usage of proteome.

With this definition, we are able to refer compactly to three different cellular populations. These are illustrated in Figure 1.

- (i) We use the term *genome* when we refer to the population of open reading frames, where each ORF counts once.
- (ii) We use the term *transcriptome* when we refer to the population of mRNA transcripts. This term was originally coined by Velculescu *et al.* (1997). Note that each ORF may give rise to different numbers of transcripts. Consequently, the transcriptome is essentially the same as the genome but with each ORF weighted by its expression level.
- (iii) The next level is the cellular population of proteins. As each protein represents a translated transcript, we make an analogy with the term transcriptome and use the term *translatome* as described above to describe this third population. Thus, the translatome is a subset of the genome where each ORF is weighed by its associated level of protein abundance.

Note that one could also, less compactly call the translatome a 'weighted proteome.' However, doing so assumes one of the two aforementioned definitions of proteome. To avoid ambiguity, we studiously avoid the use of proteome altogether in the paper.

Differences between the transcriptome and the transcriptome exist given that transcripts from different genes can give rise to different numbers of proteins, due to different rates of translation and protein degradation. Post-transcriptional modifications further affect the translatome.

In our analysis of the transcriptome and translatome, we focus on global protein features rather than the comparison of individual genes. Previous analyses have shown that differences between mRNA expression and protein abundance levels can be quite dramatic for individual genes. This may either be due to the noise in the data or to fundamental biological processes. However, our analyses show that the variation between transcriptome and translatome is much smaller for global properties that are computed by averaging over the properties of many individual genes.

METHODS

Data sources used

For our analysis we culled many divergent data sets, representing protein abundance and mRNA expression experiments and also other sources of genome annotation. These are all summarized in Table 1.

Biases in the data

The databases that annotate the specific genes may not always be accurate (Ishii *et al.*, 2000). Gene Chip experiments suffer with regard to cross hybridization and the saturation of probes. SAGE data degrades for lowly expressed mRNAs. 2D gels are unable to resolve membrane proteins (approximately 30% of the genome) and basic proteins (Gerstein, 1998c; Krogh *et al.*, 2001). In addition, the procedures for identification and quantification of the protein spots are subject to uncertainties (Haynes and Yates, 2000). Human biases include the lack of low abundance proteins (Fey and Larsen, 2001; Gygi *et al.*, 2000b; Harry *et al.*, 2000) and the differences between laboratories in sample preparation. Our reference expression data set attempts to resolve these problems.

Data set scaling

A reference set for mRNA expression. With many different mRNA expression data sets available, it is worthwhile to integrate them into a single unified reference set, with the intention of reducing the noise and errors contained in the individual data sets and to obtain a unified estimate of the normal expression state in a cell.

We adopt an iterative scaling and merging formalism,

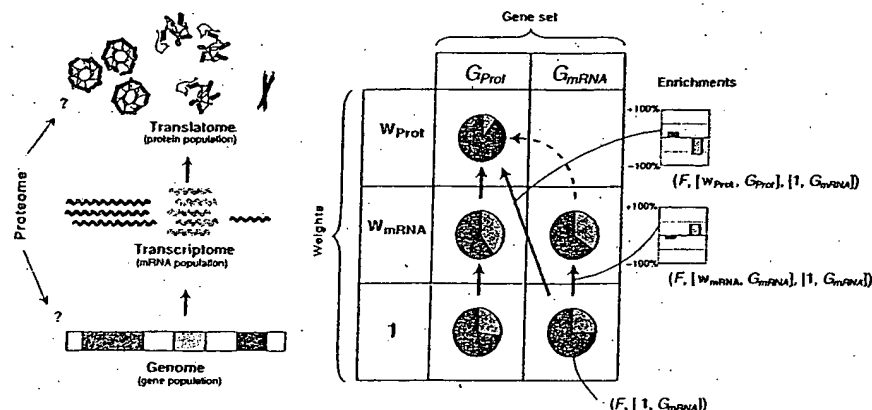


Fig. 1. Schematic overview of the analysis. On the left-side we outline the terms we use to describe the process of gene expression. The coding section of the genome is transcribed into a population of mRNA transcripts called the 'transcriptome.' The transcripts in turn are translated to a population of proteins; we use the term 'translatome' for this protein population rather than the alternative 'proteome' because the latter term may be confounded with the protein complement of the genome (which is not necessarily associated with a quantitative abundance level).

The matrix in the middle schematically shows an analysis of the three stages of expression. In general, we define a protein 'population' as a set of genes associated with a corresponding number of expression or abundance levels ('weights'): In the matrix each row represents a weight and each column a gene set. In particular, we differentiate between the mRNA reference expression set ($G_{mRNA} = G_{Gen}$), which essentially covers the complete genome, and the reference protein abundance set (G_{Prot}) which contains the proteins in data sets 2-DE #1 and 2-DE #2 (see Table 1) because the protein abundance set is a significantly smaller subset of the genome. By definition, this subset contains only proteins that can be identified by 2-D gel electrophoresis and is therefore biased in this sense. The enrichment figures throughout this paper, through a comparison of the right- and left-sides of this figure, show the results of the experimental biases of 2D gels on the data set. Each pie chart represents a composition of a particular protein feature F (for instance, an amino acid composition) in a population (represented by the symbol μ). We can further look at the 'enrichment' of this feature in one population relative to another (represented by the symbol Δ , see Section 'Methods' for an explanation of the formalism).

which we summarize below. We present a more detailed review of the methods on our web site.

We start with the values of one gene chip data set U_i where i is used throughout as a subscript to denote gene number. We then transform the values of the next Gene Chip data set X_i to Y_i with the following non-linear regression: $\min \sum_i (Y_i - U_i)^2$ with $Y_i = AX_i^B$ where A and B are the parameters of the regression. Note that two Gene Chip sets may not be defined for the same set of genes, so we have to perform the fit only over the genes common to both sets. The motivation for scaling is that the dynamic range of observed expression levels varies somewhat between different data sets, although cell types and growth conditions are very similar. Reasons for disparity may include different calibration procedures for relating fluorescence intensity to a cellular concentration (measured in copies of transcripts per cell) or different protocols for harvesting and reverse-transcribing the cellular mRNA.

We then merge and average the data to create a new

reference set V as follows:

$$\text{If } U_i \text{ and } Y_i \text{ are both defined for gene } i \text{ and } \frac{|Y_i - U_i|}{Y_i + U_i} < \alpha$$

$$\text{Then } V_i = \frac{1}{2}(Y_i + U_i)$$

$$\text{Else if only } Y_i \text{ exists, } V_i = Y_i$$

$$\text{Else } V_i = U_i$$

As presented above, where only one data set has a value for the corresponding ORF, we incorporated that value and did not exclude it. When both data sets have values for an ORF, we averaged the values if they were within 15% of each other; otherwise, we just stayed with the original chip data set U_i . We used $\alpha = 15\%$ in order to prevent outliers from skewing the result. This 15% value is a reasonable threshold for excluding outliers though other values (e.g. 10 or 20%) would give similar results (data not shown). Other data sets are subsequently included in the same procedure, continuing the iteration from the new

expression values V_i . The initial iteration starts with the Young Expression Set, as U_i , since we have the highest confidence in its accuracy.

The SAGE data (Velculescu et al., 1997) was not included in the above procedure since it is of a fundamentally different nature. An advantage of the SAGE technology over Gene Chips is that there is no possible signal saturation for high expression levels, as is possible for chips (Futcher et al., 1999). Conversely, SAGE values are less reliable for lowly expressed genes since there is a chance that one might not sequence a SAGE tag corresponding to such a gene altogether. Therefore, if after the last iteration, the average Gene Chip expression level V_i was both above a certain threshold β and below the SAGE expression level S_i for the same gene, it was replaced with the SAGE value; otherwise the average Gene Chip value was kept. This gave us our final expression set w_{mRNA} . Our treatment of the SAGE data is modeled after that in Futcher et al. (1999), and like them, we used $\beta = 16$.

This incorporation of the SAGE data into the reference data set ensures that the highly expressed outliers are as accurate as possible.

Rather than plain arithmetic averaging, this overall scaling procedure with the α cutoff avoids 'artificial averages' that combine very different values for a particular gene. Some expression values might be statistical outliers. In addition, it may be possible that the expression levels of a variety of genes can only be within mutually exclusive ranges or modes, such as when two alternative pathways are switched on or off. Simply averaging these would give values that are less representative of the particular mode values. This situation is analogous to that in averaging together an ensemble of protein structures (i.e. from NMR structure determination). Each structure could be stereochemically correct, with all side-chain atoms in predefined rotamer configurations. However, an average of all structures could yield one that is stereochemically incorrect if this involved averaging over particular side-chains in different rotameric states.

With regard to our regression analysis, we have investigated both non-linear and linear fits but found a non-linear procedure to be more advantageous. The non-linear relationship between different expression data sets perhaps reflects saturation in one or more of the Gene Chips—not an uncommon phenomenon. This non-linearity is immediately evident on scatter plots of two data sets against one another (see website). Accordingly, the non-linear fit produces a smaller residual than the linear fit: 98 297 (non-linear) versus 122 182 (linear) for the scaling of the Church data set and 59 828 (non-linear) versus 67 462 (linear) for the Samson data set.

A reference set for protein abundance. We followed a similar procedure to calculate a reference protein abundance set from the two gel electrophoresis data sets. We first scaled the two data sets against the mRNA expression reference data set, getting regression parameters C_j and D_j :

$$\min \sum_i (P_{i,j} - C_j w_{\text{mRNA},i}^{D_j})^2$$

where the subscript j indicates the data set 2-DE #1 or 2-DE #2 respectively; $P_{i,j}$ is the protein abundance value in data set j , and $w_{\text{mRNA},i}$ the corresponding reference expression value, and C_j and D_j are the parameters of the non-linear regression.

Using these parameters, we transformed the values of set 2-DE #2 onto 2-DE #1. Then we combined both sets into the reference protein set w_{Prot} by averaging them, if both values existed. Otherwise, by using the existing value, viz:

$$Q_{i,2} \equiv C_1 \left(\frac{P_{i,2}}{C_2} \right)^{D_1/D_2}$$

$w_{\text{Prot},i} = (P_{i,1} + Q_{i,2})/2$ if both $P_{i,1}$ and $Q_{i,2}$ exist.

Else if only $P_{i,1}$ exists, $w_{\text{Prot},i} = P_{i,1}$

Else if $Q_{i,2}$ exists, $w_{\text{Prot},i} = Q_{i,2}$.

Enrichment of features

Formalism. In the next part of our analysis, we want to group a number of proteins together into various categories based on common features, and characterize those features that are enriched in one population relative to another, i.e. the translome population of proteins as measured by 2D gels relative to the transcriptome population of transcripts or the genome population of genes. To this end, we set up a formalism that could be applied universally to all the attributes that we were interested in. Due to the limitations of the experiments, the translome, transcriptome, and genome populations are defined on different sets of genes, and sometimes we want to remove this 'selection bias' by forcing them to be compared on exactly the same set of genes. This is a key aspect of our formalism as presented in Figure 1.

We call an entity like $\{w, G\}$ a 'population,' where G is a set describing a particular selection of genes from the genome and w is vector of weights associated with each element of this population. In particular, we focus on three main populations here:

- (i) $\{1, G_{\text{Gen}}\}$ is the population of genes in the genome, all 6280 genes weighted once ($w = 1$);
- (ii) $\{w_{\text{mRNA}}, G_{\text{mRNA}}\}$ is the observed population of the transcripts in the transcriptome, i.e. the 6249 genes in the reference expression set weighted by their reference expression value;

- (iii) $\{w_{\text{Prot}}, G_{\text{Prot}}\}$ is the observed cellular population of the proteins in the translatome, i.e. the 181 genes in the reference abundance set weighted by their reference abundance value.

(The set of genes in the genome G_{Gen} is approximately equal to the genes in set G_{mRNA} , such that we can use both symbols interchangeably.) We can also use this notation to describe specific experiments—e.g. $\{w_{\text{lacZ}}, G_{\text{lacZ}}\}$ describes the gene set and weights relating to the transposon abundance set.

Furthermore, we define F_j as the value of a feature F in ORF j . For example, F could be the composition of leucine (a real number) or a binary value (0 or 1) indicating whether an ORF contains a trans-membrane segment. Given these definitions, the weighted average of feature F in population $\{w, G\}$ is:

$$\mu(F, \{w, G\}) \equiv \frac{\sum_{j \in G} w_j F_j}{\sum_{j \in G} w_j}$$

The weighted averages of two populations $\{w, G\}$ and $\{v, S\}$ can be compared by simply looking at their relative difference Δ :

$$\Delta(F, \{v, S\}, \{w, G\}) = \frac{\mu(F, \{v, S\}) - \mu(F, \{w, G\})}{\mu(F, \{w, G\})}$$

where v and w are weights for the sets of ORFs S and G respectively. We call Δ the 'enrichment' of feature F because it indicates whether F is enriched (if Δ is positive) or depleted (if Δ is negative) in population $\{v, S\}$ relative to $\{w, G\}$.

Usually, the gene set G is defined by the particular experiment, for which the weight w was measured. However, it is also possible to combine the gene set associated with one experiment with expression levels from another set. One may want to do this to compute the enrichment only on the genes common to both populations, for which there are defined values for both w and v , viz: $\Delta(F, \{v, S \cap G\}, \{w, S \cap G\})$. In practice, this is most relevant for comparing G_{Prot} and G_{mRNA} . Since G_{Prot} is completely a subset of G_{mRNA} , we need not explicitly deal with intersections if we calculate all statistics directly over G_{Prot} .

One can adjust the weight vectors to take into account different types of averaging. For instance, when computing the amino acid composition ($F = aa$) from the amino acid compositions of individual ORFs $F_j = aa_j$ ($\forall j \in G$), we weight by ORF length. In the case of expression weights, we have:

$$w_j = N_j w_{\text{mRNA}, j} \quad \forall j \in G$$

where N_j is a measure of the length of ORF j (such as the number of amino acids).

On the other hand, when computing the average molecular weight per amino acid, we need to normalize by the number of amino acids per ORF, which is equivalent to choosing the following weights:

$$w_j = \frac{w_{\text{mRNA}, j}}{N_j} \quad \forall j \in G$$

Application of methodology to quantitative abundance sets

Having defined our formalism, we applied it to a diverse set of protein features in yeast.

Amino acid enrichment. As shown in Figure 2a, we used our methodology to measure the enrichment of individual amino acids in both the translatome and the transcriptome relative to the genome. We found that three amino acids—valine, glycine and alanine—were consistently enriched in both transcriptome and translatome populations.

In Figure 2a we compare different gene sets. In Figure 2b we focus mainly on the variation in enrichments when all the comparisons are restricted to the set of 181 genes ($G_{\text{Prot}} \cap G_{\text{mRNA}} = G_{\text{Prot}}$) common to all data sets. Thus, the differences between the populations now only reflect the effects of differential transcription of certain genes and differential translation of certain transcripts. We find here an enrichment specifically of cysteine in the translatome in relation to the transcriptome.

To measure the statistical significance of the results on amino acid enrichment, we have performed a control analysis on a randomized data set (Figure 2d). We randomly permuted the expression values of the ORFs 1000 times and then recomputed the enrichments. This allowed us to compute distributions for the amino acid enrichments and, from integrating these, one-sided p -values indicating the significance of the observed enrichments.

Amino acid enrichment in Transposon data set. We also tried to extend our methodology, ineffectively, to cope with the semi-quantitative Transposon set. We used only those 450 ORFs that consistently yielded either no expression or high expression, as binary data, on or off. We show the enrichments of amino acids computed from this filtered Transposon abundance set in Figure 2a. Overall, the enrichments from this set seemed to be attenuated in comparison to other data.

Biomass enrichment. A corollary to amino acid enrichments is the determination of the average biomass of the transcriptome and translatome populations (shown in Figure 2c). We found that the average molecular weight of a protein in both populations was, on average, lower than in the genome population. These preliminary observations suggest a cell preference to use less energetically expensive proteins for those that are highly transcribed or trans-

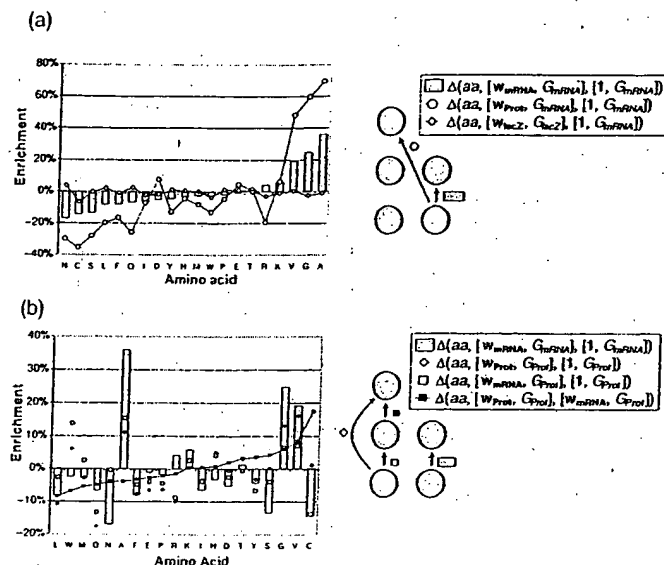


Fig. 2. Amino acid and biomass enrichment. (a) Shows the amino acid enrichments between different populations as indicated by the legend to the right of the plot (the legend is ordered in the same way as the schematic illustration in Figure 1). The bars indicate the enrichment of the transcriptome relative to the genome, whereas the circles indicate the enrichment of the translome relative to the genome. In addition, we also show the enrichment for protein abundance from the Transposon abundance set, represented by the circles with the line through them. (b) Shows a different view of amino acid enrichment from that contained in (a), now focusing on changes, and thus restricting the comparison to the genes common to all the data sets. The graph is ordered according to the enrichment from transcriptome to translome (black squares). We focus here only on the changes for the abundance gene set (G_{Prot}) to exclude the effects that arise from looking at different subsets. In this view the enrichments from genome to transcriptome (white squares) and from genome to translome (white diamonds) look more similar than do the analogous sets in (a). To make comparison with (a) easier we again show the enrichment from genome to the transcriptome for the complete gene set (G_{Gen} , shown in bars). (c) Shows biomass enrichment. The left panel depicts the average molecular weight per ORF (in units of kDa) and the right panel, the average molecular weight per amino acid (in units of Daltons) in each of the three stages of gene expression. The numbers inside the circles indicate the average molecular weights. The values next to the arrows indicate the enrichments in biomass between different populations. Both the circle diameters and the arrow widths are functions of the corresponding values (the hollow arrow indicates a positive value). It is very clear that the average molecular weight per ORF is much lower in the translome (by 20 or 15%) and transcriptome (by 29%) than in the genome. This relative depletion of biomass mainly takes place as a result of transcription; the effect of translation is less clear, depending on the populations compared. On the other hand, the depletion in the average molecular weight per amino acid (-3.3% from genome to translome) is an order of magnitude smaller than in the average weight per ORF. This shows that the yeast cell favors the expression of shorter ORFs over longer ones, and agrees with our earlier observation that there is a negative correlation between maximum ORF length and mRNA expression (Jansen and Gerstein, 2000); it seems that this effect mainly takes place during transcription rather than translation. (d) This plot shows that the amino acid enrichments are statistically significant. We have assessed significance by randomly permuting the expression levels among the genes and then recomputing the amino acid enrichments. This procedure can be repeated and used to generate distributions of random enrichments that can then be compared against the observed enrichments. In the plot the gray bars represent the observed enrichments already shown in Figure 3a. On top of the gray bars we show standard boxplots of enrichment distributions based on 1000 random permutations. (The middle line represents the distribution median. The upper and lower sides of the box coincide with the upper and lower quartiles. Outliers are shown as dots and defined as data points that are outside the range of the whiskers, the length of which is 1.5 the interquartile distance.) Based on the random distributions, we can compute one-sided p -values for the observed enrichments. Amino acids for which the p -values are less than 10^{-3} are shown in bold font.

lated. However, we also found that the average molecular weight per amino acid differed much less between the transcriptome and the translome on the one hand, and the

genome on the other hand (though it was still slightly less). This finding indicates that lower molecular weights in the translome and transcriptome relative to the genome are

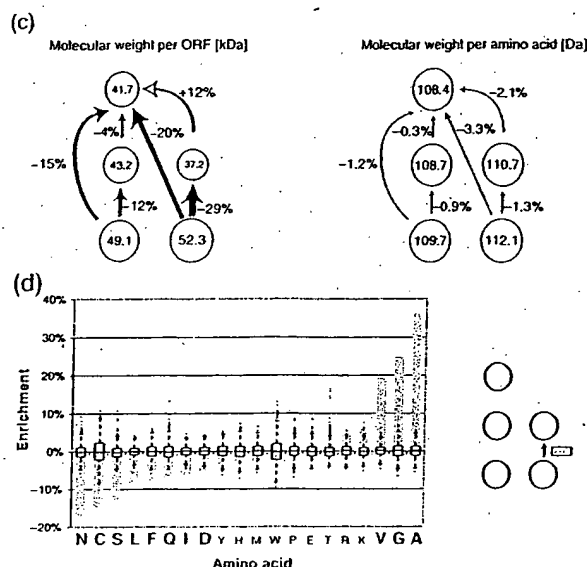


Fig. 2. Cont.

predominantly due to greater expression of shorter proteins rather than the incorporation of smaller amino acids.

Secondary structure composition. We also used our methodology to study the enrichment of secondary-structural features. Secondary structural annotation was derived from structure prediction applied uniformly to all the ORFs in the yeast genome as described in Table 1. As shown in Figure 3a, all three populations—genome, transcriptome, and translome—had a fairly similar composition of secondary structures—sheets, helices, and coils. The differences between populations were marginal and based only on the small subset of genes.

We also found that Transmembrane (TM) proteins were significantly depleted in the transcriptome (see website and caption). These results are consistent with our previous analyses (Jansen and Gerstein, 2000). The protein abundance data does not have any membrane proteins.

Subcellular localization. Figure 3c shows the enrichment of proteins associated with the various subcellular compartments. For clarity, we divided the cell into five distinct subcellular compartments. (see Table 1). We found that, in comparison to the genome, both the transcriptome and translome are enriched in cytoplasmic proteins. This is true whether we make our comparisons in

relation to the relatively large reference mRNA expression set or the smaller reference protein abundance set. As Figure 3c shows, the 2D gel experiments are clearly biased towards proteins from the cytoplasm. However, in the biased subset $G_{P_{tot}}$ transcription and translation lead to an even higher fraction of cytoplasmic proteins in the translome.

Functional categories. Finally, we compared the enrichment of various functional categories in both the translome and the transcriptome (see Figure 3b). This gives us a broad yet informative view of the cell as a whole. As described in Table 1, we used the top-level of the MIPS scheme for the functional category definitions. We found broad differences between the various populations, with some of the functional categories showing strikingly high enrichments.

DISCUSSION AND CONCLUSION

We developed: (i) a methodology for integrating many different types of gene expression and protein abundance into a common framework and applied this to a preliminary analysis; (ii) a procedure for scaling and merging different mRNA and protein sets together; and (iii) an approach for computing the enrichment of various proteomic features in the population of transcripts and proteins. We showed that by analyzing broad categories instead of individual noisy

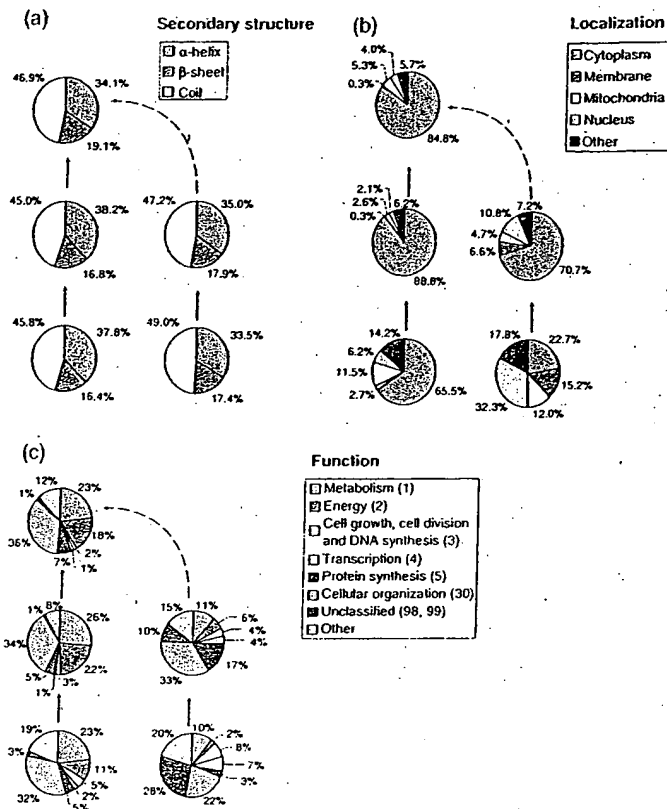


Fig. 3. Breakdown of the transcriptome and translome in terms of broad categories relating to structure, localization, and function. All of the subfigures are analogous to the schematic illustration in Figure 1. (a) Represents the composition of secondary structure in the different populations. (b) Represents the distribution of subcellular localizations associated with proteins in the various populations. We used standardized localizations developed earlier (Drawid and Gerstein, 2000), which, in turn, were derived from the MIPS, YPD, and SwissProt databases (Bairoch and Apweiler, 2000; Costanzo *et al.*, 2000; Mewes *et al.*, 2000). The subcellular localization has been experimentally determined for less than half of the yeast proteins, so our analysis applies only to this subset. (c) Shows the division of ORFs into different functional categories (according to the MIPS classification) in the various populations. Only the largest functional categories of the top level of the MIPS classification are shown. The group 'other' contains the smaller top-level categories lumped together. This 'other' group is different from the group 'unclassified,' which contains genes without any functional description.

data points, we could find logical trends in the underlying data. For example, individual transcription factors might have higher or lower protein abundance than one expects from their mRNA expression, but the category 'transcription factors' as a whole has a similar representation in the transcriptome and translome.

We found, as previously described (Futcher *et al.*, 1999; Gygi *et al.*, 1999b; Greenbaum *et al.*, 2001), a weak correlation between individual measurements of mRNA

and protein abundance. The outliers of this correlation tend to be associated with cellular organization. One might conceive of using these outliers (i.e. those with significantly different transcriptional and translational behavior) to find consensus regulatory sequences. One possible method would involve using predicted mRNA structures (Jaeger *et al.*, 1990; Zuker, 2000) to find and investigate consensus structural elements in these outliers to which the yeast translational machinery is known to be

Table 1. Data sets

Data set	Description	Size [ORFs]	Reference
mRNA expression			
Young	Gene chip profiles yeast cells with mutations that affect transcription	5455	Holstege <i>et al.</i> (1998)
Church	Gene chip profiles of yeast cells under four different conditions	6263	Roth <i>et al.</i> (1998)
Samson	Comparing gene chip profiles for yeast cells subjected to alkylating agent	6090	Jelinsky and Samson (1999)
SAGE	Yeast cells during vegetative growth	3778	Velculescu <i>et al.</i> (1997)
Reference expression	Scaling and integrating the mRNA expression set into one data source	6249	—
Protein abundance			
2-DE #1	Measurement of yeast protein abundance by 2D gel electrophoresis and mass spectrometry	156	Gygi <i>et al.</i> (1999a,b)
2-DE #2	Similar to 2-DE set #1	71	Fletcher <i>et al.</i> (1999)
Transposon	Large-scale fusions of yeast genes with <i>lacZ</i> by transposon insertion	1410	Ross-Macdonald <i>et al.</i> (1999)
Reference abundance	Scaling and integrating the 2-DE data sets into one data source	181	—
Annotation			
Annotated localization	Subcellular localizations of yeast proteins	2133 (6280)	Drawid and Gerstein (2000)
TM segments	Predicted TM and soluble proteins in yeast	2710 (6280)	Gerstein (1998a,b,c)
MIPS functions	Functional categories for yeast ORFs	3519 (6194)	Mewes <i>et al.</i> (2000)
GOR secondary structure	Predicted secondary structure yeast ORFs	6280	Gerstein (1998a,b,c)

This table provides an overview of the data sets used in our analysis. The table is divided into three sections. The top section lists different mRNA expression sets. The middle section shows the protein abundance data sets used. The bottom section contains different annotations of protein features. The column 'Data set' lists a shorthand reference to each data set used throughout this paper. The next columns contain a brief description of the data sets, the number of ORFs contained in each of them, and the literature reference. In contrast to the other data we investigated, the reference expression and abundance data sets have been calculated for the purpose of our analysis (see text). An expanded version of the table is available on our web site.

Some further information on the genome annotations:

Localization. Protein localization information from YPD, MIPS and SwissProt were merged, filtered and standardized (Bairoch and Apweiler, 2000; Costanzo *et al.*, 2000; Mewes *et al.*, 2000) into five simplified compartments—cytoplasm, nucleus, membrane, extracellular (including proteins in ER and golgi), and mitochondrial—according to the protocol in Drawid *et al.* (2000). This yielded a standardized annotation of protein subcellular localization for 2133 out of 6280 ORFs.

TM segments. In 2710 out of 6280 yeast ORFs TM segments are predicted to occur, ranging from low to high confidence (732 ORFs). The TM prediction was performed as follows: the values from the scale for amino acids in a window of size 20 (the typical size of a TM helix) were averaged and then compared against a cutoff of -1 kcal mol^{-1} . A value under this cutoff was taken to indicate the existence of a TM helix. Initial hydrophobic stretches corresponding to signal sequences for membrane insertion were excluded. (These have the pattern of a charged residue within the first seven, followed by a stretch of 14 with an average hydrophobicity under the cutoff.) These parameters have been used, tested, and refined on surveys of membrane protein in genomes. 'Sure' membrane proteins had at least two TM-segments with an average hydrophobicity less than -2 kcal mol^{-1} (Rost *et al.*, 1995; Gerstein *et al.*, 2000; Santoni *et al.*, 2000; Senes *et al.*, 2000).

Functions. MIPS functional categories have been assigned to 3519 out of 6194 ORFs. (The remainder are assigned to category '98' or '99,' which corresponds to unclassified function.)

sensitive (McCarthy, 1998).

In relation to functional categories, we found three trends that were particularly notable: (i) the 'cellular

organization,' 'protein synthesis,' and 'energy production' categories were increasingly enriched as we moved from genome to transcriptome to translatome. In the transcrip-

tome and translome population relative to the genome; (ii) proteins with 'unclassified function' are significantly depleted, perhaps reflecting a bias against studying them; (iii) proteins in the 'transcription' and 'cell growth, cell division, and DNA synthesis' categories were consistently depleted. This reflects the fact that many of these proteins, such as transcription factors, act as 'switches' such that only small quantities of the protein are necessary to activate or deactivate a process. These results concur with previous calculations (Jansen and Gerstein, 2000) wherein we found the transcriptome is enriched specifically with proteins involved in protein synthesis and energy.

Limitations given the small size of the protein abundance data

Even with the extended coverage made possible by merging many data sets together into reference sets, the analysis is still limited by the minimal data. This was most applicable to the protein abundance measurements, potentially biasing our statistical results towards certain protein families. Moreover, the 181 proteins in G_{PEI} do not represent a random sample. They are skewed towards highly expressed, well-studied proteins. Our methodology attempts to control for this gene-selection bias through our enrichment formalism, which allows one to rather precisely gauge various aspects of the bias. Conversely, many protein features in both the translome and the transcriptome are dominated by highly expressed proteins. Under these circumstances, it is often sufficient to look at this smaller number of dominating proteins to characterize the whole population. This is similar to the development of the codon adaptation index for yeast (Sharp and Li, 1987). While based on only 24 highly expressed proteins, it has proven to be robust in predicting expression levels for the entire genome.

We believe that the essential formalism and approach that we develop will remain quite relevant for future data sets (Smith, 2000).

ACKNOWLEDGEMENT

M.G. thanks the Keck foundation for support.

REFERENCES

- An, H., Scopes, R.K. et al. (1991) Gel electrophoretic analysis of *Zymomonas mobilis* glycolytic and fermentative enzymes: identification of alcohol dehydrogenase II as a stress protein. *J. Bacteriol.*, 173, 5975–5982.
- Anderson, L. and Seilhamer, J. (1997) A comparison of selected mRNA and protein abundances in human liver. *Electrophoresis*, 18, 533–537.
- Bairoch, A. (2000) Serendipity in bioinformatics, the tribulations of a Swiss bioinformatician through exciting times! *Bioinformatics*, 16, 45–64.
- Bairoch, A. and Apweiler, R. (2000) The SWISS-PROT protein sequence database and its supplement TrEMBL in 2000. *Nucleic Acids Res.*, 28, 45–48.
- Bassett, D.E. Jr., Basrai, M.A. et al. (1996) Exploiting the complete yeast genome sequence. *Curr. Opin. Genet. Dev.*, 6, 763–766.
- Batke, J., Benito, V.A. et al. (1992) A possible *in vivo* mechanism of intermediate transfer by glycolytic enzyme complexes: steady state fluorescence anisotropy analysis of an enzyme complex formation. *Arch. Biochem. Biophys.*, 296, 654–659.
- Cambillau, C. and Claverie, J.M. (2000) Structural and genomic correlates of hyperthermostability. *J. Biol. Chem.*, 275, 32383–32386.
- Cavalcoli, J.D., VanBogelen, R.A. et al. (1997) Unique identification of proteins from small genome organisms: theoretical feasibility of high throughput proteome analysis. *Electrophoresis*, 18, 2703–2708.
- Claverie, J.M. (1999) Computational methods for the identification of differential and coordinated gene expression [in process citation]. *Hum. Mol. Genet.*, 8, 1821–1832.
- Corthals, G., Wasinger, V.C., Hochstrasser, D.F. and Sanchez, J.C. (2000) The dynamic range of protein expression: a challenge for proteomic research. *Electrophoresis*, 21, 1104–1115.
- Costanzo, M.C., Hogan, J.D. et al. (2000) The Yeast Proteome Database (YPD) and *Caenorhabditis elegans* Proteome Database (WormPD): comprehensive resources for the organization and comparison of model organism protein information. *Nucleic Acids Res.*, 28, 73–76.
- Das, R. and Gerstein, M. (2000) The stability of thermophilic proteins: a study based on comprehensive genome comparison. *Funct. Int. Genom.*, 1, 33–45.
- Doolittle, W.F. (2000) The nature of the universal ancestor and the evolution of the proteome. *Curr. Opin. Struct. Biol.*, 10, 355–358.
- Drawid, A. and Gerstein, M. (2000) A Bayesian system integrating expression data with sequence patterns for localizing proteins: comprehensive application to the yeast genome. *J. Mol. Biol.*, 301, 1059–1075.
- Drawid, A., Jansen, R. et al. (2000) Gene expression levels are correlated with protein subcellular localization. *Trends Genet.*, 10, 426–430.
- Einarsson, M. and Golemis, E. (2000) Encroaching genomics: adapting large-scale science to small academic laboratories. *Physiol. Genom.*, 2, 85–92.
- Eisen, M.B. and Brown, P.O. (1999) DNA arrays for analysis of gene expression. *Meth. Enzymol.*, 303, 179–205.
- Epstein, C. and Butow, R. (2000) Microarray technology—enhanced versatility, persistent challenge. *Curr. Opin. Biotechnol.*, 11, 36–41.
- Ferea, T. and Brown, P. (1999) Observing the living genome. *Curr. Opin. Genet. Dev.*, 9, 715–722.
- Fey, S.J., Nawrocki, A. et al. (1997) Proteome analysis of *Saccharomyces cerevisiae*: a methodological outline. *Electrophoresis*, 18, 1361–72.
- Fey, S.J. and Larsen, P.M. (2001) 2D or not 2D. Two-dimensional gel electrophoresis. *Curr. Opin. Chem. Biol.*, 5, 26–33.
- Frishman, D. and Mewes, H.W. (1997) Protein structural classes in five complete genomes [letter]. *Nat. Struct. Biol.*, 4, 626–628.
- Frishman, D. and Mewes, H.W. (1999) Genome-based structural biology. *Prog. Biophys. Mol. Biol.*, 72, 1–17.

- Futcher, B., Latter, G. *et al.* (1999) A sampling of the yeast proteome. *Mol. Cell Biol.*, **19**, 7357–7368.
- Gaasterland, T. (1999) Archaeal genomics. *Curr. Opin. Microbiol.*, **2**, 542–547.
- Garrels, J.I., McLaughlin, C.S. *et al.* (1997) Proteome studies of *Saccharomyces cerevisiae*: identification and characterization of abundant proteins. *Electrophoresis*, **18**, 1347–1360.
- Gerstein, M. (1997) A structural census of genomes: comparing bacterial, eukaryotic, and archaeal genomes in terms of protein structure. *J. Mol. Biol.*, **274**, 562–576.
- Gerstein, M. (1998a) How representative are the known structures of the proteins in a complete genome? A comprehensive structural census. *Fold. Des.*, **3**, 497–512.
- Gerstein, M. (1998b) Patterns of protein-fold usage in eight microbial genomes: a comprehensive structural census. *Proteins*, **33**, 518–534.
- Gerstein, M. (1998c) Patterns of protein-fold usage in eight microbial genomes: a comprehensive structural census. *Proteins*, **33**, 518–534.
- Gerstein, M. and Hegyi, H. (1998) Comparing genomes in terms of protein structure: surveys of a finite parts list. *FEMS Microbiol. Rev.*, **22**, 277–304.
- Gerstein, M. and Jansen, R. (2000) The current excitement in bioinformatics, analysis of whole-genome expression data: how does it relate to protein structure and function. *Curr. Opin. Struct. Biol.*, **10**, 574–584.
- Gerstein, M., Lin, J. *et al.* (2000) Protein folds in the worm genome. *Pac. Symp. Biocomput.*, 30–41.
- Greenbaum, D., Luscombe, N. *et al.* (2001) Interrelating different types of genomic data, from proteome to secretome: coming in on function. *Genome Res.*, **11**, 1463–1468.
- Gygi, S.P., Rist, B. *et al.* (1999a) Quantitative analysis of complex protein mixtures using isotope-coded affinity tags. *Nature Biotechnol.*, **17**, 994–999.
- Gygi, S.P., Rochon, Y. *et al.* (1999b) Correlation between protein and mRNA abundance in yeast. *Mol. Cell Biol.*, **19**, 1720–1730.
- Gygi, S.P., Conhals, G.L. *et al.* (2000a) Evaluation of two-dimensional gel electrophoresis-based proteome analysis technology. *Proc. Natl Acad. Sci. USA*, **97**, 9390–9395.
- Gygi, S.P., Rist, B. *et al.* (2000b) Measuring gene expression by quantitative proteome analysis. *Curr. Opin. Biotechnol.*, **11**, 396–401.
- Harry, J.L., Wilkins, M.R. *et al.* (2000) Proteomics: capacity versus utility. *Electrophoresis*, **21**, 1071–1081.
- Hatzimanikatis, V., Choe, L.H. *et al.* (1999) Proteomics: theoretical and experimental considerations. *Biotechnol. Prog.*, **15**, 312–318.
- Haynes, P.A. and Yates, J.R. (2000) Proteome profiling: pitfalls and progress. *Yeast*, **17**, 81–87.
- Hegyi, H. and Gerstein, M. (1999) The relationship between protein structure and function: a comprehensive survey with application to the yeast genome. *J. Mol. Biol.*, **288**, 147–164.
- Holstege, F.C., Jennings, E.G. *et al.* (1998) Dissecting the regulatory circuitry of a eukaryotic genome. *Cell*, **95**, 717–728.
- Ishii, M., Hashimoto, S. *et al.* (2000) Direct comparison of genechip and SAGE on the quantitative accuracy in transcript profiling analysis. *Genomics*, **68**, 136–143.
- Ito, T., Tashiro, K. *et al.* (2000) Toward a protein–protein interaction map of the budding yeast: a comprehensive system to examine two-hybrid interactions in all possible combinations between the yeast proteins. *Proc. Natl Acad. Sci. USA*, **97**, 1143–1147.
- Jacger, J.A., Turner, D.H. *et al.* (1990) Predicting optimal and suboptimal secondary structure for RNA. *Meth. Enzymol.*, **183**, 281–306.
- Jansen, R. and Gerstein, M. (2000) Analysis of the yeast transcriptome with structural and functional categories: characterizing highly expressed proteins. *Nucleic Acids Res.*, **28**, 1481–1488.
- Jelinsky, S.A. and Samson, L.D. (1999) Global response of *Saccharomyces cerevisiae* to an alkylating agent. *Proc. Natl Acad. Sci. USA*, **96**, 1486–1491.
- Jones, D.T. (1998) Do transmembrane protein superfolds exist? *FEBS Lett.*, **423**, 281–285.
- Jones, D.T. (1999) GenTHREADER: an efficient and reliable protein fold recognition method for genomic sequences. *J. Mol. Biol.*, **287**, 797–815.
- Kidd, D. *et al.* (2001) Profiling serine hydrolase activities in complex proteomes. *Biochemistry*, **40**, 4005–4015.
- Klose, J. (1975) Protein mapping by combined isoelectric focusing and electrophoresis of mouse tissues. A novel approach to testing for induced point mutations in mammals. *Humangenetik*, **26**, 231–243.
- Krogh, A. *et al.* (2001) Predicting transmembrane protein topology with a hidden Markov model: application to complete genomes. *J. Mol. Biol.*, **305**, 567–580.
- Lin, J. and Gerstein, M. (2000) Whole-genome trees based on the occurrence of folds and orthologs: implications for comparing genomes on different levels. *Genome Res.*, **10**, 808–818.
- Lipshutz, R.F. S., Gingeras, T.R. and Lockhart, D.J. (1999) High density synthetic oligonucleotide arrays. *Nature Genet.*, **21**, 20–24.
- Lopez, M.F. (2000) Better approaches to finding the needle in a haystack: optimizing proteome analysis through automation. *Electrophoresis*, **21**, 1082–1093.
- MacBeath, G. and Schreiber, S.L. (2000) Printing proteins as microarrays for high-throughput function determination. *Science*, **289**, 1760–1763.
- Matton, D.P., Constabel, P. *et al.* (1990) Alcohol dehydrogenase gene expression in potato following elicitor and stress treatment. *Plant Mol. Biol.*, **14**, 775–783.
- McCarthy, J.E. (1998) Posttranscriptional control of gene expression in yeast. *Microbiol. Mol. Biol. Rev.*, **62**, 1492–1553.
- Mewes, H.W., Frishman, D. *et al.* (2000) MIPS: a database for genomes and protein sequences. *Nucleic Acids Res.*, **28**, 27–40.
- Millar, A.A., Olive, M.R. *et al.* (1994) The expression and anaerobic induction of alcohol dehydrogenase in cotton. *Biochem. Genet.*, **32**, 279–300.
- Molloy, M.P. (2000) Two-dimensional electrophoresis of membrane proteins using immobilized pH gradients. *Anal. Biochem.*, **280**, 1–10.
- Nauchitel, V.V. and Somorjai, R.L. (1994) Spatial and free energy distribution patterns of amino acid residues in water soluble proteins. *Biophys. Chem.*, **51**, 327–336.
- Nelson, R.W., Nedelkov, D. *et al.* (2000) Biosensor chip mass spectrometry: a chip-based proteomics approach. *Electrophoresis*, **21**, 1155–1163.
- O'Farrell, P.H. (1975) High resolution two-dimensional elec-

- trophoresis of proteins. *J. Biol. Chem.*, 250, 4007-4021.
- Pandey, A. and Mann, M. (2000) Proteomics to study genes and genomes. *Nature*, 405, 837-846.
- Qi, S.Y., Moir, A. et al. (1996) Proteome of *Salmonella typhimurium* SL1344: identification of novel abundant cell envelope proteins and assignment to a two-dimensional reference map. *J. Bacteriol.*, 178, 5032-5038.
- Ross-Macdonald, P., Coelho, P.S. et al. (1999) Large-scale analysis of the yeast genome by transposon tagging and gene disruption. *Nature*, 402, 413-418.
- Rost, B., Casadio, R. et al. (1995) Transmembrane helices predicted at 95% accuracy. *Protein Sci.*, 4, 521-533.
- Roth, F.P., Hughes, J.D. et al. (1998) Finding DNA regulatory motifs within unaligned noncoding sequences clustered by whole-genome mRNA quantitation. *Nature Biotechnol.*, 16, 939-945.
- Rubin, G.M., Yandell, M.D. et al. (2000) Comparative genomics of the eukaryotes. *Science*, 287, 2204-2215.
- Sali, A. (1999) Functional links between proteins. *Nature*, 402, 25-26.
- Santoni, V., Molloy, M. et al. (2000) Membrane proteins and proteomics: an amour impossible? *Electrophoresis*, 21, 1054-1070.
- Schena, M., Shalon, D. et al. (1995) Quantitative monitoring of gene expression patterns with a complementary DNA microarray. *Science*, 270, 467-470.
- Searls, D.B. (2000) Using bioinformatics in gene and drug discovery. *Drug Discov. Today*, 5, 135-143.
- Senes, A., Gerstein, M. et al. (2000) Statistical analysis of amino acid patterns in transmembrane helices: the GxxxG motif occurs frequently and in association with beta-branched residues at neighboring positions. *J. Mol. Biol.*, 296, 921-936.
- Shapiro, L. and Harris, T. (2000) Finding function through structural genomics. *Curr. Opin. Biotechnol.*, 11, 31-35.
- Sharp, P.M. and Li, W.H. (1987) The codon adaptation index—a measure of directional synonymous codon usage bias, and its potential applications. *Nucleic Acids Res.*, 15, 1281-1295.
- Sherlock, G. (2000) Analysis of large-scale gene expression data. *Curr. Opin. Immunol.*, 12, 201-205.
- Shevchenko, A., Jensen, O.N. et al. (1996) Linking genome and proteome by mass spectrometry: large-scale identification of yeast proteins from two dimensional gels. *Proc. Natl Acad. Sci. USA*, 93, 14 440-14 445.
- Smith, R.D. (2000) Probing proteomes-seeing the whole picture? *Nature Biotechnol.*, 18, 1041-1042.
- Tatusov, R.L., Koonin, E.V. et al. (1997) A genomic perspective on protein families. *Science*, 278, 631-637.
- Tekaia, F., Lazzano, A. et al. (1999) The genomic tree as revealed from whole proteome comparisons. *Genome Res.*, 9, 550-557.
- Velculescu, V.E., Zhang, L. et al. (1997) Characterization of the yeast transcriptome. *Cell*, 88, 243-251.
- Wallin, E. and von Heijne, G. (1998) Genome-wide analysis of integral membrane proteins from eubacterial, archaean, and eukaryotic organisms. *Protein Sci.*, 7, 1029-1038.
- Washburn, M.P., Wolters, D. et al. (2001) Large-scale analysis of the yeast proteome by multidimensional protein identification technology. *Nature Biotechnol.*, 19, 242-247.
- Washburn, M.P. and Yates, J.R. 3rd (2000) Analysis of the microbial proteome. *Curr. Opin. Microbiol.*, 3, 292-297.
- Wittes, J. and Friedman, H.P. (1999) Searching for evidence of altered gene expression: a comment on statistical analysis of microarray data [editorial; comment]. *J. Natl Cancer Inst.*, 91, 400-401.
- Wolf, Y.I., Brenner, S.E. et al. (1999) Distribution of protein folds in the three superkingdoms of life. *Genome Res.*, 9, 17-26.
- Young, K.H. (1998) Yeast two-hybrid: so many interactions, (in) so little time *Biol. Reprod.*, 58, 302-311.
- Zhang, M.Q. (1999) Large-scale gene expression data analysis: a new challenge to computational biologists (published erratum appears in *Genome Res.*, 1999, 9, 1156). *Genome Res.*, 9, 681-688.
- Zhu, H., Klemic, J.F. et al. (2000) Analysis of yeast protein kinases using protein chips. *Nature Genet.*, 26, 283-289.
- Zuker, M. (2000) Calculating nucleic acid secondary structure. *Curr. Opin. Struct. Biol.*, 10, 303-310.

Review

Early Detection of Lung Cancer: Clinical Perspectives of Recent Advances in Biology and Radiology¹

Fred R. Hirsch,² Wilbur A. Franklin,
Adi F. Gazdar, and Paul A. Bunn, Jr.

Lung Cancer Program and Departments of Medicine and Pathology, University of Colorado Cancer Center, Denver, Colorado 80262 [F. R. H., W. A. F., P. A. B.]; Department of Pathology, University of Texas, Southwestern Medical Center, Dallas, Texas [A. F. G.]; and Department of Oncology, Finsen Center, National University Hospital, Copenhagen, Denmark [F. R. H.]

Abstract

Lung cancer is the most common cause of cancer death in developed countries. The prognosis is poor, with less than 15% of patients surviving 5 years after diagnosis. The poor prognosis is attributable to lack of efficient diagnostic methods for early detection and lack of successful treatment for metastatic disease. Most patients (>75%) present with stage III or IV disease and are rarely curable with current therapies. Within the last decade, rapid advances in molecular biology, pathology, bronchology, and radiology have provided a rational basis for improving outcome. These advancements have led to a better documentation of morphological changes in the bronchial epithelium before development of clinical evident invasive carcinomas. This has changed our concept of lung carcinogenesis and emphasized the multistep carcinogenesis approach on several levels. Combined with the technical developments in bronchoscopic techniques, e.g., laser-induced fluorescence endoscope (LIFE) bronchoscopy, we now have improved methods to localize preinvasive and early-invasive bronchial lesions. With the LIFE bronchoscope, a new morphological entity (angiogenic squamous dysplasia) has been recognized, which might be an important biomarker and target for antiangiogenic chemopreventive agents. To reduce the mortality of lung cancer, these new technologies have been taken into the clinic in different scientific settings. The use of low-dose spiral computed tomography in the screening of a high-risk population has demonstrated the possibility of diagnosing small peripheral tumors that are not seen on conventional X-ray. A shift in the therapeutic paradigm from targeting advanced clinically

manifest lung cancer toward asymptomatic preinvasive and early-invasive cancer is occurring. The present article reviews the recent advances in the diagnosis of preinvasive and early-invasive cancer to identify biomarkers for early detection of lung cancer and for chemoprevention studies.

Introduction

Lung cancer is the most common cause of cancer deaths in the countries of North America and other developed countries, accounting for 29% of all cancer deaths and more deaths than from prostate, breast, and colorectal cancer combined in the United States (1). Lung cancer will be diagnosed in ~170,000 new patients in the United States in the year 2000, and <15% of them will survive 5 years after diagnosis (1). The prognosis for the patients with lung cancer is strongly correlated to the stage of the disease at the time of diagnosis. Whereas patients with clinical stage IA disease have a 5-year survival of about 60%, the clinical stage II-IV disease 5-year survival rate ranges from 40% to less than 5% (2). Over two-thirds of the patients have regional lymph-node involvement or distant disease at the time of presentation (3). The poor prognosis is largely attributable to the lack of effective early detection methods and the inability to cure metastatic disease. The unsatisfactory cure rates supports efforts aimed at early identification and intervention in lung cancer.

Historically, the only diagnostic tests available for the detection of lung cancer in its early stages were chest radiography and sputum cytology. The efficacy of these tests as mass screening tools was evaluated in controlled trials sponsored by the NCI³ and conducted at Johns Hopkins University, Memorial Sloan-Kettering Cancer Center, and the Mayo Clinic during the 1970s (4-6). The principal goal of these studies was to determine whether a reduction in lung cancer mortality could be achieved by adding sputum cytology testing to annual screening by chest radiography. Results from these trials showed that both tests could detect presymptomatic, early-stage carcinoma, particularly of squamous cell type. Resectability and survival rates were found to be generally higher in the study groups than in the control groups. However, improvements in resectability and survival did not lead to a reduction in overall lung cancer mortality, the most critical end point. A subsequent study of 6346 Czechoslovakian male smokers also found no reduction in lung cancer mortality after dual screening by chest radiography

Received 6/29/00; revised 10/16/00; accepted 10/30/00.

The costs of publication of this article were defrayed in part by the payment of page charges. This article must therefore be hereby marked advertisement in accordance with 18 U.S.C. Section 1734 solely to indicate this fact.

¹Supported by National Cancer Institute Grants CA 58187 from the Specialized Program of Research Excellence (SPORE)-Lung and CA 85070 from the Lung Cancer Biomarkers and Chemoprevention Consortium.

²To whom requests for reprints should be addressed, at University of Colorado Cancer Center, Department of Pathology, University of Colorado Health Sciences Center, 4200 East Ninth Avenue, B 216, Denver, Colorado 80262. E-mail: Fred.Hirsch@UCHSC.edu.

³The abbreviations used are: NCI, National Cancer Institute; CIS, carcinoma *in situ*; CT, computed tomography; ASD, angiogenic squamous dysplasia; TSG, tumor suppressor gene; LOH, loss of heterozygosity; hnRNP, heterogeneous nuclear ribonucleoprotein; SPLC, second primary lung cancer; BAL, bronchoalveolar lavage; SCLC, small cell lung carcinoma; WLB, white light bronchoscopy; LIFE, laser-induced fluorescence endoscope; ELCAP, Early Lung Cancer Action Project; PET, positron emission tomography; FDG, [¹⁸F]fluoro-2-deoxyglucose.

and sputum cytology (7). The negative results from these screening studies lead the NCI and other health policy and research groups to conclude that mass screening programs involving periodic sputum cytological evaluation and chest radiographs could not be justified. However, controversies in the methodology and interpretation of the data from these studies have later been extensively discussed (8, 9). One additional study of annual chest X-ray screening is currently being conducted by the NCI; The Prostate-, Lung-, Colorectal-, and Ovarian (PLCO) screening trial. This trial includes individuals 55–74 years old, but they are not selected for this trial on the basis of high risk for lung cancer (e.g., smoking history with >20 pack-years).

The failure of clinical trials to demonstrate the efficacy of sputum cytology and chest radiography as mass screening tools has resulted in a search for better diagnostic approaches for early lung cancer detection that take advantage of recent developments in molecular biology, gene technology, and radiology (10). Furthermore, as has been the case for mammography screening for breast cancer, it has also been important to identify risk groups for lung cancer.

Although, much is known about predisposing factors, natural history, and the outcome based on histology and stage, our understanding remains very incomplete in many areas. What are the early premalignant changes molecularly, biochemically, and morphologically? Which changes are reversible and which are not? What research tools are available to provide answers to these questions? The identification of preinvasive lesions allows for developing promising methods for early intervention (11). The therapeutic paradigm and focus are today shifting from targeting only clinically verified lung cancer as previously toward targeting the premalignant and early-malignant lesions. Furthermore, the prospect of lung cancer screening has today become more meaningful as a consequence of recent developments in biology and radiology and better possibilities to define high-risk populations most suitable for lung cancer screening (12).

The present article will focus on the clinical perspectives of our biological knowledge of premalignant and early-malignant lesions and the potential of the recent technological advancement for early diagnosis of lung cancer.

Pathology of Preinvasive and Early Invasive Bronchial Lesions

Most of the efforts to classify lung cancer have been directed toward invasive carcinoma (13). However, better understanding of the pathogenesis of lung cancer aroused renewed interest in morphological abnormalities that fall short of invasive carcinoma but may indicate initiation of carcinogenesis. These morphological abnormalities are referred to as preinvasive lesions and are shown in Fig. 1. The last edition of the WHO classification of lung tumors included the classification of preinvasive lesions as a separate section. Numerous recent studies have indicated that lung cancer is not the result of a sudden transforming event in the bronchial epithelium but a multistep process in which gradually accruing sequential genetic and cellular changes result in the formation of an invasive (i.e., malignant) tumor. Mucosal changes in the large airways that

may precede or accompany invasive squamous carcinoma include hyperplasia, metaplasia, dysplasia, and CIS (14). Hyperplasia of the bronchial epithelium and squamous metaplasia have generally been considered reversible, and not premalignant in the sense of squamous dysplasia and CIS (15).

Squamous metaplasia is a common finding, especially as a response to cigarette smoking. Peters *et al.* (16) studied bronchoscopic biopsies from six sites in 106 heavy cigarette smokers; Squamous metaplasia was noted at one or more biopsy sites in approximately two-thirds of the group, and one-fourth showed squamous metaplasia in three or more biopsy sites. The incidence of squamous metaplasia increased with smoking history and was highest in individuals who had smoked more than two packs of cigarettes a day. Averbach *et al.* (17) noted similar findings in autopsy tissues: basal cell hyperplasia and squamous metaplasia are increased in smokers in proportion to smoking history. Hyperplasia and metaplasia are believed to be reactive changes in the bronchial epithelium, as opposed to true preneoplastic changes (17, 18). The reasons for this include: (a) they are frequently found in association with chronic inflammation, and may be induced by mechanical trauma; (b) they spontaneously regress after smoking cessation; (c) in chronic smokers, the molecular changes present in these lesions are similar to those present in histologically normal epithelium; and (d) there are no reports linking their presence to increased risk for developing lung cancer. In contrast, moderate-to-severe dysplasia and CIS lesions seldom regress after smoking cessation (19).

Dysplasia and CIS are changes that frequently precede squamous cell carcinoma of the lung. Saccomanno *et al.* (20) studied more than 50,000 samples from 6,000 men, many of whom had worked in the uranium mining industry. Both smoking and uranium mining (radon exposure) were found to be associated with increased incidence of dysplasia, CIS, and invasive cancer. The studies of Saccomanno *et al.* established that increasing degrees of sputum atypia may be recognized an average of 4–5 years before the development of frank lung carcinoma.

Another question is: which grades of sputum atypia progress to cancer? From the Johns Hopkins cohort of the NCI chest X-ray/sputum screening trial, we know that among individuals with moderate atypia on sputum screening, ~10% developed known cancer up to 9 years later. Among individuals with severe atypia on the sputum screening, >40% developed known cancer during the same time period (21). Although there are data in the literature showing the relationship between sputum atypia and subsequent invasive cancer, there is still very little information about the histological progression in the bronchial mucosa in the high risk populations. In a recent publication, nine patients with CIS were followed with autofluorescence bronchoscopy at regular intervals, and 5 (56%) had progression to invasive cancer despite endobronchial therapy (22). The number of invasive cancers might even have been higher if treatment had not been given. Ongoing studies of high-risk subjects (e.g., the Colorado sputum cohort study) including serial follow-up bronchoscopies will provide evidence related to the frequency of development of invasive lung cancer as it relates to smoking history, airflow obstruction, and sputum atypia.

Since the previous WHO-classification was published in

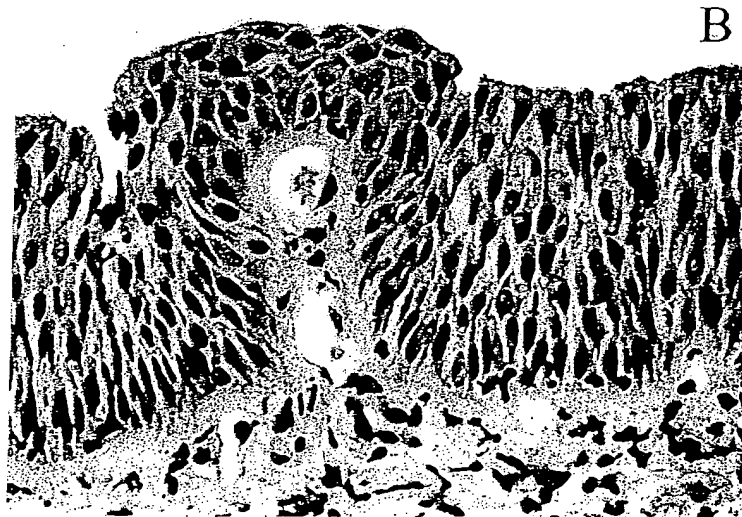
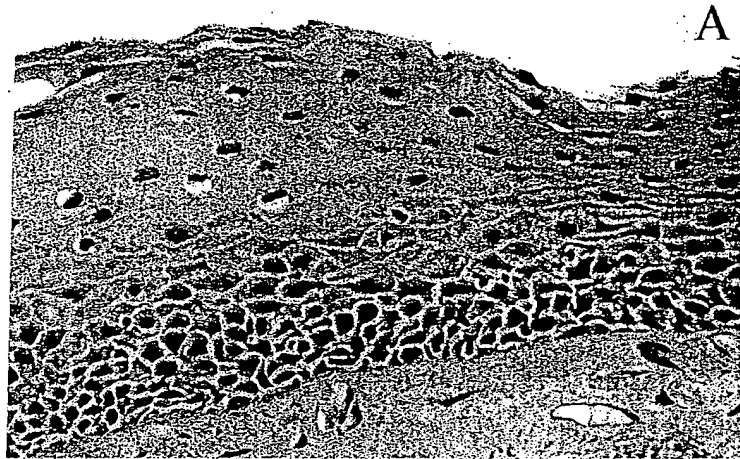


Fig. 1 A, squamous metaplasia. The cells are widely dispersed, with a regular maturation from the basal region to the top. There is keratinization, and the nuclei/cytoplasmic ratio is low. B, moderate dysplasia with ASD. Hypercellularity of the epithelium with incomplete maturation and micropapillary invasion of capillaries are seen. The nuclei/cytoplasmic ratio is high. C, severe dysplasia. There is marked pleomorphism of the cells with irregularity and prominent nucleoli.

1981, two nonsquamous lesions have been added to the WHO classification of premalignant lesions: atypical alveolar hyperplasia and diffuse idiopathic neuroendocrine cell hyperplasia (13). Both of these lesions are diagnosed rarely. The former consists of lesions <5 mm in diameter and composed of a peripheral epithelial cell proliferation with minimal cytological atypia or stromal response and resembles bronchioloalveolar carcinoma. The lesion has been seen in lung specimens resected for lung cancer, but no prospective significance of this lesion has been reported. However, this morphological lesion may play a role for the pathogenesis of peripheral lung adenocarcinomas (23, 24). The resolution of spiral CT (currently about 3 mm) approaches the diameter of these lesions, and it is anticipated that atypical alveolar hyperplasia will be increasingly encountered in subjects undergoing this procedure (25). Diffuse idiopathic neuroendocrine cell hyperplasia consists of a patchy increase in the number of well-differentiated neuroendocrine cells in the bronchioles. This process may result in the formation of small carcinoid tumors, and for this reason it is considered "preinvasive." To date, small cell carcinomas have not been associated with this lesion (13).

Recently, the use of fluorescence bronchoscopy (see below) has increased the recognition of dysplastic lesions in the large airways and a new morphological entity, ASD, was identified (26). Dysplasia of bronchial epithelium in "micropapillomatosis" and the possible link between angiogenesis and preinvasive bronchial epithelial dysplasia were recognized as early as 1983 by Muller and Muller (27), who also described the ultrastructure of these lesions. It has been suggested that this angiogenesis, which is recognized as capillary loops projecting into the dysplastic bronchial lining, is responsible for the reduced fluorescence seen in dysplastic lesions by LIFE bronchoscopes (Figs. 1 and 3; Ref. 26). Future prospective studies will show whether this morphological entity is correlated with a progression to lung cancer so as to be a target for the use of antiangiogenic agents for chemoprevention.

In general, there are several questions/problems relating to premalignant lesions, which will be addressed in future studies:

(a) The morphological criteria for premalignant and early-malignant changes, both on sputum cytology and in bronchial biopsies, have to be validated for intra- and interobserver reproducibility.

(b) Uniform and reproducible morphological/cytological criteria have to be published more extensively, and a training set of slides should be available. By the use of Internet technology, this could be more easily facilitated (28).

(c) The correlation of sputum atypia and histological changes in the bronchi in high-risk population is not well defined.

(d) The natural course of preinvasive changes in the bronchi from the high risk subjects needs to be clarified through longitudinal, prospective studies with reference to histological changes in the bronchi. Ongoing longitudinal studies with fluorescence bronchoscopy and multiple biopsies with histology and other biomarkers will define the ability of these markers to assess for risk.

(e) What is the pathology/biology of the small, often peripherally located, tumors (3 mm in diameter), which are more

often diagnosed with newer radiological techniques (e.g., low-dose spiral CT)?

(f) Optimization of the tissue procurement and processing techniques are important. Distinction of reactive from neoplastic processes is usually straightforward, but diagnostic difficulties may arise in the case of (a) inadequate or poorly prepared histological material to evaluate and (b) the presence of cytological atypia in epithelium stimulated by inflammation, viral infection, radiation, or chemotherapy.

(g) DNA array analyses of gene expression: will it be useful? How to collect proper mRNA? Can mRNA extracted from microdissected cells obtained at bronchoscopy be globally amplified and still remain representative of RNA present *in situ*?

Biology of Lung Carcinogenesis and Potential Early Detection Markers

Lung cancer is the end-stage of multiple-step carcinogenesis, in most cases driven by genetic and epigenetic damage caused by chronic exposure to tobacco carcinogens. The genetic instability in human cancers appears to exist at two levels: at the chromosomal level, including large scale losses and gains; and at the nucleotide level including single or several base changes (29). Lung cancers harbor many numerical chromosomal abnormalities (aneuploidy) and structural cytogenetic abnormalities including deletions and nonreciprocal translocations (30). At least three classes of cellular genes are involved: proto-oncogenes, TSGs, and DNA repair genes. Oncogenic activation often occurs via point mutations, gene amplification, or chromosomal rearrangement, whereas TSGs are classically inactivated by the loss of one parental allele combined with a point or small mutation or aberrant methylation of a target TSG in the remaining allele. Additionally, dysregulated gene expression (either increased or decreased expression) can occur by other, as yet unknown, mechanisms (30). Present studies have not yet confirmed a prominent role for abnormalities of DNA repair genes in lung cancer.

Preneoplastic cells contain several molecular genetic abnormalities identical to some of the abnormalities found in overt lung cancer cells (Fig. 2). These include allele loss at several loci (3p, 9p, 8p, and 17p), *myc* and *ras* up-regulation, cyclin D1 overexpression, p53 mutations, and increased immunoreactivity, bcl-2 overexpression and DNA aneuploidy (31-35). Allelotyping of precisely microdissected, preneoplastic foci of cells suggests that the earliest changes in the bronchial epithelium is allele loss at chromosome regions 3p, then 9p, 8p, 17p, 5q, and then *ras* mutations (36-39). The biological meaning of LOH is only vaguely understood. Recent evidence suggests that LOH may be a consequence of mitotic recombination, that there is only infrequent physical loss of genetic loci, and that LOH probably precedes chromosomal duplication (40). Allelic loss would thus be significant primarily in the presence of mutation in the retained allele, and gene dosage would not be expected to exert a phenotypic effect in LOH. Some reports have indicated that *ras* activation occurs at early carcinoma stages (34). Histologically normal bronchial epithelium adjacent to cancers has also been shown to have certain genetic losses. Atypical adenomatous hyperplasia, the potential precursor lesion of adenocarcinomas, often have *Ki-ras* mutations (41).

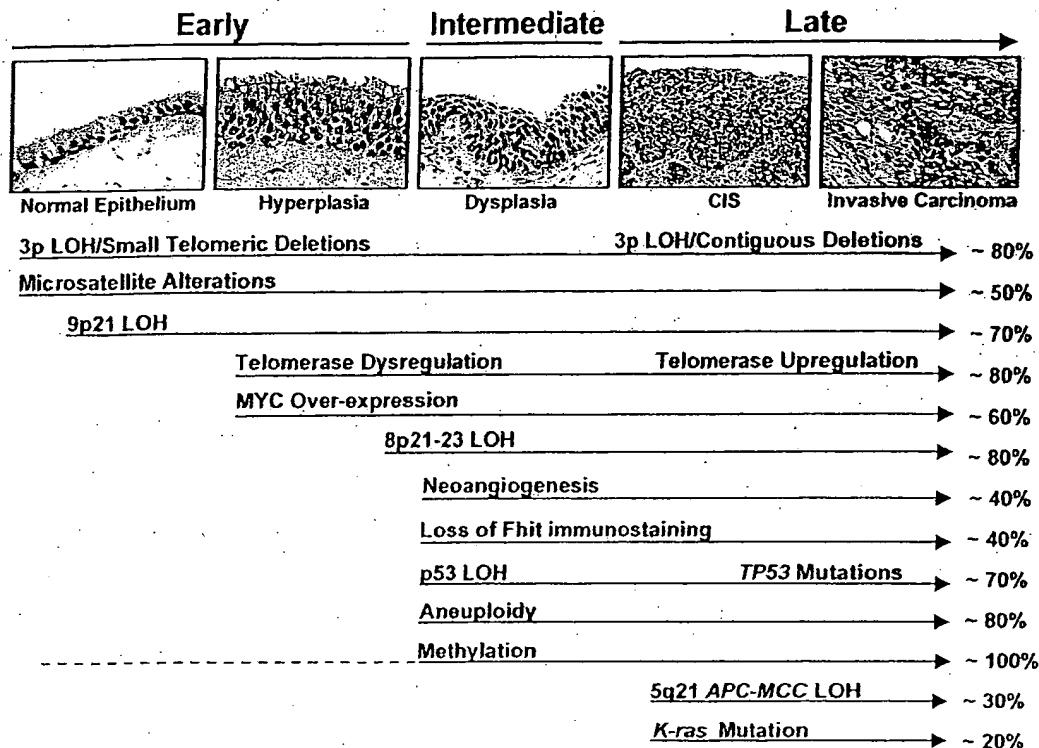


Fig. 2 Sequential changes during lung cancer pathogenesis. Although multiple genetic markers are abnormal in lung cancers, their appearance during the lengthy preneoplastic process varies. The timing of the appearance of these changes has been investigated in bronchial preneoplasia, because sequential sampling of the peripheral lung is technically difficult. Several alterations have been described in histologically normal bronchial epithelium of smokers. Other changes have been detected in slightly abnormal epithelium (hyperplasia, metaplasia) which we do not consider to be true premalignant lesions. These changes are regarded as early changes. Molecular changes detected frequently in dysplasia are regarded as intermediate in timing, whereas those usually detected at the CIS or invasive stages are regarded as late changes. It should be stressed that although there is a usual order, exceptions regarding the timing of onset may occur. Some changes are progressive, such as chromosome 3p deletions. Thus small discrete changes are present early, progressively become more extensive during pathogenesis, and frequently involve all or almost all of the arm in CIS samples. Although allelic loss at the TP53 locus may precede the onset of mutations, data on this sequence are scant. Dysregulation of the RNA component of telomerase (with its appearance in nonbasal cells) is an early event, whereas up-regulation of the gene is a relatively late event.

Molecular changes have been found not only in the lungs of patients with lung cancer, but also in the lungs of current and former smokers without lung cancer (18, 42, 43). These observations are consistent with the multistep model of carcinogenesis and "field cancerization" process, whereby the whole region is repeatedly exposed to carcinogenic damage (tobacco smoke) and is at risk for developing multiple, separate, clonally unrelated foci of neoplasia. The widespread aneuploidy that occurs throughout the respiratory tree of smokers supports this theory (44). However, the presence of the same somatic p53 point mutation at widely dispersed preneoplastic lesions in a smoker without invasive lung cancer indicates that expansion of a single progenitor clone may spread throughout the respiratory tree (45). These molecular alterations might thus be important targets for use in the early detection of lung cancer and for use as surrogate biomarkers in the follow-up of chemoprevention

studies. Detection of these mutant cells should be possible with the different molecular techniques in accessible specimens. The prospects of diagnosing these biological abnormalities in multiple types of clinical specimens are discussed below.

Specimens for Clinical Testing: Sputum

Since the 1930s, cytological examination of sputum has been used for the diagnosis of lung cancer (46). Cytological examination of sputa, especially multiple samples, is helpful for the detection of central tumors arising from the larger bronchi (e.g., squamous cell- and small cell carcinomas). Exfoliated cells from peripheral tumors, such as adenocarcinomas, arising from the smaller airways (small bronchi, bronchioles, and alveoli), especially those less than 2 cm in diameter, can be detected only occasionally in sputum samples. This has become of greater importance because the changes in cigarette exposure

(filters and decreased nicotine content) have created an increase in adenocarcinomas and a decrease in squamous carcinomas (47-49). The sensitivity of sputum cytology for early lung cancer is only in the 20%-30% range from screening studies, but by adhering to proper specimen collection, and processing and interpreting criteria, the yield can be substantially improved (50, 51). The data on the reliability of the sputum are conflicting (52-54). Browman *et al.* (52) reported interobserver agreement of 68% for exact and 82% for within - 1-category. Holliday *et al.* (54) reported low agreement within observers (27-60%) and across observers (13-50%). Within - 1-category intraobserver agreement underwent a two- or 3-fold increase in agreement, which was also the case for interobserver agreement. The variation in intra- and interobserver agreement seems to depend on experience among the cytotechnicians/cytopathologists and the composition of categories studied. A higher degree of agreement is obtained for higher grades of dysplasia (54). Risse *et al.* (55) showed that the ability to detect premalignant conditions is dependent on the number and type of cells present in the deeper airways, suggesting a mode of improvement that is unrelated to observer reliability. MacDougall *et al.* (56) concluded that sputum cytology was too insensitive and insufficiently accurate to be included in the routine work-up of any patient suspected of having lung cancer. To improve the reliability of sputum cytology examinations a simplification of the diagnostic categories from 6 (normal; squamous metaplasia; mild, moderate, and severe atypia; and carcinoma) to 2-3 categories have been proposed (54). Future clinicopathological studies will be required to validate this concept.

To improve the sensitivity of sputum examination as a population-screening tool for the detection of early lung cancer, several approaches are currently under development.

Immunostaining: Annual sputum specimens obtained from individuals screened at Johns Hopkins were obtained, and the patients were monitored for 8 years (57). Because the clinical outcome of these patients was known, archival sputum specimens were screened for the presence of biomarkers that could indicate the presence of lung tumors in an early, preinvasive stage. In an attempt to distinguish the pattern of marker expression Tockman *et al.* (58) studied two monoclonal antibodies. Positive staining predicted subsequent lung cancer approximately 2 years before clinical recognition of the disease, with a sensitivity of 91% and a specificity of 88% (58). One of these antibodies (703 D4) had a higher sensitivity and was later identified as recognizing hnRNP A2/B1 (59). The role of hnRNP A2/B1 overexpression for detecting preclinical lung cancer has been studied in a large high-risk population including 6000 Chinese tin miners who were heavy smokers and who had an extraordinary rate of lung cancer (60). The results from this study indicated that detection of hnRNP A2/B1 overexpression in sputum epithelium cells was 2- to 3-fold more sensitive for detection of lung cancer than standard chest X-ray and sputum cytology methods. The method was particularly effective in identifying early disease (60). The sensitivity was 74% versus 21% for cytology and 42% for chest X-ray. However, the biomarker had a lower specificity (70%) compared with cytology (100%) and chest radiograph (90%). An ongoing clinical trial is evaluating the performance of the A2/B1 protein as a biomarker for the early detection of SPLC. The patients at risk

for SPLC have the highest incidence of lung cancer (2-5%) among asymptomatic populations (61). In this trial, 13 SPLCs were identified by A2/B1, and the sensitivity and specificity were 77-82% and 65-81%, respectively. Among the cases identified as positive by immunocytochemistry and image cytometry, 67% developed SPLC within 1 year (62). Whereas the previous immunocytochemistry studies on material from the older screening material from the NCI-supported screening studies were made on sputum cells cytologically classified with moderately or gravely atypical metaplastic appearance, the latter studies have been done on cytologically "normal appearing" cells. More recently Sueoka *et al.* (63) reported the confirmation of the value of overexpression of hnRNP A2/B1 to detect preclinical lung cancer in Japan. Efforts to improve the sensitivity of hnRNP markers are ongoing (64).

PCR Techniques. PCR techniques have been used for the evaluation of molecular biomarkers for early lung cancer detection. In a pilot study with selected patients from the Johns Hopkins Lung Project (JHLP), 8 (53%) of 15 patients with adenocarcinoma or large cell carcinoma were detected by mutations in sputum cells from 1 to 13 months before clinical diagnosis (65). However, the method seemed to be less sensitive than the protein marker described above, and the identification of specific gene abnormalities is further limited by the need to know the specific mutation sequence with which to probe the sputum specimens. Currently, this approach is not practical for screening undiagnosed individuals. Future advances in gene chip technology may permit testing for all possible mutations of common oncogenes and TSGs in clinical specimens of asymptomatic individuals (62).

Microsatellite markers are small repeating DNA sequences found in the noncoding regions of a gene. PCR amplification of these repeat sequences provides a rapid method for assessment of LOH and facilitates the mapping of suppressor genes (66, 67). Microsatellite alterations are extension or deletions of these repeated elements. Detection of microsatellite alterations in histological or cytological specimens may facilitate the detection of clonal preneoplastic or neoplastic cell populations. Although the detection of microsatellite alterations does not indicate the specific genetic change in the tumor, detection of clonal cell populations might serve as a cancer screening marker (65). Identical alterations have been found in lung cancers and corresponding sputum samples demonstrating minimal atypia (68). The *p16* gene is located on the short arm of chromosome 9(9p21) and is frequently mutated or inactivated in tumors and cell lines derived from lung cancer (69, 70). Belinsky *et al.* (71) measured hypermethylation of the CpG islands in the sputum of lung cancer patients and demonstrated a high correlation with early stages of non-small cell lung cancer, which indicated that *p16* CpG hypermethylation could be useful in the prediction of future lung cancer. However, prospective studies are needed to evaluate the role of *p16* hypermethylation as a marker for early lung cancer detection. Multiple other genes are inactivated by hypermethylation in lung cancer (72), and the detection of hypermethylation may be useful for risk assessment and early diagnosis.

Computer-assisted Image Analysis. Computer-assisted image analysis was initially used to detect malignancy-associated changes (e.g., subvisual or nonobvious changes in the

distribution of DNA in the nuclei of histologically normal cells in the vicinity of preinvasive or invasive cancer; 73). In a retrospective analysis of sputum cytology slides, malignancy-associated changes alone correctly identified 74% of the subjects who later developed squamous cell carcinoma (74). The technique has been improved, and recent data showed sensitivities of 75% for stage 0/I lung cancer and 85% for adenocarcinomas with a specificity of 90% (75). This quantitative microscopy technique allows the examining of thousands of cells per slide within a relative short time. Similar techniques have been approved in the United States for cervical cancer screening, and might, in the future, play a role for lung cancer screening. However, no prospective clinical studies has evaluated this technology in a larger lung cancer screening setting.

High Throughput Technology. With future advances in gene chip technology, it might become feasible to probe for expression of multiple genes in sputum specimens of asymptomatic individuals. However, this requires a large amount of undegraded RNA from respiratory tract cells. With the high throughput technology, a higher sensitivity might be achieved by using multiple markers at the cost of achieving a lower specificity, which would be undesirable for a screening study.

In conclusion, we need to reevaluate the role of sputum cytology for screening and early detection of lung cancer because of advances in biomarkers and technology. Ongoing studies with standard and biomarker analysis in high-risk groups might change the previous negative attitude and provide a new perspective on sputum cytology as a mass screening tool when applied in a high-risk population. Adding different molecular diagnostic tests gives the possibility for early diagnosis far in advance of clinical presentation. However, validation of the tests in larger prospective studies is necessary, and the individual tests have to be compared with each other to define the role of early diagnosis in the overall management of high-risk subjects. Furthermore, health economic issues have to be considered.

Specimens for Clinical Testing: BAL

BAL involves the infusion and reaspiration of a sterile saline solution in distal segments of the lung via a fiberoptic bronchoscope. Ahrendt *et al.* (76) examined a series of 50 resected non-SCLC tumor patients and compared the tumor and BAL with regard to molecular markers including p53 mutations, K-ras mutation, the methylation status of the CpG island of the *p16* gene, and microsatellite alteration (Tables 1 and 2). With the possible exception of the test for microsatellite alteration, all of the tests had relatively high sensitivity and could detect mutant cells in the presence of a large excess of normal cells. The frequencies of these changes in the tumors ranged from 27% (for K-ras mutations) to 56% (for p53 mutations). As expected, p53 mutations were more frequent in central (predominantly squamous cell) tumors, and K-ras mutations were more frequent in peripheral (predominantly adenocarcinoma) tumors. The specificity was high (nearly 100%) because, with the exception of microsatellite alterations, the same genetic change in BAL sample as in tumors was always found, but the sensitivity was low, and in only 53% of tumors that contained molecular lesions were the same abnormalities detected in corresponding BAL fluids. Specifically, the tests were least helpful in the

group of patients in whom improved diagnostic abilities are most needed, those with small, peripherally located tumors (77). Unfortunately, the investigators were not able to compare the molecular tests with routine cytopathological analysis of the BAL specimens. The sensitivity of the molecular tests in BAL specimens has to be improved, and we need to know the results from subjects at increased risk (current and former smokers without lung cancer and survivors of previous cancer of the upper respiratory tract) and subjects with chronic lung diseases as well as results from healthy never smokers.

A European group has previously shown that genetic alterations detected in DNA from bronchial lavage of individuals with lung cancer were also found in individuals with no evidence of malignant disease (78), which raises the question about the specificity of such molecular damage in neoplastic conditions. To improve the sensitivity and specificity of detecting allelic imbalance in lung tumors, high throughput PCR-based microsatellite assays have been established (79). In a recent study by Fielding *et al.* (80), the up-regulation of hnRNP A2/B1 was found to be a promising marker in BAL for the detection of premalignant and malignant bronchial lesions with a diagnostic sensitivity of 96% and a specificity of 82%.

It is too early yet to make conclusions as to whether BAL examinations will add to other pathological/molecular biological clinical studies. To obtain diagnostic material for BAL bronchoscopy is required, and we do not have any data that compare BAL examinations with biopsies. Thus, we do not know whether BAL is a valuable adjunct to the biopsies taken under the same bronchoscopy procedure.

Specimens for Clinical Testing: Peripheral Blood

For many years scientists have searched for a lung cancer-specific tumor marker that could be detected in peripheral blood. Optimism was raised in the "early" immunocytochemistry era by the use of monoclonal antibodies raised against more-or-less specific epithelial epitopes. In the search for epithelial cells in peripheral blood and bone marrow, monoclonal antibodies against cytokeratin have been used. However, these reactions are clearly not cancer-specific, and some antibodies have been shown to cross-react with normal blood or bone marrow elements (81, 82). Another explanation could be that cells from the macrophage/monocyte system may contain proteins derived from the primary tumor that have undergone necrosis and apoptosis and that these processed proteins are recognized by the antibodies (82). On the basis of "traditional" immunocytochemistry, no markers have been able to detect premalignant or early-malignant disorders based on a peripheral blood sample. However, with the development of DNA technologies, new possibilities have been raised, and, with the use of PCR techniques, some promising reports have been published.

Nanogram quantities of DNA circulating in blood are present in healthy individuals (83, 84). Tumor DNA is also released into the plasma component in increased quantities (85, 86). Thus, the plasma and serum of cancer patients is enriched in DNA, an average four times the amount of free DNA as compared with normal controls (87). In a study by Chen *et al.* (88), a comparison of microsatellite alterations in tumor and plasma DNA was done in SCLC patients, and 93% of the patients with

Table 1 Tissues and other resources for the study of molecular markers

Specimen	Ref.	Comments
Tumor tissue	Numerous	Mixture of cell types, may require microdissection (139). Extensively used for most studies. Alcohol-fixed fine-needle aspirates may be used for mutational and other studies.
Sputum	65, 68, 71, 74	Respiratory cells usually in small minority. Most samples fixed in Saccomanno's fixative. Several studies have been performed on these specimens many years later.
Surrogate organ	140	Predominantly squamous epithelial cells. Buccal smears, brushings of tongue or tonsil may be explored as potential surrogate organs resulting from the field effect of tobacco damage of the entire upper aerodigestive tract. This concept needs to be confirmed.
Bronchial brush/wash	141, 142, 143	Predominantly respiratory cells. Fresh, frozen, or alcohol-fixed samples are suitable for multiple studies including FISH.*
Bronchial tissues	42, 43, 45, 144, 145	Usually from bronchial biopsies, but may be obtained from surgical resection specimens. Formalin fixation and paraffin embedding required for histological diagnosis, although EASI preps may permit identification and isolation of subpopulations. Paraffin sections may be used for genotyping polymorphisms, for allelotyping, and for <i>in situ</i> hybridization.
BAL fluids	76, 78, 146, 147, 148	BAL fluids are useful for examining the peripheral airway cells, which are the precursor cells of most adenocarcinomas. Numerous mononuclear cells present. Enrichment of epithelial cells desirable.
Blood components	72, 92, 149	Analysis of circulating tumor cells and genetic material shed by dying tumor cells into the plasma component may yield useful biological and diagnostic information. Gene mutations and presence of epithelial cell markers have been used to detect circulating tumor cells. Gene mutations, allelic loss, microsatellite alterations, and aberrant methylation have been used to identify tumor cell DNA released into the fluid compartment.
Tissue for molecular staging	150, 151	Although little data exists for lung cancers, regional lymph nodes, sentinel lymph nodes, and surgical resection margins have been used in other tumor types for molecular staging.
Tumor cell lines	152, 153	Provide an unlimited self-replicating source of high-quality molecular reagents and have been used for numerous studies. Cell lines may or may not reflect the properties of the tumors from which they were derived (26), although they probably represent cellular subpopulations (27). Aggressive metastatic tumors are more likely to be successfully cultured (28) resulting in skewed data.
Cultures of nonmalignant tissues	154, 155	Epithelial cultures may be useful for studying molecular changes during multistage pathogenesis. Temporary as well as a few immortalized cultures from nonmalignant epithelial cells have been established. B-lymphoblastoid cultures are useful for linkage analysis, for genetic susceptibility studies, and for allelotyping corresponding tumors.
Nonmalignant tissue from patients and from cancer-free relatives	156, 157, 158	Tissues such as buccal smears, tumor-free lymph nodes, and peripheral blood mononuclear cells are useful as controls for linkage analysis, for genetic susceptibility studies, and for allelotyping corresponding tumors.

* FISH, fluorescence *in situ* hybridization; EASI, epithelial aggregate separation and isolation.

microsatellite alterations in tumor DNA also had modifications in the plasma DNA. However, some patients had LOH only in the tumor DNA. Because most of the microsatellite alterations were similar in tumor DNA and plasma DNA, they concluded that some of the DNA circulating in the blood comes from the tumor. Thus, modifications of circulating DNA can be used as an early detection marker. Detection of aberrant DNA methylation in serum DNA in patients with non-SCLC has been reported (72). Although the number of patients was small and the hypermethylated DNA was found in all stages, it opens up for the possibility to be used as an early lung cancer detection marker. Furthermore, *p53* and *ras* gene mutations have been

detected in the plasma and serum of patients with colorectal cancers (89-91), pancreatic carcinomas (92, 93), and hematological malignancies (94).

In conclusion, the limited direct accessibility of lung carcinomas has led to efforts to identify tumor-associated soluble markers in serum or plasma. Many of the currently recognized soluble markers were first identified as "tumor" markers but, when evaluated in nonneoplastic tissue, have often been found in normal cells as well as in tumors. For early detection of lung cancer, we need more clinical data evaluating these new molecular biological markers from multiple sites, especially in high-risk groups.

Table 2 Molecular approaches for lung cancer investigation

Specimen	Ref.	Comment
Gene mutations	159, 160, 161	Widely used technique, especially for <i>p53</i> and <i>ras</i> genes. Often used to determine the role of a newly discovered gene in the pathogenesis of lung cancer. May be of diagnostic and prognostic significance. Multiple methodologies available.
Allelotyping	18, 158	Useful as a partial substitute for mutational analysis and for determining the chromosomal locations of putative tumor suppressor genes. Widely used to study multistage pathogenesis. Readily performed on formalin-fixed and microdissected tissues. Increasing use of genotyping using automatic sequencers.
Gene expression at RNA and protein level	145, 162, 163, 164, 165, 166	Northern blotting and reverse transcription-PCR are widely used to investigate gene expression. Western blotting often used for detection of protein expression. <i>In situ</i> hybridization for message expression can be performed on paraffin-embedded tissues and, thus, can be used to investigate multistage pathogenesis. Microarray techniques offer promise of examining all or most of the genome but currently require relatively large amount of high-quality RNA from purified cell populations. Sage technique useful for investigation and identification of expressed genes. Similarly, advances in proteomics will permit simultaneous detection of multiple proteins. Numerous immunohistochemical studies of oncogene expression have been used to study multistage pathogenesis. Of particular interest, hnRNP expression on exfoliated epithelial cells in sputum samples may predict for development of cancer.
Molecular cytogenetics	40, 167, 168, 169, 170	<i>In situ</i> hybridization studies of fixed materials or using smears has provided considerable information about numerical and structural changes.
Comparative genomic hybridization	171, 172	Useful for detection of gene amplifications. Less sensitive for the detection of regions of allelic loss.
Morphometric studies	74, 173, 174	May be applied to paraffin-embedded tissues. Useful for determining aneuploidy and for measuring a number of nuclear and cytoplasmic parameters.

Specimens for Clinical Testing: Bronchoscopy

WLB is the most commonly used diagnostic tool for obtaining a definite histological diagnosis of lung cancer. Bronchoscopy has major diagnostic limitations for premalignant lesions. Because these lesions are only a few cells thick (0.2–1 mm) and have a surface diameter of only a few millimeters, they rarely are observed as visual abnormalities. Woolner (95) reported that squamous cell CIS was visible to experienced bronchoscopists in only 29% of cases. To address this limitation, fluorescence bronchoscopy was developed. Early studies of fluorescence bronchoscopy entailed the use of fluorescent drugs (hematoporphyrin dyes) that were preferentially retained in malignant tissue (96). Although, studies evaluating this approach did, in fact, show that early invasive and *in situ* cancers could be localized, the detection of dysplasia remained problematic (97–100). Furthermore, the development of photodynamic diagnostic systems was hampered by problems including skin photosensitizing and interference with tissue autofluorescence. To overcome these problems, a new laser photodynamic diagnostic system was developed (101). This system detected tumor-specific drug fluorescence at 630 nm wavelength, which is far from normal tissue autofluorescence (500–580 nm), and interference by autofluorescence from normal tissue should then have been eliminated, but it remained a significant problem (102).

Another approach was developed by Palcic *et al.* (103), who noticed the lack of autofluorescence in the tumor lesions by using blue light (442 nm) rather than white light to illuminate the bronchial surface. They amplified the difference in autofluorescence between normal, premalignant, and tumor tissue for clinical use (103, 104). Using a high-quality-charge coupled device and special algorithm, the LIFE was developed, taking advantage of the principle that dysplastic and malignant tissues reduce autofluorescent signals compared with normal tissue (Fig. 3).

Several studies have been performed comparing the diagnostic specificity and sensitivity of LIFE bronchoscopy versus WLB in diagnosing preinvasive and early-invasive lesions (105–109; Table 3). Most of the studies reported a higher diagnostic sensitivity of LIFE bronchoscopy in the detection of premalignant and early-malignant lesions at the cost of lower specificity (i.e., more false-positive results). In most of these studies, lesions with moderate dysplasia or worse were the target of the study and rated as "positive." The prevalence of preinvasive and early lung cancer varies widely from one study to another, from 20.2% (105) to 65.8% (102). The explanation might be beyond the risk profile of genetic variations or different levels of experience among the endoscopists as well as the pathologists involved. Furthermore, there seems to be a training effect in using the LIFE bronchoscope, which has been demon-

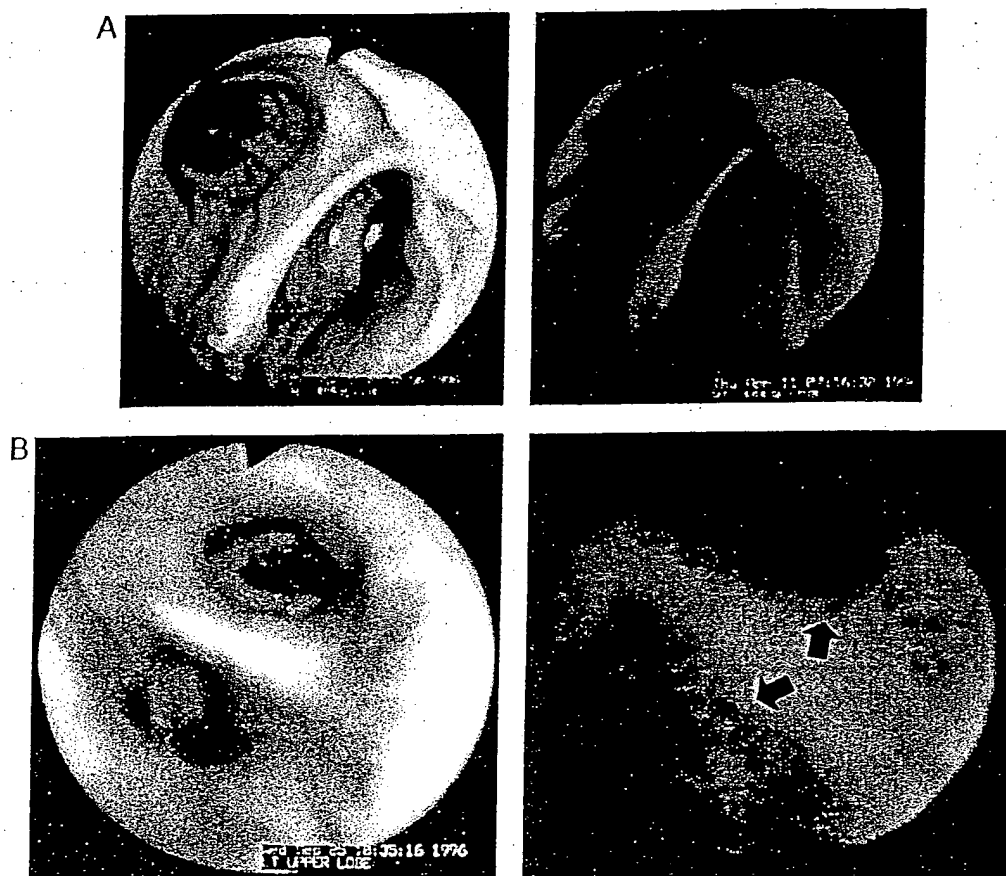


Fig 3 A, normal WLB and normal LIFE bronchoscopy. B, WLB shows inflammatory changes in the bronchial mucosa but no suspicion of malignancy (left). LIFE bronchoscopy shows diffuse reduced autofluorescence (visualized by diffuse red-brownish colorization; arrows). Biopsy demonstrated diffuse severe dysplasia.

strated by Venmans *et al.* (107). In their study, the diagnostic sensitivity increased from 67 to 80% when comparing the first and the second half of the study. The use of the LIFE device in conjunction with WLB improved the detection rate of preneoplastic lesions and CIS significantly (Table 3). Kurie *et al.* (106) looked for more subtle tissue transformation, but their study included few patients with moderate dysplasia or worse. No improvement in the evaluation of metaplasia index was observed by the use of LIFE bronchoscopy. Thus, differences in the study population might explain the different conclusion. There are still no clinical studies with sufficient long-term data showing that moderate dysplasia is the most relevant clinical predictor of eventual malignancy. Limitations in making conclusions from the existing studies are also the potential methodological bias related to the order in which the different bronchoscopy procedures are done and whether the same examiner has performed both procedures. To address these issues, a

prospective randomized study between LIFE bronchoscopy and WLB was done at the University of Colorado Cancer Center. The study design included a randomization with regard to the order of procedure as well as the order of the individual bronchoscopist (109). The order of the procedure and of the individual bronchoscopist did not affect the results. The study also demonstrated a significantly higher sensitivity in detecting premalignant lesions visualized by the LIFE, but at the cost of a lower specificity (109). The reason for the low diagnostic specificity found with the LIFE bronchoscopy in the different studies might be attributable to the visualization of more abnormal foci with the LIFE bronchoscope, with the consequence that a larger number of biopsies were taken and, thus, there was a higher risk of more false-positive results. The use of LIFE bronchoscopy has led to the identification of a new morphological entity, the ASD, which is described above. In a recent morphological study angiodysplastic changes were frequently found in preneoplastic

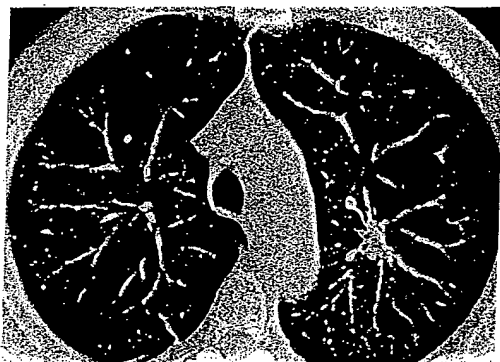


Fig. 4 Seventy-one-year-old man with a spiculated nodule in upper left lobe demonstrated on low-dose helical CT (picture), but not visible on chest X-radiography. CT-guided biopsy showed adenocarcinoma.

and early-malignant lesions in the bronchi (26). The morphological entity has been confirmed in preneoplasias among smokers, and the perspectives of this finding have been extensively discussed (110). The prognostic significance of this morphological entity is currently studied in ongoing long-term follow-up studies. Future studies have to evaluate the role of ASD as a biomarker for early lesions and whether it can be used as a marker for treatment effect or therapeutic target for chemoprevention.

The LIFE bronchoscope may play an important role in the screening and follow-up of subjects at high risk of developing lung cancer. At this stage, however, it is unknown whether the LIFE bronchoscope will lead to a reduction in lung cancer mortality. There are also no data on cost-effectiveness and cost-benefit analyses available for this new diagnostic procedure. The use of the LIFE bronchoscope may also in the future be extended to other indications, *e.g.*, patients staged as having resectable lung cancer on one side. Whether LIFE bronchoscopy of the contralateral lung will disclose abnormalities, which would change the therapeutic decision, is not yet reported.

Recent Advances in Radiology

The previous NCI-sponsored screening trials failed to demonstrate any reduction in the lung cancer mortality by sputum cytology and yearly chest radiography as mass screening tools for lung cancer screening. Limitations of design and execution of the studies, however, have been discussed extensively (8, 111, 112). An extended follow-up (median, 20.5 years) of the Mayo Lung Project was recently published (113). There was still no difference in lung cancer mortality between the intervention arm and the control arm (4.4 versus 3.9 deaths per 1000 person-years). However, the median survival for patients with resected early-stage disease was 16.0 years in the intervention arm versus 5.0 years in the usual-care arm ($P < 0.05$). The latter findings have raised the question as to whether some small lesions with limited clinical relevance may have been identified in the intervention arm, and the question of "overdiagnosis" was discussed in accompanying editorials (114).

Mass screening for lung cancer has been performed in Japan for many years and has been performed in over 500,000 people in about 80% of the local communities (115). Sobue *et al.* (116) observed that annual clinic-based chest X-ray screening for lung cancer in Japan showed reduced lung cancer mortality by about one-fourth among individuals who underwent screening once a year. In this screening program, the relative odds ratio of dying from lung cancer within 12 months was 0.535 and in the 12–24-month period was 0.638 (117). However, many studies have focused on the pitfalls in the detection of abnormalities by radiography (118–122). The limit of chest radiographic sensitivity for nodule detection is roughly 1 cm in diameter, by which time the tumor has over 10^9 cells and may already have violated bronchial epithelium and vascular epithelium. CT has been shown to be more effective in the detection of peripheral lung lesions compared with plain radiography or conventional tomography of the whole lung (123, 124).

Spiral CT scan is a relatively new technology with the ability to continuously acquire data resulting in a shorter scanning time, a lower radiation exposure, and improved diagnostic accuracy compared with those of plain radiography (125–127). Spiral CT allows the whole chest to be imaged in one or two breath-holds, reducing motion artifacts and eliminating respiratory misregistration or missing nodules. Although there is greater radiation exposure with CT than with chest radiography, low-dose techniques (lower mA of 30–50 compared with 200 for conventional CT) have achieved calculated exposure doses that are 17% that of conventional CT and 10 times that of chest radiographs. Further reduction in radiation dose while maintaining diagnostic accuracy is a topic of current research. Furthermore, for the baseline screening, low-dose spiral-CT-scan *i.v.* contrast is not administered. Nodules as small as 1–5 mm can be shown with modern spiral CT technology (25, 128). The obvious advantages with this new technology led some groups in Japan and in the United States to look to low-dose spiral CT as a tool for screening (Refs. 129–131; Tables 4 and 5).

In a Japanese report, spiral CT scans and chest radiographs were done twice a year in 1369 individuals (129). Peripheral lung cancer was detected in 15 (0.3%) of 3457 examinations, and, among the 15 lung cancer cases detected, the results of chest X-ray were negative in 11 (73%), and the tumors were detected only by low-dose spiral CT. The detection rates of low-dose spiral CT and chest X-ray were 0.43% (15 of 3457 examinations) and 0.12% (4 of 3457 examinations), respectively. Furthermore, 14 (93%) of the 15 lung cancers were stage I disease. The histology showed that 11 of the 15 lung cancer cases were adenocarcinoma, and 4 had squamous cell carcinoma. The effective exposure dose with spiral CT scan in that study was calculated to about one-sixth that of conventional CT.

The ELCAP in New York was designed to determine: (a) the frequency with which nodules were detected; (b) the frequency with which detected nodules represent malignant disease; and (c) the frequency with which malignant nodules are curable (131). In the ELCAP study, 27 lung cancers were found among 1000 subjects screened. Among the 27 patients with cancer, 85% had stage I disease (Table 5).

Another population-based study on low-dose CT screening has been published by Sone *et al.* (130), using a mobile low-dose spiral CT scanner. The detection rate was 0.48% (*i.e.*, 4–5

Table 3 Bronchoscopy versus WLB in diagnosing premalignant and early-malignant lesions

Table 3 Bronchoscopy versus WLB in diagnosing premalignant and early-malignant lesions																	
Author	No. of biopsies	Sensitivity			Specificity					Predictive values							
		LIFE+	WLB	LIFE	WLB	Relative sensitivity	LIFE+	WLB	LIFE	WLB	Relative specificity	LIFE+	WLB	PPV	NPV	PPV	NPV
Lam <i>et al.</i> (105)	700	0.67	NR	0.25	6.3 (2.7) ^c	0.66	NR	0.90	NR	NR	0.33	0.89	NR	NR	0.39	0.83	
Kurie <i>et al.</i> ^b (106)	234	NR	0.38	NR	NR	NR	0.56	NR	NR	NR	NR	NR	0.16	0.81	NR	NR	
Venmans <i>et al.</i> (107)	139	NR	0.89	0.78	1.43	NR	0.61	0.88	NR	NR	0.20	NR	0.14	0.99	0.32	0.98	
Vermulen <i>et al.</i> (108)	172	0.93	NR	0.25	3.75	0.21	NR	0.87	NR	NR	0.13	0.96	NR	NR	0.19	0.90	
Kennedy <i>et al.</i> (109)	394	0.79	0.72	0.18	4.4	0.3	0.43	0.78	0.38	NR	0.21	0.85	0.25	0.87	0.17	0.80	

^a PPV, positive predictive value; NPV, negative predictive value; NR, not reported.^b Based on reference pathologist.^c If invasive carcinoma is included.

Table 4 Results from three population-based screening studies with low-dose spiral CT (LDCT)

Authors	No. of individuals studied	True positive <i>n</i>	False positive %	Predictive value %	Detection rate %		Pack-yr	Age incl. yr
					LDCT	X-ray		
Kaneko <i>et al.</i> (129)	1369	15	15.6	6.6	0.43	0.12	>20	>50
Sone <i>et al.</i> (130)	3967	19	5.0	8.8	0.46-0.5		>30 ^b	40-74
Henschke <i>et al.</i> (131)	1000	27	20.1	11.6	2.7	0.70	>10 ^c	>60

^a Defined as individuals with "test-positive," in whom further workup gave no suspicion of malignancy.^b The study also included a group of nonsmokers.^c Average = 45 (not reported in the other studies).

Table 5 Histology, stage, and size of primary lung cancer detected by low-dose spiral CT

Table 3. Histology, stage, and size of primary lung cancer detected by low-dose spiral CT													
Author	No. of cancers/ No. screened	Histology %			TNM %				Size (mm)				
		Adeno ^a	Squam.	Other	I	II	III	IV	Average	Range	<10	11-20	>21
Kaneko <i>et al.</i> (129)	15/1369 (1.1%)	73	17		93		7		12	8-18			
Sone <i>et al.</i> (130)	19/5483 (0.3%)	63	5	32	84			16	17	6-47	4	14	3
Henschke <i>et al.</i> (131)	27/1000 (2.7%)	67	3	30	85	4	11				15	8	4

^a Adeno, adenocarcinoma; Squam., squamous cell carcinoma; TNM, tumor-node-metastasis.

cases per 1000 examinations). Surprisingly, there was no difference in the detection rate among smokers (0.52%) versus nonsmokers (0.46%). The results from the three population-based studies are summarized in Tables 4 and 5. The conclusion from these studies is that 85% of the lung cancers detected by low-dose CT were in stage I, offering improved possibility for curative treatment and better prognosis in general. However, the issue of "false-positive" scans has to be taken into consideration. Thus far, up to 20% of the participants with nodules on the scan had no malignancy during the follow-up period. The possibility that the cancers found represent incidental cancers as in the Mayo Lung Project must also be considered (114). The results from these studies confirm the expectation that low-dose CT increases the detection of small noncalcified nodules and, that lung cancer at an earlier and more curable stage are detected. The mobile CT screening study by Sone *et al.* (130) showed that low-dose CT increased the likelihood of detection of malignant disease 10 times as compared with radiography. The overall rate of malignant disease was lower in the Japanese studies (129, 130) compared with the ELCAP study (Ref. 131; detection rates 0.43-0.48% versus 2.7%). This could be because the Japanese studies screened individuals from the general population ages

40-74, whereas ELCAP screened people at high risk, ages ≥ 60 , with a tobacco history of at least 10 pack-years. Thus, as expected, the risk of the population to be screened affects the rate of cancer detection.

Questions remaining to be answered include: (a) what are the diagnostic sensitivity and specificity of this procedure; and (b) does screening reduce lung cancer mortality? The spiral CT has not been as sensitive for small central cancers as it is for small peripheral cancers (129, 131). Minute nodules of lung cancer that are near the threshold of detectability may be overlooked at spiral CT screening (132). A prospective study of the diagnostic sensitivity of spiral CT has recently shown that the diagnostic sensitivity exceeded the sensitivity of conventional CT in previous reports (25). However, there were limitations in the detection of intrapulmonary nodules smaller than 6 mm and of pleural lesions. Compared with surgery (thoracotomy with palpation of deflated lung, resection, and histology), the sensitivity of spiral CT was 60% for intrapulmonary nodules of <6 mm and 95% for nodules of ≥ 6 mm and was 100% for neoplastic lesions ≥ 6 mm. Furthermore, a marked difference in the sensitivities of two independent observers was found for nodules smaller than 6 mm, whereas agreement was much better for

6–10-mm nodules (25). Given these promising preliminary clinical results, further research is needed to determine the optimal technique for spiral CT screening, which includes collimation, reconstruction interval, pitch, and viewing methods. Decreasing the slice thickness to 3 mm, monitoring the viewing of examinations, and computer-aided diagnosis have been used to improve the diagnostic capability of spiral CT in the detection of pulmonary nodules (133–136).

Future large scale randomized studies have to confirm whether in fact spiral CT screening will lead to a reduction in lung cancer mortality. In a randomized study, the following questions arise: (a) what is the optimal high-risk group to study and what should be the control arm? (b) what should be the end points (goals) of the studies? The ultimate goal is to reduce the lung cancer mortality. However, although this is a long-term goal, intermediate end points from such studies should be evaluated. The change to more curable stages at diagnosis for the lung cancer patients is one such immediate goal; (c) what is the optimal workup and the morbidity of this program? (d) what is the cost of such a screening program? and (e) what is the false-positive rate of the screening findings? Incorporation of smoking cessation programs should be included in the future design of screening studies because it has been shown that screening with low-dose CT in participants who are still smoking provides substantial motivation for smoking cessation (137).

The studies with spiral CT-scan have demonstrated the superior diagnostic ability in the detection of small peripherally located tumors, most of the malignant ones of adenocarcinoma type of histology. The diagnostic sensitivity of spiral CT for more centrally located tumors (mostly squamous cell carcinoma) is significantly lower than for the peripherally located ones. Through these spiral CT studies, we will learn about the biology, pathology, and clinical course of these small tumors, which might be different from what we know about clinically more evident tumors detected routinely in previous studies.

Because lung cancer is so common, the introduction of any new screening technique in this area has to be underpinned by careful definition of the cost implications and must be justified by compelling evidence. The cost-effectiveness of the spiral CT approach should be assessed by evaluating the rate of over-diagnosing nonmalignant, relatively common abnormalities and comparing CT imaging to other diagnostic technologies.

PET with FDG has recently emerged as a practical and useful imaging modality in the preoperative staging of patients with lung cancer. However, whereas CT is most frequently used to provide additional anatomical and morphological information about lesions, the FDG PET imaging provides physiological and metabolic information that characterizes lesions that are indeterminate by CT. FDG PET imaging takes advantage of the increased accumulation of FDG in transformed cells and is sensitive (~95%) for the detection of cancer in patients who have indeterminate lesions on CT (138). The specificity (~85%) of PET imaging is slightly less than its sensitivity because some inflammatory processes avidly accumulate FDG. The high negative predictive value of PET suggests that lesions considered negative on the study are benign, biopsy is not needed, and radiographic follow-up is recommended. Several studies have documented the increased accuracy of PET compared with CT in the evaluation of the hilar and mediastinal lymph node status

in patients with lung cancer (138). However, the PET resolution is sufficient only for nodules ≥ 6 cm and will not be helpful in detecting the very small nodules. Compared with low-dose spiral CT, the FDG PET scan is more expensive and time consuming. The role of PET scan in early diagnosis of lung cancer in an asymptomatic high-risk population is not yet evaluated. However, future studies have to include PET evaluation to define its role in a population screening setting.

Conclusion

Recent advances in molecular biology and pathology have led to a better understanding and documentation of morphological changes in the bronchial epithelium before development of clinical evident lung carcinomas. Combined with technical developments in radiological and bronchoscopic techniques, these procedures offer great promise in diagnosing lung cancer far in advance of clinical presentation. Any of these individual procedures could be incorporated into the routine management of individuals at risk for developing primary or secondary lung cancer, and for several of these methods, clinical studies are under way. Preliminary reported data are very promising for the early detection of lung cancer. Future studies must incorporate the different methods in a multidisciplinary scientific setting to evaluate the role of the individual method in the overall management for individuals at high risk for developing lung cancer. Several of these tests might diagnose the disease at the stage of clonal expansion before invasive carcinoma has developed. A management and intervention strategy appropriate to that stage of disease have to be developed. Preliminary studies of chemoprevention agents are reported, and new agents based on other biological mechanisms are under development and ready for clinical trials. It is now time to plan clinical trials that evaluate both diagnostic and therapeutic approaches to assess their impact on the incidence of clinical lung cancer.

Acknowledgments

We thank Drs. Stephen Lam, Vancouver, British Columbia, Canada, and Kavita Garg, University of Colorado Health Sciences Center, Denver, Colorado, for a critical review of the manuscript and Drs. Timothy Kennedy and York Miller for submitting illustrations for white-light and LIFE bronchoscopy.

References

- Greenlee, R. T., Murray, T., Bolden, S., and Wingo, P. A. Cancer Statistics. 2000. *CA Cancer J. Clin.*, 50: 7–30, 2000.
- Mountain, C. T. Revision in the international system for staging of lung cancer. *Chest*, 111: 1710–1717, 1997.
- Thde, D. C. Chemotherapy of lung cancer. *N. Engl. J. Med.*, 327: 1454–1461, 1992.
- Melamed, M. R., Flehinger, B. J., Zaman, M. B., Heelan, R. T., Parchick, W. A., and Martini, N. Screening for lung cancer: results of the Memorial Sloan-Kettering study in New York. *Chest*, 86: 44–53, 1984.
- Fontana, R. S., Sanderson, D. R., Woolner, L. B., Taylor, W. F., Miller, W. E., and Muhm, J. R. Lung Cancer Screening: The Mayo program. *J. Occup. Med.*, 28: 746–750, 1986.
- Tockman, M. S. Survival and mortality from lung cancer in a screened population: The Johns Hopkins Study. *Chest*, 89: 324S–325S, 1986.

7. Kubik, A., Parkin, D. M., Khat, M., Erban, J., Polak, J., and Adamec, M. Lack of benefit from semi-annual screening for cancer of the lung: follow-up report of a randomized controlled trial on a population of high-risk males in Czechoslovakia. *Int. J. Cancer*, 45: 26-33, 1990.
8. Fontana, R. S., Sanderson, D. R., Woolner, L. B., Taylor, W. F., Miller, W. E., Muhm, J. R., Bernatz, P. E., Payne, W. S., Paisirolero, P. C., and Bergstralh, E. J. Screening of lung cancer. A critique of the Mayo Lung Project. *Cancer (Phila.)*, 67: 1155-1164, 1991.
9. Strauss, G. M., Gleason, R. E., and Sugarbaker, D. J. Screening for lung cancer. Another look: a different view. *Chest*, 111: 754-768, 1997.
10. Hirsch, F. R., Brambilla, E., Gray, N., Gritz, E., Kelloff, G. J., Linnoila, I., Pastorino, U., and Mulshine, J. L. Prevention and early detection of lung cancer—clinical aspects. *Lung Cancer (Limerick)*, 17: 163-174, 1997.
11. Hong, W. K. Chemoprevention of Lung Cancer. *Oncology (Basel)*, 13 (Suppl. 5): 135-141, 1999.
12. Mulshine, J. L., and Henschke, C. I. Prospects for lung-cancer screening. *Lancet*, 355: 592-593, 2000.
13. Travis, W. D., Colby, T. V., Corrin, B., Shimosato, Y., and Brambilla, E. Histological typing of tumours of lung and pleura. In: L. H. Sobin (ed.), *World Health Organization International Classification of Tumours*, Ed. 3. New York: Springer-Verlag, 1999.
14. Franklin, W. A. Pathology of lung cancer. *J. Thorac. Imaging*, 15: 3-12, 2000.
15. Colby, T. V. Precursor lesions to pulmonary neoplasia. In: C. Brambilla and E. Brambilla (eds.), *Lung Tumors. Fundamental Biology and Clinical Management*, pp. 61-87. New York: Marcel Dekker Inc., 1999.
16. Peters, E. J., Morice, R., Benner, S. E., Lippman, S., Lukeman, J., Lee, J. S., Ro, J. L., and Hong, W. K. Squamous metaplasia of the bronchial mucosa and its relationship to smoking. *Chest*, 103: 1429-1432, 1993.
17. Auerbach, O., Gere, B., Forman, J. B., Petrick, T. G., Smolin, H. J., Muchsam, G. E., Kassouny, D. Y., and Stout, A. P. Changes in bronchial epithelium in relation to smoking and cancer of the lung. *N. Engl. J. Med.*, 256: 97-104, 1957.
18. Wistuba, I. I., Behrens, C., Milchgrub, S., Bryant, D., Hung, J., Minna, J. D., and Gazdar, A. F. Sequential molecular abnormalities are involved in the multistage development of squamous cell lung carcinoma. *Oncogene*, 18: 643-650, 1999.
19. Lam, S., LeRiche, J. C., Zheng, Y., Coldman, A., MacAulay, C., Hawk, E., Kelloff, G., and Gazdar, A. F. Sex-related differences in bronchial epithelial changes associated with tobacco smoking. *J. Natl. Cancer Inst.*, 91: 691-696, 1999.
20. Saccomanno, G., Archer, V. E., Auerbach, O., Saunders, R. P., and Brennan, L. M. Development of carcinoma of the lung as reflected in exfoliated cells. *Cancer (Phila.)*, 32: 256-270, 1974.
21. Frost, J. K., Ball, W. C., Jr., Levin, M. L., Tockman, M. S., Erozan, Y. S., Gupta, K., Eggleston, J. C., Pressman, N. J., Donithan, M. P., and Kimball, A. W. Sputum cytopathology: use and potential in monitoring the workplace environment by screening for biological effects of exposure. *J. Occup. Med.*, 28: 692-703, 1986.
22. Venman, B. J. W., van Boxem, T. J. M., Smit, E. F., Postmus, P. E., and Sutedja, T. G. Outcome of bronchial carcinoma *in situ*. *Chest*, 117: 1572-1576, 2000.
23. Slebos, R. J., Baas, I. O., Clement, M. J., Offerhaus, G. J., Askin, F. B., Hruban, R. H., and Westra, W. H. p53 alterations in atypical alveolar hyperplasia of the human lung. *Hum. Pathol.*, 29: 801-808, 1998.
24. Kitamura, H., Kameda, Y., Ito, T., and Hayashi, H. Atypical adenomatous hyperplasia of the lung. Implications for the pathogenesis of peripheral lung adenocarcinoma. *Am. J. Clin. Pathol.*, 111: 610-622, 1999.
25. Diedrich, S., Semik, M., Lentschig, M. G., Winter, F., Scheld, H. H., Roos, N., and Bongartz, G. Helical CT of pulmonary nodules in patients with extrathoracic malignancy: CT-surgical correlation. *Am. J. Roentgenol.*, 172: 353-360, 1999.
26. Keith, R. L., Miller, Y. E., Gemmill, R. M., Drabkin, H. A., Dempsey, E. C., Kennedy, T. C., Prindiville, S., and Franklin, W. A. Angiogenic squamous dysplasia in bronchi of individuals at high risk for lung cancer. *Clin. Cancer Res.*, 6: 1616-1625, 2000.
27. Muller, K. M., and Muller, G. The ultrastructure of preneoplastic changes in bronchial mucosa. *Curr. Top. Pathol.*, 73: 233-263, 1983.
28. Hirsch, F. R., Gazdar, A. F., Gabrielson, E., Lam, S., and Franklin, W. A. Histopathologic evaluation of premalignant and early malignant bronchial lesions: an interactive program based on internet digital images to improve WHO criteria for early diagnosis of lung cancer and for monitoring chemoprevention studies—a SPOR collaborative project. *Lung Cancer (Limerick)*, 29 (Suppl. 2): 209, 2000.
29. Lengauer, C., Kinzler, K. W., and Vogelstein, B. Genetic instabilities in human cancers. *Nature (Lond.)*, 396: 643-649, 1998.
30. Fong, K. M., Sekido, Y., and Minna, J. D. Molecular pathogenesis of lung cancer. *J. Thorac. Cardiovasc. Surg.*, 118: 1136-1152, 1999.
31. Hirano, T., Franzen, B., Kato, H., Ebihara, Y., and Auer, G. Genesis of squamous cell lung carcinoma: sequential changes of proliferation, DNA ploidy, and p53 expression. *Am. J. Pathol.*, 144: 296-302, 1994.
32. Beiticher, D. C., Heighway, J., Thatcher, N., and Hasleton, P. S. Abnormal expression of CCND1 and RB1 in resection margin epithelia of lung cancer patients. *Br. J. Cancer*, 75: 1761-1768, 1997.
33. Satoh, Y., Ishikawa, Y., Nakagawa, K., Hirano, T., and Tsuchiya, E. A follow-up study of progression from dysplasia to squamous cell carcinoma with immunohistochemical examination of p53 protein overexpression in the bronchi of ex-chromate workers. *Br. J. Cancer*, 75: 678-683, 1997.
34. Li, Z. H., Zheng, J., Weiss, L. M., and Shibata D. c-k ras, and p53 mutations occur very early in adenocarcinoma of the lung. *Am. J. Pathol.*, 144: 303-309, 1994.
35. Brambilla, E., Gazzeri, S., Lantuejoul, S., Coll, J. L., Moro, D., Negoescu, A., and Brambilla, C. p53 mutant immunophenotype and deregulation of p53 transcription pathway (Bcl2, Bax, and Waf1) in precursor bronchial lesions of lung cancer. *Clin. Cancer Res.*, 4: 1609-1618, 1998.
36. Hung, J., Kishimoto, Y., Sugio, K., Virmani, A., McIntire, D. D., Minna, J. D., and Gazdar, A. F. Allele-specific chromosome 3p deletions occur at an early stage in the pathogenesis of lung carcinoma. *J. Am. Med. Assoc.*, 273: 558-563, 1995.
37. Kishimoto, Y., Sugio, K., Hung, J. Y., Virmani, A. K., McIntire, D. D., Minna, J. D., and Gazdar, A. F. Allele-specific loss in chromosome 9p loci in preneoplastic lesions accompanying non-small cell lung cancers. *J. Natl. Cancer Inst.*, 87: 1224-1229, 1995.
38. Sugio, K., Kishimoto, Y., Virmani, A. K., Hung, J. Y., and Gazdar, A. F. K-ras mutations are a relatively late event in the pathogenesis of lung carcinomas. *Cancer Res.*, 54: 5811-5815, 1994.
39. Wistuba, I. I., Behrens, C., Virmani, A. K., Milchgrub, S., Syed, S., Lam, S., Mackay, B., Minna, J. D., and Gazdar, A. F. Allelic losses at chromosome 8p21-23 are early and frequent events in the pathogenesis of lung cancer. *Cancer Res.*, 59: 1973-1979, 1999.
40. Varela-Garcia, M., Gemmill, R. M., Rabenhorst, S. H., Lott, A., Drabkin, H. A., Archer, P. A., and Franklin, W. A. Chromosomal duplication accompanies allelic loss in non-small cell lung carcinoma. *Cancer Res.*, 58: 4701-4707, 1998.
41. Westra, W. H., Baas, I. O., Hruban, R. H., Askin, F. B., Wilson, K., Offerhaus, G. J., Slebos, R. J. K-ras oncogene activation in atypical alveolar hyperplasias of the human lung. *Cancer Res.*, 56: 2224-2228, 1996.
42. Wistuba, I. I., Lam, S., Behrens, C., Virmani, A. K., Fong, K. M., LeRiche, J., Samet, J. M., Srivastava, S., Minna, J. D., and Gazdar, A. F. Molecular damage in the bronchial epithelium of current and former smokers. *J. Natl. Cancer Inst.*, 89: 1366-1377, 1997.
43. Mao, L., Lee, J. S., Kurie, J. M., Fan, Y. H., Lippman, S. M., Lee, J. J., Ro, J. Y., Broxson, A., Yu, R., Morice, R. C., Kemp, B. L., Khuri, F. R., Walsh, G. L., Hittelman, W. N., and Hong, W. K. Clonal genetic

- alterations in the lungs of current and former smokers. *J. Natl. Cancer Inst.*, 89: 857-862, 1997.
44. Smith, A. L., Hung, J., Walker, L., Rogers, T. E., Vuitch, F., Lee, E., and Gazdar, A. F. Extensive areas of aneuploidy are present in the respiratory epithelium of lung cancer patients. *Br. J. Cancer*, 73: 203-209, 1996.
 45. Franklin, W. A., Gazdar, A. F., Haney, J., Wistuba, I. I., La Rosa, F. G., Kennedy, T., Ritchey, D. M., and Miller, Y. E. Widely dispersed p53 mutation in respiratory epithelium: a novel mechanism for field carcinogenesis. *J. Clin. Invest.*, 100: 2133-2137, 1997.
 46. Johnston, W. W., and Elson, C. E. Respiratory tract. In: M. Bibbo (ed.), *Comprehensive Cytopathology*, pp. 325-401. Philadelphia: Saunders, 1997.
 47. Travis, W. D., Travis, L. B., and Devesa, S. S. Lung cancer. *Cancer (Phila.)*, 75 (Suppl. 1): 191-202, 1995.
 48. Wynder, E. L., and Muscat, J. E. The changing epidemiology of smoking and lung cancer histology. *Environ. Health Perspect.*, 103 (Suppl. 8): 143-148, 1995.
 49. Thun, M. J., Lally, C. A., Flannery, J. T., Calle, E. E., Flanders, W. D., and Heath, C. W., Jr. Cigarette smoking and changes in the histopathology of lung cancer. *J. Natl. Cancer Inst.*, 89: 1580-1586, 1997.
 50. Lam, S., and Shibuya, H. Early diagnosis of lung cancer. *Clin. Chest Med.*, 20: 53-61, 1999.
 51. Kennedy, T. C., Proudfoot, S., Piantadosi, S., Wu, L., Saccomanno, G., Petty, T. L., and Tockman, M. S. Efficacy of two sputum collection techniques in patients with air flow obstruction. *Acta Cytol.*, 43: 630-636, 1999.
 52. Browman, G. P., Arnold, A., Levine, M. N., and D'Souza, T. Use of screening phase data to evaluate observer variation of sputum cytodiagnosis as an outcome measure in a chemoprevention trial. *Cancer Res.*, 50: 1216-1219, 1990.
 53. Cantaboni, A., Pezzotta, M. G., Sironi, M., and Porcellati, M. Quality assurance in pathology: cytologic and histologic correlation. *Acta Cytol.*, 36: 717-721, 1992.
 54. Holiday, D. B., McLarty, J. W., Farley, M. L., Mabry, L. C., Cozens, D., Roby, T., Waldron, E., Underwood, R. D., Anderson, E., and Culbreth, W. Sputum cytology within and across laboratories. A reliability study. *Acta Cytol.*, 39: 195-206, 1995.
 55. Risse, E. K., Vooijs, G. P., and van't Hoff, M. A. Relationship between the cellular composition of sputum and the cytologic diagnosis of lung cancer. *Acta Cytol.*, 31: 170-176, 1987.
 56. MacDougall, B., and Weinerman, B. The value of sputum cytology. *J. Gen. Intern. Med.*, 7: 11-12, 1992.
 57. Tockman, M. S., Erozan, Y. S., Gupta, P., Piantadosi, S., Mulshine, J. L., and Ruckdeschel, J. C. The early detection of second primary lung cancers by sputum immunostaining. *Chest*, 106 (Suppl.): 385S-390S, 1994.
 58. Tockman, M. S., Gupta, P. K., Myriss, J. D., Frost, J. K., Baylin, S. B., Gold, E. B., Chase, A. M., Wilkinson, P. H., and Mulshine, J. L. Sensitive and specific monoclonal antibody recognition of human lung cancer antigen on preserved sputum cells: a new approach to early lung cancer detection. *J. Clin. Oncol.*, 6: 1685-1693, 1988.
 59. Zhou, J., Mulshine, J. L., Unsworth, E. J., Scott, F. M., Avis, I. M., Vos, M. D., and Treston, A. M. Purification and characterization of a protein that permits early detection of lung cancer. *J. Biol. Chem.*, 271: 10760-10766, 1996.
 60. Qiao Y-L., Tockman, M. S., Li, L., Erozan, Y. S., Yao, S. X., Barrett, M. J., Zhou, W. H., Giffen, C. A., Luo, X. C., and Taylor, P. R. A case-cohort study of an early biomarker of lung cancer in a screening cohort of Yunnan tin miners in China. *Cancer Epidemiol. Biomark. Prev.*, 6: 893-900, 1997.
 61. Grover, F. L., and Piantadosi, S. Recurrence and survival following resection of bronchioloalveolar carcinoma of the lung: the Lung Cancer Study Group experience. *Ann. Surg.*, 209: 779-790, 1989.
 62. Tockman, M. S. Advances in sputum analysis for screening and early detection of lung cancer. *Cancer Control*, 7: 19-24, 2000.
 63. Sueoka, E., Goto, Y., Sueoka, N., Kai, Y., Koza, T., and Fujiki, H. Heterogeneous nuclear ribonucleoprotein B1 as a new marker of early detection for human lung cancers. *Cancer Res.*, 59: 1404-1407, 1999.
 64. Mulshine, J. L. Reducing lung cancer risk. Early detection. *Chest*, 116: 493S-496S, 1999.
 65. Mao, L., Hruban, R. H., Boyle, J. O., Tockman, M., and Sidransky, D. Detection of oncogene mutations in sputum precedes diagnosis of lung cancer. *Cancer Res.*, 54: 1634-1637, 1994.
 66. Ruppert, J. M., Tokino, K., and Sidransky, D. Evidence for two bladder cancer suppressor loci on chromosome 9. *Cancer Res.*, 53: 5093-5095, 1993.
 67. Nawroz, H., van der Riet, P., Hruban, R. H., Koch, W., Ruppert, J. M., and Sidransky, D. Allelotype of head and neck squamous cell carcinoma. *Cancer Res.*, 54: 1152-1155, 1994.
 68. Miozzo, M., Sozzi, G., Musso, K., Pilotti, S., Incarbone, M., Pastorino, U., and Pierotti, M. A. Microsatellite alterations in bronchial and sputum specimens of lung cancer patients. *Cancer Res.*, 56: 2285-2288, 1996.
 69. Shapiro, G. I., Park, J. E., Edwards, C. D., Mao, L., Merlo, A., Sidransky, D., Ewen, M. E., and Rollins, B. J. Multiple mechanisms of p16^{INK4a} inactivation in non-small cell lung cancer cell lines. *Cancer Res.*, 55: 6200-6209, 1995.
 70. Hamada, K., Kohno, T., Kawanishi, M., Ohwada, S., and Yokota, J. Association of CDKN2A(p16)/CDKN2B(p15) alterations and homozygous chromosome arm 9p deletions in human lung carcinoma. *Genes Chromosomes Cancer*, 22: 232-240, 1998.
 71. Belinsky, S. A., Nikula, K. J., Palmisano, W. A., Michels, R., Saccomanno, G., Gabrielson, E., Baylin, S. B., and Herman, J. G. Aberrant methylation of p16^{INK4a} is an early event in lung cancer and a potential biomarker for early diagnosis. *Proc. Natl. Acad. Sci. USA*, 95: 11891-11896, 1998.
 72. Esteller, M., Sanchez-Cespedes, M., Rosell, R., Sidransky, D., Baylin, S. B., and Herman, J. G. Detection of aberrant promoter hypermethylation of tumor suppressor genes in serum DNA from non-small cell lung cancer patients. *Cancer Res.*, 59: 67-70, 1999.
 73. Nieburgs, H. E. Recent progress in the interpretation of malignancy associated changes (MAC). *Acta Cytol.*, 12: 445-453, 1968.
 74. Payne, P. W., Sebo, T. J., Doulikine, A., Garner, D., MacAulay, C., Lam, S., LeRiche, J. C., and Palcic, B. Sputum screening by quantitative microscopy: a reexamination of a portion of the National Cancer Institute Cooperative Early Lung Cancer Study. *Mayo Clin. Proc.*, 72: 697-704, 1997.
 75. Lam, S., Palcic, B., Garner, D., Beveridge, J., MacAulay, C., LeRiche, J., and Goldman, A. Lung Cancer Control Strategy in the New Millennium. *Lung Cancer*, 29 (Suppl. 2): 145, 2000.
 76. Ahrendt, S. A., Chow, J. T., Xu, L. H., Yang, S. C., Eisenberger, C. F., Esteller, M., Herman, J. G., Wu, L., Decker, P. A., Jen, J., and Sidransky, D. Molecular detection of tumor cells in bronchoalveolar lavage fluid from patients with early stage lung cancer. *J. Natl. Cancer Inst.*, 91: 332-339, 1999.
 77. Gazdar, A. F., and Minna, J. D. Molecular detection of early lung cancer. *J. Natl. Cancer Inst.*, 91: 299-301, 1999.
 78. Field, J. K., Liloglou, T., Xinarianos, G., Prime, W., Fielding, P., Walshaw, M. J., and Turnbull, L. Genetic alterations in bronchial lavage as a potential marker for individuals with a high risk of developing lung cancer. *Cancer Res.*, 59: 2690-2695, 1999.
 79. Liloglou, T., Maloney, P., Xinarianos, G., Fear, S., and Field, J. K. Sensitivity and limitations of high throughput fluorescent microsatellite analysis for the detection of allelic imbalance. Application in lung tumors. *Int. J. Oncol.*, 16: 5-14, 2000.
 80. Fielding, P., Turnbull, L., Prime, W., Walshaw, M., and Field, J. K. Heterogeneous nuclear ribonucleoprotein A2/B1 up-regulation in bronchial lavage specimens: a clinical marker of early lung cancer detection. *Clin. Cancer Res.*, 5: 404S-405S, 1999.
 81. Pantel, K., Schlimok, G., Angstwurm, M., Weckermann, D., Schmaus, W., Gath, H., Passlick, B., Izbicke, J. R., and Riethmüller, G. Methodological analysis of immunocytochemical screening for dissem-

- inated epithelial tumor cells in bone marrow. *J. Hematother.*, 3: 165-173, 1994.
82. Lambrecht, A. C., van't Veer, L. J., and Rodenhuis, S. The detection of minimal numbers of contaminating epithelial tumor cells in blood or bone marrow: use, limitations and future of RNA-based methods. *Ann. Oncol.*, 9: 1269-1276, 1998.
83. Steinman, C. R. Free DNA in serum and plasma from normal adults. *J. Clin. Investig.*, 66: 1391-1399, 1980.
84. Raptis, L., and Menard, H. A. Quantitation and characterization of plasma DNA in normals and patients with lupus erythematosus. *J. Clin. Investig.*, 66: 1391-1399, 1980.
85. Leon, S. A., Shapiro, B., Sklaroff, D. M., and Yaros, M. J. Free DNA in the serum of cancer patients and the effect of therapy. *Cancer Res.*, 37: 646-650, 1977.
86. Stroun, M., Anker, P., Maurice, P., Lyautey, J., Lederrey, C., and Beljanski, M. Neoplastic characteristics of the DNA found in the plasma of cancer patients. *Oncology*, 46: 318-322, 1989.
87. Shapiro, B., Chakrabaty, M., Cohn, E., and Leon, S. A. Determination of circulating DNA levels in patients with benign or malignant gastrointestinal disease. *Cancer (Phila.)*, 51: 2116-2120, 1983.
88. Chen, X. Q., Stroun, M., Magnenat, J.-L., Nicod, L. P., Kurt, A. M., Lyautey, J., Lederrey, C., and Anker, P. Microsatellite alterations in plasma DNA of small cell lung cancer patients. *Nat. Med.*, 2: 1033-1037, 1996.
89. Anker, P., Lefort, F., Vasioukhin, V., Lyautey, J., Lederrey, C., Chen, X. Q., Stroun, M., Mulcahy, H. E., and Farthing, M. J. K-ras mutations are found in DNA extracted from the plasma of colorectal cancer patients. *Gastroenterology*, 112: 1114-1129, 1997.
90. Kopreski, M. S., Benko, F. A., Kwee, C., Leitzel, K. E., Eskander, E., Lipton, A., and Gocke, C. D. Detection of mutant K-ras DNA in plasma or serum of patients with colorectal cancer. *Br. J. Cancer*, 76: 1293-1299, 1997.
91. Hibi, K., Robinson, R., Wu, L., Hamilton, S. R., Sidransky, D., and Jen, J. Molecular detection of genetic alterations in the serum of colorectal cancer patients. *Cancer Res.*, 58: 1405-1407, 1998.
92. Sorenson, G. D., Pribish, D. M., Valone, F. H., Memoli, V. A., Dzik, D. J., and Yao, S. L. Soluble normal and mutated DNA sequences from single copy genes in human blood. *Cancer Epidemiol. Biomark. Prev.*, 3: 67-71, 1994.
93. Mulcahy, H. E., Lyautey, J., Lederrey, C., qi Chen, X., Anker, P., Alstead, E. M., Ballinger, A., Farthing, M. J., and Stroun, M. A prospective study of K-ras mutations in the plasma of pancreatic cancer patients. *Clin. Cancer Res.*, 4: 271-275, 1998.
94. Vasioukhin, V., Anker, P., Maurice, P., Lyautey, J., Lederrey, C., and Stroun, M. Point mutations of the N-ras in the blood plasma DNA of patients with myelodysplastic syndrome or acute myelogenous leukaemia. *Br. J. Haematol.*, 86: 774-779, 1994.
95. Woolner, L. B. Pathology of cancer detected cytologically. In: *Atlas of Early Lung Cancer*. National Cancer Institute, NIH, United States Department of Health and Human Services, pp. 107-203. Tokyo: Igaku-Shoin, 1983.
96. Kato, H., and Cortese, D. A. Early detection of lung cancer by means of hematoporphyrin derivative fluorescence and laser photoradiation. *Clin. Chest Med.*, 6: 237-253, 1985.
97. Profio, A. E., Deiron, D. R., and King, E. G. L. Laser fluorescence bronchoscopy for localization of occult lung tumors. *Med. Phys. (NY)*, 6: 532-535, 1979.
98. Kinsey, J. H., and Cortese, D. A. Endoscopic system for simultaneous visual examination and electronic detection of fluorescence. *Rev. Sci. Instrum.*, 51: 1403-1406, 1980.
99. Profio, A. E., Deiron, D. R., and Sarmaik, J. Fluorometer for endoscopic diagnosis of tumors. *Med. Phys. (NY)*, 11: 516-520, 1984.
100. Montan, S., Svanberg, K., and Svanberg, S. Multicolor imaging and contrast enhancement in cancer-tumor localization using laser-induced fluorescence in hematoporphyrin-derivative-bearing tissue. *Optics Lett.*, 10: 56-58, 1985.
101. Kato, H., Imaizumi, T., Aizawa, K., Iwabuchi, H., Yamamoto, H., Ikeda, N., Tsuchida, T., Tamachi, Y., Ito, T., and Hayata, Y. Photodynamic diagnosis in respiratory tract malignancy, using an excimer dye laser system. *J. Photochem. Photobiol. Biol.*, 6: 189-196, 1990.
102. Kato, H., and Ikeda, N. The role of fluorescence diagnosis in the early detection of high-risk bronchial lesions. *J. Bronchol.*, 5: 273-274, 1998.
103. Palcic, B., Lam, S., Hung, J., and MacAulay, C. Detection and localization of early lung cancer by imaging techniques. *Chest*, 99: 742-743, 1991.
104. Hung, J., Lam, S., LeRiche, J. C., and Palcic, B. Autofluorescence of normal and malignant bronchial tissue. *Lasers Surg. Med.*, 11: 99-105, 1991.
105. Lam, S., Kennedy, T., Unger, M., Miller, Y. E., Gelmont, D., Rusch, V., Gipe, B., Howard, D., LeRiche, J. C., Coldman, A., and Gazdar, A. F. Localization of bronchial intraepithelial neoplastic lesions by fluorescence bronchoscopy. *Chest*, 113: 696-702, 1998.
106. Kurie, J. M., Lee, J. S., Morice, R. C., Walsh, G. L., Khuri, F. R., Broxson, A., Ro JY, Franklin, W. A., Yu, R., and Hong, W. K. Autofluorescence bronchoscopy in the detection of squamous metaplasia and dysplasia in current and former smokers. *J. Natl. Cancer Inst.*, 90: 991-995, 1998.
107. Venmans, B. J., van der Linden, J. C., van Boxem, A. J., Postmus, P. E., Smit, E. F., and Sutedja, G. Early detection of pre-invasive lesions in high risk patients. A comparison of conventional fiberoptic and fluorescence bronchoscopy. *J. Bronchol.*, 5: 280-283, 1998.
108. Vermeylen, P., Pierard, P., Roufosse, C., Bosschaerts, T., Verhest, A., Sculier, J.-P., and Ninane, V. Detection of bronchial preneoplastic lesions and early lung cancer with fluorescence bronchoscopy: a study about its ambulatory feasibility under local anaesthesia. *Lung Cancer (Limerick)*, 25: 161-168, 1999.
109. Kennedy, T., Hirsch, F. R., Miller, Y., Prindiville, S., Bunn, P. A., Jr., and Franklin, W. A randomized study of fluorescence bronchoscopy versus white-light bronchoscopy for early detection of lung cancer in high risk patients. *Lung Cancer (Limerick)*, 29 (Suppl. 2): 244, 2000.
110. Gazdar, A. F., and Minna, J. D. Angiogenesis and the multistage development of lung cancers. *Clin. Cancer Res.*, 6: 1611-1612, 2000.
111. Henschke, C. I., Miettinen, O. S., Yankelevitz, D. F., Libby, D. M., and Smith, J. P. Radiographic screening for cancer: proposed paradigm for requisite research. *Clin. Imaging*, 18: 6-20, 1994.
112. Miettinen, O. S. Screening for lung cancer. *Radiol. Clin. N. Am.*, 38: 479-486, 2000.
113. Marcus, P. M., Bergstralh, E. J., Fagerstrom, M., Williams, D. E., Fontana, R., Taylor, W. F., and Prorok, P. C. Lung cancer mortality in the Mayo Lung Project: impact of extended follow-up. *J. Natl. Cancer Inst.*, 92: 1308-1316, 2000.
114. Black, W. C. Overdiagnosis. An underrecognized cause of confusion and harm in cancer screening. *J. Natl. Cancer Inst.*, 92: 1280-1282, 2000.
115. The Health, and Welfare Statistics Foundation. The current issue on the screening project for elderly people by the Ministry of Health and Welfare Japan. *J. Health Welfare*, 42: 37, 1995.
116. Sobue, T., Suzuki, T., and Naruke, T. The Japanese Lung Cancer Screening Research Group: a case-control study for evaluating lung cancer screening in Japan. *Int. J. Cancer*, 50: 230-237, 1992.
117. Okamoto, N., Suzuki, T., Hasegawa, H., Goreh, T., Hagiwara, S., Sekimoto, M., and Kaneko, M. Evaluation of a clinic-based screening program for lung cancer with a case-control design in Kanagawa. *Lung Cancer (Limerick)*, 25: 77-85, 1999.
118. Muhm, J. R., Miller, W. F., Fontana, R. S., Sanderson, D. R., and Uhlenhuth, M. A. Lung cancer detected during a screening program using four-month chest radiographs. *Radiology*, 148: 609-615, 1983.
119. Hayabuchi, N., Russell, W. J., and Murakami, J. Problems in radiographic detection and diagnosis of lung cancer. *Acta Radiol. (CPII)*, 30: 163-167, 1989.
120. Woodring, J. H. Pitfalls in the radiologic diagnosis of lung cancer. *Am. J. Roentgenol.*, 154: 1165-1175, 1990.

121. Greene, R. E. Missed lung nodules: lost opportunities for cancer care. *Radiology*, 182: 8-9, 1992.
122. Austin, J. H. M., Romney, B. M., Goldsmith, L. S. Missed bronchogenic carcinoma: radiographic findings in 27 patients with a potentially resectable lesions evident in retrospect. *Radiology*, 182: 115-122, 1992.
123. Schaner, E. G., Chang, A. E., Doppan, J. L., Conkle, D. M., Flye, M. W., and Rosenberg, S. A. Comparison of computed and conventional whole lung tomography in detecting pulmonary nodules. *Am. J. Roentgenol.*, 131: 51-54, 1978.
124. Webb, W. R. Radiologic evaluation of solitary pulmonary nodule. *Am. J. Roentgenol.*, 154: 701-708, 1990.
125. Kalender, W. A., Seissler, W., Klotz, E., and Vock, P. Spiral volumetric CT with single-breath-hold technique, continuous transport, and continuous scanner rotation. *Radiology*, 176: 181-183, 1990.
126. Costello, P., Anderson, W. A., and Blume, D. Pulmonary nodule: evaluation with spiral volumetric CT. *Radiology*, 179: 875-876, 1991.
127. Remy-Jardin, M., Giraud, F., and Marquette, C. H. Pulmonary nodules: detection with thick section spiral CT versus conventional CT. *Radiology*, 187: 513-520, 1993.
128. Davis, S. CT evaluation for pulmonary metastases in patients with extrathoracic malignancy. *Radiology*, 180: 1-12, 1991.
129. Kaneko, M., Eguchi, K., Ohmatsu, H., Kakinuma, R., Naruke, T., Suemasu, K., and Moriyama, N. Peripheral lung cancer: screening and detection with low-dose spiral CT versus radiography. *Radiology*, 201: 798-802, 1996.
130. Sone, S., Takashima, S., Li, F., Yang, Z., Honda, T., Maruyama, Y., Hasegawa, M., Yamada, T., Kubo, K., Hanamura, K., and Asakura, K. Mass screening for lung cancer with mobile spiral computed tomography scanner. *Lancet*, 351: 1242-1245, 1998.
131. Henschke, C. I., McCauley, D. I., Yankelevitz, D. F., Naidich, D. P., McGuinness, G., Miettinen, O. S., Libby, D. M., Pasmantier, M. W., Koizumi, J., Altorki, N. K., and Smith, J. P. Early Lung Cancer Action Project: overall design and findings from baseline screening. *Lancet*, 354: 99-105, 1999.
132. Kakinuma, R., Ohmatsu, H., Kaneko, M., Eguchi, K., Naruke, T., Nagai, K., Nishiwaki, Y., Suzuki, A., and Moriyama, N. Detection failures in spiral CT screening for lung cancer: analysis of CT findings. *Radiology*, 212: 61-66, 1999.
133. Paranjpe, D. V., and Bergin, C. J. Spiral CT of the lungs: optimal technique and resolution compared with conventional CT. *Am. J. Roentgenol.*, 162: 561-567, 1994.
134. Seltzer, S. E., Judy, P. F., Adams, D. F., Jacobson, F. L., Stark, P., Kikinis, R., Swenson, R. G., Hooton, S., Head, B., and Feldman, U. Spiral CT of the chest: comparison of cine and film-based viewing. *Radiology*, 197: 73-78, 1995.
135. Croisille, P., Souto, M., Cova, M., Wood, S., Afework, Y., Kuhlman, J. E., and Zerhouni, E. A. Pulmonary nodules: improved detection with vascular segmentation and extraction with spiral CT. *Radiology*, 197: 397-401, 1995.
136. Kanazawa, K., Kawata, Y., Niki, N., Satoh, H., Ohmatsu, H., Kakinuma, R., and Kaneko, M. Computer-aided diagnosis for pulmonary nodules based on helical CT images. *Comput. Med. Imaging Graph.*, 22: 157-167, 1998.
137. Buckshee, N., Agnello, K., Yankelevitz, D. F., Mancuso, C., and Henschke, C. I. Smoking habits and overall satisfaction after early lung cancer screening using low-dose CT. *ALA/ATS International Conference*, 1999.
138. Coleman, R. E. PET in lung cancer. *J. Nucl. Med.*, 40: 814-820, 1999.
139. Maitra, A., Wisnub, I. I., Virmani, A. K., Sakaguchi, M., Park, J., Shuck, A., Milchgrub, S., Gibbons, D., Minna, J. D., and Gazdar, A. F. Enrichment of epithelial cells for molecular studies. *Nat. Med.*, 5: 459-463, 1999.
140. Kopelovich, L., Henson, D. E., Gazdar, A. F., Dubb, B., Srivastava, S., Kelloff, G. J., and Greenwald, P. Surrogate anatomic/functional sites for evaluating cancer risk: an extension of the field effect. *Clin. Cancer Res.*, 5: 3899-3905, 1999.
141. Crowell, R. E., Gilliland, F. D., Temes, R. T., Harms, H. J., Neft, R. E., Heaphy, E., Auckley, D. H., Crooks, L. A., Jordan, S. W., Samet, J. M., Lechner, J. F., and Belinsky, S. A. Detection of trisomy 7 in nonmalignant bronchial epithelium from lung cancer patients and individuals at risk for lung cancer. *Cancer Epidemiol. Biomark. Prev.*, 5: 631-637, 1996.
142. Somers, V. A., van Herten, A. M., ten Velde, G. P., Arends, J. W., and Thunnissen, F. B. Additional value of K-ras point mutations in bronchial wash fluids for diagnosis of peripheral lung tumours. *Eur. Respir. J.*, 13: 1120-1124, 1999.
143. Yahata, N., Ohyashiki, K., Ohyashiki, J. H., Iwama, H., Hayashi, S., Ando, K., Hirano, T., Tsuchida, T., Kato, H., Shay, J. W., and Toyama, K. Telomerase activity in lung cancer cells obtained from bronchial washings. *J. Natl. Cancer Inst.*, 90: 684-690, 1998.
144. Wistuba, I. I., and Gazdar, A. F. Molecular abnormalities in the sequential development of lung carcinoma. In: S. Srivastava, D. E. Henson, and A. F. Gazdar (eds.), *Molecular Pathology of Early Cancer*, pp. 265-276. Amsterdam: IOS Press, 1999.
145. Yashima, K., Litzky, L. A., Kaiser, L., Rogers, T., Lam, S., Wistuba, I. I., Milchgrub, S., Srivastava, S., Piotyszek, M. A., Shay, J. W., and Gazdar, A. F. Telomerase expression in respiratory epithelium during the multistage pathogenesis of lung carcinomas. *Cancer Res.*, 57: 2373-2377, 1997.
146. Scott, F. M., Treston, A. M., Shaw, G. L., Avis, I., Sorenson, J., Kelly, K., Dempsey, E. C., Cantor, A. B., Tockman, M., and Mulshine, J. L. Peptide amidating activity in human bronchoalveolar lavage fluid. *Lung Cancer (Limerick)*, 14: 239-251, 1996.
147. Scott, F. M., Modali, R., Lehman, T. A., Seddon, M., Kelly, K., Dempsey, E. C., Wilson, V., Tockman, M. S., and Mulshine, J. L. High frequency of K-ras codon 12 mutations in bronchoalveolar lavage fluid of patients at high risk for second primary lung cancer. *Clin. Cancer Res.*, 3: 479-482, 1997.
148. Mills, N. E., Fishman, C. L., Rom, W. N., and Jacobson, D. R. *Ras* oncogene detection in bronchoalveolar lavage fluid from patients with lung cancer. *Lung Cancer (Limerick)*, 1 (Suppl.): 11, 1994.
149. Nawroz, H., Koch, W., Anker, P., Stroun, M., and Sidransky, D. Microsatellite alterations in serum DNA of head and neck cancer patients. *Nat. Med.*, 2: 1035-1037, 1996.
150. Brennan, J. A., Mao, L., Hruban, R. H., Boyle, J. O., Eby, Y. J., Koch, W. M., Goodman, S. N., and Sidransky, D. Molecular assessment of histopathological staging in squamous-cell carcinoma of the head and neck. *N. Engl. J. Med.*, 332: 429-435, 1995.
151. Ahrendt, S. A., Yang, S. C., Wu, L., Westra, W. H., Jen, J., Califano, J. A., and Sidransky, D. Comparison of oncogene mutation detection and telomerase activity for the molecular staging of non-small cell lung cancer. *Clin. Cancer Res.*, 3: 1207-1214, 1997.
152. Gazdar, A. F., and Minna, J. D. NCI series of cell lines: an historical perspective. *J. Cell. Biochem.*, 24 (Suppl.): 1-11, 1996.
153. Wistuba, I. I., Bryant, D., Behrens, C., Milchgrub, S., Virmani, A. K., Ashfaq, R., Minna, J. D., and Gazdar, A. F. Comparison of features of human lung cancer cell lines and their corresponding tumors. *Clin. Cancer Res.*, 5: 991-1000, 1999.
154. Amstad, P., Reddel, R. R., Pfeifer, A., Malan, S. L., Mark, G. D., and Harris, C. C. Neoplastic transformation of a human bronchial epithelial cell line by a recombinant retrovirus encoding viral Harvey ras. *Mol. Carcinog.*, 1: 151-160, 1988.
155. Franklin, W. A., Folkvord, J. M., Varela-Garcia, M., Kennedy, T., Proudfoot, S., Cook, R., Dempsey, E. C., Helm, K., Bunn, P. A., and Miller, Y. E. Expansion of bronchial epithelial cell populations by in vitro culture of explants from dysplastic and histologically normal sites. *Am. J. Respir. Cell Mol. Biol.*, 15: 297-304, 1996.
156. Kelsey, K., Spitz, M., Zuo, A., and Wiencke, J. Deletion of glutathione S-transferase class μ and class θ genes interacts to enhance susceptibility to lung cancer in minority populations. *Cancer Causes Control*, 1997.

157. Wu, X., Zhao, Y., Hoon, S. E., Tomlinson, G. E., Minna, J. D., Hong, W. K., and Spitz, M. R. Benzo[a]pyrene diol epoxide-induced 3p21.3 aberrations and genetic predisposition to lung cancer. *Cancer Res.*, 58: 1605-1608, 1998.
158. Virmani, A. K., Fong, K. M., Kodagoda, D., McIntire, D., Hung, J., Tonk, V., Minna, J. D., and Gazdar, A. F. Allelotyping demonstrates common and distinct patterns of chromosomal loss in human lung cancer types. *Genes Chromosomes Cancer*, 21: 308-319, 1998.
159. Takahashi, T., Nau, M. M., Chiba, I., Birrer, M. J., Rosenberg, R. K., Vinocour, M., Levitt, M., Pass, H., Gazdar, A. F., and Minna, J. D. p53: a frequent target for genetic abnormalities in lung cancer. *Science (Washington DC)*, 246: 491-494, 1989.
160. Forgacs, E., Biesterveld, E. J., Sekido, Y., Fong, K. M., Muneer, S., Wistuba, I., Mielchgrub, S., Brezinschek, R., Virmani, A., Gazdar, A. F., and Minna, J. D. Mutation analysis of the *PTEN/MMAC1* gene in lung cancer. *Oncogene*, 17: 1557-1565, 1998.
161. Mitsudomi, T., Steinberg, S., Oie, H. K., Mulshine, J. L., Phelps, R., Viallet, J., Pass, H., Minna, J. D., and Gazdar, A. F. *ras* gene mutations in non-small cell lung cancers are associated with shortened survival irrespective of treatment intent. *Cancer Res.*, 51: 4999-5002, 1991.
162. Sozzi, G., Veronese, M. L., Negrini, M., Baffa, R., Corticelli, M. G., Inoue, H., Tornielli, S., Pilotti, S., Ohta, M., Huebner, K., and Croce, C. M. The *FHIT* gene at 3p14.2 is abnormal in lung cancer. *Cell*, 85: 17-26, 1996.
163. Anbazhagan, R., Tihan, T., Borman, D. M., Johnston, J. C., Saltz, J. H., Weigering, A., Piantadosi, S., and Gabrielson, E. Classification of small cell lung cancer and pulmonary carcinoid by gene expression profiles. *Cancer Res.*, 59: 5119-5122, 1999.
164. Hibi, K., Liu, Q., Beaudry, G. A., Madden, S. L., Westra, W. H., Wehage, S. L., Yang, S. C., Heilmiller, R. F., Bertelsen, A. H., Sidransky, D., and Jen, J. Serial analysis of gene expression in non-small cell lung cancer. *Cancer Res.*, 58: 5690-5694, 1998.
165. Sozzi, G., Pastorino, U., Moiraghi, L., Tagliabue, E., Pezzella, F., Ghirelli, C., Tornielli, S., Sard, L., Huebner, K., Pierotti, M. A., Croce, C. M., and Pilotti, S. Loss of *FHIT* function in lung cancer and preinvasive bronchial lesions. *Cancer Res.*, 58: 5032-5037, 1998.
166. Tockman, M. S., and Mulshine, J. L. Sputum screening by quantitative microscopy: a new dawn for detection of lung cancer? *Mayo Clin. Proc.*, 72: 788-790, 1997.
167. Izzo, J., and Hittelman, W. N. Characterization of multistep tumorigenesis by *in situ* hybridization. In: M. Andreeff and D. Finkel (eds.), *Introduction to FISH*. In press, 2001.
168. Neft, R. E., Crowell, R. E., Gilliland, F. D., Murphy, M. M., Lane, J. L., Harms, H., Coons, T., Heaphy, E., Belinsky, S. A., and Lechner, J. F. Frequency of trisomy 20 in nonmalignant bronchial epithelium from lung cancer patients and cancer-free former uranium miners and smokers. *Cancer Epidemiol. Biomark. Prev.*, 7: 1051-1054, 1998.
169. Heppell-Parton, A. C., Nacheva, E., Carter, N. P., and Rabbitts, P. H. A combined approach of conventional and molecular cytogenetics for detailed karyotypic analysis of the small cell lung carcinoma cell line U2020. *Cancer Genet. Cytogenet.*, 108: 110-119, 1999.
170. Lechner, J. F., Neft, R., Gilliland, F. D., Crowell, R. E., Auckely, D. H., Temes, R. T., and Belinsky, S. A. Individuals at high risk for lung cancer have airway epithelial cells with chromosome aberrations frequently found in lung tumor cells. *In Vivo* 12: 23-26, 1998.
171. Walch, A. K., Zitzelsberger, H. F., Aubele, M. M., Mattis, A. E., Bauchinger, M., Candidus, S., Prauer, H. W., Werner, M., and Hofler, H. Typical and atypical carcinoid tumors of the lung are characterized by 11q deletions as detected by comparative genomic hybridization. *Am. J. Pathol.*, 153: 1089-1098, 1998.
172. Petersen, I., Bujard, M., Petersen, S., Wolf, G., Goeze, A., Schwendel, A., Langreck, H., Gellert, K., Reichel, M., Just, K., du Manoir, S., Cremer, T., Dietel, M., and Ried, T. Patterns of chromosomal imbalances in adenocarcinoma and squamous cell carcinoma of the lung. *Cancer Res.*, 57: 2331-2335, 1997.
173. Smith, A. L., Hung, J., Walker, L., Rogers, T. E., Vuitich, F., Lee, E., and Gazdar, A. F. Extensive areas of aneuploidy are present in the respiratory epithelium of lung cancer patients. *Br. J. Cancer*, 73: 203-209, 1996.
174. MacAulay, C. E., Lam, S., Kein-Parker, H., Gazdar, A., Guillaud, M., Payne, P., LeRiche, J., Dawe, C., Band, P., and Palcic, B. Intermediate endpoint biomarkers for lung cancer chemoprevention. *SPJ*, 3260: 207-211, 1998.

MOLECULAR BIOLOGY OF **THE CELL**

THIRD EDITION

Bruce Alberts • Dennis Bray
Julian Lewis • Martin Raff • Keith Roberts
James D. Watson



Garland Publishing, Inc.
New York & London

GARLAND STAFF

Text Editor: Miranda Robertson

Managing Editor: Ruth Adams

Illustrator: Nigel Orme

Molecular Model Drawings: Kate Hesketh-Moore

Director of Electronic Publishing: John M. Roblin

Computer Specialist: Chuck Bartelt

Disk Preparation: Carol Winter

Copy Editor: Shirley M. Cobert

Production Editor: Douglas Goertzen

Production Coordinator: Perry Bessas

Indexer: Majja Hinkle

Bruce Alberts received his Ph.D. from Harvard University and is currently President of the National Academy of Sciences and Professor of Biochemistry and Biophysics at the University of California, San Francisco. *Dennis Bray* received his Ph.D. from the Massachusetts

Institute of Technology and is currently a Medical Research Council Fellow in the Department of Zoology, University of Cambridge. *Julian Lewis* received his D.Phil. from the University of Oxford and is

currently a Senior Scientist in the Imperial Cancer Research Fund Developmental Biology Unit, University of Oxford. *Martin Raff* received his M.D. from McGill University and is currently a Professor in the MRC

Laboratory for Molecular Cell Biology and the Biology Department, University College, London. *Keith Roberts* received his Ph.D. from the University of Cambridge and is currently Head of the Department of Cell

Biology, the John Innes Institute, Norwich. *James D. Watson* received his Ph.D. from Indiana University and is currently Director of the Cold Spring Harbor Laboratory. He is the author of *Molecular Biology of the Gene* and,

with Francis Crick and Maurice Wilkins, won the Nobel Prize in Medicine and Physiology in 1962.

© 1983, 1989, 1994 by Bruce Alberts, Dennis Bray, Julian Lewis, Martin Raff, Keith Roberts, and James D. Watson.

All rights reserved. No part of this book covered by the copyright hereon may be reproduced or used in any form or by any means—graphic, electronic, or mechanical, including photocopying, recording, taping, or information storage and retrieval systems—without permission of the publisher.

Library of Congress Cataloging-in-Publication Data

Molecular biology of the cell / Bruce Alberts, ... [et al.]. — 3rd ed.
p. cm.

Includes bibliographical references and index.

ISBN 0-8153-1619-1 (hard cover) — ISBN 0-8153-1620-3 (pbk.)

1. Cytology. 2. Molecular biology. I. Alberts, Bruce.

II. DNLAF 1. C-4J5. 2. Molecular Biology. — QH531.2 M713 (1994)

QH531.2 M64 — 1994

574.37—dc20

DNL/M/DLC

for Library of Congress

93-45907

CJP

Published by Garland Publishing, Inc.
717 Fifth Avenue, New York, NY 10022

Printed in the United States of America

15 14 13 12 10 9 8 7 6 5 4 3 2 1

Front cover: The photograph shows a rat nerve cell in culture. It is labeled with a fluorescent antibody that stains its cell body and dendritic processes (yellow). Nerve terminals (green) from other neurons (not visible), which have made synapses on the cell, are labeled with a different antibody (courtesy of Olaf Mundigl and Pietro de Camilli.)

Dedication page: Gavin Borden, late president of Garland Publishing, weathered in during his mid-1980s climb near Mount McKinley with MBot, author Bruce Alberts, and famous mountaineer guide Mugs Mump (1940-1992).

Back cover: The authors, in alphabetical order, crossing Abbey Road in London on their way to lunch. Much of this third edition was written in a house just around the corner. (Photograph by Richard Oliver.)

extracts. If these minor cell proteins differ among cells to the same extent as the more abundant proteins, as is commonly assumed, only a small number of protein differences (perhaps several hundred) suffice to create very large differences in cell morphology and behavior.

A Cell Can Change the Expression of Its Genes in Response to External Signals³

Most of the specialized cells in a multicellular organism are capable of altering their patterns of gene expression in response to extracellular cues. If a liver cell is exposed to a glucocorticoid hormone, for example, the production of several specific proteins is dramatically increased. Glucocorticoids are released during periods of starvation or intense exercise and signal the liver to increase the production of glucose from amino acids and other small molecules; the set of proteins whose production is induced includes enzymes such as tyrosine aminotransferase, which helps to convert tyrosine to glucose. When the hormone is no longer present, the production of these proteins drops to its normal level.

Other cell types respond to glucocorticoids in different ways. In fat cells, for example, the production of tyrosine aminotransferase is reduced, while some other cell types do not respond to glucocorticoids at all. These examples illustrate a general feature of cell specialization—different cell types often respond in different ways to the same extracellular signal. Underlying this specialization are features that do not change, which give each cell type its permanently distinctive character. These features reflect the persistent expression of different sets of genes.

Gene Expression Can Be Regulated at Many of the Steps in the Pathway from DNA to RNA to Protein⁴

If differences between the various cell types of an organism depend on the particular genes that the cells express, at what level is the control of gene expression exercised? There are many steps in the pathway leading from DNA to protein, and all of them can in principle be regulated. Thus a cell can control the proteins it makes by (1) controlling when and how often a given gene is transcribed (**transcriptional control**), (2) controlling how the primary RNA transcript is spliced or otherwise processed (**RNA processing control**), (3) selecting which completed mRNAs in the cell nucleus are exported to the cytoplasm (**RNA transport control**), (4) selecting which mRNAs in the cytoplasm are translated by ribosomes (**translational control**), (5) selectively destabilizing certain mRNA molecules in the cytoplasm (**mRNA degradation control**), or (6) selectively activating, inactivating, or compartmentalizing specific protein molecules after they have been made (**protein activity control**) (Figure 9-2).

For most genes transcriptional controls are paramount. This makes sense because, of all the possible control points illustrated in Figure 9-2, only transcriptional control ensures that no superfluous intermediates are synthesized. In the

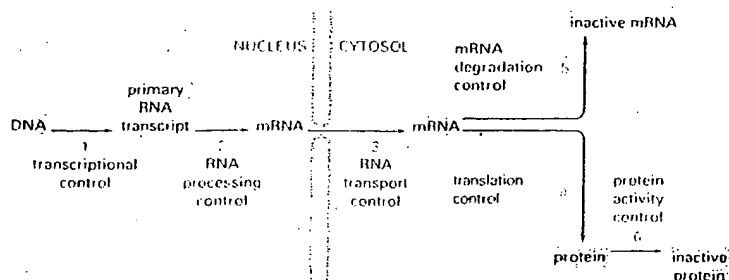


Figure 9-2 Six steps at which eucaryote gene expression can be controlled. Only controls that operate at steps 1 through 5 are discussed in this chapter. The regulation of protein activity (step 6) is discussed in Chapter 5; this includes reversible activation or inactivation by protein phosphorylation as well as irreversible inactivation by proteolytic degradation.

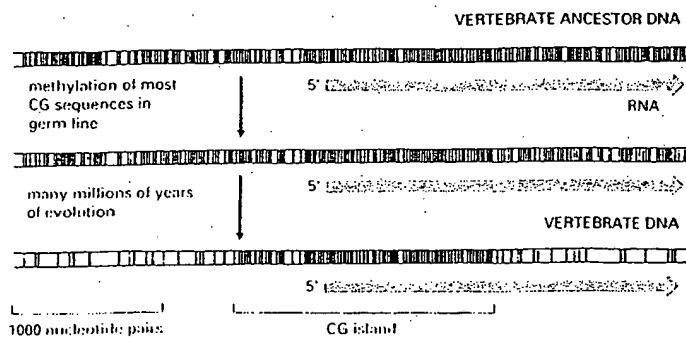


FIGURE 9-71 A mechanism to explain both the marked deficiency of CG sequences and the presence of CG islands in vertebrate genomes. A black line marks the location of an unmethylated CG dinucleotide in the DNA sequence, while a red line marks the location of a methylated CG dinucleotide.

Summary

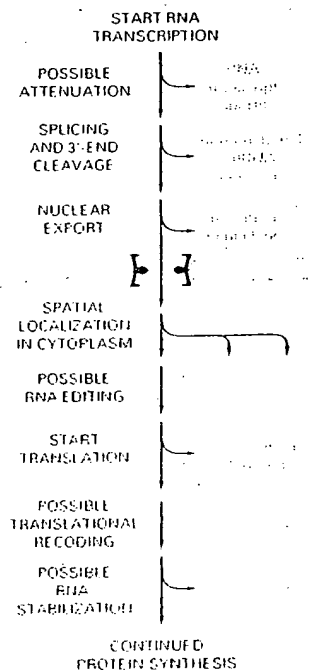
The many types of cells in animals and plants are created largely through mechanisms that cause different genes to be transcribed in different cells. Since many specialized animal cells can maintain their unique character when grown in culture, the gene regulatory mechanisms involved in creating them must be stable once established and heritable when the cell divides, endowing the cell with a memory of its developmental history. Prokaryotes and yeasts provide unusually accessible model systems in which to study gene regulatory mechanisms, some of which may be relevant to the creation of specialized cell types in higher eucaryotes. One such mechanism involves a competitive interaction between two (or more) gene regulatory proteins, each of which inhibits the synthesis of the other; this can create a flip-flop switch that switches a cell between two alternative patterns of gene expression. Direct or indirect positive feedback loops, which enable gene regulatory proteins to perpetuate their own synthesis, provide a general mechanism for cell memory.

In eucaryotes gene transcription is generally controlled by combinations of gene regulatory proteins. It is thought that each type of cell in a higher eucaryotic organism contains a specific combination of gene regulatory proteins that ensures the expression of only those genes appropriate to that type of cell. A given gene regulatory protein may be expressed in a variety of circumstances and typically is involved in the regulation of many genes.

In addition to diffusible gene regulatory proteins, inherited states of chromatin condensation are also utilized by eucaryotic cells to regulate gene expression. In vertebrates DNA methylation also plays a part, mainly as a device to reinforce decisions about gene expression that are made initially by other mechanisms.

Although controls on the initiation of gene transcription are the predominant form of regulation for most genes, other controls can act later in the pathway from RNA to protein to modulate the amount of gene product that is made. Although these **posttranscriptional controls**, which operate after RNA polymerase has bound to the gene's promoter and begun RNA synthesis, are less common than **transcriptional control**, for many genes they are crucial. It seems that every step in gene expression that could be controlled in principle is likely to be regulated under some circumstances for some genes.

We consider the varieties of posttranscriptional regulation in temporal order, according to the sequence of events that might be experienced by an RNA molecule after its transcription has begun (Figure 9-72).



Possible posttranscriptional controls on gene expression. Only a few of these controls are likely to be used for any one gene.

MOLECULAR BIOLOGY OF
THE CELL

fourth edition

Bruce Alberts

Alexander Johnson

Julian Lewis

Martin Raff

Keith Roberts

Peter Walter

 **Garland Science**
Taylor & Francis Group

Garland

Vice President: Denise Schanck
Managing Editor: Sarah Gibbs
Senior Editorial Assistant: Kirsten Jenner
Managing Production Editor: Emma Hunt
Proofreader and Layout: Emma Hunt
Production Assistant: Angela Bennett
Text Editors: Marjorie Singer Anderson and Betsy Dileria
Copy Editor: Bruce Goatly
Word Processors: Fran Dependahl, Misty Landers and Carol Winter
Designer: Blink Studio, London
Illustrator: Nigel Orme
Indexer: Janine Ross and Sherry Granum
Manufacturing: Nigel Eyre and Marion Morrow

Cell Biology Interactive

Artistic and Scientific Direction: Peter Walter
Narrated by: Julie Theriot
Production, Design, and Development: Mike Morales

Bruce Alberts received his Ph.D. from Harvard University and is President of the National Academy of Sciences and Professor of Biochemistry and Biophysics at the University of California, San Francisco. **Alexander Johnson** received his Ph.D. from Harvard University and is a Professor of Microbiology and Immunology at the University of California, San Francisco. **Julian Lewis** received his D.Phil. from the University of Oxford and is a Principal Scientist at the Imperial Cancer Research Fund, London. **Martin Raff** received his M.D. from McGill University and is at the Medical Research Council Laboratory for Molecular Cell Biology and Cell Biology Unit and in the Biology Department at University College London. **Keith Roberts** received his Ph.D. from the University of Cambridge and is Associate Research Director at the John Innes Centre, Norwich. **Peter Walter** received his Ph.D. from The Rockefeller University in New York and is Professor and Chairman of the Department of Biochemistry and Biophysics at the University of California, San Francisco, and an Investigator of the Howard Hughes Medical Institute.

© 2002 by Bruce Alberts, Alexander Johnson, Julian Lewis, Martin Raff, Keith Roberts, and Peter Walter.
© 1983, 1989, 1994 by Bruce Alberts, Dennis Bray, Julian Lewis, Martin Raff, Keith Roberts, and James D. Watson.

All rights reserved. No part of this book covered by the copyright hereon may be reproduced or used in any form in any form or by any means—graphic, electronic, or mechanical, including photocopying, recording, taping, or information storage and retrieval systems—without permission of the publisher.

Library of Congress Cataloging-in-Publication Data
Molecular biology of the cell / Bruce Alberts ... [et al.]. -- 4th ed.
p. cm
Includes bibliographical references and index.
ISBN 0-8153-3218-1 (hardbound) -- ISBN 0-8153-4072-9 (pbk.)
1. Cytology. 2. Molecular biology. I. Alberts, Bruce
[DNLM: 1. Cells. 2. Molecular Biology.]
Q153.2 .M64 2002
571.6--dc21

2001054473 CIP

Published by Garland Science, a member of the Taylor & Francis Group,
29 West 35th Street, New York, NY 10001-2299

Printed in the United States of America

15 11 13 12 11 10 9 8 7 6 5 4 3 2 1

Front cover Human Genome: Reprinted by permission from *Nature*, International Human Genome Sequencing Consortium, 409:860-921, 2001 © Macmillan Magazines Ltd. Adapted from an image by Francis Collins, NHGRI; Jim Kent, UCSC; Evan Birney, EBI; and Darryl Leja, NHGRI; showing a portion of Chromosome 1 from the initial sequencing of the human genome.

Back cover In 1967, the British artist Peter Blake created a design classic. Nearly 35 years later Nigel Orme (illustrator), Richard Denyer (photographer), and the authors have together produced an affectionate tribute to Mr Blake's image. With its gallery of icons and influences, its assembly created almost as much complexity, intrigue and mystery as the original. *Drosophila*, *Arabidopsis*, Dolly and the assembled company tempt you to dip inside where, as in the original, "a splendid time is guaranteed for all." (Gunter Blobel, courtesy of The Rockefeller University; Marie Curie, Keystone Press Agency Inc; Darwin bust, by permission of the President and Council of the Royal Society; Rosalind Franklin, courtesy of Cold Spring Harbor Laboratory Archives; Dorothy Hodgkin, © The Nobel Foundation, 1964; James Joyce, etching by Peter Blake; Robert Johnson, photo booth self-portrait early 1930s, © 1986 Delta Haze Corporation all rights reserved, used by permission; Albert L. Lehninger, (unidentified photograph) courtesy of The Alan Mason Chesney Medical Archives of The Johns Hopkins Medical Institutions; Linus Pauling, from Ava Helen and Linus Pauling Papers, Special Collections, Oregon State University; Nicholas Poussin, courtesy of ArtToday.com; Barbara McClintock, © David Micklos, 1983; Andrei Sakharov, courtesy of Elena Bonner; Frederick Sanger, © The Nobel Foundation, 1958.)

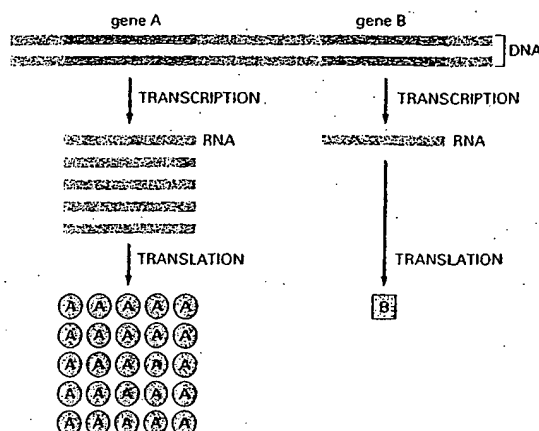


Figure 6-3 Genes can be expressed with different efficiencies. Gene A is transcribed and translated much more efficiently than gene B. This allows the amount of protein A in the cell to be much greater than that of protein B.

FROM DNA TO RNA

Transcription and translation are the means by which cells read out, or express, the genetic instructions in their genes. Because many identical RNA copies can be made from the same gene, and each RNA molecule can direct the synthesis of many identical protein molecules, cells can synthesize a large amount of protein rapidly when necessary. But each gene can also be transcribed and translated with a different efficiency, allowing the cell to make vast quantities of some proteins and tiny quantities of others (Figure 6-3). Moreover, as we see in the next chapter, a cell can change (or regulate) the expression of each of its genes according to the needs of the moment—most obviously by controlling the production of its RNA.

Portions of DNA Sequence Are Transcribed into RNA

The first step a cell takes in reading out a needed part of its genetic instructions is to copy a particular portion of its DNA nucleotide sequence—a gene—into an RNA nucleotide sequence. The information in RNA, although copied into another chemical form, is still written in essentially the same language as it is in DNA—the language of a nucleotide sequence. Hence the name **transcription**.

Like DNA, RNA is a linear polymer made of four different types of nucleotide subunits linked together by phosphodiester bonds (Figure 6-4). It differs from DNA chemically in two respects: (1) the nucleotides in RNA are *ribonucleotides*—that is, they contain the sugar ribose (hence the name *ribonucleic acid*) rather than deoxyribose; (2) although, like DNA, RNA contains the bases adenine (A), guanine (G), and cytosine (C), it contains the base uracil (U) instead of the thymine (T) in DNA. Since U, like T, can base-pair by hydrogen-bonding with A (Figure 6-5), the complementary base-pairing properties described for DNA in Chapters 4 and 5 apply also to RNA (in RNA, G pairs with C, and A pairs with U). It is not uncommon, however, to find other types of base pairs in RNA: for example, G pairing with U occasionally.

Despite these small chemical differences, DNA and RNA differ quite dramatically in overall structure. Whereas DNA always occurs in cells as a double-stranded helix, RNA is single-stranded. RNA chains therefore fold up into a variety of shapes, just as a polypeptide chain folds up to form the final shape of a protein (Figure 6-6). As we see later in this chapter, the ability to fold into complex three-dimensional shapes allows some RNA molecules to have structural and catalytic functions.

Transcription Produces RNA Complementary to One Strand of DNA

All of the RNA in a cell is made by DNA transcription, a process that has certain similarities to the process of DNA replication discussed in Chapter 5.

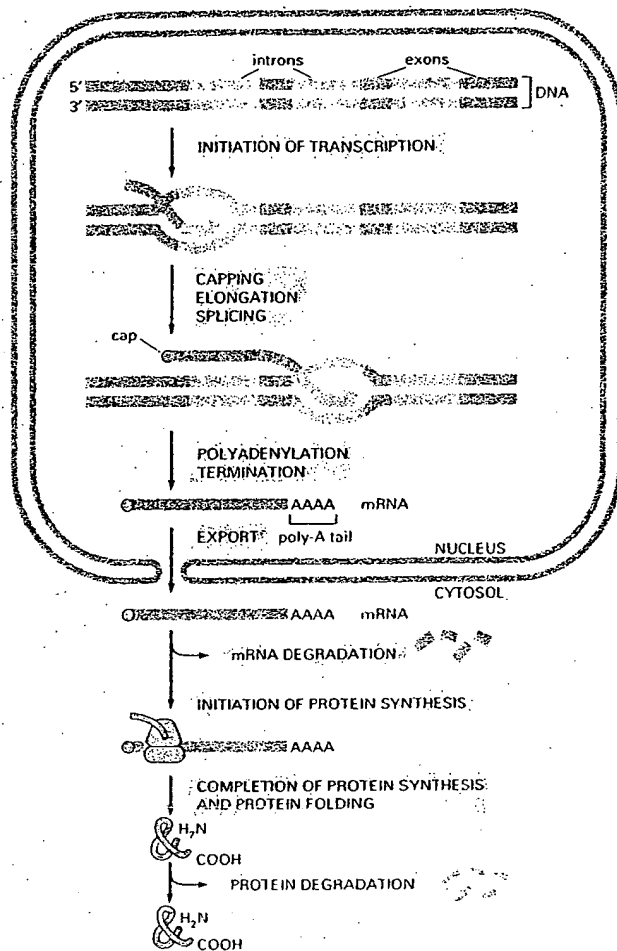


Figure 6-90 The production of a protein by a eucaryotic cell. The final level of each protein in a eucaryotic cell depends upon the efficiency of each step depicted.

ure 6-90) could be regulated by the cell for each individual protein. However, as we shall see in Chapter 7, the initiation of transcription is the most common point for a cell to regulate the expression of each of its genes. This makes sense, inasmuch as the most efficient way to keep a gene from being expressed is to block the very first step—the transcription of its DNA sequence into an RNA molecule.

Summary

The translation of the nucleotide sequence of an mRNA molecule into protein takes place in the cytoplasm on a large ribonucleoprotein assembly called a ribosome. The amino acids used for protein synthesis are first attached to a family of tRNA molecules, each of which recognizes, by complementary base-pair interactions, particular sets of three nucleotides in the mRNA (codons). The sequence of nucleotides in the mRNA is then read from one end to the other in sets of three according to the genetic code.

To initiate translation, a small ribosomal subunit binds to the mRNA molecule at a start codon (AUG) that is recognized by a unique initiator tRNA molecule. A large ribosomal subunit binds to complete the ribosome and begin the elongation phase of protein synthesis. During this phase, aminoacyl tRNAs—each bearing a specific amino acid bind sequentially to the appropriate codon in mRNA by forming complementary base pairs with the tRNA anticodon. Each amino acid is added to the C-terminal end of the growing polypeptide by means of a cycle of three sequential

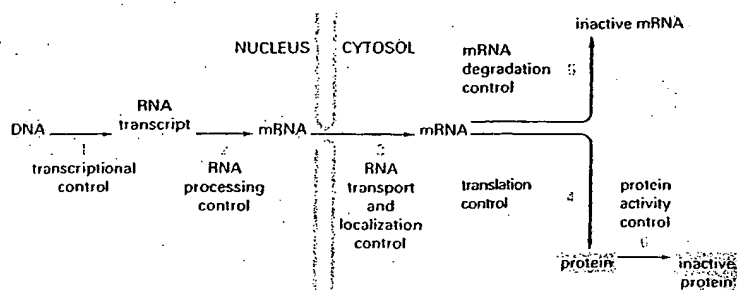


Figure 7-5 Six steps at which eucaryotic gene expression can be controlled. Controls that operate at steps 1 through 5 are discussed in this chapter. Step 6, the regulation of protein activity, includes reversible activation or inactivation by protein phosphorylation (discussed in Chapter 3) as well as irreversible inactivation by proteolytic degradation (discussed in Chapter 6).

Gene Expression Can Be Regulated at Many of the Steps in the Pathway from DNA to RNA to Protein

If differences among the various cell types of an organism depend on the particular genes that the cells express, at what level is the control of gene expression exercised? As we saw in the last chapter, there are many steps in the pathway leading from DNA to protein, and all of them can in principle be regulated. Thus a cell can control the proteins it makes by (1) controlling when and how often a given gene is transcribed (**transcriptional control**), (2) controlling how the RNA transcript is spliced or otherwise processed (**RNA processing control**), (3) selecting which completed mRNAs in the cell nucleus are exported to the cytosol and determining where in the cytosol they are localized (**RNA transport and localization control**), (4) selecting which mRNAs in the cytoplasm are translated by ribosomes (**translational control**), (5) selectively destabilizing certain mRNA molecules in the cytoplasm (**mRNA degradation control**), or (6) selectively activating, inactivating, degrading, or compartmentalizing specific protein molecules after they have been made (**protein activity control**) (Figure 7-5).

For most genes transcriptional controls are paramount. This makes sense because, of all the possible control points illustrated in Figure 7-5, only transcriptional control ensures that the cell will not synthesize superfluous intermediates. In the following sections we discuss the DNA and protein components that perform this function by regulating the initiation of gene transcription. We shall return at the end of the chapter to the additional ways of regulating gene expression.

Summary

The genome of a cell contains in its DNA sequence the information to make many thousands of different protein and RNA molecules. A cell typically expresses only a fraction of its genes, and the different types of cells in multicellular organisms arise because different sets of genes are expressed. Moreover, cells can change the pattern of genes they express in response to changes in their environment, such as signals from other cells. Although all of the steps involved in expressing a gene can in principle be regulated, for most genes the initiation of RNA transcription is the most important point of control.

How does a cell determine which of its thousands of genes to transcribe? As mentioned briefly in Chapters 4 and 6, the transcription of each gene is controlled by a regulatory region of DNA relatively near the site where transcription begins. Some regulatory regions are simple and act as switches that are thrown by a single signal. Many others are complex and act as tiny microprocessors, responding to a variety of signals that they interpret and integrate to switch the neighboring gene on or off. Whether complex or simple, these switching devices

GENIES

Benjamin Lewin

Oxford New York Tokyo
Oxford University Press
1997

CHAPTER 29

Regulation of transcription

The phenotypic differences that distinguish the various kinds of cells in a higher eukaryote are largely due to differences in the expression of genes that code for proteins, that is, those transcribed by RNA polymerase II. In principle, the expression of these genes might be regulated at any one of several stages. The concept of the "level of control" implies that gene expression is not necessarily an automatic process once it has begun. It could be regulated in a gene-specific way at any one of several sequential steps. We can distinguish (at least) five potential control points, forming the series:

Activation of gene structure
↓
Initiation of transcription
↓
Processing the transcript
↓
Transport to cytoplasm
↓
Translation of mRNA

The existence of the first step is implied by the discovery that genes may exist in either of two structural conditions. Relative to the state of most of the genome, genes are found in an "active" state in the cells in which they are expressed (see Chapter 27). The change of structure is distinct from the act of transcription, and indicates that the gene is "transcribable." This suggests that acquisition of the "active" structure must be the first step in gene expression.

Transcription of a gene in the active state is

controlled at the stage of initiation, that is, by the interaction of RNA polymerase with its promoter. This is now becoming susceptible to analysis in the *in vitro* systems (see Chapter 28). For most genes, this is a major control point; probably it is the most common level of regulation.

There is at present no evidence for control at subsequent stages of transcription in eukaryotic cells, for example, via antitermination mechanisms.

The primary transcript is modified by capping at the 5' end, and usually also by polyadenylation at the 3' end. Introns must be spliced out from the transcripts of interrupted genes. The mature RNA must be exported from the nucleus to the cytoplasm. Regulation of gene expression by selection of sequences at the level of nuclear RNA might involve any or all of these stages, but the one for which we have most evidence concerns changes in splicing; some genes are expressed by means of alternative splicing patterns whose regulation controls the type of protein product (see Chapter 30).

Finally, the translation of an mRNA in the cytoplasm can be specifically controlled. There is little evidence for the employment of this mechanism in adult somatic cells, but it does occur in some embryonic situations, as described in Chapter 7. The mechanism is presumed to involve the blocking of initiation of translation of some mRNAs by specific protein factors.

But having acknowledged that control of gene expression can occur at multiple stages, and that production of RNA cannot inevitably be equated with production of protein, it is clear

that the overwhelming majority of regulatory events occur at the initiation of transcription. Regulation of tissue-specific gene transcription lies at the heart of eukaryotic differentiation; indeed, we see examples in Chapter 38 in which proteins that regulate embryonic development prove to be transcription factors. A regulatory transcription factor serves to provide

common control of a large number of target genes, and we seek to answer two questions about this mode of regulation: what identifies the common target genes to the transcription factor; and how is the activity of the transcription factor itself regulated in response to intrinsic or extrinsic signals?

Response elements identify genes under common regulation

The principle that emerges from characterizing groups of genes under common control is that *they share a promoter element that is recognized by a regulatory transcription factor*. An element that causes a gene to respond to such a factor is called a **response element**; examples are the HSE (heat shock response element), GRE (glucocorticoid response element), SRE (serum response element).

The properties of some inducible transcription factors and the elements that they recognize are summarized in Table 29.1. Response elements have the same general characteristics as upstream elements of promoters or enhancers. They contain short consensus sequences, and copies of the response elements found in different genes are closely related, but not necessarily identical. The region bound by the factor extends for a short distance on either side of

the consensus sequence. In promoters, the elements are not present at fixed distances from the startpoint, but are usually <200 bp upstream of it. The presence of a single element usually is sufficient to confer the regulatory response, but sometimes there are multiple copies.

Response elements may be located in promoters or in enhancers. Some types of elements are typically found in one rather than the other: usually an HSE is found in a promoter, while a GRE is found in an enhancer. We assume that all response elements function by the same general principle. *A gene is regulated by a sequence at the promoter or enhancer that is recognized by a specific protein. The protein functions as a transcription factor needed for RNA polymerase to initiate. Active protein is available only under conditions when the gene is to be expressed; its absence means that the promoter is not activated by this particular circuit.*

An example of a situation in which many genes are controlled by a single factor is provided by the heat shock response. This is common to a wide range of prokaryotes and eukaryotes and involves multiple controls of gene expression: an increase in temperature turns off transcription of some genes, turns on transcription of the heat shock genes, and causes changes in the translation of mRNAs. The control of the heat shock genes illustrates the differences between prokaryotic and eukaryotic modes of control. In bacteria, a new sigma factor is synthesized that directs RNA polymerase holoenzyme to recognize an alter-

Table 29.1 Inducible transcription factors bind to response elements that identify groups of promoters or enhancers subject to coordinate control.

Regulatory Agent	Module	Consensus	Factor
Heat shock	HSE	CNNGAANNTCCNNG	HSTF
Glucocorticoid	GRE	TGGTACAAATGTTCT	Receptor
Phorbol ester	TRE	TGACTCA	AP1
Serum	SRE	CCATATTAGG	SRF



World Journal of Surgical
Oncology
Volume 2

Viewing options:

- Abstract
- Full text
- PDF (778KB)

Associated material:

- Readers' comments
- PubMed record

Related literature:

- Articles citing this article on BioMed Central on Google Scholar
- Other articles by authors
- Similar articles (PubMed)

Tools:

- E-mail to a friend
- Download references
- Post a comment

Key:

- ✉ E-mail
- ✉ Corresponding author

Research

Prostate stem cell antigen (PSCA) expression in human prostate cancer tissues and its potential role in prostate carcinogenesis and progression of prostate cancer

Zhao Zhigang¹ ✉ and Shen Wenlv² ✉

¹Department of Urology, Shantou University Medical College, Shantou, Guangdong, China

²Department of Urology, No 2. Affiliated Hospital of Shantou University Medical College, Shantou, Guangdong, China

World Journal of Surgical Oncology 2004, 2:13 doi:10.1186/1477-7819-2-13

The electronic version of this article is the complete one and can be found online at: <http://www.wjso.com/content/2/1/13>

Received 30 March 2004

Accepted 10 May 2004

Published 10 May 2004

© 2004 Zhigang and Wenlv; licensee BioMed Central Ltd. This is an Open Access article: verbatim copying and redistribution of this article are permitted in all media for any purpose, provided this notice is preserved along with the article's original URL.

Keywords: Prostate, Neoplasm, Prostate stem cell antigen (PSCA)

Outline

Abstract

Background

Prostate stem cell antigen (PSCA) is a recently defined homologue of the Thy-1/Ly-6 family of glycosylphosphatidylinositol (GPI)-anchored cell surface antigens. The purpose of the present study was to examine the expression status of PSCA protein and mRNA in clinical specimens of human prostate cancer (Pca) and to validate it as a potential molecular target for diagnosis and treatment of Pca.

Materials and Methods

Immunohistochemical (IHC) and *in situ* hybridization (ISH) analyses of PSCA expression were simultaneously performed on paraffin-embedded sections from 20 benign prostatic hyperplasia (BPH), 20 prostatic intraepithelial neoplasm (PIN) and 48 prostate cancer (Pca) tissues, including 9 androgen-independent prostate cancers. The level of PSCA expression was semiquantitatively scored by assessing both the percentage and intensity of PSCA-positive staining cells in the specimens. Then compared PSCA expression between BPH, PIN and Pca tissues and analysed the correlations

of PSCA expression level with pathological grade, clinical stage and progression to androgen-independence in Pca.

Results

In BPH and low grade PIN, PSCA protein and mRNA staining were weak or negative and less intense and uniform than that seen in HGPIN and Pca. There were moderate to strong PSCA protein and mRNA expression in 8 of 11 (72.7%) HGPIN and in 40 of 48 (83.4%) Pca specimens examined by IHC and ISH analyses, with statistical significance compared with BPH (20%) and low grade PIN (22.2%) samples ($p < 0.05$, respectively). The expression level of PSCA increased with high Gleason grade, advanced stage and progression to androgen-independence ($p < 0.05$, respectively). In addition, IHC and ISH staining showed a high degree of correlation between PSCA protein and mRNA overexpression.

Conclusions

Our data demonstrate that PSCA as a new cell surface marker is overexpressed by a majority of human Pca. PSCA expression correlates positively with adverse tumor characteristics, such as increasing pathological grade (poor cell differentiation), worsening clinical stage and androgen-independence, and speculatively with prostate carcinogenesis. PSCA protein overexpression results from upregulated transcription of PSCA mRNA. PSCA may have prognostic utility and may be a promising molecular target for diagnosis and treatment of Pca.

Outline Introduction

Abstract
Introduction
Materials and methods
Results
Discussion
Competing interests
References

Prostate cancer (Pca) is the second leading cause of cancer-related death in American men and is becoming a common cancer increasing in China. Despite recently great progress in the diagnosis and management of localized disease, there continues to be a need for new diagnostic markers that can accurately discriminate between indolent and aggressive variants of Pca. There also continues to be a need for the identification and characterization of potential new therapeutic targets on Pca cells. Current diagnostic and therapeutic modalities for recurrent and metastatic Pca have been limited by a lack of specific target antigens of Pca.

Although a number of prostate-specific genes have been identified (i.e. prostate specific antigen, prostatic acid phosphatase, glandular kallikrein 2), the majority of these are secreted proteins not ideally suited for many immunological strategies. So, the identification of new cell surface antigens is critical to the development of new diagnostic and therapeutic approaches to the management of Pca.

Reiter RE et al [1] reported the identification of prostate stem cell antigen (PSCA), a cell surface antigen that is predominantly prostate specific. The PSCA gene encodes a 123 amino acid glycoprotein, with 30% homology to stem cell antigen 2 (Sca 2). Like Sca-2, PSCA also belongs to a member of the Thy-1/Ly-6 family and is anchored by a glycosylphosphatidylinositol (GPI) linkage. mRNA *in situ* hybridization (ISH) localized PSCA expression in

normal prostate to the basal cell epithelium, the putative stem cell compartment of prostatic epithelium, suggesting that PSCA may be a marker of prostate stem/progenitor cells.

In order to examine the status of PSCA protein and mRNA expression in human Pca and validate it as a potential diagnostic and therapeutic target for Pca, we used immunohistochemistry (IHC) and *in situ* hybridization (ISH) simultaneously, and conducted PSCA protein and mRNA expression analyses in paraffin-embedded tissue specimens of benign prostatic hyperplasia (BPH, n = 20), prostate intraepithelial neoplasm (PIN, n = 20) and prostate cancer (Pca, n = 48). Furthermore, we evaluated the possible correlation of PSCA expression level with Pca tumorigenesis, grade, stage and progression to androgen-independence.

Outline Materials and methods

Abstract
Introduction
Materials and methods
Results
Discussion
Competing interests
References

Tables

Table 1
Correlation of PSCA expression with Gleason score

Table 2
Correlation of PSCA expression with clinical stage

Tissue samples

All of the clinical tissue specimens studied herein were obtained from 80 patients of 57–84 years old by prostatectomy, transurethral resection of prostate (TURP) or biopsies. The patients were classified as 20 cases of BPH, 20 cases of PIN, 40 cases of primary Pca, including 9 patients with recurrent Pca and a history of androgen ablation therapy (orchiectomy and/or hormonal therapy), who were referred to as androgen-independent prostate cancers. Eight specimens were harvested from these androgen-independent Pca patients prior to androgen ablation treatment. Each tissue sample was cut into two parts, one was fixed in 10% formalin for IHC and the other treated with 4% paraformaldehyde/0.1 M PBS PH 7.4 in 0.1% DEPC for 1 h for ISH analysis, and then embedded in paraffin. All paraffin blocks examined were then cut into 5 μ m sections and mounted on the glass slides specific for IHC and ISH respectively in the usual fashion. H&E-stained section of each Pca was evaluated and assigned a Gleason score by the experienced urological pathologist at our institution based on the criteria of Gleason score [2]. The Gleason sums are summarized in Table 1. Clinical staging was performed according to Jewett-whitmore-prout staging system, as shown in Table 2. In the category of PIN, we graded the specimens into two groups, i.e. low grade PIN (grade I – II) and high grade PIN (HGPIN, grade III) on the basis of literatures [3,4].

Immunohistochemical (IHC) analysis

Briefly, tissue sections were deparaffinized, dehydrated, and subjected to microwaving in 10 mmol/L citrate buffer, PH 6.0 (Boshide, Wuhan, China) in a 900 W oven for 5 min to induce epitope retrieval. Slides were allowed to cool at room temperature for 30 min. A primary mouse antibody specific to human PSCA (Boshide, Wuhan, China) with a 1:100 dilution was applied to incubate with the slides at room temperature for 2 h. Labeling was detected by sequentially adding biotinylated secondary antibodies and streptavidin-peroxidase, and localized using 3,3'-diaminobenzidine reaction. Sections were then counterstained with hematoxylin. Substitution of the primary antibody with phosphate-buffered-saline (PBS) served as a negative-staining control.

mRNA *in situ* hybridization (ISH)

Five- μ m-thick tissue sections were deparaffinized and dehydrated, then digested in pepsin solution (4 mg/ml in 3% citric acid) for 20 min at 37.5°C, and further processed for ISH. Digoxigenin-labeled sense and antisense human PSCA RNA probes (obtained from Boshide, Wuhan, China) were hybridized to the sections at 48°C overnight. The posthybridization wash with a high stringency was performed sequentially at 37°C in 2 × standard saline citrate (SSC) for 10 min, in 0.5 × SSC for 15 min and in 0.2 × SSC for 30 min. The slides were then incubated to biotinylated mouse anti-digoxigenin antibody at 37.5°C for 1 h followed by washing in 1 × PBS for 20 min at room temperature, and then to streptavidin-peroxidase at 37.5°C for 20 min followed by washing in 1 × PBS for 15 min at room temperature. Subsequently, the slides were developed with diaminobenzidine and then counterstained with hematoxylin to localize the hybridization signals. Sections hybridized with the sense control probes routinely did not show any specific hybridization signal above background. All slides were hybridized with PBS to substitute for the probes as a negative control.

Scoring methods

To determine the correlation between the results of PSCA immunostaining and mRNA *in situ* hybridization, the same scoring manners are taken in the present study for PSCA protein staining by IHC and PSCA mRNA staining by ISH. Each slide was read and scored by two independently experienced urological pathologists using Olympus BX-41 light microscopes. The evaluation was done in a blinded fashion. For each section, five areas of similar grade were analyzed semiquantitatively for the fraction of cells staining. Fifty percent of specimens were randomly chosen and rescored to determine the degree of interobserver and intraobserver concordance. There was greater than 95% intra- and interobserver agreement.

The intensity of PSCA expression evaluated microscopically was graded on a scale of 0 to 3+ with 3 being the highest expression observed (0, no staining; 1+, mildly intense; 2+, moderately intense; 3+, severely intense). The staining density was quantified as the percentage of cells staining positive for PSCA with the primary antibody or hybridization probe, as follows: 0 = no staining; 1 = positive staining in <25% of the sample; 2 = positive staining in 25%–50% of the sample; 3 = positive staining in >50% of the sample. Intensity score (0 to 3+) was multiplied by the density score (0–3) to give an overall score of 0–9 [1,5]. In this way, we were able to differentiate specimens that may have had focal areas of increased staining from those that had diffuse areas of increased staining [6]. The overall score for each specimen was then categorically assigned to one of the following groups: 0 score, negative expression; 1–2 scores, weak expression; 3–6 scores, moderate expression; 9 score, strong expression.

Statistical analysis

Intensity and density of PSCA protein and mRNA expression in BPH, PIN and Pca tissues were compared using the Chi-square and Student's *t*-test. Univariate associations between PSCA expression and Gleason score, clinical stage and progression to androgen-independence were calculated using Fisher's Exact Test. For all analyses, $p < 0.05$ was considered statistically significant.

Outline Results

Abstract
Introduction
Materials and methods
Results
Discussion
Competing interests
References

Figures

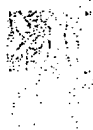


Figure 1
Representatives of PSCA
IHC and ISH staining in Pca
(A. IHC staining, B. ISH
staining, x200
magnification)

PSCA expression in BPH

In general, PSCA protein and mRNA were expressed weakly in individual samples of BPH. Some areas of prostate expressed weak levels (composite score 1–2), whereas other areas were completely negative (composite score 0). Four cases (20%) of BPH had moderate expression of PSCA protein and mRNA (composite score 4–6) by IHC and ISH. In 2/20 (10%) BPH specimens, PSCA mRNA expression was moderate (composite score 3–6), but PSCA protein expression was weak (composite score 2) in one and negative (composite score 0) in the other. PSCA expression was localized to the basal and secretory epithelial cells, and prostatic stroma was almost negative staining for PSCA protein and mRNA in all cases examined.

PSCA expression in PIN

In this study, we detected weak or negative expression of PSCA protein and mRNA (≤ 2 scores) in 7 of 9 (77.8%) low grade PIN and in 2 of 11 (18.2%) HGPIN, and moderate expression (3–6 scores) in the rest 2 low grade PIN and 5 of 11 (45.5%) HGPIN. One HGPIN with moderate PSCA mRNA expression (6 score) was found weak staining for PSCA protein (2 score) by IHC. Strong PSCA protein and mRNA expression (9 score) were detected in the remaining 3 of 11 (27.3%) HGPIN. There was a statistically significant difference of PSCA protein and mRNA expression levels observed between HGPIN and BPH ($p < 0.05$), but no statistical difference reached between low grade PIN and BPH ($p > 0.05$).

PSCA expression in Pca

In order to determine if PSCA protein and mRNA can be detected in prostate cancers and if PSCA expression levels are increased in malignant compared with benign glands, Forty-eight paraffin-embedded Pca specimens were analysed by IHC and ISH. It was shown that 19 of 48 (39.6%) Pca samples stained very strongly for PSCA protein and mRNA with a score of 9 and another 21 (43.8%) specimens displayed moderate staining with scores of 4–6 (Figure 1). In addition, 4 specimens with moderate to strong PSCA mRNA expression (scores of 4–9) had weak protein staining (a score of 2) by IHC analyses. Overall, Pca expressed a significantly higher level of PSCA protein and mRNA than any other specimen category in this study ($p < 0.05$, compared with BPH and PIN respectively). The result demonstrates that PSCA protein and mRNA are overexpressed by a majority of human Pca.

Correlation of PSCA expression with Gleason score in Pca

Using the semi-quantitative scoring method as described in Materials and Methods, we compared the expression level of PSCA protein and mRNA with Gleason grade of Pca, as shown in Table 1. Prostate adenocarcinomas were graded by Gleason score as 2–4 scores = well-differentiation, 5–7 scores = moderate-differentiation and 8–10 scores = poor-differentiation [7]. Seventy-two percent of Gleason scores 8–10 prostate cancers had very

strong staining of PSCA compared to 21% with Gleason scores 5-7 and 17% with 2-4 respectively, demonstrating that poorly differentiated Pca had significantly stronger expression of PSCA protein and mRNA than moderately and well differentiated tumors ($p < 0.05$). As depicted in Figure 1, IHC and ISH analyses showed that PSCA protein and mRNA expression in several cases of poorly differentiated Pca were particularly prominent, with more intense and uniform staining. The results indicate that PSCA expression increases significantly with higher tumor grade in human Pca.

Correlation of PSCA expression with clinical stage in Pca

With regards to PSCA expression in every stage of Pca, we showed the results in Table 2. Seventy-five percent of locally advanced and node positive cancers (i.e. C-D stages) expressed statistically high levels of PSCA versus 32.5% that were organ confined (i.e. A-B stages) ($p < 0.05$). The data demonstrate that PSCA expression increases significantly with advanced tumor stage in human Pca.

Correlation of PSCA expression with androgen-independent progression of Pca

All 9 specimens of androgen-independent prostate cancers stained positive for PSCA protein and mRNA. Eight specimens were obtained from patients managed prior to androgen ablation therapy. Seven of eight (87.5%) of these androgen-independent prostate cancers were in the strongest staining category (score = 9), compared with three out of eight (37.5%) of patients with androgen-dependent cancers ($p < 0.05$). The results demonstrate that PSCA expression increases significantly with progression to androgen-independence of human Pca.

It is evident from the results above that within a majority of human prostate cancers the level of PSCA protein and mRNA expression correlates significantly with increasing grade, worsening stage and progression to androgen-independence.

Correlation of PSCA immunostaining and mRNA *in situ* hybridization

In all 88 specimens surveyed herein, we compared the results of PSCA IHC staining with mRNA ISH analysis. Positive staining areas and its intensity and density scores evaluated by IHC were identical to those seen by ISH in 79 of 88 (89.8%) specimens (18/20 BPH, 19/20 PIN and 42/48 Pca respectively). Importantly, 27/27 samples with PSCA mRNA composite scores of 0-2, 32/36 samples with scores of 3-6 and 22/24 samples with a score of 9 also had PSCA protein expression scores of 0-2, 3-6 and 9 respectively. However, in 5 samples with PSCA mRNA overall scores of 3-6 and in 2 with scores of 9 there were less or negative PSCA protein expression (i.e. scores of 0-4), suggesting that this may reflect posttranscriptional modification of PSCA or that the epitopes recognized by PSCA mAb may be obscured in some cancers. The data demonstrate that the results of PSCA immunostaining were consistent with those of mRNA ISH analysis, showing a high degree of correlation between PSCA protein and mRNA expression.

Outline Discussion

Abstract
Introduction
Materials and methods
Results
Discussion
Competing interests
References

PSCA is homologous to a group of cell surface proteins that mark the earliest phase of hematopoietic development. PSCA mRNA expression is prostate-specific in normal male tissues and is highly up-regulated in both androgen-dependent and-independent Pca xenografts (LAPC-4 tumors). We hypothesize that PSCA may play a role in Pca tumorigenesis and progression, and may serve as a target for Pca diagnosis and treatment. In this study, IHC and ISH showed that in general there were weak or absent PSCA protein and mRNA expression in BPH and low grade PIN tissues. However, PSCA protein and mRNA are widely expressed in HGPIN, the putative precursor of invasive Pca, suggesting that up-regulation of PSCA is an early event in prostate carcinogenesis. Recently, Reiter RE et al [1], using ISH analysis, reported that 97 of 118 (82%) HGPIN specimens stained strongly positive for PSCA mRNA. A very similar finding was seen on mouse PSCA (mPSCA) expression in mouse HGPIN tissues by Tran C. P et al [8]. These data suggest that PSCA may be a new marker associated with transformation of prostate cells and tumorigenesis.

We observed that PSCA protein and mRNA are highly expressed in a large percentage of human prostate cancers, including advanced, poorly differentiated, androgen-independent and metastatic cases. Fluorescence-activated cell sorting and confocal/ immunofluorescent studies demonstrated cell surface expression of PSCA protein in Pca cells [9]. Our IHC expression analysis of PSCA shows not only cell surface but also apparent cytoplasmic staining of PSCA protein in Pca specimens (Figure 1). One possible explanation for this is that anti-PSCA antibody can recognize PSCA peptide precursors that reside in the cytoplasm. Also, it is possible that the positive staining that appears in the cytoplasm is actually from the overlying cell membrane [5]. These data seem to indicate that PSCA is a novel cell surface marker for human Pca.

Our results show that elevated level of PSCA expression correlates with high grade (i.e. poor differentiation), increased tumor stage and progression to androgen-independence of Pca. These findings support the original IHC analyses by Gu Z et al [9], who reported that PSCA protein expressed in 94% of primary Pca and the intensity of PSCA protein expression increased with tumor grade, stage and progression to androgen-independence. Our results also collaborate the recent work of Han KR et al [10], in which the significant association between high PSCA expression and adverse prognostic features such as high Gleason score, seminal vesicle invasion and capsular involvement in Pca was found. It is suggested that PSCA overexpression may be an adverse predictor for recurrence, clinical progression or survival of Pca. Hara H et al [11] used RT-PCR detection of PSA, PSMA and PSCA in 1 ml of peripheral blood to evaluate Pca patients with poor prognosis. The results showed that among 58 Pca patients, each PCR indicated the prognostic value in the hierarchy of PSCA>PSA>PSMA RT-PCR, and extraprostatic cases with positive PSCA PCR indicated lower disease-progression-free survival than those with negative PSCA PCR, demonstrating that PSCA can be used as a prognostic factor. Dubey P et al [12] reported that elevated numbers of PSCA + cells correlate positively with the onset and development of prostate carcinoma over a long time span in the prostates of the TRAMP and PTEN +/- models compared with its

normal prostates. Taken together with our present findings, in which PSCA is overexpressed from HGPIN to almost frank carcinoma, it is reasonable and possible to use increased PSCA expression level or increased numbers of PSCA-positive cells in the prostate samples as a prognostic marker to predict the potential onset of this cancer. These data raise the possibility that PSCA may have diagnostic utility or clinical prognostic value in human Pca.

The cause of PSCA overexpression in Pca is not known. One possible mechanism is that it may result from PSCA gene amplification. In humans, PSCA is located on chromosome 8q24.2 [1], which is often amplified in metastatic and recurrent Pca and considered to indicate a poor prognosis [13-15]. Interestingly, PSCA is in close proximity to the c-myc oncogene, which is amplified in >20% of recurrent and metastatic prostate cancers [16,17]. Reiter RE et al [18] reported that PSCA and MYC gene copy numbers were co-amplified in 25% of tumors (five out of twenty), demonstrating that PSCA overexpression is associated with PSCA and MYC coamplification in Pca. Gu Z et al [9] recently reported that in 102 specimens available to compare the results of PSCA immunostaining with their previous mRNA ISH analysis, 92 (90.2%) had identically positive areas of PSCA protein and mRNA expression. Taken together with our findings, in which we detected moderate to strong expression of PSCA protein and mRNA in 34 of 40 (85%) Pca specimens examined simultaneously by IHC and ISH analyses, it is demonstrated that PSCA protein and mRNA overexpressed in human Pca, and that the increased protein level of PSCA was resulted from the upregulated transcription of its mRNA.

At present, the regulation mechanisms of human PSCA expression and its biological function are yet to be elucidated. PSCA expression may be regulated by multiple factors [18]. Watabe T et al [19] reported that transcriptional control is a major component regulating PSCA expression levels. In addition, induction of PSCA expression may be regulated or mediated through cell-cell contact and protein kinase C (PKC) [20]. Homologues of PSCA have diverse activities, and have themselves been involved in carcinogenesis. Signalling through SCA-2 has been demonstrated to prevent apoptosis in immature thymocytes [21]. Thy-1 is involved in T cell activation and transduces signals through src-like tyrosine kinases [22]. Ly-6 genes have been implicated both in tumorigenesis and in cell-cell adhesion [23-25]. Cell-cell or cell-matrix interaction is critical for local tumor growth and spread to distal sites. From its restricted expression in basal cells of normal prostate and its homology to SCA-2, PSCA may play a role in stem/progenitor cell function, such as self-renewal (i.e. anti-apoptosis) and/or proliferation [1]. Taken together with the results in the present study, we speculate that PSCA may play a role in tumorigenesis and clinical progression of Pca through affecting cell transformation and proliferation. From our results, it is also suggested that PSCA as a new cell surface antigen may have a number of potential uses in the diagnosis, therapy and clinical prognosis of human Pca. PSCA overexpression in prostate biopsies could be used to identify patients at high risk to develop recurrent or metastatic disease, and to discriminate cancers from normal glands in prostatectomy samples. Similarly, the detection of PSCA-overexpressing cells in bone marrow or peripheral blood may identify and predict metastatic progression better than current assays, which identify only PSA-positive or PSMA-positive prostate cells.

In summary, we have shown in this study that PSCA protein and mRNA are maintained in expression from HGPIN through all stages of Pca in a majority of cases, which may be associated with prostate carcinogenesis and correlate positively with high tumor grade (poor cell differentiation), advanced stage and androgen-independent progression. PSCA protein overexpression is due to the upregulation of its mRNA transcription. The results suggest that PSCA may be a promising molecular marker for the clinical prognosis of human Pca and a valuable target for diagnosis and therapy of this tumor.

Competing interests

None declared.

Outline References

Abstract
Introduction
Materials and methods
Results
Discussion
Competing interests
References

1. Reiter RE, Gu Z, Watabe T, Thomas G, Szigeti K, David E, Wahl M, Nisitani S, Yamashiro J, Le Beau MM, Loda M, Witte ON: **Prostate stem cell antigen: a cell surface marker overexpressed in prostate cancer.** *Proc Natl Acad Sci USA* 1998, **95**:1735-1740. [PubMed Abstract] [Publisher Full Text]
Return to citation in text: [1] [2] [3] [4] [5]
2. Gleason DF: **Histologic grading and clinical staging of prostatic carcinoma.** *In: Urologic Pathology: The Prostate (Edited by: Tannebaum M).* Philadelphia, Lea & Febiger 1977, 171-197.
Return to citation in text: [1]
3. Brawer MK: **Prostatic intraepithelial neoplasia: a premalignant lesion.** *Hum Pathol* 1992, **23**:242-248. [PubMed Abstract]
Return to citation in text: [1]
4. Amin MB, Ro JY, Ayala AC: **Prostatic intraepithelial neoplasia: relationship to adenocarcinoma of prostate.** *Pathol Annu* 1994, **29**:1-30. [PubMed Abstract]
Return to citation in text: [1]
5. Amara N, Palapattu GS, Schrage M, Gu Z, Thomas GV, Dorey F, Said J, Reiter RE: **Prostate stem cell antigen is overexpressed in human transitional cell carcinoma.** *Cancer Res* 2001, **61**:4660-4665. [PubMed Abstract] [Publisher Full Text]
Return to citation in text: [1] [2]
6. Hanas JS, Lerner MR, Lightfoot SA, Raczkowski C, Kastens DJ, Brackett DJ, Postier RG: **Expression of the cyclin-dependent kinase inhibitor p21 (WAF1/CIP1) and p53 tumor suppressor in dysplastic progression and adenocarcinoma in Barrett esophagus.** *Cancer (Phila)* 1999, **86**:756-763. [Publisher Full Text]
Return to citation in text: [1]
7. Egevad L, Gramfors T, Karlberg L: **Prognostic value of the Gleason score in prostate cancer.**


BJU Int 2002, **89**:538-542. [PubMed Abstract] [Publisher Full Text]
Return to citation in text: [1]

8. Tran CP, Lin C, Yamashiro J, Reiter RE: **Prostate stem cell antigen is a marker of late intermediate prostate epithelial cells.**
Mol Cancer Res 2002, **1**:113-121. [PubMed Abstract] [Publisher Full Text]
Return to citation in text: [1]
9. Gu Z, Thomas G, Yamashiro J, Shintaku IP, Dorey F, Raitano A, Witte ON, Said JW, Loda M, Reiter RE: **Prostate stem cell antigen (PSCA) expression increases with high Gleason score, advanced stage and bone metastasis in prostate cancer.**
Oncogene 2000, **19**:1288-1296. [PubMed Abstract] [Publisher Full Text]
Return to citation in text: [1] [2] [3]
10. Han KR, Seligson DB, Liu X, Horvath S, Shintaku PI, Thomas GV, Said JW, Reiter RE: **Prostate stem cell antigen expression is associated with gleason score, seminal vesicle invasion and capsular invasion in prostate cancer.**
J Urol 2004, **171**:1117-1121. [PubMed Abstract] [Publisher Full Text]
Return to citation in text: [1]
11. Hara H, Kasahara T, Kawasaki T, Bilim V, Obara K, Takahashi K, Tomita Y: **Reverse Transcription-Polymerase Chain Reaction Detection of Prostate-specific Antigen, Prostate-specific Membrane Antigen, and Prostate Stem Cell Antigen in One Milliliter of Peripheral Blood.**
Clin Cancer Res 2002, **8**:1794-1799. [PubMed Abstract] [Publisher Full Text]
Return to citation in text: [1]
12. Dubey P, Wu H, Reiter RE, Witte ON: **Alternative pathways to prostate carcinoma activate prostate stem cell antigen expression.**
Cancer Res 2001, **61**:3256-3261. [PubMed Abstract] [Publisher Full Text]
Return to citation in text: [1]
13. Visa korpi T, Kallioniemi AH, Syvanen AC, Hyytinen ER, Karhu R, Tammela T, Isola JJ, Kallioniemi OP: **Genetic changes in primary and recurrent prostate cancer by comparative genomic hybridization.**
Cancer Res 1995, **55**:342-347. [PubMed Abstract]
Return to citation in text: [1]
14. Sato K, Qian J, Slezak JM, Lieber MM, Bostwick DG, Bergstralh EJ, Jenkins RB: **Clinical significance of alterations of chromosome 8 in high-grade, advanced, nonmetastatic prostate carcinoma.**
J Natl Cancer Inst 1999, **91**:1574-1580. [PubMed Abstract] [Publisher Full Text]
Return to citation in text: [1]
15. Van Den Berg C, Guan XY, Von Hoff D, Jenkins R, Bittner J, Griffin C, Kallioniemi O, Visakorpi T, McGill J, Herath J, Epstein J, Sarosdy M, Meltzer P, Trent J: **DNA sequence amplification in human prostate cancer identified by chromosome microdissection: potential prognostic implications.**
Clin Cancer Res 1995, **1**:11-18. [PubMed Abstract]
Return to citation in text: [1]
16. Jenkins RB, Qian J, Lieber MM, Bostwick DG: **Detection of c-myc oncogene amplification and chromosomal anomalies in metastatic prostatic carcinoma by fluorescence in situ hybridization.**
Cancer Res 1997, **57**:524-531. [PubMed Abstract]
Return to citation in text: [1]

17. Nupponen NN, Kakkola L, Koivisto P, Visakorpi T: **Genetic alterations in hormone-refractory recurrent prostate carcinomas.**
Am J Pathol 1998, **153**:141-148. [PubMed Abstract] [Publisher Full Text]
Return to citation in text: [1]
18. Reiter RE, Sato I, Thomas G, Qian J, Gu Z, Watabe T, Loda M, Jenkins RB: **Coamplification of prostate stem cell antigen (PSCA) and MYC in locally advanced prostate cancer.**
Genes Chromosomes Cancer 2000, **27**:95-103. [PubMed Abstract] [Publisher Full Text]
Return to citation in text: [1] [2]
19. Watabe T, Lin M, Donjacour AA, Cunha GR, Witte ON, Reiter RE: **Growth, regeneration, and tumorigenesis of the prostate activates the PSCA promoter.**
Proc Natl Acad Sci USA 2002, **99**:401-406. [PubMed Abstract] [Publisher Full Text]
Return to citation in text: [1]
20. Bahrenberg G, Brauers A, Joost HG, Jakse G: **PSCA expression is regulated by phorbol ester and cell adhesion in the bladder carcinoma cell line RT112.**
Cancer Lett 2001, **168**:37-43. [PubMed Abstract] [Publisher Full Text]
Return to citation in text: [1]
21. Noda S, Kosugi A, Saitoh S, Narumiya S, Hamaoka T: **Protection from anti-TCR/CD3-induced apoptosis in immature thymocytes by a signal through thymic shared antigen-1/stem cell antigen-2.**
J Exp Med 1996, **183**:2355-2360. [PubMed Abstract]
Return to citation in text: [1]
22. Thomas PM, Samelson LE: **The glycoposphatidylinositol-anchored Thy-1 molecule interacts with the p60fyn protein tyrosine kinase in T cells.**
J Biol Chem 1992, **267**:12317-12322. [PubMed Abstract] [Publisher Full Text]
Return to citation in text: [1]
23. Bamezai A, Rock KL: **Overexpressed Ly-6A.2 mediated cell-cell adhesion by binding a ligand expressed on lymphoid cells.**
Proc Natl Acad Sci USA 1995, **92**:4294-4298. [PubMed Abstract] [Publisher Full Text]
Return to citation in text: [1]
24. Katz BZ, Eshel R, Sagi-Assif O, Witz IP: **An association between high Ly-6A/E expression on tumor cells and a highly malignant phenotype.**
Int J Cancer 1994, **59**:684-691. [PubMed Abstract]
Return to citation in text: [1]
25. Brakenhoff RH, Gerretsen M, Knippels EM, van Dijk M, van Essen H, Weghuis DO, Sinke RJ, Snow GB, van Dongen GA: **The human E48 antigen, highly homologous to the murine Ly-6 antigen ThB, is a GPI-anchored molecule apparently involved in keratinocyte cell-cell adhesion.**
J Cell Biol 1995, **129**:1677-1689. [PubMed Abstract] [Publisher Full Text]
Return to citation in text: [1]

Have something to say? Post a comment on the article!



Published by  BioMed Central

© 1999-2006 BioMed Central Ltd unless otherwise stated < info@biomedcentral.com > Terms and conditions

Review

Translation Initiation in Cancer: A Novel Target for Therapy¹

Funda Meric² and Kelly K. Hunt

Department of Surgical Oncology, The University of Texas M. D. Anderson Cancer Center, Houston, Texas 77030

Abstract

Translation initiation is regulated in response to nutrient availability and mitogenic stimulation and is coupled with cell cycle progression and cell growth. Several alterations in translational control occur in cancer. Variant mRNA sequences can alter the translational efficiency of individual mRNA molecules, which in turn play a role in cancer biology. Changes in the expression or availability of components of the translational machinery and in the activation of translation through signal transduction pathways can lead to more global changes, such as an increase in the overall rate of protein synthesis and translational activation of the mRNA molecules involved in cell growth and proliferation. We review the basic principles of translational control, the alterations encountered in cancer, and selected therapies targeting translation initiation to help elucidate new therapeutic avenues.

Introduction

The fundamental principle of molecular therapeutics in cancer is to exploit the differences in gene expression between cancer cells and normal cells. With the advent of cDNA array technology, most efforts have concentrated on identifying differences in gene expression at the level of mRNA, which can be attributable either to DNA amplification or to differences in transcription. Gene expression is quite complicated, however, and is also regulated at the level of mRNA stability, mRNA translation, and protein stability.

The power of translational regulation has been best recognized among developmental biologists, because transcription does not occur in early embryogenesis in eukaryotes. For example, in *Xenopus*, the period of transcriptional quiescence continues until the embryo reaches midblastula transition, the 4000-cell stage. Therefore, all necessary mRNA molecules are transcribed during oogenesis and stockpiled in a translationally inactive, masked form. The mRNA are translationally activated at appropriate times during oocyte maturation, fertilization, and

early embryogenesis and thus, are under strict translational control.

Translation has an established role in cell growth. Basically, an increase in protein synthesis occurs as a consequence of mitogenesis. Until recently, however, little was known about the alterations in mRNA translation in cancer, and much is yet to be discovered about their role in the development and progression of cancer. Here we review the basic principles of translational control, the alterations encountered in cancer, and selected therapies targeting translation initiation to elucidate potential new therapeutic avenues.

Basic Principles of Translational Control

Mechanism of Translation Initiation

Translation initiation is the main step in translational regulation. Translation initiation is a complex process in which the initiator tRNA and the 40S and 60S ribosomal subunits are recruited to the 5' end of a mRNA molecule and assembled by eukaryotic translation initiation factors into an 80S ribosome at the start codon of the mRNA (Fig. 1). The 5' end of eukaryotic mRNA is capped, i.e., contains the cap structure m⁷GpppN (7-methyl-guanosine-triphospho-5'-ribonucleoside). Most translation in eukaryotes occurs in a cap-dependent fashion, i.e., the cap is specifically recognized by the eIF4E,³ which binds the 5' cap. The eIF4F translation initiation complex is then formed by the assembly of eIF4E, the RNA helicase eIF4A, and eIF4G, a scaffolding protein that mediates the binding of the 40S ribosomal subunit to the mRNA molecule through interaction with the eIF3 protein present on the 40S ribosome. eIF4A and eIF4B participate in melting the secondary structure of the 5' UTR of the mRNA. The 43S initiation complex (40S/eIF2/Met-tRNA/GTP complex) scans the mRNA in a 5'→3' direction until it encounters an AUG start codon. This start codon is then base-paired to the anticodon of initiator tRNA, forming the 48S initiation complex. The initiation factors are then displaced from the 48S complex, and the 60S ribosome joins to form the 80S ribosome.

Unlike most eukaryotic translation, translation initiation of certain mRNAs, such as the picornavirus RNA, is cap independent and occurs by internal ribosome entry. This mechanism does not require eIF4E. Either the 43S complex can bind the initiation codon directly through interaction with the IRES in the 5' UTR such as in the encephalomyocarditis virus, or it can

Received 5/16/02; revised 7/12/02; accepted 7/22/02.

¹ F. M. is supported by The University of Texas M. D. Anderson Cancer Center Physician-Scientist Program and by NIH Grant 1K08-CA 91895-01. K. K. H. is supported by Department of Defense Award DAMD-17-97-1-7162.

² To whom requests for reprints should be addressed, at Department of Surgical Oncology, Box 444, The University of Texas M. D. Anderson Cancer Center, 1515 Holcombe Boulevard, Houston, TX 77030. Phone: (713) 745-4453; Fax: (713) 745-4926; E-mail: fmeric@mdanderson.org.

³ The abbreviations used are: eIF4E, eukaryotic initiation factor 4E; UTR, untranslated region; IRES, internal ribosome entry site; 4E-BP1, eukaryotic initiation factor 4E-binding protein 1; SGK, ribosomal p70 S6 kinase; mTOR, mammalian target of rapamycin; ATM, ataxia telangiectasia mutated; PI3K, phosphatidylinositol 3-kinase; PTEN, phosphatase and tensin homolog deleted from chromosome 10; PP2A, protein phosphatase 2A; TGF- β 3, transforming growth factor- β 3; PAP, poly(A) polymerase; EPA, eicosapentaenoic acid; mda-7, melanoma differentiation-associated gene 7.

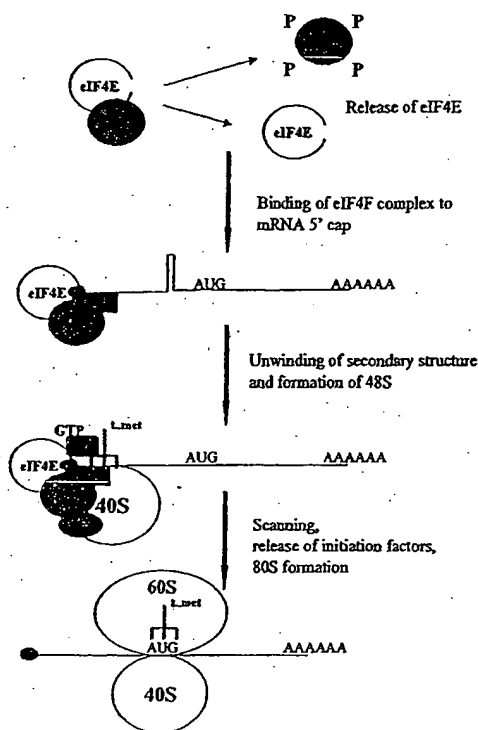


Fig. 1. Translation initiation in eukaryotes. The 4E-BPs are hyperphosphorylated to release eIF4E so that it can interact with the 5' cap, and the eIF4F initiation complex is assembled. The interaction of poly(A) binding protein with the initiation complex and circularization of the mRNA is not depicted in the diagram. The secondary structure of the 5' UTR is melted, the 40S ribosomal subunit is bound to eIF3, and the ternary complex consisting of eIF2, GTP, and the Met-tRNA are recruited to the mRNA. The ribosome scans the mRNA in a 5'→3' direction until an AUG start codon is found in the appropriate sequence context. The initiation factors are released, and the large ribosomal subunit is recruited.

initially attach to the IRES and then reach the initiation codon by scanning or transfer, as is the case with the poliovirus (1).

Regulation of Translation Initiation

Translation initiation can be regulated by alterations in the expression or phosphorylation status of the various factors involved. Key components in translational regulation that may provide potential therapeutic targets follow.

eIF4E. eIF4E plays a central role in translation regulation. It is the least abundant of the initiation factors and is considered the rate-limiting component for initiation of cap-dependent translation. eIF4E may also be involved in mRNA splicing, mRNA 3' processing, and mRNA nucleocytoplasmic transport (2). eIF4E expression can be increased at the transcriptional level in response to serum or growth factors (3). eIF4E overexpression may cause preferential translation of mRNAs containing excessive secondary structure in their 5' UTR that are normally discriminated against by the trans-

lational machinery and thus are inefficiently translated (4–7). As examples of this, overexpression of eIF4E promotes increased translation of vascular endothelial growth factor, fibroblast growth factor-2, and cyclin D1 (2, 8, 9).

Another mechanism of control is the regulation of eIF4E phosphorylation. eIF4E phosphorylation is mediated by the mitogen-activated protein kinase-interacting kinase 1, which is activated by the mitogen-activated pathway activating extracellular signal-related kinases and the stress-activated pathway acting through p38 mitogen-activated protein kinase (10–13). Several mitogens, such as serum, platelet-derived growth factor, epidermal growth factor, insulin, angiotensin II, src kinase overexpression, and ras overexpression, lead to eIF4E phosphorylation (14). The phosphorylation status of eIF4E is usually correlated with the translational rate and growth status of the cell; however, eIF4E phosphorylation has also been observed in response to some cellular stresses when translational rates actually decrease (15). Thus, further study is needed to understand the effects of eIF4E phosphorylation on eIF4E activity.

Another mechanism of regulation is the alteration of eIF4E availability by the binding of eIF4E to the eIF4E-binding proteins (4E-BP, also known as PHAS-I). 4E-BPs compete with eIF4G for a binding site in eIF4E. The binding of eIF4E to the best characterized eIF4E-binding protein, 4E-BP1, is regulated by 4E-BP1 phosphorylation. Hypophosphorylated 4E-BP1 binds to eIF4E, whereas 4E-BP1 hyperphosphorylation decreases this binding. Insulin, angiotensin, epidermal growth factor, platelet-derived growth factor, hepatocyte growth factor, nerve growth factor, insulin-like growth factors I and II, interleukin 3, granulocyte-macrophage colony-stimulating factor + steel factor, gastrin, and the adenovirus have all been reported to induce phosphorylation of 4E-BP1 and to decrease the ability of 4E-BP1 to bind eIF4E (15, 16). Conversely, deprivation of nutrients or growth factors results in 4E-BP1 dephosphorylation, an increase in eIF4E binding, and a decrease in cap-dependent translation.

p70 S6 Kinase. Phosphorylation of ribosomal 40S protein S6 by S6K is thought to play an important role in translational regulation. S6K $-/-$ mouse embryonic cells proliferate more slowly than do parental cells, demonstrating that S6K has a positive influence on cell proliferation (17). S6K regulates the translation of a group of mRNAs possessing a 5' terminal oligopyrimidine tract (5' TOP) found at the 5' UTR of ribosomal protein mRNAs and other mRNAs coding for components of the translational machinery. Phosphorylation of S6K is regulated in part based on the availability of nutrients (18, 19) and is stimulated by several growth factors, such as platelet-derived growth factor and insulin-like growth factor I (20).

eIF2 α Phosphorylation. The binding of the initiator tRNA to the small ribosomal unit is mediated by translation initiation factor eIF2. Phosphorylation of the α -subunit of eIF2 prevents formation of the eIF2/GTP/Met-tRNA complex and inhibits global protein synthesis (21, 22). eIF2 α is phosphorylated under a variety of conditions, such as viral infection, nutrient deprivation, heme deprivation, and apoptosis (22). eIF2 α is phosphorylated by heme-regulated inhibitor, nutrient-regulated protein kinase, and the IFN-induced, double-stranded RNA-activated protein kinase (PKR; Ref. 23).

The mTOR Signaling Pathway. The macrolide antibiotic rapamycin (Siralimus; Wyeth-Ayerst Research, Collegeville, PA) has been the subject of intensive study because it inhibits signal transduction pathways involved in T-cell activation. The rapamycin-sensitive component of these pathways is mTOR (also called FRAP or RAFT1). mTOR is the mammalian homologue of the yeast TOR proteins that regulate G_1 progression and translation in response to nutrient availability (24). mTOR is a serine-threonine kinase that modulates translation initiation by altering the phosphorylation status of 4E-BP1 and S6K (Fig. 2; Ref. 25).

4E-BP1 is phosphorylated on multiple residues. mTOR phosphorylates the Thr-37 and Thr-46 residues of 4E-BP1 *in vitro* (26); however, phosphorylation at these sites is not associated with a loss of eIF4E binding. Phosphorylation of Thr-37 and Thr-46 is required for subsequent phosphorylation at several COOH-terminal, serum-sensitive sites; a combination of these phosphorylation events appears to be needed to inhibit the binding of 4E-BP1 to eIF4E (25). The product of the ATM gene, p38/MSK1 pathway, and protein kinase C α also play a role in 4E-BP1 phosphorylation (27-29).

S6K and 4E-BP1 are also regulated, in part, by PI3K and its downstream protein kinase Akt. PTEN is a phosphatase that negatively regulates PI3K signaling. PTEN null cells have constitutively active Akt, with increased S6K activity and S6 phosphorylation (30). S6K activity is inhibited both by PI3K inhibitors wortmannin and LY294002 and by mTOR inhibitor rapamycin (24). Akt phosphorylates Ser-2448 in mTOR *in vitro*, and this site is phosphorylated upon Akt activation *in vivo* (31-33). Thus, mTOR is regulated by the PI3K/Akt pathway; however, this does not appear to be the only mode of regulation of mTOR activity. Whether the PI3K pathway also regulates S6K and 4E-BP1 phosphorylation independent of mTOR is controversial.

Interestingly, mTOR autophosphorylation is blocked by wortmannin but not by rapamycin (34). This seeming inconsistency suggests that mTOR-responsive regulation of 4E-BP1 and S6K activity occurs through a mechanism other than intrinsic mTOR kinase activity. An alternate pathway for 4E-BP1 and S6K phosphorylation by mTOR activity is by the inhibition of a phosphatase. Treatment with calyculin A, an inhibitor of phosphatases 1 and 2A, reduces rapamycin-induced dephosphorylation of 4E-BP1 and S6K by rapamycin (35). PP2A interacts with full-length S6K but not with a S6K mutant that is resistant to dephosphorylation resulting from rapamycin. mTOR phosphorylates PP2A *in vitro*; however, how this process alters PP2A activity is not known. These results are consistent with the model that phosphorylation of a phosphatase by mTOR prevents dephosphorylation of 4E-BP1 and S6K, and conversely, that nutrient deprivation and rapamycin block inhibition of the phosphatase by mTOR.

Polyadenylation. The poly(A) tail in eukaryotic mRNA is important in enhancing translation initiation and mRNA stability. Polyadenylation plays a key role in regulating gene expression during oogenesis and early embryogenesis. Some mRNA that are translationally inactive in the oocyte are polyadenylated concomitantly with translational activation in oocyte maturation, whereas other mRNAs that are translationally active during oogenesis are deadenylated and trans-

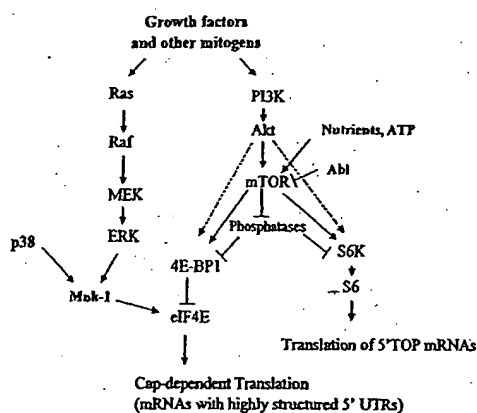


Fig. 2. Regulation of translation initiation by signal transduction pathways. Signaling via p38, extracellular signal-related kinase, PI3K, and mTOR can all activate translation initiation.

lationally silenced (36-38). Thus, control of poly(A) tail synthesis is an important regulatory step in gene expression. The 5' cap and poly(A) tail are thought to function synergistically to regulate mRNA translational efficiency (39, 40).

RNA Packaging. Most RNA-binding proteins are assembled on a transcript at the time of transcription, thus determining the translational fate of the transcript (41). A highly conserved family of Y-box proteins is found in cytoplasmic messenger ribonucleoprotein particles, where the proteins are thought to play a role in restricting the recruitment of mRNA to the translational machinery (41-43). The major mRNA-associated protein, YB-1, destabilizes the interaction of eIF4E and the 5' mRNA cap *in vitro*, and overexpression of YB-1 results in translational repression *in vivo* (44). Thus, alterations in RNA packaging can also play an important role in translational regulation.

Translation Alterations Encountered in Cancer

Three main alterations at the translational level occur in cancer: variations in mRNA sequences that increase or decrease translational efficiency, changes in the expression or availability of components of the translational machinery, and activation of translation through aberrantly activated signal transduction pathways. The first alteration affects the translation of an individual mRNA that may play a role in carcinogenesis. The second and third alterations can lead to more global changes, such as an increase in the overall rate of protein synthesis, and the translational activation of several mRNA species.

Variations in mRNA Sequence

Variations in mRNA sequence affect the translational efficiency of the transcript. A brief description of these variations and examples of each mechanism follow.

Mutations. Mutations in the mRNA sequence, especially in the 5' UTR, can alter its translational efficiency, as seen in the following examples.

c-myc. Saito *et al.* proposed that translation of full-length *c-myc* is repressed, whereas in several Burkitt lymphomas that have deletions of the mRNA 5' UTR, translation of *c-myc* is more efficient (45). More recently, it was reported that the 5' UTR of *c-myc* contains an IRES, and thus *c-myc* translation can be initiated by a cap-independent as well as a cap-dependent mechanism (46, 47). In patients with multiple myeloma, a C→T mutation in the *c-myc* IRES was identified (48) and found to cause an enhanced initiation of translation via internal ribosomal entry (49).

BRCA1. A somatic point mutation (117 G→C) in position -3 with respect to the start codon of the *BRCA1* gene was identified in a highly aggressive sporadic breast cancer (50). Chimeric constructs consisting of the wild-type or mutated *BRCA1* 5' UTR and a downstream luciferase reporter demonstrated a decrease in the translational efficiency with the 5' UTR mutation.

Cyclin-dependent Kinase Inhibitor 2A. Some inherited melanoma kindreds have a G→T transversion at base -34 of cyclin-dependent kinase inhibitor-2A, which encodes a cyclin-dependent kinase 4/cyclin-dependent kinase 6 kinase inhibitor important in G₁ checkpoint regulation (51). This mutation gives rise to a novel AUG translation initiation codon, creating an upstream open reading frame that competes for scanning ribosomes and decreases translation from the wild-type AUG.

Alternate Splicing and Alternate Transcription Start Sites. Alterations in splicing and alternate transcription sites can lead to variations in 5' UTR sequence, length, and secondary structure, ultimately impacting translational efficiency.

ATM. The *ATM* gene has four noncoding exons in its 5' UTR that undergo extensive alternative splicing (52). The contents of 12 different 5' UTRs that show considerable diversity in length and sequence have been identified. These divergent 5' leader sequences play an important role in the translational regulation of the *ATM* gene.

mdm. In a subset of tumors, overexpression of the oncoprotein *mdm2* results in enhanced translation of the *mdm2* mRNA. Use of different promoters leads to two *mdm2* transcripts that differ only in their 5' leaders (53). The longer 5' UTR contains two upstream open reading frames, and this mRNA is loaded with ribosomes inefficiently compared with the short 5' UTR.

BRCA1. In a normal mammary gland, *BRCA1* mRNA is expressed with a shorter leader sequence (5' UTRa), whereas in sporadic breast cancer tissue, *BRCA1* mRNA is expressed with a longer leader sequence (5' UTRb); the translational efficiency of transcripts containing 5' UTRb is 10 times lower than that of transcripts containing 5' UTRa (54).

TGF-β3. *TGF-β3* mRNA includes a 1.1-kb 5' UTR, which exerts an inhibitory effect on translation. Many human breast cancer cell lines contain a novel *TGF-β3* transcript with a 5' UTR that is 870 nucleotides shorter and has a 7-fold greater translational efficiency than the normal *TGF-β3* mRNA (55).

Alternate Polyadenylation Sites. Multiple polyadenylation signals leading to the generation of several transcripts with differing 3' UTR have been described for several mRNA species, such as the *RET* proto-oncogene (56), *ATM* gene (52), tissue inhibitor of metalloproteinases-3 (57), *RHOA*

proto-oncogene (58), and calmodulin-1 (59). Although the effect of these alternate 3' UTRs on translation is not yet known, they may be important in RNA-protein interactions that affect translational recruitment. The role of these alterations in cancer development and progression is unknown.

Alterations in the Components of the Translation Machinery

Alterations in the components of translation machinery can take many forms.

Overexpression of eIF4E. Overexpression of eIF4E causes malignant transformation in rodent cells (60) and the deregulation of HeLa cell growth (61). Polunovsky *et al.* (62) found that eIF4E overexpression substitutes for serum and individual growth factors in preserving viability of fibroblasts, which suggests that eIF4E can mediate both proliferative and survival signaling.

Elevated levels of eIF4E mRNA have been found in a broad spectrum of transformed cell lines (63). eIF4E levels are elevated in all ductal carcinoma *in situ* specimens and invasive ductal carcinomas, compared with benign breast specimens evaluated with Western blot analysis (64, 65). Preliminary studies suggest that this overexpression is attributable to gene amplification (66).

There are accumulating data suggesting that eIF4E overexpression can be valuable as a prognostic marker. eIF4E overexpression was found in a retrospective study to be a marker of poor prognosis in stages I to III breast carcinoma (67). Verification of the prognostic value of eIF4E in breast cancer is now under way in a prospective trial (67). However, in a different study, eIF4E expression was correlated with the aggressive behavior of non-Hodgkin's lymphomas (68). In a prospective analysis of patients with head and neck cancer, elevated levels of eIF4E in histologically tumor-free surgical margins predicted a significantly increased risk of local-regional recurrence (9). These results all suggest that eIF4E overexpression can be used to select patients who might benefit from more aggressive systemic therapy. Furthermore, the head and neck cancer data suggest that eIF4E overexpression is a field defect and can be used to guide local therapy.

Alterations in Other Initiation Factors. Alterations in a number of other initiation factors have been associated with cancer. Overproduction of eIF4G, similar to eIF4E, leads to malignant transformation *in vitro* (69). eIF-2α is found in increased levels in bronchioloalveolar carcinomas of the lung (3). Initiation factor eIF-4A1 is overexpressed in melanoma (70) and hepatocellular carcinoma (71). The p40 subunit of translation initiation factor 3 is amplified and overexpressed in breast and prostate cancer (72), and the eIF3-p110 subunit is overexpressed in testicular seminoma (73). The role that overexpression of these initiation factors plays on the development and progression of cancer, if any, is not known.

Overexpression of S6K. S6K is amplified and highly overexpressed in the MCF7 breast cancer cell line, compared with normal mammary epithelium (74). In a study by Barlund *et al.* (74), S6K was amplified in 59 of 668 primary breast tumors, and a statistically significant association was observed between amplification and poor prognosis.

Overexpression of PAP. PAP catalyzes 3' poly(A) synthesis. PAP is overexpressed in human cancer cells compared with normal and virally transformed cells (75). PAP enzymatic activity in breast tumors has been correlated with PAP protein levels (76) and, in mammary tumor cytosols, was found to be an independent factor for predicting survival (76). Little is known, however, about how PAP expression or activity affects the translational profile.

Alterations in RNA-binding Proteins. Even less is known about alterations in RNA packaging in cancer. Increased expression and nuclear localization of the RNA-binding protein YB-1 are indicators of a poor prognosis for breast cancer (77), non-small cell lung cancer (78), and ovarian cancer (79). However, this effect may be mediated at least in part at the level of transcription, because YB-1 increases chemoresistance by enhancing the transcription of a multidrug resistance gene (80).

Activation of Signal Transduction Pathways

Activation of signal transduction pathways by loss of tumor suppressor genes or overexpression of certain tyrosine kinases can contribute to the growth and aggressiveness of tumors. An important mutant in human cancers is the tumor suppressor gene *PTEN*, which leads to the activation of the PI3K/Akt pathway. Activation of PI3K and Akt induces the oncogenic transformation of chicken embryo fibroblasts. The transformed cells show constitutive phosphorylation of S6K and of 4E-BP1 (81). A mutant Akt that retains kinase activity but does not phosphorylate S6K or 4E-BP1 does not transform fibroblasts, which suggests a correlation between the oncogenicity of PI3K and Akt and the phosphorylation of S6K and 4E-BP1 (81).

Several tyrosine kinases such as platelet-derived growth factor, insulin-like growth factor, HER2/neu, and epidermal growth factor receptor are overexpressed in cancer. Because these kinases activate downstream signal transduction pathways known to alter translation initiation, activation of translation is likely to contribute to the growth and aggressiveness of these tumors. Furthermore, the mRNA for many of these kinases themselves are under translational control. For example, HER2/neu mRNA is translationally controlled both by a short upstream open reading frame that represses HER2/neu translation in a cell type-independent manner and by a distinct cell type-dependent mechanism that increases translational efficiency (82). HER2/neu translation is different in transformed and normal cells. Thus, it is possible that alterations at the translational level can, in part, account for the discrepancy between *HER2/neu* gene amplification detected by fluorescence *in situ* hybridization and protein levels detected by immunohistochemical assays.

Translation Targets of Selected Cancer Therapy

Components of the translation machinery and signal pathways involved in the activation of translation initiation represent good targets for cancer therapy.

Targeting the mTOR Signaling Pathway: Rapamycin and Temstatin

Rapamycin inhibits the proliferation of lymphocytes. It was initially developed as an immunosuppressive drug for organ

transplantation. Rapamycin with FKBP 12 (FK506-binding protein, *M*, 12,000) binds to mTOR to inhibit its function.

Rapamycin causes a small but significant reduction in the initiation rate of protein synthesis (83). It blocks cell growth in part by blocking S6 phosphorylation and selectively suppressing the translation of 5' TOP mRNAs, such as ribosomal proteins, and elongation factors (83–85). Rapamycin also blocks 4E-BP1 phosphorylation and inhibits cap-dependent but not cap-independent translation (17, 86).

The rapamycin-sensitive signal transduction pathway, activated during malignant transformation and cancer progression, is now being studied as a target for cancer therapy (87). Prostate, breast, small cell lung, glioblastoma, melanoma, and T-cell leukemia are among the cancer lines most sensitive to the rapamycin analogue CCI-779 (Wyeth-Ayerst Research; Ref. 87). In rhabdomyosarcoma cell lines, rapamycin is either cytostatic or cytotoxic, depending on the p53 status of the cell; p53 wild-type cells treated with rapamycin arrest in the G₁ phase and maintain their viability, whereas p53 mutant cells accumulate in G₁ and undergo apoptosis (88, 89). In a recently reported study using human primitive neuroectodermal tumor and medulloblastoma models, rapamycin exhibited more cytotoxicity in combination with cisplatin and camptothecin than as a single agent. *In vivo*, CCI-779 delayed growth of xenografts by 160% after 1 week of therapy and 240% after 2 weeks. A single high-dose administration caused a 37% decrease in tumor volume. Growth inhibition *in vivo* was 1.3 times greater, with cisplatin in combination with CCI-779 than with cisplatin alone (90). Thus, preclinical studies suggest that rapamycin analogues are useful as single agents and in combination with chemotherapy.

Rapamycin analogues CCI-779 and RAD001 (Novartis, Basel, Switzerland) are now in clinical trials. Because of the known effect of rapamycin on lymphocyte proliferation, a potential problem with rapamycin analogues is immunosuppression. However, although prolonged immunosuppression can result from rapamycin and CCI-779 administered on continuous-dose schedules, the immunosuppressive effects of rapamycin analogues resolve in ~24 h after therapy (91). The principal toxicities of CCI-779 have included dermatological toxicity, myelosuppression, infection, mucositis, diarrhea, reversible elevations in liver function tests, hyperglycemia, hypokalemia, hypocalcemia, and depression (87, 92–94). Phase II trials of CCI-779 have been conducted in advanced renal cell carcinoma and in stage III/IV breast carcinoma patients who failed with prior chemotherapy. In the results reported in abstract form, although there were no complete responses, partial responses were documented in both renal cell carcinoma and in breast carcinoma (94, 95). Thus, CCI-779 has documented preliminary clinical activity in a previously treated, unselected patient population.

Active investigation is under way into patient selection for mTOR inhibitors. Several studies have found an enhanced efficacy of CCI-779 in PTEN-null tumors (30, 96). Another study found that six of eight breast cancer cell lines were responsive to CCI-779, although only two of these lines lacked PTEN (97). There was, however, a positive correlation between Akt activation and CCI-779 sensitivity (97). This correlation suggests that activation of the PI3K-Akt pathway,

regardless of whether it is attributable to a PTEN mutation or to overexpression of receptor tyrosine kinases, makes cancer cell amenable to mTOR-directed therapy. In contrast, lower levels of the target of mTOR, 4E-BP1, are associated with rapamycin resistance; thus, a lower 4E-BP1/eIF4E ratio may predict rapamycin resistance (98).

Another mode of activity for rapamycin and its analogues appears to be through inhibition of angiogenesis. This activity may be both through direct inhibition of endothelial cell proliferation as a result of mTOR inhibition in these cells or by inhibition of translation of such proangiogenic factors as vascular endothelial growth factor in tumor cells (99, 100).

The angiogenesis inhibitor tustatin, another anticancer drug currently under study, was also found recently to inhibit translation in endothelial cells (101). Through a requisite interaction with integrin, tustatin inhibits activation of the PI3K/Akt pathway and mTOR in endothelial cells and prevents dissociation of eIF4E from 4E-BP1, thereby inhibiting cap-dependent translation. These findings suggest that endothelial cells are especially sensitive to therapies targeting the mTOR-signaling pathway.

Targeting eIF2 α EPA, Clotrimazole, mda-7, and Flavonoids

EPA is an n-3 polyunsaturated fatty acid found in the fish-based diets of populations having a low incidence of cancer (102). EPA inhibits the proliferation of cancer cells (103), as well as in animal models (104, 105). It blocks cell division by inhibiting translation initiation (105). EPA releases Ca²⁺ from intracellular stores while inhibiting their refilling, thereby activating PKR. PKR, in turn phosphorylates and inhibits eIF2 α , resulting in the inhibition of protein synthesis at the level of translation initiation. Similarly, clotrimazole, a potent antiproliferative agent *in vitro* and *in vivo*, inhibits cell growth through depletion of Ca²⁺ stores, activation of PKR, and phosphorylation of eIF2 α (106). Consequently, clotrimazole preferentially decreases the expression of cyclins A, E, and D1, resulting in blockage of the cell cycle in G₁.

mda-7 is a novel tumor suppressor gene being developed as a gene therapy agent. Adenoviral transfer of mda-7 (Ad-mda7) induces apoptosis in many cancer cells including breast, colorectal, and lung cancer (107–109). Ad-mda7 also induces and activates PKR, which leads to phosphorylation of eIF2 α and induction of apoptosis (110).

Flavonoids such as genistein and quercetin suppress tumor cell growth. All three mammalian eIF2 α kinases, PKR, heme-regulated inhibitor, and PERK/PEK, are activated by flavonoids, with phosphorylation of eIF2 α and inhibition of protein synthesis (111).

Targeting eIF4A and eIF4E: Antisense RNA and Peptides

Antisense expression of eIF4A decreases the proliferation rate of melanoma cells (112). Sequestration of eIF4E by overexpression of 4E-BP1 is proapoptotic and decreases tumorigenicity (113, 114). Reduction of eIF4E with antisense RNA decreases soft agar growth, increases tumor latency, and increases the rates of tumor doubling times (7). Antisense eIF4E RNA treat-

ment also reduces the expression of angiogenic factors (115) and has been proposed as a potential adjuvant therapy for head and neck cancers, particularly when elevated eIF4E is found in surgical margins. Small molecule inhibitors that bind the eIF4G/4E-BP1-binding domain of eIF4E are proapoptotic (116) and are also being actively pursued.

Exploiting Selective Translation for Gene Therapy

A different therapeutic approach that takes advantage of the enhanced cap-dependent translation in cancer cells is the use of gene therapy vectors encoding suicide genes with highly structured 5' UTR. These mRNA would thus be at a competitive disadvantage in normal cells and not translate well, whereas in cancer cells, they would translate more efficiently. For example, the introduction of the 5' UTR of fibroblast growth factor-2'5' to the coding sequence of herpes simplex virus type-1 thymidine kinase gene, allows for selective translation of herpes simplex virus type-1 thymidine kinase gene in breast cancer cell lines compared with normal mammary cell lines and results in selective sensitivity to ganciclovir (117).

Toward the Future

Translation is a crucial process in every cell. However, several alterations in translational control occur in cancer. Cancer cells appear to need an aberrantly activated translational state for survival, thus allowing the targeting of translation initiation with surprisingly low toxicity. Components of the translational machinery, such as eIF4E, and signal transduction pathways involved in translation initiation, such as mTOR, represent promising targets for cancer therapy. Inhibitors of the mTOR have already shown some preliminary activity in clinical trials. It is possible that with the development of better predictive markers and better patient selection, response rates to single-agent therapy can be improved. Similar to other cytostatic agents, however, mTOR inhibitors are most likely to achieve clinical utility in combination therapy. In the interim, our increasing understanding of translation initiation and signal transduction pathways promise to lead to the identification of new therapeutic targets in the near future.

Acknowledgments

We thank Gayle Nesom from The University of Texas M. D. Anderson Cancer Center Department of Scientific Publications for editorial assistance and Dr. Elmer Bernstam for assistance with manuscript preparation.

References

1. Pestova, T. V., Kolupaeva, V. G., Lomakin, I. B., Plipenko, E. V., Shatsky, I. N., Agol, V. I., and Hellen, C. U. Molecular mechanisms of translation initiation in eukaryotes. *Proc. Natl. Acad. Sci. USA*, 98: 7029–7036, 2001.
2. Rosenwald, I. B., Kaspar, R., Rousseau, D., Gehrike, L., Leboulch, P., Chen, J. J., Schmidt, E. V., Sonenberg, N., and London, I. M. Eukaryotic translation initiation factor 4E regulates expression of cyclin D1 at transcriptional and post-transcriptional levels. *J. Biol. Chem.*, 270: 21176–21180, 1995.
3. Rosenwald, I. B., Hutzler, M. J., Wang, S., Savas, L., and Fraire, A. E. Expression of eukaryotic translation initiation factors 4E and 2 α is increased frequently in bronchioloalveolar but not in squamous cell carcinomas of the lung. *Cancer (Phila.)*, 92: 2164–2171, 2001.

4. Darveau, A., Pelletier, J., and Sonenberg, N. Differential efficiencies of *in vitro* translation of mouse c-myc transcripts differing in the 5' untranslated region. *Proc. Natl. Acad. Sci. USA*, 82: 2315-2319, 1985.
5. Kozak, M. Influences of mRNA secondary structure on initiation by eukaryotic ribosomes. *Proc. Natl. Acad. Sci. USA*, 83: 2850-2854, 1986.
6. Koromilas, A. E., Lazaris-Karatzas, A., and Sonenberg, N. mRNAs containing extensive secondary structure in their 5' non-coding region translate efficiently in cells overexpressing initiation factor eIF-4E. *EMBO J.*, 11: 4153-4158, 1992.
7. Finkler-Schaeffer, C. W., Graff, J. R., De Benedetti, A., Zimmer, S. G., and Rhoads, R. E. Decreasing the level of translation initiation factor 4E with antisense RNA causes reversal of ras-mediated transformation and tumorigenesis of cloned rat embryo fibroblasts. *Int. J. Cancer*, 55: 841-847, 1993.
8. Kevill, C. G., De Benedetti, A., Payne, D. K., Coe, L. L., Laroux, F. S., and Alexander, J. S. Translational regulation of vascular permeability factor by eukaryotic initiation factor 4E: implications for tumor angiogenesis. *Int. J. Cancer*, 65: 785-790, 1996.
9. Nathan, C. A., Franklin, S., Abreo, F. W., Nassar, R., De Benedetti, A., and Glass, J. Analysis of surgical margins with the molecular marker eIF4E: a prognostic factor in patients with head and neck cancer. *J. Clin. Oncol.*, 17: 2909-2914, 1999.
10. Fukunaga, R., and Hunter, T. MNK1, a new MAP kinase-activated protein kinase, isolated by a novel expression screening method for identifying protein kinase substrates. *EMBO J.*, 16: 1921-1933, 1997.
11. Waskiewicz, A. J., Flynn, A., Proud, C. G., and Cooper, J. A. Mitogen-activated protein kinases activate the serine/threonine kinases Mnk1 and Mnk2. *EMBO J.*, 16: 1909-1920, 1997.
12. Wang, X., Flynn, A., Waskiewicz, A. J., Webb, B. L., Vries, R. G., Baines, I. A., Cooper, J. A., and Proud, C. G. The phosphorylation of eukaryotic initiation factor eIF4E in response to phorbol esters, cell stresses, and cytokines is mediated by distinct MAP kinase pathways. *J. Biol. Chem.*, 273: 9373-9377, 1998.
13. Pyronnet, S., Imataka, H., Gingras, A. C., Fukunaga, R., Hunter, T., and Sonenberg, N. Human eukaryotic translation initiation factor 4G (eIF4G) recruits Mnk1 to phosphorylate eIF4E. *EMBO J.*, 18: 270-279, 1999.
14. Kleijn, M., Scheper, G. C., Voorma, H. O., and Thomas, A. A. Regulation of translation initiation factors by signal transduction. *Eur. J. Biochem.*, 253: 531-544, 1998.
15. Raught, B., and Gingras, A. C. eIF4E activity is regulated at multiple levels. *Int. J. Biochem. Cell Biol.*, 31: 43-57, 1999.
16. Takeuchi, K., Shibamoto, S., Nagamine, K., Shigemori, I., Omura, S., Kitamura, N., and Ito, F. Signaling pathways leading to transcription and translation cooperatively regulate the transient increase in expression of c-Fos protein. *J. Biol. Chem.*, 276: 26077-26083, 2001.
17. Kawasome, H., Papst, P., Webb, S., Keller, G. M., Johnson, G. L., Gelfand, E. W., and Terada, N. Targeted disruption of p70(s6k) defines its role in protein synthesis and rapamycin sensitivity. *Proc. Natl. Acad. Sci. USA*, 95: 5033-5038, 1998.
18. Christie, G. R., Hajdich, E., Hundal, H. S., Proud, C. G., and Taylor, P. M. Intracellular sensing of amino acids in *Xenopus laevis* oocytes stimulates p70 S6 kinase in a target of rapamycin-dependent manner. *J. Biol. Chem.*, 277: 9952-9957, 2002.
19. Hara, K., Yonezawa, K., Weng, Q. P., Kozlowski, M. T., Belham, C., and Avruch, J. Amino acid sufficiency and mTOR regulate p70 S6 kinase and eIF-4E BP1 through a common effector mechanism. *J. Biol. Chem.*, 273: 14484-14494, 1998.
20. Graves, L. M., Bornfeldt, K. E., Argast, G. M., Krebs, E. G., Kong, X., Lin, T. A., and Lawrence, J. C., Jr. cAMP- and rapamycin-sensitive regulation of the association of eukaryotic initiation factor 4E and the translational regulator PHAS-I in aortic smooth muscle cells. *Proc. Natl. Acad. Sci. USA*, 92: 7222-7226, 1995.
21. Merrick, W. C., and Hershey, J. W. B. The pathway and mechanism of eukaryotic protein synthesis. In: J. W. B. Hershey and M. B. Mathews (eds.), *Translational Control*, pp. 31-69. Cold Spring Harbor, NY: Cold Spring Harbor Laboratory, 1996.
22. Kimball, S. R. Eukaryotic initiation factor eIF2. *Int. J. Biochem. Cell Biol.*, 31: 25-29, 1999.
23. Jagus, R., Joshi, B., and Barber, G. N. PKR, apoptosis and cancer. *Int. J. Biochem. Cell Biol.*, 31: 123-138, 1999.
24. Thomas, G., and Hall, M. N. TOR signalling and control of cell growth. *Curr. Opin. Cell Biol.*, 9: 782-787, 1997.
25. Gingras, A. C., Raught, B., and Sonenberg, N. Regulation of translation initiation by FRAP/mTOR. *Genes Dev.*, 15: 807-826, 2001.
26. Gingras, A. C., Gygi, S. P., Raught, B., Polakiewicz, R. D., Abraham, R. T., Hoekstra, M. F., Aebersold, R., and Sonenberg, N. Regulation of 4E-BP1 phosphorylation: a novel two-step mechanism. *Genes Dev.*, 13: 1422-1437, 1999.
27. Kumar, V., Pandey, P., Sabatini, D., Kumar, M., Majumder, P. K., Bharti, A., Carmichael, G., Kufe, D., and Karbhandia, S. Functional interaction between RAFT1/FRAP/mTOR and protein kinase C δ in the regulation of cap-dependent initiation of translation. *EMBO J.*, 19: 1087-1097, 2000.
28. Yang, D. Q., and Kastan, M. B. Participation of ATM in insulin signaling through phosphorylation of eIF-4E-binding protein 1. *Nat. Cell Biol.*, 2: 893-898, 2000.
29. Liu, G., Zhang, Y., Bode, A. M., Ma, W. Y., and Dong, Z. Phosphorylation of 4E-BP1 is mediated by the p38/MSK1 pathway in response to UVB irradiation. *J. Biol. Chem.*, 277: 8810-8816, 2002.
30. Neshat, M. S., Mellinghoff, I. K., Tran, C., Stiles, B., Thomas, G., Petersen, R., Frost, P., Gibbons, J. J., Wu, H., and Sawyers, C. L. Enhanced sensitivity of PTEN-deficient tumors to inhibition of FRAP/mTOR. *Proc. Natl. Acad. Sci. USA*, 98: 10314-10319, 2001.
31. Sekulic, A., Hudson, C. C., Homme, J. L., Yin, P., Ottensmess, D. M., Karnitz, L. M., and Abraham, R. T. A direct linkage between the phosphoinositide 3-kinase-AKT signaling pathway and the mammalian target of rapamycin in mitogen-stimulated and transformed cells. *Cancer Res.*, 60: 3504-3513, 2000.
32. Scott, P. H., and Lawrence, J. C., Jr. Attenuation of mammalian target of rapamycin activity by increased cAMP in 3T3-L1 adipocytes. *J. Biol. Chem.*, 273: 34496-34501, 1998.
33. Reynolds, I. T., Bodine, S. C., and Lawrence, J. C., Jr. Control of Ser2448 phosphorylation in the mammalian target of rapamycin by insulin and skeletal muscle load. *J. Biol. Chem.*, 277: 17657-17662, 2002.
34. Peterson, R. T., Beal, P. A., Comb, M. J., and Schreiber, S. L. FKBP12-rapamycin-associated protein (FRAP) autophosphorylates at serine 2481 under translationally repressive conditions. *J. Biol. Chem.*, 275: 7416-7423, 2000.
35. Peterson, R. T., Desai, B. N., Hardwick, J. S., and Schreiber, S. L. Protein phosphatase 2A interacts with the 70-kDa S6 kinase and is activated by inhibition of FKBP12-rapamycin-associated protein. *Proc. Natl. Acad. Sci. USA*, 96: 4438-4442, 1999.
36. McGrew, L. L., Dworkin-Rastl, E., Dworkin, M. B., and Richter, J. D. Poly(A) elongation during *Xenopus* oocyte maturation is required for translational recruitment and is mediated by a short sequence element. *Genes Dev.*, 3: 803-815, 1989.
37. Sheets, M. D., Wu, M., and Wickens, M. Polyadenylation of c-mos mRNA as a control point in *Xenopus* meiotic maturation. *Nature (Lond.)*, 374: 511-516, 1995.
38. Varnum, S. M., and Wormington, W. M. Deadenylation of maternal mRNAs during *Xenopus* oocyte maturation does not require specific cis-sequences: a default mechanism for translational control. *Genes Dev.*, 4: 2278-2286, 1990.
39. Gafie, D. R. The cap and poly(A) tail function synergistically to regulate mRNA translational efficiency. *Genes Dev.*, 5: 2108-2116, 1991.
40. Sachs, A. B., and Varani, G. Eukaryotic translation initiation: there are (at least) two sides to every story. *Nat. Struct. Biol.*, 7: 356-361, 2000.
41. Wolffe, A. P., and Meric, F. Coupling transcription to translation: a novel site for the regulation of eukaryotic gene expression. *Int. J. Biochem. Cell Biol.*, 28: 247-257, 1996.
42. Evdokimova, V. M., Wei, C. L., Sitkov, A. S., Simonenko, P. N., Lazarev, O. A., Vasilenko, K. S., Ustinov, V. A., Hershey, J. W., and Ovchinnikov, L. P. The major protein of messenger ribonucleoprotein particles in somatic cells is a member of the Y-box binding transcription factor family. *J. Biol. Chem.*, 270: 3186-3192, 1995.
43. Matsumoto, K., Meric, F., and Wolffe, A. P. Translational repression dependent on the interaction of the *Xenopus* Y-box protein FRGY2 with mRNA. Role of the cold shock domain, tail domain, and selective RNA sequence recognition. *J. Biol. Chem.*, 271: 22706-22712, 1996.

44. Eydokimova, V., Ruzanov, P., Imataka, H., Raught, B., Svitkin, Y., Ovchinnikov, L. P., and Sonenberg, N. The major mRNA-associated protein YB-1 is a potent 5' cap-dependent mRNA stabilizer. *EMBO J.*, 20: 5491-5502, 2001.
45. Saito, H., Hayday, A. C., Wiman, K., Hayward, W. S., and Tonegawa, S. Activation of the c-myc gene by translocation: a model for translational control. *Proc. Natl. Acad. Sci. USA*, 80: 7476-7480, 1983.
46. Nanbru, C., Lafon, I., Audigier, S., Gensac, M. C., Vagner, S., Huez, G., and Prats, A. C. Alternative translation of the proto-oncogene c-myc by an internal ribosome entry site. *J. Biol. Chem.*, 272: 32061-32066, 1997.
47. Stoneley, M., Paulin, F. E., Le Quesne, J. P., Chappell, S. A., and Willis, A. E. c-Myc 5' untranslated region contains an internal ribosome entry segment. *Oncogene*, 16: 423-428, 1998.
48. Paulin, F. E., West, M. J., Sullivan, N. F., Whitney, R. L., Lyne, L., and Willis, A. E. Aberrant translational control of the c-myc gene in multiple myeloma. *Oncogene*, 13: 505-513, 1996.
49. Chappell, S. A., LeQuesne, J. P., Paulin, F. E., de Schoolmeester, M. L., Stoneley, M., Soutar, R. L., Ralston, S. H., Hellrich, M. H., and Willis, A. E. A mutation in the c-myc IRES leads to enhanced internal ribosome entry in multiple myeloma: a novel mechanism of oncogene de-regulation. *Oncogene*, 19: 4437-4440, 2000.
50. Signori, E., Bagni, C., Papa, S., Primerano, B., Rinaldi, M., Amaldi, F., and Fazio, V. M. A somatic mutation in the 5'UTR of *BRCA1* gene in sporadic breast cancer causes down-modulation of translation efficiency. *Oncogene*, 20: 4596-4600, 2001.
51. Liu, L., Diworich, D., Gao, L., Monzon, J., Summers, A., Lassam, N., and Hogg, D. Mutation of the CDKN2A 5' UTR creates an aberrant initiation codon and predisposes to melanoma. *Nat. Genet.*, 21: 128-132, 1999.
52. Savitsky, K., Platzer, M., Uziel, T., Gilad, S., Sarti, A., Rosenthal, A., Elroy-Stein, O., Shih, Y., and Rotman, G. Ataxia-telangiectasia: structural diversity of untranslated sequences suggests complex post-transcriptional regulation of *ATM* gene expression. *Nucleic Acids Res.*, 25: 1678-1684, 1997.
53. Brown, C. Y., Mize, G. J., Pineda, M., George, D. L., and Morris, D. R. Role of two upstream open reading frames in the translational control of oncogene *mdm2*. *Oncogene*, 18: 5631-5637, 1999.
54. Sobczak, K., and Krzyzosiak, W. J. Structural determinants of *BRCA1* translational regulation. *J. Biol. Chem.*, 277: 17349-17358, 2002.
55. Arrick, B. A., Grendell, R. L., and Griffin, L. A. Enhanced translational efficiency of a novel transforming growth factor $\beta 3$ mRNA in human breast cancer cells. *Mol. Cell. Biol.*, 14: 619-628, 1994.
56. Myers, S. M., Eng, C., Ponder, B. A., and Mulligan, L. M. Characterization of *RET* proto-oncogene 3' splicing variants and polyadenylation sites: a novel C-terminus for *RET*. *Oncogene*, 11: 2039-2045, 1995.
57. Byrne, J. A., Tomasello, C., Rouyer, N., Bellocq, J. P., Rio, M. C., and Basset, P. The tissue inhibitor of metalloproteinases-3 gene in breast carcinoma: identification of multiple polyadenylation sites and a stromal pattern of expression. *Mol. Med.*, 7: 418-427, 1995.
58. Moscow, J. A., He, R., Gudas, J. M., and Cowan, K. H. Utilization of multiple polyadenylation signals in the human *RHOA* protooncogene. *Gene (Amst.)*, 144: 229-236, 1994.
59. Senterre-Lesentants, S., Alag, A. S., and Sobel, M. E. Multiple mRNA species are generated by alternate polyadenylation from the human *calmodulin-1* gene. *J. Cell. Biochem.*, 58: 445-454, 1995.
60. Lazaris-Karatzas, A., Montine, K. S., and Sonenberg, N. Malignant transformation by a eukaryotic initiation factor subunit that binds to mRNA 5' cap. *Nature (Lond.)*, 345: 544-547, 1990.
61. De Benedetti, A., and Rhoads, R. E. Overexpression of eukaryotic protein synthesis initiation factor 4E in HeLa cells results in aberrant growth and morphology. *Proc. Natl. Acad. Sci. USA*, 87: 8212-8216, 1990.
62. Potunovsky, V. A., Rosenwald, I. B., Tan, A. T., White, J., Chiang, L., Sonenberg, N., and Blitman, P. B. Translational control of programmed cell death: eukaryotic translation initiation factor 4E blocks apoptosis in growth-factor-restricted fibroblasts with physiologically expressed or de-regulated Myc. *Mol. Cell. Biol.*, 16: 6573-6581, 1996.
63. Miyagi, Y., Sugiyama, A., Asai, A., Okazaki, T., Kuchino, Y., and Kerr, S. J. Elevated levels of eukaryotic translation initiation factor eIF-4E mRNA in a broad spectrum of transformed cell lines. *Cancer Lett.*, 97: 247-252, 1995.
64. Kerekatte, V., Smiley, K., Hu, B., Smith, A., Gelder, F., and De Benedetti, A. The proto-oncogene/translation factor eIF4E: a survey of its expression in breast carcinomas. *Int. J. Cancer*, 64: 27-31, 1995.
65. Li, B. D., Liu, L., Dawson, M., and De Benedetti, A. Overexpression of eukaryotic initiation factor 4E (eIF4E) in breast carcinoma. *Cancer (Phila.)*, 79: 2385-2390, 1997.
66. Sorrells, D. L., Black, D. R., Meschonat, C., Rhoads, R., De Benedetti, A., Gao, M., Williams, B. J., and Li, B. D. Detection of eIF4E gene amplification in breast cancer by competitive PCR. *Ann. Surg. Oncol.*, 5: 232-237, 1998.
67. Li, B. D., McDonald, J. C., Nassar, R., and De Benedetti, A. Clinical outcome in stage I to III breast carcinoma and eIF4E overexpression. *Ann. Surg.*, 227: 756-761; discussion, 761-763, 1998.
68. Wang, S., Rosenwald, I. B., Hutzler, M. J., Pihan, G. A., Savas, L., Chen, J. J., and Woda, B. A. Expression of the eukaryotic translation initiation factors 4E and 2a in non-Hodgkin's lymphomas. *Am. J. Pathol.*, 155: 247-255, 1999.
69. Fukuchi-Shimogori, T., Ishii, I., Kashiwagi, K., Mashiba, H., Ekimoto, H., and Igarashi, K. Malignant transformation by overproduction of translation initiation factor eIF4G. *Cancer Res.*, 57: 5041-5044, 1997.
70. Eberle, J., Krasagakis, K., and Orfanos, C. E. Translation initiation factor eIF-4A1 mRNA is consistently overexpressed in human melanoma cells *in vitro*. *Int. J. Cancer*, 71: 396-401, 1997.
71. Shuda, M., Kondoh, N., Tanaka, K., Ryo, A., Wakatsuki, T., Hada, A., Goseki, N., Igari, T., Hatsuse, K., Aihara, T., Horiuchi, S., Shichita, M., Yamamoto, N., and Yamamoto, M. Enhanced expression of translation factor mRNAs in hepatocellular carcinoma. *Anticancer Res.*, 20: 2489-2494, 2000.
72. Nupponen, N. N., Porkka, K., Kakkola, L., Tanner, M., Persson, K., Borg, A., Isola, J., and Visakorpi, T. Amplification and overexpression of p40 subunit of eukaryotic translation initiation factor 3 in breast and prostate cancer. *Am. J. Pathol.*, 154: 1777-1783, 1999.
73. Rothe, M., Ko, Y., Albers, P., and Wernert, N. Eukaryotic initiation factor 3 p110 mRNA is overexpressed in testicular seminomas. *Am. J. Pathol.*, 157: 1597-1604, 2000.
74. Barkind, M., Forozan, F., Kononen, J., Bubendorf, L., Chen, Y., Bittner, M. L., Thorhorst, J., Haas, P., Bucher, C., Sauter, G., Kallioniemi, O. P., and Kallioniemi, A. Detecting activation of ribosomal protein S6 kinase by complementary DNA and tissue microarray analysis. *J. Natl. Cancer Inst. (Bethesda)*, 92: 1252-1259, 2000.
75. Topalian, S. L., Kaneko, S., Gonzales, M. I., Bond, G. L., Ward, Y., and Manley, J. L. Identification and functional characterization of neo-poly(A) polymerase, an RNA processing enzyme overexpressed in human tumors. *Mol. Cell. Biol.*, 21: 5614-5623, 2001.
76. Scorilas, A., Taleri, M., Ardavanis, A., Courtis, N., Dimitriadis, E., Yotis, J., Tsiapalis, C. M., and Tringias, T. Polyadenylate polymerase enzymatic activity in mammary tumor cytosols: a new independent prognostic marker in primary breast cancer. *Cancer Res.*, 60: 5427-5433, 2000.
77. Janz, M., Harbeck, N., Dettmar, P., Berger, U., Schmidt, K., Jurchott, K., Schmitt, M., and Royer, H. D. Y-box factor YB-1 predicts drug resistance and patient outcome in breast cancer independent of clinically relevant tumor biologic factors HER2, uPA and PAI-1. *Int. J. Cancer*, 97: 278-282, 2002.
78. Shibahara, K., Sugio, K., Osaki, T., Uchiyama, T., Maehara, Y., Kohno, K., Yasumoto, K., Sugimachi, K., and Kuwano, M. Nuclear expression of the Y-box binding protein, YB-1, as a novel marker of disease progression in non-small cell lung cancer. *Clin. Cancer Res.*, 7: 3151-3155, 2001.
79. Kamura, T., Yahata, H., Amada, S., Ogawa, S., Sonoda, T., Kobayashi, H., Mitumoto, M., Kohno, K., Kuwano, M., and Nakano, H. Is nuclear expression of Y box-binding protein-1 a new prognostic factor in ovarian serous adenocarcinoma? *Cancer (Phila.)*, 85: 2450-2454, 1999.
80. Borgov, R. C., Jurchott, K., Wagener, C., Bergmann, S., Metzner, S., Bonmert, K., Mapara, M. Y., Winzer, K. J., Dietel, M., Dorken, B., and Royer, H. D. Nuclear localization and increased levels of transcription factor YB-1 in primary human breast cancers are associated with intrinsic *MDR1* gene expression. *Nat. Med.*, 3: 447-450, 1997.
81. Aoki, M., Blazek, E., and Vogt, P. K. A role of the kinase mTOR in cellular transformation induced by the oncoproteins P3k and Akt. *Proc. Natl. Acad. Sci. USA*, 98: 136-141, 2001.
82. Child, S. J., Miller, M. K., and Geballe, A. P. Cell type-dependent and -independent control of HER-2/neu translation. *Int. J. Biochem. Cell Biol.*, 31: 201-213, 1999.

83. Jefferies, H. B., Reinhard, C., Kozma, S. C., and Thomas, G. Rapamycin selectively represses translation of the "polypyrimidine tract" mRNA family. *Proc. Natl. Acad. Sci. USA*, 91: 4441-4445, 1994.
84. Terada, N., Patel, H. R., Takase, K., Kohno, K., Naim, A. C., and Gelfand, E. W. Rapamycin selectively inhibits translation of mRNAs encoding elongation factors and ribosomal proteins. *Proc. Natl. Acad. Sci. USA*, 91: 11477-11481, 1994.
85. Jefferies, H. B., Fumagalli, S., Dennis, P. B., Reinhard, C., Pearson, R. B., and Thomas, G. Rapamycin suppresses 5' TOP mRNA translation through inhibition of p70S6k. *EMBO J.*, 16: 3693-3704, 1997.
86. Beretta, L., Gingras, A. C., Svltin, Y. V., Hall, M. N., and Sonenberg, N. Rapamycin blocks the phosphorylation of 4E-BP1 and inhibits cap-dependent initiation of translation. *EMBO J.*, 15: 658-664, 1996.
87. Hidalgo, M., and Rowinsky, E. K. The rapamycin-sensitive signal transduction pathway as a target for cancer therapy. *Oncogene*, 19: 6680-6686, 2000.
88. Hosoi, H., Dilling, M. B., Shikata, T., Liu, L. N., Shu, L., Ashmun, R. A., Germain, G. S., Abraham, R. T., and Houghton, P. J. Rapamycin causes poorly reversible inhibition of mTOR and induces p53-independent apoptosis in human rhabdomyosarcoma cells. *Cancer Res.*, 59: 886-894, 1999.
89. Huang, S., and Houghton, P. J. Resistance to rapamycin: a novel anticancer drug. *Cancer Metastasis Rev.*, 20: 69-78, 2001.
90. Georger, B., Kerr, K., Tang, C. B., Fung, K. M., Powell, B., Sutton, L. N., Phillips, P. C., and Janss, A. J. Antitumor activity of the rapamycin analog CCI-779 in human primitive neuroectodermal tumor/medulloblastoma models as single agent and in combination chemotherapy. *Cancer Res.*, 61: 1527-1532, 2001.
91. Gibbons, J. J., Discalini, C., Peterson, R., Hernandez, R., Skotnicki, J., and Frost, P. The effect of CCI-779, a novel macrolide anti-tumor agent, on the growth of human tumor cells *in vitro* and in nude mouse xenografts *in vivo*. *Proc. Am. Assoc. Cancer Res.*, 40: 301, 1999.
92. Hidalgo, M., Rowinsky, E., Erlichman, C., Marshall, B., Marks, R., Edwards, T., and Buckner, J. J. A Phase I and pharmacological study of CCI-779 cycle inhibitor. *Ann. Oncol.*, 11 (Suppl. 4): 133, 2001.
93. Alexandre, J., Raymond, E., Depenbrock, H., Mekhaldi, S., Angevin, E., Paillet, C., Hanauske, A., Frisch, J., Feussner, A., and Armand, J. P. CCI-779, a new rapamycin analog, has antitumor activity at doses inducing only mild cutaneous effects and mucositis: early results of an ongoing Phase I study. *Proceedings of the 1999 AACR-NCI-EORTC International Conference, Clin. Cancer Res.*, 5 (Suppl.): 3730s, 1999.
94. Chan, S., Johnston, S., Scheulen, M. E., Mross, K., Morant, A., Lahr, A., Feussner, A., Berger, M., and Kirsch, T. First report: a Phase 2 study of the safety and activity of CCI-779 for patients with locally advanced or metastatic breast cancer failing prior chemotherapy. *Proc. Am. Soc. Clin. Oncol.*, 21: 44a, 2002.
95. Atkins, M. B., Hidalgo, M., Stadler, W., Logan, T., Dutcher, J. P., Hudes, G., Park, Y., Marshall, B., Boni, J., and Dukat, G. A randomized double-blind Phase 2 study of intravenous CCI-779 administered weekly to patients with advanced renal cell carcinoma. *Proc. Am. Soc. Clin. Oncol.*, 21: 10a, 2002.
96. Smith, S. G., Trinh, C. M., Inge, L. J., Thomas, G., Cloughesy, T. F., Sawyers, C. L., and Mischel, P. S. PTEN expression status predicts glioblastoma cell sensitivity to CCI-779. *Proc. Am. Assoc. Cancer Res.*, 43: 335, 2002.
97. Yu, K., Toral-Barza, L., Discalini, C., Zhang, W. G., Skotnicki, J., Frost, P., and Gibbons, J. J. mTOR, a novel target in breast cancer: the effect of CCI-779, an mTOR inhibitor, in preclinical models of breast cancer. *Endocr. Relat. Cancer*, 8: 249-258, 2001.
98. Dilling, M. B., Germain, G. S., Dudkin, L., Jayaraman, A. L., Zhang, X., Harwood, F. C., and Houghton, P. J. 4E-binding proteins, the suppressors of eukaryotic initiation factor 4E, are downregulated in cells with acquired or intrinsic resistance to rapamycin. *J. Biol. Chem.*, 277: 13907-13917, 2002.
99. Guba, M., von Breitenbuch, P., Steinhilber, M., Koehl, G., Flegel, S., Hornung, M., Bruns, C. J., Zuelke, C., Farkas, S., Anthuber, M., Jauch, K. W., and Geissler, E. K. Rapamycin inhibits primary and metastatic tumor growth by antiangiogenesis: involvement of vascular endothelial growth factor. *Nat. Med.*, 8: 128-135, 2002.
100. Lane, H. A., Schell, C., Theuer, A., O'Reilly, T., and Wood, J. Anti-angiogenic activity of RAD001, an orally active anticancer agent. *Proc. Am. Assoc. Cancer Res.*, 43: 184, 2002.
101. Maeshima, Y., Suchak, A., Lively, J. C., Ueki, K., Kharbada, S., Kahn, C. R., Sonenberg, N., Hynes, R. O., and Kalluri, R. Tumstatin, an endothelial cell-specific inhibitor of protein synthesis. *Science (Wash. DC)*, 295: 140-143, 2002.
102. Caygill, C. P., Charlett, A., and Hill, M. J. Fat, fish oil and cancer. *Br. J. Cancer*, 74: 159-164, 1996.
103. Falconer, J. S., Ross, J. A., Fearon, K. C., Hawkins, R. A., O'Riordan, M. G., and Carter, D. C. Effect of eicosapentaenoic acid and other fatty acids on the growth *in vitro* of human pancreatic cancer cell lines. *Br. J. Cancer*, 69: 826-832, 1994.
104. Noguchi, M., Minami, M., Yagasaki, R., Kinoshita, K., Earschi, M., Kitagawa, H., Taniya, T., and Miyazaki, I. Chemoprevention of DMBA-induced mammary carcinogenesis in rats by low-dose EPA and DHA. *Br. J. Cancer*, 75: 348-353, 1997.
105. Palakurthi, S. S., Fluckiger, R., Aktas, H., Changolkar, A. K., Shah-safaei, A., Hameil, S., Klic, E., and Halperin, J. A. Inhibition of translation initiation mediates the anticancer effect of the n-3 polyunsaturated fatty acid eicosapentaenoic acid. *Cancer Res.*, 60: 2919-2925, 2000.
106. Aktas, H., Fluckiger, R., Acosta, J. A., Savage, J. M., Palakurthi, S. S., and Halperin, J. A. Depletion of intracellular Ca^{2+} stores, phosphorylation of eIF2 α , and sustained inhibition of translation initiation mediate the anticancer effects of clonazepam. *Proc. Natl. Acad. Sci. USA*, 95: 8280-8285, 1998.
107. Mhashilkar, A. M., Schrock, R. D., Hindi, M., Liao, J., Sieger, K., Kourouma, F., Zou-Yang, X. H., Onishi, E., Takhi, O., Vedvick, T. S., Fanger, G., Stewart, L., Watson, G. J., Snary, D., Fisher, P. B., Saeki, T., Roth, J. A., Ramesh, R., and Chada, S. Melanoma differentiation associated gene-7 (*mda-7*): a novel anti-tumor gene for cancer gene therapy. *Mol. Med.*, 7: 271-282, 2001.
108. Su, Z. Z., Madreddi, M. T., Lin, J. J., Young, C. S., Kladu, S., Reed, J. C., Goldstein, N. I., and Fisher, P. B. The cancer growth suppressor gene *mda-7* selectively induces apoptosis in human breast cancer cells and inhibits tumor growth in nude mice. *Proc. Natl. Acad. Sci. USA*, 95: 14400-14405, 1998.
109. Saeki, T., Mhashilkar, A., Chada, S., Branch, C., Roth, J. A., and Ramesh, R. Tumor-suppressive effects by adenovirus-mediated *mda-7* gene transfer in non-small cell lung cancer cell *in vitro*. *Gene Ther.*, 7: 2051-2057, 2000.
110. Palta, A., Vorburger, S. A., Barber, G. N., Chada, S., Mhashilkar, A. M., Zou-Yang, H., Stewart, A. L., Balachandran, S., Roth, J. A., Hunt, K. K., and Swisher, S. G. Adenoviral transfer of the melanoma differentiation-associated gene 7 (*mda-7*) induces apoptosis of lung cancer cells via up-regulation of the double-stranded RNA-dependent protein kinase (PKR). *Cancer Res.*, 62: 2239-2243, 2002.
111. Ito, T., Warnken, S. P., and May, W. S. Protein synthesis inhibition by flavonoids: roles of eukaryotic initiation factor 2 α kinases. *Biochem. Biophys. Res. Commun.*, 265: 589-594, 1999.
112. Eberle, J., Fecker, L. F., Bittner, J. U., Orfanos, C. E., and Geilen, C. C. Decreased proliferation of human melanoma cell lines caused by antisense RNA against translation factor eIF-4A1. *Br. J. Cancer*, 86: 1957-1962, 2002.
113. Polunovsky, V. A., Gingras, A. C., Sonenberg, N., Peterson, M., Tan, A., Rubins, J. B., Manivel, J. C., and Bitterman, P. B. Translational control of the antiapoptotic function of Ras. *J. Biol. Chem.*, 275: 24776-24780, 2000.
114. D'Cunha, J., Kratzke, M. G., Alter, M. D., Polunovsky, V. A., Bitterman, P. B., and Kratzke, R. A. Over-expression of the translational repressor 4E-BP1 inhibits NSCLC tumorigenicity *in vivo*. *Proc. Am. Assoc. Cancer Res.*, 43: 816-817, 2002.
115. DeFatta, R. J., Nathan, C. A., and De Benedetti, A. Antisense RNA to eIF4E suppresses oncogenic properties of a head and neck squamous cell carcinoma cell line. *Laryngoscope*, 110: 928-933, 2000.
116. Herbert, T. P., Fahraeus, R., Prescott, A., Lane, D. P., and Proud, C. G. Rapid induction of apoptosis mediated by peptides that bind initiation factor eIF4E. *Curr. Biol.*, 10: 793-796, 2000.
117. DeFatta, R. J., Li, Y., and De Benedetti, A. Selective killing of cancer cells based on translational control of a suicide gene. *Cancer Gene Ther.*, 9: 573-578, 2002.

Genome-wide Study of Gene Copy Numbers, Transcripts, and Protein Levels in Pairs of Non-invasive and Invasive Human Transitional Cell Carcinomas*

Torben F. Ørntoft†§, Thomas Thykjaer¶, Frederic M. Waldman||, Hans Wolf**, and Julio E. Celis‡†

Gain and loss of chromosomal material is characteristic of bladder cancer, as well as malignant transformation in general. The consequences of these changes at both the transcription and translation levels is at present unknown partly because of technical limitations. Here we have attempted to address this question in pairs of non-invasive and invasive human bladder tumors using a combination of technology that included comparative genomic hybridization, high density oligonucleotide array-based monitoring of transcript levels (5600 genes), and high resolution two-dimensional gel electrophoresis. The results showed that there is a gene dosage effect that in some cases superimposes on other regulatory mechanisms. This effect depended ($p < 0.015$) on the magnitude of the comparative genomic hybridization change. In general (18 of 23 cases), chromosomal areas with more than 2-fold gain of DNA showed a corresponding increase in mRNA transcripts. Areas with loss of DNA, on the other hand, showed either reduced or unaltered transcript levels. Because most proteins resolved by two-dimensional gels are unknown it was only possible to compare mRNA and protein alterations in relatively few cases of well focused abundant proteins. With few exceptions we found a good correlation ($p < 0.005$) between transcript alterations and protein levels. The implications, as well as limitations, of the approach are discussed. *Molecular & Cellular Proteomics* 1:37–45, 2002.

Aneuploidy is a common feature of most human cancers (1), but little is known about the genome-wide effect of this

phenomenon at both the transcription and translation levels. High throughput array studies of the breast cancer cell line BT474 has suggested that there is a correlation between DNA copy numbers and gene expression in highly amplified areas (2), and studies of individual genes in solid tumors have revealed a good correlation between gene dose and mRNA or protein levels in the case of c-erb-B2, cyclin D1, *ems1*, and N-myc (3–5). However, a high cyclin D1 protein expression has been observed without simultaneous amplification (4), and a low level of c-myc copy number increase was observed without concomitant c-myc protein overexpression (6).

In human bladder tumors, karyotyping, fluorescent *in situ* hybridization, and comparative genomic hybridization (CGH)¹ have revealed chromosomal aberrations that seem to be characteristic of certain stages of disease progression. In the case of non-invasive pTa transitional cell carcinomas (TCCs), this includes loss of chromosome 9 or parts of it, as well as loss of Y in males. In minimally invasive pT1 TCCs, the following alterations have been reported: 2q–, 11p–, 1q+, 11q13+, 17q+, and 20q+ (7–12). It has been suggested that these regions harbor tumor suppressor genes and oncogenes; however, the large chromosomal areas involved often contain many genes, making meaningful predictions of the functional consequences of losses and gains very difficult.

In this investigation we have combined genome-wide technology for detecting genomic gains and losses (CGH) with gene expression profiling techniques (microarrays and proteomics) to determine the effect of gene copy number on transcript and protein levels in pairs of non-invasive and invasive human bladder TCCs.

EXPERIMENTAL PROCEDURES

Material—Bladder tumor biopsies were sampled after informed consent was obtained and after removal of tissue for routine pathology examination. By light microscopy tumors 335 and 532 were staged by an experienced pathologist as pTa (superficial papillary),

From the †Department of Clinical Biochemistry, Molecular Diagnostic Laboratory and ‡Department of Urology, Aarhus University Hospital, Skejby, DK-8200 Aarhus N, Denmark, §AROS Applied Biotechnology ApS, Gustav Wiedsvvej 10, DK-8000 Aarhus C, Denmark, ¶UCSF Cancer Center and Department of Laboratory Medicine, University of California, San Francisco, CA 94143-0808, and ||Institute of Medical Biochemistry and Danish Centre for Human Genome Research, Ole Worms Allé 170, Aarhus University, DK-8000 Aarhus C, Denmark

Received, September 26, 2001, and in revised form, November 7, 2001

Published, MCP Papers in Press, November 13, 2001, DOI 10.1074/mcp.M100019-MCP200

¹ The abbreviations used are: CGH, comparative genomic hybridization; TCC, transitional cell carcinoma; LOH, loss of heterozygosity; PA-FABP, psoriasis-associated fatty acid-binding protein; 2D, two-dimensional.

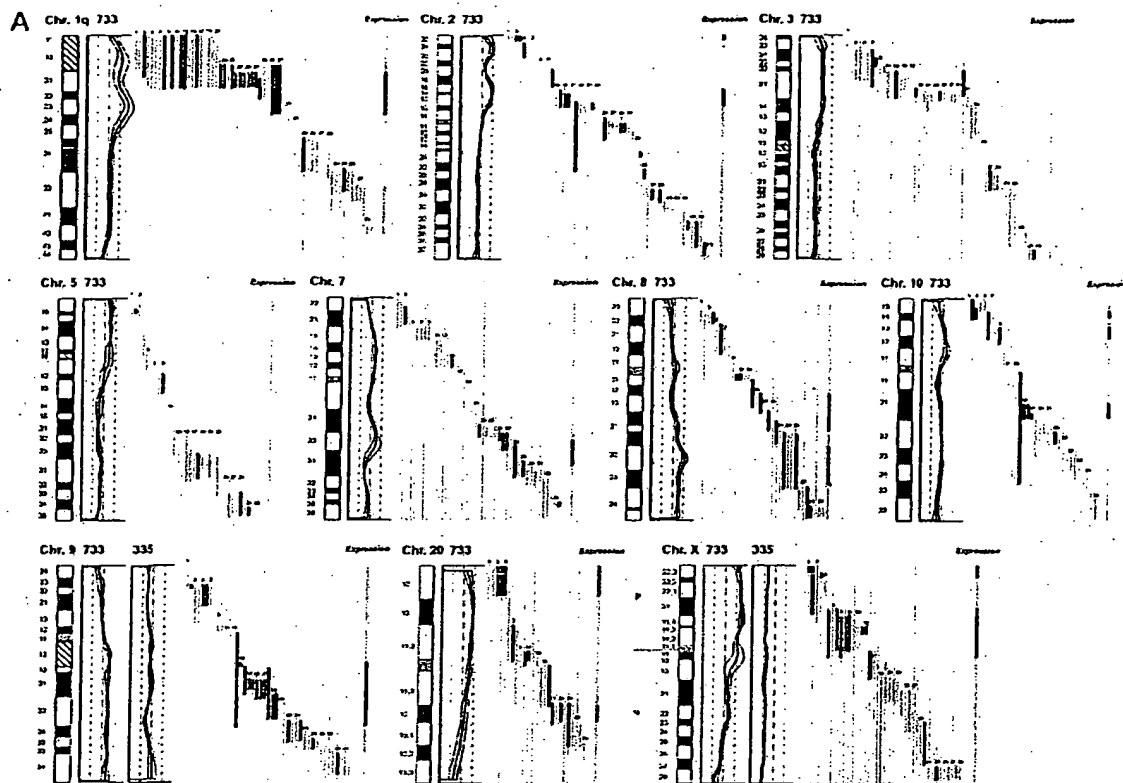


Fig. 1. DNA copy number and mRNA expression level. Shown from left to right are chromosome (Chr.), CGH profiles, gene location and expression level of specific genes, and overall expression level along the chromosome. **A**, expression of mRNA in invasive tumor 733 as compared with the non-invasive counterpart tumor 335. **B**, expression of mRNA in invasive tumor 827 compared with the non-invasive counterpart tumor 532. The average fluorescent signal ratio between tumor DNA and normal DNA is shown along the length of the chromosome (left). The bold curve in the ratio profile represents a mean of four chromosomes and is surrounded by thin curves indicating one standard deviation. The central vertical line (broken) indicates a ratio value of 1 (no change), and the vertical lines next to it (dotted) indicate a ratio of 0.5 (left) and 2.0 (right). In chromosomes where the non-invasive tumor 335 used for comparison showed alterations in DNA content, the ratio profile of that chromosome is shown to the right of the invasive tumor profile. The colored bars represents one gene each, identified by the running numbers above the bars (the name of the gene can be seen at www.MDL.DK/sdata.html). The bars indicate the purported location of the gene, and the colors indicate the expression level of the gene in the invasive tumor compared with the non-invasive counterpart; >2-fold increase (black), >2-fold decrease (blue), no significant change (orange). The bar to the far right, entitled *Expression* shows the resulting change in expression along the chromosome; the colors indicate that at least half of the genes were up-regulated (black), at least half of the genes down-regulated (blue), or more than half of the genes are unchanged (orange). If a gene was absent in one of the samples and present in another, it was regarded as more than a 2-fold change. A 2-fold level was chosen as this corresponded to one standard deviation in a double determination of ~1800 genes. Centromeres and heterochromatic regions were excluded from data analysis.

grade I and II, respectively, tumors 733 and 827 were staged as pT1 (invasive into submucosa), 733 was staged as solid, and 827 was staged as papillary, both grade III.

mRNA Preparation—Tissue biopsies, obtained fresh from surgery, were embedded immediately in a sodium-guanidinium thiocyanate solution and stored at -80°C . Total RNA was isolated using the RNeasy B RNA isolation method (WAK-Chemie Medical GmbH). poly(A)⁺ RNA was isolated by an oligo(dT) selection step (Oligotex mRNA kit; Qiagen).

cRNA Preparation—1 μg of mRNA was used as starting material. The first and second strand cDNA synthesis was performed using the SuperScript[®] choice system (Invitrogen) according to the manufacturer's instructions but using an oligo(dT) primer containing a T7 RNA polymerase binding site. Labeled cRNA was prepared using the ME-GAScript[®] *in vitro* transcription kit (Ambion). Biotin-labeled CTP and

UTP (Enzo) was used, together with unlabeled NTPs in the reaction. Following the *in vitro* transcription reaction, the unincorporated nucleotides were removed using RNeasy-columns (Qiagen).

Array Hybridization and Scanning—Array hybridization and scanning was modified from a previous method (13). 10 μg of cRNA was fragmented at 94°C for 35 min in buffer containing 40 mM Tris acetate, pH 8.1, 100 mM KOAc, 30 mM MgOAc. Prior to hybridization, the fragmented cRNA in a 6 \times SSPE-T hybridization buffer (1 M NaCl, 10 mM Tris, pH 7.6, 0.005% Triton), was heated to 95°C for 5 min, subsequently cooled to 40°C , and loaded onto the Affymetrix probe array cartridge. The probe array was then incubated for 16 h at 40°C at constant rotation (60 rpm). The probe array was exposed to 10 washes in 6 \times SSPE-T at 25°C followed by 4 washes in 0.5 \times SSPE-T at 50°C . The biotinylated cRNA was stained with a streptavidin-phycoerythrin conjugate, 10 $\mu\text{g}/\text{ml}$ (Molecular Probes) in 6 \times SSPE-T

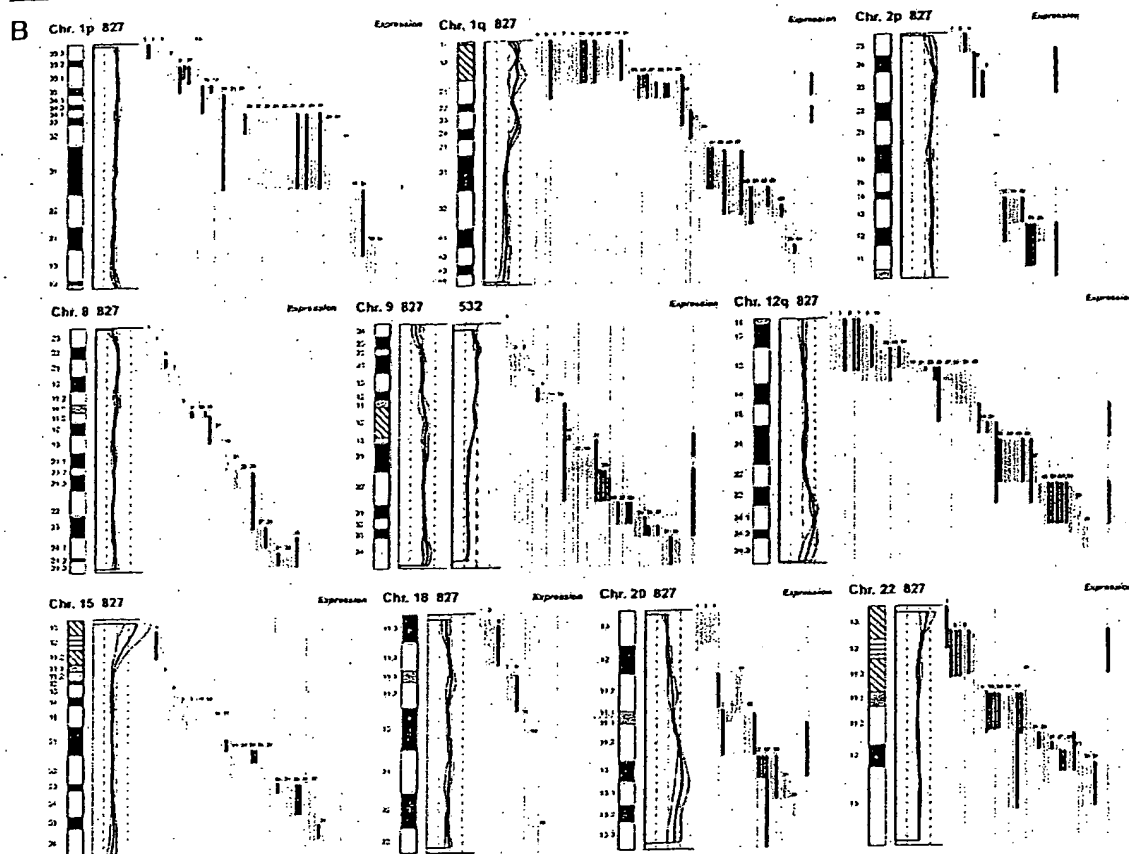


FIG. 1—continued

for 30 min at 25 °C followed by 10 washes in 6× SSPE-T at 25 °C. The probe arrays were scanned at 560 nm using a confocal laser scanning microscope (made for Affymetrix by Hewlett-Packard). The readings from the quantitative scanning were analyzed by Affymetrix gene expression analysis software.

Microsatellite Analysis—Microsatellite Analysis was performed as described previously (14). Microsatellites were selected by use of www.ncbi.nlm.nih.gov/genemap98, and primer sequences were obtained from the genome data base at www.gdb.org. DNA was extracted from tumor and blood and amplified by PCR in a volume of 20 μ l for 35 cycles. The amplicons were denatured and electrophoresed for 3 h in an ABI Prism 377. Data were collected in the Gene Scan program for fragment analysis. Loss of heterozygosity was defined as less than 33% of one allele detected in tumor amplicons compared with blood.

Proteomic Analysis—TCCs were minced into small pieces and homogenized in a small glass homogenizer in 0.5 ml of lysis solution. Samples were stored at -20 °C until use. The procedure for 2D gel electrophoresis has been described in detail elsewhere (15, 16). Gels were stained with silver nitrate and/or Coomassie Brilliant Blue. Proteins were identified by a combination of procedures that included microsequencing, mass spectrometry, two-dimensional gel Western immunoblotting, and comparison with the master two-dimensional gel image of human keratinocyte proteins; see biobase.dk/cgi-bin/celis.

CGH—Hybridization of differentially labeled tumor and normal DNA to normal metaphase chromosomes was performed as described previously (10). Fluorescein-labeled tumor DNA (200 ng), Texas Red-

labeled reference DNA (200 ng), and human Cot-1 DNA (20 μ g) were denatured at 37 °C for 5 min and applied to denatured normal metaphase slides. Hybridization was at 37 °C for 2 days. After washing, the slides were counterstained with 0.15 μ g/ml 4,6-diamidino-2-phenylindole in an anti-fade solution. A second hybridization was performed for all tumor samples using fluorescein-labeled reference DNA and Texas Red-labeled tumor DNA (inverse labeling) to confirm the aberrations detected during the initial hybridization. Each CGH experiment also included a normal control hybridization using fluorescein- and Texas Red-labeled normal DNA. Digital image analysis was used to identify chromosomal regions with abnormal fluorescence ratios, indicating regions of DNA gains and losses. The average green:red fluorescence intensity ratio profiles were calculated using four images of each chromosome (eight chromosomes total) with normalization of the green:red fluorescence intensity ratio for the entire metaphase and background correction. Chromosome identification was performed based on 4,6-diamidino-2-phenylindole banding patterns. Only images showing uniform high intensity fluorescence with minimal background staining were analyzed. All centromeres, p arms of acrocentric chromosomes, and heterochromatic regions were excluded from the analysis.

RESULTS

Comparative Genomic Hybridization—The CGH analysis identified a number of chromosomal gains and losses in the

Gene Copy Numbers, Transcripts, and Protein Levels

TABLE I
Correlation between alterations detected by CGH and by expression monitoring

Top, CGH used as independent variable (if CGH alteration – what expression ratio was found); bottom, altered expression used as independent variable (if expression alteration – what CGH deviation was found).

CGH alterations	Tumor 733 vs. 335	Concordance	CGH alterations	Tumor 827 vs. 532	Concordance
	Expression change clusters			Expression change clusters	
13 Gain	10 Up-regulation 0 Down-regulation 3 No change	77%	10 Gain	8 Up-regulation 0 Down-regulation 2 No change	80%
10 Loss	1 Up-regulation 5 Down-regulation 4 No change	50%	12 Loss	3 Up-regulation 2 Down regulation 7 No change	17%
Expression change clusters	Tumor 733 vs. 335	Concordance	Expression change clusters	Tumor 827 vs. 532	Concordance
	CGH alterations			CGH alterations	
16 Up-regulation	11 Gain 2 Loss 3 No change	69%	17 Up-regulation	10 Gain 5 Loss 2 No change	59%
21 Down-regulation	1 Gain 8 Loss 12 No change	38%	9 Down-regulation	0 Gain 3 Loss 6 No change	33%
15 No change	3 Gain 3 Loss 9 No change	60%	21 No change	1 Gain 3 Loss 17 No change	81%

two invasive tumors (stage pT1, TCCs 733 and 827), whereas the two non-invasive papillomas (stage pTa, TCCs 335 and 532) showed only 9p–, 9q22–q33–, and X–, and 7+, 9q–, and Y–, respectively. Both invasive tumors showed changes (1q22–24+, 2q14.1–qter–, 3q12–q13.3–, 6q12–q22–, 9q34+, 11q12–q13+, 17+, and 20q11.2–q12+) that are typical for their disease stage, as well as additional alterations, some of which are shown in Fig. 1. Areas with gains and losses deviated from the normal copy number to some extent, and the average numerical deviation from normal was 0.4-fold in the case of TCC 733 and 0.3-fold for TCC 827. The largest changes, amounting to at least a doubling of chromosomal content, were observed at 1q23 in TCC 733 (Fig. 1A) and 20q12 in TCC 827 (Fig. 1B).

mRNA Expression in Relation to DNA Copy Number—The mRNA levels from the two invasive tumors (TCCs 827 and 733) were compared with the two non-invasive counterparts (TCCs 532 and 335). This was done in two separate experiments in which we compared TCCs 733 to 335 and 827 to 532, respectively, using two different scaling settings for the arrays to rule out scaling as a confounding parameter. Approximately 1,800 genes that yielded a signal on the arrays were searched in the Unigene and Genemap data bases for chromosomal location, and those with a known location (1096) were plotted as bars covering their purported locus. In that way it was possible to construct a graphic presentation of DNA copy number and relative mRNA levels along the individual chromosomes (Fig. 1).

For each mRNA a ratio was calculated between the level in the invasive versus the non-invasive counterpart. Bars, which represent chromosomal location of a gene, were color-coded according to the expression ratio, and only differences larger

than 2-fold were regarded as informative (Fig. 1). The density of genes along the chromosomes varied, and areas containing only one gene were excluded from the calculations. The resolution of the CGH method is very low, and some of the outlier data may be because of the fact that the boundaries of the chromosomal aberrations are not known at high resolution.

Two sets of calculations were made from the data. For the first set we used CGH alterations as the independent variable and estimated the frequency of expression alterations in these chromosomal areas. In general, areas with a strong gain of chromosomal material contained a cluster of genes having increased mRNA expression. For example, both chromosomes 1q21–q25, 2p and 9q, showed a relative gain of more than 100% in DNA copy number that was accompanied by increased mRNA expression levels in the two tumor pairs (Fig. 1). In most cases, chromosomal gains detected by CGH were accompanied by an increased level of transcripts in both TCCs 733 (77%) and 827 (80%) (Table I, top). Chromosomal losses, on the other hand, were not accompanied by decreased expression in several cases, and were often registered as having unaltered RNA levels (Table I, top). The inability to detect RNA expression changes in these cases was not because of fewer genes mapping to the lost regions (data not shown).

In the second set of calculations we selected expression alterations above 2-fold as the independent variable and estimated the frequency of CGH alterations in these areas. As above, we found that increased transcript expression correlated with gain of chromosomal material (TCC 733, 69% and TCC 827, 59%), whereas reduced expression was often detected in areas with unaltered CGH ratios (Table I, bottom). Furthermore, as a control we looked at areas with no alter-

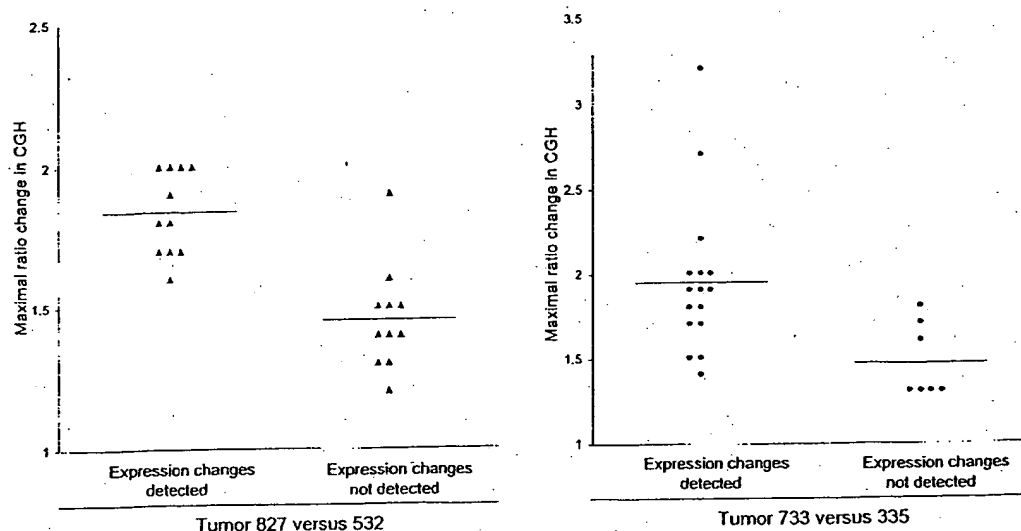


FIG. 2. Correlation between maximum CGH aberration and the ability to detect expression change by oligonucleotide array monitoring. The aberration is shown as a numerical -fold change in ratio between invasive tumors 827 (▲) and 733 (◆) and their non-invasive counterparts 532 and 335. The expression change was taken from the *Expression* line to the *right* in Fig. 1, which depicts the resulting expression change for a given chromosomal region. At least half of the mRNAs from a given region have to be either up- or down-regulated to be scored as an expression change. All chromosomal arms in which the CGH ratio plus or minus one standard deviation was outside the ratio value of one were included.

ation in expression. No alteration was detected by CGH in most of these areas (TCC 733, 60% and TCC 827, 81%; see Table I, *bottom*). Because the ability to observe reduced or increased mRNA expression clustering to a certain chromosomal area clearly reflected the extent of copy number changes, we plotted the maximum CGH aberrations in the regions showing CGH changes against the ability to detect a change in mRNA expression as monitored by the oligonucleotide arrays (Fig. 2). For both tumors TCC 733 ($p < 0.015$) and TCC 827 ($p < 0.00003$) a highly significant correlation was observed between the level of CGH ratio change (reflecting the DNA copy number) and alterations detected by the array based technology (Fig. 2). Similar data were obtained when areas with altered expression were used as independent variables. These areas correlated best with CGH when the CGH ratio deviated 1.6- to 2.0-fold (Table I, *bottom*) but mostly did not at lower CGH deviations. These data probably reflect that loss of an allele may only lead to a 50% reduction in expression level, which is at the cut-off point for detection of expression alterations. Gain of chromosomal material can occur to a much larger extent.

Microsatellite-based Detection of Minor Areas of Losses—In TCC 733, several chromosomal areas exhibiting DNA amplification were preceded or followed by areas with a normal CGH but reduced mRNA expression (see Fig. 1, TCC 733 chromosome 1q32, 2p21, and 7q21 and q32, 9q34, and 10q22). To determine whether these results were because of undetected loss of chromosomal material in these regions or

because of other non-structural mechanisms regulating transcription, we examined two microsatellites positioned at chromosome 1q25-32 and two at chromosome 2p22. Loss of heterozygosity (LOH) was found at both 1q25 and at 2p22 indicating that minor deleted areas were not detected with the resolution of CGH (Fig. 3). Additionally, chromosome 2p in TCC 733 showed a CGH pattern of gain/no change/gain of DNA that correlated with transcript increase/decrease/increase. Thus, for the areas showing increased expression there was a correlation with the DNA copy number alterations (Fig. 1A). As indicated above, the mRNA decrease observed in the middle of the chromosomal gain was because of LOH, implying that one of the mechanisms for mRNA down-regulation may be regions that have undergone smaller losses of chromosomal material. However, this cannot be detected with the resolution of the CGH method.

In both TCC 733 and TCC 827, the telomeric end of chromosome 11p showed a normal ratio in the CGH analysis; however, clusters of five and three genes, respectively, lost their expression. Two microsatellites (D11S1760, D11S922) positioned close to MUC2, IGF2, and cathepsin D indicated LOH as the most likely mechanism behind the loss of expression (data not shown).

A reduced expression of mRNA observed in TCC 733 at chromosomes 3q24, 11p11, 12p12.2, 12q21.1, and 16q24 and in TCC 827 at chromosome 11p15.5, 12p11, 15q11.2, and 18q12 was also examined for chromosomal losses using microsatellites positioned as close as possible to the gene loci

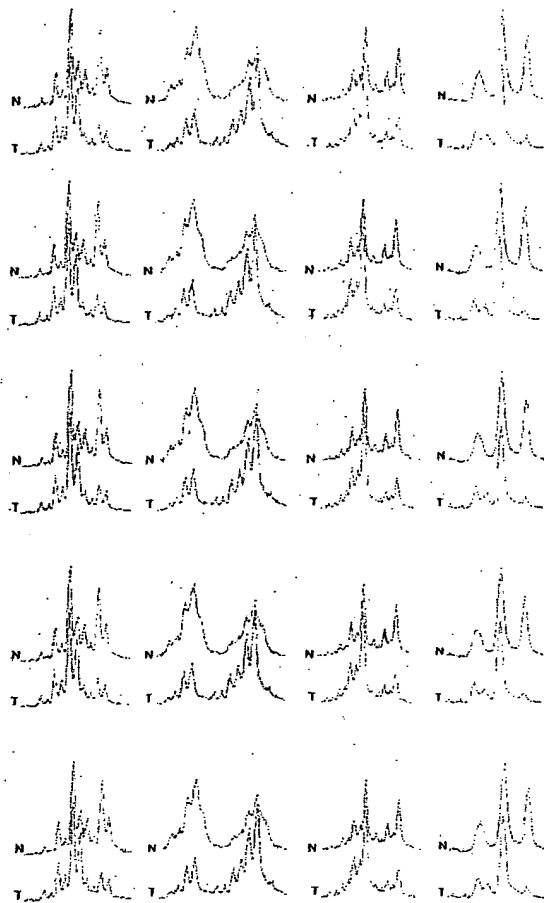


FIG. 3. Microsatellite analysis of loss of heterozygosity. Tumor 733 showing loss of heterozygosity at chromosome 1q25, detected (a) by D1S215 close to Hu class I histocompatibility antigen (gene number 38 in Fig. 1), (b) by D1S2735 close to cathepsin E (gene number 41 in Fig. 1), and (c) at chromosome 2p23 by D2S2251 close to general β -spectrin (gene number 11 on Fig. 1) and of (d) tumor 827 showing loss of heterozygosity at chromosome 18q12 by S18S1118 close to mitochondrial 3-oxoacyl-coenzyme A thiolase (gene number 12 in Fig. 1). The upper curves show the electropherogram obtained from normal DNA from leukocytes (N), and the lower curves show the electropherogram from tumor DNA (T). In all cases one allele is partially lost in the tumor amplicon.

showing reduced mRNA transcripts. Only the microsatellite positioned at 18q12 showed LOH (Fig. 3), suggesting that transcriptional down-regulation of genes in the other regions may be controlled by other mechanisms.

Relation between Changes in mRNA and Protein Levels—2D-PAGE analysis, in combination with Coomassie Brilliant Blue and/or silver staining, was carried out on all four tumors using fresh biopsy material. 40 well resolved abundant known proteins migrating in areas away from the edges of the pH

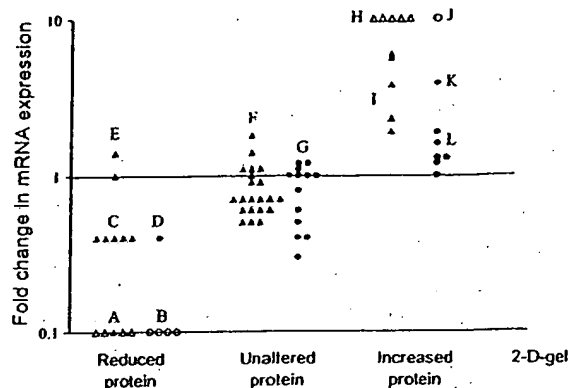


FIG. 4. Correlation between protein levels as judged by 2D-PAGE and transcript ratio. For comparison proteins were divided in three groups, unaltered in level or up- or down-regulated (horizontal axis). The mRNA ratio as determined by oligonucleotide arrays was plotted for each gene (vertical axis). Δ , mRNAs that were scored as present in both tumors used for the ratio calculation; ∇ , mRNAs that were scored as absent in the invasive tumors (along horizontal axis) or as absent in non-invasive reference (top of figure). Two different scalings were used to exclude scaling as a confounder, TCCs 827 and 532 (Δ) were scaled with background suppression, and TCCs 733 and 335 (\bullet) were scaled without suppression. Both comparisons showed highly significant ($p < 0.005$) differences in mRNA ratios between the groups. Proteins shown were as follows: Group A (from left), phosphoglucomutase 1, glutathione transferase class μ number 4, fatty acid-binding protein homologue, cytochrome 15, and cytochrome 13; B (from left), fatty acid-binding protein homologue, 28-kDa heat shock protein, cytochrome 13, and calnexin; C (from left), α -enolase, hnRNP B1, 28-kDa heat shock protein, 14-3-3- ϵ , and pre-mRNA splicing factor; D, mesothelial keratin K7 (type II); E (from top), glutathione S-transferase- π and mesothelial keratin K7 (type II); F (from top and left), adenylate cyclase-associated protein, E-cadherin, keratin 19, calnexin, phosphoglycerate mutase, annexin IV, cytoskeletal γ -actin, hnRNP A1, integral membrane protein calnexin (IP90), hnRNP H, brain-type clathrin light chain-a, hnRNP F, 70-kDa heat shock protein, heterogeneous nuclear ribonucleoprotein A/B, translationally controlled tumor protein, liver glyceraldehyde-3-phosphate dehydrogenase, keratin 8, aldehyde reductase, and Na,K-ATPase β -1 subunit; G, (from top and left), TCP20, calnexin, 70-kDa heat shock protein, calnexin, hnRNP H, cytochrome 15, ATP synthase, keratin 19, triosephosphate isomerase, hnRNP F, liver glyceraldehyde-3-phosphate dehydrogenase, glutathione S-transferase- π , and keratin 8; H (from left), plasma gelsolin, autoantigen calreticulin, thioredoxin, and NAD+-dependent 15 hydroxyprostaglandin dehydrogenase; I (from top), prolidase 4-hydroxylase β -subunit, cytochrome 20, cytochrome 17, prolidase, and fructose 1,6-bisphosphatase; J, annexin II; K, annexin IV; L (from top and left), 90-kDa heat shock protein, prolidase 4-hydroxylase β -subunit, α -enolase, GRP 78, cyclophilin, and cofilin.

gradient, and having a known chromosomal location, were selected for analysis in the TCC pair 827/532. Proteins were identified by a combination of methods (see "Experimental Procedures"). In general there was a highly significant correlation ($p < 0.005$) between mRNA and protein alterations (Fig. 4). Only one gene showed disagreement between transcript alteration and protein alteration. Except for a group of cyto-

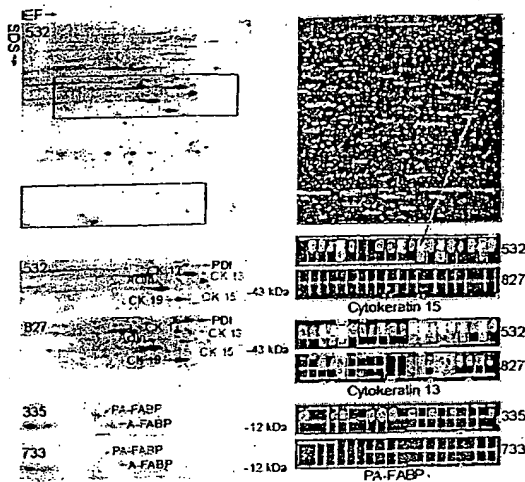


FIG. 5. Comparison of protein and transcript levels in invasive and non-invasive TCCs. The upper part of the figure shows a 2D gel (left) and the oligonucleotide array (right) of TCC 532. The red rectangles on the upper gel highlight the areas that are compared below. Identical areas of 2D gels of TCCs 532 and 827 are shown below. Clearly, cytokeratins 13 and 15 are strongly down-regulated in TCC 827 (red annotation). The tile on the array containing probes for cytokeratin 15 is enlarged below the array (red arrow) from TCC 532 and is compared with TCC 827. The upper row of squares in each tile corresponds to perfect match probes; the lower row corresponds to mismatch probes containing a mutation (used for correction for unspecific binding). Absence of signal is depicted as black, and the higher the signal the lighter the color. A high transcript level was detected in TCC 532 (6151 units) whereas a much lower level was detected in TCC 827 (absence of signals). For cytokeratin 13, a high transcript level was also present in TCC 532 (15659 units), and a much lower level was present in TCC 827 (623 units). The 2D gels at the bottom of the figure (left) show levels of PA-FABP and adipocyte-FABP in TCCs 335 and 733 (invasive), respectively. Both proteins are down-regulated in the invasive tumor. To the right we show the array tiles for the PA-FABP transcript. A medium transcript level was detected in the case of TCC 335 (1277 units) whereas very low levels were detected in TCC 733 (166 units). IEF, isoelectric focusing.

keratins encoded by genes on chromosome 17 (Fig. 5) the analyzed proteins did not belong to a particular family. 26 well focused proteins whose genes had a known chromosomal location were detected in TCCs 733 and 335, and of these 19 correlated ($p < 0.005$) with the mRNA changes detected using the arrays (Fig. 4). For example, PA-FABP was highly expressed in the non-invasive TCC 335 but lost in the invasive counterpart (TCC 733; see Fig. 5). The smaller number of proteins detected in both 733 and 335 was because of the smaller size of the biopsies that were available.

11 chromosomal regions where CGH showed aberrations that corresponded to the changes in transcript levels also showed corresponding changes in the protein level (Table II). These regions included genes that encode proteins that are found to be frequently altered in bladder cancer, namely cytokeratins 17 and 20, annexins II and IV, and the fatty acid-binding proteins PA-FABP and FBP1. Four of these proteins were encoded by genes in chromosome 17q, a frequently amplified chromosomal area in invasive bladder cancers.

DISCUSSION

Most human cancers have abnormal DNA content, having lost some chromosomal parts and gained others. The present study provides some evidence as to the effect of these gains and losses on gene expression in two pairs of non-invasive and invasive TCCs using high throughput expression arrays and proteomics, in combination with CGH. In general, the results showed that there is a clear individual regulation of the mRNA expression of single genes, which in some cases was superimposed by a DNA copy number effect. In most cases, genes located in chromosomal areas with gains often exhibited increased mRNA expression, whereas areas showing losses showed either no change or a reduced mRNA expression. The latter might be because of the fact that losses most often are restricted to loss of one allele, and the cut-off point for detection of expression alterations was a 2-fold change, thus being at the border of detection. In several cases, how-

TABLE II
Proteins whose expression level correlates with both mRNA and gene dose changes

Protein	Chromosomal location	Tumor TCC	CGH alteration	Transcript alteration*	Protein alteration
Annexin II	1q21	733	Gain	Abs to Pres*	Increase
Annexin IV	2p13	733	Gain	3.9-Fold up	Increase
Cytokeratin 17	17q12-q21	827	Gain	3.8-Fold up	Increase
Cytokeratin 20	17q21.1	827	Gain	5.6-Fold up	Increase
(PA)-FABP	8q21.2	827	Loss	10-Fold down	Decrease
FBP1	9q22	827	Gain	2.3-Fold up	Increase
Plasma gelsolin	9q31	827	Gain	Abs to Pres	Increase
Heat shock protein 28	15q12-q13	827	Loss	2.5-Fold up	Decrease
Prohibitin	17q21	827/733	Gain	3.7-/2.5-Fold up*	Increase
Prolyl-4-hydroxyl	17q25	827/733	Gain	5.7-/1.6-Fold up	Increase
hnRNPB1	7p15	827	Loss	2.5-Fold down	Decrease

* Abs, absent; Pres, present.

* In cases where the corresponding alterations were found in both TCCs 827 and 733 these are shown as 827/733.

ever, an increase or decrease in DNA copy number was associated with *de novo* occurrence or complete loss of transcript, respectively. Some of these transcripts could not be detected in the non-invasive tumor but were present at relatively high levels in areas with DNA amplifications in the invasive tumors (e.g. in TCC 733 transcript from cellular ligand of annexin II gene (chromosome 1q21) from absent to 2670 arbitrary units; in TCC 827 transcript from small proline-rich protein 1 gene (chromosome 1q12-q21.1) from absent to 1326 arbitrary units). It may be anticipated from these data that significant clustering of genes with an increased expression to a certain chromosomal area indicates an increased likelihood of gain of chromosomal material in this area.

Considering the many possible regulatory mechanisms acting at the level of transcription, it seems striking that the gene dose effects were so clearly detectable in gained areas. One hypothetical explanation may lie in the loss of controlled methylation in tumor cells (17-19). Thus, it may be possible that in chromosomes with increased DNA copy numbers two or more alleles could be demethylated simultaneously leading to a higher transcription level, whereas in chromosomes with losses the remaining allele could be partly methylated, turning off the process (20, 21). A recent report has documented a ploidy regulation of gene expression in yeast, but in this case all the genes were present in the same ratio (22), a situation that is not analogous to that of cancer cells, which show marked chromosomal aberrations, as well as gene dosage effects.

Several CGH studies of bladder cancer have shown that some chromosomal aberrations are common at certain stages of disease progression, often occurring in more than 1 of 3 tumors. In pTa tumors, these include 9p-, 9q-, 1q+, Y- (2, 6), and in pT1 tumors, 2q-, 11p-, 11q-, 1q+, 5p+, 8q+, 17q+, and 20q+ (2-4, 6, 7). The pTa tumors studied here showed similar aberrations such as 9p- and 9q22-q33- and 9q- and Y-, respectively. Likewise, the two minimal invasive pT1 tumors showed aberrations that are commonly seen at that stage, and TCC 827 had a remarkable resemblance to the commonly seen pattern of losses and gains, such as 1q22-24 amplification (seen in both tumors), 11q14-q22 loss, the latter often linked to 17 q+ (both tumors), and 1q+ and 9p-, often linked to 20q+ and 11 q13+ (both tumors) (7-9). These observations indicate that the pairs of tumors used in this study exhibit chromosomal changes observed in many tumors, and therefore the findings could be of general importance for bladder cancer.

Considering that the mapping resolution of CGH is of about 20 megabases it is only possible to get a crude picture of chromosomal instability using this technique. Occasionally, we observed reduced transcript levels close to or inside regions with increased copy numbers. Analysis of these regions by positioning heterozygous microsatellites as close as possible to the locus showing reduced gene expression revealed loss of heterozygosity in several cases. It seems likely that multiple and different events occur along each chromosomal

arm and that the use of cDNA microarrays for analysis of DNA copy number changes will reach a resolution that can resolve these changes, as has recently been proposed (2). The outlier data were not more frequent at the boundaries of the CGH aberrations. At present we do not know the mechanism behind chromosomal aneuploidy and cannot predict whether chromosomal gains will be transcribed to a larger extent than the two native alleles. A mechanism as genetic imprinting has an impact on the expression level in normal cells and is often reduced in tumors. However, the relation between imprinting and gain of chromosomal material is not known.

We regard it as a strength of this investigation that we were able to compare invasive tumors to benign tumors rather than to normal urothelium, as the tumors studied were biologically very close and probably may represent successive steps in the progression of bladder cancer. Despite the limited amount of fresh tissue available it was possible to apply three different state of the art methods. The observed correlation between DNA copy number and mRNA expression is remarkable when one considers that different pieces of the tumor biopsies were used for the different sets of experiments. This indicate that bladder tumors are relatively homogenous, a notion recently supported by CGH and LOH data that showed a remarkable similarity even between tumors and distant metastasis (10, 23).

In the few cases analyzed, mRNA and protein levels showed a striking correspondence although in some cases we found discrepancies that may be attributed to translational regulation, post-translational processing, protein degradation, or a combination of these. Some transcripts belong to undertranslated mRNA pools, which are associated with few translationally inactive ribosomes; these pools, however, seem to be rare (24). Protein degradation, for example, may be very important in the case of polypeptides with a short half-life (e.g. signaling proteins). A poor correlation between mRNA and protein levels was found in liver cells as determined by arrays and 2D-PAGE (25), and a moderate correlation was recently reported by Ideker *et al.* (26) in yeast.

Interestingly, our study revealed a much better correlation between gained chromosomal areas and increased mRNA levels than between loss of chromosomal areas and reduced mRNA levels. In general, the level of CGH change determined the ability to detect a change in transcript. One possible explanation could be that by losing one allele the change in mRNA level is not so dramatic as compared with gain of material, which can be rather unlimited and may lead to a severalfold increase in gene copy number resulting in a much higher impact on transcript level. The latter would be much easier to detect on the expression arrays as the cut-off point was placed at a 2-fold level so as not to be biased by noise on the array. Construction of arrays with a better signal to noise ratio may in the future allow detection of lesser than 2-fold alterations in transcript levels, a feature that may facilitate the analysis of the effect of loss of chromosomal areas on transcript levels.

In eleven cases we found a significant correlation between DNA copy number, mRNA expression, and protein level. Four of these proteins were encoded by genes located at a frequently amplified area in chromosome 17q. Whether DNA copy number is one of the mechanisms behind alteration of these eleven proteins is at present unknown and will have to be proved by other methods using a larger number of samples. One factor making such studies complicated is the large extent of protein modification that occurs after translation, requiring immunoidentification and/or mass spectrometry to correctly identify the proteins in the gels.

In conclusion, the results presented in this study exemplify the large body of knowledge that may be possible to gather in the future by combining state of the art techniques that follow the pathway from DNA to protein (26). Here, we used a traditional chromosomal CGH method, but in the future high resolution CGH based on microarrays with many thousand radiation hybrid-mapped genes will increase the resolution and information derived from these types of experiments (2). Combined with expression arrays analyzing transcripts derived from genes with known locations, and 2D gel analysis to obtain information at the post-translational level, a clearer and more developed understanding of the tumor genome will be forthcoming.

Acknowledgments—We thank Mie Madsen, Hanne Steen, Inge Lis Thorsen, Hans Lund, Nikolaj Ørntoft, and Lynn Bjerke for technical help and Thomas Gingeras, Christine Harrington, and Morten Østergaard for valuable discussions.

* This work was supported by grants from The Danish Cancer Society, the University of Aarhus, Aarhus County, Novo Nordic, the Danish Biotechnology Program, the Frenkels Foundation, the John and Birthe Meyer Foundation, and NCI, National Institutes of Health Grant CA47537. The costs of publication of this article were delayed in part by the payment of page charges. This article must therefore be hereby marked "advertisement" in accordance with 18 U.S.C. Section 1734 solely to indicate this fact.

§ To whom correspondence should be addressed: Dept. of Clinical Biochemistry, Molecular Diagnostic Laboratory, Aarhus University Hospital, Skejby, DK-8200 Aarhus N, Denmark. Tel.: 45-89495100/45-86156201 (private); Fax: 45-89496018; E-mail: orntoft@kba.sks.au.dk.

REFERENCES

- Lengauer, C., Kinzler, K. W., and Vogelstein, B. (1998) Genetic instabilities in human cancers. *Nature* 396, 643–649.
- Pollack, J. R., Perou, C. M., Alizadeh, A. A., Eisen, M. B., Pergamenschikov, A., Williams, C. F., Jeffrey, S. S., Bolstein, D., and Brown, P. O. (1999) Genome-wide analysis of DNA copy-number changes using cDNA microarrays. *Nat. Genet.* 23, 41–45.
- de Cremoux, P., Martin, E. C., Vincent-Salomon, A., Dieras, V., Barbaroux, C., Liva, S., Pouillart, P., Sastre-Garau, X., and Magdelenat, H. (1999) Quantitative PCR analysis of c-erb B-2 (HER2/neu) gene amplification and comparison with p185(HER2/neu) protein expression in breast cancer drill biopsies. *Int. J. Cancer* 83, 157–161.
- Brungier, P. P., Tamimi, Y., Shuring, E., and Schalken, J. (1996) Expression of cyclin D1 and EMS1 in bladder tumors; relationship with chromosome 11q13 amplifications. *Oncogene* 12, 1747–1753.
- Slavc, I., Ellenbogen, R., Jung, W. H., Vawter, G. F., Kretschmar, C., Grier, H., and Korf, B. R. (1990) *myc* gene amplification and expression in primary human neuroblastoma. *Cancer Res.* 50, 1459–1463.
- Sauter, G., Carroll, P., Moch, H., Kallioniemi, A., Kerschmann, R., Narayan, P., Mihatsch, M. J., and Waldman, F. M. (1995) *c-myc* copy number gains in bladder cancer detected by fluorescence *in situ* hybridization. *Am. J. Pathol.* 146, 1131–1139.
- Richter, J., Jiang, F., Gorog, J. P., Sartorius, G., Egenter, C., Gasser, T. C., Moch, H., Mihatsch, M. J., and Sauter, G. (1997) Marked genetic differences between stage pTa and stage pT1 papillary bladder cancer detected by comparative genomic hybridization. *Cancer Res.* 57, 2860–2864.
- Richter, J., Boffa, L., Wagner, U., Schraml, P., Gasser, T. C., Moch, H., Mihatsch, M. J., and Sauter, G. (1998) Patterns of chromosomal imbalances in advanced urinary bladder cancer detected by comparative genomic hybridization. *Am. J. Pathol.* 153, 1615–1621.
- Bruch, J., Wehr, G., Hautmann, R., Mattfeldt, T., Bruderlein, S., Moller, P., Sauter, S., Harneiser, H., Vogel, W., and Paiss, T. (1998) Chromosomal changes during progression of transitional cell carcinoma of the bladder and delineation of the amplified interval on chromosome arm 8q. *Genes Chromosomes Cancer* 23, 167–174.
- Hovey, R. M., Chu, L., Balazs, M., De Vries, S., Moore, D., Sauter, G., Carroll, P. R., and Waldman, F. M. (1998) Genetic alterations in primary bladder cancers and their metastases. *Cancer Res.* 58, 3555–3560.
- Simon, R., Burger, H., Brinkschmidt, C., Bocker, W., Hertle, L., and Terpe, H. J. (1998) Chromosomal aberrations associated with invasion in papillary superficial bladder cancer. *J. Pathol.* 185, 345–351.
- Koo, S. H., Kwon, K. C., Ihm, C. H., Jeon, Y. M., Park, J. W., and Sul, C. K. (1999) Detection of genetic alterations in bladder tumors by comparative genomic hybridization and cytogenetic analysis. *Cancer Genet. Cytogenet.* 110, 87–93.
- Wodicka, L., Dong, H., Mittmann, M., Ho, M. H., and Lockhart, D. J. (1997) Genome-wide expression monitoring in *Saccharomyces cerevisiae*. *Nat. Biotechnol.* 15, 1359–1367.
- Christensen, M., Sunde, L., Bolund, L., and Orntoft, T. F. (1999) Comparison of three methods of microsatellite detection. *Scand. J. Clin. Lab. Invest.* 59, 167–177.
- Celis, J. E., Ostergaard, M., Basse, B., Celis, A., Lauridsen, J. B., Ratz, G. P., Andersen, L., Hein, B., Wolf, H., Orntoft, T. F., and Rasmussen, H. H. (1996) Loss of adipocyte-type fatty acid binding protein and other protein biomarkers is associated with progression of human bladder transitional cell carcinomas. *Cancer Res.* 56, 4782–4790.
- Celis, J. E., Ratz, G., Basse, B., Lauridsen, J. B., and Celis, A. (1994) in *Cell Biology: A Laboratory Handbook* (Celis, J. E., ed) Vol. 3, pp. 222–230, Academic Press, Orlando, FL.
- Ohlsson, R., Tycko, B., and Sapienza, C. (1998) Monoallelic expression: 'there can only be one'. *Trends Genet.* 14, 435–438.
- Hollander, G. A., Zuklys, S., Morel, C., Mizoguchi, E., Mobisson, K., Simpson, S., Terhorst, C., Wishart, W., Golan, D. E., Bhan, A. K., and Burakoff, S. J. (1998) Monoallelic expression of the interleukin-2 locus. *Science* 279, 2118–2121.
- Brannan, C. I., and Bartolomei, M. S. (1999) Mechanisms of genomic imprinting. *Curr. Opin. Genet. Dev.* 9, 164–170.
- Ohlsson, R., Cui, H., He, L., Pfeifer, S., Malmikumpu, H., Jiang, S., Feinberg, A. P., and Hedborg, F. (1999) Mosaic allelic insulin-like growth factor 2 expression patterns reveal a link between Wilms' tumorigenesis and epigenetic heterogeneity. *Cancer Res.* 59, 3889–3892.
- Cui, H., Hedborg, F., He, L., Nordenskjold, A., Sandstedt, B., Pfeifer-Ohlsson, S., and Ohlsson, R. (1997) Inactivation of H19, an imprinted and putative tumor repressor gene, is a preneoplastic event during Wilms' tumorigenesis. *Cancer Res.* 57, 4469–4473.
- Galitski, T., Saldanha, A. J., Styles, C. A., Lander, E. S., and Fink, G. R. (1999) Ploidy regulation of gene expression. *Science* 285, 251–254.
- Tsao, J., Yatabe, Y., Markl, I. D., Haiyan, K., Jones, P. A., and Shibata, D. (2000) Bladder cancer genotype stability during clinical progression. *Genes Chromosomes Cancer* 29, 26–32.
- Zong, Q., Schummer, M., Hood, L., and Morris, D. R. (1999) Messenger RNA translation state: the second dimension of high-throughput expression screening. *Proc. Natl. Acad. Sci. U. S. A.* 96, 10632–10636.
- Anderson, L., and Seilhamer, J. (1997) Comparison of selected mRNA and protein abundances in human liver. *Electrophoresis* 18, 533–537.
- Ideker, T., Thorsson, V., Ranish, J. A., Christmas, R., Buhler, J., Eng, J. K., Bumgarner, R., Goodlett, D. R., Aebersold, R., and Hood, L. (2001) Integrated genomic and proteomic analyses of a systematically perturbed metabolic network. *Science* 292, 929–934.

FREE full text article at
www.mspenline.org

Genome-wide study of gene copy numbers, transcripts, and protein levels in pairs of non-invasive and invasive human transitional cell carcinomas.

Orntoft TE, Thykjaer T, Waldman FM, Wolf H, Celis JE.

Department of Clinical Biochemistry, Molecular Diagnostic Laboratory, Aarhus University Hospital, Skejby, DK-8200 Aarhus N, Denmark. orntoft@kba.sks.au.dk

Gain and loss of chromosomal material is characteristic of bladder cancer, as well as malignant transformation in general. The consequences of these changes at both the transcription and translation levels is at present unknown partly because of technical limitations. Here we have attempted to address this question in pairs of non-invasive and invasive human bladder tumors using a combination of technology that included comparative genomic hybridization, high density oligonucleotide array-based monitoring of transcript levels (5600 genes), and high resolution two-dimensional gel electrophoresis. The results showed that there is a gene dosage effect that in some cases superimposes on other regulatory mechanisms. This effect depended ($p < 0.015$) on the magnitude of the comparative genomic hybridization change. In general (18 of 23 cases), chromosomal areas with more than 2-fold gain of DNA showed a corresponding increase in mRNA transcripts. Areas with loss of DNA, on the other hand, showed either reduced or unaltered transcript levels. Because most proteins resolved by two-dimensional gels are unknown it was only possible to compare mRNA and protein alterations in relatively few cases of well focused abundant proteins. With few exceptions we found a good correlation ($p < 0.005$) between transcript alterations and protein levels. The implications, as well as limitations, of the approach are discussed.

PMID: 12096139 [PubMed - indexed for MEDLINE]



Expression of cadherins and catenins in paired tumor and non-neoplastic primary prostate cultures and corresponding prostatectomy specimens.

Wang J, Krill D, Torbenson M, Wang Q, Bisceglia M, Stoner J, Thomas A, DeFlavia P, Dhir R, Becich MJ.

Department of Pathology, University of Pittsburgh Medical Center, PA, USA.

Cadherins are a family of transmembrane proteins that play a crucial role in cell differentiation, cell migration, and intercellular adhesion. Cadherins are associated with catenins through their highly conserved cytoplasmic domain. Down-regulation of E-cadherin protein has been shown in various human cancers. This study examined the expression of cadherins and associated catenins at the mRNA level. Paired tumor and nonneoplastic primary prostate cultures were obtained from surgical specimens. Quantitative multiplex fluorescence reverse transcriptase-polymerase chain reaction (QMF RT-PCR) and quantitative analysis were performed and correlated with immunostain results. Six of seven cases of neoplastic cultures showed moderately-to-markedly decreased levels of E-cadherin and P-cadherin mRNA. Similar losses of alpha-catenin and beta-catenin mRNA were also observed. The results of QMF RT-PCR showed good correlation with the results of immunohistochemical studies based on corresponding formalin-fixed sections. In conclusion, this paper presents a coordinated down-regulation in the expression of E-cadherin and associated catenins at the mRNA and protein level in most of the cases studied. This down-regulation may play an important role in the pathogenesis of prostate cancer.

PMID: 11127708 [PubMed - indexed for MEDLINE]

ORIGINAL PAPER

Jianzhou Wang · Diane Krill · Michael Torbenson
Qi Wang · Michelle Bisceglia · Judy Stoner
Angela Thomas · Petrina DeFlavia · Rajiv Dhir
Michael J. Becich

Expression of cadherins and catenins in paired tumor and non-neoplastic primary prostate cultures and corresponding prostatectomy specimens

Received: 6 March 2000 / Accepted: 23 May 2000

Abstract Cadherins are a family of transmembrane proteins that play a crucial role in cell differentiation, cell migration, and intercellular adhesion. Cadherins are associated with catenins through their highly conserved cytoplasmic domain. Down-regulation of E-cadherin protein has been shown in various human cancers. This study examined the expression of cadherins and associated catenins at the mRNA level. Paired tumor and non-neoplastic primary prostate cultures were obtained from surgical specimens. Quantitative multiplex fluorescence reverse transcriptase-polymerase chain reaction (QMF RT-PCR) and quantitative analysis were performed and correlated with immunostain results. Six of seven cases of neoplastic cultures showed moderately-to-markedly decreased levels of E-cadherin and P-cadherin mRNA. Similar losses of α -catenin and β -catenin mRNA were also observed. The results of QMF RT-PCR showed good correlation with the results of immunohistochemical studies based on corresponding formalin-fixed sections. In conclusion, this paper presents a coordinated down-regulation in the expression of E-cadherin and associated catenins at the mRNA and protein level in most of the cases studied. This down-regulation may play an important role in the pathogenesis of prostate cancer.

Key words Prostate adenocarcinoma · Cadherin · Catenin · Adhesion molecules

J. Wang · D. Krill · M. Torbenson
Q. Wang · M. Bisceglia · J. Stoner · A. Thomas
P. DeFlavia · R. Dhir · M. J. Becich
Department of Pathology,
University of Pittsburgh Medical Center, Pittsburgh, PA
M. J. Becich (✉)
UPMC Shadyside,
Department of Pathology,
5230 Centre Avenue, Pittsburgh, PA 15232, USA
e-mail: becich@pitt.edu
Tel.: +1-412-6233941; Fax: +1-412-6232814

Introduction

Prostate cancer is the most common malignant tumor and the second leading cause of cancer death in men. The clinical course of patients with prostate cancer varies widely, and different factors contribute to this marked clinical variability, including genetic background, hormonal environment, and the invasive potential of the tumor. Invasion and metastasis are the hallmarks of malignancy and have been closely linked to alterations in cell-to-cell adhesion, cell migration, and interactions with extracellular matrix components [22].

Cadherins are a family of transmembrane glycoproteins responsible for maintaining the integrity of tissue and are involved in cell differentiation, cell migration, and intercellular adhesion through a calcium-dependent mechanism characterized by homotypic adhesion [35–37]. Their highly conserved cytoplasmic domains associate with catenins, a group of intracellular proteins that mediate contact between the cadherins and the microfilaments of the cytoskeleton. Each cadherin subclass shows a unique tissue distribution: E-cadherin is predominantly expressed in epithelial cells and P-cadherin is restricted to decidua tissue and the basal or lower layers of stratified epithelium [30].

The accumulating evidence suggests a decrease or loss of function in E-cadherin and P-cadherin in several human carcinomas [3, 9, 23, 32]. Loss of heterozygosity (LOH) at chromosome 16 in the location of the E-cadherin gene is present in a high percentage of prostate cancers [6, 21, 26, 28]. Decreased expression of E-cadherin is seen in various human malignant tumor cell lines, and the level of decrease correlates with the invasive potential of the tumor cell lines [1, 9, 12, 24, 40, 42]. In addition, many, but not all, immunohistochemical studies using formalin-fixed, paraffin-embedded tissue have shown that the E-cadherin protein is decreased in prostate cancer and the decrease is correlated with tumor grade [4, 8, 13, 27, 38]. Other studies have shown decreased-to-absent P-cadherin levels, but variable E-cadherin levels [33].

α - and β -catenins bind the cytoplasmic domain of E-cadherin and link it to the cytoskeleton [16, 31]. Down-regulation of expression and deletion of α -catenin genes were identified in several human cancer cell lines [19, 24, 42]. Immunohistochemical studies showed decreased α -catenin staining, which correlated well with the loss of E-cadherin staining and patient survival [25, 29, 39]. In addition, decreased β -catenin protein expression appears to be associated with malignant transformation of epithelial tissue [34]. These results suggest that cadherins and catenins may function as tumor invasion-suppressor genes. However, most of these results were obtained in studies using transformed tumor cell lines and formalin-fixed, paraffin-embedded tissue. To our knowledge, no studies to date have examined the co-expression of cadherins and catenins at the mRNA level using material derived from surgical specimens.

Recently, we have developed the methodology to cultivate primary epithelial cells under defined conditions from surgical prostatectomy specimens [20]. Areas of both carcinoma and non-neoplastic tissue are identified grossly, verified histologically, and then cultured separately, resulting in paired primary cultures of both non-neoplastic and neoplastic epithelium from the same patient. The non-neoplastic tissue cultures serve as an important control of any person-to-person variability in the expression of the genes of interest.

In this study, we investigated the co-expression of cadherin and catenin mRNA from multiple paired primary prostate cultures derived from surgical prostatectomy specimens using quantitative multiplex fluorescence reverse transcriptase-polymerase chain reaction (QMF RT-PCR) [41, 44]. Immunohistochemistry studies of cadherins and catenins were performed on the corresponding paraffin-embedded prostate tissue.

Materials and methods

Tissue specimen and primary prostate cultures

We studied patients with adenocarcinoma of the prostate who underwent prostatectomy at the University of Pittsburgh Medical Center during the time interval January 1996–January 1998. No patient had received treatment prior to surgery. Fresh prostatectomy specimens were sectioned and grossly examined, representative samples of neoplastic and non-neoplastic tissue were collected, and the diagnoses were confirmed by examination of hematoxylin and eosin (H&E)-stained sections. Epithelial cells from tumor and

non-neoplastic areas of the specimen were isolated and then cultured with a chemically defined medium (CDM) without addition of growth factors as previously described. Tissue fragments were cut into small pieces and underwent a series of collagenous digestions. Following each digestion, the cells were pelleted by centrifugation at 1,000 rpm for 4 MIN [20]. To selectively promote epithelial cell growth, the pellets were resuspended and maintained in serum-free CDM supplemented with epithelial growth factor (EGF) [20]. The culture's morphology was examined daily, and epithelial cells were allowed to grow until confluence was reached, between days 7 and 10.

Isolation of total RNA and synthesis of cDNA

Total RNA was extracted from the cultured primary prostate epithelial cells at first passage according to the Trizol solution (Gibco BRL, Rockville, MD) modified method of Chomczynski and Sacchi [7]. The RNA was then quantitated spectrophotometrically. Two micrograms of total RNA were used for first strand cDNA synthesis using oligo-dT primers and MMLV reverse transcriptase (Gibco BRL, Rockville, MD).

PCR primers and quantitative multiplex fluorescence PCR

PCR primers for hepatocyte growth factor (HGF) and c-myc were synthesized as previously described [17]. PCR primers for E-cadherin, P-cadherin, α -catenin, β -catenin, and β -actin cDNA were designed according to cDNA sequences provided by the GeneBank (WWW2.ncbi.nlm.gov/genbank/query). The primers were selected to amplify 150–250 bp target genes and the PCR products from each target gene were designed to have a different size (Table 1). The reverse primers were synthesized with fluorescent molecules covalently attached to the 5' end (BRL, Rockville, MD). Twenty-five microliters of PCR reactions for QMF-PCR contained primers (20 μ M each), cDNA corresponding to 50 ng of total RNA, dNTPs, and reaction buffer. The reactions were amplified for 21 cycles at 94 °C for 1 min, 57 °C for 2 min, and 72 °C for 2 min. Five microliters of QMF-PCR reactions were mixed with an equal volume of sequencing gel loading buffer, denatured, and aliquots were electrophoresed on an ABI 373A automated sequencer (Applied Biosystems, Foster City, CA) using a matrix specific for fluorescein (Fig. 1A).

Automated sequencer gels were run for 6 h at 30 W using Genescan software (ABI, Foster City, CA). Lane assignments and areas of the peaks corresponding to fluorescent peaks were assigned and quantitated by the Genescan software using Photomultiplier tube (PMT) voltages (Fig. 1B). All experiments were done in triplicate and the results presented as means and standard deviations (SD).

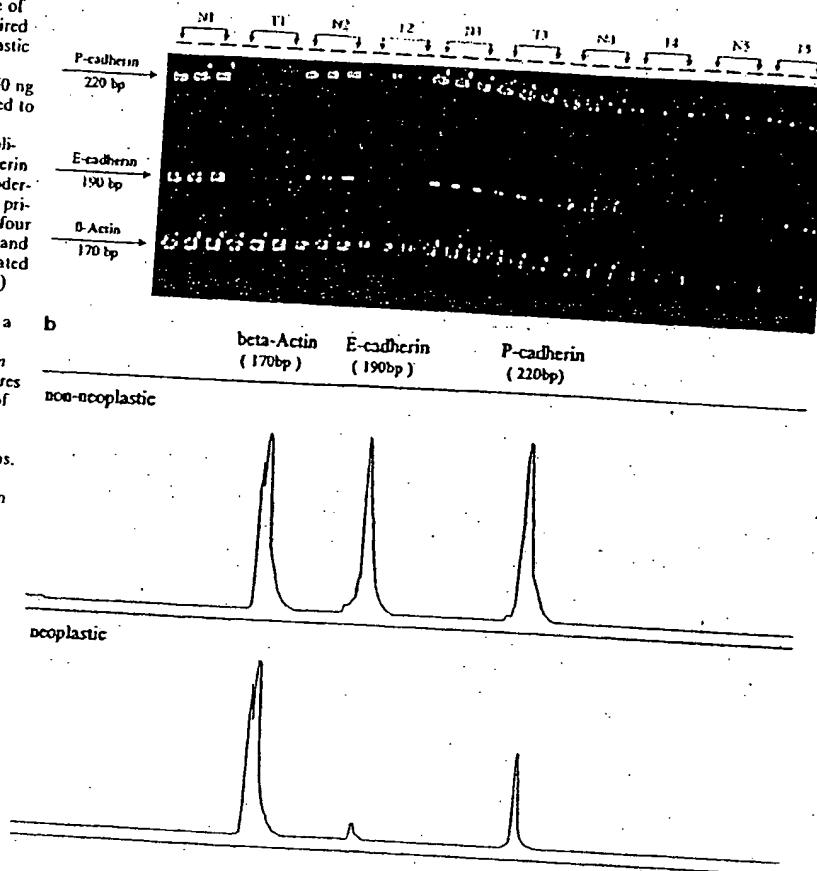
Antibodies and immunohistochemistry

Five-micron sections were obtained from formalin-fixed, paraffin-embedded tissue blocks. They were deparaffinized and hydrated with graduated ethanols. Slides were then microwaved in 1.1 M

Table 1 Summary of PCR primer sequences and PCR products

Primer	Sequence	Target gene	Size of PCR product (bp)
1	Forward ccacactgtgccatctacg	β -Actin	170
2	Reverse gcttctcttaagtcacgc		
3	Forward caaagtggccatagatggtag	E-cadherin	190
4	Reverse ctgcttgatccagaaacgg		
5	Forward gcaagagccagctctgttagc	P-cadherin	220
6	Reverse acttgagctgattcagctctgg		
7	Forward gatggacaactatgagccagg	α -Catenin	182
8	Reverse tataccaggcgggaagcctcg		
9	Forward ttctgggtgccactaccacagc	β -Catenin	218
10	Reverse tgcatacctcatctaatgic		

Fig. 1 A Genescan image of QMF RT-PCR of five paired non-neoplastic and neoplastic primary prostate cultures. cDNA corresponding to 50 ng of total RNA was subjected to 21 cycles of PCR, and all reactions were done in triplicate. RNA of both E-cadherin and P-cadherin showed moderate-to-marked reduction in primary neoplastic cultures in four of five cases (Cases 1, 2, 4, and 5). B Representative automated sequencer traces (ABI 373A) from 21 cycles of QMF RT-PCR using cDNA from a paired non-neoplastic (top panel) and neoplastic (bottom panel) primary prostate cultures (Case 2), and copy number of PCR products (α -actin, E-cadherin, and P-cadherin) was calculated using peak areas. Neoplastic culture showed markedly decreased expression of both E-cadherin and P-cadherin



citrate buffer (pH 6.0) for antigen retrieval. The avidin-biotin complex method for immunohistochemistry was utilized from Vector Laboratories (Burlingame, Calif., USA). The E-cadherin, P-cadherin, α -catenin, and β -catenin antibodies, all mouse monoclonal antibodies, were purchased from Transduction Laboratories (Lexington, Ky., USA).

Evaluation of immunostaining

The percentage of positive cells, intensity of the staining, and cellular localization of the staining were examined by two independent observers using normal prostate epithelium from the same specimen as an internal control. The intensity of the signal was graded as strong, moderate, weak, and negative. The staining pattern of the tumor was compared with that of normal epithelium from the same specimens.

Results

Expression of E-cadherin and P-cadherin

Since many prostate cancers are known to be histologically heterogeneous, adjacent H&E-stained sections of the tissue fragments sent to culture were reviewed

to assess tissue homogeneity and to rule out the presence of other diseases. The paired primary cultures for this study were selected based on the following histologic features: (1) non-neoplastic tissue showed no cancerous foci or high-grade prostatic intraepithelial neoplasia (PIN); (2) neoplastic sections contained less than 5% non-cancerous epithelium. Seven out of 38 pairs of cultures met the selection criteria and were included in this study. Histologically, all seven cases were moderately differentiated adenocarcinomas, with Gleason scores ranging from 5 to 7 (median = 6). In six of these cases, adjacent sections of tumor contained no benign prostate epithelium, and in one case (specimen 4), there was less than 5% non-cancerous epithelium. Prostate stromal cells express HGF, whereas the epithelial cells express c-met, the receptor for HGF [17, 20]. The cases included in this study showed no detectable HGF expression after 21 cycles of QMF RT-PCR (data not shown). This indicates there was no significant stromal cell contamination in the current epithelial cultures. QMF-PCR is an accurate method of measuring the relative levels of mRNA in small tissue samples [41]. In

In this study, we used this method to quantitate the mRNA levels of E-cadherin and P-cadherin, relative to β -actin. All the RNA samples contained no DNA contamination, as shown by the absence of automated signals when RT was omitted from the RT-PCR reactions. We observed the expected linear increases in β -actin, E-cadherin, and P-cadherin signal intensities between cycle numbers 18 and 24, with a cDNA input corresponding to 50 ng of total RNA. The ratios of β -actin to E-cadherin and P-cadherin were constant, as was the E-cadherin/P-cadherin ratio. These results indicated that the target genes were consistently amplified in the reactions. Twenty-one cycles of PCR were chosen for all subsequent experiments. In addition, the raw sequence quantitation of peak areas for β -actin using the same cDNA input was similar among the paired primary prostate cultures (data not shown).

When compared with the paired non-neoplastic primary cultures and normalized with the β -actin internal controls, four of the neoplastic cultures showed marked (>85%) reduction of E-cadherin mRNA levels, with one case showing no detectable E-cadherin mRNA. The other three neoplastic cultures showed mild-to-moderate reductions (Table 2).

Six of seven neoplastic cultures showed moderately to markedly decreased P-cadherin mRNA levels when compared with non-neoplastic cultures. Interestingly,

the four cases showing marked reduction in levels of E-cadherin mRNA, and also demonstrated significant losses of P-cadherin mRNA. The case with no detectable E-cadherin mRNA also demonstrated near total loss of P-cadherin mRNA (Case 1). Another case (Case 3), with only mild reduction in E-cadherin mRNA, showed no significant change in P-cadherin mRNA. Genetic variations among the patients were evident in the marked differences in the baseline levels of E-cadherin and P-cadherin expression seen in the non-neoplastic primary prostate cultures.

Expression of α -catenin and β -catenin

The highly conserved intracytoplasmic domain of the cadherins interacts with α - and β -catenins, with the catenins serving as a link between the cadherins and the microfilaments of the cytoskeleton. Six cases of neoplastic cultures showed mild-to-moderate reductions in α -catenin mRNA levels, ranging from 26 to 62%. These cases also demonstrated more severe reductions of β -catenin mRNA levels and generally correlated with the changes of cadherins in the same specimen (Table 3). Interestingly, the case with no significant change of P-cadherin mRNA and only a mild loss of E-cadherin mRNA also showed no change in mRNA levels of both

Table 2 E-cadherin and P-cadherin expression in paired non-neoplastic and neoplastic primary prostate cultures derived from prostatectomy specimens

Case	E-cadherin ^a		Percentage loss in tumor ^b	P-cadherin ^a		Percentage loss in tumor ^b
	Non-neoplastic	Tumor		Non-neoplastic	Tumor	
1	71.0 \pm 2.2	ND ^c	100	65.7 \pm 2.0	0.8 \pm 0.1	99
2	27.4 \pm 6.4	3.7 \pm 0.3	86	53.4 \pm 6.5	17.8 \pm 1.3	67
3	18.0 \pm 0.2	12.6 \pm 1.9	30	88.8 \pm 6.5	86.4 \pm 9.5	3
4	93.5 \pm 12.0	5.4 \pm 0.9	94	87.8 \pm 7.0	25.5 \pm 2.5	71
5	41.5 \pm 3.0	24.4 \pm 4.0	41	30.5 \pm 1.4	18.1 \pm 2.4	41
6	56.7 \pm 1.1	8.1 \pm 1.0	86	71.8 \pm 2.9	17.1 \pm 2.2	76
7	53.8 \pm 6.1	22.2 \pm 0.7	59	62.7 \pm 3.5	19.4 \pm 2.2	69

^a Level of E-cadherin and P-cadherin are normalized with β -actin from the same sample: (E-cadherin or P-cadherin)/actin \times 100

^b Percentage loss in tumor primary culture: [(N - T)/N] \times 100%

^c ND, not detectable

Table 3 α -Catenin and β -catenin expression in paired non-neoplastic and neoplastic primary prostate cultures derived from prostatectomy specimens

Case	α -catenin ^a		Percentage loss in tumor ^b	β -catenin ^a		Percentage loss in tumor ^b
	Non-neoplastic	Tumor		Non-neoplastic	Tumor	
1	45.1 \pm 7.1	17.3 \pm 0.5	62	19.7 \pm 3.6	ND ^c	100
2	49.2 \pm 1.6	36.2 \pm 4.0	26	21.7 \pm 1.5	3.9 \pm 0.2	82
3	48.0 \pm 5.9	47.8 \pm 9.0	<1	40.1 \pm 5.3	38.9 \pm 6.2	3
4	61.1 \pm 2.5	40.8 \pm 2.6	33	36.8 \pm 1.8	22.1 \pm 1.9	40
5	58.2 \pm 1.8	27.8 \pm 1.6	52	29.8 \pm 2.0	15.2 \pm 1.1	49
6	46.7 \pm 4.7	33.6 \pm 4.7	28	31.5 \pm 4.2	13.5 \pm 1.6	57
7	43.2 \pm 2.6	26.4 \pm 1.7	39	22.3 \pm 1.5	11.6 \pm 1.4	48

^a Level of α -catenin and β -catenin are normalized with β -actin from the same sample: (catenin/actin) \times 100

^b Percentage loss in tumor primary culture: [(N - T)/N] \times 100%

^c ND, not detectable

α - and β -catenins. Moderate interspecimen variation was observed in the baseline expression of α -catenin and β -catenin mRNA levels in the non-neoplastic cultures.

Immunohistochemical studies of cadherins and catenins

In benign prostate tissue, E-cadherin was, in all cases, uniformly localized to the membranes of luminal glandular epithelial cells, predominantly at cell-cell junctions (Fig. 3A). One case of prostate cancer showed complete negative staining for E-cadherin (Fig. 3B), and the remaining six cases demonstrated reduced immunostaining for E-cadherin, with 25–75% of cancer cells positive (Fig. 3C). The cancerous glands generally showed reduced signal intensity and an altered heterogeneous staining pattern, which included focal cytoplasmic staining and reduced membranous staining (Fig. 3C, Table 4).

Benign prostate tissue showed uniform basal cell immunoreactivity for P-cadherin, with principally cytoplasmic and focal membranous pattern staining. The

benign, glandular non-basal epithelial cells and stromal cells were negative for P-cadherin (Fig. 3D). P-cadherin immunoreactivity was completely absent in two cases of prostate cancer (Fig. 3E), and the remaining five cases showed variable focal positivity, which was predominantly cytoplasmic (Fig. 3F). This focal P-cadherin immunostaining positivity was confirmed by staining multiple sections and by using different monoclonal antibodies. In some cases, serial sections also appeared to show immunostaining for both E- and P-cadherins with the same neoplastic cells.

In all cases of benign prostate tissue, α - and β -catenin protein expression showed strong homogeneous staining of the luminal glandular epithelium and the basal cells. In a pattern similar to that of normal E-cadherin, the α - and β -catenins were localized predominantly at luminal epithelial cell-cell borders (Fig. 2A, C). In all cases of prostate cancer, there was a mild-to-moderate reduction in staining for both catenins with 50–75% of cells positive, and the staining tended to be heterogeneous (Fig. 2B, D; Table 4).

Table 4 Immunohistochemical expression of cadherins and catenins in prostatectomy specimens corresponding to primary prostate culture

Case	E-cadherin	P-cadherin	α -catenin	β -catenin
1	–	–	++	++
2	++	+	++	++
3	+++	++	+++	+++
4	+	–	++	+++
5	+++	+	+++	+++
6	++	+	+++	+++
7	++	+	++	+++

–, Negative; +, < 25% positive; ++, 25–50% positive; +++, 50–75% positive; +++, > 75% positive

Discussion

In this study, we observed a coordinated down-regulation of the expression in the genes involved in the cadherin and catenin mediated cell-cell pathway at the mRNA level. The protein levels, as demonstrated by the immunohistochemical studies on the corresponding tissue sections, were generally consistent with the mRNA data as well as with that reported in the literature [18, 33, 34, 38, 39].

E-cadherin showed the most consistent loss of expression at both the mRNA level and the protein level.

Fig. 2A–D Immunohistochemical staining of α - and β -catenin in non-neoplastic prostate and in prostate adenocarcinoma. Original magnification $\times 115$. **A, C** Normal membranous expression of α -catenin and β -catenin in non-neoplastic prostatic epithelium (Case 1). **B** Decreased immunostaining for α -catenin in prostate adenocarcinoma (Case 1). **D** Decreased and heterogeneous immunostaining for β -catenin in prostate adenocarcinoma (Case 1)

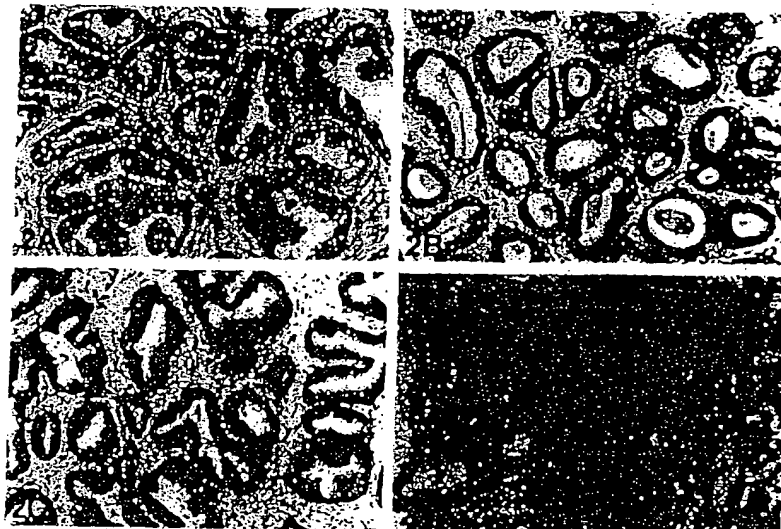
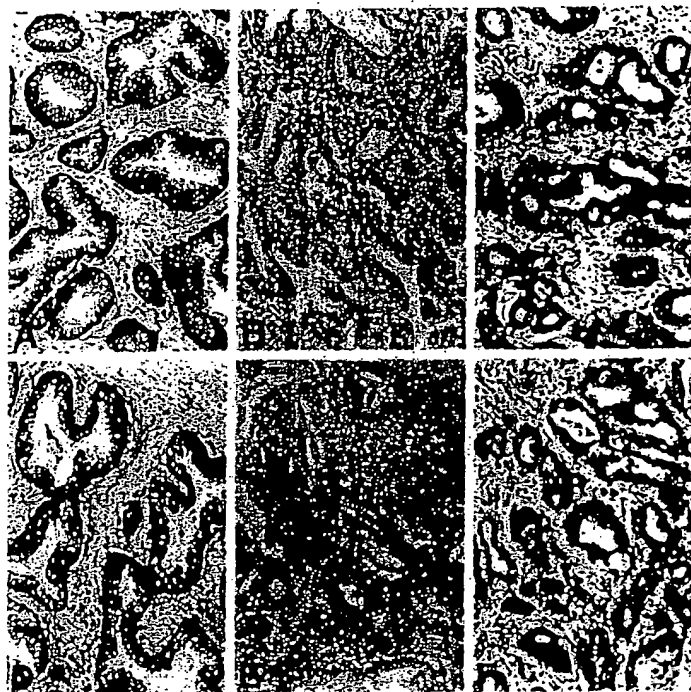


Fig. 3 A Immunohistochemical staining of E- and P-cadherin in non-neoplastic prostate and in prostate adenocarcinoma. Original magnification $\times 115$. A Normal membranous expression of E-cadherin in non-neoplastic prostatic epithelium (Case 1). B, C Complete negative (Case 1) and focal heterogeneous (Case 3) immunostaining for E-cadherin in prostate adenocarcinoma. D Normal continuous basal layer expression of P-cadherin in a portion of non-neoplastic prostatic epithelium (Case 1). E, F Complete negative (Case 1) and mild focal heterogeneous (Case 3) immunostaining for P-cadherin in prostate adenocarcinoma



LOH at chromosome 16q, where both E-cadherin and P-cadherin are located, occurs in up to 30% of prostate cancers. Four of our cases showed a greater than 50% reduction in mRNA, ranging from 87 to 100%, suggesting that mechanisms in addition to LOH may play a role in the reduction of E-cadherin mRNA levels below that of the 50% predicted by LOH alone.

Previous studies have suggested that P-cadherin could serve as a specific marker for basal cell differentiation and was not expressed in prostate cancer, although a recent study has shown focal P-cadherin expression in some prostate tumors [18]. In this study, we demonstrated P-cadherin mRNA in six of seven neoplastic cultures, although it was significantly reduced in all six cases. It is impossible to rule out the possibility that some of the P-cadherin mRNA expression may have resulted from potential contamination by small numbers of non-neoplastic basal cells admixed with the neoplastic cells within the culture material. However, we favor the interpretation that low levels of P-cadherins are expressed in cultured tumor cells, as well as weakly in some tumors in vivo owing to disruption of normal gene regulation. This interpretation is favored by the presence of focal immunostaining for P-cadherin protein in histologically neoplastic cells in five of seven cases. The histologic selection criteria (requiring minimal to no benign prostate glands) should also have minimized major contamination. Despite the presence of mRNA in primary tumor cultures and focal positive immuno-

staining, P-cadherin immunostaining may still serve as a useful basal cell marker because the staining pattern was distinctly abnormal in the cases where it was focally present.

In this study, the levels of α - and β -catenin mRNA were also lower than normal in six of seven cases, though the reductions were relatively less than those of cadherins, especially for the α -catenins. Catenin protein expression was generally moderate to weak by immunohistochemistry and showed a heterogeneous cytoplasmic and weak membranous staining pattern. The immunopositivity was generally similar in most cases, with 25–75% cells showing positivity. The results of the immunohistochemical studies were generally consistent with the mRNA data; although not in all cases (e.g., Case 1); perhaps due to tumor heterogeneity.

In this study, we also observed a coordinated down-regulation of E-cadherin and the catenins in most cases; this was most observable at the mRNA level. The cadherins are tightly regulated during embryogenesis and appear to serve the need for precise spatio-temporal regulation. The promoter sequences of both E-cadherin and P-cadherin have been cloned and functionally analyzed [2, 5, 10, 15]. Both promoters have similar regulatory elements, such as GC-rich regions and CCAAT boxes. Although the two promoters share similar sequences, in vitro binding studies suggest that the two promoters are regulated by different transcriptional factors [11]. The tissue specificity of these promoters

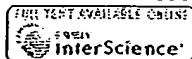
appears to be derived by different combinations of a relatively few factors common to many types of tissues, and does not appear to be derived from transcription factors specific for each type of tissue. In our study, the degree of loss of expression of α - and β -catenins at the mRNA level was correlated with reductions in the levels of E-cadherin expression. Although the exact mechanism of this coordinated down-regulation is not known, the coordinated pattern supports the hypothesis that loss or alteration of some regulatory factors occurs during prostate tumor progression. Possible mechanisms include transcriptional factor alterations or hypermethylation of the promoter region [14, 43]. Limited information is available on the transcriptional regulation of the catenins, but it is possible that similar mechanisms may play a role.

In summary, this is the first comparative study of the expression of the genes involved in the cadherin-mediated cell-cell adhesion pathway at the mRNA level using paired neoplastic and non-neoplastic primary cultures derived from prostatectomy specimens. Our results indicate that (1) there is a marked patient-to-patient variation in the normal levels of the cadherins and catenins; (2) mRNA levels of E-cadherin as well as catenins are significantly reduced in some prostate cancer primary cultures, and the reduction tends to be to the same degree in each tumor, suggesting a defect in a regulating mechanism common to all of these genes; (3) P-cadherin appears to be present at both the mRNA level and the protein level in some prostate cancers. This coordinated down-regulation of E-cadherin and catenin-mediated adhesion pathways may play a crucial role in tumor pathogenesis and metastasis.

References

- Behrens J, Mareel M, Fiers W, van Roy F, Birchmeier W (1989) Dissecting tumor cell invasion: epithelial cells acquire invasive properties after the loss of uvomorulin-mediated cell-cell adhesion. *J Cell Biol* 108: 2435
- Behrens J, Lowrick O, Klein-Hitpass L, Birchmeier W (1991) The E-cadherin promoter: functional analysis of the GC-rich region and an epithelial cell-specific palindromic regulatory element. *Proc Natl Acad Sci USA* 88: 11,495
- Birchmeier W, Behrens J (1994) Cadherin expression in carcinomas: role in the formation of cell junctions and prevention of invasiveness. *Biochem Biophys Acta* 1198: 11
- Bussemakers MJ, van Moorselaar RJ, Girolodi LA, Ichikawa T, Isaacs JT, Takeichi M, Debruyne FM, Schalken JA (1992) Decreased expression of E-cadherin in the progression of rat prostate cancer. *Cancer Res* 52: 2916
- Bussemakers MJ, Girolodi LA, van Bokhoven A, Schalken JA (1994) Transcriptional regulation of the human E-cadherin gene in human prostate cell lines: characterization of the human E-cadherin promoter. *Biochem Biophys Res Commun* 203: 1284
- Carter BS, Ewing CM, Ward WS, Teiger BF, Alders TW, Scalken JA, Epstein JI, Isaacs WB (1990) Allelic loss of chromosomes 16q and 10q in human prostate cancer. *Proc Natl Acad Sci USA* 87: 8751
- Chomczynski P, Sacchi N (1987) Single-step method of RNA isolation by acid guanidinium thiocyanate-phenol-chloroform extraction. *Ann Biochem* 162: 156
- Cohen M, Griebling T, Ahaghotu C, Rokhlin O, Ross J (1997) Cellular adhesion molecules in urologic malignancies. *Am J Clin Pathol* 107: 56
- Doki Y, Shiozaki H, Tahara H, Inoue M, Oka H, Iihara K, Kadowaki T, Takeichi M, Mori T (1993) Correlation between E-cadherin expression and invasiveness in vitro in a human esophageal cancer cell line. *Cancer Res* 53: 3421
- Faraldo ML, Cano A (1993) The 5' flanking sequences of the mouse P-cadherin gene: homologies to 5' sequences of the E-cadherin gene and identification of a first 215 base-pair intron. *J Mol Biol* 231: 935
- Faraldo ML, Rodrigo I, Behrens J, Birchmeier W, Cano A (1997) Analysis of the E-cadherin and P-cadherin promoters in murine keratinocyte cell lines from different stages of mouse skin carcinogenesis. *Mol Carcinog* 20: 33
- Frixen UH, Behrens J, Sachs M, Eberle G, Voss B, Ward A, Lochner D, Birchmeier W (1991) E-cadherin-mediated cell-cell adhesion prevents invasiveness of human carcinoma cells. *J Cell Biol* 113: 173
- Girolodi LA, Schalken JA (1993) Decreased expression of the intracellular adhesion molecule E-cadherin in prostate cancer: biologic significance and clinical implications. *Cancer Metastasis Rev* 12: 29
- Graff JR, Herman JG, Lapidus RG, Chopra H, Xu R, Jarrard DF, Isaacs WB, Pitha PM, Davidson NE, Baylin SB (1995) E-cadherin expression is silenced by DNA hypermethylation in human breast and prostate carcinomas. *Cancer Res* 55: 5195
- Hatta M, Takeichi M (1994) Complex cell type-specific transcriptional regulation by the promoter and an intron of the mouse P-cadherin gene. *Dev Growth Differ* 36: 509
- Hinck L, Nathke IS, Papkoff J, Nelson WJ (1994) Dynamics of cadherin/catenin complex formation: novel protein interactions and pathways of complex assembly. *J Cell Biol* 125: 1327
- Humphrey PA, Zhu X, Zarnegar R, Swanson PD, Ratliff TL, Vollmer RT, Day ML (1995) Hepatocyte growth factor and its receptor (c-MET) in prostatic carcinoma. *Am J Pathol* 147: 386
- Jarrard DF, Paul R, Vanbokhoven A, Nguyen SH, Bova GS, Wheelock MJ, Johnson KR, Schalken J, Bussemakers M, Isaacs WB (1997) P-cadherin is a basal cell-specific epithelial marker that is not expressed in prostate cancer. *Clin Cancer Res* 3: 2121
- Kadowaki T, Shiozaki H, Inoue M, Tamura S, Oka H, Doki Y, Iihara K, Matsui S, Iwazawa T, Nagafuchi A (1994) E-cadherin and α -catenin expression in human esophageal cancer. *Cancer Res* 54: 291
- Krill D, Shuman M, Thompson MT, Becich MJ, Strom SC (1997) A simple method for the isolation and culture of epithelial and stromal cells from benign and neoplastic prostates. *Urology* 49: 981
- Kunimi K, Bergerheim US, Larsson IL, Ekman P, Collins VP (1991) Allelotyping of prostate carcinoma. *Genomics* 11: 530
- Liotta LA (1986) Tumor invasion and metastasis: role of extracellular matrix. *Cancer Res* 46: 1
- Mayer B, Johnson JP, Leill F, Jauch KW, Heiss MM, Schildberg FW, Birchmeier W, Funke I (1993) E-cadherin expression in primary and metastatic gastric cancer: down-regulation correlates with cellular dedifferentiation and glandular disintegration. *Cancer Res* 53: 1690
- Morton R, Ewing C, Nagafuchi A, Tsukita S, Isaacs W (1993) Reduction of E-cadherin levels and deletion of the α -catenin gene in human prostate cancer cells. *Cancer Res* 53: 3585
- Murant SJ, Handley J, Stower M, Reid N, Cussenot O, Maitland NJ (1997) Coordinated changes in expression of cell-cell adhesion molecules in prostate cancer. *Eur J Cancer* 33: 263
- Nati E, Magenis RE, Zimmer J, Mansouri A, Scherer G (1989) Regional assignment of the human foci for uvomorulin and chymotrypsinogen B with the help of two overlapping deletions on the long arm of chromosome 16. *Cytogenet Cell Genet* 50: 145
- Paul R, Ewing C, Jarrard D, Isaacs W (1997) The cadherin cell-cell adhesion pathway in prostate cancer progression. *Br J Urol* 79: 37

28. Philips SM, Kinsella AR, Lee SJ, Morton DG (1994) Chromosome 16q and E-cadherin loss in prostate cancer. *Br J Cancer* (69 Suppl) 21: 19
29. Richmond PJ, Karayiannakis AJ, Nagafuchi A, Kaisary AV, Pignatelli M (1997) Aberrant E-cadherin and α -catenin expression in prostate cancer: correlation with patient survival. *Cancer Res* 57: 3189
30. Sakaki T, Wato M, Kaji R, Mushimoto K, Shirasu R, Tanaka A (1994) Correlation of E- and P-cadherin expression with differentiation grade and mode of invasion in gingival carcinoma. *Pathol Int* 44: 280
31. Shiozaki H, Oka H, Inoue M, Tamura S, Monden M (1996) E-cadherin mediated adhesion system in cancer cells. *Cancer Suppl* 77: 1605
32. Siitonen S, Kononen J, Helin H, Rantala I, Holli K, Isola J (1996) Reduced E-cadherin expression is associated with invasiveness and unfavorable prognosis in breast cancer. *Am J Clin Pathol* 105: 394
33. Solaer AP, Harner GD, Knudsen KA, McBrearty FX, Grujic E, Salazar H, Han AC, Keshgegian AA (1997) Expression of P-cadherin identifies prostate-specific-negative cells in epithelial tissues of male sexual accessory organs and in prostate carcinomas. *Am J Pathol* 151: 471
34. Takayama T, Shiozaki H, Shibamoto S, Oka H, Kimura Y, Tamura S, Inoue M, Monden T, Ito F, Monden M (1996) β -catenin expression in human cancers. *Am J Pathol* 148: 39
35. Takeichi M (1988) Cell-cell adhesion molecules controlling animal morphogenesis. *Development* 102: 639
36. Takeichi M (1990) Cadherins: a molecular family important in selective cell-cell adhesion. *Annu Rev Biochem* 61: 147
37. Takeichi M (1991) Cadherin cell adhesion receptor as a morphogenetic regulator. *Science* 251: 1451
38. Umbas R, Isaacs WB, Bringuier PP, Schaafama HE, Karthaus HF, Oosterhof GO, Debruyne FM, Schalken JA (1994) Decreased E-cadherin expression is associated with poor prognosis in patients with prostate cancer. *Cancer Res* 49: 2128
39. Umbas R, Isaacs W, Bringuier P, Xue Y, Debruyne F, Schalken J (1997) Relation between aberrant α -catenin expression and loss of E-cadherin function in prostate cancer. *Int J Cancer* 74: 374
40. Vlemmings K, Vakaet JL, Marcel M, Fiers W, van Roy F (1991) Genetic manipulation of E-cadherin expression by epithelial cell tumor cells reveals an invasion suppressor role. *Cell* 66: 107
41. Wang J, Pegoraro E, Menegazzo E, Gennarelli M, Hoop RC, Angelini C, Hoffman EP (1995) Myotonic dystrophy: evidence for a possible dominant-negative RNA mutation. *Hum Mol Genet* 4: 599
42. Watabe M, Nagafuchi A, Tsukita S, Takeichi M (1994) Induction of polarized cell-cell association and retardation of growth by activation of the E-cadherin-catenin adhesion system in a dispersed carcinoma line. *J Cell Biol* 127: 247
43. Yoshiura K, Kanai Y, Ochiai A, Shimoyama Y, Sugimura T, Hirohashi S (1995) Silencing of the E-cadherin invasion-suppressor gene by CpG methylation in human carcinomas. *Proc Natl Acad Sci USA* 92: 7416
44. Zhou J, Spier SJ, Beech J, Hoffman EP (1994) Pathophysiology of sodium channelopathies: correlation of normal/mutant mRNA ratios with clinical phenotype in dominantly inherited periodic paralysis. *Hum Mol Genet* 3: 1599



Vascular endothelial growth factor expression correlates with matrix metalloproteinases MT1-MMP, MMP-2 and MMP-9 in human glioblastomas.

Munaut C, Noel A, Hougrand O, Foidart JM, Boniver J, Deprez M.

Laboratory of Tumour and Development Biology, University of Liege, Liege, Belgium.

Vascular endothelial growth factor (VEGF) is the major endothelial mitogen in central nervous system neoplasms and it is expressed in 64-95% of glioblastomas (GBMs). Tumour cells are the main source of VEGF in GBMs whereas VEGF receptors (VEGFR-1, its soluble form sVEGFR-1, VEGFR-2 and neuropilin-1) are expressed predominantly by endothelial cells. Infiltrating tumour cells and newly-formed capillaries progress through the extracellular matrix by local proteolysis involving matrix metalloproteinases (MMPs). Recent studies have shown that VEGF expression and bioavailability can be modulated by MMPs. We reported previously that the expression of MT1-MMP in human breast cancer cells was associated with an enhanced VEGF expression. We used quantitative RT-PCR, Western blot, gelatin zymography and immunohistochemistry to study the expression of VEGF, VEGFR-1, VEGFR-2, sVEGFR-1, neuropilin-1, MT1-MMP, MMP-2, MMP-9 and TIMP-2 in 20 human GBMs and 5 normal brains. The expression of these MMPs was markedly increased in most GBMs with excellent correlation between mRNA and protein levels; activated forms of MMP-2 and MMP-9 were present in 8/18 and 7/18 of GBMs. A majority of GBMs (17/20) also expressed high levels of VEGF, as previously reported, with strong correlation between VEGF and MT1-MMP gene expression levels, and double-immunostaining showed that VEGF and MT1-MMP peptides co-localize in tumour and endothelial cells. Our results suggest that the interplay between metalloproteinases and VEGF previously described in experimental tumours may also be operative in human GBMs. Because of its dual ability to activate MMP-2 and to up-regulate VEGF, MT1-MMP might be of central importance in the growth of GBMs and represent an interesting target for anti-cancer treatments. Copyright 2003 Wiley-Liss, Inc.

PMID: 12918061 [PubMed - indexed for MEDLINE]

Real-time quantitative RT-PCR of cyclin D1 mRNA in mantle cell lymphoma: comparison with FISH and immunohistochemistry.

Hui P, Howe JG, Crouch J, Nimmakayalu M, Oumsiyeh MB, Tallini G, Flynn SD, Smith BR.

Department of Laboratory Medicine, Yale University School of Medicine, 333 Cedar Street, P.O. Box 208035, New Haven, CT 06520-8035, USA.

Presence of the balanced translocation t(11;14)(q13;q32) and the consequent overexpression of cyclin D1 found in mantle cell lymphoma (MCL) has been shown to be of important diagnostic value. Although many molecular and immunohistochemical approaches have been applied to analyze cyclin D1 status, correlative studies to compare different methods for the diagnosis of MCL are lacking. In this study, we examined 39 archived paraffin specimens from patients diagnosed with a variety of lymphoproliferative diseases including nine cases meeting morphologic and immunophenotypic criteria for MCL by: (1) real-time quantitative RT-PCR to evaluate cyclin D1 mRNA expression; (2) dual fluorescence in situ hybridization (FISH) to evaluate the t(11;14) translocation in interphase nuclei; and (3) tissue array immunohistochemistry to evaluate the cyclin D1 protein level. Among the nine cases of possible MCL, seven cases showed overexpression of cyclin D1 mRNA (cyclin D1 positive MCL) and two cases showed no cyclin D1 mRNA increase (cyclin D1 negative "MCL-like"). In six of seven cyclin D1 positive cases, the t(11;14) translocation was demonstrated by FISH analysis; in one case FISH was unsuccessful. Six of the seven cyclin D1 mRNA overexpressing cases showed increased cyclin D1 protein on tissue array immunohistochemistry; one was technically suboptimal. Among the two cyclin D1 negative MCL-like cases, FISH confirmed the absence of the t(11;14) translocation in both cases. All other lymphoproliferative diseases studied were found to have low or no cyclin D1 mRNA expression and were easily distinguishable from the cyclin D1 overexpressing MCLs by all three techniques. In addition, to confirming the need to assess cyclin D1 status, as well as, morphology and immunophenotyping to establish the diagnosis of MCL, this study demonstrates good correlation and comparability between measure of cyclin D1 mRNA, the 11;14 translocation and cyclin D1 protein.

Publication Types:

- Evaluation Studies

PMID: 12952233 [PubMed - indexed for MEDLINE]



Increased expression of proteasome subunits in skeletal muscle of cancer patients with weight loss.

Khal J, Hine AV, Fearon KC, Dejong CH, Tisdale MJ.

Pharmaceutical Sciences Research Institute, Aston University, Birmingham B4 7ET, UK.

Atrophy of skeletal muscle is common in patients with cancer and results in increased morbidity and mortality. In order to design effective therapy the mechanism by which this occurs needs to be elucidated. Most studies suggest that the ubiquitin-proteasome proteolytic pathway is most important in intracellular proteolysis, although there have been no reports on the activity of this pathway in patients with different extents of weight loss. In this report the expression of the ubiquitin-proteasome pathway in rectus abdominis muscle has been determined in cancer patients with weight loss of 0-34% using a competitive reverse transcriptase polymerase chain reaction to measure expression of mRNA for proteasome subunits C2 and C5, while protein expression has been determined by western blotting. Overall, both C2 and C5 gene expression was increased by about three-fold in skeletal muscle of cachectic cancer patients (average weight loss 14.5 \pm 2.5%), compared with that in patients without weight loss, with or without cancer. The level of gene expression was dependent on the amount of weight loss, increasing maximally for both proteasome subunits in patients with weight loss of 12-19%. Further increases in weight loss reduced expression of mRNA for both proteasome subunits, although it was still elevated in comparison with patients with no weight loss. There was no evidence for an increase in expression at weight losses less than 10%. There was a good correlation between expression of proteasome 20S α subunits, detected by western blotting, and C2 and C5 mRNA, showing that increased gene expression resulted in increased protein synthesis. Expression of the ubiquitin conjugating enzyme, E2(14k), with weight loss followed a similar pattern to that of proteasome subunits. These results suggest variations in the expression of key components of the ubiquitin-proteasome pathway with weight loss of cancer patients, and suggest that another mechanism of protein degradation must be operative for patients with weight loss less than 10%.

PMID: 16125116 [PubMed - in process]

ELSEVIER
SCIENCE DIRECT

Increased expression of proteasome subunits in skeletal muscle of cancer patients with weight loss.

Khal J, Hine AV, Fearon KC, Dejong CH, Tisdale MJ.

Pharmaceutical Sciences Research Institute, Aston University, Birmingham B4 7ET, UK.

Atrophy of skeletal muscle is common in patients with cancer and results in increased morbidity and mortality. In order to design effective therapy the mechanism by which this occurs needs to be elucidated. Most studies suggest that the ubiquitin-proteasome proteolytic pathway is most important in intracellular proteolysis, although there have been no reports on the activity of this pathway in patients with different extents of weight loss. In this report the expression of the ubiquitin-proteasome pathway in rectus abdominis muscle has been determined in cancer patients with weight loss of 0-34% using a competitive reverse transcriptase polymerase chain reaction to measure expression of mRNA for proteasome subunits C2 and C5, while protein expression has been determined by western blotting. Overall, both C2 and C5 gene expression was increased by about three-fold in skeletal muscle of cachectic cancer patients (average weight loss 14.5 \pm 2.5%), compared with that in patients without weight loss, with or without cancer. The level of gene expression was dependent on the amount of weight loss, increasing maximally for both proteasome subunits in patients with weight loss of 12-19%. Further increases in weight loss reduced expression of mRNA for both proteasome subunits, although it was still elevated in comparison with patients with no weight loss. There was no evidence for an increase in expression at weight losses less than 10%. There was a good correlation between expression of proteasome 20S α subunits, detected by western blotting, and C2 and C5 mRNA, showing that increased gene expression resulted in increased protein synthesis. Expression of the ubiquitin conjugating enzyme, E2(14k), with weight loss followed a similar pattern to that of proteasome subunits. These results suggest variations in the expression of key components of the ubiquitin-proteasome pathway with weight loss of cancer patients, and suggest that another mechanism of protein degradation must be operative for patients with weight loss less than 10%.

PMID: 16125116 [PubMed - in process]



Id-1 and Id-2 are overexpressed in pancreatic cancer and in dysplastic lesions in chronic pancreatitis.

Maruyama H, Kleeff J, Wildi S, Friess H, Buchler MW, Israel MA, Korc M.

Division of Endocrinology, Department of Medicine, University of California, Irvine, USA.

Id proteins antagonize basic helix-loop-helix proteins, inhibit differentiation, and enhance cell proliferation. In this study we compared the expression of Id-1, Id-2, and Id-3 in the normal pancreas, in pancreatic cancer, and in chronic pancreatitis (CP). Northern blot analysis demonstrated that all three Id mRNA species were expressed at high levels in pancreatic cancer samples by comparison with normal or CP samples. Pancreatic cancer cell lines frequently coexpressed all three Ids, exhibiting a good correlation between Id mRNA and protein levels, as determined by immunoblotting with highly specific anti-Id antibodies. Immunohistochemistry using these antibodies demonstrated the presence of faint Id-1 and Id-2 immunostaining in pancreatic ductal cells in the normal pancreas, whereas Id-3 immunoreactivity ranged from weak to strong. In the cancer tissues, many of the cancer cells exhibited abundant Id-1, Id-2, and Id-3 immunoreactivity. Scoring on the basis of percentage of positive cells and intensity of immunostaining indicated that Id-1 and Id-2 were increased significantly in the cancer cells by comparison with the respective controls. Mild to moderate Id immunoreactivity was also seen in the ductal cells in the CP-like areas adjacent to these cells and in the ductal cells of small and interlobular ducts in CP. In contrast, in dysplastic and atypical papillary ducts in CP, Id-1 and Id-2 immunoreactivity was as significantly elevated as in the cancer cells. These findings suggest that increased Id expression may be associated with enhanced proliferative potential of pancreatic cancer cells and of proliferating or dysplastic ductal cells in CP.

PMID: 10487839 [PubMed - indexed for MEDLINE]

Id-1 and Id-2 Are Overexpressed in Pancreatic Cancer and in Dysplastic Lesions in Chronic Pancreatitis

Haruhisa Maruyama,* Jörg Kleeff,* Stefan Wildi,*
Helmut Friess,[†] Markus W. Büchler,[†]
Mark A. Israel,[‡] and Murray Korc*

From the Division of Endocrinology, Diabetes, and Metabolism,*
Departments of Medicine, Biological Chemistry and
Pharmacology, University of California, Irvine, California; the
Department of Visceral and Transplantation Surgery,[†] University
of Bern, Bern, Switzerland; and the Preuss Laboratory,[‡]
Department of Neurological Surgery, University of California,
San Francisco, California

Id proteins antagonize basic helix-loop-helix proteins, inhibit differentiation, and enhance cell proliferation. In this study we compared the expression of Id-1, Id-2, and Id-3 in the normal pancreas, in pancreatic cancer, and in chronic pancreatitis (CP). Northern blot analysis demonstrated that all three Id mRNA species were expressed at high levels in pancreatic cancer samples by comparison with normal or CP samples. Pancreatic cancer cell lines frequently coexpressed all three Ids, exhibiting a good correlation between Id mRNA and protein levels, as determined by immunoblotting with highly specific anti-Id antibodies. Immunohistochemistry using these antibodies demonstrated the presence of faint Id-1 and Id-2 immunostaining in pancreatic ductal cells in the normal pancreas, whereas Id-3 immunoreactivity ranged from weak to strong. In the cancer tissues, many of the cancer cells exhibited abundant Id-1, Id-2, and Id-3 immunoreactivity. Scoring on the basis of percentage of positive cells and intensity of immunostaining indicated that Id-1 and Id-2 were increased significantly in the cancer cells by comparison with the respective controls. Mild to moderate Id immunoreactivity was also seen in the ductal cells in the CP-like areas adjacent to these cells and in the ductal cells of small and interlobular ducts in CP. In contrast, in dysplastic and atypical papillary ducts in CP, Id-1 and Id-2 immunoreactivity was as significantly elevated as in the cancer cells. These findings suggest that increased Id expression may be associated with enhanced proliferative potential of pancreatic cancer cells and of proliferating or dysplastic ductal cells in CP. (*Am J Pathol* 1999, 155:815-822)

Basic helix-loop-helix (bHLH) proteins play an important role as transcription factors in cellular development, proliferation, and differentiation.^{1,2} The basic domain of the bHLHs is required for binding to an E-box DNA sequence, thus promoting transcription of specific target genes. The HLH domain promotes dimer formation with various members of the bHLH protein family.^{1,2} Homodimers of the class B family of bHLH proteins, including MyoD, NeuroD, and numerous other proteins, are known to activate tissue-specific genes.³⁻⁵ These tissue-specific bHLHs typically form heterodimers with widely expressed class A bHLHs, which include proteins encoded by E2A, E2-2, HEB, and other genes (also termed E-proteins).⁶⁻⁹ These heterodimers activate transcription of genes that are associated with differentiation.

Id genes encode a family of four HLH proteins that lack the basic DNA binding domain.^{1,10} They act as dominant-negative HLH proteins by forming high affinity heterodimers with other bHLH proteins, thereby preventing them from binding to DNA and inhibiting transcription of differentiation-associated genes.¹⁰⁻¹² Id gene expression is down-regulated on differentiation in many cell types *in vitro* and *in vivo*.¹³⁻¹⁸ In addition, Id proteins seem to be required for cell cycle progression through G₁/S phase in certain cell types, and interaction between Id-2 and pRB is associated with enhanced proliferation in some cell lines *in vitro*.¹⁹⁻²³

Pancreatic cancer is the fifth leading cause of cancer death in the United States, with a mortality rate that virtually equals its incidence rate.²⁴ This malignancy is often associated with the overexpression of a variety of mitogenic growth factors and their receptors, and by oncogenic mutations of K-ras and inactivation of the p53 tumor suppressor gene.²⁵ We have recently reported that pancreatic cancers overexpress the HLH protein Id-2, and that enhanced expression of this protein is evident in the cytoplasm of the cancer cells within the pancreatic tumor mass.²⁶ It is not known, however, whether the expression of other Id proteins is altered in this malignancy, or whether their expression is altered in chronic pancreatitis

Contract grant sponsor: National Cancer Institute. Contract grant number: U.S. Public Health Service grant CA-40162.

Accepted for publication May 24, 1999.

Address reprint requests to Dr. Murray Korc, Division of Endocrinology, Diabetes and Metabolism, Medical Sciences I, C240, University of California, Irvine, CA 92697. E-mail: mkorc@uci.edu.

(CP), an inflammatory disease that is characterized by dysplastic ducts, foci of proliferating ductal cells, acinar cell degeneration, and fibrosis.²⁷ We now report that there is a five- to sixfold increase in Id-1 and Id-2 mRNA levels and a twofold increase in Id-3 mRNA levels in pancreatic cancer by comparison with the normal pancreas. In contrast, overall Id mRNA levels are not increased in CP.

Patients and Methods

Normal human pancreatic tissue samples from 7 male and 5 female donors (median age 41.8 years, range 14–68 years), CP tissues from 13 males and 1 female (median age 42.1 years; range 30–56 years), and pancreatic cancer tissues from 10 male and 6 female donors (median age 62.6 years; range 53–83 years) were obtained through an organ donor program and from surgical specimens from patients with severe symptomatic chronic pancreatitis or pancreatic cancer. A partial duodenopancreatectomy (Whipple/pylorus-preserving Whipple; $n = 13$), a left resection of the pancreas ($n = 2$), or a total pancreatectomy ($n = 1$) were carried out in the pancreatic cancer patients. According to the TNM classification of the Union Internationale Contre le Cancer (UICC) 6 tumors were stage 1, 1 was stage 2, and 9 were stage 3 ductal cell adenocarcinoma. Freshly removed tissue samples were fixed in 10% formaldehyde solution for 12 to 24 hours and paraffin-embedded for histological analysis. In addition, tissue samples were frozen in liquid nitrogen immediately on surgical removal and maintained in -80°C until use for RNA extraction. All studies were approved by the Ethics Committee of the University of Bern, Bern, Switzerland, and by the Human Subjects Committee at the University of California, Irvine, California.

Northern Blot Analysis

Northern blot analysis was carried out as described previously.^{26,28} Briefly, total RNA was extracted by the single step acid guanidinium thiocyanate phenol chloroform method. RNA was size-fractionated on 1.2% agarose/1.8 mol/L formaldehyde gels; electrotransferred onto nylon membranes, and cross-linked by UV irradiation. Blots were prehybridized and hybridized with cDNA probes and washed under high stringency conditions. The following cDNA probes were used: a 979-bp human Id-1 cDNA probe, a 440-bp human Id-2 cDNA probe, and a 450-bp human Id-3 cDNA probe, covering the entire coding regions of Id-1, Id-2, and Id-3, respectively. A *Bam*HI 190-bp fragment of mouse 7S cDNA that hybridizes with human cytoplasmic RNA was used to confirm equal RNA loading and transfer. Blots were then exposed at -80°C to Kodak BioMax-MS films and the resulting autoradiographs were scanned to quantify the intensity of the radiographic bands.^{26,28} For each sample the ratio of Id mRNA expression to 7S expression was calculated. To compare the relative increase in expression of the respective Id mRNA species in the cancer and CP samples, the same normal samples were used for normal/

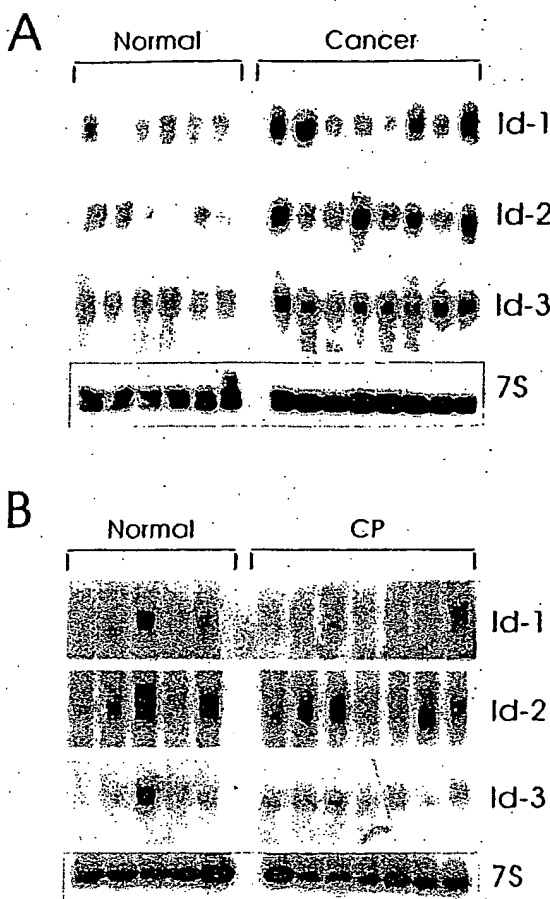


Figure 1. mRNA expression of Id-1, Id-2, and Id-3 in pancreatic cancer and chronic pancreatitis. Total RNA (20 $\mu\text{g}/\text{lane}$) from six normal, eight cancerous, and seven chronic pancreatitis tissue samples were subjected to Northern blot analysis using ^{32}P -labeled cDNA probes (500,000 cpm/ml) specific for Id-1, Id-2, and Id-3, respectively. A 7S cDNA probe (50,000 cpm/ml) was used as a loading and transfer control. Exposure times of the normal/cancer blots were 1 day for all Id probes, and 2 days for the normal/CP blots. Exposure time was 4 hours for mouse 7S cDNA. By comparison with the normal samples, Id-1 and Id-3 mRNA levels were elevated in 8 and 9 cancer samples, respectively, whereas Id-2 was elevated in 6 cancer samples.

cancer and normal/CP membranes. The median score for Id-1, Id-2, and Id-3 mRNA levels in these normal samples was set to 100. Statistical analysis was performed with SigmaStat software (Jandel Scientific, San Raphael, CA). The rank sum test was used, and $P < 0.05$ was taken as the level of significance.

Cell Culture and Western Blot Analysis

PANC-1, MIA-PaCa-2, ASPC-1, and CAPAN-1 human pancreatic cell lines were obtained from ATCC (Manassas, VA). COLO-357 human pancreatic cells were a gift from Dr. R. S. Metzger (Durham, NC). Cells were routinely grown in DMEM (COLO-357, MIA-PaCa-2, PANC-1) or RPMI (ASPC-1, CAPAN-1) supplemented with 10% fetal bovine serum, 100 U/ml penicillin, and 100 $\mu\text{g}/\text{ml}$ streptomycin. For immunoblot analysis, exponentially growing

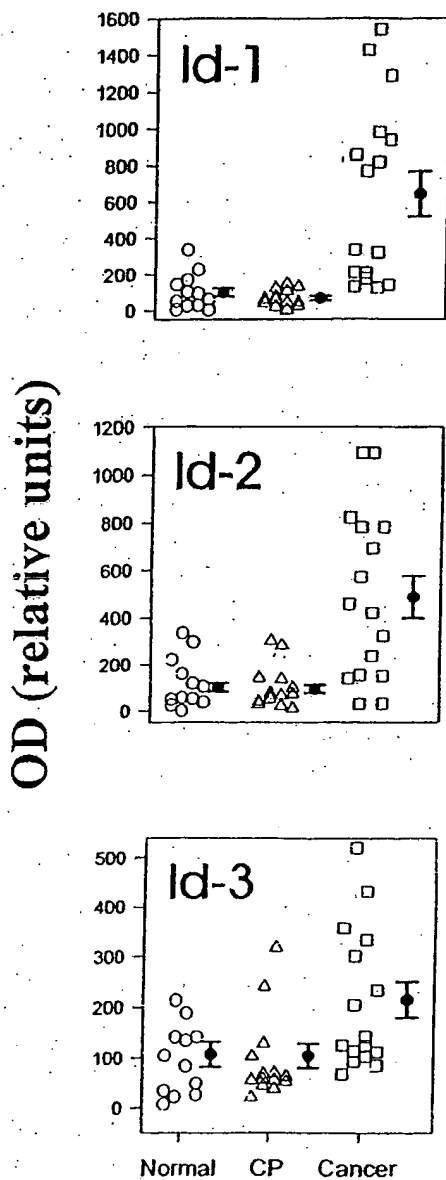


Figure 2. Densitometric analysis of Northern blots. Autoradiographs of Northern blots from 12 normal, 14 CP; and 16 pancreatic cancers were analyzed by densitometry. mRNA levels were determined by calculating the ratio of the optical density for the respective Id mRNA species in relation to the optical density of mouse 7S cDNA. To compare the relative increase in expression of the respective Id mRNA species in the cancer and CP samples, the same normal samples were used for normal/cancer and normal/CP membranes. Normal pancreatic tissues are indicated by circles, CP tissues by triangles, and cancer tissues by squares. Data are expressed as median scores \pm SD. By comparison with the normal samples, only the cancer samples exhibited significant increases: 6.5-fold ($P < 0.01$) for Id-1, fivefold ($P < 0.01$) for Id-2, and twofold ($P = 0.027$) for Id-3.

cells (60–70% confluent) were solubilized in lysis buffer containing 50 mmol/L Tris-HCl, pH 7.4, 150 mmol/L NaCl, 1 mmol/L EDTA, 1 μ g/ml pepstatin A, 1 mmol/L phenylmethylsulfonyl fluoride (PMSF), and 1% Triton X-100. Proteins were subjected to sodium dodecyl sulfate polyacryl-

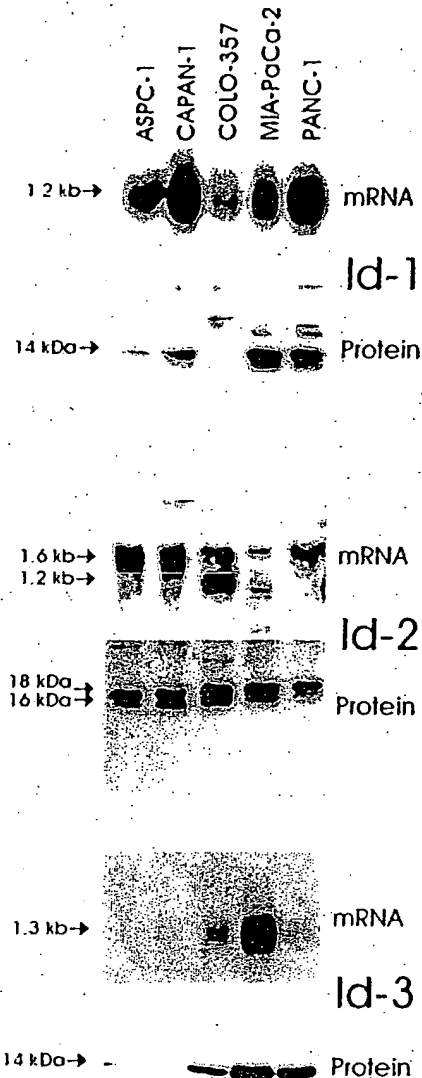


Figure 3. Id mRNA and protein expression in pancreatic cancer cell lines. Upper panels: Total RNA (20 μ g/lane) from 5 pancreatic cancer cell lines were subjected to Northern blot analysis using 32 P-labeled cDNA probes (500,000 cpm/ml) specific for Id-1, Id-2, and Id-3, respectively. Exposure times were 1 day for all Id probes. Lower panels: Immunoblotting. Cell lysates (30 μ g/lane) were subjected to SDS-PAGE. Membranes were probed with specific Id-1, Id-2, and Id-3 antibodies. Visualization was performed by enhanced chemiluminescence.

amide gel electrophoresis (SDS-PAGE), transferred to Immobilon P membranes, and incubated for 90 minutes with the indicated antibodies and for 60 minutes with secondary antibodies against rabbit IgG. Visualization was performed by enhanced chemiluminescence.

Immunohistochemistry

Specific rabbit anti-human Id-1 (C-20), Id-2 (C-20), and Id-3 (C-20; all from Santa Cruz Biotechnology, Santa

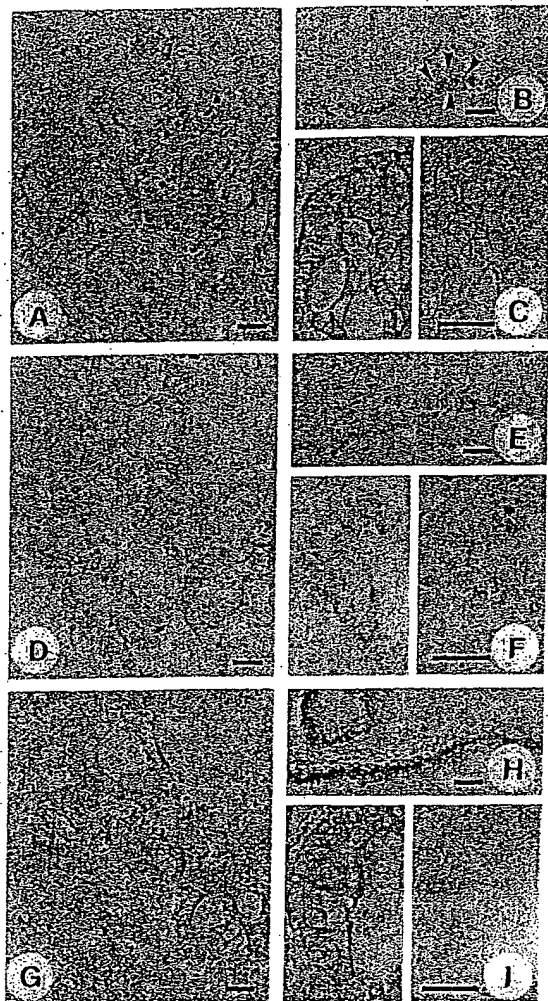


Figure 4. Normal and cancerous pancreatic tissues were subjected to immunostaining using highly specific anti-Ig-1 (A-C), anti-Ig-2 (D-F), and anti-Ig-3 (G-I) antibodies as described in the Methods section. Moderate to strong Ig-1 immunoreactivity was present in the cytoplasm of duct-like cancer cells (A and C, left panel). In the normal pancreas there was weak Ig-1 immunoreactivity in the ductal cells (B). Preabsorption with the Ig-1-specific blocking peptide abolished the Ig-1 immunoreactivity (C, right panel). Strong Ig-2 immunoreactivity was observed in the cytoplasm of the cancer cells that exhibited duct-like structures (D and F, left panel), whereas in the normal pancreas, there was only weak Ig-2 immunoreactivity in the ductal cells (E). Preabsorption with the Ig-2-specific blocking peptide abolished the Ig-2 immunoreactivity (F, right panel). Moderate to strong Ig-3 immunoreactivity was present in the duct-like cancer cells (G and I, left panel). Moderate to strong Ig-3 immunoreactivity was also present in the ductal cells of normal pancreatic tissue samples (H). Ig-3 immunoreactivity was completely abolished by preabsorption with the Ig-3 specific blocking peptide (I, right panel). A, D, and G constitute serial sections of a pancreatic cancer sample, revealing coexpression of the three Ig proteins. Scale bars, 25 μ m.

Cruz, CA) polyclonal antibodies were used for immunohistochemistry. These affinity-purified rabbit polyclonal antibodies specifically react with Ig-1, Ig-2, and Ig-3, respectively, of human origin, as determined by Western blotting. Paraffin-embedded sections (4 μ m) were subjected to immunostaining using the streptavidin-peroxidase technique. Where indicated, immunostaining for all three Ig proteins was performed on serial sections. En-

dogenous peroxidase activity was blocked by incubation for 30 minutes with 0.3% hydrogen peroxide in methanol. Tissue sections were incubated for 15 minutes (23°C) with 10% normal goat serum and then incubated for 16 hours at 4°C with the indicated antibodies in PBS containing 1% bovine serum albumin. Bound antibodies were detected with biotinylated goat anti-rabbit IgG secondary antibodies and streptavidin-peroxidase complex, using diaminobenzidine tetrahydrochloride as the substrate. Sections were counterstained with Mayer's hematoxylin. Preabsorption with Ig-1-, Ig-2-, or Ig-3-specific blocking peptides completely abolished immunoreactivity of the respective primary antibody. The immunohistochemical results were semiquantitatively analyzed as described previously.^{29,30} The percentage of positive cancer cells was stratified into four groups: 0, no cancer cells exhibiting immunoreactivity; 1, <33% of the cancer cells exhibiting immunoreactivity; 2, 33 to 67% of the cancer cells exhibiting immunoreactivity; 3 >67% of the cancer cells exhibiting immunoreactivity. The intensity of the immunohistochemical signal was also stratified into four groups: 0, no immunoreactivity; 1, weak immunoreactivity; 2, moderate immunoreactivity; 3, strong immunoreactivity. Finally, the sum of the results of the cell score and the intensity score was calculated. Statistical analysis was performed with SigmaStat software. The rank sum test was used, and $P < 0.05$ was taken as the level of significance.

Results

Northern blot analysis of total RNA isolated from 12 normal pancreatic tissues and 16 pancreatic cancers revealed the presence of the 1.2-kb Ig-1 transcript and the 1.6-kb Ig-2 mRNA transcript in 11 of the 12 normal pancreatic samples, and the 1.3-kb Ig-3 mRNA transcript in all normal pancreatic samples (Figure 1A, 2). In the cancer tissues, Ig-1 mRNA levels were elevated in 8 of 16 samples, Ig-2 mRNA levels were elevated in 9 of these samples, and Ig-3 mRNA levels were elevated in 6 of these samples (Figure 1A, 2). Concomitant overexpression of all three Ig species was observed in 6 of the cancer samples (38%). In contrast, none of the Ig mRNA species were overexpressed in CP by comparison with normal controls (Figure 1B, 2). Densitometric analysis of all of the autoradiograms indicated that there was a 6.5-fold increase ($P < 0.01$) in Ig-1 mRNA levels, a fivefold increase ($P < 0.01$) in Ig-2 mRNA levels, and a twofold increase ($P = 0.027$) in Ig-3 mRNA levels in the pancreatic cancer samples in comparison to normal controls (Figure 2). In contrast, there was no statistically significant difference in the expression levels of Ig-1, Ig-2, and Ig-3, in CP tissues in comparison to the corresponding levels in the normal pancreas (Figure 2).

Next, we assessed the expression of the three Ig genes in 5 human pancreatic cancer cell lines by Northern and Western blot analyses. Ig-1 mRNA was present at varying levels in all 5 cell lines (Figure 3). ASPC-1, CAPAN-1, MIA-PaCa-2, and PANC-1 expressed moderate to high levels of Ig-1 mRNA, whereas COLO-357 cells

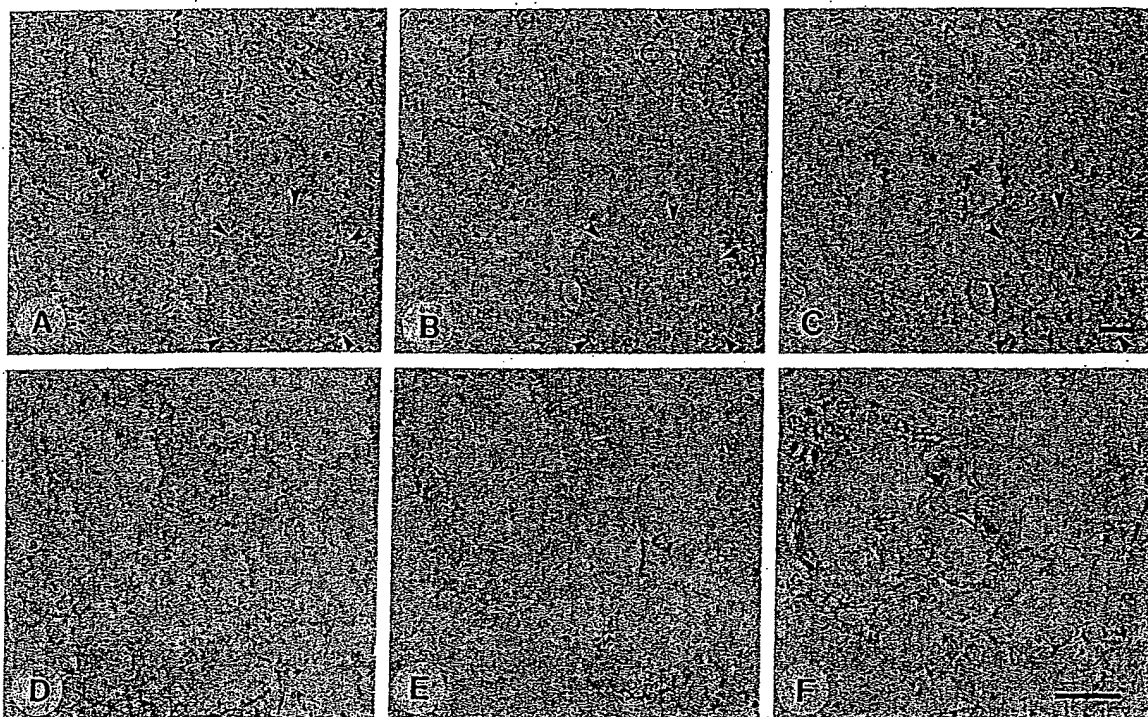


Figure 5. Immunohistochemistry of pancreatic cancer and dysplastic ducts in CP tissues. In the pancreatic cancer tissues (A-C) there was moderate to strong Id-1 (A), Id-2 (B), and Id-3 (C) immunoreactivity in the ductal cells in the areas adjacent to the cancer cells that exhibited CP-like alterations. Islet cells did not exhibit Id immunoreactivity (outlined by solid arrowheads). In the CP samples, moderate to strong Id-1 (D), Id-2 (E), and Id-3 (F) immunoreactivity was present in the cytoplasm of epithelial cells forming large dysplastic ducts. Scale bar, 25 μ m.

expressed relatively low levels of this mRNA moiety. Western blotting with a highly specific anti-Id-1 antibody confirmed the presence of the approximately 14-kd Id-1 protein in the 4 cell lines that expressed high levels of Id-1 mRNA (Figure 3). Furthermore, the three cell lines with the highest Id-1 mRNA expression (CAPAN-1, MIA-PaCa-2, and PANC-1) also exhibited the highest Id-1 protein expression. Variable levels of the 1.6-kb Id-2 mRNA transcript were present in all 5 cell lines. In addition, a minor band of approximately 1.2 kb was visible in COLO-357 and MIA-PaCa-2 cells. Immunoblot analysis with a highly specific anti-Id-2 antibody revealed two bands of approximately 16 and 18 kd at relatively high levels in all of the cell lines with exception of PANC-1 cells, in which the 16-kd band was relatively faint (Figure 3). With the exception of MIA-PaCa-2 cells, there was a good correlation between Id-2 mRNA and protein levels (Figure 3). Id-3 mRNA was present at high levels in MIA-PaCa-2 cells, at moderate levels in COLO-357 cells, and at low levels in PANC-1 cells. Id-3 mRNA was not detectable in ASPC-1 and CAPAN-1 cells (Figure 3). Immunoblot analysis with a highly specific anti-Id-3 antibody revealed an approximately 14-kd band that was most abundant in MIA-PaCa-2 cells, and was also readily apparent in COLO-357 and PANC-1 cells. In contrast, only a faint Id-3 band was seen in ASPC-1 and CAPAN-1 cells. Thus, with the exception of PANC-1 cells, there was a good correlation between Id-3 mRNA and protein levels.

To determine the localization of Id-1, Id-2, and Id-3, immunostaining was carried out using the same highly specific anti-Id antibodies. In the pancreatic cancers, moderate to strong Id-1 immunoreactivity was present in the cancer cells in 9 of 10 randomly selected cancer samples. An example of moderate Id-1 immunoreactivity is shown in Figure 4A, and of strong immunoreactivity in Figure 4C (left panel). In contrast, in the normal pancreas, faint Id-1 immunoreactivity was present only in the ductal cells of pancreatic ducts (Figure 4B, arrowheads). Preabsorption with the Id-1-specific blocking peptide completely abolished the Id-1 immunoreactivity (Figure 4C, right panel). The cancer cells also exhibited strong Id-2 (Figure 4, D and F, left panel) and moderate to strong Id-3 immunoreactivity. An example of moderate Id-3 immunoreactivity is shown in Figure 4G, and of strong immunoreactivity in Figure 4I (left panel). In contrast, only faint Id-2 immunoreactivity was present in the ductal cells in the normal pancreas (Figure 4E), whereas Id-3 immunoreactivity in these cells was more variable and ranged from moderate to occasionally strong (Figure 4H). Islet cells and acinar cells were always devoid of Id immunoreactivity: Preabsorption of the respective antibody with the blocking peptides specific for Id-2 (Figure 4F, right panel) and Id-3 (Figure 4I, right panel) completely abolished immunoreactivity. Analysis of serial pancreatic cancer sections revealed that there was often colocalization of the

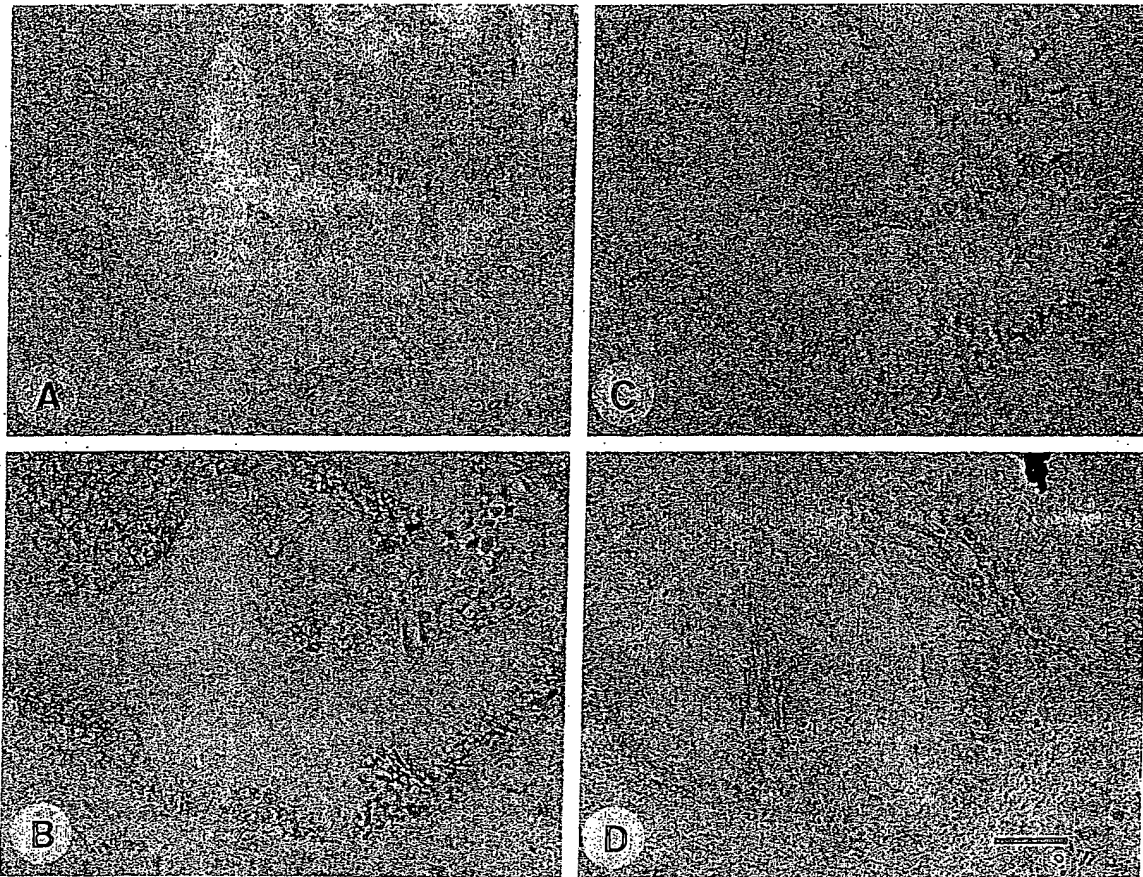


Figure 6. Immunohistochemistry of atypical papillary epithelium in CP tissues. Serial section analysis of some CP samples revealed the presence of large duct-like structures with atypical papillary epithelium. Mild to moderate Id-1 (A) and Id-2 (B) immunoreactivity and weak Id-3 (C) immunoreactivity was present in the cytoplasm of the cells forming these large ducts with papillary structures. Some CP samples also exhibited moderate Id-3 immunoreactivity in these cells (D). Scale bar, 25 μ m.

three Id proteins. An example of serial sections from a pancreatic cancer tissue is shown in Figure 4, A, D, and G.

Id-1, Id-2, and Id-3 immunoreactivity was also present at moderate levels in the cytoplasm of ductal cells within CP-like areas adjacent to the cancer cells (Figure 5, A-C). As in the normal pancreas, islet cells (outlined by arrowheads) did not exhibit Id immunoreactivity. In 4 of 9 CP samples, there were foci of ductal cell dysplasia of relatively large interlobular ducts, all of which exhibited moderate to strong Id-1, Id-2, and Id-3 immunoreactivity (Figure 5, D-F). Five of 9 CP samples also contained foci of large ducts exhibiting atypical papillary epithelium. Serial section analysis of one of those CP samples revealed mild to moderate Id-1 and Id-2 immunoreactivity and weak Id-3 immunoreactivity in the cells of these atypical papillary ducts (Figure 6, A-C). In contrast, in some of these CP samples, moderate to strong Id-3 immunoreactivity was also observed (Figure 6D). However, most of the ductal cells forming the typical ductular structures of CP, such as large interlobular ducts and small proliferating ducts, exhibited generally only weak to occasionally moderate Id immunoreactivity (data not shown).

The immunohistochemical data for Id-1, Id-2, and Id-3 are summarized in Table 1. In the case of Id-1 and Id-2, the cancer cells as well as the dysplastic and atypical papillary ducts in CP exhibited a significantly higher score than the ductal cells in the normal pancreas. In contrast, due to the marked variability in Id-3 immunostaining in the normal pancreas, the differences between normal and cancer cells and normal and dysplastic cells did not achieve statistical significance.

Discussion

Id proteins constitute a family of HLH transcription factors that are important regulators of cellular differentiation and proliferation.^{1,2} To date, four members of the human Id family have been identified.^{1,10-12} Their expression is enhanced during cellular proliferation and in response to mitogenic stimuli,^{19,31} and overexpression of Id genes inhibits differentiation and/or enhances proliferation in several different cell types.^{15,32-34} The forced expression of Id-1 in mouse small intestinal epithelium results in

Table 1. Histological Scoring

		Id-1	Id-2	Id-3
Normal (n = 6)	Ductal cells	2.0 ± 0.4	2.3 ± 0.2	2.5 ± 0.9
Cancer (n = 10)	Cancer cells	4.5* ± 0.5	5.2 [§] ± 0.3	4.5 ± 0.6
CP (n = 9)	Typical CP lesions (n = 9)	2.7 ± 0.5	3.1 ± 0.6	3.4 ± 0.7
	Dysplastic ducts (n = 4)	5.3 [†] ± 0.2	5.8 [†] ± 0.2	5.3 ± 0.4
	Atypical papillary ducts (n = 5)	4.4 [‡] ± 0.2	5.2 [‡] ± 0.2	5.0 ± 0.4

Scoring of the histological specimens was performed as described in the Patients and Methods section. Values are the means ± SD of the number of samples indicated in parenthesis. P values are based on comparisons with the respective controls in the normal samples.

*P < 0.02; [†]P < 0.01; [‡]P = 0.004; [§]P = 0.001.

adenoma formation in these animals.³⁵ The growth-promoting effects of Id genes are thought to occur through several mechanisms. For example, Id-2 can bind to members of the pRB tumor suppressor family, thus blocking their growth-suppressing activity,^{20,21} and Id-1 and Id-2 can antagonize the bHLH-mediated activation of known inhibitors of cell cycle progression such as the cyclin-dependent kinase inhibitor p21.²³

In the present study, we determined by Northern blot analysis that a significant percentage of human pancreatic cancers expressed increased Id-1, Id-2, and Id-3 mRNA levels. Increased expression was most evident for Id-1 (6.5-fold) and Id-2 (fivefold). In contrast, Id-3 mRNA levels were only twofold increased in the cancer samples, partly because this mRNA was present at relatively high levels in the normal pancreas. Immunohistochemical analysis confirmed the presence of Id-1, Id-2, and Id-3 in the cancer cells within the tumor mass, whereas in the normal pancreas faint Id-1 and Id-2 immunoreactivity and moderate to occasionally strong Id-3 immunoreactivity was present in some ductal cells. Pancreatic acinar and islet cells in the normal pancreas were devoid of Id-1, Id-2, and Id-3 immunoreactivity. In the cancer samples, all three Id proteins often colocalized in the cancer cells. Coexpression of all three Id genes was also observed in cultured pancreatic cancer cell lines, which often exhibited a close correlation between Id mRNA and protein expression. However, in MIA-PaCa-2 there was a divergence of Id-2 mRNA and protein levels, and in PANC-1 cells, Id-3 mRNA levels did not correlate well with Id-3 protein expression. These observations suggest that in these cells, the half-life of either Id mRNA or Id protein may be altered by comparison with the other cell lines. Interestingly, Id-2 immunoblotting revealed two closely spaced bands of approximately 16 and 18 kd in 4 of 5 cell lines. In view of the fact that two possible initiation codons have been reported for the Id-2 gene,³⁶ our observation raises the possibility that the two Id-2-immunoreactive bands may represent separate translation products of the Id-2 gene.

Pancreatic cancers often harbor p53 tumor suppressor gene mutations³⁷ and exhibit alterations in apoptosis pathways. Thus, these cancers often exhibit increased expression of anti-apoptotic proteins such as Bcl-2³⁸ and abnormal resistance to Fas-ligand-mediated apoptosis.³⁹ It has been shown recently that forced constitutive expression of Id genes together with the expression of anti-apoptotic genes such as Bcl-2 or Bcl-X_L can result in

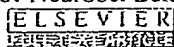
malignant transformation of human fibroblasts,¹¹ raising the possibility that the enhanced Id expression in pancreatic cancers together with increased expression of anti-apoptotic genes may contribute to the malignant potential of pancreatic cancer cells *in vivo*.

In the CP tissues there was no significant increase in Id-1, Id-2, and Id-3 mRNA levels in comparison to the normal pancreas. Immunohistochemical analysis of pancreatic cancer samples revealed colocalization of weak to moderate Id-1, Id-2, and Id-3 immunoreactivity in proliferating ductal cells in the CP-like regions adjacent to the cancer cells, indicating that Id expression was not restricted to the cancer cells. Similarly, analysis of CP samples indicated weak Id-1, Id-2, and Id-3 immunoreactivity in the cells of small proliferating ducts and large ducts without dysplastic changes. In general, there was a correlation between weak immunoreactivity and low Id mRNA levels. However, in samples that harbored large ducts with papillary structures there was moderate Id immunoreactivity, and in the cells forming dysplastic ducts there was moderate to strong Id immunoreactivity. In these CP samples, Id mRNA levels were relatively higher than in the CP samples that were devoid of these histological changes. Overall, however, increased Id expression, most notably of Id-1 and Id-2, distinguished a subgroup of pancreatic cancers from CP (Table 1).

Epidemiological studies have shown that the risk of developing pancreatic cancer is increased up to 16-fold in patients with pre-existing CP in comparison to the general population.⁴⁰ The mechanisms that contribute to neoplastic transformation in CP are not known. Although there is no established tumor progression model for pancreatic cancer, such as the adenoma-carcinoma sequence of colorectal carcinoma,⁴¹ it is generally accepted that K-ras and p16 mutations occur relatively early in pancreatic carcinogenesis, whereas p53 mutations occur late in this process.^{37,41-43} Increased Id expression may contribute to malignant transformation of cultured cell lines *in vitro*¹¹ and has been linked to cell invasion in a murine mammary epithelial cell line.⁴⁴ In view of the current findings that Id-1, Id-2, and Id-3 are overexpressed in pancreatic cancer and in dysplastic/metaplastic ducts in CP, these observations raise the possibility that elevated levels of Id-1, Id-2, and, to a lesser extent, Id-3 may represent relatively early markers of pancreatic malignant transformation and may contribute to the pathobiology of pancreatic cancer.

References

- Jan YN, Jan LY: HLH proteins, fly neurogenesis, and vertebrate myogenesis. *Cell* 1993, 75:827-830
- Olson EN, Klein WH: bHLH factors in muscle development: dead lines and commitments, what to leave in and what to leave out. *Genes Dev* 1994, 8:1-8
- Begley CG, Aplan PD, Denning SM, Haynes BF, Waldmann TA, Kirsch IR: The gene SCL is expressed during early hematopoiesis and encodes a differentiation-related DNA-binding motif. *Proc Natl Acad Sci USA* 1989, 86:10128-10132
- Johnson JE, Birren SJ, Anderson DJ: Two rat homologues of *Drosophila achaete-scute* specifically expressed in neuronal precursors. *Nature* 1990, 346:858-861
- Weintraub H: The MyoD family and myogenesis: redundancy, networks, and thresholds. *Cell* 1993, 75:1241-1244
- Hu JS, Olson EN, Kingston RE: HEB, a helix-loop-helix protein related to E2A, and ITF2 that can modulate the DNA-binding ability of myogenic regulatory factors. *Mol Cell Biol* 1992, 12:1031-1042
- Langlands K, Yin X, Anand G, Prochownik EV: Differential interactions of Id proteins with basic-helix-loop-helix transcription factors. *J Biol Chem* 1997, 272:19785-19793
- Murre C, Bain G, van Dijk MA, Engel I, Furnari BA, Massari ME, Matthews JR, Quong MW, Rivera RR, Stuiver MH: Structure and function of helix-loop-helix proteins. *Biochim Biophys Acta* 1994, 1218:129-135
- Murre C, McCaw PS, Vaessin H, Caudy M, Jan LY, Jan YN, Cabrera CV, Buskin JN, Hauschka SD, Lassar AB, Baltimore D: Interactions between heterologous helix-loop-helix proteins generate complexes that bind specifically to a common DNA sequence. *Cell* 1989, 58:537-544
- Benezra R, Davis RL, Lockshon D, Turner DL, Weintraub H: The protein Id: a negative regulator of helix-loop-helix DNA binding proteins. *Cell* 1990, 61:49-59
- Norton JD, Atherton GT: Coupling of cell growth control and apoptosis functions of Id proteins. *Mol Cell Biol* 1998, 18:2371-2381
- Norton JD, Deed RW, Craggs G, Sablitzky F: Id helix-loop-helix proteins in cell growth and differentiation. *Trends Cell Biol* 1998, 8:58-65
- Christy BA, Sanders LK, Lau LF, Copeland NG, Jenkins NA, Nathans D: An Id-related helix-loop-helix protein encoded by a growth factor-inducible gene. *Proc Natl Acad Sci USA* 1991, 88:1815-1819
- Kawaguchi N, DeLuca HF, Noda M: Id gene expression and its suppression by 1,25-dihydroxyvitamin D3 in rat osteoblastic osteosarcoma cells. *Proc Natl Acad Sci USA* 1992, 89:4569-4572
- Kreider BL, Benezra R, Rovera G, Kadesch T: Inhibition of myeloid differentiation by the helix-loop-helix protein Id. *Science* 1992, 255:1700-1702
- Le Jossic C, Ilyin GP, Loyer P, Glaise D, Cariou S, Guguen-Guillouzo C: Expression of helix-loop-helix factor Id-1 is dependent on the hepatocyte proliferation and differentiation status in rat liver and in primary culture. *Cancer Res* 1994, 54:6065-6068
- Sun XH, Copeland NG, Jenkins NA, Baltimore D: Id proteins Id1 and Id2 selectively inhibit DNA binding by one class of helix-loop-helix proteins. *Mol Cell Biol* 1991, 11:5603-5611
- Wilson RB, Kiledjian M, Shen CP, Benezra R, Zwollo P, Dymecki SM, Desiderio SV, Kadesch T: Repression of immunoglobulin enhancers by the helix-loop-helix protein Id: implications for B-lymphoid-cell development. *Mol Cell Biol* 1991, 11:6185-6191
- Hara E, Yamaguchi T, Nojima H, Ide T, Campisi J, Okayama H, Oda K: Id-related genes encoding helix-loop-helix proteins are required for G1 progression and are repressed in senescent human fibroblasts. *J Biol Chem* 1994, 269:2139-2145
- Iavarone A, Garg P, Lasorella A, Hsu J, Israel MA: The helix-loop-helix protein Id-2 enhances cell proliferation and binds to the retinoblastoma protein. *Genes Dev* 1994, 8:1270-1284
- Lasorella A, Iavarone A, Israel MA: Id2 specifically alters regulation of the cell cycle by tumor suppressor proteins. *Mol Cell Biol* 1996, 16:2570-2578
- Peverali FA, Ramqvist T, Saffrich R, Pepperkok R, Barone MV, Philipson L: Regulation of G1 progression by E2A and Id helix-loop-helix proteins. *EMBO J* 1994, 13:4291-4301
- Prabhu S, Ignatova A, Park ST, Sun XH: Regulation of the expression of cyclin-dependent kinase inhibitor p21 by E2A and Id proteins. *Mol Cell Biol* 1997, 17:5888-5896
- Warshaw AL, Fernandez-del Castillo C: Pancreatic carcinoma. *N Engl J Med* 1992, 326:455-465
- Korc M: Role of growth factors in pancreatic cancer. *Surg Oncol Clin North Am* 1998, 7:25-41
- Kleeff J, Ishiwata T, Friess H, Büchler MW, Israel MA, Korc M: The helix-loop-helix protein Id2 is overexpressed in human pancreatic cancer. *Cancer Res* 1998, 58:3769-3772
- Oertel JE, Heffes CS, Oertel YC: *Pancreas. Diagnostic Surgical Pathology*. Edited by SS Sternberg. New York, Raven Press, 1989, pp 1057-1093
- Korc M, Chandrasekar B, Yamanaka Y, Friess H, Büchler MW, Beger HG: Overexpression of the epidermal growth factor receptor in human pancreatic cancer is associated with concomitant increase in the levels of epidermal growth factor and transforming growth factor α . *J Clin Invest* 1992, 90:1352-1360
- Saeki T, Stromberg K, Qi CF, Gullick WJ, Tahara E, Normanno N, Ciardiello F, Kenney N, Johnson GR, Salomon DS: Differential immunohistochemical detection of amphiregulin and cripto in human normal colon and colorectal tumors. *Cancer Res* 1992, 52:3467-3473
- Cantero D, Friess H, Delforin J, Zimmermann A, Bründler MA, Riesle E, Korc M, Büchler MW: Enhanced expression of urokinase plasminogen activator and its receptor in pancreatic carcinoma. *Br J Cancer* 1997, 75:388-395
- Desprez PY, Hara E, Bissell MJ, Campisi J: Suppression of mammary epithelial cell differentiation by the helix-loop-helix protein Id-1. *Mol Cell Biol* 1995, 15:3398-3404
- Shoji W, Yamamoto T, Obinata M: The helix-loop-helix protein Id inhibits differentiation of murine erythroleukemia cells. *J Biol Chem* 1994, 269:5078-5084
- Cross JC, Flannery ML, Blonar MA, Steingrimsson E, Jenkins NA, Copeland NG, Rutter WJ, Werb Z: Hxl encodes a basic helix-loop-helix transcription factor that regulates trophoblast cell development. *Development* 1995, 121:2513-2523
- Sun XH: Constitutive expression of the Id1 gene impairs mouse B cell development. *Cell* 1994, 79:893-900
- Wice BM, Gordon JI: Forced expression of Id-1 in the adult mouse small intestinal epithelium is associated with development of adenomas. *J Biol Chem* 1998, 273:25310-25319
- Barone MV, Pepperkok R, Peverali FA, Philipson L: Id proteins control growth induction in mammalian cells. *Proc Natl Acad Sci USA* 1994, 91:4965-4968
- Barton CM, Sladdon SL, Hughes CM, Hall PA, O'Sullivan C, Kloppel G, Theis B, Russell RC, Neoptolmos J, Williamson RCN, Lane DP, Lemoine NR: Abnormalities of the p53 tumour suppressor gene in human pancreatic cancer. *Br J Cancer* 1991, 64:1076-1082
- Ohshio G, Suwa H, Imamura T, Yamaki K, Tanaka T, Hashimoto Y, Imamura M: An immunohistochemical study of bcl-2 and p53 protein expression in pancreatic carcinomas. *Scand J Gastroenterol* 1998, 33:535-539
- Ungeloren H, Voss M, Jansen M, Roeder C, Henne-Bruns D, Kremer B, Kallhoff H: Human pancreatic adenocarcinomas express Fas and Fas ligand yet are resistant to Fas-mediated apoptosis. *Cancer Res* 1998, 58:1741-1749
- Niederer C, Niederer MC, Heintges T, Lüthen R: *Epidemiology: relation between chronic pancreatitis and pancreatic carcinoma. Cancer of the Pancreas*. Edited by HG Beger, MW Büchler, MH Schoenberg. Ulm, Germany: Universitätsverlag Ulm GmbH, 1996, pp 6-9
- Moskaluk CA, Kern SE: *Molecular genetics of pancreatic carcinoma. Pancreatic Cancer: Pathogenesis, Diagnosis, and Treatment*. Edited by HA Reber. Totowa, NJ, Humana Press, 1998, pp 3-20
- Moskaluk CA, Hruban RH, Kern SE: p16 and K-ras gene mutations in the intraductal precursors of human pancreatic adenocarcinoma. *Cancer Res* 1997, 57:2140-2143
- Tada M, Ohashi M, Shiratori Y, Okudaira T, Komatsu Y, Kawabe T, Yoshida H, Machinami R, Kishi K, Ornata M: Analysis of K-ras gene mutation in hyperplastic duct cells of the pancreas without pancreatic disease. *Gastroenterology* 1996, 110:227-231
- Desprez PY, Lin CO, Thomasset N, Sympton CJ, Bissell MJ, Campisi J: A novel pathway for mammary epithelial cell invasion induced by the helix-loop-helix protein Id-1. *Mol Cell Biol* 1998, 18:4577-4588



Alterations in neuropeptide Y levels and Y1 binding sites in the Flinders Sensitive Line rats, a genetic animal model of depression.

Caberlotto L, Jimenez P, Overstreet DH, Hurd YL, Mathe AA, Fuxe K.

Department of Neuroscience, Karolinska Institute, Stockholm, Sweden.

Previously, we observed specific alterations of neuropeptide Y (NPY) and Y1 receptor mRNA expression in discrete regions of the Flinders Sensitive Line rats (FSL), an animal model of depression. In order to clarify the correlation between mRNA expression and protein content, radioimmunoassay and receptor autoradiography were currently performed. In the FSL rats, NPY-like immunoreactivity (NPY-LI) was decreased in the hippocampal CA region, while Y1 binding sites were increased; NPY-LI was increased in the arcuate nucleus. Fluoxetine treatment elevated NPY-LI in the arcuate and anterior cingulate cortex and increased Y1 binding sites in the medial amygdala and occipital cortex in both strains. No differences were found regarding the Y2 binding sites. The results demonstrate a good correlation between NPY peptide and mRNA expression, and sustain the possible involvement of NPY and Y1 receptors in depression.

PMID: 10327163 [PubMed - indexed for MEDLINE]

FREE full text article at
www.biolreprod.org

Follicle-stimulating hormone receptor and its messenger ribonucleic acid are present in the bovine cervix and can regulate cervical prostanoid synthesis.

Mizrachi D, Shemesh M.

Department of Hormone Research, Kimron Veterinary Institute, Bet Dagan, Israel 50250.

The hypothesis that FSH regulates the bovine cervical prostaglandin E(2) (PGE(2)) synthesis that is known to be associated with cervical relaxation and opening at the time of estrus was investigated. Cervical tissue from pre-estrous/estrous, luteal, and postovulatory cows were examined for 1) the presence of bovine (b) FSH receptor (R) and its corresponding mRNA and 2) the effect of FSH on the PGE(2) regulatory pathway in vitro. The presence of bFSHR mRNA in the cervix (maximal during pre-estrus/estrus) was demonstrated by the expression of a reverse transcription (RT) polymerase chain reaction (PCR) product (384 base pairs) specific for bFSHR mRNA and sequencing. Northern blotting revealed three transcripts (2.5, 3.3, and 3.8 kilobases [kb]) in cervix from pre-estrous/estrous cows. The level of FSHR (75 kDa) was significantly higher ($p < 0.01$) in Western blots of pre-estrous/estrous cervix than in other cervical tissues. There was a good correlation between the 75-kDa protein expression and its corresponding transcript of 2.55 kb throughout the estrous cycle as described by Northern blot analysis as well as RT-PCR. Incubation of FSH (10 ng/ml) with pre-estrous/estrous cervix resulted in a 3-fold increase in the expression of FSHR and a 2-fold increase in both G protein ($\alpha(s)$) and cyclooxygenase II. FSH (5-20 ng/ml) significantly increased ($p < 0.01$) cAMP, inositol phosphate ($p < 0.01$), and PGE(2) ($p < 0.01$) production by pre-estrous/estrous cervix but not by cervix at the other stages. We conclude that bovine cervix at the time of the peripheral plasma FSH peak (pre-estrus/estrus) contains high levels of FSHR and responds to FSH by increasing the PGE(2) production responsible for cervical relaxation at estrus.

PMID: 10456856 [PubMed - indexed for MEDLINE]



The decompensated detrusor III: impact of bladder outlet obstruction on sarcoplasmic endoplasmic reticulum protein and gene expression.

Stein R, Gong C, Hutcheson JC, Canning DA, Zderic SA.

Division of Urology, Children's Hospital of Philadelphia, Philadelphia, Pennsylvania, USA.

PURPOSE: Regulation of calcium ion homeostasis has a significant role in smooth muscle contractility. The sarcoplasmic endoplasmic reticulum, calcium, magnesium, adenosine triphosphatase (SERCA) is a regulatory ion pump that may have a role in the functional outcome after outlet obstruction. We investigate what correlation if any existed between SERCA protein and gene expression, and the contractile properties in the same bladder. **MATERIALS AND METHODS:** Standardized partial bladder outlet obstructions were created in adult New Zealand white rabbits, which were divided into control, sham operated and obstructed groups. Muscle strip studies subcategorized the obstructed group into compensated (force greater than 50% of control) and decompensated (force less than 50% of control). Microsomal membrane and total RNA fractions were prepared from the same bladder tissue. Membrane proteins were used for Western blot analysis using a SERCA specific monoclonal antibody, and total RNA was assessed with Northern blot analysis. **RESULTS:** The relative intensities of signals for the Western and Northern blots demonstrated a strong correlation between protein and gene expression. Furthermore there was a strong association between the loss of SERCA messenger RNA and protein expression and loss of bladder function. **CONCLUSIONS:** Bladder contractility after outlet obstruction is influenced in part by smooth muscle cell ability to maintain calcium homeostasis via SERCA. The loss of SERCA protein expression is mediated by down-regulation in gene expression in the same bladder. These data suggest that smooth muscle ion pump gene expression is in part mechanically (pressure work) regulated.

PMID: 10958733 [PubMed - indexed for MEDLINE]

141: Zhonghua Jie He He Hu Xi Za Zhi. 2002 Jun;25(6):337-40.

[Related Articles](#), [Links](#)

[The pathogenic role of macrophage migration inhibitory factor in acute respiratory distress syndrome]

[Article in Chinese]

Guo Y, Xie C.

Department of Respiratory Medicine, First Affiliated Hospital of Zhongshan University, Guangzhou 510080 China.

OBJECTIVE To investigate the expression and pathogenic role of macrophage migration inhibitory factor (MIF) in human acute respiratory distress syndrome (ARDS). **METHODS** The serum level of MIF in ARDS patients and normal persons were measured by ELISA method. Peripheral blood mononuclear cell (PBMC) MIF expression was determined by flow-cytometry. The expression of MIF mRNA and protein in the lung tissues were detected by using double immunohistochemistry labeling and in situ hybridization. **RESULTS** The serum level of MIF increased significantly in ARDS patients as compared with normal persons ($P < 0.01$). The percentage of PBMC MIF expression was higher in ARDS patients than in normal controls ($P < 0.01$). In situ hybridization and immunohistochemistry showed undetectable or weak MIF mRNA and protein expression in normal lungs. In contrast, there was marked upregulation of MIF mRNA and protein expression in the ARDS lungs. In ARDS macrophages infiltrated the alveolar space and interstitium, most of which also expressed MIF. Infiltrating macrophages were almost restricted to the areas of severe tissue damage. The MIF expression level showed a strong correlation with the number of infiltrating macrophages. **CONCLUSIONS** The serum level of MIF and PBMC MIF expression increased in ARDS patients with enhanced pulmonary MIF expression and macrophage infiltration, which suggests that MIF plays a pivotal role in the pathogenesis of ARDS.

PMID: 12126556 [PubMed - indexed for MEDLINE]



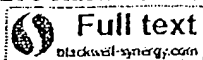
An increased high-mobility group A2 expression level is associated with malignant phenotype in pancreatic exocrine tissue.

Abe N, Watanabe T, Suzuki Y, Matsumoto N, Masaki T, Mori T, Sugiyama M, Chiappetta G, Fusco A, Atomi Y.

First Department of Surgery, Kyorin University School of Medicine, 6-20-2, Shinkawa, Mitaka, Tokyo 181-8611, Japan. abenbtg@kyorin-u.ac.jp

The altered form of the high-mobility group A2 (HMGA2) gene is somehow related to the generation of human benign and malignant tumours of mesenchymal origin. However, only a few data on the expression of HMGA2 in malignant tumour originating from epithelial tissue are available. In this study, we examined the HMGA2 expression level in pancreatic carcinoma, and investigated whether alterations in the HMGA2 expression level are associated with a malignant phenotype in pancreatic tissue. High-mobility group A2 mRNA and protein expression was determined in eight surgically resected specimens of non-neoplastic tissue (six specimens of normal pancreatic tissue and two of chronic pancreatitis tissue) and 27 pancreatic carcinomas by highly sensitive reverse transcriptase-polymerase chain reaction (RT-PCR) techniques and immunohistochemical staining, respectively. Reverse transcriptase-polymerase chain reaction analysis revealed the expression of the HMGA2 gene in non-neoplastic pancreatic tissue, although its expression level was significantly lower than that in carcinoma. Immunohistochemical analysis indicated that the presence of the HMGA2 gene in non-neoplastic pancreatic tissue observed in RT-PCR reflects its abundant expression in islet cells, together with its focal expression in duct epithelial cells. Intense and multifocal or diffuse HMGA2 immunoreactivity was noted in all the pancreatic carcinoma examined. A strong correlation between HMGA2 overexpression and the diagnosis of carcinoma was statistically verified. Based on these findings, we propose that an increased expression level of the HMGA2 protein is closely associated with the malignant phenotype in the pancreatic exocrine system, and accordingly, HMGA2 could serve as a potential diagnostic molecular marker for distinguishing pancreatic malignant cells from non-neoplastic pancreatic exocrine cells.

PMID: 14647145 [PubMed - indexed for MEDLINE]



Selective apoptosis of natural killer-cell tumours by l-asparaginase.

Ando M, Sugimoto K, Kitoh T, Sasaki M, Mukai K, Ando J, Egashira M, Schuster SM, Oshimi K.

Department of Haematology, Juntendo University School of Medicine, Tokyo, Japan.

We examined the effectiveness of various anti-tumour agents to natural killer (NK)-cell tumour cell lines and samples, which are generally resistant to chemotherapy, using flow cytometric terminal deoxynucleotidyl transferase-mediated dUTP-biotin nick end-labelling (TUNEL) assay. Although NK-YS and NK-92 were highly resistant to various anti-tumour agents, l-asparaginase induced apoptosis in these two NK-cell lines. NK-cell leukaemia/lymphoma and acute lymphoblastic leukaemia (ALL) samples were selectively sensitive to l-asparaginase and to doxorubicin (DXR) respectively. Samples of chronic NK lymphocytosis, an NK-cell disorder with an indolent clinical course, were resistant to both drugs. Our study clearly separated two major categories of NK-cell disorders and ALL according to the sensitivity to DXR and l-asparaginase. We examined asparagine synthetase levels by real-time quantitative polymerase chain reaction (RQ-PCR) and immunostaining in these samples. At least in nasal-type NK-cell lymphoma, there was a good correlation among asparagine synthetase expression, in vitro sensitivity and clinical response to l-asparaginase. In aggressive NK-cell leukaemia, although asparagine synthetase expression was high at both mRNA and protein levels, l-asparaginase induced considerable apoptosis. Furthermore, samples of each disease entity occupied a distinct area in two-dimensional plotting with asparagine synthetase mRNA level (RQ-PCR) and in vitro l-asparaginase sensitivity (TUNEL assay). We confirmed rather specific anti-tumour activity of l-asparaginase against NK-cell tumours in vitro, which provides an experimental background to the clinical use of l-asparaginase for NK-cell tumours.

PMID: 16156856 [PubMed - in process]

Comment in:

- [Cancer Res. 2002 Jan 15;62\(2\):618-9.](#)

[FREE full text article at
cancerres.aacrjournals.org](#)

BMI-1 gene amplification and overexpression in hematological malignancies occur mainly in mantle cell lymphomas.

Bea S, Tort F, Pinyol M, Puig X, Hernandez L, Hernandez S, Fernandez PL, van Lohuizen M, Colomer D, Campo E.

The Hematopathology Section, Laboratory of Anatomic Pathology, Hospital Clinic, Institut d'Investigacions Biomediques August Pi i Sunyer (IDIBAPS), University of Barcelona, Spain.

The BMI-1 gene is a putative oncogene belonging to the Polycomb group family that cooperates with c-myc in the generation of mouse lymphomas and seems to participate in cell cycle regulation and senescence by acting as a transcriptional repressor of the INK4a/ARF locus. The BMI-1 gene has been located on chromosome 10p13, a region involved in chromosomal translocations in infant leukemias, and amplified in occasional non-Hodgkin's lymphomas (NHLs) and solid tumors. To determine the possible alterations of this gene in human malignancies, we have examined 160 lymphoproliferative disorders, 13 myeloid leukemias, and 89 carcinomas by Southern blot analysis and detected BMI-1 gene amplification (3- to 7-fold) in 4 of 36 (11%) mantle cell lymphomas (MCLs) with no alterations in the INK4a/ARF locus. BMI-1 and p16INK4a mRNA and protein expression were also studied by real-time quantitative reverse transcription-PCR and Western blot, respectively, in a subset of NHLs. BMI-1 expression was significantly higher in chronic lymphocytic leukemia and MCL than in follicular lymphoma and large B cell lymphoma. The four tumors with gene amplification showed significantly higher mRNA levels than other MCLs and NHLs with the BMI-1 gene in germline configuration. Five additional MCLs also showed very high mRNA levels without gene amplification. A good correlation between BMI-1 mRNA levels and protein expression was observed in all types of lymphomas. No relationship was detected between BMI-1 and p16INK4a mRNA levels. These findings suggest that BMI-1 gene alterations in human neoplasms are uncommon, but they may contribute to the pathogenesis in a subset of malignant lymphomas, particularly of mantle cell type.

PMID: 11289106 [PubMed - indexed for MEDLINE]

BMI-1 Gene Amplification and Overexpression in Hematological Malignancies Occur Mainly in Mantle Cell Lymphomas¹

Silvia Beà, Frederic Tort, Magda Pinyol, Xavier Puig, Luis Hernández, Silvia Hernández, Pedro L. Fernández, Maarten van Lohuizen, Dolors Colomer,² and Elias Campo²

The Hematopathology Section, Laboratory of Anatomic Pathology, Hospital Clinic, Institut d'Investigacions Biomèdiques "August Pi i Sunyer" (IDIBAPS), University of Barcelona, 08036 Barcelona, Spain [S. B., F. T., M. P., X. P., L. H., S. H., P. L. F., D. C., E. C.], and Division of Molecular Carcinogenesis, The Netherlands Cancer Institute, 1066 CX Amsterdam, Netherlands [M. v. L.]

Abstract

The *BMI-1* gene is a putative oncogene belonging to the Polycomb group family that cooperates with *c-myc* in the generation of mouse lymphomas and seems to participate in cell cycle regulation and senescence by acting as a transcriptional repressor of the *INK4a/ARF* locus. The *BMI-1* gene has been located on chromosome 10p13, a region involved in chromosomal translocations in infant leukemias, and amplified in occasional non-Hodgkin's lymphomas (NHLs) and solid tumors. To determine the possible alterations of this gene in human malignancies, we have examined 160 lymphoproliferative disorders, 13 myeloid leukemias, and 89 carcinomas by Southern blot analysis and detected *BMI-1* gene amplification (3- to 7-fold) in 4 of 36 (11%) mantle cell lymphomas (MCLs) with no alterations in the *INK4a/ARF* locus. *BMI-1* and *p16^{INK4a}* mRNA and protein expression were also studied by real-time quantitative reverse transcription-PCR and Western blot, respectively, in a subset of NHLs. *BMI-1* expression was significantly higher in chronic lymphocytic leukemia and MCL than in follicular lymphoma and large B cell lymphoma. The four tumors with gene amplification showed significantly higher mRNA levels than other MCLs and NHLs with the *BMI-1* gene in germline configuration. Five additional MCLs also showed very high mRNA levels without gene amplification. A good correlation between *BMI-1* mRNA levels and protein expression was observed in all types of lymphomas. No relationship was detected between *BMI-1* and *p16^{INK4a}* mRNA levels. These findings suggest that *BMI-1* gene alterations in human neoplasms are uncommon, but they may contribute to the pathogenesis in a subset of malignant lymphomas, particularly of mantle cell type.

Introduction

The *BMI-1*³ gene is a putative oncogene of the Polycomb group originally identified by retroviral insertional mutagenesis in *Eμ-c-myc* transgenic mice infected with the Moloney murine leukemia virus (1, 2). These animals had a rapid development of pre-B cell lymphomas showing frequent proviral insertions near the *BMI-1* gene. This integration resulted in *BMI-1* overexpression suggesting a cooperative effect between *C-MYC* and *BMI-1* in the development of these tumors (3, 4). Recent studies have indicated that the *BMI-1* gene may also participate in cell cycle control and senescence through the

INK4a/ARF locus by acting as an upstream negative regulator of *p16^{INK4a}* and *p14/p19^{ARF}* gene expression (5). The human *BMI-1* gene has been mapped to chromosome 10p13 (6), a region involved in chromosomal translocations in infant leukemias (7) and rearrangements in malignant T cell lymphomas (8, 9). More recently, high-level DNA amplifications of this region have been found by comparative genomic hybridization in NHLs and solid tumors (10, 11). However, the possible implication of the *BMI-1* gene in these alterations and its role in the pathogenesis of human tumors is not known. The aim of this study was to analyze the possible *BMI-1* gene alterations and expression in a large series of human neoplasms and to determine the relationship with *INK4a/ARF* locus aberrations.

Materials and Methods

Case Selection. A series of 262 human tumors, including 173 hematological malignancies and 89 carcinomas (Table 1), matched normal tissues from all carcinomas, 11 samples of normal peripheral mononuclear cells, and 5 reactive lymph nodes and tonsils, were selected based on the availability of frozen samples for molecular analysis.

DNA Extraction and Southern Blot Analysis. Genomic DNA was obtained using Proteinase K/RNase treatment. 15 μg were digested with *EcoRI* and *HindIII* restriction enzymes (Life Technologies, Inc., Gaithersburg, MD), for Southern blot analysis and hybridized with a 1.5-kb *PstI* fragment of the partial *BMI-1* cDNA (6).

RNA Extraction and Real-time Quantitative RT-PCR. Total RNA was obtained from 67 lymphoid neoplasms (10 CLLs, 27 MCLs, 8 FLs, and 22 LCLs) using guanidine/isothiocyanate extraction and cesium/chloride gradient centrifugation. One μg of total RNA was transcribed into cDNA using MMLV-reverse transcriptase (Life Technologies, Inc.) and random hexamers, following manufacturer's directions. Sequences of the *BMI-1* and the *p16* detection probes and primers were designed using the Primer Express program (Applied Biosystems, Foster City) as follows: *BMI-1* sense, 5'-CTGGTTGCCATTGACAGC-3'; *BMI-1* antisense, 5'-CAGAAAATGAATGCGAGCCA-3'; *p16* sense, 5'-CAACGCACCGAATAGTTACGG-3'; *p16* antisense, 5'-AACTTCGTCCTCCAGAGTCGC-3'. The probes *BMI-1*, 5'-CAGCTCGCTTCAAGATGGCCGC-3', and *p16*, 5'-CGGAGGCCGATCCAGGTGGTA-3', were labeled with 6-carboxy-fluorescein as the reporter dye. The TaqMan-GAPDH Control Reagents (Applied Biosystems) were used to amplify and detect the *GAPDH* gene, as recommended by the manufacturer. The quantitative assay amplified 1 μl of cDNA in two to four replicates using the primers and probes described above and the standard master mix (Applied Biosystems). All reactions were performed in an ABI PRISM 7700 Sequence Detector System (Applied Biosystems). *GAPDH*, *BMI-1*, and *p16^{INK4a}* expression was related to a standard curve derived from serial dilutions of Raji cDNA. The RUs of *BMI-1* and *p16^{INK4a}* expression were defined as the mRNA levels of these genes normalized to the *GAPDH* expression level in each case.

Protein Analysis. Whole-cell protein extracts were obtained from additional frozen tissue available in 31 cases (7 CLLs, 12 MCLs, 8 FLs, and 4 LCLs), loaded onto a 10% SDS-polyacrylamide gel, and electroblotted to a nitrocellulose membrane (Amersham). Blocked membranes were incubated sequentially with the monoclonal antibody BMI-F6 (12), antimouse conju-

Received 10/16/00; accepted 1/29/01.

The costs of publication of this article were defrayed in part by the payment of page charges. This article must therefore be hereby marked advertisement in accordance with 18 U.S.C. Section 1734 solely to indicate this fact.

¹ Supported by Grant SAF 99/20 from Comisión Interministerial de Ciencia y Tecnología, European Union Contract QLGI-CT-2000-689, the Asociación Española contra el Cáncer, and Generalitat de Catalunya 98SGR21. S. B. and F. T. were fellows supported by Spanish Ministerio de Educación y Cultura, and S. H. was supported by the Asociación Española contra el Cáncer and the Fundació Rius i Virgili.

² To whom requests for reprints should be addressed, at the Department of Pathology, Hospital Clinic, University of Barcelona, Villarroel 170, 08036-Barcelona, Spain. Phone: 34 93 227 5450; Fax: 34 93 227 5572; E-mail: campo@medicina.ub.es.

³ The abbreviations used are: *BMI-1*, B cell-specific Moloney murine leukemia virus integration site 1; NHL, non-Hodgkin's lymphoma; CLL, chronic lymphocytic leukemia; FL, follicular lymphoma; LCL, large B cell lymphoma; MCL, mantle cell lymphoma; RT-PCR, reverse-transcription-PCR; RU, relative units.

Table 1 Hematological malignancies and solid tumor samples analyzed for BMI-1 gene alterations

Tissue samples	No. of cases
Hematological malignancies	
Hodgkin's disease	2
B cell lymphoproliferative disorders	
B-Acute lymphoblastic leukemia	14
CLL	29
Hairy cell leukemia	4
FL	15
MCL	36
LCL	40
T cell lymphoproliferative disorders	
T-Acute lymphoblastic leukemia	8
Large granular cell leukemia	4
Peripheral T-cell lymphoma	8
Myeloproliferative disorders	
Acute myeloid leukemia	7
Chronic myeloid leukemia	6
Solid tumors	
Colon carcinoma	26
Breast carcinoma	29
Laryngeal squamous cell carcinoma	34
Total	262

gated to horseradish peroxidase (Amersham), and detected by enhanced chemiluminescence (Amersham) according to the manufacturer's recommendations.

Statistical Analysis. Because of the non-normal distribution of the samples and the small size of some subsets of tumors, the statistical evaluation was performed using nonparametric tests (SPSS, version 9.0). Comparison between mRNA expression levels in the different groups of NHLs was performed using the Kruskal-Wallis Test, with a *P* for significance set at 0.05. For differences between particular groups, the conservative Bonferroni procedure was performed, and the *P* was set at 0.005. The remaining statistical analyses were carried out using the Mann-Whitney nonparametric *U* test (significance, *P* < 0.05). The comparison between BMI-1 and p16^{INK4a} quantitative mRNA levels was also performed using the Pearson's correlation coefficient.

Results

BMI-1 Gene Amplification. The BMI-1 gene was examined by Southern blot in a large series of human tumors and normal samples (Table 1). The cDNA probe used in the study detected three *Eco*RI fragments of 7.3, 3.8, and 2.6 kb and three *Hind*III fragments of 6.2, 4, and 3.5 kb. BMI-1 gene amplification (3- to 7-fold) was detected in 4 of 36 (11%) MCLs (Fig. 1). The amplifications were confirmed with both restriction enzymes. The amplified MCLs were two blastoid and two typical variants. No amplifications were observed in any of the solid tumors when compared with their respective matched non-neoplastic mucosa. No BMI-1 gene rearrangements were observed in any of the samples examined.

BMI-1 mRNA Expression. To determine the BMI-1 expression pattern in NHL we analyzed BMI-1 mRNA levels by real-time quantitative RT-PCR in 67 lymphomas (10 CLLs, 27 MCLs, 8 FLs, and 22 LCLs), including the four tumors with gene amplification. A distinct BMI-1 mRNA expression pattern was observed in the different types of lymphomas (Fig. 2; Kruskal-Wallis Test; *P* < 0.001). The BMI-1 mRNA levels in CLLs (mean, 2.2 RU; SD, 1.3) and MCLs with no BMI-1 gene amplification (mean, 2.5 RU; SD, 2.3) were significantly higher than in FLs (mean, 0.9 RU; SD, 0.8) and LCLs (mean, 0.6 RU; SD, 0.4; Mann-Whitney nonparametric *U* test; *P* < 0.01). The 4 MCLs with BMI-1 gene amplification showed significantly higher levels of expression than all other groups of tumors (mean, 5.1 RU; SD, 1.6; *P* < 0.005). In addition, five typical MCLs with no structural alterations of the gene also showed very high levels of BMI-1 mRNA expression ranging from 4 to 9.8 RU, similar to cases with gene amplification (Fig. 2A).

BMI-1 Protein Expression. BMI-1 protein expression was examined by Western blot in 31 tumors (7 CLLs; 12 MCLs, including two

cases with BMI-1 gene amplification and 4 cases with mRNA overexpression and no structural alteration of the gene; 8 FLs, and 4 LCLs) in which additional frozen tissue was available. The monoclonal antibody against BMI-1 detected three closely migrating proteins of *M_r* 45,000–48,000 (2). The two more slowly migrating bands probably represent phosphorylated isoforms of the protein (12). The two MCLs with gene amplification and three of four cases with mRNA overexpression without amplification of the gene showed very high levels of protein expression. The remaining MCLs and CLLs showed intermediate levels of protein expression, whereas low- or no-expression signals were detected in the LCLs and FLs included in the study (Fig. 3). These results indicate that BMI-1 protein expression in NHL is concordant with the mRNA levels observed by real-time quantitative RT-PCR.

Relationship between BMI-1 and p16^{INK4a} Gene Alterations. The *INK4a/ARF* locus has been recently identified as a downstream target of the transcriptional repressing activity of the BMI-1 gene, suggesting that this gene may contribute to human neoplasias with wild type *INK4a/ARF* (5). Most of the lymphoproliferative disorders analyzed in the present study, including the four cases with BMI-1 gene amplification, had been previously examined for *p53* gene mutations and *INK4a/ARF* locus alterations, including gene deletions, mutations, hypermethylation, and expression (13, 14). The four MCLs with BMI-1 gene amplification and mRNA overexpression and the five tumors with BMI-1 mRNA overexpression with no structural alterations of the gene showed a wild-type configuration of the *INK4a/ARF* locus (13). However, one case with BMI-1 gene amplification and one case with mRNA overexpression with no alteration of the gene showed *p53* gene mutations associated with allelic deletions.

To determine the possible relationship between BMI-1 and p16^{INK4a} mRNA expression, p16^{INK4a} mRNA levels were evaluated by real-time quantitative RT-PCR in 50 tumors (10 CLLs, 27 MCLs, and 13 LCLs), including 6 cases with alterations in the *INK4a/ARF* locus (2 MCLs and 1 LCL with p16^{INK4a} gene deletion, 2 LCLs with p16 promoter hypermethylation, and 1 CLL with p16^{INK4a} gene mutation), and the 4 lymphomas with BMI-1 amplification. Negative or negligible levels of p16^{INK4a} were observed in the 6 tumors with *INK4a/ARF* locus alterations. These cases were not included in the comparisons between BMI-1 and p16^{INK4a} mRNA expression. The p16^{INK4a} expression levels were relatively similar in the different types of tumors. Only LCLs tended to have lower levels of expression, but the differences did not reach statistical significance (Fig. 2B). No differences were observed in the p16^{INK4a} mRNA levels between tumors with BMI-1 gene amplification and overexpression and lymphomas with germline configuration of the gene.

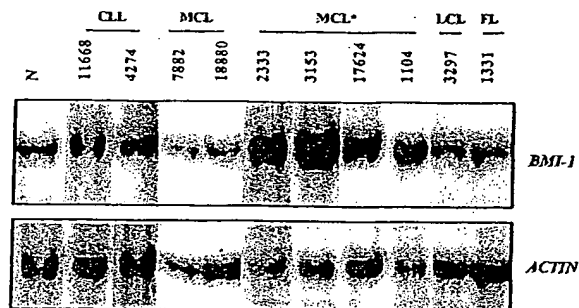


Fig. 1. Southern blot analysis of BMI-1 gene. Four MCLs (MCL*) showed BMI-1 gene amplification (3- to 7-fold) compared with non-neoplastic tissues (N) and other NHLs. No amplifications or gene rearrangements were detected in the remaining NHLs and carcinomas included in the study.

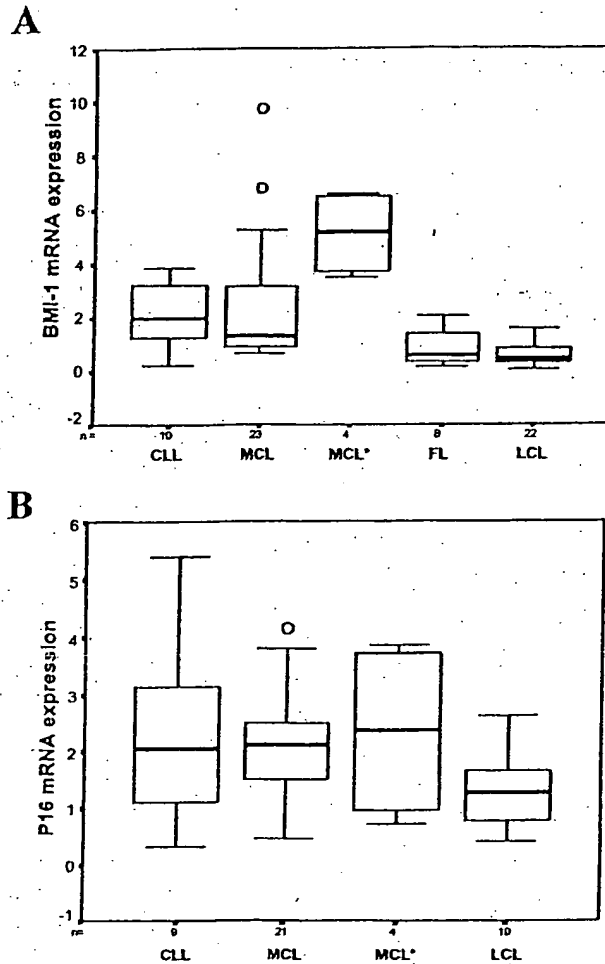


Fig. 2. A, quantitative BMI-1 mRNA transcript analysis (median and range) using real-time RT-PCR in a series of NHLs. MCLs with *BMI-1* gene amplification (MCL*) revealed significantly higher overall BMI-1 mRNA levels than all other types of NHLs, including MCLs with no structural alterations of the gene ($P < 0.005$). MCLs and CLLs expressed significantly higher levels than FLs and LCLs ($P < 0.001$). Results are depicted as the ratio of absolute BMI-1:GADPH mRNA transcript numbers (RU). Bars, SD. B, quantitative p16^{INK4a} mRNA transcript analysis (median and range) using real-time RT-PCR in a series of NHLs. Expression levels were relatively similar in the different types of tumors. Results are depicted as the ratio of absolute p16^{INK4a}:GADPH mRNA transcript numbers (RU). Bars, SD.

Discussion

In the present study, we have examined a large series of human tumors for the presence of gene alterations and mRNA expression of the *BMI-1* gene. Gene amplification was identified in four MCLs. These tumors showed significantly higher levels of mRNA and protein expression compared with other lymphomas with *BMI-1* in germ-line configuration. BMI-1 expression levels were also highly up-regulated in a subset of MCLs with no apparent structural alterations of the gene. No alterations were detected in any of the different types of carcinomas included in the study. *BMI-1* is considered an oncogene belonging to the Polycomb group family of genes. These proteins mainly act as transcriptional regulators, controlling specific target genes involved in development, cell differentiation, proliferation, and senescence. Different studies have shown the implication of BMI-1 overexpression in the development of lymphomas in murine and feline animal models (3, 4). The findings of the present study indicate

for the first time that *BMI-1* gene alterations in human neoplasms are an uncommon phenomenon, but they seem to occur mainly in a subset of NHLs, particularly of mantle cell type.

The human *BMI-1* gene has been mapped to chromosome 10p13. High-level DNA amplifications and gains in this region have been identified by comparative genomic hybridization in occasional solid tumors and NHLs (10, 11). Different chromosomal translocations involving the 10p13 region have also been identified in infant leukemias and T cell lymphoproliferative disorders (7, 8, 15). Most acute leukemias with this chromosomal alteration occur in children <12 months of age, whereas it seems to be extremely rare in adults. 10p translocations in T-cell lymphoproliferative disorders have been observed mainly in adult T cell leukemia/lymphomas and occasional cutaneous T cell lymphomas. In our study, we did not observe *BMI-1* rearrangements or amplifications in any of the acute leukemias or T cell lymphomas. However, all of the acute leukemias in this study were diagnosed in patients over 16 years, and no adult T cell leukemia/lymphomas or cutaneous lymphomas could be included in the series. Similarly, high-level DNA amplifications at the 10p13 region have been detected in head and neck carcinomas and other solid tumors. Although we found no evidence for *BMI-1* gene rearrangements or amplifications in a substantial set of carcinomas, this does not exclude the possibility of increased gene expression or protein levels in these tumors. Additional studies are required to elucidate the possible involvement of *BMI-1* in these particular groups of human neoplasms.

In human hematopoietic cells, BMI-1 is preferentially expressed in primitive CD34+ bone marrow cells, whereas it is negative or very low in more mature CD34- cells (16). In peripheral lymphocytes, and particularly in follicular B cells, BMI-1 protein expression has been detected in resting cells of the mantle zone, whereas it is down-regulated in proliferating germinal center cells (17, 18). These observations indicate that BMI-1 expression in normal hematopoietic cells is tightly regulated in relation with cell differentiation in bone marrow and antigen-specific response in peripheral lymphocytes. BMI-1 expression in human tumors has not been examined previously. In this study, we have demonstrated that BMI-1 mRNA and protein expression show a distinct pattern in different types of lymphomas. Thus, BMI-1 levels were low in LCLs and FLs and significantly higher in MCLs and CLLs. These findings suggest that BMI-1 expression patterns in B cell lymphomas maintain in part the expression profile of their normal cell counterparts; because FLs and at least a subgroup of LCLs are considered lymphomas derived from follicular germinal center cells, whereas MCLs and CLLs are tumors mainly derived from naive pregerminal center cells. However, the four MCLs with *BMI-1* gene amplification expressed significantly higher mRNA levels than all other tumors. In addition, five MCLs with no structural alterations of the gene showed high mRNA levels similar to those observed in tumors with *BMI-1* gene amplification, suggesting that other mechanisms may be involved in up-regulation of the gene in these lymphomas. Different studies using animal models have shown a dose-dependent effect of *BMI-1* gene expression on skeleton development

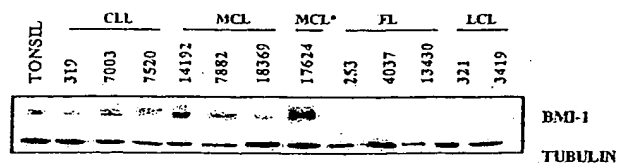


Fig. 3. Western blot analysis of BMI-1 protein in NHLs. The amplified MCL (17624) showed the highest BMI-1 protein levels, whereas other MCLs and CLLs had intermediate levels of expression. Very low or negative signal was observed in FLs and LCLs.

and lymphomagenesis (1, 3). These observations suggest that the high mRNA and protein levels detected in a subset of MCLs may play a role in the pathogenesis of these neoplasms.

Recent studies have identified the *INK4a/ARF* locus as a downstream target of the BMI-1 transcriptional repressor activity, suggesting that BMI-1 overexpression may contribute to human neoplasias that retain the wild-type *INK4a/ARF* locus (5). Interestingly, in our study, *BMI-1* amplification and overexpression appeared in tumors with no alterations in *p16^{INK4a}* and *p14^{ARF}* genes. However, we could not detect differences in the expression levels of *p16^{INK4a}* in tumors with and without *BMI-1* gene alterations. The reasons for this apparent discrepancy with experimental observations are not clear. One possibility may be that genes other than *INK4a/ARF* are the main targets of BMI-1 repressor activity in these tumors. Particularly, different genes of the HOX family are regulated by BMI-1 and may also be involved in lymphomagenesis (19, 20).

In conclusion, the findings of this study indicate that *BMI-1* gene expression is differentially regulated in B cell lymphomas. Alterations of the gene seem to be an uncommon phenomenon in human neoplasms, but they may contribute to the pathogenesis in a subset of MCLs. Although, *BMI-1* gene alterations occurred in tumors with wild-type *INK4a/ARF* locus, the possible cooperation between these genes and the oncogenic mechanisms of BMI-1 in human neoplasms require additional analysis.

Acknowledgments

The authors thank Iracema Nayach for her excellent technical assistance.

References

- Haupt, Y., Alexander, W. S., Barri, G., Klinken, S. P., and Adams, J. M. Novel zinc finger gene implicated as myc collaborator by retrovirally accelerated lymphomagenesis in E μ -myc transgenic mice. *Cell*, 65: 753-763, 1991.
- van Lohuizen, M., Verbeck, S., Scheijen, B., Wientjens, E., van der Gulden, H., and Berns, A. Identification of cooperating oncogenes in E μ -myc transgenic mice by provirus tagging. *Cell*, 65: 737-752, 1991.
- Alkema, M. J., Jacobs, H., van Lohuizen, M., and Berns, A. Perturbation of B and T cell development and predisposition to lymphomagenesis in E μ Bmi1 transgenic mice require the Bmi1 RING finger. *Oncogene*, 15: 899-910, 1997.
- Haupt, Y., Bath, M. L., Harris, A. W., and Adams, J. M. *Bmi-1* transgene induces lymphomas and collaborates with myc in tumorigenesis. *Oncogene*, 8: 3161-3164, 1993.
- Jacobs, J. J., Kieboom, K., Marino, S., DePinho, R. A., and van Lohuizen, M. The oncogene and Polycomb-group gene *bmi-1* regulates cell proliferation and senescence through the *ink4a* locus. *Nature (Lond.)*, 397: 164-168, 1999.
- Alkema, M. J., Wiegant, J., Raap, A. K., Berns, A., and van Lohuizen, M. Characterization and chromosomal localization of the human proto-oncogene *BMI-1*. *Hum. Mol. Genet.*, 2: 1597-1603, 1993.
- Pui, C. H., Raimondi, S. C., Murphy, S. B., Ribeiro, R. C., Kalwinsky, D. K., Dahl, G. V., Crist, W. M., and Williams, D. L. An analysis of leukemic cell chromosomal features in infants. *Blood*, 69: 1289-1293, 1987.
- Berger, R., Baranger, L., Bernheim, A., Valensi, F., Flandrin, G., and Berheim, A. T. Cytogenetics of T-cell malignant lymphoma. Report of 17 cases and review of the chromosomal breakpoints. *Cancer Genet. Cytogenet.*, 36: 123-130, 1988.
- D'Alessandro, E., Paterlini, P., Lo Re, M. L., Di Cola, M., Ligas, C., Quaglini, D., and Del Porto, G. Cytogenetic follow-up in a case of Sezary syndrome. *Cancer Genet. Cytogenet.*, 45: 231-236, 1990.
- Bea, S., Ribas, M., Hernandez, J. M., Bosch, F., Pinyol, M., Hernandez, L., Garcia, J. L., Flores, T., Gonzalez, M., Lopez-Guillermo, A., Piris, M. A., Cardesa, A., Montserrat, E., Miro, R., and Campo, E. Increased number of chromosomal imbalances and high-level DNA amplifications in mantle cell lymphoma are associated with blastoid variants. *Blood*, 93: 4365-4374, 1999.
- Knuutila, S., Bjorkqvist, A. M., Autio, K., Tarkkanen, M., Wolf, M., Monni, O., Szymanska, J., Larramendy, M. L., Tapper, J., Pere, H., el-Rifai, W., Hemmer, S., Wasenius, V. M., Vidgren, V., and Zhu, Y. DNA copy number amplifications in human neoplasms: review of comparative genomic hybridization studies. *Am. J. Pathol.*, 152: 1107-1123, 1998.
- Alkema, M. J., Bronk, M., Verhoeven, E., Otte, A., van't Veer, L. J., Berns, A., and van Lohuizen, M. Identification of Bmi1-interacting proteins as constituents of a multimeric mammalian polycomb complex. *Genes Dev.*, 11: 226-240, 1997.
- Pinyol, M., Hernandez, L., Martinez, A., Cobo, F., Hernandez, S., Beà, S., López-Guillermo, A., Nayach, I., Palacin, A., Nadal, A., Fernández, P., Montserrat, E., Cardesa, A., and Campo, E. *INK4a/ARF* locus alterations in human non-Hodgkin's lymphomas mainly occur in tumors with wild type *p53* gene. *Am. J. Pathol.*, 156: 1987-1996, 2000.
- Pinyol, M., Cobo, F., Beà, S., Jares, P., Nayach, I., Fernández, P. L., Montserrat, E., Cardesa, A., and Campo, E. *p16^{INK4a}* gene inactivation by deletions, mutations, and hypermethylation is associated with transformed and aggressive variants of non-Hodgkin's lymphomas. *Blood*, 91: 2977-2984, 1998.
- Foot, A. B., Oakhill, A., and Kitchen, C. Acute monoblastic leukemia of infancy in Klinefelter's syndrome. *Cancer Genet. Cytogenet.*, 61: 99-100, 1992.
- Lessard, J., Baban, S., and Sauvageau, G. Stage-specific expression of polycomb group genes in human bone marrow cells. *Blood*, 91: 1216-1224, 1998.
- Raaphorst, F. M., van Kemenade, F. J., Fieret, E., Hamer, K. M., Satijn, D. P., Otte, A. P., and Meijer, C. J. Cutting edge: polycomb gene expression patterns reflect distinct B cell differentiation stages in human germinal centers. *J. Immunol.*, 164: 1-4, 2000.
- Raaphorst, F. M., van Kemenade, F. J., Blokzijl, T., Fieret, E., Hamer, K. M., Satijn, D. P., Otte, A. P., and Meijer, C. J. Coexpression of *BMI-1* and *EZH2* polycomb group genes in Reed-Sternberg cells of Hodgkin's disease. *Am. J. Pathol.*, 157: 709-715, 2000.
- Gould, A. Functions of mammalian Polycomb group and trithorax group related genes. *Curr. Opin. Genet. Dev.*, 7: 488-494, 1997.
- van Oostveen, J., Bijl, J., Raaphorst, F., Walboomers, J., and Meijer, C. The role of homeobox genes in normal hematopoiesis and hematological malignancies. *Leukemia*, 13: 1675-1690, 1999.

Human thyroid carcinoma cell lines and normal thyrocytes: expression and regulation of matrix metalloproteinase-1 and tissue matrix metalloproteinase inhibitor-1 messenger-RNA and protein.

Aust G, Hofmann A, Laue S, Rost A, Kohler T, Scherbaum WA.

Institut of Anatomy, University of Leipzig, Germany.

Matrix metalloproteinase-1 (MMP-1) and tissue matrix metalloproteinase inhibitor 1 (TIMP-1) play an important role in remodeling the extracellular matrix in normal and pathological processes. The effect of phorbol-myristate acetate (PMA), interleukin-1 (IL-1), and tumor necrosis factor-alpha (TNF-alpha) on MMP-1 and TIMP-1 expression was studied on highly purified thyrocytes and undifferentiated 8505 C, C 643, HTh 74, SW 1736 thyroid carcinoma cells compared with thyroid-derived fibroblasts. Messenger RNA (mRNA) levels were monitored by competitive semiquantitative reverse transcriptase polymerase chain reaction (RT-PCR) after 24 hours. Culture supernatants were assayed for free and/or complexed MMP-1 and TIMP-1 after 48 hours using enzyme-linked immunosorbent assay (ELISA) systems (detection limit: <2 ng/mL). MMP-1 and TIMP-1 mRNA were present in all cell types, although thyrocytes showed MMP-1 mRNA levels near the detection limit. 8505 C expressed MMP-1 mRNA levels of up to 10(6) times those of the other cells analyzed. PMA and IL-1 increased MMP-1 mRNA in most cell types. TIMP-1 mRNA increased after treatment with PMA in all cells except 8505 C, whereas only slight effects were shown after IL-1 stimulation. MMP-1 protein was undetectable in normal thyrocyte cultures, but was secreted spontaneously by all cell lines ([ng/mL]; C 643: 15+/-7; HTh 74: 81+/-1; SW 1736: 13+/-2; 8505 C: 2097+/-320). There was a strong correlation between levels of MMP-1 mRNA and protein ($r = 0.99$, $p < .0001$). PMA and IL-1 increased MMP-1 secretion in all cell types after 48 hours. Fibroblasts ([ng/mL] 517+/-55) and the cell lines (C 643: 142+/-48; HTh 74: 115+/-13; SW 1736: 202+/-14; 8505C: 120+/-19) secreted TIMP-1 in unstimulated cultures, whereas only a trace amount was detected in thyrocyte cultures, even after PMA treatment. IL-1 upregulated TIMP-1 secretion after 48 hours in SW 1736, HTh 74, and C 643 cells. Our data suggest that in contrast to normal thyrocytes, dedifferentiated thyroid carcinoma cell lines are potential producers of MMP-1 as well as TIMP-1. High MMP-1 or MMP-1/TIMP-1 expression may play a role in tissue invasion of undifferentiated thyroid cancer cells.

PMID: 9349574 [PubMed - indexed for MEDLINE]



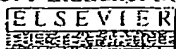
Expression of embryonic fibronectin isoform EIIIA parallels alpha-smooth muscle actin in maturing and diseased kidney.

Barnes VL, Musa J, Mitchell RJ, Barnes JL.

Department of Medicine, Division of Nephrology, University of Texas Health Science Center, San Antonio, Texas, USA.

In this study we examined if an association exists between expression of an alternatively spliced "embryonic" fibronectin isoform EIIIA (Fn-EIIIA) and alpha-smooth muscle actin (alpha-SMA) in the maturing and adult rat kidney and in two unrelated models of glomerular disease, passive accelerated anti-glomerular basement membrane (GBM) nephritis and Habu venom (HV)-induced proliferative glomerulonephritis, using immunohistochemistry and in situ hybridization. Fn-EIIIA and alpha-SMA proteins were abundantly expressed in mesangium and in periglomerular and peritubular interstitium of 20-day embryonic and 7-day (D-7) postnatal kidneys in regions of tubule and glomerular development. Staining was markedly reduced in these structures in maturing juvenile (D-14) kidney and was largely lost in adult kidney. Expression of Fn-EIIIA and alpha-SMA was reinitiated in the mesangium and the periglomerular and peritubular interstitium in both models and was also observed in glomerular crescents in anti-GBM nephritis. Increased expression of Fn-EIIIA mRNA by in situ hybridization corresponded to the localization of protein staining. Dual labeling experiments verified co-localization of Fn-EIIIA and alpha-SMA, showing a strong correlation of staining between location and staining intensity during kidney development, maturation, and disease. Expression of EIIIA mRNA corresponded to protein expression in developing and diseased kidneys and was lost in adult kidney. These studies show a recapitulation of the co-expression of Fn-EIIIA and alpha-SMA in anti-GBM disease and suggest a functional link for these two proteins.

PMID: 10330455 [PubMed - indexed for MEDLINE]



Rapid quantitation of proinflammatory and chemoattractant cytokine expression in small tissue samples and monocyte-derived dendritic cells: validation of a new real-time RT-PCR technology.

Blaschke V, Reich K, Blaschke S, Zipprich S, Neumann C.

Department of Dermatology, von-Siebold-Str. 3, D-37075, Goettingen, Germany.
vblasch@gwdg.de

The analysis of cytokine profiles plays a central part in the characterization of disease-related inflammatory pathways and the identification of functional properties of immune cell subpopulations. Because tissue biopsy samples are too small to allow the detection of cytokine protein, the detection of mRNA by RT-PCR analysis is often used to investigate the cytokine milieu in inflammatory lesions. RT-PCR itself is a qualitative method, indicating the presence or absence of specific transcripts. With the use of internal or external standards it may also serve as a quantitative method. The most widely accepted method is quantitative competitive RT-PCR, based on internal shortened standards. Recently, online real-time PCR has been introduced (LightCycler), which allows quantitation in less than 30 min. Here, we have tested its use for the analysis of cytokine gene expression in different experimental in vitro and ex vivo settings. First, we compared quantitative competitive RT-PCR with real-time RT-PCR in the quantitation of transcription levels of the CD4(+) cell-specific chemoattractant Interleukin-16 during the maturation of monocyte-derived dendritic cells, and found a good correlation between both methods. Second, differences in the amounts of IL-16 mRNA in synovial tissue from patients with rheumatoid arthritis and osteoarthritis as assessed by real-time RT-PCR paralleled differences in the level of IL-16 protein in the synovial fluid. Finally, we employed real-time RT-PCR to study the cutaneous expression of several cytokines during experimental immunomodulatory therapy of psoriasis by Interleukin-10, and demonstrate that the technique is suitable for pharmacogenomic monitoring. In summary, real-time RT-PCR is a sensitive and rapid tool for quantifying mRNA expression even with small quantities of tissue. The results obtained do not differ from those generated by quantitative competitive RT-PCR.

Publication Types:

- Evaluation Studies

PMID: 11121549 [PubMed - indexed for MEDLINE]

74: Apoptosis. 1997;2(6):518-28.

Related Articles, Links



Butyrate-induced reversal of dexamethasone resistance in autonomous rat Nb2 lymphoma cells.

Buckley AR, Krumenacker JS, Buckley DJ, Leff MA, Magnuson NS, Reed JC, Miyashita T, de Jong G, Gout PW.

Department of Pharmacology and Toxicology, University of North Dakota School of Medicine and Health Sciences, Grand Forks 58202-9037, USA.
abuckley@mail.med.und.nodak.edu

The parental rat Nb2 lymphoma is a prolactin (PRL)-dependent T cell line. Exposure of a PRL-independent subline, Nb2-SFJCD1, to sodium butyrate (NaBT) causes transient reversal of their growth factor-independent proliferation in association with constitutive expression of protooncogenes pim-1 and c-myc. In the present study, we investigated the effect of NaBT treatment on the sensitivity of Nb2-SFJCD1 cells to dexamethasone (DEX)-induced apoptosis. Pretreatment with NaBT (2 mM, 72 h) partially reversed resistance to apoptosis in Nb2-SFJCD1 cells exposed to DEX (100 nM) for 12 h, assessed by flow cytometric analyses of DNA fragmentation. However, the cytolytic effect of DEX was abrogated by PRL in a time- and concentration-dependent manner. Evaluation of apoptosis-associated gene expression in NaBT-pre-treated cultures incubated with DEX or DEX+PRL indicated that the apoptosis resistance did not stem from altered bcl-2 or bax expression. However, there was a strong correlation between the resistance to DEX-activated apoptosis and their enhanced expression of pim-1 mRNA and protein. The results show that it is possible to reverse DEX-induced apoptosis of Nb2 pre-T cells and suggest the pim-1 gene product has an important role as a suppressor of this process, perhaps functioning as a mediator of PRL action.

PMID: 14646523 [PubMed]



Characterization of cyclin D2 expression in human endometrium.

Choi D, Yoon S, Lee E, Hwang S, Song S, Kim J, Yoon BK, Lee JH.

Department of Obstetrics and Gynecology, Samsung Medical Center, Sungkyunkwan University School of Medicine, Seoul, South Korea. dschoi@smc.samsung.co.kr

OBJECTIVE: This study was undertaken to investigate cyclin D2 mRNA and protein expression in human endometrium during the menstrual cycle. **METHODS:** Endometrial samples were obtained from 15 premenopausal nonpregnant women who had hysterectomies for benign gynecologic reasons. They were divided into the following five groups according to histologic dating: early proliferative (n = 3), mid to late proliferative (n = 3), early secretory (n = 3), mid secretory (n = 3), and late secretory (n = 3). Cyclin D2 mRNA and protein expression were analyzed using reverse transcriptase-polymerase chain reaction, Western blotting, and immunohistochemistry. **RESULTS:** Cyclin D2 mRNA and protein were expressed in human endometrial tissue throughout the menstrual cycle. Cyclin D2 mRNA and protein expression of proliferative phase endometrium were significantly higher than those of secretory phase endometrium ($P < .05$). The staining intensity of cyclin D2 in proliferative phase endometrium was higher than that in secretory phase ($P < .05$). Cyclin D2 mRNA level showed good correlation with cyclin D2 protein level ($R = 0.579$, $P < .03$), and cyclin D2 protein also showed good correlation with immunohistochemical staining intensity ($R = 0.562$, $P < .03$). **CONCLUSION:** Cyclin D2 was expressed in human endometrium throughout the menstrual cycle. Cyclin D2 mRNA and protein were expressed at high levels in proliferative phase endometrium, especially in the early proliferative phase, and then decreased in the secretory phase.

PMID: 11839508 [PubMed - indexed for MEDLINE]

□ 86: Am J Physiol Lung Cell Mol Physiol. 2004 Feb;286(2):L301-11.
Epub 2003 Sep 26.

Related Articles,
Links

FREE full text article at
ajplung.physiology.org

Downregulation of ENaC activity and expression by TNF-alpha in alveolar epithelial cells.

Dagenais A, Fr  chette R, Yamagata Y, Yamagata T, Carmel JF, Clermont ME, Brochiero E, Masse C, Berthiaume Y.

Centre de recherche, CHUM-H  tel-Dieu, 3850 St-Urbain, Montreal, Quebec, Canada H2W 1T7. andre.dagenais.chum@ssss.gouv.qc.ca

Sodium absorption by an amiloride-sensitive channel is the main driving force of lung liquid clearance at birth and lung edema clearance in adulthood. In this study, we tested whether tumor necrosis factor-alpha (TNF-alpha), a proinflammatory cytokine involved in several lung pathologies, could modulate sodium absorption in cultured alveolar epithelial cells. We found that TNF-alpha decreased the expression of the alpha-, beta-, and gamma-subunits of epithelial sodium channel (ENaC) mRNA to 36, 43, and 16% of the controls after 24-h treatment and reduced to 50% the amount of alpha-ENaC protein in these cells. There was no impact, however, on alpha(1) and beta(1) Na(+)-K(+)-ATPase mRNA expression. Amiloride-sensitive current and ouabain-sensitive Rb(+) uptake were reduced, respectively, to 28 and 39% of the controls. A strong correlation was found at different TNF-alpha concentrations between the decrease of amiloride-sensitive current and alpha-ENaC mRNA expression. All these data show that TNF-alpha, a proinflammatory cytokine present during lung infection, has a profound influence on the capacity of alveolar epithelial cells to transport sodium.

PMID: 14514522 [PubMed - indexed for MEDLINE]



Inhibin and activin production and subunit expression in human placental cells cultured in vitro.

Debieve F, Pampfer S, Thomas K

Department of Obstetrics and Gynecological Endocrinology, Université Catholique de Louvain, 1200 Brussels, Belgium.

Inhibins and activins are dimeric proteins, with each subunit being one of three related protein subunits (alpha, betaA or betaB). The mRNA levels of these subunits were studied quantitatively during in-vitro differentiation of human cytotrophoblast cells into syncytium, using Northern blot analysis and semi-quantitative reverse transcription-polymerase chain reaction (RT-PCR) analysis. The corresponding protein concentrations were determined by specific enzyme-linked immunosorbent assays for inhibin A, B, pro alphaC and activin A in cellular protein extracts and culture medium (n = 5).

Immunofluorescence studies showed syncytium formation after 48 h. The alpha subunit was present before plating and increased at 48 h ($P < 0.001$) while the betaA subunit was weak before plating and increased at 24 h. The betaB subunit was not detected. With respect to corresponding protein synthesis, inhibin A (alpha + betaA) had risen after 48 h in cellular protein extract and after 72 h in culture medium, while activin A (betaA + betaB) was detected after 24 h, with no significant variations in culture medium. There was a good correlation between inhibin A and alpha subunit expression ($r = 0.736$, $P < 0.001$), as well as between activin A and betaA subunit expression ($r = 0.755$, $P < 0.001$). This study showed that mRNA expression parallels protein synthesis of inhibin and activin in trophoblast cells. Inhibin A synthesis appears to be dependent on alpha subunit mRNA expression, rather than on the betaA subunit which controls activin A synthesis. This study has also shown that isolated cytotrophoblast cells do not produce dimeric inhibin. However, during the transformation of cytotrophoblast cells into syncytium, betaA subunit mRNA expression may be an indicator of cell aggregation, while alpha subunit mRNA expression may be an indicator of cell fusion.

PMID: 10908285 [PubMed - indexed for MEDLINE]

Involvement of the CCND1 gene in hairy cell leukemia.

de Boer CJ, Kluin-Nelemans JC, Dreef E, Kester MG, Kluin PM, Schuurung E, van Krieken JH.

Department of Pathology, University of Leiden, The Netherlands.

BACKGROUND: Previous results suggested increased mRNA expression of CCND1 in hairy cell leukemia (HCL). The CCND1 gene is involved in the t(11;14)(q13;q32) chromosomal rearrangement, a characteristic abnormality in mantle cell lymphoma (MCL). We and others reported that, in contrast to other B-cell lymphomas, almost all MCL have over-expression of the CCND1 gene with a good correlation between RNA and protein analysis. Recent studies showed that overexpression of the cyclin D1 protein can be easily detected by immunohistochemistry (IHC) on formalin-fixed, paraffin embedded tissues. **PATIENTS AND METHODS:** To investigate whether the CCND1 gene is involved in HCL, we performed IHC on a series of 22 cases using formalin-fixed paraffin embedded splenectomy specimens. For IHC the sections were boiled in citrate buffer. The presence of rearrangements within the BCL-1 locus and the CCND1 gene was analyzed in 13 of 22 cases by Southern blot analysis using all available break-point probes. Expression of CCND1 was analyzed at the mRNA level (Northern blot) and protein level (IHC). **RESULTS:** Overexpression of the cyclin D1 protein using IHC was observed in all cases, with strong expression in 5 cases. Pre-existing B- and T-cell areas of the spleen did not express significant levels of the cyclin D1 protein. Seven of 9 cases analyzed by both IHC and Northern blotting showed overexpression of the CCND1 gene with both methods. No genomic abnormalities were observed in any of the 13 cases studied by Southern blot analysis. Additionally, no 11q13 abnormalities were detected by banding analysis of 19 of 22 cases. **CONCLUSIONS:** The elevated levels of CCND1 mRNA and protein in conjunction with the absence of overt rearrangements within the BCL-1 locus distinguish HCL from MCL and other B-cell malignancies. This suggests that activation of the CCND1 gene in HCL is due to mechanisms other than chromosomal rearrangement.

PMID: 8740788 [PubMed - indexed for MEDLINE]

FREE full text article at
www.iovs.org

Expression of membrane-type matrix metalloproteinases 4, 5, and 6 in mouse corneas infected with *P. aeruginosa*.

Dong Z, Katar M, Alousi S, Berk RS.

Department of Immunology and Microbiology, Wayne State University School of Medicine, 540 E. Canfield, Detroit, MI 48201, USA.

PURPOSE: To investigate the expression and regulation of membrane-type matrix metalloproteinases (MT-MMPs) 4, 5, and 6 in the mouse corneas infected with *Pseudomonas aeruginosa*. **METHODS:** C57BL/6J mice were intracorneally infected with *P. aeruginosa*. The expression of MT4-, MT5-, and MT6-MMP was detected at both the mRNA and protein levels by RT-PCR and immunoblot analysis. Immunohistochemical staining was performed to localize the expression of MT4- and MT5-MMP in the mouse corneas. **RESULTS:** Expression of MT4- and MT5-MMP was detected in the normal (uninfected) cornea by RT-PCR and immunoblot analysis. When infected with *P. aeruginosa*, the corneas showed significant induction of each MT-MMP. Localization of MT4- and MT5-MMP revealed that the expression of MT5-MMP was restricted to the epithelial tissue in the normal cornea, whereas the induced expression of MT4- and MT5-MMP was predominantly in the substantia propria, which contained most of the infiltrating cells. MT6-MMP expression was not detected in the uninfected cornea but was upregulated in the infected corneas. **CONCLUSIONS:** Expression of MT4-, MT5-, and MT6-MMP was induced in corneas infected with *P. aeruginosa*. Immunohistochemistry showed predominant immunoreactivity of MT4- and MT5-MMP in the substantia propria. Previous histologic studies have revealed different patterns of inflammatory cell infiltration with an increased number of polymorphonuclear neutrophils (PMNs) during the early stage of inflammation and increased macrophages during the late stage. These results indicate a good correlation between the overexpression of the MT-MMPs in the infected corneas and the inflammatory response—that is, leukocyte infiltration—indicating that inflammatory cells such as macrophages and PMNs may play a role in the upregulation of MT-MMPs during corneal infection, which in turn can cause the destruction of corneal tissue.

PMID: 11726626 [PubMed - indexed for MEDLINE]



Suppressors of cytokine signaling proteins are differentially expressed in Th1 and Th2 cells: implications for Th cell lineage commitment and maintenance.

Egwuagu CE, Yu CR, Zhang M, Mahdi RM, Kim SJ, Gery I.

Laboratory of Immunology, National Eye Institute, National Institutes of Health, Bethesda, MD 20892, USA. emeka@helix.nih.gov

Positive regulatory factors induced by IL-12/STAT4 and IL-4/STAT6 signaling during T cell development contribute to polarized patterns of cytokine expression manifested by differentiated Th cells. These two critical and antagonistic signaling pathways are under negative feedback regulation by a multimember family of intracellular proteins called suppressor of cytokine signaling (SOCS). However, it is not known whether these negative regulatory factors also modulate Th1/Th2 lineage commitment and maintenance. We show here that CD4(+) naive T cells constitutively express low levels of SOCS1, SOCS2, and SOCS3 mRNAs. These mRNAs and their proteins increase significantly in nonpolarized Th cells after activation by TCR signaling. We further show that differentiation into Th1 or Th2 phenotype is accompanied by preferential expression of distinct SOCS mRNA transcripts and proteins. SOCS1 expression is 5-fold higher in Th1 than in Th2 cells, whereas Th2 cells contain 23-fold higher levels of SOCS3. We also demonstrate that IL-12-induced STAT4 activation is inhibited in Th2 cells that express high levels of SOCS3 whereas IL-4/STAT6 signaling is constitutively activated in Th2 cells, but not Th1 cells, with high SOCS1 expression. These results suggest that mutually exclusive use of STAT4 and STAT6 signaling pathways by differentiated Th cells may derive in part, from SOCS3- or SOCS1-mediated repression of IL-12/STAT4- or IL-4/STAT6 signaling in Th2 and Th1 cells, respectively. Given the strong correlation between distinct patterns of SOCS expression and differentiation into the Th1 or Th2 phenotype, SOCS1 and SOCS3 proteins are therefore Th lineage markers that can serve as therapeutic targets for immune modulation therapy.

PMID: 11907070 [PubMed - indexed for MEDLINE]

Altered levels of scavenging enzymes in embryos subjected to a diabetic environment.

Forsberg H, Borg LA, Cagliero E, Eriksson UJ.

Department of Medical Cell Biology, University of Uppsala, Sweden.

Maternal diabetes during pregnancy is associated with an increased rate of congenital malformations in the offspring. The exact molecular etiology of the disturbed embryogenesis is unknown, but an involvement of radical oxygen species in the teratological process has been suggested. Oxidative damage presupposes an imbalance between the activity of the free oxygen radicals and the antioxidant defence mechanisms on the cellular level. The aim of the present study was to investigate if maternal diabetes *in vivo*, or high glucose *in vitro* alters the expression of the free oxygen radical scavenging enzymes superoxide dismutase (CuZnSOD and MnSOD), catalase and glutathione peroxidase in rat embryos during late organogenesis. We studied offspring of normal and diabetic rats on gestational days 11 and 12, and also evaluated day-11 embryos after a 48 hour culture period in 10 mM or 50 mM glucose concentration. Both maternal diabetes and high glucose culture caused growth retardation and increased rate of congenital malformations in the embryos. The CuZnSOD and MnSOD enzymes were expressed on gestational day 11 and both CuZnSOD, MnSOD and catalase were expressed on day 12 with increased concentrations of MnSOD transcripts when challenged by a diabetic milieu. There was a good correlation between mRNA, protein, and activity levels, suggesting that the regulation of these enzymes occurs primarily at the pretranslational level. Maternal diabetes *in vivo* and high glucose concentration *in vitro* induced increased MnSOD expression, concomitant with increased total SOD activity, and a tentative decrease in catalase expression and activity in the embryos. These findings support the notion of enhanced oxidative stress in the embryo as an etiologic agent in diabetic teratogenesis.

PMID: 8804988 [PubMed - indexed for MEDLINE]

Induction of the estrogen receptor by growth hormone and glucocorticoid substitution in primary cultures of rat hepatocytes.

Freyschuss B, Stavreus-Evers A, Sahlin L, Eriksson H.

Department of Reproductive Endocrinology, Karolinska Hospital, Stockholm, Sweden.

Hepatic estrogen receptors (ER) mediate estrogenic effects on mammalian liver metabolism and are thereby involved in the regulation of important physiological/pathological processes, such as coagulation, atherosclerosis, and hypertension. The regulation of the formation of the ER in primary cultures of rat hepatocytes was studied by assaying ER and ER mRNA under different endocrine conditions. The ER concentration was measured using two different methods, a ligand-binding technique and an ER enzyme immunoassay. The results obtained by the two methods showed good correlation, and linear regression analysis gave a correlation coefficient of 0.95. ER concentrations fell to low steady state levels within 16 h after establishing the cell culture and remained low in the absence of hormonal substitution. Upon medium supplementation with pituitary GH and the glucocorticoid dexamethasone (DEX) in combination, the ER concentration increased 6-fold from 4.2 ± 1.0 to 25.8 ± 7.0 fmol/mg cytosolic protein. ER mRNA was measured by solution hybridization. Substitution with GH and DEX in combination increased ER mRNA to $210 \pm 14\%$ of control levels. No effect on ER mRNA stability was seen after hormone treatment. It is concluded that the regulatory effects of GH and DEX on the hepatic ER in this in vitro system are very similar to the effects of these hormones under in vivo conditions. The inducible expression of the ER has never before, to our knowledge, been demonstrated in any mammalian liver cell culture system.

PMID: 8404593 [PubMed - indexed for MEDLINE]

Oxytocin receptors in bovine cervix: distribution and gene expression during the estrous cycle.

Fuchs AR, Ivell R, Fields PA, Chang SM, Fields MJ.

Department of Obstetrics and Gynecology, Cornell University Medical College, New York, New York 10021, USA.

Oxytocin (OT) receptor (OTR) concentrations were determined in the cervix of nonpregnant cows on cycle Days 0, 3, 7-8, 17, and 19 (n = 3-4 cows each day); [3H]OT was used as the labeled ligand. Mucosal and muscle layers of the cervix were also analyzed separately for both ligand binding and expression of the OTR gene using a newly developed RNase protection assay (RAP). Cellular localization of OTR protein was determined by immunohistochemistry. All regions of cervix from cows at estrus had high concentrations of OTR; in the luteal phase, all were sharply down-regulated. At estrus the mucosal layer had about 30-fold higher concentrations than the muscle layer. OTR mRNA was readily detected by RAP in the mucosa from estrous cows, while much weaker signals were found in the muscle. On Days 7-17, the OTR mRNA signals in both mucosa and muscle were very faint or nondetectable. Thus, there was a good correlation between ligand binding and mRNA expression, which suggests that OTR concentrations are mainly regulated at the transcriptional level. The epithelial cells at the luminal surface of the mucosa were the principal site of immunoreactive OTR; muscle cells showed significantly weaker signals. Previously, OT was found to stimulate prostaglandin (PG) E₂ output in vitro in bovine cervical tissues. Since PGE₂ is capable of softening the cervix, our findings suggest that OT may have a novel physiological function to cause softening of the bovine cervix mediated by the release of PGE₂.

PMID: 8835394 [PubMed - indexed for MEDLINE]



Silencing of the thrombomodulin gene in human malignant melanoma.

Furuta J, Kaneda A, Umebayashi Y, Otsuka F, Sugimura T, Ushijima T.

Carcinogenesis Division, National Cancer Center Research Institute, Tokyo, Japan.

The loss of thrombomodulin (TM) expression is associated with tumour growth, infiltration and lymph node metastasis in human tumours. In melanoma cell lines, TM is reported to mediate cell adhesion, and its introduction into TM-negative melanoma cell lines suppresses their growth. In this study, we analysed TM expression in surgical melanoma specimens and the role of its promoter methylation in the loss of its expression. In 15 (75%) of the 20 specimens (five from a primary site and 15 from metastatic sites), melanoma cells lacked TM immunoreactivity. Methylation of the TM promoter region was detected in 10 (67%) of the 15 TM-negative specimens by methylation-specific polymerase chain reaction, whereas methylation was detected in two (40%) of the five TM-positive specimens. In cell lines, complete methylation of the TM promoter CpG island was detected in six (46%) of 13 melanoma cell lines, whereas no methylation was detected in two cultured normal melanocytes. There was a good correlation between the methylated status of the CpG island and the loss of TM messenger RNA (mRNA) expression. Treatment of melanoma cell lines with a demethylating agent, 5-aza-2'-deoxycytidine, induced demethylation of the promoter CpG island and the restoration of mRNA and protein expression. These findings suggest that most human melanomas lack TM expression, and that methylation of the promoter CpG island is one of the mechanisms responsible.

PMID: 15714116 [PubMed - indexed for MEDLINE]

FREE full text article at
www.jimmunol.org

Cyclooxygenase-2 expression in macrophages: modulation by protein kinase C- α .

Giroux M, Descoteaux A.

Institut National de la Recherche Scientifique-Institut Armand-Frappier, Universite du Quebec, Laval, Canada.

Cyclooxygenase-2 (COX-2) is an inducible enzyme responsible for high levels of PG production during inflammation and immune responses. Previous studies with pharmacological inhibitors suggested a role for protein kinase C (PKC) in PG production possibly by regulating COX-2 expression. In this study, we addressed the role of PKC- α in the modulation of COX-2 expression and PGE2 synthesis by the overexpressing of a dominant-negative (DN) mutant of this isoenzyme in the mouse macrophage cell line RAW 264.7. We investigated the effect of various stimuli on COX-2 expression, namely, LPS, IFN- γ , and the intracellular parasite *Leishmania donovani*. Whereas LPS-induced COX-2 mRNA and protein expression were down-regulated in DN PKC- α -overexpressing clones, IFN- γ -induced COX-2 expression was up-regulated in DN PKC- α -overexpressing clones with respect to normal RAW 264.7 cells. Measurements of PGE2 levels revealed a strong correlation between PGE2 secretion and IFN- γ -induced COX-2 mRNA and protein levels in DN PKC- α -overexpressing clones. Taken together, these results suggest a role for PKC- α in the modulation of LPS- and IFN- γ -induced COX-2 expression, as well as in IFN- γ -induced PGE2 secretion.

PMID: 11034408 [PubMed - indexed for MEDLINE]

Society for Endocrinology
FREE FULL TEXT

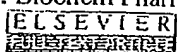
Modulation of gap junction mediated intercellular communication in TM3 Leydig cells.

Goldenberg RC, Fortes FS, Cristancho JM, Morales MM, Franci CR, Varanda WA, Campos de Carvalho AC.

Institute of Biophysics Carlos Chagas Filho, UFRJ, Brazil.

Long-term modulation of intercellular communication via gap junctions was investigated in TM3 Leydig cells, under low and high confluence states, and upon treatment of the cells for different times with activators of protein kinase A (PKA) and protein kinase C (PKC). Cells in low confluence were readily coupled, as determined by transfer of the dye Lucifer Yellow; on reaching confluence, the cells uncoupled. Western blots and RT-PCR revealed that connexin 43 (Cx43) was abundantly expressed in TM3 Leydig cells and its expression was decreased after the cells achieved confluence. Stimulation of PKA or PKC induced a decrease in cell-cell communication. Staurosporin, an inhibitor of protein kinases, increased coupling and was able to prevent and reverse the uncoupling actions of dibutyryl cAMP and 12-O-tetradecanoyl-phorbol-13-acetate (TPA). Under modulation by confluence, Cx43 was localized to the appositional membranes when cells were coupled and was mainly in the cytoplasm when they were uncoupled. In addition, cAMP and TPA reduced the surface membrane labeling for Cx43, whereas staurosporin increased it. These data show a strong correlation between functional coupling and the membrane distribution of Cx43, implying that this connexin has an important role in intercellular communication between TM3 cells. Furthermore, increased testosterone secretion in response to luteinizing hormone was accompanied by a decrease in intercellular communication, suggesting that gap junction mediated coupling may be a modulator of hormone secretion in TM3 cells.

PMID: 12740021 [PubMed - indexed for MEDLINE]



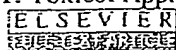
Restored expression and activity of organic ion transporters rOAT1, rOAT3 and rOCT2 after hyperuricemia in the rat kidney.

Habu Y, Yano I, Okuda M, Fukatsu A, Inui K.

Department of Pharmacy, Kyoto University Hospital, Faculty of Medicine, Kyoto University, Sakyo-ku, Kyoto 606-8507, Japan.

We previously reported that in hyperuricemic rats, renal impairment occurred and organic ion transport activity decreased, accompanied with a specific decrease in the expression of rat organic anion transporters, rOAT1 and rOAT3, and organic cation transporter, rOCT2. In the present study, we investigated the reversibility of the organic ion transport activity and expression of organic ion transporters (slc22a) during recovery from hyperuricemia. Hyperuricemia was induced by the administration of a chow containing uric acid and oxonic acid, an inhibitor of uric acid metabolism. Four days after discontinuance of the chow, the plasma uric acid concentration returned to the normal level, and renal functions such as creatinine clearance and BUN levels were restored, although the recovery of tubulointerstitial injury was varied in sites of the kidney. Basolateral uptake of p-aminohippurate (PAH) and tetraethylammonium (TEA), and both protein and mRNA levels of rOAT1, rOAT3 and rOCT2 in the kidney gradually improved during 14 days of recovery from hyperuricemia. Basolateral PAH transport showed a higher correlation with the protein level of rOAT1 ($r(2)=0.80$) than rOAT3 ($r(2)=0.34$), whereas basolateral TEA transport showed a strong correlation with rOCT2 protein ($r(2)=0.91$). The plasma testosterone concentration, which is a dominant factor in the regulation of rOCT2, was gradually restored during the recovery from hyperuricemia, but the correlation between the plasma testosterone level and rOCT2 protein expression in the kidney was not significant. These results suggest that the regulation of organic ion transporters, rOAT1, rOAT3 and rOCT2, by hyperuricemia is reversible, and the organic ion transport activity restores according to the expression levels of these transporters.

PMID: 15748710 [PubMed - indexed for MEDLINE]



Regulation of cytochrome P4501A1 in teleosts: sustained induction of CYP1A1 mRNA, protein, and catalytic activity by 2,3,7,8-tetrachlorodibenzofuran in the marine fish *Stenotomus chrysops*.

Hahn ME, Stegeman JJ.

Biology Department, Woods Hole Oceanographic Institution, Massachusetts 02543.

Cytochrome P4501A1 (CYP1A1) is known to play important roles in the activation and detoxification of carcinogens and other toxicants in vertebrate animals, including fish. Although extensively studied in mammalian systems, the regulation of CYP1A forms in other vertebrates is less well understood. We examined the time course and dose-response relationships for induction of CYP1A1 mRNA, protein, and catalytic activity by 2,3,7,8-tetrachlorodibenzofuran (TCDF) in the marine fish *Stenotomus chrysops* (scup). The time course of CYP1A1 induction was determined following a single ip dose (10 nmol/kg) of 2,3,7,8-TCDF. Hepatic ethoxyresorufin-O-deethylase activity was increased after 1 day, reached a maximum by 8 days, and was still elevated 14 days after treatment. The content of immunodetectable CYP1A1 protein in liver was elevated on Day 1 and continued to increase through 14 days. CYP1A1 protein content was also strongly induced in heart and gill beginning at 2 days after treatment and extending through Day 14. Hepatic CYP1A1 mRNA was strongly induced by 1 day after dosing and remained elevated through 14 days. The sustained induction of CYP1A1 mRNA by 2,3,7,8-TCDF contrasts with the transient induction seen previously in fish treated with nonhalogenated inducers and most likely reflects differences in persistence of the inducers. Dose-response studies indicated that induction of CYP1A1 mRNA, protein, and catalytic activity occurred following doses of 2,3,7,8-TCDF as low as 0.4 nmol/kg (120 ng/kg), within the range of whole-body contents of this congener measured in fish from contaminated environments. The estimated dose producing half-maximal CYP1A1 induction in scup was approximately 2-10 nmol/kg, suggesting that the sensitivity of these fish to induction may be as great as or greater than that of rats. In contrast to previous results obtained with 3,3',4,4'-tetrachlorobiphenyl (TCB) and beta-naphthoflavone, which appear to inhibit or inactivate CYP1A1 in fish and other vertebrates, there was a good correlation among levels of CYP1A1 mRNA, protein, and catalytic activity in individual fish following various doses of 2,3,7,8-TCDF. The difference in response to 2,3,7,8-TCDF versus 3,3',4,4'-TCB may reflect differences in the inducing potencies of the two compounds relative to their similar potencies as inhibitors of CYP1A1 catalytic activity. In additional studies to evaluate structure-activity relationships for CYP1A1 induction by chlorinated dibenzofurans in fish, scup were treated with 2,3,6,8-tetrachlorodibenzofuran (2,3,6,8-TCDF). At 10 or 50 nmol/kg, 2,3,6,8-TCDF was inactive as an inducer of CYP1A1 mRNA, protein, or catalytic activity. (ABSTRACT TRUNCATED AT 400 WORDS)

PMID: 8048062 [PubMed - indexed for MEDLINE]



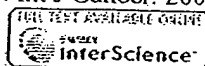
The role of the epidermal growth factor receptor in sustaining neutrophil inflammation in severe asthma.

Hamilton LM, Torres-Lozano C, Puddicombe SM, Richter A, Kimber I, Dearman RJ, Vrugt B, Aalbers R, Holgate ST, Djukanovic R, Wilson SJ, Davies DE.

Division of Infection, Inflammation & Repair, School of Medicine, University of Southampton, UK.

BACKGROUND: The extent of epithelial injury in asthma is reflected by expression of the epidermal growth factor receptor (EGFR), which is increased in proportion to disease severity and is corticosteroid refractory. Although the EGFR is involved in epithelial growth and differentiation, it is unknown whether it also contributes to the inflammatory response in asthma. **OBJECTIVES:** Because severe asthma is characterized by neutrophilic inflammation, we investigated the relationship between EGFR activation and production of IL-8 and macrophage inhibitory protein-1 alpha (MIP-1alpha) using in vitro culture models and examined the association between epithelial expression of IL-8 and EGFR in bronchial biopsies from asthmatic subjects. **METHODS:** H292 or primary bronchial epithelial cells were exposed to EGF or H2O2 to achieve ligand-dependent and ligand-independent EGFR activation; IL-8 mRNA was measured by real-time PCR and IL-8 and MIP-1alpha protein measured by enzyme-linked immunosorbent assay (ELISA). Epithelial IL-8 and EGFR expression in bronchial biopsies from asthmatic subjects was examined by immunohistochemistry and quantified by image analysis. **RESULTS:** Using H292 cells, EGF and H2O2 increased IL-8 gene expression and release and this was completely suppressed by the EGFR-selective tyrosine kinase inhibitor, AG1478, but only partially by dexamethasone. MIP-1alpha release was not stimulated by EGF, whereas H2O2 caused a 1.8-fold increase and this was insensitive to AG1478. EGF also significantly stimulated IL-8 release from asthmatic or normal primary epithelial cell cultures established from bronchial brushings. In bronchial biopsies, epithelial IL-8, MIP-1alpha, EGFR and submucosal neutrophils were all significantly increased in severe compared to mild disease and there was a strong correlation between EGFR and IL-8 expression ($r = 0.70$, $P < 0.001$). **CONCLUSIONS:** These results suggest that in severe asthma, epithelial damage has the potential to contribute to neutrophilic inflammation through enhanced production of IL-8 via EGFR-dependent mechanisms.

PMID: 12580917 [PubMed - indexed for MEDLINE]



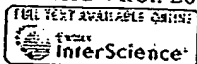
Localization of tissue inhibitor of metalloproteinases 1 (TIMP-1) in human colorectal adenoma and adenocarcinoma.

Holten-Andersen MN, Hansen U, Brunner N, Nielsen HJ, Illemann M, Nielsen BS.

The Finsen Laboratory, Rigshospitalet, Denmark.

Tissue inhibitor of matrix metalloproteinases 1 (TIMP-1) inhibits the proteolytic activity of matrix metalloproteinases and hereby prevents cancer invasion. However, TIMP-1 also possesses other functions such as inhibition of apoptosis, induction of malignant transformation and stimulation of cell-growth. We have previously demonstrated that TIMP-1 is elevated in blood from colorectal cancer patients and that high TIMP-1 levels predict poor prognosis. To clarify the role of TIMP-1 in colorectal tumorigenesis, the expression pattern of TIMP-1 in benign and malignant colorectal tumors was studied. In all of 24 cases of colorectal adenocarcinoma TIMP-1 mRNA was detected by in situ hybridization. In all cases TIMP-1 expression was found in fibroblast-like cells located at the invasive front but was seen only sporadically in normal mucosa. No TIMP-1 mRNA was seen in any of the cases in benign or malignant epithelial cells, in vascular cells or smooth muscle cells. Comparison of sections processed for TIMP-1 in situ hybridization with sections immunohistochemically stained with antibodies against TIMP-1 showed good correlation between TIMP-1 mRNA and immunoreactivity. Combining TIMP-1 in situ hybridization with immunohistochemical staining for alpha-smooth muscle actin or CD68 showed TIMP-1 mRNA in myofibroblasts but not in macrophages. TIMP-1 mRNA was detected in 2 of 7 adenomatous polyps in the adenoma area: in both cases associated with focal stromal inflammation at the epithelial-stromal interface. In conclusion, TIMP-1 expression is a rare event in benign human colon tissue but is highly expressed by myofibroblasts in association with invading colon cancer cells.

PMID: 15386409 [PubMed - indexed for MEDLINE]



Tissue plasminogen activator induced by dengue virus infection of human endothelial cells.

Huang YH, Lei HY, Liu HS, Lin YS, Chen SH, Liu CC, Yeh TM.

Department of Microbiology and Immunology, College of Medicine, National Cheng Kung University, Tainan, Taiwan, ROC.

Dengue hemorrhagic fever and dengue shock syndrome (DHF/DSS) are severe complications of dengue virus (DV) infection. However, the pathogenesis of hemorrhage induced by dengue virus infection is poorly understood. Since endothelial cells play a pivotal role in the regulation of hemostasis, we studied the effect of DV infection on the production of tissue plasminogen activator (tPA) and plasminogen activator inhibitor 1 (PAI-1) in vitro using both primary isolated endothelial cells; human umbilical cord veins cells, and a human microvascular endothelial cell line. DV infection significantly induced the secretion of tPA but not PAI-1 of human endothelial cells. In addition, tPA mRNA of endothelial cells was induced by DV as demonstrated by RT-PCR. Antibody against IL-6 but not control antibody inhibited DV-induced tPA production of endothelial cells. Furthermore, a good correlation between sera levels of IL-6 and tPA was found in DHF but not DF patients. These results suggest that IL-6 can regulate DV-induced tPA production of endothelial cells, which may play important roles in the pathogenic development of DHF/DSS. Copyright 2003 Wiley-Liss, Inc.

PMID: 12794725 [PubMed - indexed for MEDLINE]

Neu oncogene expression in ovarian tumors: a quantitative study.

Huettner PC, Carney WP, Naber SP, DeLellis RA, Membrino W, Wolfe HJ.

Department of Pathology, Tufts University School of Medicine, Massachusetts.

We studied neu mRNA expression by slot blot analysis and protein product expression by capture ELISA and immunohistochemistry in 57 primary and metastatic ovarian neoplasms, two paraovarian leiomyosarcomas, and eight normal ovaries. Some 61% of ovarian tumors but none of the paraovarian neoplasms or normal ovaries overexpressed neu mRNA. A total of 96% of the ovarian tumors that overexpressed neu were of epithelial type. Epithelial ovarian tumors had significantly higher amounts of the neu oncogene product as determined by capture ELISA than either germ cell and stromal tumors or normal ovaries (p less than 0.025). Different subtypes of ovarian carcinomas had significantly different amounts of neu oncogene product as measured by capture ELISA; endometrioid tumors had the highest, and poorly differentiated carcinomas not otherwise specified had the lowest (p less than 0.025). ELISA values, mRNA overexpression, and immunohistochemical staining intensity did not correlate with stage at diagnosis or architectural or nuclear grade in ovarian tumors. We conclude that capture ELISA is a simple, effective way to measure the neu oncogene protein product and that there is a good correlation between ELISA levels and immunohistochemical staining intensity. However, ELISA values did not correlate with stage or histologic prognostic factors in ovarian neoplasms.

PMID: 1353878 [PubMed - indexed for MEDLINE]

Elevation of topoisomerase I messenger RNA, protein, and catalytic activity in human tumors: demonstration of tumor-type specificity and implications for cancer chemotherapy.

Husain I, Mohler JL, Seigler HF, Besterman JM.

Department of Cell Biology, Glaxo Inc. Research Institute, Research Triangle Park, North Carolina 27709.

Topoisomerase I has been identified as an intracellular target of camptothecin, a plant alkaloid with anticancer activity. Various lines of evidence suggest that the sensitivity of cells to this drug is directly related to the topoisomerase I content. In humans, the levels of topoisomerase I have been shown to be elevated in colorectal tumors, compared to normal colon mucosa. The aim of our study was to determine whether (a) topoisomerase I levels are elevated in other solid tumors, (b) the elevated enzyme is catalytically active in these tumors, and (c) the increase in topoisomerase I levels in colorectal tumors is a result of increased transcription or translation. Topoisomerase I levels were quantitated in crude extracts from colorectal, prostate, and kidney tumors and their matched normal counterparts by Western blotting and by direct determination of catalytic activity, and mRNA levels were determined by Northern blotting. By Western blotting, colorectal tumors showed 5-35-fold increases in topoisomerase I levels, compared to their normal colon mucosa. In the case of prostate tumors, the increase was 2-10-fold, compared with benign hyperplastic prostate tissue from the same patients. However, no difference was observed in topoisomerase I levels in kidney tumors, compared to their normal counterparts. The catalytic activity of topoisomerase I was determined by a quantitative ³²P-transfer assay in crude homogenates, without isolating nuclei. Colorectal and prostate tumors exhibited 11-40- and 4-26-fold increases, respectively, in catalytic activity. However, kidney tumors did not show any alteration in catalytic activity, compared to their normal matched samples. Thus, for all three tumor types there was a good correlation between enzyme levels and catalytic activity. Finally, colorectal tumors were analyzed for steady state mRNA levels. A 2-33-fold increase in mRNA levels was found in colorectal tumors, compared to normal colon mucosa. These results suggest that alterations in topoisomerase I expression in humans are tumor type specific and that the increase in topoisomerase I levels results from either increased transcription of the topoisomerase I gene or increased mRNA stability.

PMID: 8275492 [PubMed - indexed for MEDLINE]

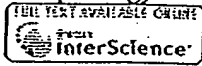
Developmental regulation of acidic fibroblast growth factor (aFGF) expression in bovine retina.

Jacquemin E, Jonet L, Oliver L, Bugra K, Laurent M, Courtois Y, Jeanny JC.

Unite de Recherches Gerontologiques, U. 118 INSERM, Paris, France.

Acidic fibroblast growth factor (aFGF) is a signalling molecule implicated in a wide variety of biological processes such as cell growth, differentiation and survival. It has been purified from bovine retina. The present study was carried out to detect which cells in the bovine retina expressed aFGF at the different stages of embryonic and post-natal development. The specific aFGF mRNA and protein were detected by in situ hybridization employing riboprobes and immunocytochemistry using affinity purified polyclonal human recombinant aFGF antibodies respectively. No signal was detected by either technique until 4-5 months and then there was progressive expression of aFGF with terminal morphogenesis of the retina. By 8-9 months of embryonic development, nuclei of the 3 neuronal layers (ganglion cell layer, inner and outer nuclear layers) were all uniformly and intensely labeled. A slight labeling of the pigmented epithelium of the retina was also visible throughout development and maturation. These results showed a good correlation between message and protein expression in these cell types. In contrast, glial cells in the nerve fiber layer and vascular endothelial cells displayed a nuclear immunostaining for the protein in the absence of message. These data suggest that aFGF plays a role in the late steps of retinal differentiation by autocrine and paracrine mechanisms.

PMID: 7507349 [PubMed - indexed for MEDLINE]



The p21(Cip1) protein, a cyclin inhibitor, regulates the levels and the intracellular localization of CDC25A in mice regenerating livers.

Jaime M, Pujol MJ, Serratos J, Pantoja C, Canela N, Casanovas O, Serrano M, Agell N, Bachs O.

Department of Cell Biology and Pathology, Faculty of Medicine, Institut d'Investigacions Biomediques August Pi Sunyer (IDIBAPS), University of Barcelona, Barcelona, Spain.

Liver cells from p21(Cip1^{-/-}) mice subjected to partial hepatectomy (PH) progress into DNA synthesis faster than those from wild-type mice. These cells also show a premature induction of cyclin E/cyclin-dependent kinase (CDK) 2 activity. We studied the mechanisms whereby cells lacking p21(Cip1) showed a premature induction of this activity. Whereas the levels of CDK2, cyclin E, and p27(Kip1) were similar in both wild-type and p21(Cip1^{-/-}) mice, those of the activator CDC25A were much higher in p21(Cip1^{-/-}) quiescent and regenerating livers than in wild-type animals. Moreover, p21(Cip1^{-/-}) cells also showed a premature translocation of CDC25A from cytoplasm into the nucleus. The ectopic expression of p21(Cip1) into mice embryo fibroblasts from p21(Cip1^{-/-}) mice decreased the levels of CDC25A and delayed its nuclear translocation. The levels of CDC25A messenger RNA in p21(Cip1^{-/-}) cells were higher than in wild-type cells, suggesting that this increase might be responsible, at least in part, for the high levels of CDC25A protein in these cells. Thus, the results reported here indicate that p21(Cip1) regulates the levels and the intracellular localization of CDC25A. We also found a good correlation between CDC25A nuclear translocation and cyclin E/CDK2 activation. In conclusion, premature translocation of CDC25A to the nucleus might be involved in the advanced induction of cyclin E/CDK2 activity and DNA replication in cells from animals lacking p21(Cip1).

PMID: 11981756 [PubMed - indexed for MEDLINE]



Alteration of frizzled expression in renal cell carcinoma.

Janssens N, Andries L, Janicot M, Perera T, Bakker A.

Department of Biochemistry, University of Antwerp, Wilrijk, Belgium.
njansse9@prdbe.jnj.com

To evaluate the involvement of frizzled receptors (Fzds) in oncogenesis, we investigated mRNA expression levels of several human Fzds in more than 30 different human tumor samples and their corresponding (matched) normal tissue samples, using real-time quantitative PCR. We observed that the mRNA level of Fzd5 was markedly increased in 8 of 11 renal carcinoma samples whilst Fzd8 mRNA was increased in 7 of 11 renal carcinoma samples. Western blot analysis of crude membrane fractions revealed that Fzd5 protein expression in the matched tumor/normal kidney samples correlated with the observed mRNA level. Wnt/beta-catenin signaling pathway activation was confirmed by the increased expression of a set of target genes. Using a kidney tumor tissue array, Fzd5 protein expression was investigated in a broader panel of kidney tumor samples. Fzd5 membrane staining was detected in 30% of clear cell carcinomas, and there was a strong correlation with nuclear cyclin D1 staining in the samples. Our data suggested that altered expression of certain members of the Fzd family, and their downstream targets, could provide alternative mechanisms leading to activation of the Wnt signaling pathway in renal carcinogenesis. Fzd family members may have a role as a biomarker.

PMID: 15557753 [PubMed - indexed for MEDLINE]

1010-4283
054
v. 25
no. 4
2004

Jul-Aug

1010-4283

Received on: 01-23
Tumour biology: the journal
of the International Society
for Oncodevelopmental
Biology and Medicine.

2004 | 4 | 04

July-August 2004
(Released November 2004)
ISSN 1010-4283
25(4) 157-220 (2004)

The Journal of the International Society for
Oncodevelopmental Biology and Medicine

Tumor Biology

Tumor Markers, Tumor Targeting
and Translational Cancer Research

Research Articles

- 157 Tissue Microarray Analysis of Cyclin D1 Gene Amplification and Gain in Colorectal Carcinomas
Toncheva, D.; Petrova, D.; Tzenova, V.; Dimova, I.; Yankova, R.; Yordanov, V.; Damjanov, D.; Todorov, T.; Zaharieva, B. (Sofia)
- 161 Alteration of Frizzled Expression in Renal Cell Carcinoma
Janssens, N. (Wilrijk/Beerse); Andries, L. (Edegem); Janicot, M.; Perera, T.; Bakker, A. (Beerse)
- 172 Antisense and Dominant-Negative AKT2 cDNA Inhibits Glioma Cell Invasion
Pu, P.; Kang, C.; Li, J. (Tianjin); Jiang, H. (Detroit, Mich.)
- 179 Production and Characterization of a New Antibody Specific for the Mutant EGF Receptor, EGFRvIII, in *Camelus bactrianus*
Omidfar, K.; Rasace, M.J. (Tehran); Modjtahedi, H. (Guilford); Forouzandeh, M.; Taghikhani, M.; Bakhtiani, A.; Paknejad, M.; Kashanian, S. (Tehran)
- 188 Matrix Metalloproteinases 2 and 9 and Their Tissue Inhibitors in Low Malignant Potential Ovarian Tumors
Määttä, M.; Santala, M.; Soini, Y.; Talvensaari-Mattila, A.; Turpeenniemi-Hujanen, T. (Oulu)

- 193 Human Kallikrein 6 Degrades Extracellular Matrix Proteins and May Enhance the Metastatic Potential of Tumour Cells
Ghosh, M.C.; Grass, L.; Soosaipillai, A. (Toronto); Sotiropoulou, G. (Patras); Diamandis, E.P. (Toronto)

Mini Reviews

- 200 The TP53 Tumor Suppressor Gene and Melanoma Tumorigenesis: Is There a Relationship?
Hussein, M.R. (Assuit)
- 208 Strategies to Endow Cytotoxic T Lymphocytes or Natural Killer Cells with Antibody Activity against Carcinoembryonic Antigen
Kuroki, M.; Kuroki, M.; Shibaguchi, H.; Badran, A.; Hachimine, K.; Zhang, J.; Kinugasa, T. (Fukuoka)

Research Commentary

- 217 Up Close and Personal: Molecular Diagnostics in Oncology
Rye, P.D. (Oslo); Nilsson, O. (Göteborg); Rittenhouse, H. (San Diego, Calif.); Stigbrand, T. (Umeå)

S. Karger
Medical and Scientific
Publishers
Basel · Freiburg
Paris · London
New York · Bangalore
Bangkok · Singapore
Tokyo · Sydney

KARGER

Online

Access to full text and tables of contents,
including tentative ones for forthcoming issues:
www.karger.com/tbi_issues

Alteration of Frizzled Expression in Renal Cell Carcinoma

Nico Janssens^{a,c} Luc Andries^b Michel Janicot^c Tim Perera^c
Annette Bakker^c

^aDepartment of Biochemistry, University of Antwerp, Wilrijk, ^bHistoGeneX, Edegem, and ^cOncology Discovery Research, Johnson & Johnson Pharmaceutical Research and Development, Beerse, Belgium

Key Words

β -Catenin · Cyclin D1 · Frizzled receptor · Renal cell carcinoma · Wnt

Abstract

To evaluate the involvement of frizzled receptors (Fzds) in oncogenesis, we investigated mRNA expression levels of several human Fzds in more than 30 different human tumor samples and their corresponding (matched) normal tissue samples, using real-time quantitative PCR. We observed that the mRNA level of Fzd5 was markedly increased in 8 of 11 renal carcinoma samples whilst Fzd8 mRNA was increased in 7 of 11 renal carcinoma samples. Western blot analysis of crude membrane fractions revealed that Fzd5 protein expression in the matched tumor/normal kidney samples correlated with the observed mRNA level. Wnt/ β -catenin signaling pathway activation was confirmed by the increased expression of a set of target genes. Using a kidney tumor tissue array, Fzd5 protein expression was investigated in a broader panel of kidney tumor samples. Fzd5 membrane staining was detected in 30% of clear cell carcinomas, and there was a strong correlation with nuclear cyclin D1 staining in the samples. Our data suggested that altered expression of certain members of the

Fzd family, and their downstream targets, could provide alternative mechanisms leading to activation of the Wnt signaling pathway in renal carcinogenesis. Fzd family members may have a role as a biomarker.

Copyright © 2004 S. Karger AG, Basel

Introduction

The Wnt signaling pathway is evolutionary conserved and controls many events during embryonic development. Members of the Wnt gene family of secreted glycoproteins are involved in embryonic induction, generation of cell polarity, cell proliferation and the determination of cell fate [1, 2]. Recently, it has become evident that the Wnt pathway is also deregulated in a range of tumors [3].

The Wnt signaling pathway is activated when Wnt proteins bind to a cell surface receptor complex consisting of a member of the frizzled receptor (Fzd) family and either low-density-lipoprotein receptor-related protein (LRP)5 or LRP6 [4, 5]. A detailed characterization of the Fzds and the immediate downstream events after Wnt binding has been hampered by the lack of pure biologically active Wnts.

Downstream of the receptor complex, three pathways may be initiated, depending on the composition of the

KARGER

Fax +41 61 306 12 34
E-Mail karger@karger.ch
www.karger.com

© 2004 S. Karger AG, Basel
1010-4233/04/0254-0161\$21.00/0

Accessible online at:
www.karger.com/tbi

Nico Janssens
Oncology Discovery Research, JAJPRD
Turnhoutseweg 30
BE-2340 Beerse (Belgium)
Tel. +32 14 605831, Fax +32 14 605403, E-Mail njansse9@prdbe.jnj.com

ligand and receptor complex. The 'Wnt/ β -catenin pathway', the 'Wnt/ Ca^{2+} pathway' or the 'Wnt polarity pathway' [6]. The Wnt/ β -catenin pathway has been linked to carcinogenesis. Genetic alterations in components of this pathway (adenomatous polyposis coli, APC, axin and β -catenin) can result in the accumulation of non-phosphorylated β -catenin [3, 7] and this can promote carcinogenesis. Conversely, neither the Wnt/ Ca^{2+} pathway nor the Wnt polarity pathway involves the activation of β -catenin [for review, see ref. 1, 6].

Mutations in one of the three regulatory genes (APC, β -catenin and axin), overexpression of Wnts and Fzds or the expression of a constitutively active Fzd have been linked to Wnt/ β -catenin pathway activation in various tumors [8, 9].

To evaluate the involvement of Fzds in oncogenesis, we investigated mRNA expression levels of several human Fzds (Fzd2, 3, 5, 6, 7, 8 and 9) in more than 30 different human tumor samples using real-time quantitative PCR. Each sample was compared with its corresponding (matched) normal tissue sample. The most striking observation was the dramatically increased Fzd5 and Fzd8 mRNA expression seen in the renal carcinoma samples. This was confirmed at the protein level using Western blotting. Kidney tumor tissue arrays confirmed Fzd5 membrane staining in 30% of clear cell carcinomas, with nuclear cyclin D1 showing a strong correlation with the Fzd5 membrane labeling. Fzd8 protein expression analysis was not performed due to the lack of suitable reagents. These data suggest that Fzd5 may have a role in renal cell carcinogenesis due to its frequent overexpression observed in these tumor samples. Potential future applications could include uses in tumor targeting or as a potential biomarker.

Materials and Methods

Tissue Samples

Frozen tumor tissue samples with corresponding normal tissue from the same patient were derived either from human biopsy or autopsy material (Department of Pathology, University of Antwerp, kindly provided by Prof. E. Van Marck). Tissue specimens were snap-frozen in liquid nitrogen and kept at -80°C until use. Frozen sections of kidney tumor and normal tissue samples were stained with hematoxylin-eosin to support the pathologist's observations and to confirm the type of kidney tumor. Paraffin-embedded tissue slides of renal carcinoma, lung carcinoma, breast and colon carcinoma were obtained, after encryption, from the Department of Pathology (Middelheim Hospital, Antwerp, Belgium). The CL1 human kidney cancer (SuperBioChips Laboratories) tissue array used in this study contained 59 tissue samples consisting of 9 normal kidney tissues,

30 clear cell renal carcinoma samples and another 20 renal cell tumor types (chromophil, chromophobe, papillary type, collecting duct carcinoma and samples with mixed types).

RNA Isolation and Reverse Transcription

Total RNA was extracted from tissue specimens using Ultraspec Reagent (Biotecx, USA) according to the manufacturer's instructions. All total RNA was routinely treated with DNase (DNA-free kit, Ambion, USA). 1 μg of total RNA was used to synthesize cDNA using oligo-dT primers (Superscript; Invitrogen, Merelbeke, Belgium). Reverse transcription was performed at 42°C for 60 min, followed by 70°C for 10 min.

Real-Time PCR

Real-time PCR was performed on either an ABI Prism 7700 or 7900 Sequence detection system (Perkin-Elmer Applied Biosystems, Foster City, Calif., USA) using the 5' nuclease assay (TaqmanTM). Primer and probe sequences were designed using Primer Express (PE Applied Biosystems) and are shown in table 1. Quantitative values were obtained from the threshold cycle number (Ct) at which the increase in the signal associated with exponential growth of PCR products is detected using PE Biosystems analysis software, according to the manufacturer's instructions.

We have used the $2^{-\Delta\Delta\text{Ct}}$ method to analyze the relative changes in gene expression of the different genes between tumor and corresponding normal tissue samples. We used the mitochondrial ATP synthase 6 (ATP5b) as the endogenous RNA control [10; Janssens et al., in prep.], and each sample was normalized to its ATP5b content. The relative expression of the target gene was also normalized to the corresponding normal tissue sample (calibrator). Results, expressed as the amount of target sample relative to the ATP5b gene and the calibrator, were determined as follows: $N = 2^{-10(\text{Ct}_{\text{sample}} - \Delta\text{Ct}_{\text{calibrator}})}$, where the ΔCt values of the sample and calibrator were determined by subtracting the average Ct value of the sample and the calibrator from the average Ct value of the ATP5b gene. Amplification was done essentially as described previously [10]. Briefly, 50 μl of reaction mixture containing 1 μl of cDNA template were amplified as follows: incubation at 50°C for 2 min, denaturation at 95°C for 10 min, and 50 cycles at 95°C for 15 s and 60°C for 1 min.

Membrane Preparation, Gel Electrophoresis and Immunoblotting

Tissue samples were weighed, suspended at a 40 times dilution [$= 40$ volumes/original wet weight of tissue (v/w)] in 50 mM Tris-HCl buffer, pH 7.4, and homogenized with an Ultra-Turrax homogenizer. After centrifugation for 10 min, 24,000 g at 4°C , the pellet was washed three times by resuspension in the Tris-HCl buffer followed by centrifugation. The final membrane pellets were stored at -80°C in the Tris-HCl buffer at a concentration of 0.5–1 mg/ml. The Bradford protein assay (Pierce, Aalst, Belgium) was used for protein determination. Proteins (50 μg) were separated by 8% SDS-PAGE and transferred to nitrocellulose membranes. After primary and secondary antibody incubation, the antigen-antibody-peroxidase complex was detected by chemiluminescence (Pierce, Aalst, Belgium) according to the manufacturer's instructions.

Immunohistochemistry

Immunohistochemistry was performed on 10- μm -thick cryosections of unfixed tumor tissue and on 6- μm -thick paraffin sections from renal tumor tissue fixed by formalin or by an alcohol-based fixative. Adjacent tissue blocks from renal tumors were processed with

Table 1. Real-time PCR primer and probe sequences

Target cDNA	Primer/probe sequences ^a	Fragment position ^b	Accession No. ^c
FZD2	(a) 5'-atcccggtgcccg-3' (b) 5'-gtatttgatcatgagccgtgaagtc-3' (c) 5'-FAM-tacacgccgcgcatgctgc-TAMRA-3'	1,548-1,613	AB017364
FZD3	(a) 5'-tcacgcccagtcgctggg-3' (b) 5'-ttgtacattcaattttatcctgc-3' (c) 5'-FAM-caiccccggaactctaacatcatttt-TAMRA-3'	1,473-1,547	AB039723
FZD5	(a) 5'-tgccaaggcacttccgtt-3' (b) 5'-tcctcaagtcgcccgc-3' (c) 5'-FAM-ctttcatggctgtgtccccc-TAMRA-3'	2,143-2,204	HSU43318
FZD6	(a) 5'-ctagcaccctcaggtaagagaa-3' (b) 5'-cccagagagtcggagatggal-3' (c) 5'-FAM-tgtgtgaacctgcctcgcag-TAMRA-3'	2,094-2,170	AF072873
FZD7	(a) 5'-ctgtggaaaggcataactgtg-3' (b) 5'-aaccaacgggaaccicaga-3' (c) 5'-FAM-aagcaactttataggcaagcagcga-TAMRA-3'	2,687-2,762	AB017365
FZD8	(a) 5'-tggtgctggctgcttctt-3' (b) 5'-cgctccatgctgataaggaa-3' (c) 5'-FAM-ccacctcgcacgccttcca-TAMRA-3'	853-919	AB043703
FZD9	(a) 5'-cccgggagctacggac-3' (b) 5'-tagtcatgtgcaagaccagg-3' (c) 5'-FAM-tggcgcgcactgcactataaggct-TAMRA-3'	1,696-1,763	HSU82169
ATP5b	(a) 5'-gggtgagggtgcttgggt-3' (b) 5'-gggcgcagtgattataggctt-3' (c) 5'-FAM-aagtgggctaggcattttatcttagagc-TAMRA-3'	580-503	AF368271
c-myc	(a) 5'-accacgagcagcgcctga-3' (b) 5'-tccagcagaaggatccagact-3' (c) 5'-FAM-acccttggcaggagcctcct-TAMRA-3'	1,297-1,413	HSMYCI
Cyclin D1	(a) 5'-gaacctggccgcaatgac-3' (b) 5'-cgctctggcattttgga-3' (c) 5'-FAM-ccgcacgatttcattgaacatt-TAMRA-3'	4,148-4,211	AF511593
PPAR δ	(a) 5'-agcatctcaccggcaaa-3' (b) 5'-gtctcgatgctggatcaca-3' (c) 5'-FAM-ccagccacacggccct-TAMRA-3'	932-990	NM-006238

^a (a) = Sense primer; (b) = antisense primer; (c) = probe.
^b Fragment positions are given according to the EMBL/GenBank accession No. of cloned sequence.
^c EMBL/GenBank accession No. of cloned sequence.

formalin and with the alcohol-based fixative. Paraffin and cryosections were mounted on poly-L-lysine or 3-aminopropyltriethoxysilane-gelatin-coated slides. The 59 tissue samples on the CLI human renal cancer tissue array slides were all fixed with formalin and embedded in paraffin, and the sections were mounted on silane-coated slides (SuperBioChips Laboratories). In addition to renal carcinoma tissue, sections from 10 formalin-fixed paraffin-embedded lung carcinomas were stained for Fzd5. Colon and breast tumors

were used as positive controls for β -catenin and cyclin D1 immunostaining.

The following primary antibodies were used: Fzd5 (Upstate Biotechnology), β -catenin (Zymed), cyclin D1 (Zymed), E-cadherin (Novocastra) and cytokeratin 8 (Biogenex). Cryosections were fixed in 4% paraformaldehyde for 5 min; acetone for 5 min at -20°C and 70% ethanol for 5 min. Endogenous peroxidase activity was quenched using 3% H_2O_2 . Paraffin sections of formalin- and alcohol-

Table 2. Fzd mRNA expression in tumor samples

Sample ^a	Tissue	Tumor type	x-fold expression increase ^b						
			FZD2	FZD3	FZD5	FZD6	FZD7	FZD8	FZD9
133702	kidney	adenocarcinoma	0.17	0.5	3.72	2.13	0.06	1.32	—
137770	kidney	renal cell carcinoma	1.23	3.56	8.26	2.61	1.3	8.21	5.44
138844	kidney	renal cell carcinoma	0.31	0.11	6.84	1.18	0.23	3.18	2.8
137146	kidney	renal cell carcinoma	0.47	0.45	3.16	2.23	0.73	4.42	1.37
137564	kidney	renal cell carcinoma	3.43	2.95	9.6	1.57	7.64	3.52	—
133408	kidney	renal cell carcinoma	23.97	0.98	6.39	2.48	5.05	16.72	—
139188	kidney	renal cell carcinoma	3.7	0.56	0.66	1.33	0.37	4.41	1.53
135699	kidney	renal cell carcinoma	2.6	0.36	4.83	0.9	0.34	2.54	2.31
139064	kidney	renal cell carcinoma	5.16	1.82	1.25	2.36	1.8	2.19	2.85
134585	kidney	renal cell carcinoma	1.47	0.72	1.38	0.47	0.09	0.6	—
140279	kidney	renal cell carcinoma	7.33	18.17	3.93	6.05	6.41	4.65	7.91
137252	ovary	carcinosarcoma	0.4	3.39	0.49	0.44	0.92	0.54	0.53
138256	ovary	papillary carcinoma	0.7	5.17	1.22	2.19	0.4	0.11	—
146472	ovary	serous papillary carcinoma	0.39	3.29	2.56	1.34	3.94	0.67	0.59
145845	colon	adenocarcinoma	3.45	3.36	0.58	1.22	1.67	1.24	1.99
146145	colon	adenocarcinoma	5.46	6.74	4.42	6.57	3.36	6.08	0.15
146630	colon	adenocarcinoma	4.01	4.73	0.3	1.16	0.54	0.55	0.12
146633	colon	adenocarcinoma	1.87	1.07	1.62	1.47	0.51	2.07	—
147055	colon	adenocarcinoma	0.66	1.41	1.01	1.33	0.24	0.79	4.87
142253	lung	adenocarcinoma	0.67	5.17	0.43	1.87	0.33	0.59	0.41
143036	lung	adenocarcinoma	0.67	1.24	2.63	1.13	1.11	1.04	9.19
138938	lung	adenocarcinoma	0.93	0.88	1.07	1.3	1.73	0.38	0.76
133563	lung	adenocarcinoma	2.76	1.23	0.31	1.34	0.99	0.78	4.97
144387	lung	adenocarcinoma	12.85	0.43	0.49	0.25	2.73	0.54	—
137304	lung	acinary adenocarcinoma	0.54	9.15	1.65	1.25	0.63	3.41	2.64
144546	lung	epithelial carcinoma	0.1	0.67	0.21	8.11	0.27	0.97	1.32
137621	lung	epithelial carcinoma	1.52	2.19	0.37	2.26	0.52	0.45	1.06
145552	lung	epithelial carcinoma	1.09	—	0.16	0.91	1.47	0.13	0.5
143987	testis	embryonal carcinoma	0.24	0.6	19.43	1.33	23.12	2.43	0.33
137332	stomach	leiomyoma	19.32	3.91	0.45	1.53	18.98	32.82	16.7
139026	stroma	gastrointestinal carcinoma	66.1	3.51	0.03	6.67	8.44	2.28	20.82
136049	rectum	adenocarcinoma	1.71	0.52	0.4	0.54	0.29	0.88	0.28
140794	gall bladder	adenosquamous carcinoma	0.19	—	0.93	3.02	0.2	—	—

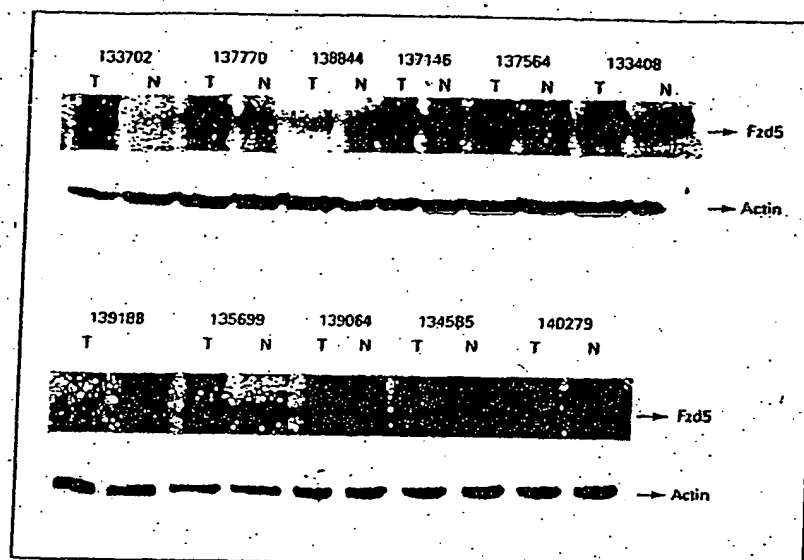
^a Sample identification numbers were given by the pathologist.

^b Results are expressed as x-fold increase of the gene in the tumor tissue sample compared to its matched normal tissue sample after normalizing both samples on the basis of their ATP5b content. A cutoff of 3-fold was used to define differential expression. Significant (>3-fold) increases in the expression level of the Fzd receptor are shown in italics. — = Expression of the target gene undetectable in one or both samples (tumor and/or normal).

fixed tissue were processed with a trypsin-tritrate-microwave pretreatment or with an EDTA-microwave pretreatment to unmask epitopes, respectively. Sections were then sequentially processed with primary antibodies, biotinylated secondary antibodies and streptavidin-biotin-peroxidase (Fzd5, E-cadherin and cytokeratin 8). For β -catenin, polyclonal rabbit antibody with the EnVision detection system (DAKO) was used. The slides were further developed using 3-amino-9-ethylcarbazole, counterstained with hemalaun and mount-

ed with glycerin gelatin. Stained sections were observed with an Axioplan 2 microscope equipped with an Axiocam digital camera. Staining intensity for β -catenin was scored as no staining (value 0), weak and fragmentary staining of cell membranes (value 1), moderate membrane staining of less than 50% of the tumor cells (value 2), moderate membrane staining of more than 50% of tumor cells (value 3) and strong membrane staining of more than 75% of tumor cells (value 4). The cyclin D1 staining was quantified as a percentage of

Fig. 1. Fzd5 protein expression in matched tumor/normal kidney samples. T = Tumor sample; N = matched normal sample. Sample identification numbers are given by the pathologist.



cyclin D1-immunoreactive nuclei in tumor cells in three fields (area: 18,641 μm^2) of each tumor sample. The total number of tumor nuclei ranged from 51 to 164. The correlation between Fzd5 and β -catenin staining, and between Fzd5 and cyclin D1 staining was evaluated by the Mann-Whitney U test.

Results

Fzd mRNA Expression in Matched Human Tumor/Normal Tissue Samples

Fzd expression in tumor tissue was compared with Fzd expression in matched normal tissue samples and normalized to the expression of the housekeeping gene mitochondrial ATP5b (table 2). A 3-fold increase was considered significant.

In the kidney tumor samples, in which 10 of 11 samples were clear cell carcinomas, Fzd5 was upregulated in 8 of the 11 samples. A similar observation was made for Fzd8 and Fzd2, which were upregulated in 7 and 5 renal tumor samples, respectively. None of the other Fzds showed consistent upregulation.

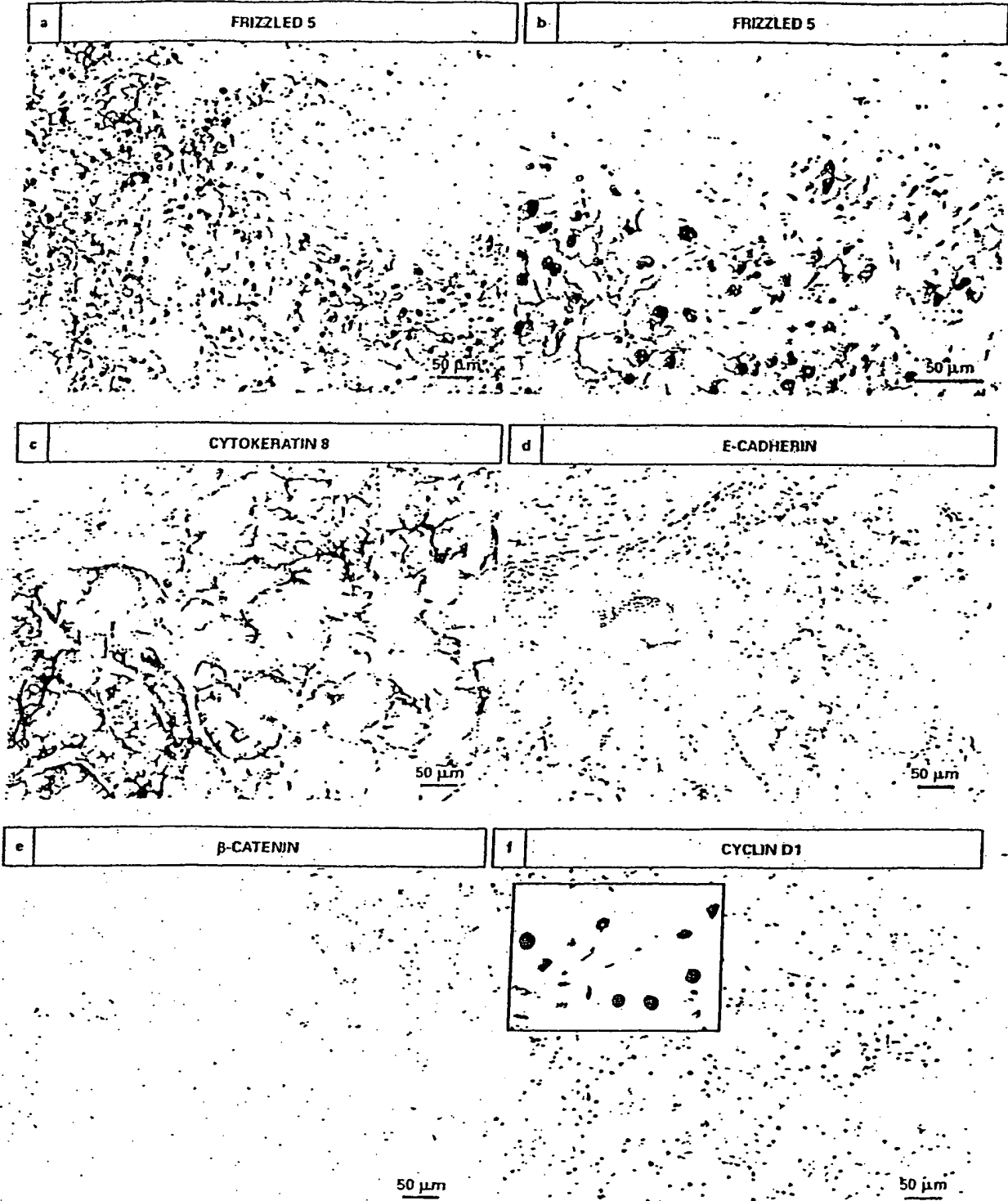
Both Fzd2 and Fzd3 were upregulated in 3 of 5 colon adenocarcinoma samples. No other Fzd expression was significantly different compared to the normal colon tissue sample. Fzd3 showed an increased expression in all 3 ovarian carcinoma samples. Fzd expression was not altered in any of the lung tumor samples. The Fzd expres-

sion level was observed to be relatively low in these lung tissues compared to the other tissues investigated.

Western Blot and Immunohistochemistry Analysis on Renal Carcinomas

Western blotting was used to evaluate Fzd5 protein expression in the renal tissue samples used for mRNA expression analysis. Membrane fractions of the renal carcinoma and corresponding normal tissue samples were prepared. As previously shown (table 2), Fzd5 mRNA upregulation was detected in 8 of the 11 matched tumor/normal samples. Increased expression of Fzd5 protein was seen in membrane fractions from 9 of 11 samples (fig. 1). In most cases, concomitant increases in Fzd5 mRNA and protein levels were observed.

Hematoxylin-eosin staining of the cryosectioned tumors confirmed the presence of clear cell carcinoma. Fzd5 immunostaining in clear cell carcinoma (fig. 2a, b) was observed to be localized to cell membranes and to nuclei. Cytokeratin 8 (fig. 2c) and E-cadherin (fig. 2d) were also detected. E-cadherin labeling of cell membranes in clear cell carcinoma was less intense and patchy compared to epithelial cells of normal renal tissue. β -Catenin staining was confined to the cell membrane. β -Catenin levels in the clear cell carcinoma membranes were highly variable. Nuclear β -catenin staining was not observed in any of the samples. Epithelial cells in normal renal tissue showed intense membrane staining and some cytoplasmic



staining. In addition, weak β -catenin staining of endothelial cells was observed. A high number of cyclin D1-immunoreactive nuclei was observed in clear cell carcinoma (fig. 2f).

On the CL1 human kidney cancer tissue array, 30% ($n = 9$) of the clear cell carcinoma tumor samples ($n = 30$) showed Fzd5 immunoreactivity (fig. 3a). Membrane-associated β -catenin staining was observed in 33% of the Fzd5-positive tumor samples and 57% of Fzd5-negative clear renal cell carcinoma samples (table 3; fig. 3c, d). Again, nuclear β -catenin staining was never observed. Statistical analysis did not reveal a difference in the expression of β -catenin between Fzd5-positive and Fzd5-negative tumor samples (fig. 4a).

Nuclear cyclin D1 was observed in 89% of the Fzd5-positive clear cell carcinoma samples (table 3; fig. 3e). Only 38% of the Fzd5-negative clear cell carcinoma samples contained nuclear cyclin D1. Statistical analysis showed a significantly higher cyclin D1 expression in Fzd5-positive compared to Fzd5-negative tumor samples (fig. 4b).

c-myc, Cyclin D1 and Peroxisome Proliferator-Activated Receptor δ Expression in Renal Carcinomas

Wnt/ β -catenin pathway activation in the kidney tissue samples was investigated looking at the expression of a number of target genes, which have previously been shown to be upregulated when the pathway is active. Gene expression of *c-myc*, cyclin D1 and peroxisome proliferator-activated receptor δ (PPAR δ) was analyzed. Increased expression of both *c-myc* and cyclin D1 genes have been implicated in cell proliferation, and carcinogenesis, and they represent two of the more important and closely studied target genes of the Wnt signaling pathway.

Fig. 2. Distribution of Fzd5 (a, b), cytokeratin 8 (c), E-cadherin (d) and β -catenin (e) immunoreactivity in paraffin sections from a renal tumor processed by an alcohol fixative. From the same tumor, a formalin-fixed block was used for cyclin D1 immunostaining (f). Fzd5 immunostaining shows distinct immunoreactivity in cell membranes and in nuclei of clear cell renal carcinoma. Clear cells are immunoreactive for cytokeratin 8. β -Catenin and E-cadherin staining of membranes is rather weak, and not uniform, in clear cell renal carcinoma. Nuclear β -catenin immunoreactivity was not observed. In clear cell renal carcinoma, many nuclei showed cyclin D1 immunoreactivity. The inset in f shows a detailed view of the cyclin D1 labeling of nuclei in clear cell renal carcinoma.

Expression of PPAR δ was investigated because it represents a direct target of the β -catenin pathway with T cell factor binding sites in its promoter. Expression of *c-myc* was found to be upregulated in 7 of 11, whilst cyclin D1 was upregulated in 10 of 11 kidney tumor samples (table 4). PPAR δ was upregulated in 9 cases. All three selected target genes showed a marked upregulation in the majority of renal tumors, which suggested that the Wnt/ β -catenin pathway was activated in these samples.

Discussion

Fzd family member overexpression has been postulated to play key roles in different tumor types such as esophageal carcinoma [11], gastric cancer [12] and head and neck squamous cell carcinoma [13]. The current study evaluated the potential implication of Fzds as tumor-associated antigens in different tumor types. We screened a number of matched normal/tumor tissue samples for the expression of a variety of Fzds using real-time quantitative PCR.

Results obtained revealed that both Fzd5 and Fzd8 mRNA were overexpressed in the majority of renal carcinoma samples when compared to the matched normal kidney samples. Fzd2 and Fzd3 were upregulated in 3 of 5 colon adenocarcinoma samples. Fzd3 was also upregulated in the ovarian tumor tissue samples compared to the matched normal tissue samples. None of the other Fzds evaluated showed a specific differential expression pattern in any of the samples studied. Fzd5 and Fzd8 show 69.1% similarity and belong to the same subgroup of Fzds [14]. The significantly higher expression of Fzd5 and Fzd8 in the renal tumor samples, as compared to the normal renal samples, suggests a higher probability that this subgroup may be implicated in the progression of renal cancer. Therefore, we decided to further examine the possible role of Fzd5 in renal carcinoma.

We observed, using Western blotting, that protein levels were mostly consistent with mRNA levels in the tumor samples. In order to be able to determine the Fzd5 expression in a broader range of kidney tissues, we utilized a tissue array. Fzd5 membrane staining was detected in 9 of 30 (30%) clear cell carcinomas, and importantly, membrane staining was not detected in the matched 9 normal kidney tissue samples.

Since the Wnt signaling pathway appears to play an important role in embryonic development, in particular embryonic kidney induction [15, 16], activation of this pathway in the adult kidney due to mutation or overex-

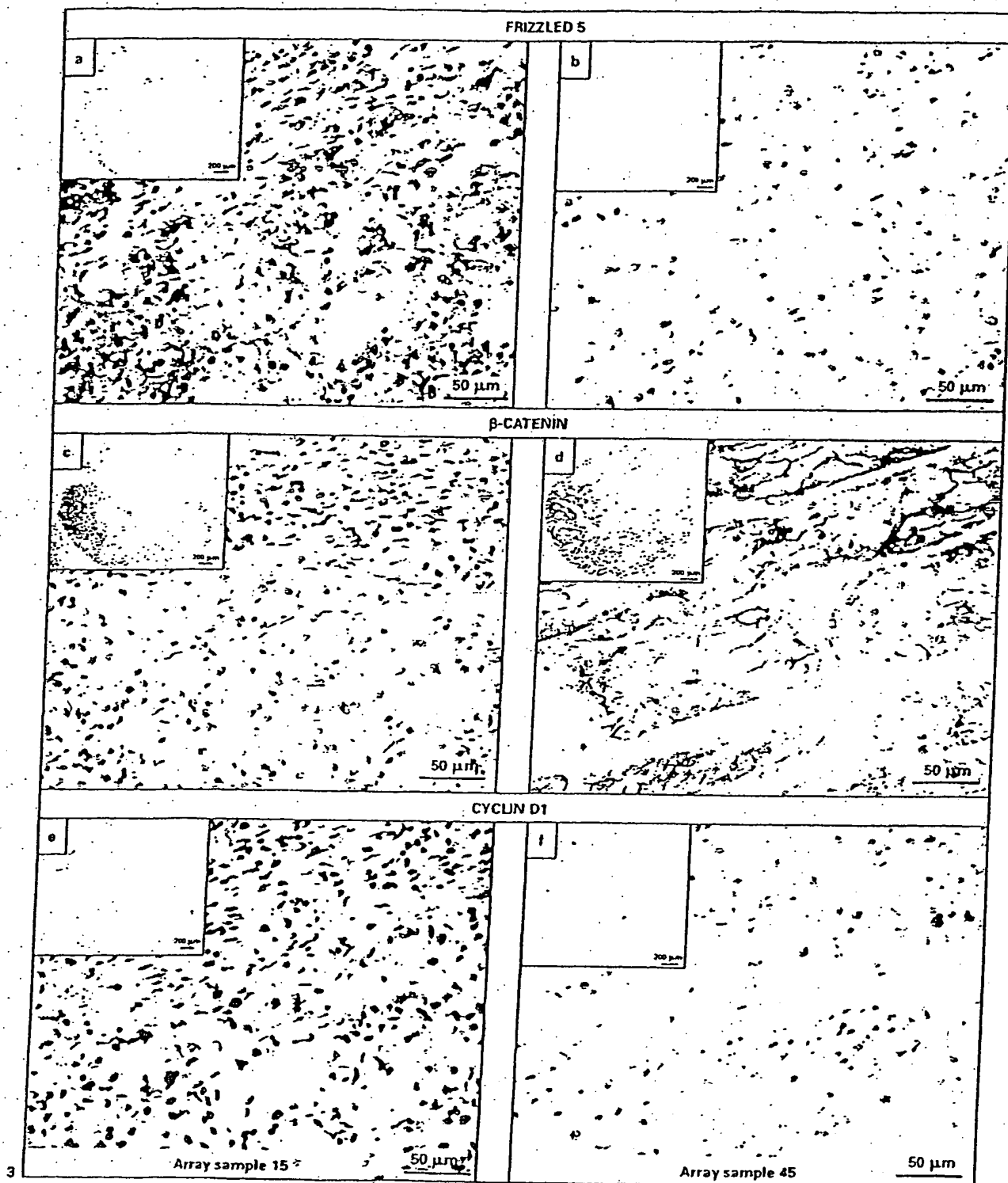


Table 3. Correlation between Fzd5 and β -catenin or cyclin D1 expression

	Fzd5, %	
	+	-
β -Catenin +	33	57
β -Catenin -	67	43
Cyclin D1 +	89	38
Cyclin D1 -	11	62

pression of one of the components of the pathway could be a determining factor in the development of renal cancers. Therefore, several studies have looked into the possible function the Wnt/ β -catenin pathway plays in renal carcinogenesis. APC gene mutations have been demonstrated not to be involved in renal carcinoma [17, 18]. In addition, β -catenin mutations are rare events in renal carcinoma [19, 20]. Nevertheless, cytoplasmic accumulation of β -catenin has been reported in a number of renal cell carcinomas [19], and thus the Wnt signaling pathway

Table 4. Wnt/ β -catenin target gene mRNA expression in tumor samples

Sample ^a	Tissue	Tumor type	x-fold expression increase ^b		
			c-myc	cyclin D1	PPAR δ
133702	kidney	adenocarcinoma	0.54	4.52	0.52
137770	kidney	renal cell carcinoma	13.9	28.91	5.53
138844	kidney	renal cell carcinoma	2.39	31.49	7.48
137146	kidney	renal cell carcinoma	7.62	15.38	3.15
137564	kidney	renal cell carcinoma	33.82	19.65	8.65
133408	kidney	renal cell carcinoma	7.8	8.92	4.86
139188	kidney	renal cell carcinoma	2.22	9.92	11.67
135699	kidney	renal cell carcinoma	12.18	22.73	5.53
139064	kidney	renal cell carcinoma	22.11	5.04	6.33
134585	kidney	renal cell carcinoma	1.79	1.14	1.67
140279	kidney	renal cell carcinoma	61.68	54.95	14.62

^a Sample identification numbers were given by the pathologist.

^b Results are expressed as x-fold increase of the gene in the tumor tissue sample compared to its matched normal tissue sample after normalizing both samples on the basis of their ATP5 β content. A cutoff of 3-fold was used to define differential expression. Significant (> 3-fold) increases in the expression level of the Fzd receptors are in italics.

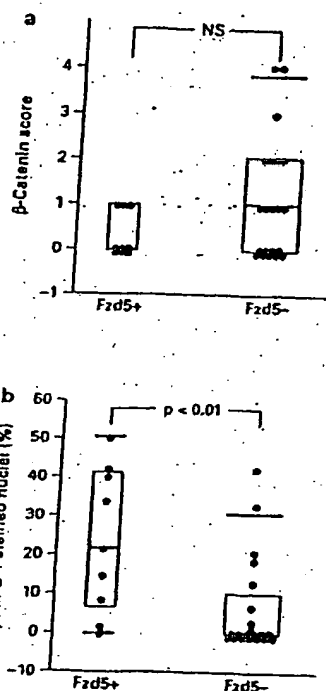


Fig. 3. Fzd5, β -catenin and cyclin D1 immunostaining of the CL1 renal carcinoma tissue arrays. The left column of images represents serial sections from tumor sample 15. Insets show an overview of each tumor section on the serial tissue arrays. The Fzd5-immunoreactive clear cell renal carcinoma (a) of this tumor sample does not express β -catenin (c). Immunostaining for cyclin D1 (e) detects distinct labeling of nuclei in clear cell renal carcinoma. The right column of images is taken from serial sections of tumor sample 45. Clear cell renal carcinoma from this tumor sample does not express Fzd5 (b) and cyclin D1 (f) but does show distinct membrane β -catenin staining (d).

Fig. 4. Box plot charts (thick black line = median) illustrating the relationship between Fzd5 immunostaining and β -catenin (a) and cyclin D1 (b) expression in clear cell renal carcinoma. No significant correlation was observed between the β -catenin scores of Fzd5-positive and -negative clear cell renal carcinoma. Nuclear cyclin D1 staining in clear cell renal carcinoma showed a significant difference between Fzd5-positive and Fzd5-negative tumor samples.

might act as an inducer of tumorigenesis in the kidney. This view is supported by the observation that aberrant activity of the Wnt signaling pathway has been reported in renal-cancer-derived cell lines. Zang et al. [21] observed a higher expression level of Wnt5a and Fzd5 mRNA in the renal cancer cell line GRC-1 than in the normal renal cell line HK-2. Expression of β -catenin was also higher in GRC-1 than in HK-2.

To determine the status of the canonical Wnt signaling pathway in our renal carcinoma samples, we have quantitated the mRNA levels of three important target genes of T cell factor/lymphoid enhancer factor activation by β -catenin. The mRNA levels of these three target genes (c-myc, cyclin D1 and PPAR δ) correlated largely with the expression of Fzd5 in these samples, suggesting that the canonical pathway is activated. On the kidney tissue array, cyclin D1 protein expression showed a highly significant correlation with the Fzd5 expression in the tumor samples (table 3). Cyclin D1 protein is frequently overexpressed in various tumors, but in only a proportion of the cases is it due to amplification of the cyclin D1 gene [22]. Therefore, other mechanisms such as upregulation of gene transcription may play a substantial role in the overexpression of cyclin D1 [23–26]. Our data, showing increased cyclin D1 expression in renal carcinoma samples, are consistent with the results of Stassar et al. [27]. They studied genes that are associated with human renal carcinoma by suppression subtractive hybridization and reported 14 differentially expressed genes, including cyclin D1. Although we would have expected an increased nuclear β -catenin staining, nuclear accumulation of β -cate-

nin was not observed in any of the tumors or on the tissue array. This result is consistent with the data presented for renal cell carcinomas by Kim et al. [19]. They did not detect nuclear β -catenin staining in the 52 renal cell carcinomas examined. The lack of nuclear β -catenin staining has also been reported by others in tumors that might have arisen from Wnt/ β -catenin pathway activation [28–31].

While expression of both Wnt5a and Fzd5 does induce duplication of the *Xenopus* head, exogenous expression of Fzd5 in a *Xenopus* model does not induce duplication of the head [32]. Fzd5 does not activate the β -catenin signaling pathway on its own, as the presence of its endogenous ligand is also required. Our results suggest that Fzd5 may have a role in renal cell carcinogenesis due to its frequent overexpression observed in these tumor samples, and we hypothesize that if Fzd5 is overexpressed, it has a rather limited effect on β -catenin signaling. However, in the presence of its endogenous still unknown ligand, it activates the canonical Wnt signaling pathway. The elucidation of this ligand and its binding characteristics is still under investigation. Ultimately, knowledge of the specific expression patterns of both Wnt and Fzd members could lead to directed tumor targeting or could be used as a tumor marker.

Acknowledgment

We are grateful to Prof. E. Van Marck (University of Antwerp) for providing us with the tissue samples.

References

- Pandur P, Maurus D, Kuhl M: Increasingly complex: New players enter the Wnt signaling network. *Bioessays* 2002;24:881–884.
- Dale TC: Signal transduction by the Wnt family of ligands. *Biochem J* 1998;329:209–223.
- Oving JM, Clevers HC: Molecular causes of colon cancer. *Eur J Clin Invest* 2002;32:448–457.
- Pinson KI, Brennan J, Monkley S, Avery BJ, Skarnes WC: An LDL-receptor-related protein mediates Wnt signalling in mice. *Nature* 2000;407:535–538.
- Tamai K, Semenov M, Kato Y, Spokony R, Liu CM, Katsuyama Y, Hess F, Saint-Jeannet JP, He X: LDL-receptor-related proteins in Wnt signal transduction. *Nature* 2000;407:530–535.
- Miller JR: The Wnts. *Genome Biol* 2002, vol 3.
- Satoh S, Daigo Y, Furukawa Y, Kato T, Miwa N, Nishiwaki T, Kawasoe T, Ishiguro H, Fujita M, Tokino T, Sasaki Y, Imaoka S, Murata M, Shimano T, Yamaoka Y, Nakamura Y: AXIN1 mutations in hepatocellular carcinomas, and growth suppression in cancer cells by virus-mediated transfer of AXIN1. *Nat Genet* 2000;24:245–250.
- Vider BZ, Zimmer A, Chastre E, Prevot S, Gerspach C, Estlin D, Wolloch Y, Tronick SR, Gazit A, Yaniv A: Evidence for the involvement of the Wnt 2 gene in human colorectal cancer. *Oncogene* 1996;12:153–158.
- Iozzo RV, Eichstetter I, Danielson KG: Aberrant expression of the growth factor Wnt-5A in human malignancy. *Cancer Res* 1995;55:3495–3499.
- Gerard CJ, Andrejka LM, Macina RA: Mitochondrial ATP synthase 6 as an endogenous control in the quantitative RT-PCR analysis of clinical cancer samples. *Mol Diagn* 2000;5:39–46.
- Tanaka S, Akiyoshi T, Mori M, Wands JR, Sugimachi K: A novel frizzled gene identified in human esophageal carcinoma mediates APC/beta-catenin signals. *Proc Natl Acad Sci USA* 1998;95:10164–10169.
- To KF, Chan MW, Leung WK, Yu J, Tong JH, Lee TL, Chan FK, Sung JJ: Alterations of frizzled (FzE3) and secreted frizzled related protein (hsFRP) expression in gastric cancer. *Life Sci* 2001;70:483–489.
- Rhee CS, Sen M, Lu D, Wu C, Leoni L, Rubin J, Corr M, Carson DA: Wnt and frizzled receptors as potential targets for immunotherapy in head and neck squamous cell carcinomas. *Oncogene* 2002;21:6598–6605.

- 14 Saitoh T, Hirai M, Katoh M: Molecular cloning and characterization of human frizzled-8 gene on chromosome 10p11.2. *Int J Oncol* 2001;18:991-996.
- 15 Dressler GR: Tubulogenesis in the developing mammalian kidney. *Trends Cell Biol* 2003;12:390-395.
- 16 Vainio SJ, Itaranta PV, Perasaari JP, Uusitalo MS: Wnts as kidney tubule inducing factors. *Int J Dev Biol* 1999;43:419-423.
- 17 Bohm M, Wieland I, Stinhofer C, Otto T, Rubben H: Detection of loss of heterozygosity in the APC tumor suppressor gene in nonpapillary renal cell carcinoma by microdissection and polymerase chain reaction. *Urol Res* 1997;25:161-165.
- 18 Suzuki H, Ueda T, Komiya A, Okano T, Isaka S, Shimazaki J, Ito H: Mutational state of von Hippel-Lindau and adenomatous polyposis coli genes in renal tumors. *Oncology* 1997;54:252-257.
- 19 Kim YS, Kang YK, Kim JB, Han SA, Kim KII, Paik SR: Beta-catenin expression and mutational analysis in renal cell carcinomas. *Pathol Int* 2000;50:725-730.
- 20 Ueda M, Gemmill RM, West J, Winn R, Sugita M, Tanaka N, Ueki M, Drabkin HA: Mutations of the β - and γ -catenin genes are uncommon in human lung, breast, kidney, cervical and ovarian carcinomas. *Br J Cancer* 2001;85:64-68.
- 21 Zang T, Zhuang L, Zhang Z, Xin D, Guo Y: Aberrant activity of WNT/frizzled signaling pathway in renal cancer cell lines. *Chin Sci Bull* 2000;45:1703-1707.
- 22 Ozturk M: Genetic aspects of hepatocellular carcinogenesis. *Semin Liver Dis* 1999;19:235-242.
- 23 Aktas H, Cai H, Cooper GM: Ras links growth factor signaling to the cell cycle machinery via regulation of cyclin D1 and the Cdk inhibitor p27KIP1. *Mol Cell Biol* 1997;17:3850-3857.
- 24 Weber JD, Raben DM, Phillips PJ, Baldassare JJ: Sustained activation of extracellular-signal-regulated kinase 1 (ERK1) is required for the continued expression of cyclin D1 in G1 phase. *Biochem J* 1997;326:61-68.
- 25 Lavoie JN, L'Allemain G, Brunet A, Muller R, Pouyssegur J: Cyclin D1 expression is regulated positively by the p42/p44MAPK and negatively by the p38/HOGMAPK pathway. *J Biol Chem* 1996;271:20608-20616.
- 26 Treinies I, Paterson HF, Hooper S, Wilson R, Marshall CJ: Activated MEK stimulates expression of AP-1 components independently of phosphatidylinositol 3-kinase (PI3-kinase) but requires a PI3-kinase signal to stimulate DNA synthesis. *Mol Cell Biol* 1999;19:321-329.
- 27 Stassar MJ, Devitt G, Brosius M, Rinnab L, Prang J, Schradin T, Simon J, Petersen S, Kopp-Schneider A, Zoller M: Identification of human renal cell carcinoma associated genes by suppression subtractive hybridization. *Br J Cancer* 2001;85:1372-1382.
- 28 Wong SC, Lo SF, Lee KC, Yam JW, Chan JK, Wendy Hsiao WL: Expression of frizzled-related protein and Wnt-signalling molecules in invasive human breast tumours. *J Pathol* 2002;196:145-153.
- 29 Ueta T, Ikeguchi M, Hirooka Y, Kaibara N, Terada T: Beta-catenin and cyclin D1 expression in human hepatocellular carcinoma. *Oncol Rep* 2002;9:1197-1203.
- 30 Tanaka Y, Kato K, Notohara K, Nakatani Y, Miyake T, Ijiri R, Nishimata S, Ishida Y, Kigasawa H, Ohama Y, Tsukayama C, Kobayashi Y, Horie H: Significance of aberrant (cytoplasmic/nuclear) expression of beta-catenin in pancreaticoblastoma. *J Pathol* 2003;199:185-190.
- 31 Qiao Q, Ramadani M, Gansauge S, Gansauge F, Leder G, Beger HG: Reduced membranous and ectopic cytoplasmic expression of beta-catenin correlate with cyclin D1 overexpression and poor prognosis in pancreatic cancer. *Int J Cancer* 2001;95:194-197.
- 32 He X, Saint-Jeannet JP, Wang Y, Nathans J, Dawid I, Varmus H: A member of the frizzled protein family mediating axis induction by Wnt-5A. *Science* 1997;275:1652-1654.

Full text article at
www.biolreprod.org

Multidrug resistance phosphoglycoprotein (ABCB1) in the mouse placenta: fetal protection.

Kalabis GM, Kostaki A, Andrews MH, Petropoulos S, Gibb W, Matthews SG.

Department of Physiology, University of Toronto, Ontario, Canada.

The multidrug resistance phosphoglycoprotein ATP-binding cassette subfamily B (ABCB1) actively extrudes a range of structurally and functionally diverse xenobiotics as well as glucocorticoids. ABCB1 is present in many cancer cell types as well as in normal tissues. Although it has been localized within the mouse placenta, virtually nothing is known about its regulation. In the mouse, two genes, *Abcb1a* and *Abcb1b*, encode ABCB1. We hypothesized that there are changes in placental *Abcb1a* and *Abcb1b* gene expression and ABCB1 protein levels during pregnancy. Using in situ hybridization, we demonstrated that *Abcb1b* mRNA is the predominant placental isoform and that there are profound gestational changes in the expression of both *Abcb1a* and *Abcb1b* mRNA. Placentas from pregnant mice were analyzed between Embryonic Days (E) 9.5 and 19 (term approximately 19.5d). *Abcb1b* mRNA was detected in invading trophoblast cells by E9.5, peaked within the placental labyrinth at E12.5, and then progressively decreased toward term ($P < 0.0001$). *Abcb1a* mRNA, although lower than that of *Abcb1b* at midgestation, paralleled changes in *Abcb1b* mRNA. Changes in *Abcb1* mRNA were reflected by a significant decrease in ABCB1 protein ($P < 0.05$). A strong correlation existed between placental *Abcb1b* mRNA and maternal progesterone concentrations, indicating a potential role of progesterone in regulation of placental *Abcb1b* mRNA. In conclusion, there are dramatic decreases in *Abcb1a* and *Abcb1b* mRNA and in ABCB1 at the maternal-fetal interface over the second half of gestation, suggesting that the fetus may become increasingly susceptible to the influences of xenobiotics and natural steroids in the maternal circulation.

PMID: 15917342 [PubMed - in process]

Expression of human telomerase reverse transcriptase gene and protein, and of estrogen and progesterone receptors, in breast tumors: Preliminary data from neo-adjuvant chemotherapy.

Kamimori M, Izumiyama N, Hashimoto M, Nakamura K, Okano T, Kurabayashi R, Naoki H, Honma N, Ogawa T, Kaminishi M, Takubo K.

Division of Breast and Endocrine Surgery, Department of Surgery, Graduate School of Medicine, The University of Tokyo, Bunkyo-ku, Tokyo 113-8655, Japan. kamori-dis@umin.ac.jp.

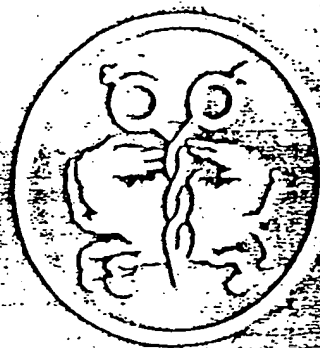
Human telomerase reverse transcriptase (hTERT), the catalytic subunit of telomerase, is very closely associated with telomerase activity. Telomerase has been implicated in cellular immortalization and carcinogenesis. In situ detection of hTERT will aid in determining the localization of telomerase-positive cells. The aim of this study was to detect expression of hTERT mRNA, hTERT protein, estrogen receptor (ER) and progesterone receptor (PR) in paraffin-embedded breast tissue samples and to investigate the relationship between hTERT expression and various clinicopathological parameters in breast tumorigenesis. We used in situ hybridization (ISH) to examine hTERT gene expression, and immunohistochemistry (IHC) to examine expression of hTERT protein, ER and PR, in breast tissues including 64 adenocarcinomas, 2 phyllode tumors and their adjacent normal breast tissues. hTERT gene expression was detected by ISH in 56 (88%) carcinomas, but in neither of the 2 phyllode tumors. hTERT protein expression was detected by IHC in 52 (81%) carcinomas, but in neither of the 2 phyllode tumors. Moreover, ER and PR were expressed in 42 (66%) and 42 (66%) carcinomas, respectively, and in neither of the 2 phyllode tumors. In 4 cases of breast carcinoma that strongly expressed hTERT gene and protein before treatment, neo-adjuvant chemotherapy led to disappearance of gene and protein expression in all cases. There was a strong correlation between detection of hTERT gene expression by ISH and of hTERT protein by ICH in tissue specimens from breast tumors. These results suggest that detection of hTERT protein by ICH can be used to distinguish breast cancers as a potential diagnostic and therapeutic marker.

PMID: 16211220 [PubMed - in process]

161
v. 27
no. 5
2005 Nov

Received on: 05-10-20
International journal of
oncology.

Journal of Oncology



ISSN 1079-6115

An international journal devoted to Oncology Research and Cancer Treatment

VOLUME 27, NUMBER 5, NOVEMBER 2005



Expression of human telomerase reverse transcriptase gene and protein, and of estrogen and progesterone receptors, in breast tumors: Preliminary data from neo-adjuvant chemotherapy

MAKOTO KAMMORI^{1,2}, NAOTAKA IZUMIYAMA², MASANORI HASHIMOTO¹, KEN-ICHI NAKAMURA²,
TADAO OKANO³, RIE KURABAYASHI¹, HIKI NAOKI¹, NAOKO HONMA², TOSHIHISA OGAWA¹,
MICHIO KAMINISHI¹ and KAIYO TAKUBO²

¹Division of Breast and Endocrine Surgery, Department of Surgery, Graduate School of Medicine,
The University of Tokyo; ²Human Tissue Research Group, Tokyo Metropolitan Institute of Gerontology;

³Tokyo Metropolitan Tama Cancer Detection Center, Tokyo, Japan

Received January 25, 2005; Accepted March 24, 2005

Abstract. Human telomerase reverse transcriptase (hTERT), the catalytic subunit of telomerase, is very closely associated with telomerase activity. Telomerase has been implicated in cellular immortalization and carcinogenesis. *In situ* detection of hTERT will aid in determining the localization of telomerase-positive cells. The aim of this study was to detect expression of hTERT mRNA, hTERT protein, estrogen receptor (ER) and progesterone receptor (PR) in paraffin-embedded breast tissue samples and to investigate the relationship between hTERT expression and various clinicopathological parameters in breast tumorigenesis. We used *in situ* hybridization (ISH) to examine hTERT gene expression, and immunohistochemistry (IHC) to examine expression of hTERT protein, ER and PR, in breast tissues including 64 adenocarcinomas, 2 phyllode tumors and their adjacent normal breast tissues. hTERT gene expression was detected by ISH in 56 (88%) carcinomas, but in neither of the 2 phyllode tumors. hTERT protein expression was detected by IHC in 52 (81%) carcinomas, but in neither of the 2 phyllode tumors. Moreover, ER and PR were expressed in 42 (66%) and 42 (66%) carcinomas, respectively, and in neither of the 2 phyllode tumors. In 4 cases of breast carcinoma that strongly expressed hTERT gene and protein before treatment, neo-adjuvant chemotherapy led to disappearance of gene and protein expression in all cases. There was a strong correlation between detection of hTERT gene expression by ISH and of hTERT protein by ICH in tissue specimens from breast tumors. These results suggest that detection of hTERT

protein by ICH can be used to distinguish breast cancers as a potential diagnostic and therapeutic marker.

Introduction

Breast cancer is the most frequent malignancy in women, affecting up to one in every eight females worldwide. The most important clinicopathological prognostic parameter so far identified is the absence or presence of lymph node metastasis, but the identification of further parameters for both lymph node-positive and -negative patients would facilitate an individually based risk-directed therapy (1). A promising emerging molecular marker is telomerase, a ribonucleoprotein enzyme complex, which when activated or upregulated allows tumor cells to escape from cellular senescence and to proliferate indefinitely (2). The human telomere is a simple repeat sequence of six bases (TTAGGG) that is located at the ends of each chromosome (3). Telomeres are believed to protect against degeneration, reconstruction, fusion, and loss (4) and to promote the homologous pairing of chromosomes (5). The end-to-end chromosome fusions observed in some tumors may result from the loss of telomeres and may be partly responsible for the genetic instability associated with tumorigenesis. Telomerase catalyzes the synthesis of telomere DNA and facilitates cell immortalization through the stabilization of chromosomal structure (6-8). Although the expression of the human RNA component of telomerase (hTERC) is widespread, the restricted expression pattern of the mRNA of hTERT, the human telomerase catalytic subunit gene, is correlated with telomerase activity (8-13). As telomerase activity seems to be the key player in tumor cell immortality, it has importance as a target molecule for anti-cancer therapy. Telomerase activity has been shown to correlate with poor clinical outcome in neuroblastomas and other tumors (14). For breast cancer, however, telomerase activity is a controversial prognostic marker: some studies suggest that telomerase activity, clinicopathological parameters and disease outcome are linked, whereas others do not find this association (14-23).

Correspondence to: Dr Makoto Kamitori, Division of Breast and Endocrine Surgery, Department of Surgery, Graduate School of Medicine, The University of Tokyo, 7-3-1 Hongo, Bunkyo-ku, Tokyo 113-8655, Japan
E-mail: kamitori-dis@umin.ac.jp

Key words: human telomerase reverse transcriptase, telomerase, estrogen receptor, breast cancer, chemotherapy

We have succeeded in very clearly and sensitively demonstrating hTERT mRNA in thyroid, colorectal, parathyroid and lung tissues by use of an oligonucleotide probe (13,24-26). Strong correlation has been observed between hTERT mRNA and/or protein expression and telomerase in a variety of malignant tumors (13,14,24,25,27,28). In the present study, we used ISH to examine expression of the hTERT gene, and IHC to examine expression of hTERT protein, ER and PR, in 64 carcinomas and 2 phyllodes tumors of breast to determine whether hTERT protein can be used to differentiate breast cancers. We also analyzed hTERT mRNA and protein expression with special reference to clinical features and histological findings to investigate the potential role of hTERT mRNA expression analysis in predicting the biological characteristics of breast cancers. Since hTERT expression in breast tumors has not previously been analysed by ISH or IHC, our investigation also examined various clinicopathological parameters, including age, histopathological type, tumor size, lymph node status, relapses, and the expression of ER and PR.

Materials and methods

Tissue collection. Sixty-six samples were obtained during 66 mastectomies: 64 breast carcinomas, 2 phyllodes tumors and 66 specimens of the adjacent normal breast gland. In 4 cases, samples were obtained during core needle biopsies (CNB) before neo-adjuvant therapy and again during mastectomies after neo-adjuvant therapy; for these cases, all measurements and examinations were performed both before and after the neo-adjuvant therapy. The patients ranged in age from 32 to 90 years. The patients with carcinomas ranged in age from 37 to 90, mean 56, years and were all women. The women with phyllode tumors were aged 32 and 38 years, respectively. The surgical and CNB tissue samples were frozen rapidly with liquid nitrogen and stored at -80°C until fixation. Then, they were fixed in 10% buffer formalin solution and embedded in paraffin. Surgical and CNB samples were collected from the patients after obtaining their informed consent, and the study protocol was approved by the Medical Department of the University of Tokyo Ethics Committee. The pathologic diagnoses were made by the surgical pathological specialists at our institute on the basis of examination of hematoxylin-eosin stained slides. A pathological review was performed for all breast tumors according to the BRE score. pT and pN staging were assigned according to the 1997 WHO classification (7th edition).

MCF-7 human breast cancer cells, kindly provided by the Cell Resource Center for Biomedical Research, Institute of Development, Aging and Cancer, Tohoku University, were used as positive controls. The cells were incubated in RPMI-1640 medium with 25 mM HEPES buffer, L-glutamine, and 10% fetal bovine serum (Gibco, Grand Island, NY) on a chamber-attached slideglass (Lab-Tek® Chamber Slide™; Nalge Nunc International, Naperville, IL) in a humidified 5% CO₂ atmosphere at 37°C. The cells were then fixed with 10% buffered neutral formalin (Sigma Chemical Co., St. Louis, MO). The cultured MCF-7 cell line that was used as a positive control was tested for telomerase with a PCR-based standard TRAP assay (6,13). These cells were also used to prepare cell blocks. Briefly, the cells were fixed in 10% buffered neutral

formalin, resuspended in molten agarose and then embedded in paraffin. Sections from these cell blocks were used as positive procedural controls in ISH and IHC. The negative control in ISH was obtained by replacing the oligonucleotide probe with RNase. The negative control in IHC was obtained by replacing the primary antibody with Tris-buffered saline (TBS).

Oligonucleotide probe for ISH. The specificity of the oligonucleotide sequence was initially determined by a GenEMBL database search using the Genetics Computer Group Sequence Analysis Program (GCG, Madison, WI) based on the fastA algorithm (29); the sequence exhibited 100% homology with the hTERT gene sequence. A d(T)₃₀ oligonucleotide was used to verify the integrity and lack of degradation of the mRNA in each sample. All oligonucleotide probes were synthesized with a hapten-labeled nucleotide, such as digoxigenin-dUTP (Boehringer-Mannheim), at the 3' end via direct coupling by using standard phosphoramidite chemistry (Research Genetics, Huntsville, AL) (30). The probe used for detection of hTERT by ISH was generated from the original sequence for *Homo sapiens* telomerase reverse transcriptase (AF015950); 2766-2800: 5'-GCCTCGTCTTCTACAGGGAAGTTCACCACTGTCTT-3' (13,24-26).

ISH. ISH was performed with the GenPoint nucleic acid hyper-detection system (Dako, Carpinteria, CA) (31). Formalin-fixed, paraffin-embedded tissue sections (5 µm thick) were deparaffinized in xylene and a graded alcohol series. Tissue sections and CNB samples were then pretreated with target retrieval solution (Dako, S1700) at 95°C and proteinase K (Dako, S3004) at room temperature. Next, the tissues and CNB samples were fixed in 0.3% hydrogen peroxide followed by a methyl alcohol series at room temperature. Digoxigenin-labeled anti-sense oligonucleotide in mRNA *in situ* hybridization solution (Dako, S3304) was placed over the tissues and CNB samples. After hybridization at 37°C overnight, the slides were washed in stringent wash solution (Dako, GenPoint System Kit) at 45°C. The tissues and CNB samples were exposed to avidin blocking solution (Dako, X0590) at room temperature followed by biotin blocking solution (Dako, X0590) at room temperature. The tissues and samples were then incubated at room temperature with a sheep monoclonal hapten-labeled anti-digoxigenin antibody (Dako, p5104), and the slides were then fixed with biotinyl tyramine (Dako, GenPoint System Kit) at room temperature. Finally, the slides were incubated with HRP-conjugated streptavidin (Dako, GenPoint System Kit) at room temperature. Since 3,3'-diaminobenzidine tetrahydrochloride (DAB) was used as the substrate, a positive reaction was visible as a brown color under a light microscope. The sections were weakly counter-stained with 0.1% hematoxylin.

IHC. IHC was performed by the avidin-biotin complex/horseradish peroxidase method. Tissue sections were stained for hTERT with a commercially available monoclonal antibody (NCL-L-hTERT; Novocastra, Newcastle upon Tyne, UK). Sections were dewaxed in xylene. Antigen retrieval was done by incubating sections immersed in 0.01 M citrate buffer at pH 6.0 in a microwave oven at 99°C. The sections were allowed to cool down at room temperature. The sections

MCF-7 Lysis Case 6 Case 14 Case 23 Case 44 Case 59

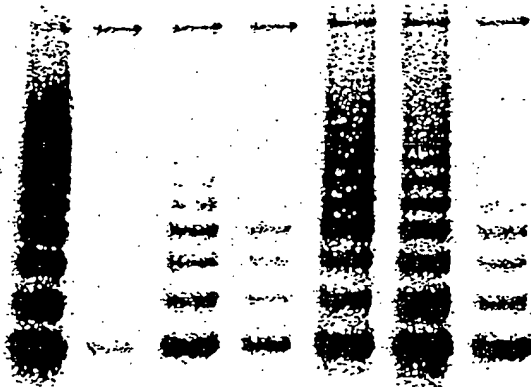


Figure 1. Representative results of the TRAP assay. If functional telomerase is present, the enzyme adds DNA to the substrate in 6-base-pair (bp) increments, resulting in a ladder-like distribution of products. The 6-bp ladder signals are apparent for MCF-7 and breast cancers (case nos. 6, 14, 23, 44 and 59) and are not apparent for lysis buffer as the negative control. An extract of MCF-7 was used as a positive control for the TRAP assay and as an Internal Telomerase Assay Standard (ITAS) positive control for PCR amplification, with lysis buffer as the negative control (Lysis).

were then immersed in 1% hydrogen peroxide (H_2O_2) in methanol to block endogenous peroxidase activity. Following that, the sections were washed in TBS (pH 7.6) before being incubated in normal rabbit serum for 20 min to block non-specific binding. After draining off the excess serum, the sections were incubated with the primary antibody at room temperature. The sections were washed in TBS before being incubated with the secondary antibody (biotinylated rabbit anti-mouse, Dako). The sections were washed again with TBS and incubated with avidin biotin complex/horseradish peroxidase. After washing the sections with TBS, peroxidase activity was visualized under light microscopy by applying DAB chromogen (Dako). The sections were counterstained with hematoxylin, dehydrated in increasing grades of alcohol and finally mounted in dibutyl phthalate (DPX) mountant.

Homogeneous staining or a speckled/dotted pattern in the nucleus was considered positive staining, and absence of distinct nuclear staining was taken as negative staining. Grading of the percentage of stained cells (hTERT labeling index) was performed by previously published criteria (1) as follows: Grade 1, negative staining; Grade 2, 1-10% positive staining nuclei; Grade 3, 11-50% positive nuclei; and Grade 4, >50% positive nuclei. Immunostained slides for ER and PR were scored as previously described (32,33). In brief, each entire slide was evaluated by light microscopy. First, a proportion score was assigned, which represents the estimated proportion of positive-staining tumor cells (0, none; 1, <1/100; 2, 1/100 to 1/10; 3, 1/10 to 1/3; 4, 1/3 to 2/3; and 5, >2/3). Next, an intensity score was assigned, which represents the average intensity of positive tumor cells (0, none; 1, weak; 2, intermediate; and 3, strong). The proportion and intensity scores were then added to obtain a total score, which ranged from 0 to 8. Slides were scored by pathologists who did not have knowledge of ligand-binding results or patient outcome.

Table 1. Relationships between mRNA status (negative/positive) by ISH and standard clinical, pathological, and biological factors in the 66 tumors.

	Total population (%)	No. of patients (%)		P-value ^a
		hTERT negative	hTERT positive	
Total	66	10 (15.2)	56 (84.8)	
Age				NS
≤50	26	6 (23.1)	20 (76.9)	
>50	40	6 (15.0)	34 (85.0)	
Histopathological type				NS
Scirrhous	32	2 (6.4)	30 (93.6)	
Papillonubular	20	2 (10.0)	18 (90.0)	
Solid tubular	6	1 (16.7)	5 (83.3)	
Mucinous	2	1 (50.0)	1 (50.0)	
Non-invasive	4	2 (50.0)	2 (50.0)	
Phyllodes	2	2 (100)	0 (0)	
Tumor size (cm) ^b				NS
T1 (<2.0)	20	0 (0)	20 (100)	
T2 (2.0-5.0)	34	6 (17.6)	28 (82.4)	
T3 (>5.0)	10	2 (20.0)	8 (80.0)	
Lymph node status ^b				NS
pN0	34	6 (17.6)	28 (82.4)	
pN1	26	2 (7.7)	24 (92.3)	
pN2+pNM	4	0 (0)	4 (100)	
Relapse				NS
+	10	0 (0)	10 (100)	
-	56	10 (17.6)	46 (82.4)	
ER expression				NS
+ (≥2)	42	6 (14.3)	36 (85.7)	
- (<2)	24	4 (16.7)	20 (83.3)	
PR expression				NS
+ (≥2)	42	4 (9.5)	38 (90.5)	
- (<2)	24	6 (25.0)	18 (75.0)	

^a χ^2 test. NS, not significant; ^bInformation available for 64 patients.

Statistical analysis. Differences in p-values were analyzed with the χ^2 test for independence, and Fisher's test was used for correlations. In all comparisons, $p < 0.05$ was considered significant.

Results

Representative results of the TRAP assay are shown in Fig. 1. The cultured cells, which were tested for telomerase activity

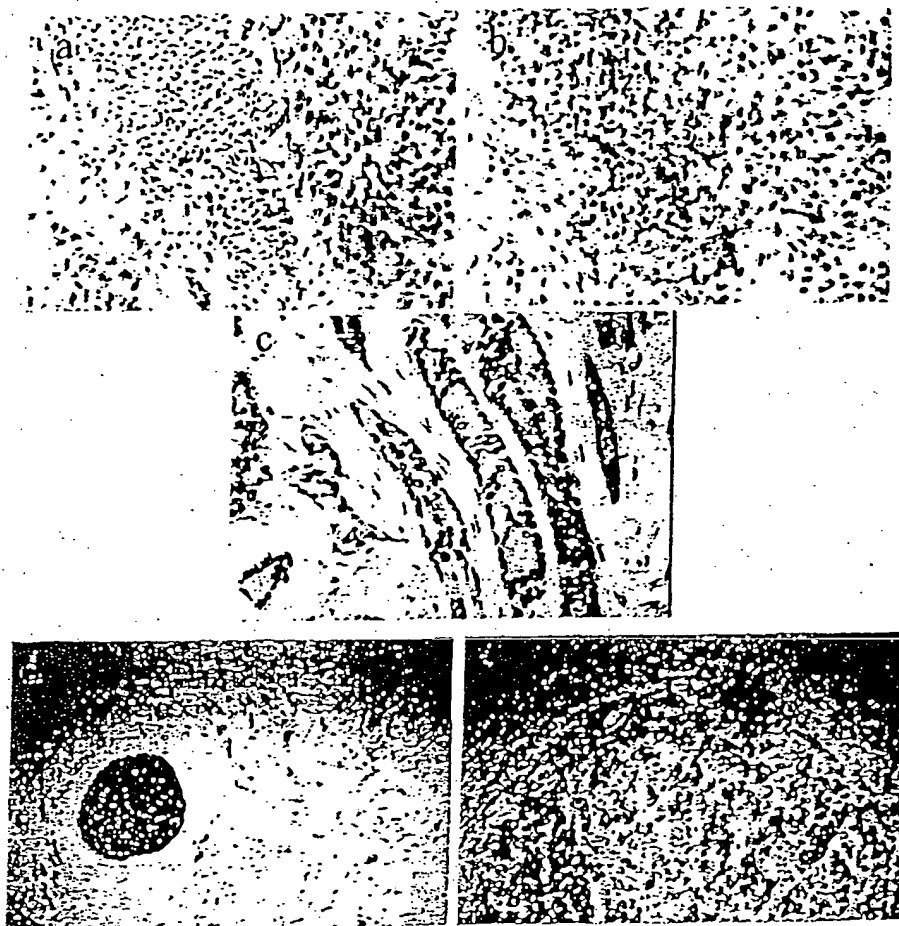


Figure 2. Correlation between histologic diagnosis, human telomerase reverse transcriptase (hTERT) mRNA by ISH, hTERT protein by IHC, estrogen receptor (ER) by IHC and progesterone receptor (PR) by IHC in breast cancers. (a, H&E); (b, hTERT mRNA); (c, hTERT protein); (d, ER) and (e, PR).

with the TRAP assay, gave positive results with all procedural controls (MCF-7 and 5 breast cancer samples) (Fig. 1).

ISH revealed that hTERT mRNA was strongly expressed in the nuclei and cytoplasm of almost all of the MCF-7 human cancer cells (data not shown). Expression of hTERT mRNA was detected in 56 (88%) of the 64 breast cancers and in none of the phyllodes tumors of the breast (Table I) with the anti-sense probe, whereas no expression was detected with the anti-sense probe treated with RNase (data not shown). The levels of expression were heterogeneous within the carcinomatous regions. Strong expression of hTERT mRNA was not confined to the carcinomatous regions but was also detected in infiltrating lymphocytes (Fig. 2a and b). Higher expression levels of both signals of hTERT mRNA were detected in some sections containing both carcinomas and lymphocytes, compared with the adjacent non-cancerous mammary gland, but no clear differences in signal intensity were observed between carcinomas and lymphocytes. The signals in both the normal and cancer tissues were mainly present in the lymphocytes, and the signal intensity was similar in both, although a precise quantitative comparison of the *in situ* signals was impossible.

IHC revealed that hTERT protein was strongly expressed in the nuclei, nuclear membrane and cytoplasm of almost all of the MCF-7 human cancer cells (data not shown). Expression of hTERT protein was detected in 52 (81%) of the 64 breast cancers and in none of the phyllode tumors of the breast (Table II). The levels of expression were heterogeneous within the carcinomatous regions. As shown in Fig. 2c, strong expression of hTERT protein was observed in nuclei, nuclear membrane and cytoplasm, similar to the pattern in MCF-7 human cancer cells. Normal mammary gland and stromal cells generally showed negative immunoreactivity against hTERT protein antibody.

A nuclear signal for the ER (Fig. 2d), as assessed by IHC, was observed in 36 (56%) of the 64 breast cancers and in none of the phyllode tumors of the breast, with positive scores ranging from 2 to 8 (Tables I and II). A nuclear signal for the PR (Fig. 2e), as assessed by IHC, was observed in 38 (59%) of the 64 breast cancers and in none of the phyllode tumors of the breast, with positive scores ranging from 2 to 8 (Tables I and II).

We used ISH and IHC to examine hTERT expression in 4 cases of breast cancer before and after neo-adjuvant

Table II. Relationships between mRNA status (negative/positive) by IHC and standard clinical, pathological, and biological factors in the 66 tumors.

	Total	No. of patients (%)		P-value ^a
		hTERT negative	hTERT positive	
Total	66	14 (21.2)	52 (78.8)	
Age				NS
≤50	26	10 (38.5)	16 (61.5)	
>50	40	4 (10.0)	36 (90.0)	
Histopathological type				NS
Scirrhous	32	2 (6.4)	30 (93.6)	
Papillotubular	20	4 (20.0)	16 (80.0)	
Solid tubular	6	4 (66.7)	2 (33.3)	
Mucinous	2	0 (0)	2 (100)	
Non-invasive	4	2 (50.0)	2 (50.0)	
Phyllodes	2	2 (100)	0 (0)	
Tumor size (cm) ^b				NS
T1 (<2.0)	20	4 (20.0)	16 (80.0)	
T2 (2.0-5.0)	34	6 (17.6)	28 (82.4)	
T3 (>5.0)	10	2 (20.0)	8 (80.0)	
Lymph node status ^b				NS
pN0	34	6 (17.6)	28 (82.4)	
pN1	26	6 (23.1)	20 (76.9)	
pN2+pNM	4	0 (0)	4 (100)	
Relapse				NS
+	10	1 (10.0)	9 (90.0)	
-	56	13 (23.2)	43 (79.6)	
ER expression				NS
+ (≥2)	42	6 (14.3)	36 (85.7)	
- (<2)	24	8 (33.3)	16 (66.7)	
PR expression				NS
+ (≥2)	42	6 (14.3)	36 (85.7)	
- (<2)	24	8 (33.3)	16 (66.7)	

^aχ² test. NS, not significant. ^bInformation available for 64 patients.

chemotherapy. Before chemotherapy, all 4 of the breast carcinomas strongly expressed hTERT by both ISH and IHC. After chemotherapy, hTERT expression completely disappeared in all 4 cases (Table III). hTERT expression by lymphocytes was detectable by ISH and IHC both before and after chemotherapy in all 4 cases, and the level of expression did not appear to be altered by treatment.

No correlation was observed between hTERT mRNA expression and any of the clinicopathological parameters age, histopathological type, tumor size, lymph node status,

Table III. Relationship of hTERT mRNA and protein expression before and after neoadjuvant chemotherapy.

Case	Age	Neoadjuvant	hTERT mRNA		hTERT protein	
			Before	After	Before	After
1	80	Anastrozole	+	-	+	-
2	78	Anastrozole	+	-	+	-
3	35	FEC ^a	+	-	+	-
4	37	AC ^b	+	-	+	-

^aFEC, 5FU (500 mg/m²), Epirubicin (70 mg/m²), Cyclophosphamide (500 mg/m²). ^bAC, Doxorubicin (60 mg/m²), Cyclophosphamide (500 mg/m²). Before, before neoadjuvant chemotherapy. After, after neoadjuvant chemotherapy. +, positive; -, negative.

relapses, and the expression of ER and PR. Similarly, there was no correlation between hTERT protein expression and any of these clinicopathological parameters. There was a correlation between hTERT mRNA expression and hTERT protein expression in breast cancers ($p < 0.005$).

Discussion

This study reports a comparison of hTERT mRNA expression by ISH and hTERT protein expression by IHC in tissue sections from breast tumors. hTERT mRNA was detected by ISH in 56 of the 64 breast cancers and in MCF-7 human breast cancer cells. Breast cancer cell nuclei stained strongly positive with the specific anti-sense probe but not with the anti-sense probe treated with RNase (data not shown). Tissue lymphocytes also stained positively with the anti-sense probe, but the stromal cells did not. Expression of hTERT protein was observed by IHC in 52 of the 64 breast cancers. hTERT mRNA and protein expressions were highly correlated in breast cancers ($p < 0.005$). Detection of the hTERT protein by IHC has permitted further analysis of carcinogenesis and cancer diagnosis (34).

In recent years, there has been disagreement over the suitability of telomerase activity as a prognostic biologic marker in breast cancer that may help to differentiate patients for individually based risk-related therapy. Hiyama *et al* (15), in a study of 140 breast cancer specimens with the TRAP assay, found a strong association between telomerase activity and stage classification and observed telomerase activity in 68% of stage I tumors and 95% of stage IV tumors. Poremba *et al* (1), using tissue microarrays, found a statistically significant correlation between tumor-specific survival (overall survival) and hTERT expression in breast cancer. However, some problems in interpretation may affect this apparent consensus. First, some samples of breast cancer tissue may be extensively contaminated by infiltrating lymphocytes during operative manipulations, especially in advanced disease, causing overestimation of telomerase activity and/or hTERT expression. In our previous reports, higher expression levels

of signals for both hTERT mRNA and protein were detected in some sections containing both carcinoma and lymphocytes in thyroid and colorectal cancers (13,24). Secondly, Poremba *et al* (1) used polyclonal antibodies against hTERT protein as a signal for expression. In our hands, polyclonal antibodies against hTERT protein give rise to strong background signals and are not clearly specific for measuring expression in cancer tissues. We have carefully compared the reactivity against hTERT protein of the monoclonal antibody used in the present study with that of some polyclonal antibodies. Use of the monoclonal antibody in IHC allowed clear demonstration of hTERT protein expression, with results similar to those of ISH for hTERT mRNA expression. Furthermore, IHC is technically much easier to perform than ISH, since contamination of samples by RNase is not an issue in IHC.

To the best of our knowledge, this report is the first on the study of hTERT expression in breast cancer as a function of neo-adjuvant treatment. We examined hTERT expression in 4 cases of breast cancer before and after chemotherapy. Before chemotherapy, hTERT was strongly expressed in all 4 carcinomas, but after chemotherapy hTERT expression had completely disappeared in all 4 cases. hTERT expression by lymphocytes was detectable by ISH and IHC both before and after chemotherapy in all 4 cases, and the level of expression did not appear to be altered by treatment.

In conclusion, determination of hTERT mRNA expression by ISH and hTERT protein expression by IHC can be used to obtain information contributing to a histopathological diagnosis during screening of breast cancers. By use of a monoclonal antibody, we could very clearly and sensitively demonstrate hTERT protein expression in breast cancer tissues but not in non-cancerous tissues. We also demonstrated that 4 carcinomas with originally positive immunoreactivity against hTERT protein became negative after neo-adjuvant chemotherapy. These results suggest that determination of hTERT protein by IHC can be used as a potential diagnostic and therapeutic marker to distinguish breast cancers.

Acknowledgments

We thank Ms. Sachiko Nishimura for her expert technical assistance.

References

- Poremba C, Heine B, Diallo R, Heinecke A, Wai D, Schaefer KL, Braun Y, Schuck A, Lanvers C, Bankfalvi A, Kneif S, Thorhorst J, Zuber M, Kochli OR, Mross F, Dieterich H, Sauter G, Stein H, Fogt F and Boecker W: Telomerase as a prognostic marker in breast cancer: high-throughput tissue microarray analysis of hTERT and hTR. *J Pathol* 198: 181-189, 2002.
- Healy KC: Telomere dynamics and telomerase activation in tumor progression: prospects for prognosis and therapy. *Oncol Res* 7: 121-130, 1995.
- Shampay J and Blackburn EH: Tetrahymena micronuclear sequences that function as telomeres in yeast. *Nucleic Acids Res* 17: 3247-3260, 1989.
- Levy MZ, Allsopp RC, Fuhrer AB, Greider CW and Harley CB: Telomere end-replication problem and cell aging. *J Mol Biol* 225: 951-960, 1992.
- Moyzis RK, Buckingham JM, Cram LS, Dani M, Deaven LL, Jones MD, Meyne J, Ratliff RL and Wu JR: A highly conserved repetitive DNA sequence, (TTAGGG)_n, present at the telomeres of human chromosomes. *Proc Natl Acad Sci USA* 85: 6622-6626, 1988.
- Kim NW, Piatyszek MA, Prowse KR, Harley CB, West MD, Ho PL, Coviello GM, Wright WE, Weinrich SL and Shay JW: Specific association of human telomerase activity with immortal cells and cancer. *Science* 266: 2011-2015, 1994.
- Blackburn EH: Telomerase. *Annu Rev Biochem* 61: 113-129, 1992.
- Shay JW and Bacchetti S: A survey of telomerase activity in human cancer. *Eur J Cancer* 33: 787-791, 1997.
- Meyerson M, Counter CM, Eaton EN, Ellison LW, Steiner P, Caddle SD, Ziaugra L, Beijersbergen RL, Davidoff MJ, Liu Q, Bacchetti S, Haber DA and Weinberg RA: hEST2, the putative human telomerase catalytic subunit gene, is up-regulated in tumor cells and during immortalization. *Cell* 90: 785-795, 1997.
- Nakamura TM, Morin GB, Chapman KB, Weinrich SL, Andrews WH, Lingner J, Harley CB and Cech TR: Telomerase catalytic subunit homologs from fission yeast and human. *Science* 277: 955-959, 1997.
- Kilian A, Bowtell DD, Abud HE, Hime GR, Venter DJ, Keese PK, Duncan EL, Reddel RR and Jefferson RA: Isolation of a candidate human telomerase catalytic subunit gene, which reveals complex splicing patterns in different cell types. *Hum Mol Genet* 6: 2011-2019, 1997.
- Kamori M, Nakamura KI, Kanauchi H, Obara T, Kawahara M, Mimura Y, Kaminishi M and Takubo K: Consistent decrease in telomere length in parathyroid tumors but alteration in telomerase activity limited to malignancies: a preliminary report. *World J Surg* 26: 1083-1087, 2002.
- Kamori M, Nakamura K, Hashimoto M, Ogawa T, Kaminishi M and Takubo K: Clinical application of human telomerase reverse transcriptase gene expression in thyroid follicular tumors by fine-needle aspirations using *in situ* hybridization. *Int J Oncol* 22: 985-991, 2003.
- Poremba C, Scheel C, Hero B, Christiansen H, Schaefer KL, Nakayama J, Berthold F, Juergens H, Boecker W and Dockhorn-Dworniczak B: Telomerase activity and telomerase subunits gene expression patterns in neuroblastoma: a molecular and immunohistochemical study establishing prognostic tools for fresh-frozen and paraffin-embedded tissues. *J Clin Oncol* 18: 2582-2592, 2000.
- Hiyama E, Gollahon L, Kataoka T, Kuroi K, Yokoyama T, Gazdar AF, Hiyama K, Piatyszek MA and Shay JW: Telomerase activity in human breast tumors. *J Natl Cancer Inst* 88: 116-122, 1996.
- Sugino T, Yoshida K, Bolodczuk J, Tahara H, Buley J, Manek S, Wells C, Goodison S, Ide T, Suzuki T, Tahara E and Tarin D: Telomerase activity in human breast cancer and benign breast lesions: diagnostic applications in clinical specimens, including fine needle aspirates. *Int J Cancer* 69: 301-306, 1996.
- Nawaz S, Hashizumi TL, Markham NE, Shroyer AL and Shroyer KR: Telomerase expression in human breast cancer with and without lymph node metastases. *Am J Clin Pathol* 107: 542-547, 1997.
- Clark GM, Osborne CK, Levitt D, Wu F and Kim NW: Telomerase activity and survival of patients with node-positive breast cancer. *J Natl Cancer Inst* 89: 1874-1881, 1997.
- Poremba C, Boecker W, Willenbring H, Schaefer KL, Otterbach F, Burger H, Diallo R and Dockhorn-Dworniczak B: Telomerase activity in human proliferative breast lesions. *Int J Oncol* 12: 641-648, 1998.
- Hoos A, Hepp HH, Kaul S, Ahlert T, Basten G and Wallwiener D: Telomerase activity correlates with tumor aggressiveness and reflects therapy effect in breast cancer. *Int J Cancer* 79: 8-12, 1998.
- Roos G, Nilsson P, Cajander S, Nielsen NH, Arnerlov C and Landberg G: Telomerase activity in relation to p53 status and clinico-pathological parameters in breast cancer. *Int J Cancer* 79: 343-348, 1998.
- Mokbel K, Parris CN, Ghilchik M, Williams G and Newbold RF: The association between telomerase, histopathological parameters, and Ki-67 expression in breast cancer. *Am J Surg* 178: 69-72, 1999.
- Umbricht CB, Sherman ME, Dome J, Carey LA, Marks J, Kim N and Sukumar S: Telomerase activity in ductal carcinoma *in situ* and invasive breast cancer. *Oncogene* 18: 3407-3414, 1999.
- Kamori M, Kanauchi H, Nakamura KI, Kawahara M, Weber TK, Mafune KI, Kaminishi M and Takubo K: Demonstration of human telomerase reverse transcriptase (hTERT) in human colorectal carcinomas by *in situ* hybridization. *Int J Oncol* 20: 15-21, 2002.

25. Kammori M, Nakamura KI, Ogawa T, Mafune KI, Tatutomi Y, Obara T, Onoda N, Fujiwara M, Izumiyama-Shimomura N, Mori M, Kaminishi M and Takubo K: Demonstration of human telomerase reverse transcriptase (hTERT) in human parathyroid tumors by *in situ* hybridization with a new oligonucleotide probe. *Clin Endocrinol* 58: 43-48, 2003.
26. Fukushima M, Shimomura N, Nakamura KI, Kammori M, Koizumi K, Shimizu K and Takubo K: Demonstration of human telomerase reverse transcriptase by *in situ* hybridization in lung carcinoma. *Oncol Rep* 12: 1227-1232, 2004.
27. Frost M, Bobak JB, Gianani R, Kim N, Weinrich S, Spalding DC, Cass LG, Thompson LC, Enomoto T, Uribe-Lopez D and Shroyer KR: Localization of telomerase hTERT protein and hTR in benign mucosa, dysplasia, and squamous cell carcinoma of the cervix. *Am J Clin Pathol* 114: 726-734, 2000.
28. Kawakami Y, Kitamoto M, Nakanishi T, Yasui W, Tahara E, Nakayama J, Ishikawa F, Tahara H, Ide T and Kajiyama G: Immuno-histochemical detection of human telomerase reverse transcriptase in human liver tissues. *Oncogene* 19: 3888-3893, 2000.
29. Pearson WR and Lipman DJ: Improved tools for biological sequence comparison. *Proc Natl Acad Sci USA* 85: 2444-2448, 1988.
30. Caruthers MH, Beaucage SL, Efcavitch JW, Fisher EF, Goldman RA, De Haseth PL, Mandeck W, Matteucci MD, Rosendahl MS and Stabinsky Y: Chemical synthesis and biological studies on mutated gene-control regions. *Cold Spring Harbor Symp Quant Biol* 47: 411-418, 1982.
31. Tani Y: PCR *In situ* amplification and catalyzed signal amplification: approaches of higher sensitive, non-radioactive *in situ* hybridization. *Acta Histochem Cytochem* 32: 261-270, 1999.
32. Harvey JM, Clark GM, Osborne CK and Allred DC: Estrogen receptor status by immunohistochemistry is superior to the ligand-binding assay for predicting response to adjuvant endocrine therapy in breast cancer. *J Clin Oncol* 17: 1474-1481, 1999.
33. Allred DC, Harvey JM, Berardo M and Clark GM: Prognostic and predictive factors in breast cancer by immunohistochemical analysis. *Mod Pathol* 11: 155-168, 1998.
34. Tahara H, Yasui W, Tahara E, Fujimoto J, Ito K, Tamai K, Nakayama J, Ishikawa F, Tahara E and Ide T: Immunohistochemical detection of human telomerase catalytic component, hTERT, in human colorectal tumor and non-tumor tissue sections. *Oncogene* 18: 1561-1567, 1999.



Expression of the ubiquitin-proteasome pathway and muscle loss in experimental cancer cachexia.

Khal J, Wyke SM, Russell ST, Hine AV, Tisdale MJ.

Pharmaceutical Sciences Research Institute, Aston University, Birmingham, UK.

Muscle protein degradation is thought to play a major role in muscle atrophy in cancer cachexia. To investigate the importance of the ubiquitin-proteasome pathway, which has been suggested to be the main degradative pathway mediating progressive protein loss in cachexia, the expression of mRNA for proteasome subunits C2 and C5 as well as the ubiquitin-conjugating enzyme, E2(14k), has been determined in gastrocnemius and pectoral muscles of mice bearing the MAC16 adenocarcinoma, using competitive quantitative reverse transcriptase polymerase chain reaction. Protein levels of proteasome subunits and E2(14k) were determined by immunoblotting, to ensure changes in mRNA were reflected in changes in protein expression. Muscle weights correlated linearly with weight loss during the course of the study. There was a good correlation between expression of C2 and E2(14k) mRNA and protein levels in gastrocnemius muscle with increases of 6-8-fold for C2 and two-fold for E2(14k) between 12 and 20% weight loss, followed by a decrease in expression at weight losses of 25-27%, although loss of muscle protein continued. In contrast, expression of C5 mRNA only increased two-fold and was elevated similarly at all weight losses between 7.5 and 27%. Both proteasome functional activity, and proteasome-specific tyrosine release as a measure of total protein degradation was also maximal at 18-20% weight loss and decreased at higher weight loss. Proteasome expression in pectoral muscle followed a different pattern with increases in C2 and C5 and E2(14k) mRNA only being seen at weight losses above 17%, although muscle loss increased progressively with increasing weight loss. These results suggest that activation of the ubiquitin-proteasome pathway plays a major role in protein loss in gastrocnemius muscle, up to 20% weight loss, but that other factors such as depression in protein synthesis may play a more important role at higher weight loss.

PMID: 16160695 [PubMed - in process]



Cell type-specific occurrence of caveolin-1alpha and -1beta in the lung caused by expression of distinct mRNAs.

Kogo H, Aiba T, Fujimoto T.

Department of Anatomy and Molecular Cell Biology, Nagoya University Graduate School of Medicine, Showa-ku, Nagoya 466-8550, Japan. hkogo@fujita-hu.ac.jp

Two isoforms of caveolin-1, alpha and beta, had been thought to be generated by alternative translation initiation of an mRNA (FL mRNA), but we showed previously that a variant mRNA (5'V mRNA) encodes the beta isoform specifically. In the present study, we demonstrated strong correlation between the expression of the caveolin-1 protein isoforms and mRNA variants in culture cells and the developing mouse lung. The alpha isoform protein and FL mRNA were expressed constantly during the lung development, whereas expression of the beta isoform protein and 5'V mRNA was negligible in the fetal lung before 17.5 days post coitum, and markedly increased simultaneously at 18.5 days post coitum, when the alveolar type I cells started to differentiate. Immunohistochemical analysis revealed the cell type-specific expression of the two isoforms; the alveolar type I cell expresses the beta isoform predominantly, while the endothelium harbors the alpha isoform chiefly. The mutually exclusive expression of caveolin-1 isoforms was verified by Western blotting of the selective plasma membrane preparation obtained from the endothelial and alveolar epithelial cells. The present result indicates that the two caveolin-1 isoforms are generated from distinct mRNAs in vivo and that their production is regulated independently at the transcriptional level. The result also suggests that the alpha and beta isoforms of caveolin-1 may have unique physiological functions.

PMID: 15067006 [PubMed - indexed for MEDLINE]

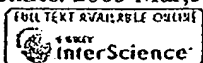
Oncogene and growth factor expression in ovarian cancer.

Konmoss F, Bauknecht T, Birmelin G, Kohler M, Tesch H, Pfeiderer A.

Department of Gynaecology, Albert-Ludwig University, Freiburg, Germany.

The varying tumor-biological behavior of ovarian carcinomas probably influences both their operability and response to chemotherapy, which are the most relevant prognostic factors. The phenotype of different ovarian carcinomas is obviously associated with an activation of the EGF/TGF-alpha signal pathway, including c-myc and c-jun expression. Analysis of EGF-R, TGF-alpha, c-myc and c-jun expression in 33 stage III/IV, and 2 stage I/II ovarian carcinomas with biochemical, molecular-chemical and immunohistochemical methods showed a correlation between the mRNA and protein levels of EGF-R and TGF-alpha for tumors with low or high expressing rates. However, the concentration of measurable free EGF-Rs seems to depend on the amount of TGF-alpha expression by the tumors. The EGF-R binding ligand TGF-alpha is produced by epithelial tumor cells; stromal cells are usually TGF-alpha-negative, as shown by immunohistochemistry. High expression rates of EGF-R, TGF-alpha and c-myc were detected in 6, 7, and 10 out of 35 ovarian carcinomas, respectively. C-jun mRNA was detected in 18/19 cases studied. Non-malignant tissues originating from myometrium or ovary expressed no (or only small amounts of) EGF-R or TGF-alpha mRNA, whereas a high c-myc expression was found in 1/7 normal myometria, and in 2/5 normal ovaries. There was no strong correlation between EGF-R/TGF-alpha and c-myc/c-jun expression.(ABSTRACT TRUNCATED AT 250 WORDS)

PMID: 1502888 [PubMed - indexed for MEDLINE]



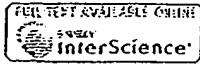
A transcriptomic and proteomic analysis of the effect of CpG-ODN on human THP-1 monocytic leukemia cells.

Kuo CC, Kuo CW, Liang CM, Liang SM.

Institute of BioAgricultural Sciences, Academia Sinica, Taipei, Taiwan.

The CpG motif of bacterial DNA (CpG-DNA) is a potent immunostimulating agent whose mechanism of action is not yet clear. Here, we used both DNA microarray and proteomic approaches to investigate the effects of oligodeoxynucleotides containing the CpG motif (CpG-ODN) on gene transcription and protein expression profiles of CpG-ODN responsive THP-1 cells. Microarray analysis revealed that 2 h stimulation with CpG-ODN up-regulated 50 genes and down-regulated five genes. These genes were identified as being associated with inflammation, antimicrobial defense, transcriptional regulation, signal transduction, tumor progression, cell differentiation, proteolysis and metabolism. Longer stimulation (8 h) with CpG-ODN enhanced transcriptional expression of 58 genes. Among these 58 genes, none except one, namely WNT1 inducible signaling pathway protein 2, was the same as those induced after 2 h stimulation. Proteomic analysis by two-dimensional gel electrophoresis, followed by mass spectrometry identified several proteins up-regulated by CpG-ODN. These proteins included heat shock proteins, modulators of inflammation, metabolic proteins and energy pathway proteins. Comparison of microarray and proteomic expression profiles showed poor correlation. Use of more reliable and sensitive analyses, such as reverse transcriptase polymerase chain reaction, Western blotting and functional assays, on several genes and proteins, nonetheless, confirmed that there is indeed good correlation between mRNA and protein expression after CpG-ODN treatment. This study also revealed that several anti-apoptotic and neuroprotective related proteins, not previously reported, are activated by CpG-DNA. These findings have extended our knowledge on the activation of cells by CpG-DNA and may contribute to further understanding of mechanisms that link innate immunity with acquired immune response(s).

PMID: 15693060 [PubMed - indexed for MEDLINE]



Quantification of CK20 gene and protein expression in colorectal cancer by RT-PCR and immunohistochemistry reveals inter- and intratumour heterogeneity.

Lassmann S, Bauer M, Soong R, Schreglmann J, Tabiti K, Nahrig J, Ruger R, Hofer H, Werner M.

Pathologisches Institut, Universitätsklinikum Freiburg, Albertstrasse 19, 79104 Freiburg, Germany. lassmann@ukl.uni-freiburg.de

Cytokeratin 20 (CK20) is an epithelial protein expressed almost exclusively in the gastrointestinal (GI) tract and is widely used as immunohistochemical marker for routine diagnosis. In contrast, CK20 gene expression is not an established marker for the classification of tumours and the detection of disseminated cancer cells in colorectal cancer. Recently, real-time reverse transcriptase polymerase chain reaction (RT-PCR) has provided the means for reproducible and quantitative investigation of molecular markers. This report directly compares CK20 mRNA and protein expression in serial sections of archival, formalin-fixed, paraffin-embedded (FFPE) colorectal adenocarcinomas. CK20 expression was detected by immunohistochemistry (IHC) in 60/63 (95.2%) cases, by conventional RT-PCR in 58/60 (96.7%) and by quantitative RT-PCR using the LightCycler (LightCycler is a trademark of a Member of the Roche Group) System in 29/32 (90.6%) microdissected cases, one case yielding variable results. Despite the high detection rate of all three techniques, marked heterogeneity of CK20 expression was seen between different cases and also within individual cases. CK20 expression profiles were not related to particular histopathological features of the tumours. A good correlation ($r = 0.8964$) was found between CK20 mRNA and protein expression by comparing quantitative RT-PCR with IHC in 32 cases. This was also true for selected heterogeneous tumour cells within individual cases. Both RT-PCR and IHC are therefore valuable tools for CK20 detection in colorectal adenocarcinoma, with real-time RT-PCR providing supplementary quantitative information. This suggests a promising supportive role for quantitative RT-PCR in molecular pathology. Copyright 2002 John Wiley & Sons, Ltd.

Publication Types:

- Evaluation Studies

PMID: 12237879 [PubMed - indexed for MEDLINE]



Enhanced expressions of arachidonic acid-sensitive tandem-pore domain potassium channels in rat experimental acute cerebral ischemia.

Li ZB, Zhang HX, Li LL, Wang XL.

Institute of Materia Medica, Chinese Academy of Medical Sciences and Peking Union Medical College, Beijing 100050, China.

To further explore the pathophysiological significance of arachidonic acid-sensitive potassium channels, RT-PCR and Western blot analysis were used to investigate the expression changes of TREK channels in cortex and hippocampus in rat experimental acute cerebral ischemia in this study. Results showed that TREK-1 and TRAAK mRNA in cortex, TREK-1 and TREK-2 mRNA in hippocampus showed significant increases 2 h after middle cerebral artery occlusion (MCAO). While the mRNA expression levels of the all three channel subtypes increased significantly 24 h after MCAO in cortex and hippocampus. At the same time, the protein expressions of all the three channel proteins showed significant increase 24 h after MCAO in cortex and hippocampus, but only TREK-1 showed increased expression 2 h after MCAO in cortex and hippocampus. Immunohistochemical experiments verified that all the three channel proteins had higher expression levels in cortical and hippocampal neurons 24 h after MCAO. These results suggested a strong correlation between TREK channels and acute cerebral ischemia. TREK channels might provide a neuroprotective mechanism in the pathological process.

PMID: 15652517 [PubMed - indexed for MEDLINE]



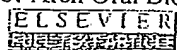
Retinal preconditioning and the induction of heat-shock protein 27.

Li Y, Roth S, Laser M, Ma JX, Crosson CE.

Department of Ophthalmology, Medical University of South Carolina, Charleston, South Carolina 29425, USA.

PURPOSE: Brief periods of ischemia have been shown to protect the retina from potentially damaging periods of ischemia. This phenomenon has been termed ischemic preconditioning or ischemic tolerance. In the present study the cellular changes in levels of heat shock protein (Hsp)27, -70, and -90 mRNA and expression of Hsp in the rat retina associated with ischemic preconditioning were evaluated. **METHODS:** Unilateral retinal ischemia was created in Long-Evans and Sprague-Dawley rats for 5 minutes. Rats were then left for 1 hour to 7 days, to allow the retina to reperfuse. Retinas were dissected, the mRNA and protein isolated, and Northern and Western blot analyses conducted to detect changes in expression of Hsp27, -70, and -90. Immunohistochemical studies were used to identify retinal regions where Hsp changes occurred. Selected animals were subjected to a second ischemic event, 60 minutes in duration, to correlate the changes in expression of Hsp with functional protection of the retina from ischemic injury. **RESULTS:** In control and sham-treated animals retinal Hsp27, -70, and -90 mRNAs were detectable. Five hours after retinal preconditioning, levels of Hsp27 mRNA were elevated above control levels, and 24 hours later, mRNA levels increased 200% over basal levels. Hsp27 expression remained elevated for up to 72 hours and then began to return to control levels. Hsp27 protein levels were increased by 200% over basal levels 24 hours after retinal preconditioning, remained at this level for 72 hours, and then returned to control levels. In contrast, no consistent change in Hsp70 or -90 mRNA or protein levels was observed during the course of the study. Immunohistochemical studies demonstrated that the increase in expression of Hsp27 was localized to neuronal and non-neuronal cells in the inner layers of the retina. Electroretinography studies demonstrated a strong correlation between the protection of retinal function from ischemic injury and the expression of Hsp27. **CONCLUSIONS:** These results provide evidence that the induction of Hsp27 is a gene-specific event associated with ischemic preconditioning in the retina. This increase in expression of Hsp27 occurs in both neuronal and non-neuronal retinal cells, and appears to be one component of the neuroprotective events induced by ischemic preconditioning in the retina.

PMID: 12601062 [PubMed - indexed for MEDLINE]



Increasing expression of tissue plasminogen activator and plasminogen activator inhibitor type 2 in dog gingival tissues with progressive inflammation.

Lindberg P, Kinnby B, Lecander I, Lang NP, Matsson L.

Center for Oral Health Sciences, Malmo University, S-214 21 Malmo, Sweden.
pia.lindberg@od.mah.se

Urokinase and tissue-type plasminogen activators (u-PA and t-PA) are serine proteases that convert plasminogen into plasmin, which degrades matrix proteins and activates metalloproteinases. The PAs are balanced by specific inhibitors (PAI-1 and PAI-2). Local production of t-PA and PAI-2 was recently demonstrated in human gingival tissues. The aim now was to investigate the production and localization of t-PA and PAI-2 in gingival tissues from dogs in three well-defined periodontal conditions; clinically healthy gingiva, chronic gingivitis and an initial stage of ligature-induced loss of attachment. At the start of the experiment the gingiva showed clear signs of inflammation. Clinically healthy gingiva were obtained after 21 days period of intense oral hygiene. Attachment loss was induced by placing rubber ligatures around the neck of some teeth. Biopsies were taken from areas representing the different conditions and prepared for in situ hybridization and immunohistochemistry. In clinically healthy gingiva both t-PA mRNA and antigen were expressed in a thin outer layer of the sulcular and junctional epithelia. No t-PA signals or staining were seen in connective tissue. Both mRNA signaling and immunostaining for t-PA were stronger in chronic gingivitis. In areas with loss of attachment, t-PA mRNA as well as antigen were found in the sulcular and junctional epithelia to a similar degree as in gingivitis. Occasionally the connective tissue was involved, especially in connection with vessels. PAI-2 mRNA was seen in a thin outer layer of the sulcular and junctional epithelia in clinically healthy gingiva, but no signals were seen in connective tissue. PAI-2 antigen was found primarily in the outer layer of the sulcular and junctional epithelia. Some cells in the connective tissue were stained. In gingivitis, PAI-2 signals were mainly found in the same locations, but more intense and extending towards the connective tissue. Immunostaining was seen in the outer half of the sulcular and junctional epithelia as well as in the upper part of the connective tissue, close to the sulcular epithelium. In sites with loss of attachment, PAI-2 mRNA was found throughout the sulcular and junctional epithelia, as was the antigen, which stained intensely. No PAI-2 mRNA was seen in connective tissue; the antigen was found scattered, especially near vessels. This study shows that the expression of both t-PA and PAI-2 increases with experimental gingival inflammation in the dog, and furthermore, the two techniques demonstrate a strong correlation between the topographical distribution of the site of protein synthesis and the tissue location of the antigens for both t-PA and PAI-2. The distribution correlates well with previous findings in humans.

Effect of duration of fixation on quantitative reverse transcription polymerase chain reaction analyses.

Macabeo-Ong M, Ginzinger DG, Dekker N, McMillan A, Regezi JA, Wong DT, Jordan RC.

Oral Pathology, Department of Stomatology, University of California San Francisco, California 94143-0424, USA.

Increasingly, there is the need to analyze gene expression in tumor tissues and correlate these findings with clinical outcome. Because there are few tissue banks containing enough frozen material suitable for large-scale genetic analyses, methods to isolate and quantify messenger RNA (mRNA) from formalin-fixed, paraffin-embedded tissue sections are needed. Recovery of RNA from routinely processed biopsies and quantification by the polymerase chain reaction (PCR) has been reported; however, the effects of formalin fixation have not been well studied. We used a proteinase K-salt precipitation RNA isolation protocol followed by TaqMan quantitative PCR to compare the effect of formalin fixation for 24, 48, and 72 hours and for 1 week in normal (2), oral epithelial dysplasia (3), and oral squamous cell carcinoma (4) specimens yielding 9 fresh and 36 formalin-fixed samples. We also compared mRNA and protein expression levels using immunohistochemistry for epidermal growth factor receptor (EGFR), matrix metalloproteinase (MMP)-1, p21, and vascular endothelial growth factor (VEGF) in 15 randomly selected and routinely processed oral carcinomas. We were able to extract RNA suitable for quantitative reverse transcription (RT) from all fresh (9/9) and formalin-fixed (36/36) specimens fixed for differing lengths of time and from all (15/15) randomly selected oral squamous cell carcinoma. We found that prolonged formalin fixation (>48 h) had a detrimental effect on quantitative RT polymerase chain reaction results that was most marked for MMP-1 and VEGF but less evident for p21 and EGFR. Comparisons of quantitative RT polymerase chain reaction and immunohistochemistry showed that for all markers, except p21, there was good correlation between mRNA and protein levels. p21 mRNA was overexpressed in only one case, but protein levels were elevated in all but one tumor, consistent with the established translational regulation of p21. These results show that RNA can be reliably isolated from formalin-fixed, paraffin-embedded tissue sections and can produce reliable quantitative RT-PCR data. However, results for some markers are adversely affected by prolonged formalin fixation times.

PMID: 12218216 [PubMed - indexed for MEDLINE]



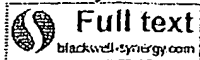
Tightly regulated and inducible expression of a yoked hormone-receptor complex in HEK 293 cells.

Meehan TP, Puett D, Narayan P.

Department of Biochemistry and Molecular Biology, University of Georgia, Athens, Georgia 30602, USA.

We have previously reported the construction of a constitutively active luteinizing hormone receptor by covalently linking a fused heterodimeric hormone to the extracellular domain of the G protein-coupled receptor. This yoked hormone-receptor complex (YHR) was found to produce high levels of cAMP in the absence of exogenous hormone. Stable lines expressing YHR were generated in HEK 293 cells to obtain lines with different expression levels; however, in a relatively short time of continued passage, it was found that YHR expression was greatly reduced. Herein, we describe the development of clonal lines of HEK 293 cells in which the expression of YHR is under the control of a tetracycline-regulated system. Characterization of clonal lines revealed tight control of YHR expression both by dose and time of incubation with doxycycline. These experiments demonstrated a good correlation between expression levels of the receptor and basal cAMP production. Moreover, the reduction in receptor expression following doxycycline removal revealed that YHR mRNA and protein decayed at similar rates, again suggesting a strong linkage between mRNA and protein levels. The controlled expression of YHR in this cell system will allow for a more detailed analysis of the signaling properties associated with constitutive receptor activation and may prove to be advantageous in developmental studies with transgenic animals.

PMID: 14766006 [PubMed - indexed for MEDLINE]



Overexpression of chemokines, fibrogenic cytokines, and myofibroblasts in human membranous nephropathy.

Mezzano SA, Droguett MA, Burgos ME, Ardiles LG, Aros CA, Caorsi I, Egido J.

Division of Nephrology, School of Medicine, Universidad Austral, Valdivia, Chile.
smezzano@uach.cl

Overexpression of chemokines, fibrogenic cytokines, and myofibroblasts in human membranous nephropathy. **BACKGROUND:** Proteinuria plays a central role in the progression of glomerular disease, and there is growing evidence suggesting that it may determine tubular cell activation with release of chemokines and fibrogenic factors, leading to interstitial inflammatory reaction. However, most studies on this subject have been performed in experimental models, and the experience in human kidney biopsies has been scarce. We analyzed the tissue sections of patients with idiopathic membranous nephropathy (IMN), a noninflammatory glomerular disease that may follow a progressive disease with heavy persistent proteinuria, interstitial cell infiltration, and decline of renal function. **METHODS:** Paraffin-embedded biopsy specimens from 25 patients with IMN (13 progressive and 12 nonprogressive) were retrospectively studied by immunohistochemistry [monocyte chemoattractant protein-1 (MCP-1), regulated on activation normal T-cell expressed and secreted chemokine (RANTES), osteopontin (OPN), platelet-derived growth factor-BB (PD-GF-BB)] and in situ hybridization [MCP-1, RANTES, PDGF-BB, transforming growth factor-beta1 (TGF-beta1)]. Moreover, we studied the presence of myofibroblasts, which were identified by the expression of alpha-smooth muscle actin (alpha-SMA), the monocytes/macrophages (CD68-positive cells), and T-cell infiltration (CD4+ and CD8+ cells). All of the patients were nephrotic and without treatment at time of the biopsy. **RESULTS:** A strong up-regulation of MCP-1, RANTES, and OPN expression was observed, mainly in tubular epithelial cells, with a significant major intensity in the progressive IMN patients. A strong correlation between the mRNA expression and the corresponding protein was noted. The presence of these chemokines and OPN was associated with interstitial cell infiltration. TGF-beta and PDGF were also up-regulated, mainly in tubular epithelial cells, with a stronger expression in the progressive IMN, and an association with the presence of myofibroblasts was found. **CONCLUSIONS:** Patients with severe proteinuria and progressive IMN have an overexpression in tubular epithelial cells of the chemokines MCP-1, RANTES, and OPN and the profibrogenic cytokines PDGF-BB and TGF-beta. Because this up-regulation was associated with an interstitial accumulation of mononuclear cells and an increase in myofibroblastic activity, it is suggested that those mediators are potential predictors of progression in IMN. Finally, based on experimental data and the findings of this article, we speculate that severe proteinuria is the main factor responsible for the up-regulation of these factors in tubular epithelial cells.

FREE full text article at
www.obesityresearch.org

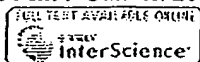
Decreased uncoupling protein expression and intramyocytic triglyceride depletion in formerly obese subjects.

Mingrone G, Rosa G, Greco AV, Manco M, Vega N, Hesselink MK, Castagneto M, Schrauwen P, Vidal H.

Istituto di Clinica Medica and. Clinica Chirurgica and Centro CNR Fisiopatologia Shock, Universita Cattolica S Cuore, Rome, Italy. gmingrone@rm.unicatt.it

OBJECTIVE: To examine the muscular uncoupling protein expression 2 (UCP2) and UCP3 gene expression in morbid obese subjects before and after bariatric surgery [bilio-pancreatic diversion (BPD)]. **RESEARCH METHODS AND PROCEDURES:** Eleven obese subjects (BMI = 49 ± 2 kg/m²) were studied before BPD and 24 months after BPD. Skeletal muscle UCP2 and UCP3 mRNA was measured using reverse transcriptase-competitive polymerase chain reaction and UCP3 protein by Western blotting. Intramyocytic triglycerides were quantified by high-performance liquid chromatography. Twenty-four-hour energy expenditure and respiratory quotient (RQ) were measured in a respiratory chamber. **RESULTS:** After BPD, the average weight loss was approximately 38%. Nonprotein RQ was increased in the postobese subjects (0.73 ± 0.00 vs. 0.83 ± 0.02 , $p < 0.001$). The intramyocytic triglyceride level dropped (3.66 ± 0.16 to 1.60 ± 0.29 mg/100 mg of fresh tissue, $p < 0.0001$) after BPD. Expression of UCP2 and UCP3 mRNA was significantly reduced (from $35.9 \pm 6.1\%$ to $18.6 \pm 4.5\%$ of cyclophilin, $p = 0.02$; from $60.2 \pm 14.0\%$ to $33.4 \pm 8.5\%$, $p = 0.03$; respectively). UCP3 protein content was also significantly reduced (272.19 ± 84.13 vs. 175.78 ± 60.31 , AU, $p = 0.04$). A multiple regression analysis ($R^2 = 0.90$) showed that IMTG levels ($p = 0.007$) represented the most powerful independent variable for predicting UCP3 variation. **DISCUSSION:** The strong correlation of UCP expression and decrease in IMTG levels suggests that triglyceride content plays an even more important role in the regulation of UCP gene expression than the circulating levels of free fatty acids or the achieved degree of weight loss.

PMID: 12740453 [PubMed - indexed for MEDLINE]



Urokinase-mediated posttranscriptional regulation of urokinase-receptor expression in non small cell lung carcinoma.

Montuori N, Mattiello A, Mancini A, Taglialatela P, Caputi M, Rossi G, Ragno P.

Istituto di Endocrinologia ed Oncologia Sperimentale, Consiglio Nazionale delle Ricerche, Naples, Italy.

The urokinase-type plasminogen activator (uPA) and its cellular receptor (uPAR) are involved in the proteolytic cascade required for tumor cell dissemination and metastasis, and are highly expressed in many human tumors. We have recently reported that uPA, independently of its enzymatic activity, is able to increase the expression of its own receptor in uPAR-transfected kidney cells at a posttranscriptional level. In fact, uPA, upon binding uPAR, modulates the activity and/or the level of a mRNA-stabilizing factor that binds the coding region of uPAR-mRNA. We now investigate the relevance of uPA-mediated posttranscriptional regulation of uPAR expression in non small cell lung carcinoma (NSCLC), in which the up-regulation of uPAR expression is a prognostic marker. We show that uPA is able to increase uPAR expression, both at protein and mRNA levels, in primary cell cultures obtained from tumor and adjacent normal lung tissues of patients affected by NSCLC, thus suggesting that the enzyme can exert its effect in lung cells. We investigated the relationship among the levels of uPA, uPAR and uPAR-mRNA binding protein(s) in NSCLC. Lung tissue analysis of 35 NSCLC patients shows an increase of both uPA and uPAR in tumor tissues, as compared to adjacent normal tissues, in 27 patients (77%); 19 of these 27 patients also show a parallel increase of the level and/or binding activity of a cellular protein capable of binding the coding region of uPAR-mRNA. Therefore, in tumor tissues, a strong correlation is observed among these 3 parameters; uPA, uPAR and the level and/or the activity of a uPAR-mRNA binding protein. We then suggest that uPA regulates uPAR expression in NSCLC at a posttranscriptional level by increasing uPAR-stability through a cellular factor that binds the coding region of uPAR-mRNA. Copyright 2003 Wiley-Liss, Inc.

PMID: 12704669 [PubMed - indexed for MEDLINE]



DNA hypermethylation is a mechanism for loss of expression of the HLA class I genes in human esophageal squamous cell carcinomas.

Nie Y, Yang G, Song Y, Zhao X, So C, Liao J, Wang LD, Yang CS.

Laboratory for Cancer Research, College of Pharmacy, Rutgers-The State University of New Jersey, 164 Frelinghuysen Road, Piscataway, NJ 08854-8020, USA.

The three human leukocyte antigen (HLA) class I antigens, HLA-A, HLA-B and HLA-C, play important roles in the elimination of transformed cells by cytotoxic T cells. Frequent loss of expression of these antigens at the cell surface has been observed in many human cancers. Various mechanisms for post-transcriptional regulation have been proposed and tested but the molecular mechanisms for transcriptional regulation are not clear. We show by immunohistochemistry that the HLA class I antigens are absent in 26 of 29 (89%) samples of human esophageal squamous cell carcinomas (ESCC). Eleven of the 26 ESCC samples lost mRNA expression for at least one of the HLA genes, as shown by RT-PCR. DNA from the 29 pairs of ESCC and neighboring normal epithelium were examined for CpG island hypermethylation, homozygous deletion, microsatellite instability (MSI) and loss of heterozygosity (LOH). DNA from normal epithelial tissues had no detectable methylation of the CpG islands of any of these gene loci. Thirteen of 29 ESCC samples (45%) exhibited methylation of one or more of the three HLA loci and six samples (21%) exhibited methylation of all three loci. The HLA-B gene locus was most frequently methylated (38%). HLA-B mRNA expression in an ESCC cell line, where HLA-B was hypermethylated and did not express mRNA, was activated after treatment with 5-aza-2'-deoxycytidine. Homozygous deletion of these three gene loci was not observed. Relatively low rates of LOH and MSI were observed for the microsatellite markers D6S306, D6S258, D6S273 and D6S1666, close to the HLA-A, -B and -C loci, although a high ratio of LOH was observed at a nearby locus (represented by the markers D6S1051 and D6S1560), where the tumor suppressor gene p21(Waf1) resides. A strong correlation between genetic alterations and mRNA inactivation was observed in the ESCC samples. Our results indicate that HLA class I gene expression was frequently down-regulated in ESCC at both the protein and mRNA levels and that hypermethylation of the promoter regions of the HLA-A, -B and -C genes is a major mechanism of transcriptional inactivation.

PMID: 11577000 [PubMed - indexed for MEDLINE]

Comment in:

- [Hum Pathol. 2003 Jul;34\(7\):635-8.](#)

Human Pathology

Molecular and immunohistochemical analysis of HER2/neu oncogene in synovial sarcoma.

Nuciforo PG, Pellegrini C, Fasani R, Maggioni M, Coggi G, Parafioriti A, Bosari S.

Department of Medicine, Surgery and Dental Sciences, University of Milan, A.O.S. Paolo and IRCCS Ospedale Maggiore, Italy.

Amplification and/or overexpression of HER2/neu have been documented in many types of epithelial tumor and recently has been reported in sarcomas, particularly in osteosarcomas. But the role of HER2/neu alterations in soft tissue tumors remains poorly understood. Thus the present study investigates the expression of HER2/neu in 13 patients with synovial sarcoma (SS). In this study, HER2/neu mRNA levels were measured in frozen tissue samples using a real-time reverse transcription-polymerase chain reaction assay; protein expression was assessed by immunohistochemistry using an anti-HER2/neu polyclonal antibody. Six normal skeletal muscle specimens were used to establish basal levels of HER2/neu mRNA. HER2/neu transcripts were detected in all normal tissues and SSs. Four of 13 sarcomas (31%) demonstrated HER2/neu mRNA levels above the mean value, whereas 3 tumors (23%) displayed HER2/neu protein overexpression. Both membranous and cytoplasmic patterns of immunostaining were observed, and a strong correlation was found between protein expression and mRNA level ($P = 0.01$). Increased HER2/neu mRNA levels were significantly associated with a lower risk of developing recurrences ($P = 0.02$). Moreover, none of the patients with HER2/neu overexpression developed metastasis. Our data demonstrate that HER2/neu is expressed in SSs and that both membrane and cytoplasmic HER2/neu expression correlate with mRNA levels. Our results show that the presence of increased levels of HER2/neu in SSs is associated with a more favorable clinical course. Further studies are needed to assess the role of this oncogene in SSs and to evaluate the application of inhibitory humanized monoclonal antibodies in the treatment regimens for this malignancy.

PMID: 12874758 [PubMed - indexed for MEDLINE]

Original Contributions

Molecular and Immunohistochemical Analysis of HER2/neu Oncogene in Synovial Sarcoma

PAOLO GIOVANNI NUCIFORO, MD, CATERINA PELLEGRINI, PhD,
ROBERTA FASANI, MD, MARCO MAGGIONI, MD,
GUIDO COGGI, MD, ANTONINA PARAFIORITI, MD,
AND SILVANO BOSARI, MD

Amplification and/or overexpression of HER2/neu have been documented in many types of epithelial tumor and recently has been reported in sarcomas, particularly in osteosarcomas. But the role of HER2/neu alterations in soft tissue tumors remains poorly understood. Thus the present study investigates the expression of HER2/neu in 13 patients with synovial sarcoma (SS). In this study, HER2/neu mRNA levels were measured in frozen tissue samples using a real-time reverse transcription-polymerase chain reaction assay; protein expression was assessed by immunohistochemistry using an anti-HER2/neu polyclonal antibody. Six normal skeletal muscle specimens were used to establish basal levels of HER2/neu mRNA. HER2/neu transcripts were detected in all normal tissues and SSs. Four of 13 sarcomas (31%) demonstrated HER2/neu mRNA levels above the mean value, whereas 3 tumors (23%) displayed HER2/neu protein overexpression. Both membranous and cytoplasmic patterns of immunostaining were observed, and a strong correlation was

found between protein expression and mRNA level ($P = 0.01$). Increased HER2/neu mRNA levels were significantly associated with a lower risk of developing recurrences ($P = 0.02$). Moreover, none of the patients with HER2/neu overexpression developed metastasis. Our data demonstrate that HER2/neu is expressed in SSs and that both membrane and cytoplasmic HER2/neu expression correlate with mRNA levels. Our results show that the presence of increased levels of HER2/neu in SSs is associated with a more favorable clinical course. Further studies are needed to assess the role of this oncogene in SSs and to evaluate the application of inhibitory humanized monoclonal antibodies in the treatment regimens for this malignancy. HUM PATHOL 34:639-645. © 2003 Elsevier Inc. All rights reserved.

Key Words: HER2/neu, synovial sarcoma, real-time RT-PCR, immunohistochemistry.

Abbreviations: FISH, fluorescence *in situ* hybridization, RT-PCR, reverse transcription-polymerase chain reaction, SS, synovial sarcoma.

Synovial sarcoma (SS) is an aggressive soft tissue tumor that accounts for up to 10% of sarcomas, with a peak incidence in adolescents and young adults. This tumor occurs in 2 major forms, biphasic and monophasic, and it is cytogenetically characterized by the t(X;18)(p11;q11) translocation, found in >95% of cases. Although traditionally considered to be a high-grade neoplasm, recent investigations have suggested that different factors influence prognosis, including morphological and cytogenetic features, treatment strategies, the ploidy status, and the apoptotic index.¹

The development of new therapeutic advancements, such as the specific targeting of molecular alterations present in human malignancies, has brought to light the

need to identify not only prognostic factors, but also tumor features that are predictive of response to therapy.

One of the most extensively studied molecular targets for therapy is the HER-2/neu proto-oncogene. The HER-2/neu oncogene (also known as c-erbB-2), located on chromosome 17q21, is a member of the tyrosine kinase receptor family and encodes for a 185-kilodalton protein that shows 50% homology with the epidermal growth factor receptor.^{2,3} This gene is amplified and/or overexpressed in 20% to 30% of breast carcinomas^{4,5} and in various other tumors,⁶ and usually is associated with tumor aggressiveness and poor prognosis.^{7,8} Several studies have supported the value of HER-2/neu to predict the response to chemotherapy in breast cancer, and the use of recombinant humanized antibodies to HER-2/neu protein (Trastuzumab) in the care of patients with advanced, metastatic breast tumors has been approved.⁹

The role of HER-2/neu activation in soft tissue tumors remains poorly understood, and scarce molecular data backing immunohistochemical studies have been reported. HER-2/neu protein expression was immunohistochemically studied in 204 sarcomas, including 6 SSs, and overexpression was absent in all these malignant mesenchymal neoplasms.¹⁰

Recently, HER-2/neu alterations have been described in osteosarcoma, with a high incidence of pro-

From the Department of Medicine, Surgery and Dental Sciences, University of Milan, A.O.S. Paolo and IRCCS Ospedale Maggiore, Milan, Italy; Department of Pathology, Orthopedic Institute Gaetano Pini, Milan, Italy; and Interuniversity Center of Cancer Research, Milan, Italy. Accepted for publication March 5, 2003.

Supported by grants from Ministero dell'Istruzione, dell'Università e della Ricerca (MIUR-cofin 1999) and Associazione Italiana per la Ricerca sul Cancro (AIRC).

Address correspondence and reprint requests to Paolo Giovanni Nuciforo, MD, Division of Anatomic Pathology, A.O.S. Paolo, Via A. Di Rudini 8, 20142, Milano, Italy.

© 2003 Elsevier Inc. All rights reserved.

0046-8177/03/3407-0002\$30.00/0

doi:10.1016/S0046-8177(03)00238-7

RT-PCR were purchased from Applied Biosystems (Foster City, CA).

Primers and Probes

Primers and probes for β -actin and HER2/neu mRNA were chosen using the computer program Primer Express (Applied Biosystems). Sequences of the forward primer for HER2/neu mRNA (GenBank accession number X03363) were 5'-TCC TGT CTG CAC CTG GAT GAC-3' and the reverse primer 5'-CCA AAG ACC ACC CCC AAG A-3'; the sequence of the TaqMan probe was 5'-(FAM)-ACC ACA ATG CCA ACC ACC GCA GA-(TAMRA)-3'. Sequences of the forward primer for β -actin mRNA (GenBank accession number X00351) were 5'-TCC TTC CTG GCC ATG GAG-3' and the reverse primer 5'-AGG AGG ACC AAT GAT CTT GAT CTT-3'; the sequence of the TaqMan probe was 5'-(FAM)-CCT GTG CCA TCC ACC AAA CTA CCT TC-(TAMRA)-3'. Probes were purchased from Applied Biosystems.

Real-Time RT-PCR

To measure HER2/neu expression in these tumors we used a real-time quantitative RT-PCR based on TaqMan methodology, as previously described,¹⁷ with minor modifications. Briefly, this technique allows, by means of fluorescence emission, to find the cycling point when PCR product is detectable (Ct value or threshold cycle). As previously reported, the Ct value correlates to the starting quantity of the target mRNA.¹⁸ To normalize the amount of total RNA present in each reaction, we amplified the housekeeping gene β -actin, which is assumed to be constant in both normal samples and tumor tissues.

Our results are expressed as relative levels of HER2/neu mRNA, referred to a sample, called a "calibrator," chosen to represent 1X expression of this gene. The calibrator was a breast cancer cellular line (MCF-7)¹⁹ that was analyzed on every assay plate with the unknown samples. All of the analyzed tumors expressed n-fold HER2/neu mRNA relative to the calibrator.

The amount of target, normalized to an endogenous reference (β -actin) and relative to the calibrator, was defined by the $\Delta\Delta C_t$ method as described by Livak K (Sequence Detector User Bulletin 2; Applied Biosystems). Specifically, the formula is applied as follows:

$$\text{target amount} = 2^{-\Delta\Delta C_t}$$

where $\Delta\Delta C_t = [C_t(\text{HER2/neu sample}) - C_t(\beta\text{-actin sample})] - [C_t(\text{HER2/neu calibrator}) - C_t(\beta\text{-actin calibrator})]$.

Immunohistochemistry

Formalin-fixed, paraffin-embedded tissue sections were deparaffinized, rehydrated, and exposed to the primary antibody using the EnVision+ system (Dako, Carpinteria, CA). Primary anti-HER2/neu antibody (rabbit polyclonal antibody, catalog number A0485; Dako) was applied in a dilution of 1:2000 for 60 minutes at room temperature. Before exposure to the primary antibody, sections were microwave-pretreated in EDTA, pH 8.0, to retrieve antigenicity, and incubated with endogenous peroxidase-blocking solution for 10 minutes at room temperature. Positive control, constituted by a breast carcinoma showing more than 80% positive staining for HER2/neu, as well as negative control, in which the primary antibody was omitted, were stained in parallel.

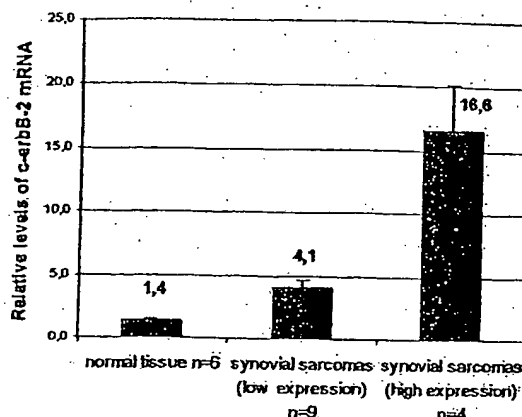


FIGURE 1. Distribution of HER2/neu mRNA levels in normal muscle tissues, and in low- and high-expression sarcomas. Data are expressed as mean and standard error of the mean for each group.

All cases were examined for both cytoplasmic and membrane immunoreactivity. Cytoplasmic staining was evaluated on a semiquantitative scale, according to Kilpatrick et al with minor modifications,²⁰ and reported as 0 (no staining or staining in <10% of cells), 1+ (weak staining in >10% of cells), 2+ (moderate staining in >10% of cells), or 3+ (strong staining in >10% of cells). The presence of a membranous pattern of staining was recorded separately and scored as absent (no staining or weak staining in <10% of cells) or present (complete and/or incomplete staining in >10% of cells). Tumors with a cytoplasmic score of 3+ were considered to have high HER2/neu protein expression.

Statistical Analysis

Statistical differences were calculated by Fisher's exact test. The *t*-test method was used to evaluate the differences between groups. Differences were considered statistically significant when *P* was <0.05.

RESULTS

HER2/neu mRNA Evaluation

All of the tissues analyzed contained detectable levels of HER2/neu mRNA. Six normal tissue samples (skeletal muscle) were used to establish basal level of HER2/neu mRNA. All the normal samples expressed very low levels of HER2/neu mRNA, ranging from 0.9 to 1.9 n (mean, 1.4 n). Among the 13 tumor samples, HER2/neu levels varied greatly, ranging from 2.1 to 24 n. Setting a cutoff level at 7.9 n (a value that represents the mean value of expression distribution of the SSs), 9 cases (69%) had low HER2/neu expression and 4 cases (31%) had high HER2/neu expression (Fig 1; Table 1). The difference between the 2 groups (low and high HER2/neu tumors) was statistically significant (*P* = 0.0001).

TABLE 2. Correlation Between Clinicopathologic Features and HER2/neu Expression as Detected by IHC and RT-PCR

Variable	HER2/neu					
	IHC			PCR		
	L	H	P value	L	H	P value
Age (years)						
<40	3	3		3	3	
>40	7	0	NS	6	1	NS
Sex						
Female	8	0		7	1	
Male	2	3	0.03	2	3	NS
Tumor size (cm)						
<5	3	2		3	2	
>5	7	1	NS	6	2	NS
Histological grade						
II	3	0		3	0	
III	7	3	NS	6	4	NS
Histological type						
MF	5	1		5	1	
BF	2	1		2	1	
PD	3	1	NS	2	2	NS
Chemo/Radiotherapy*						
Yes	4	2		3	3	
No	5	1	NS	5	1	NS
Recurrence†						
Yes	5	0		5	0	
No	2	3	NS	1	4	0.02
Metastasis†						
Yes	3	0		3	0	
No	4	3	NS	3	4	NS

Abbreviations: L, low expression; H, high expression; NS, not significant; MF, monophasic fibrous; BF, biphasic; PD, poorly differentiated (including MF and BF with poorly differentiated areas).

*Information not available for case 7.

†Cases 7, 12, and 13 were excluded from the analysis.

clinicopathologic features, including local recurrence and metastatic disease. Two cases (cases 12 and 13) with follow-up less than 12 months and 1 case (case 7) for which clinical information was not available were excluded from the analysis of recurrences and metastatic behavior.

No correlation was observed between HER2/neu mRNA expression and age, sex, tumor size, tumor grade, histotype, and metastasis. A correlation between sex of the patients and HER2/neu protein expression was found. In fact, none of the female patients showed high HER2/neu protein expression ($P = 0.03$). Patients with high Her2/neu mRNA levels had a lower risk of recurrence than those with low Her2/neu mRNA levels ($P = 0.02$). None of the cases with high HER2/neu mRNA levels developed metastatic foci, although the small number of observations precluded reaching statistical significance ($P = 0.1$). Results are detailed in Table 2.

DISCUSSION

The present work provides the first combined molecular by real-time RT-PCR and immunohistochemical evidence that HER2/neu overexpression occurs in SSs.

Our results indicate that this parameter may provide prognostic information and suggest that a specific therapy with humanized monoclonal antibodies against HER2/neu may be considered in a significant number of SSs.

The HER2/neu oncogene has been extensively investigated as a prognostic factor and more recently as a predictor of response to therapy. It has been demonstrated in breast cancer, where HER2/neu overexpression is usually associated with gene amplification,²¹ and in other epithelial tumors, including ovarian, gastric, lung, and urinary bladder carcinomas.

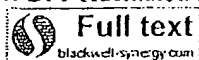
HER2/neu amplification/overexpression appears to be an early event in oncogenic transformation by interacting with other members of the HER family.³ In breast cancer, it is involved in cell cycle and apoptotic pathways through the antiapoptotic effects mediated by p53 and p21 deregulation.^{22,23}

Whether HER2/neu overexpression plays an important role in mesenchymal neoplasms remains controversial. An immunohistochemical study of sarcomas, using a monoclonal antibody, reported no evidence of immunoreactivity for HER-2/neu in 6 SSs as well as in other 197 mesenchymal tumors, with cytoplasmic reactivity observed only in 1 case of peripheral neuroepithelioma.¹⁰ A recent investigation reported gene expression profiles of 41 soft tissue tumors with cDNA microarray analysis. Among these sarcomas, 6 monophasic SSs were characterized by a unique expression pattern of a cluster of 104 genes, including the epidermal growth factor receptor, which shows 50% homology with the HER2/neu gene.²⁴ These data also suggest that the erb-B receptor family plays a significant role in SS. It has been demonstrated that a variable number of osteosarcomas overexpress HER2/neu.¹¹⁻¹⁵ However, more recent studies^{20,25,26} were unable to detect any HER2/neu gene amplification and/or overexpression using fluorescence in situ hybridization (FISH), RT-PCR, and immunohistochemistry.

Differences in the techniques used may play an important role and explain (at least in part) these discrepancies. HER2/neu alterations can be evaluated using different techniques including immunohistochemistry, FISH, Southern hybridization, Northern blot, and competitive, differential, or real-time PCR.²⁷ Immunohistochemistry is the most common method for detection of HER2/neu overexpression, but it is significantly affected by the sensitivity and specificity of the antibodies used, the type of tissue (frozen versus formalin-fixed), and the various interpretative criteria and scoring systems used to evaluate cases. Indeed, most studies of HER2/neu expression in osteosarcoma used immunohistochemical techniques, with different monoclonal or polyclonal antibodies. The discrepancy in results may stem from the use of different antibodies, as well as a lack of standardized evaluation.

For these reasons, to evaluate HER2/neu immunoreactivity in our study, we used a polyclonal antibody (Dako, Carpinteria, CA), arguably the most diffuse and thoroughly tested antibody for HER2/neu assessment. Furthermore, we investigated HER2/neu mRNA ex-

- breast cancer that overexpress Her2/neu. *N Engl J Med* 344:783-792, 2001
10. George E, Nichans GA, Swanson PE, et al: Overexpression of the c-erbB-2 oncogene in sarcomas and small round cell tumors of childhood. An immunohistochemical investigation. *Arch Pathol Lab Med* 116:1033-1035, 1992
11. Onda M, Matsuda S, Higaki S, et al: ErbB-2 expression is correlated with poor prognosis for patients with osteosarcoma. *Cancer* 77:71-78, 1996
12. Gorlick R, Huvois AG, Heller G, et al: Expression of HER2/erbB-2 correlates with survival in osteosarcoma. *J Clin Oncol* 17:2781-2788, 1999
13. Akatsuka T, Wada T, Kokai Y, et al: Loss of ErbB2 expression in pulmonary metastatic lesions in osteosarcoma. *Oncology* 60:361-366, 2001
14. Morris CD, Gorlick R, Huvois G, et al: Human epidermal growth factor receptor 2 as a prognostic indicator in osteogenic sarcoma. *Clin Orthop* 382:59-65, 2001
15. Akatsuka T, Wada T, Kokai Y, et al: ErbB2 expression is correlated with increased survival of patients with osteosarcoma. *Cancer* 94:1397-1404, 2002
16. Coindre JM, Trojani M, Contesso G, et al: Reproducibility of a histopathologic grading system for adult soft tissue sarcoma. *Cancer* 58:306-309, 1986
17. Marchetti A, Pellegrini C, Butti F, et al: Prediction of survival in stage I lung carcinoma patients by telomerase function evaluation. *Lab Invest* 82:729-736, 2002
18. Heid CA, Stevens J, Livak KJ, et al: Real time quantitative PCR. *Genome Res* 6:986-994, 1996
19. Kraus MH, Popescu NC, Amsbaugh SC, et al: Overexpression of the EGF receptor-related proto-oncogene erbB-2 in human mammary tumor cell lines by different molecular mechanisms. *EMBO J* 6:605-610, 1987
20. Kilpatrick SE, Geisinger KR, King TS, et al: Clinicopathologic analysis of HER-2/neu immunoreactivity among various histologic subtypes and grades of osteosarcoma. *Mod Pathol* 14:1277-1283, 2001
21. Slamon DJ, Godolphin W, Jones LA, et al: Studies of the HER-2/neu proto-oncogene in human breast and ovarian cancer. *Science* 244:707-712, 1989
22. Harari D, Yarden Y: Molecular mechanisms underlying ErbB2/HER2 action in breast cancer. *Oncogene* 19:6102-6114, 2000
23. Zhou BP, Liao Y, Xia W, et al: HER-2/neu induces p53 ubiquitination via Akt-mediated MDM2 phosphorylation. *Nat Cell Biol* 3:973-982, 2001
24. Nielsen OT, West RB, Linn SC, et al: Molecular characterization of soft tissue tumours: A gene expression study. *Lancet* 359:1301-1307, 2002
25. Thomas DG, Giordano TJ, Sanders D, et al: Absence of HER2/neu gene expression in osteosarcoma and skeletal Ewing's sarcoma. *Clin Cancer Res* 8:788-793, 2002
26. Maitra A, Wanzer D, Weinberg AG, et al: Amplification of the Her-2/neu oncogene is uncommon in pediatric osteosarcomas. *Cancer* 92:677-683, 2001
27. Hanna W, Kahn HJ, Trudeau M: Evaluation of HER-2/neu (erbB-2) status in breast cancer: From bench to bedside. *Mod Pathol* 12:827-834, 1999
28. Naber SP, Tsutsumi Y, Yin S, et al: Strategies for the analysis of oncogene overexpression. Studies of the neu oncogene in breast carcinoma. *Am J Clin Pathol* 94:125-136, 1990
29. Tetu B, Brisson J: Prognostic significance of HER-2/neu oncoprotein expression in node-positive breast cancer. The influence of the pattern of immunostaining and adjuvant therapy. *Cancer* 73:2359-2365, 1994
30. Coombs LM, Pigott DA, Sweeney E, et al: Amplification and over-expression of c-erbB-2 in transitional cell carcinoma of the urinary bladder. *Br J Cancer* 63:601-608, 1991
31. Kay EW, Mulcahy H, Walsh CB, et al: Cytoplasmic c-erbB-2 protein expression correlates with survival in Dukes' B colorectal carcinoma. *Histopathology* 25:455-461, 1994
32. Roychowdhury DF, Tseng A Jr, Fu KK, et al: New prognostic factors in nasopharyngeal carcinoma: Tumor angiogenesis and c-erbB-2 expression. *Cancer* 77:1419-1426, 1996
33. Hall PA, Hughes CM, Staddon SL, et al: The c-erb B2 proto-oncogene in human pancreatic cancer. *J Pathol* 161:195-200, 1990
34. Sugg SL, Ezzat S, Zheng L, et al: Cytoplasmic staining of erbB-2 but not mRNA levels correlates with differentiation in human thyroid neoplasia. *Clin Endocrinol (Oxf)* 49:629-637, 1998
35. Keshgegian AA, Cnaan A: erbB-2 oncoprotein expression in breast carcinoma. Poor prognosis associated with high degree of cytoplasmic positivity using CB-11 antibody. *Am J Clin Pathol* 108:456-463, 1997
36. Kawauchi S, Fukuda T, Oda Y, et al: Prognostic significance of apoptosis in synovial sarcoma: Correlation with clinicopathologic parameters, cell proliferative activity, and expression of apoptosis-related proteins. *Mod Pathol* 13:755-765, 2000
37. Rosen G, Forscher C, Lowenbraun S, et al: Synovial sarcoma: Uniform response of metastasis to high dose ifosfamide. *Cancer* 73:2506-2511, 1994
38. Muss HB, Thor AD, Berry DA, et al: c-erbB-2 expression and response to adjuvant therapy in women with node-positive early breast cancer. *N Engl J Med* 330:1260-1266, 1994



Expression of bcr-abl mRNA in individual chronic myelogenous leukaemia cells as determined by in situ amplification.

Pachmann K, Zhao S, Schenk T, Kantarjian H, El-Naggar AK, Siciliano MJ, Guo JQ, Arlinghaus RB, Andreeff M.

The University of Texas M.D. Anderson Cancer Center, Department of Molecular Haematology and Therapy, 1515 Holcombe Boulevard, Houston, TX 77030, USA.

We present the results of a novel method developed for evaluation of in situ amplification, a molecular genetic method at the cellular level. Reverse transcription polymerase chain reaction (RT-PCR) was used to study bcr-abl transcript levels in individual cells from patients with chronic myelogenous leukaemia (CML). After hybridizing a fluorochrome-labelled probe to the cell-bound RT-PCR product, bcr-abl mRNA-positive cells were determined using image analysis. A dilution series of bcr-abl-positive BV173 into normal cells showed a good correlation between expected and actual values. In 25 CML samples, the percentage of in situ PCR-positive cells showed an excellent correlation with cytogenetic results ($r = 0.94$, $P < 0.0001$), interphase fluorescence in situ hybridization (FISH) ($r = 0.95$, $P = 0.001$) and hypermetaphase FISH ($r = 0.81$, $P < 0.001$). The fluorescence intensity was higher in residual CML cells after interferon (IFN) treatment than in newly diagnosed patients ($P = 0.004$), and was highest in late-stage CML resistant to IFN therapy and lowest in CML blast crisis ($P = 0.001$). Mean fluorescence values correlated with bcr-abl protein levels, as determined by Western blot analysis ($r = 0.62$). Laser scanning cytometry allowing automated analysis of large numbers of cells confirmed the results. Thus, fluorescence in situ PCR provides a novel and quantitative approach for monitoring tumour load and bcr-abl transcript levels in CML.

PMID: 11260080 [PubMed - indexed for MEDLINE]



Correlative immunohistochemical and reverse transcriptase polymerase chain reaction analysis of somatostatin receptor type 2 in neuroendocrine tumors of the lung.

Papotti M, Croce S, Macri L, Funaro A, Pecchioni C, Schindler M, Bussolati G.

Department of Biomedical Sciences and Oncology, University of Turin, Italy.

Somatostatin receptors type 2 (sst2) have been frequently detected in neuroendocrine tumors and bind somatostatin analogues, such as octreotide, with high affinity. Receptor autoradiography, specific mRNA detection and, more recently, antisst2 polyclonal antibodies are currently employed to reveal sst2. The aim of the present study was to investigate by three different techniques the presence of sst2 in a series of 26 neuroendocrine tumors of the lung in which fresh frozen tissue and paraffin sections were available. It was possible, therefore, to compare, in individual cases, RNA analysis studied by reverse transcriptase polymerase chain reaction (RT-PCR), in situ hybridization (ISH), and immunohistochemistry. A series of 20 nonneuroendocrine lung carcinoma samples served as controls. RT-PCR was positive for sst2 in 22 of 26 samples, including 15 of 15 typical carcinoids, 5 of 6 atypical carcinoids, and 2 of 5 small-cell carcinomas. The sst2 mRNA signal obtained by RT-PCR was strong in the majority (87%) of typical carcinoids and of variable intensity in atypical carcinoids and small-cell carcinomas. A weakly positive signal was observed in 5 of 20 control samples. In immunohistochemistry, two different antibodies (anti-sst2) were employed, including a monoclonal antibody, generated in the Department of Pathology, University of Turin. In the majority of samples a good correlation between sst2 mRNA (as detected by RT-PCR) and sst2 protein expression (as detected by immunohistochemistry) was observed. However, one atypical carcinoid and one small-cell carcinoma had focal immunostaining but no RT-PCR signal. ISH performed in selected samples paralleled the results obtained with the other techniques. A low sst2 expression was associated with high grade neuroendocrine tumors and with aggressive behavior. It is concluded that 1) neuroendocrine tumors of the lung express sst2, and there is a correlation between the mRNA amount and the degree of differentiation; 2) immunohistochemistry and ISH are reliable tools to demonstrate sst2 in these tumors; and 3) sst2 identification in tissue sections may provide information on the diagnostic or therapeutic usefulness of somatostatin analogues in individual patients with neuroendocrine tumors.

PMID: 10718213 [PubMed - indexed for MEDLINE]

Volume 9, Number 1, March 2000

[Diagnostic Molecular Pathology

WESTON LIBRARY

MAR 07 2000

35120 CLINICAL SCIENCE CENTER
800 HIGHLAND AVE MADISON WI 53792

Co-Editors

Ronald A. DeLeellis, M.D.

Robert J. Wolfe, M.D.



LIPPINCOTT WILLIAMS & WILKINS

Diagnostic Molecular Pathology

Volume 9 □ Number 1 □ March 2000

ORIGINAL ARTICLES

- 1 Strong Association of SYT-SSX Fusion Type and Morphologic Epithelial Differentiation in Synovial Sarcoma
Cristina R. Antonescu, Akira Kawai, Denis H. Leung, Fulvio Lonardo, James M. Woodruff, John H. Healey, and Marc Ladanyi
- 9 Clinical Relevance of Molecular Diagnosis in Childhood Rhabdomyosarcoma
Ana Tobar, Smadar Avigad, Meira Zoldan, Celia Mor, Yakov Gosben, and Rina Zaizov
- 14 Accumulation of Chromosomal Imbalances From Intraductal Proliferative Lesions to Adjacent In Situ and Invasive Ductal Breast Cancer
Michaela M. Aubele, Margaret C. Cummings, Anita E. Mattis, Horst F. Zitzelsberger, Axel K. Walch, Markus Kremer, Heinz Höfler, and Martin Werner
- 20 Routine Analysis of p53 Mutation in Clinical Breast Tumor Specimens Using Fluorescence-Based Polymerase Chain Reaction and Single Strand Conformation Polymorphism
Barry Iacopetta, Hany Elsaleh, Fabienne Grieu, David Joseph, Greg Sterrett, and Peter Robbins
- 26 Tumor-Associated Overexpression of the Soluble T1-S Receptor in Lymph Node-Negative Breast Cancer
Anne Katrin Werenskiold, Dieter Prechtel, Nadia Harbeck, and Heinz Höfler

(continued on next page)

Listed in *Index Medicus*, *Current Awareness in Biological Sciences*, *EMBASE/Excerpta Medica*,
Current Contents/Life Sciences, and *Science Citation Index*.

Diagnostic Molecular Pathology (ISSN 1052-9551) is published four times per year in March, June, September, and December by Lippincott Williams & Wilkins, Inc., 12107 Insurance Way, Hagerstown, MD 21740. Business offices are located at 530 Walnut Street, Philadelphia, PA 19106-3621. Printed in the U.S.A. Periodicals postage paid at Hagerstown, MD, and at additional mailing offices.

Copyright © 2000 by Lippincott Williams & Wilkins, Inc. All rights reserved.

Address for subscription information, orders, or changes of address: (except Japan) 12107 Insurance Way, Hagerstown, MD 21740, or call 1-800-638-3030; in Maryland, call collect 301-714-2300. In Japan, contact Igaku-Shoin, Ltd., 1-28-36 Hongo, Bunkyo-ku, Tokyo 113, Japan; phone: 81-3-3817-5675; fax: 81-3-3815-6776.

Annual subscription rates: U.S.: \$143.00 individual, \$309.00 institution; Canada and Mexico: \$165.00 individual, \$232.00 institution. (The Canadian GST Tax of 7% will be added to the subscription price of all orders shipped to Canada. The Lippincott Williams & Wilkins, Inc. GST Identification No. is 895524239.) Canada Post International Publications Mail Product Sales Agreement No. 0616168; all other countries (except Japan): \$171.00 individual, \$258.00 institution. (Prices outside North America include \$6.00 for air freight shipping; air freight delivery occurs within 7-21 days worldwide.) International subscriptions must be prepaid. Single copies, when available, may be ordered from the publisher. Single copies \$58.00. Prices are subject to change without notice. Copies will be replaced without charge if the publisher receives a request within 90 days of the mailing date, both in the U.S. and worldwide.

Postmaster: Send changes of address to *Diagnostic Molecular Pathology*, P.O. Box 1550, Hagerstown, MD 21740.

WESTON LIBRARY
MAR 07 2000
J51120 CLINICAL SCIENCE CENTER
600 HIGHLAND AVE MADISON WI 53782

This material may be protected by Copyright law (Title 17 U.S. Code)

Correlative Immunohistochemical and Reverse Transcriptase Polymerase Chain Reaction Analysis of Somatostatin Receptor Type 2 in Neuroendocrine Tumors of the Lung

Mauro Papotti, M.D., Sabrina Croce, M.D., Luigia Macri, M.D.,
Aola Funaro, Ph.D., Carla Pecchioni, Marcus Schindler, M.D., and
Gianni Bussolati, M.D., F.R.C.Path.

Somatostatin receptors type 2 (sst2) have been frequently detected in neuroendocrine tumors and bind somatostatin analogues, such as octreotide, with high affinity. Receptor autoradiography, specific mRNA detection and, more recently, anti-sst2 polyclonal antibodies are currently employed to reveal sst2. The aim of the present study was to investigate by three different techniques the presence of sst2 in a series of 26 neuroendocrine tumors of the lung in which fresh frozen tissue and paraffin sections were available. It was possible, therefore, to compare, in individual cases, RNA analysis studied by reverse transcriptase polymerase chain reaction (RT-PCR), *in situ* hybridization (ISH), and immunohistochemistry. A series of 20 nonneuroendocrine lung carcinoma samples served as controls. RT-PCR was positive for sst2 in 22 of 26 samples, including 15 of 15 typical carcinoids, 5 of 6 atypical carcinoids, and 2 of 5 small-cell carcinomas. The sst2 mRNA signal obtained by RT-PCR was strong in the majority (87%) of typical carcinoids and of variable intensity in atypical carcinoids and small-cell carcinomas. A weakly positive signal was observed in 5 of 20 control samples. In immunohistochemistry, two different antibodies (anti-sst2) were employed, including a monoclonal antibody, generated in the Department of Pathology, University of Turin. In the majority of samples a good correlation between sst2 mRNA (as detected by RT-PCR) and sst2 protein expression (as detected by immunohistochemistry) was observed. However, one atypical carcinoid and one small-cell carcinoma had focal immunostaining but no RT-PCR signal. ISH performed in selected samples paralleled the results obtained with the other techniques. A low sst2 expression was associated with

high grade neuroendocrine tumors and with aggressive behavior. It is concluded that 1) neuroendocrine tumors of the lung express sst2, and there is a correlation between the mRNA amount and the degree of differentiation; 2) immunohistochemistry and ISH are reliable tools to demonstrate sst2 in these tumors; and 3) sst2 identification in tissue sections may provide information on the diagnostic or therapeutic usefulness of somatostatin analogues in individual patients with neuroendocrine tumors.

Key Words: Neuroendocrine—Lung—Tumors—Somatostatin receptors—Immunohistochemistry—Small cell carcinoma—Reverse transcriptase polymerase chain reaction.

Diagn Mol Pathol 9(1): 47-57, 2000.

The somatostatin receptor family (sst) includes at least five isoforms that have been recently identified and characterized (18,32,41). The ssts are widely distributed in normal human tissues and in human tumors. Sst type 2 is more commonly detected in neuroendocrine tumors (32,37) and binds the somatostatin analogue octreotide with high affinity.

Sst localization had originally been demonstrated by means of binding assays of radiolabeled somatostatin analogues (20,25,31). Subsequently, specific sst messenger RNA (mRNA) detection was obtained by means of *in situ* hybridization (ISH) and reverse transcriptase polymerase chain reaction (RT-PCR) (14,32,37). Recently, polyclonal antibodies specific for different isoforms of sst were produced and used in immunohistochemistry (10,12,15,18,30,35,36). Given the well-known heterogeneity of neoplastic populations, *in situ* methods (immunohistochemistry and ISH) allow a more definite mapping of the distribution of the receptor in such tissues.

From the Department of Biomedical Sciences and Oncology (M.P., S.C., L.M., A.F., C.P., G.B.), University of Turin, Italy; and Glaxo Institute of Applied Pharmacology (M.S.), University of Cambridge, United Kingdom.

Supported by grants from the Regione Piemonte (grant no. 165 of Research Project DGR 34-23230) and Ministry of University (Rome), Italy.

A.F. is the recipient of a Research Contract by the University of Turin.

Address correspondence and reprint requests to Prof. M. Papotti, Department of Pathology, University of Turin, Via Santena 7, I-10126 Torino.

This is potentially useful for predicting the responsiveness of a given neoplastic cell population to medical treatment with somatostatin analogues, which are used in the clinical setting for both diagnostic and therapeutic purposes with special reference to neuroendocrine tumors.

The spectrum of neuroendocrine tumors of the lung includes well-differentiated neoplasms (so-called typical carcinoids) and poorly differentiated small-cell carcinomas (SCCs). Intermediate forms sharing features of both the aforementioned types also belong to this spectrum (so-called atypical carcinoids or well-differentiated neuroendocrine carcinomas). Finally, large-cell neuroendocrine carcinoma has been identified and included in this tumor group (4,40). The tissue distribution of *sst2* in neuroendocrine tumors of the lung has not been thoroughly characterized, although individual samples of bronchial carcinoids were found to express *sst2* (30). SCCs (but not non-small-cell types) were also shown to be *sst2* positive by receptor binding assay (33). Moreover, *sst2* has been detected in *in vitro* cell cultures of human SSC of the lung (39,42). No study on a series of neuroendocrine tumors of the lung including all neuroendocrine lung tumor types has been reported to date.

The aim of this study was therefore to investigate the presence of *sst2* mRNA and protein in a series of 26 neuroendocrine tumors of the lung, employing different technical approaches, such as RT-PCR, ISH, and immunohistochemistry. To this purpose a monoclonal antibody to *sst2* (N-terminal) was generated in the Department of Pathology, University of Turin. The results were then compared and related to the tumor grade and to other clinicopathologic parameters.

MATERIALS AND METHODS

Case Series and RNA Extraction

Twenty-six samples of neuroendocrine tumors of the lung, in which fresh frozen tissue was available, were retrieved from the surgical pathology file of the University of Turin, Italy. All samples were reviewed applying currently accepted criteria of classification (4,40), and the neuroendocrine nature was confirmed by positive immunostaining for chromogranin A (CgA) (with or without antigen retrieval) or synaptophysin, and by positive RT-PCR for CgA mRNA. According to the classifications described here, these included 15 well-differentiated neuroendocrine tumors (typical carcinoids), 6 well-differentiated neuroendocrine carcinomas (atypical carcinoids), and 5 SCCs.

A series of 20 non-small-cell lung carcinomas (10 squamous, 9 adenocarcinomas, and 1 large-cell anaplastic) lacking neuroendocrine differentiation, as demonstrated by negative immunohistochemistry and RT-PCR for CgA (1), served as a control group. Clinicopathologic data and follow-up information were obtained for all patients.

For hybridization analysis, total RNA was extracted using the guanidine thiocyanate-cesium chloride method (5). The concentration of RNA was estimated by spectrophotometry, and RNA degradation was assessed by agarose gel electrophoresis, as previously reported (37).

Reverse Transcriptase Polymerase Chain Reaction for *sst2* and Chromogranin A

Total RNA (2 µg) was first digested, with 10 units of RNase-free DNase (Boehringer, Mannheim, Germany) in a 10-µL solution containing 20 mmol/L MgCl₂, to avoid DNA contamination. The solution was kept at room temperature for 10 minutes, then heated for 5 minutes at 70°C to inactivate the DNase molecules; 40 pmol/L of oligodeoxythymidine primers (oligo-dT16) were added and the solution was heated again at 70°C for 10 minutes, then chilled on ice to allow the primer hybridization. The resulting solution was reverse transcribed using 100 units of reverse transcriptase (Gibco BRL, Gaithersburg, MD). Complementary DNA (cDNA) was generated in a 50-µL final reaction volume containing 50 mmol/L Tris-HCl pH 8.3, 75 mmol/L KCl, 3 mmol/L MgCl₂, 10 mmol/L dithiothreitol, 1 mmol/L deoxynucleotide triphosphates (dNTPs), and 20 units of RNasin (Promega, Madison, WI). The solution was heated at 37°C for 90 minutes. Finally, the enzymes were inactivated by heating to 70°C for 10 minutes.

The efficiency of the reverse transcription was determined by performing a PCR reaction having the β_2 -microglobulin "housekeeping gene" as a target. PCR was carried out in a 10-µL final reaction volume containing 1 µL of cDNA template, 10 pmol of sense and antisense oligonucleotide primers, 67 mmol/L Tris-HCl pH 8.8, 16 mmol/L (NH₄)₂SO₄, 0.01% polysorbate 20, 2 mmol/L dNTPs, 1 mmol/L MgCl₂, and 0.5 units of Taq polymerase. β_2 -Microglobulin, *sst2*, and CgA PCR reactions were performed using the same protocol at the following PCR conditions: 35 cycles, each cycle consisting of denaturation at 94°C for 2 minutes, annealing at 55°C for 1 minute for β_2 -microglobulin, at 61°C for *sst2*, and at 68°C for CgA; extension was performed at 72°C for 1 minute. The primers used for RT-PCR (9,11,23,37) are reported in Table 1.

The amplified fragments were run in a 1% agarose gel, containing ethidium bromide. Strict precautions against contamination were undertaken (19) and negative controls (a no-template control and a no-reverse transcriptase control and distilled water to replace the RNA) were included. The RNA extracted from an H716 neuroendocrine colon carcinoma cell line and from a neuroblastoma (37) served as positive controls for CgA and *sst2*, respectively.

Antibodies

Two different antibodies specific for *sst2* were employed: The first one was a monoclonal antibody raised

TABLE 1. Sequences of primers used for reverse transcriptase polymerase chain reaction

	Size of PCR product (bp)	Position	Study
1) β_2 -microglobulin sense: 5' ACC CCC ACT GAA AAA GAT GA 3'	120	286-305	Gussow et al. (9)
2) β_2 -microglobulin antisense: 5' ATC TTC AAA CCT CCA TGA TG 3'		389-408	
3) SSTR2 sense: 5' CAG TCA TGA GCA TCG ACC GA 3'	284	402-421	Sestini et al. (37)
4) SSTR2 antisense: 5' GCA AAG ACA GAT GAT GGT GA 3'		665-684	
5) CgA sense: 5' GCT CCA AGA CCT CGC TCT CC 3'	583	316-335	Helman et al. (11)
6) CgA antisense: 5' GAC CGA CTC TCG CCT TTC CG 3'		878-897	

PCR, polymerase chain reaction.

in the Department of Pathology (University of Turin) specific for an N-terminal sequence of the sst2 (shared by both A and B receptor isoforms). The octapeptide EPYYDLTS, corresponding to amino acids 35 to 42 of the human receptor (and differing by one amino acid from the mouse sequence), was synthesized, having a lysin added to the N-terminal. This sequence was similar to that used by other groups to produce polyclonal antibodies (17,18,27). This sequence was rather short but made it possible to avoid extensive homology with sst1. In addition, according to a genbank search using FASTA (28), this protein sequence is unique to human sst2 and has a partial homology only with rat and human nuclear receptor retinoid orphan nuclear receptor-beta (a protein having nuclear localization). Three Balb/c mice were immunized with the peptide conjugated to keyhole limpets hemocyanin (KLH) (Sigma, St. Louis, MO) following the standard procedure. After the first intrasplenic injection (100 μ g of protein) at time 0, the mice were intraperitoneally injected six times with the peptide-KLH conjugate (150 μ g) in the presence of Freund adjuvant. The reactivity of the sera from each animal was evaluated using an enzyme-linked immunosorbent assay, using the peptide coated onto the plastic. The hybridomas were produced by somatic fusion of immunized splenocytes with the mouse myeloma cell line Ag8.X63.653, following the standard technique (21). The monoclonal antibodies of interest were selected on the basis of the reactivity with the target peptide and with appropriate tissue sections. The latter included formalin-fixed and paraffin-embedded sections of pituitary gland and pancreatic islets and were analyzed by means of immunoperoxidase staining. Parallel control experiments were also performed by staining serial sections of these tissues, omitting the primary antibody or with the preimmune serum or with the antibody preadsorbed with high concentrations (1 mg/mL) of the antigenic peptide. In addition, the selected monoclonal antibodies (coded 10C6 and 10G4), both of IgM isotype, were further characterized by Western blotting. Membranes were prepared from stable transfected Chinese hamster ovary (CHO)-K1 cells, individually expressing recombinant human somatostatin receptors (sst1 to sst5). Western blotting was performed as previously described (36). The monoclonal

antibody was used as culture supernatant at 1:3 dilution for 2 hours at room temperature in Tris-buffered saline (TBS), supplemented with 0.1% polysorbate 20. Blots were washed in TTBS and incubated with peroxidase-conjugated goat antimouse IgM, diluted 1:1,500 for 90 minutes at room temperature. Then, blots were washed in TTBS and immunocomplexes were visualized using ECL following manufacturer's instructions (Amersham, Bucks, UK).

A second polyclonal antibody was produced that had been characterized previously (35,36). This antibody (coded K230) was raised in sheep and was specific for a sequence of the C-terminal portion of the sst2A (KSRL-NETTETQRTLLNEDLQ, amino acids 347 to 366).

Immunohistochemistry

Sections 4 or 5 μ thick, adjacent to those used for conventional histopathologic examination and immunostaining for neuroendocrine markers, were collected onto poly-L-lysine-coated slides. The proliferative activity of the tumors was assessed by means of Ki67 immunostaining (clone MIB1, Immunotech, Marseille, France), diluted 1:10 after microwave-based antigen retrieval in citrate buffer). The ascitic fluid of monoclonal antibody 10G4 was used in this study and was applied to tissue sections with prior antigen retrieval (three 3-minute passages in a microwave oven at 800 W in citrate buffer pH 6.0), at the dilution of 1:10,000 or 1:12,000 for 30 minutes at room temperature. The antiserum coded K230 was applied overnight at a dilution of 1:300 with no prior antigen retrieval. The immune reactions were then revealed with the immunoperoxidase technique (13) using the streptavidin-peroxidase kit and diaminobenzidine as chromogen. A weak nuclear counterstain or no counterstain was used in parallel sections. Control stainings for both antibodies included immunoperoxidase of serial sections using preimmune serum or antibody preadsorbed with the antigen or buffer instead of the primary antibody.

In Situ Hybridization

Selected tumors (12 samples) were also analyzed for sst2 mRNA expression by means of a nonradioactive, tyramide deposition-based ISH technique. The proce-

duration of amplification was modified from procedures reported by Kerstens et al. (16), Speel et al. (38), and the GenPoint (biotinyl-tyramide) manufacturer (Dako, Glostrup, Denmark). Briefly, 5- μ m-thick paraffin sections were collected onto silane-coated slides and deparaffinized through xylene and graded alcohols to phosphate buffer saline (PBS). The slides were then incubated for 5 minutes in a microwave oven at 800 W in citrate buffer pH 6.0. After washing in PBS, they were digested with proteinase K (1 μ g/mL) for 10 minutes at 23°C. Endogenous peroxidase activity was blocked with 3% hydrogen peroxide and endogenous biotin was blocked using avidin-blocking reagent for 15 minutes followed by washing in PBS and biotin-blocking reagent for 15 minutes (3). Sections were then prehybridized for 1 hour at room temperature in a mixture composed of 4 \times SSC, 50% formamide, Denhardt's 1 \times , dextran sulfate 5 \times , 500 μ g/mL salmon sperm DNA, and 250 μ g/mL tRNA. Hybridization took place overnight at 42°C in a solution containing the specific probe at a concentration of 1 pmol/mL. The probe was a digoxigenin-labeled 48-base oligonucleotide (32), complementary to positions 91 to 139 of the human *sst2* gene (41). After hybridization, excess hybridization buffer and coverslips were removed by a rapid wash in 4 \times SSC followed by stringent washing in 0.1 \times SSC for 10 minutes at 42°C. The hybrids were revealed by the following incubation steps: peroxidase-labeled antidigoxigenin (diluted 1:100 in PBS) for 30 minutes at room temperature, biotinylated tyramide (diluted 1:5 in PBS) for 15 minutes at room temperature, and peroxidase-labeled streptavidin for 15 minutes at room temperature. Diaminobenzidine was used as chromogen. Controls for ISH included staining of serial sections with sense probe, an unrelated probe (EBER-1 of the Epstein-Barr virus), and omission of the probe in the hybridization mixture, with all other experimental conditions identical to the procedure described here.

RESULTS

Reverse Transcriptase Polymerase Chain Reaction

All neuroendocrine tumors, but no nonneuroendocrine lung carcinomas, were positive for CgA mRNA (Fig. 1). *Sst2* mRNA was amplified in 22 of 26 samples of neuroendocrine tumor. The signals had variable intensities (Fig. 2) and were weak in moderately or poorly differentiated tumors (mostly in SCCs). No amplification was obtained in no-template or no-reverse transcriptase experiments. Control samples (nonneuroendocrine lung carcinomas proven by negative CgA RT-PCR) were weakly positive for *sst2* in 5 of 20 samples only (including 3 adenocarcinomas, 1 squamous, and the large-cell anaplastic carcinoma) (Fig. 3). These differences were statistically significant ($P < 0.01$) by χ^2 test.

Characterization of Monoclonal Antibodies to *sst2*

Several clones were identified having a positive binding by enzyme-linked immunosorbent assay and a parallel immunoreactivity on formalin-fixed paraffin-embedded human endocrine tissues (pituitary and pancreatic islets). In Western blotting experiments, two clones (coded 10C6 and 10G4) specifically developed a band at approximately 70 kD. When the antibodies were used against CHO-transfected cells expressing recombinant somatostatin receptors 1 through 5, a specific band corresponding to *sst2* (at approximately 70 kD) was revealed by the monoclonal antibody 10G4. Monoclonal antibody 10C6 developed a strong band with *sst2* but displayed a weaker reactivity also with *sst1*, 3, and 5, at least in the present experimental conditions (Fig. 4 A,B). The same antibodies were also tested by means of immunoperoxidase staining on formalin-fixed, paraffin-embedded samples of normal human pituitary gland and pancreas. Monoclonal antibody 10G4 gave good results in immunohistochemistry and was used at increasing di-

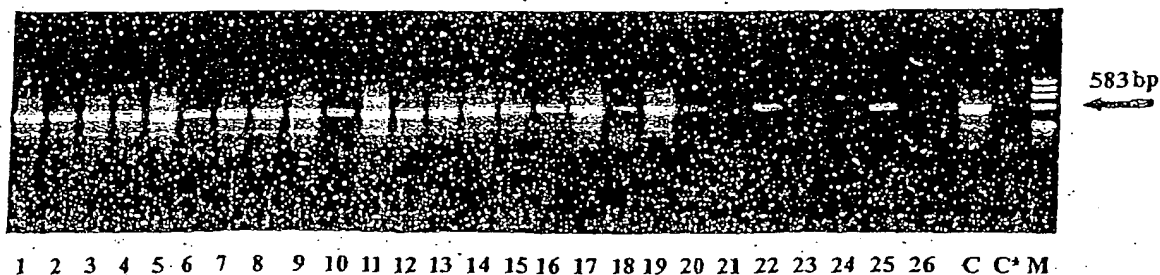


FIG. 1. Reverse transcriptase polymerase chain reaction for chromogranin A (CgA) mRNA in 26 samples of neuroendocrine tumor of the lung. Numbers in each lane correspond to sample numbers in Table 2. CgA mRNA is amplified at 429 bp. C and C* stand for positive (neuroendocrine colon carcinoma cell line, H716) and negative (distilled water) controls, respectively. The last column to the right represents the molecular weight marker. All samples are positive with a variable intensity of the amplification band.

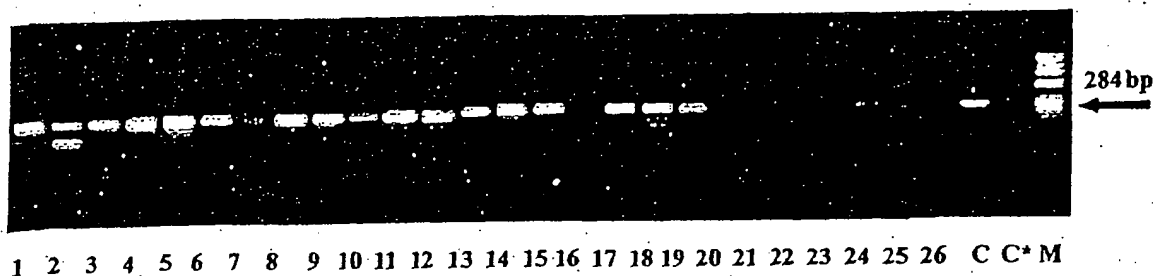


FIG. 2. Reverse transcriptase polymerase chain reaction for *sst2* mRNA in 26 samples of neuroendocrine tumor of the lung. Numbers in each lane correspond to sample numbers in Table 2. *sst2* mRNA is amplified at 284 bp. C and C* stand for positive (a neuroblastoma) and negative (distilled water) controls, respectively. The last column to the right represents the molecular weight marker. Twenty-two of 26 samples are positive with a variable intensity of the amplification band.

lutions (up to 1:15,000) with specific staining. Using thin sections (approximately 4 μ m), a strong membrane-bound and peripheral cytoplasmic immunoreactivity was found in an adenohypophyseal cell population (corresponding to growth hormone-secreting cells, as confirmed by double immunohistochemical analyses) and in pancreatic islets (Fig. 4 C,D). In the latter, the staining was apparently not restricted to a specific hormone-producing cell type and had a peripheral cytoplasmic or membrane distribution. Exocrine pancreatic cells (both acinar and ductal) were only occasionally immunostained. Immunohistochemistry performed on serial control sections, either omitting the primary antibody or using the preimmune serum or antibodies preabsorbed with the synthetic peptide, was negative in both tissues. Monoclonal antibody 10C6 had a relatively higher background staining at similar dilutions.

Immunohistochemistry

The antibodies to *sst2* (monoclonal antibody 10G4 and polyclonal K230) gave slightly different immunoreactions in 25 samples, and staining was not done in 1 sample because of lack of residual paraffin blocks. The monoclonal antibody 10G4 stained 21 of 25 samples, the

negative samples being 1 atypical carcinoid and 3 SCCs (Fig. 5). The tumors had 5% to 25% of the neoplastic cells immunoreactive. The staining was at the periphery of the cytoplasm, and omitting the counterstain its membrane-bound distribution was better outlined in most samples (Fig. 6). One sample of atypical carcinoid (no. 21) was focally immunoreactive for *sst2*, despite negative RT-PCR findings. Conversely, sample no. 26 was immunohistochemistry negative and RT-PCR positive. The antiserum anti-*sst2A* (code K230) gave positive signal in 19 of 25 samples, in 5% to 60% of the neoplastic cell population (Fig. 7). The location of the staining was at the membrane level associated with a weak cytoplasmic reactivity. The same pattern was seen in positive controls, e.g., pancreatic islets (Fig. 7, inset). Two samples (nos. 19 and 26) were negative in spite of a positive RT-PCR signal. Two other tumors (nos. 21 and 22), apparently devoid of *sst2* mRNA, showed a small percentage of immunoreactive cells. Incidentally, one of these latter samples (no. 21) was also immunoreactive with monoclonal antibody 10G4 (Table 2).

The five control samples positive by RT-PCR were also reactive with the antibodies. The type of immunocytochemical location of *sst2* receptors was similar to that described here, being a peripheral cytoplasmic stain-

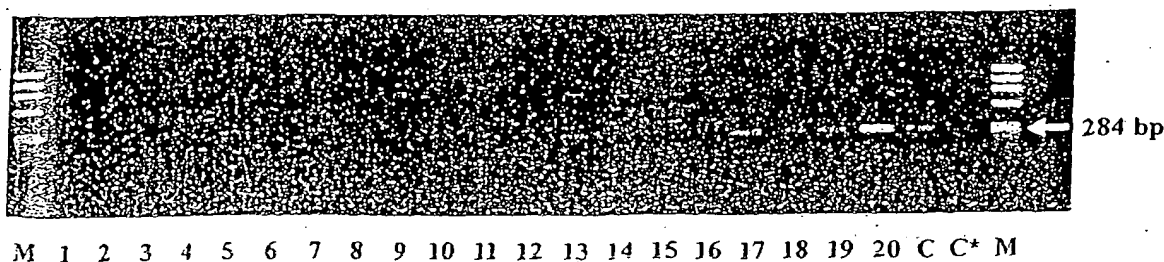


FIG. 3. Reverse transcriptase polymerase chain reaction for *sst2* mRNA in 20 control samples of nonneuroendocrine lung carcinoma. Five of 20 samples show a weak band at 284 bp corresponding to *sst2* mRNA. Control columns (C and C*) are identical to those in Fig. 2.

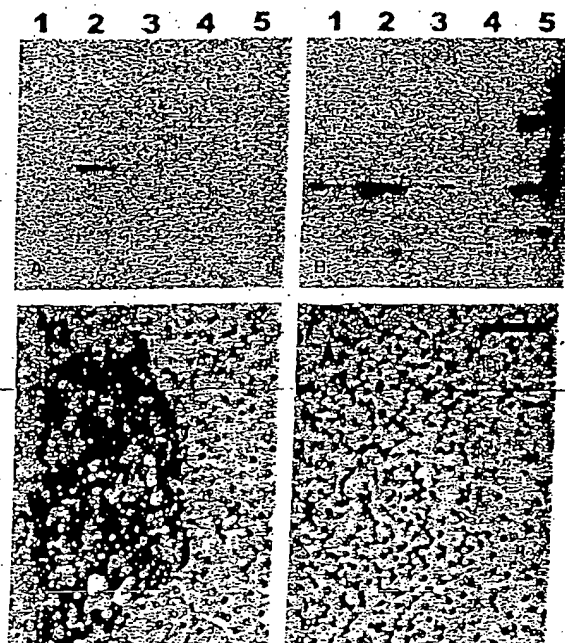


FIG. 4. Western blot analysis of monoclonal antibody clones 10G4 and 10C6 against sst2 in Chinese hamster ovary cells transfected with recombinant sst 1 through 5 (numbers of each column correspond to receptor type). Monoclonal antibody 10G4 shows a specific band at approximately 70 kD for sst2 only (A) as opposed to monoclonal antibody 10C6, which strongly reacts with sst2 but also has some degrees of cross-reactivity with sst 1, 3, and 5 (B). The lower figures show control formalin-fixed paraffin-embedded pancreatic islets immunostained with monoclonal antibody 10G4 without (C) and with (D) preadsorption with the peptide antigen, respectively. The majority of endocrine cells show a membrane-bound immunoreactivity (C) (immunoperoxidase). Bar: 90 µm.

ing present in 40% to 70% of neoplastic cells. A weak and focal staining was also observed in five of the remaining RT-PCR-negative samples, when the antibody K230 was used (but not when the monoclonal was employed).

Several cells in peritumoral tissues were occasionally stained. Ciliated cells of bronchial mucosa had a peripheral staining at the cilia border. Mucous glands were negative. Rare chondrocytes had a membrane staining. The wall of peritumoral as well as of occasional distant vessels was stained at the endothelium level and in occasional smooth muscle cells.

The reactivity of both antibodies was abolished in serial sections when the reagents were preabsorbed with the respective synthetic peptides, but not when an unrelated peptide was used. The peritumoral bronchial mucosa had a focal staining of ciliated cells with both antibodies. This reactivity disappeared when the preabsorbed antibody was applied.

In Situ Hybridization

Eight of 12 samples stained by ISH were positive for sst2 mRNA. The mRNA was present in a percentage of cells (ranging from 10% to 40%) and gave a weak signal (Fig. 8), despite the amplification provided by the tyramide-based procedure. The background level was minimal using diluted biotinylated tyramide. Control sections stained with sense probe or an unrelated probe, or omitting the probe, were consistently negative.

Clinical Data

Clinicopathologic data are summarized in Table 2. At follow-up, the majority of patients with typical carcinoids are free from disease 1 to 11 years after surgery. Two patients are alive with stable metastatic disease. Patients affected by atypical carcinoids had disease progression in one third of samples. Finally, patients with SCC had fatal outcomes within 1 year from diagnosis (except the recent sample). Eight patients had preoperative octreotide scintigraphy performed at the time of diagnosis. All patients had positive octreoscan findings, and, in these patients, also the tumor was positive by RT-PCR and immu-



FIG. 5. sample no. 25 (small cell carcinoma). Absence of immunoreactivity for sst2 with the monoclonal 10G4. This sample was also negative by reverse transcriptase polymerase chain reaction and in situ hybridization. (Immunoperoxidase in a formalin-fixed paraffin-embedded sample. Nuclei slightly counterstained with hemalum.) Bar: 45 µm.

nohistochemistry or ISH. In addition, three of these patients received octreotide therapy administered at the time of tumor recurrence or metastatic spread. Stable disease is recorded at follow-up more than 5 years after diagnosis.

Correlations

Overall, complete overlapping (i.e., RT-PCR, ISH, and immunohistochemistry with two antibodies) between *sst2* gene and protein expression was obtained in 21 of 25 samples (84%) and between RT-PCR results and immunohistochemical findings with at least one of the antibodies in 24 of 25 samples (96%). The monoclonal antibody 10G4 looked highly sensitive, being able to stain all but one sample (no. 26) (95%) positive for *sst2* mRNA by RT-PCR. *Sst2* expression, at mRNA as well as at protein levels, was reduced in high grade tumors, with SCCs being weakly positive in only two of five samples. Decreasing expression of *sst2* appears to cor-



FIG. 6. sample no. 16 (typical carcinoid). Immunohistochemical detection of *sst2* by means of monoclonal antibody 10G4. The neoplastic cells have a peripheral cytoplasmic staining and membrane positivity in some cells, whereas the peribronchial gland adjacent to the tumor is unreactive. (Immunoperoxidase in a formalin-fixed paraffin-embedded sample. Nuclei slightly counterstained with hemalum.) Bar: 45 μ m. The membrane-bound distribution of the immunostaining is better outlined in a parallel section stained for monoclonal antibody 10G4 omitting nuclear counterstain (inset).



FIG. 7. Same sample as in Fig. 6. Immunohistochemical detection of *sst2* by means of the polyclonal antibody K230. The immunostaining is more intense at the cell border (arrows), as observed with the monoclonal antibody. In the inset, a pancreatic islet, used as positive control, shows a predominant membrane-bound immunostaining of many neuroendocrine cells. (Immunoperoxidase in a formalin-fixed paraffin-embedded sample. Nuclei slightly counterstained with hemalum.) Bar: 45 μ m.

relate with high tumor grade and elevated proliferative activity, but not with other parameters such sex, age, or tumor size.

DISCUSSION

In this study, the presence of *sst2* mRNA has been demonstrated in a series of resected neuroendocrine tumors of the lung by means of RT-PCR and confirmed by a sensitive nonradioactive tyramide-based ISH procedure and by immunohistochemistry with anti-*sst2* antibodies. Samples of both carcinoid tumors and SCCs were *sst2* positive, although a reduced or absent signal was observed in poorly differentiated (small-cell) carcinomas. This is the first study of *sst2* expression in a relatively large series of neuroendocrine tumors of the lung. Single samples of human carcinoids and SCCs (including cell lines of the latter) had previously been analyzed and found to express *sst2* (7,15,30,32,33,39,42). Several methods have been used to detect these receptors and partially overlapping results were obtained.

In the present study, the expression of high amounts of

TABLE 2. Clinicopathologic data and somatostatin receptor type 2 (sst2) expression in 26 cases of neuroendocrine lung tumors

Patient no.	Diagnosis	Sex/age	Size (cm)	Follow-up (mo)	CgA IHC	CgA RT-PCR	SYP IHC	Ki67 IHC*	sst2 RT-PCR	sst2 IHC Mab(10G4)	sst2 IHC (K230 Ab)
1	WD NET	F/35	3.5	NED 90	+	+++	+ F	1.5	+++	+	+
2	WD NET	F/29	4	NED 45	+	++	+ F	3	++	+	+
3	WD NET	F/41	2.5	NED 70	+	++	+	0.1	+++	+	+ F
4	WD NET†	F/25	4	NED 21	+	++	+	2.6	+++	+ F	+ F
5	WD NET†	M/58	3.8	NED 23	+	+++	+	13	+++	+ F	+
6	WD NET	M/52	2.5	NED 42	+	++	+	4.5	+++	+ F	+ F
7	WD NET	F/69	3.5	NED 47	+	++	+	1	+	+	+
8	WD NET	M/29	3	NED 70	+	+++	+	1.5	+++	+	+
9	WD NET	M/27	4	NED 108	+	+++	+	NT	+++	+	+
10	WD NE Ca†	M/66	8	AWD 55	+	++	+ F	1.1	++	+ F	+
11	WD NET†	F/29	2	AWD 56	+	+++	+	2.5	+++	+	+
12	WD NET*	F/32	3	NED 26	+	++	+	4	+++	+	+
13	WD NE Ca	M/60	3	NED 133	+	+++	+	1	+++	NT	NT
14	WD NET	M/28	4	NED 130	+	+++	+	1	+++	+	+
15	WD NET†	M/41	1.3	AWD 53	+	+++	+	1.5	+++	+	+
16	WD NET†	F/31	1	NED 13	+	++	++	2.6	+	+	+
17	WD NET	F/53	4	NED 24	+	+++	+ F	4	+++	+ F	+
18	WD NE Ca	M/62	3	NED 6	-	++	-	13	+++	+	+ F
19	WD NE CA	F/73	5	DOD 20	+	+++	+	3	++	+	-
20	SCC	M/57	6	DOD 12	+	++	+	45	+	+ F	+ F
21	SCC	M/51	4.5	DOD 5	+	+	+	35	-	+ F	+ F
22	WD NE Ca	M/60	6	NED 51	+	++	+	1.5	-	-	+
23	SCC	F/56	6	DOD 11	+	+	+	50	-	-	-
24	WD NE Ca	M/77	2.5	NED 21	+	+	+	24	+	+ F	+ F
25	SCC	M/57	5	DOD 10	+	++	++	80	-	-	-
26	SCC†	M/68	.11	recent case	+	+	++	71	+	-	-

AWD, alive with disease; CgA, chromogranin A; DOD, died of disease; + F, focal; positive in <5% of cells; IHC, immunohistochemistry; Mab, monoclonal antibody; NECa, Neuroendocrine carcinoma; NED, no evidence of disease; NET, neuroendocrine tumor; NT, not tested; RT-PCR, reverse transcriptase polymerase chain reaction; SCC, Small-cell lung carcinoma; SYP, synaptophysin; WD, well differentiated.

* Ki67 IHC: values correspond to percentage of positive nuclei of neoplastic cells.

† Patients who had preoperative octreoscan performed.

‡ Patients who had octreoscan performed and octreotide treatment.

sst2 mRNA was confirmed in well to moderately differentiated neuroendocrine tumors, in agreement with the results obtained by Reubi et al. (32) by means of radioactive ISH. The presence of sst2 mRNA in SCC had never been reported in human specimens, except for two samples included in Reubi et al.'s series (32). Although the data on cell lines support the observation that SCCs contain sst2 (42), slightly discrepant results were found in some of samples described here. Unfortunately, SCCs are rarely operated on, and therefore it is difficult to collect a large number of surgical specimens. The five samples studied in the current series by means of RT-PCR had a low amount (two samples) or absent (three samples) sst2 mRNA. This could be the result of the extensive necrosis commonly present in such tumor types. However, because care was taken to freeze fragments that were macroscopically devoid of necrotic areas, a more likely hypothesis is that sst2 expression is reduced in poorly differentiated tumors. Recently, Reisinger et al. (29) showed that the uptake of somatostatin analogues in patients with SCC undergoing chemotherapy is significantly lower, and therapeutic external factors may affect the receptor status of individual tumors. In addition, the uptake of somatostatin analogues

in metastatic deposits of SCC has been shown to be low or absent (29,2). The present findings suggest that the sst2 mRNA content is related to the degree of tumor differentiation. These data must be confirmed in larger series of nonneuroendocrine tumors to ascertain whether the observed loss or decrease of sst2 expression in neuroendocrine tumors is a common event linked to neoplastic dedifferentiation. In addition, further studies are needed to assess the functionality of such receptors, by comparing the profile of sst2 expression in tumor tissues with binding assays employing labeled somatostatin and with the clinical response to diagnostic and therapeutic administration of somatostatin analogues.

To this purpose, several investigators have demonstrated a correlation between clinical imaging or response to somatostatin analogue treatment and sst2 mRNA content in single samples of carcinoid tumors (15,22). Northern blotting and ISH were the techniques used for sst2 mRNA identification. This kind of correlation is useful for selecting patients for somatostatin analogue treatment, although the demonstration of receptor mRNA in a cell does not imply per se that the receptor is fully functional.

The present study relied on a highly sensitive tech-

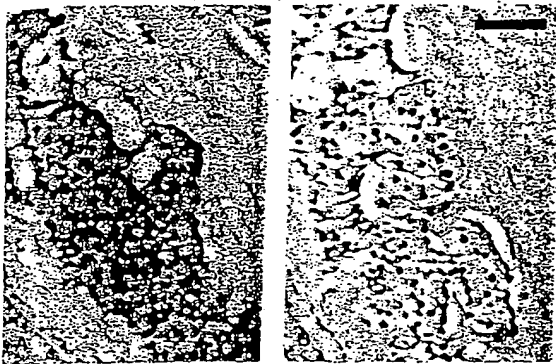


FIG. 8. sample no. 11 (typical carcinoid). In situ hybridization (ISH) for sst2 mRNA shows a weak cytoplasmic staining (A) in most tumor cells. An ISH performed with an unrelated probe was negative in a serial section of the same tumor (B). This sample was strongly positive by reverse transcriptase polymerase chain reaction for sst2 mRNA and by immunohistochemistry. (Nonradioactive ISH revealed by peroxidase and diaminobenzidine, as substrate. Nuclei counterstained with hemalum.) Bar: 75 μ m.

nique, RT-PCR, to identify all samples bearing even small amounts of sst2 mRNA. Indeed, in a previous study, single samples exhibiting octreotide-binding sites had no demonstrable sst2 mRNA by means of ISH, possibly due to the low sensitivity of the ISH procedure (34). The RT-PCR has shown sst2 mRNA transcripts in the majority of samples here studied. Only four samples were negative, all belonging to poorly differentiated high grade tumors, which usually follow an aggressive course. A decrease of sst2 mRNA expression in association with neuroendocrine tumor dedifferentiation had also been reported in neuroblastomas (37). In the above report, as well as in the current study, samples having an unfavorable prognosis were found to contain a relatively low amount of sst2 mRNA, as compared with well-differentiated tumors.

In the current sample series, eight samples were investigated before surgery with radiolabeled octreotide. Despite the low figures, all the samples positive at the diagnostic procedure had a strong RT-PCR signal for sst2 mRNA. Three of eight patients were also responsive to octreotide treatment administered at the time of relapse or metastatic spread. More extensive correlative clinicopathologic studies on the sst status are needed to better define the tissue distribution of somatostatin binding sites and their potential clinical role in the treatment of patients.

Sst2 evaluation by means of ISH (14,32) or RT-PCR (26,37) is a highly sensitive and reliable procedure. Unfortunately, these techniques have limitations because frozen tissue is needed for some of them, and radioactive material or costly and time-consuming methods are nec-

essary for others. Immunohistochemical analysis of sst2 by means of specific antibodies represents an ideal, cheap, and rapid alternative, easily applicable to archival material. For these reasons, several investigators have raised polyclonal antibodies specific for sst (8,10,15,17, 18). In the current study, tested tumor fragments adjacent to those snap frozen for RT-PCR analysis were tested with a polyclonal antibody against a C-terminal portion of the sst2A splice variant (35,36). In addition, a monoclonal antibody was produced in the Department of Pathology (University of Turin) against an N-terminal sequence of the human sst2. This antibody was the first monoclonal developed against sst2 and was shown to be highly specific for sst2 in Western blot and immunohistochemical analysis. Both the monoclonal and the polyclonal antibodies specifically reacted with all samples also positive by RT-PCR (with minor discrepancies in two samples, likely due to tumor heterogeneity). The observed correlation between RT-PCR and immunohistochemistry indicates that the latter may be a reliable diagnostic tool and may allow immunohistochemical investigation for sst2 even in small biopsy samples. This in turn may enable a rapid screening of sst2-positive tumors for medical treatment with somatostatin analogues.

Having confirmed in a relatively large series that the vast majority of neuroendocrine tumors of the lung contain variable amounts of sst2 mRNA, a final comment is deserved for sst2 expression in nonneuroendocrine lung carcinomas. No data have been reported thus far in the literature concerning normal human lung, although in the present study some bronchial cells of peritumoral parenchyma were positive for sst2 when immunohistochemical analysis was performed with either antibody. The staining was specific because it was abolished using preabsorbed antibodies. Therefore, it is likely that normal human lung tissue contains sst2. This might be confirmed by alternative techniques (e.g., Western blot, RT-PCR). However, *in situ* morphologic procedures, such as those employed here, have definite advantages. In fact, the lung is rich in vessels, and in several tissues (either in tumoral or in inflammatory-reactive conditions) the vessels were recently shown to contain sst (6).

A low expression of sst2 was found in 25% of lung carcinomas of nonneuroendocrine type investigated in the present study by means of RT-PCR. Therefore, sst type 2, at least, does not appear to be extensively expressed in nonneuroendocrine carcinomas of the lung. However, because two tumors in the control group (a squamous carcinoma and an adenocarcinoma, respectively) had positive octreotide scintigraphy, but no sst2 mRNA, it is plausible that a heterogeneous distribution of sst occurs in nonneuroendocrine lung tumors. Other receptor types may be expressed in these tumors and may be responsible for the positive results in diagnostic testing. Because sst5 is also known to bind somatostatin

analogues, such as octreotide, with high affinity (24), the expression of this receptor type will be investigated in future studies. □

Acknowledgments: The authors are grateful to Dr. P.L. Filosso (Turin) for clinical data, to Mrs. M. Cerrato and Miss S. Solero for skilful technical help, and to Mr. A. Grua for the photographs.

REFERENCES

1. Abbona GC, Papotti M, Viberli L, Macri L, Stella A, Bussolati G. Chromogranin A gene expression in non-small cell lung carcinomas. *J Pathol* 1998;186:1-6.
2. Berenger N, Moretti JL, Boaziz C, Vigneron N, Morete JF, Breau JL. Somatostatin receptor imaging in small cell lung cancer. *Eur J Cancer* 1996;32:1429-31.
3. Bussolati G, Guglionia P, Volante M, Pace M, Papotti M. Retrieved endogenous biotin: a novel marker and potential pitfall in diagnostic immunohistochemistry. *Histopathology* 1997;31:400-7.
4. Capella C, Heitz PU, Hoffer H, Solcia E, Kloppel G. Revised classification of neuroendocrine tumors of the lung, pancreas and gut. *Virchows Arch* 1995;425:547-60.
5. Chirgwin JM, Przybyla AE, MacDonald RJ, Rutter W. Isolation of biologically active RNA from sources enriched in ribonuclease. *Biochemistry* 1979;18:5294-7.
6. Denzler B, Reubi JC. Expression of somatostatin receptors in peritumoral veins of human tumors. *Cancer* 1999;85:189-98.
7. Fujita T, Yamaji Y, Sato M, Murao K, Takahara J. Gene expression of somatostatin receptor subtypes, SSTR1 and SSTR2, in human lung cancer cell lines. *Life Sci* 1994;55:1797-806.
8. Gu WZ, Schonbrunn A. Coupling specificity between somatostatin receptor sst2A and G proteins: isolation of the receptor-G protein complex with a receptor antibody. *Mol Endocrinol* 1997;11:527-37.
9. Gussow D, Rein R, Ginjaar I, Hochstenbach F, Seemann G, Kottman A, Ploegh HL. The human beta 2-microglobulin gene: primary structure and definition of the transcriptional unit. *J Immunol* 1987;139:3132-8.
10. Helboe L, Moller M, Nonnegard L, Schiodt M, Sudsen CE. Development of selective antibodies against the human somatostatin receptor subtypes sst1-sst5. *Brain Res Mol Brain Res* 1997;49:82-8.
11. Helman JJ, Ahn TG, Levine MA, et al. Molecular cloning and primary structure of human chromogranin A (secretory protein I) cDNA. *J Biol Chem* 1988;263:11559-63.
12. Hofland LJ, Liu Q, Van Koetsveld PM, et al. Immunohistochemical detection of somatostatin receptor subtypes sst1 and sst2A in human somatostatin receptor positive tumors. *J Clin Endocrinol Metab* 1999;84:775-80.
13. Hsu SM, Raine L, Fanger H. Use of avidin-peroxidase complex (ABC) in immunoperoxidase techniques: comparison between ABC and unlabelled antibody (PAP) procedures. *J Histochem Cytochem* 1981;29:577-80.
14. Janson ET, Gobl A, Kalkne KM, Oberg K. A comparison between the efficacy of somatostatin receptor scintigraphy and that of in situ hybridization for somatostatin receptor subtype 2 messenger RNA to predict therapeutic outcome in carcinoid patients. *Cancer Res* 1996;56:2561-5.
15. Janson ET, Svendsberg M, Gobl A, Westlin JE, Oberg K. Determination of somatostatin receptors subtype 2 in carcinoid tumors by immunohistochemical investigation with somatostatin receptor subtype 2 antibodies. *Cancer Res* 1998;58:2375-8.
16. Kerstens HJM, Poddighe PJ, Hanselaar AGJM. A novel in situ hybridization signal amplification method based on the deposition of biotinylated tyramine. *J Histochem Cytochem* 1995;43:347-52.
17. Krisch B, Feindt J, Mentlein R. Immunoelectronmicroscopic analysis of the ligand-induced internalization of the somatostatin receptor subtype 2 in cultured human glioma cells. *J Histochem Cytochem* 1998;46:1233-42.
18. Kumar U, Laird D, Srikanth CB, Escher E, Patel YC. Expression of the five somatostatin receptors (SSTR1-5) subtypes in rat pituitary somatotrophs: quantitative analysis by double-label immunofluorescence confocal microscopy. *Endocrinology* 1997;138:4473-6.
19. Kwok S, Higuchi R. Avoiding false positives with PCR. *Nature* 1989;339:237-8.
20. Lambert SWJ, Hofland LJ, Koetsveld PM, Reubi JC, Bruining HA, Bakker WH, Krenning EP. Parallel in vivo and in vitro detection of functional somatostatin receptors in human endocrine pancreatic tumors: consequences with regard to diagnosis, localization and therapy. *J Clin Endocrinol Metab* 1990;71:566-74.
21. Malavasi F, Funaro A, Bellone G, et al. Functional and molecular characterization by the CB04 monoclonal antibody of a cell surface structure exerting C3-complement receptor activity. *J Clin Immunol* 1985;5:412-20.
22. Nilsson O, Kolby L, Wangberg B, et al. Comparative studies on the expression of somatostatin receptor subtypes, outcome of octreotide scintigraphy and response to octreotide treatment in patients with carcinoid tumours. *Br J Cancer* 1998;77:632-7.
23. Pagani A, Forai M, Tonini GP, Papotti M, Bussolati G. Expression of members of the chromogranin family in primary neuroblastomas. *Diagn Mol Pathol* 1992;1:16-24.
24. Panetta R, Greenwood MT, Warszynska A, et al. Molecular cloning, functional characterization and chromosomal localization of a human somatostatin receptor (somatostatin receptor type 5) with preferential affinity for somatostatin-28. *Mol Pharmacol* 1994;45:417-27.
25. Papotti M, Macri L, Bussolati G, Reubi JC. Correlative study on neuroendocrine differentiation and presence of somatostatin receptors in breast carcinomas. *Int J Cancer* 1989;43:365-9.
26. Papotti M, Macri L, Pagani A, Aloj F, Bussolati G. Quantitation of somatostatin receptor type 2 in neuroendocrine (Merkel cell) carcinoma of the skin by competitive RT-PCR. *Endocr Pathol* 1999;10:1-10.
27. Patel YC, Panetta R, Escher E, Greenwood M, Srikanth CB. Expression of multiple somatostatin receptor genes in AIT-20 cells: evidence for a novel somatostatin-28 selective receptor subtype. *J Biol Chem* 1994;269:1506-9.
28. Pearson WR, Lipman DJ. Improved tools for biological sequence comparison. *Proc Natl Acad Sci U S A* 1988;85:2444-8.
29. Reisinger I, Bohuslavizki KH, Brenner W, et al. Somatostatin receptor scintigraphy in small-cell lung cancer: results of a multicenter study. *J Nucl Med* 1998;39:224-7.
30. Reubi JC, Kappeler A, Waser B, Laissue J, Hipkin RW, Schonbrunn A. Immunohistochemical localization of somatostatin receptors sst2A in human tumors. *Am J Pathol* 1998;153:253-45.
31. Reubi JC, Maurer R, von Werder K, Torhorst J, Kljij JGM, Lambert SWJ. Somatostatin receptors in human endocrine tumors. *Cancer Res* 1987;47:551-8.
32. Reubi JC, Schaefer JC, Waser B, Mengod G. Expression and localization of somatostatin receptors SSTR1, SSTR2, SSTR3 messenger RNA in primary human tumors using in situ hybridisation. *Cancer Res* 1994;54:3455-9.
33. Reubi JC, Waser B, Sheppard M, Macaulay V. Somatostatin receptors are present in small-cell but not in non-small-cell primary lung carcinomas: relationship to EGF receptors. *Int J Cancer* 1990;45:269-74.
34. Schaefer JC, Waser B, Mengod G, Reubi JC. Somatostatin receptors subtypes sst1, sst2, sst3 and sst5 expression in human pituitary, gastroentero-pancreatic and mammary tumors: comparison of mRNA analysis with receptor autoradiography. *Int J Cancer* 1997;70:530-7.
35. Schindler M, Holloway S, Humphrey PPA, Waldvogel H, Faull RLM, Berger W, Emson PC. Localization of the somatostatin sst2a receptor in human cerebral cortex, hippocampus and cerebellum. *Neuroreport* 1998;9:521-5.
36. Schindler M, Sellers LA, Humphrey PPA, Emson PC. Immunohistochemical localization of the somatostatin sst2(A) receptor in the rat brain and spinal cord. *Neuroscience* 1997;76:225-40.
37. Sestini R, Orlando C, Peri A, et al. Quantification of somatostatin

- receptor type 2 gene expression in neuroblastoma cell lines and primary tumors using competitive reverse transcription-polymerase chain reaction. *Clin Cancer Res* 1996;2:1757-65.
38. Speel EJM, Saremaslani P, Roth J, Hopman AHN, Komminoth P. Improved mRNA in situ hybridization on formaldehyde-fixed and paraffin-embedded tissue using signal amplification with different baptenized tyramides. *Histochem Cell Biol* 1998;420:1-7.
39. Taylor JE, Theveniau MA, Bashirzadeh R, Reisine T, Eden PA. Detection of somatostatin receptor subtype 2 (SSTR2) in established tumors and tumor cell lines: evidence for sst2 heterogeneity. *Peptides* 1994;15:1229-36.
40. Travis WD, Gal AA, Colby TV, Klimstra DS, Falk R, Koss MN. Reproducibility of neuroendocrine lung tumor classification. *Hum Pathol* 1998;29:272-9.
41. Yamada Y, Post SR, Wang K, Tager H, Bell GI, Seino S. Cloning and functional characterization of a family of human and mouse somatostatin receptors expressed in brain, gastrointestinal tract and kidney. *Biochemistry* 1992;89:251-5.
42. Zhang CY, Yokogoshi Y, Yoshimoto K, Fujinaka Y, Matsumoto K, Saito S. Point mutation of the somatostatin receptor 2 gene in the human small cell lung cancer cell line COR-L103. *Biochem Biophys Res Commun* 1995;210:805-15.



P-cadherin overexpression is an indicator of clinical outcome in invasive breast carcinomas and is associated with CDH3 promoter hypomethylation.

Paredes J, Albergaria A, Oliveira JT, Jeronimo C, Milanezi F, Schmitt FC.

Institute of Pathology and Molecular Immunology of Porto University (IPATIMUP), Braga, Portugal. jparedes@ipatimup.pt

PURPOSE: P-cadherin overexpression has been reported in breast carcinomas, where it was associated with proliferative high-grade histological tumors. This study aimed to analyze P-cadherin expression in invasive breast cancer and to correlate it with tumor markers, pathologic features, and patient survival. Another purpose was to evaluate the P-cadherin promoter methylation pattern as the molecular mechanism underlying this gene regulation. **EXPERIMENTAL DESIGN:** Using a series of invasive breast carcinomas, P-cadherin expression was evaluated and correlated with histologic grade, estrogen receptor, MIB-1, and p53 and c-erbB-2 expression. In order to assess whether P-cadherin expression was associated with changes in CDH3 promoter methylation, we studied the methylation status of a gene 5'-flanking region in these same carcinomas. This analysis was also done for normal tissue and for a breast cancer cell line treated with a demethylating agent. **RESULTS:** P-cadherin expression showed a strong correlation with high histologic grade, increased proliferation, c-erbB-2 and p53 expression, lack of estrogen receptor, and poor patient survival. This overexpression can be regulated by gene promoter methylation because the 5-Aza-2'-deoxycytidine treatment of MCF-7/AZ cells increased P-cadherin mRNA and protein levels. Additionally, we found that 71% of P-cadherin-negative cases showed promoter methylation, whereas 65% of positive ones were unmethylated ($P = 0.005$). The normal P-cadherin-negative breast epithelial cells showed consistent CDH3 promoter methylation. **CONCLUSIONS:** P-cadherin expression was strongly associated with tumor aggressiveness, being a good indicator of clinical outcome. Moreover, the aberrant expression of P-cadherin in breast cancer might be regulated by gene promoter hypomethylation.

PMID: 16115928 [PubMed - in process]



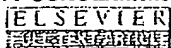
Mammary-derived growth inhibitor protein and messenger ribonucleic acid concentrations in different physiological states of the gland.

Politis I, Gorewit RC, Muller T, Grosse R.

Department of Animal Science, Cornell University, Ithaca 14853.

Expression of mammary-derived growth inhibitor in tissue from lactating and involuting bovine mammary glands was investigated. Seventeen lactating, pregnant (220 to 272 d in gestation) cows were divided in two groups of 8 and 9 cows each. Cows of the first group were slaughtered while in lactation. Cows of the second group (9 involuting cows) were slaughtered at 13 to 52 d following sudden cessation of milking. High concentrations of mammary-derived growth inhibitor (.63% of the total protein) were detected in mammary tissue of lactating cows. Mammary-derived growth inhibitor (less than .10% of the total protein) was dramatically reduced during most of the involution period (13 to 45 d following cessation of milking). Mammary-derived growth inhibitor was again detected (.28% of the total protein) during the last stage of the involution (46 to 53 d after cessation of milking), which coincided with colostrum formation. When steady state concentrations of mammary-derived growth inhibitor mRNA were examined, the results obtained mirrored those obtained at the protein concentration. These data suggest that regulation of mammary-derived growth inhibitor occurs via modulation of the steady state concentration of its mRNA. Furthermore, there is a strong correlation between mammary-derived growth inhibitor expression and lactation in dairy cows.

PMID: 1500548 [PubMed - indexed for MEDLINE]



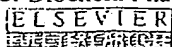
Matrilin-3 in human articular cartilage: increased expression in osteoarthritis.

Pullig O, Weseloh G, Klatt AR, Wagener R, Swoboda B.

Division of Orthopaedic Rheumatology, Department of Orthopaedics, University of Erlangen-Nuremberg, Rathsberger Str. 57, D-91054 Erlangen, Germany.
oliver.pullig@med.uni-erlangen.de

OBJECTIVE: Matrilin-3 is a member of the recently described matrilin family of extracellular matrix proteins containing von Willebrand factor A-like domains. The matrilin-3 subunit can form homo-tetramers as well as hetero-oligomers together with subunits of matrilin-1 (cartilage matrix protein). It has a restricted tissue distribution and is strongly expressed in growing skeletal tissues. Detailed information on expression and distribution of extracellular matrix proteins is important to understand cartilage function in health and in disease like osteoarthritis (OA). **METHODS:** Normal and osteoarthritic cartilage were systematically analysed for matrilin-3 expression, using immunohistochemistry, Western blot analysis, in situ hybridization, and quantitative PCR. **RESULTS:** Our results indicate that matrilin-3 is a mandatory component of mature articular cartilage with its expression being restricted to chondrocytes from the tangential zone and the upper middle cartilage zone. Osteoarthritic cartilage samples with only moderate morphological osteoarthritic degenerations have elevated levels of matrilin-3 mRNA. In parallel, we found an increased deposition of matrilin-3 protein in the cartilage matrix. Matrilin-3 staining was diffusely distributed in the cartilage matrix, with no cellular staining being detectable. In cartilage samples with minor osteoarthritic lesions, matrilin-3 deposition was restricted to the middle zone and to the upper deep zone. A strong correlation was found between enhanced matrilin-3 gene and protein expression and the extent of tissue damage. Sections with severe osteoarthritic degeneration showed the highest amount of matrilin-3 mRNA, strong signals in in situ hybridization, and prominent protein deposition in the middle and deep cartilage zone. **CONCLUSION:** We conclude that matrilin-3 is an integral component of human articular cartilage matrix and that the enhanced expression of matrilin-3 in OA may be a cellular response to the modified microenvironment in the disease. Copyright 2002 OsteoArthritis Research Society International.

PMID: 11950247 [PubMed - indexed for MEDLINE]



Up-regulation of mitochondrial peripheral benzodiazepine receptor expression by tumor necrosis factor alpha in testicular leydig cells. Possible involvement in cell survival.

Rey C, Mauduit C, Naureils O, Benahmed M, Louisot P, Gasnier F.

INSERM U. 189, Faculte de Medecine Lyon-Sud, BP12, 69921 cedex, Oullins, France.

Porcine Leydig cells in primary cultures are resistant to tumor necrosis factor alpha (TNFalpha) cytotoxicity. Here we report that these cells can be rendered sensitive to TNFalpha killing by treatment with the translational inhibitor cycloheximide, suggesting the existence of proteins that can suppress the death stimulus induced by the cytokine. In search of these cytoprotective proteins, we focused on the constituents of the mitochondrial permeability transition pore (PT pore), whose opening has been shown to play a critical role in the TNFalpha-mediated death pathway. We found that TNFalpha up-regulated mRNA and protein expression of the mitochondrial peripheral benzodiazepine receptor (PBR), an outer membrane-derived constituent of the pore. A strong correlation was established between the resistance of the cells to TNFalpha killing and the density of PBR-binding sites. Concomitantly, TNFalpha down-regulated Bcl-2 mRNA and protein expression. As Bcl-2 has been shown to be an endogenous inhibitor of the PT pore, we hypothesize that the TNFalpha-induced up-regulation of PBR expression may compensate for the decrease in Bcl-2 levels to prevent the opening of the PT pore.

PMID: 11077046 [PubMed - indexed for MEDLINE]

MetaPress

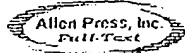
GLUT1 messenger RNA and protein induction relates to the malignant transformation of cervical cancer.

Rudlowski C, Becker AJ, Schroder W, Rath W, Buttner R, Moser M.

Dept of Gynecology and Obstetrics, University Hospital Heidelberg, Vossstr 7-9, D-69115 Heidelberg, Germany.

We studied whether induction of glucose transporters (GLUTs) 1 to 4 correlates with human papillomavirus (HPV)-dependent malignant transformation of cervical epithelium. Tissue samples of cervical intraepithelial neoplasia (CIN; grades 1 to 3), invasive carcinomas, and lymph node metastasis were examined. HPV typing was performed. Tissue sections were immunostained with GLUT1 to GLUT4 antibodies. Messenger RNA (mRNA) in situ hybridization confirmed GLUT1 protein expression. Weak expression of GLUT1 was found in nondysplastic HPV-positive and HPV-negative epithelium; significant expression was observed in preneoplastic lesions, correlating with the degree of dysplasia. In CIN 3 high-risk HPV lesions, cervical cancer, and metastasis, GLUT1 was expressed at highest levels with a strong correlation of GLUT1 mRNA and protein expression. Immunostains for GLUT2 to GLUT4 were negative. Cervical tumor cells respond to enhanced glucose utilization by up-regulation of GLUT1. The strong induction of GLUT1 mRNA and protein in HPV-positive CIN 3 lesions suggests GLUT1 overexpression as an early event in cervical neoplasia. GLUT1 is potentially relevant as a diagnostic tool and glucose metabolism as a therapeutic target in cervical cancer.

PMID: 14608894 [PubMed - indexed for MEDLINE]



UVA irradiation-induced activation of activator protein-1 is correlated with induced expression of AP-1 family members in the human keratinocyte cell line HaCaT.

Silvers AL, Bowden GT.

Department of Radiation Oncology, Arizona Cancer Center, The University of Arizona, Tucson 85724, USA.

To determine whether the transcription factor activator protein-1 (AP-1) could be modulated by ultraviolet A (UVA) exposure, we examined AP-1 DNA-binding activity and transactivation after exposure to UVA in the human immortalized keratinocyte cell line HaCaT. Maximal AP-1 transactivation was observed with 250 kJ/m² UVA between 3 and 4 h after irradiation. DNA binding of AP-1 to the target 12-O-tetradecanoylphorbol-13-acetate response element sequence was maximally induced 1-3 h after irradiation. Both de novo transcription and translation contributed to the UVA-induced AP-1 DNA binding. c-Fos was implicated as a primary component of the AP-1 DNA-binding complex. Other components of the complex included Fra-2, c-Jun, JunB and JunD. UVA irradiation induced protein expression of c-Fos, c-Jun, Fra-1 and Fra-2. Phosphorylated forms of these induced proteins were determined at specific time points. A strong correlation existed between UVA-induced AP-1 activity and accumulation of c-Fos, c-Jun and Fra-1 proteins. UVA irradiation also induced c-fos and c-jun mRNA expression and transcriptional activation of the c-fos gene promoter. These results demonstrate that UVA irradiation activates AP-1 and that c-fos induction may play a critical role in the response of these human keratinocytes to UVA irradiation.

PMID: 11950097 [PubMed - indexed for MEDLINE]

Tumor necrosis factor-alpha upregulates the prostaglandin E2 EP1 receptor subtype and the cyclooxygenase-2 isoform in cultured amnion WISH cells.

Spaziani EP, Benoit RR, Tsibris JC, Gould SF, O'Brien WF.

University of South Florida Health Science Center, Department of Obstetrics & Gynecology, Tampa 33612, USA. espazian@com1.med.usf.edu

Recent studies have demonstrated a strong correlation between infection and preterm labor. Preterm delivery is also associated with high levels of cytokines and prostaglandins in amniotic fluid. The purpose of this study was to investigate the effect of tumor necrosis factor-alpha (TNF-alpha) on the levels of cyclooxygenase, prostaglandin E2 production (PGE2), and expression of the PGE2 receptor subtype EP1 in amnion WISH cell culture. Amnion WISH cell cultures were incubated in increasing concentrations of TNF-alpha (0-50 ng/ml). Changes in cyclooxygenase and EP1 receptor proteins were evaluated by Western blot analysis. Changes in EP1 mRNA were evaluated by Northern blot, and culture fluid concentrations of PGE2 were estimated by enzyme immunoassay (EIA). EP1 protein ($p < 0.01$), EP1 mRNA ($p < 0.05$), cyclooxygenase-2 (COX-2) protein ($p < 0.001$), and PGE2 concentrations ($p < 0.01$) all increased with increasing concentrations of TNF-alpha. Changes in COX-1 protein were not observed following TNF-alpha-incubation. The results suggest that TNF-alpha may play a role in infection-induced preterm labor by its pleiotropic ability to simultaneously stimulate COX-2 activity, PGE2 concentrations, and PGE2 EP1 receptor levels in human amnion.

PMID: 9877447 [PubMed - indexed for MEDLINE]



Specific inhibition of AQP1 water channels in isolated rat intrahepatic bile duct units by small interfering RNAs.

Splinter PL, Masyuk AI, LaRusso NF.

Center for Basic Research in Digestive Diseases, Division of Gastroenterology and Hepatology, Mayo Medical School, Clinic, and Foundation, Rochester, Minnesota 55905, USA.

Cholangiocytes express water channels (i.e. aquaporins (AQPs)), proteins that are increasingly recognized as important in water transport by biliary epithelia. However, direct functional studies demonstrating AQP-mediated water transport in cholangiocytes are limited, in part because of the lack of specific AQP inhibitors. To address this issue, we designed, synthesized, and utilized small interfering RNAs (siRNAs) selective for AQP1 and investigated their effectiveness in altering AQP1-mediated water transport in intrahepatic bile duct units (IBDUs) isolated from rat liver. Twenty-four hours after transfection of IBDUs with siRNAs targeting two different regions of the AQP1 transcript, both AQP1 mRNA and protein expression were inhibited by 76.6-92.0 and 57.9-79.4%, respectively. siRNAs containing the same percent of base pairs as the AQP1-siRNAs but in random sequence (i.e. scrambled siRNAs) had no effect. Suppression of AQP1 expression in cholangiocytes resulted in a decrease in water transport by IBDUs in response to both an inward osmotic gradient (200 mosm) or a secretory agonist (forskolin), the osmotic water permeability coefficient ($P(f)$) decreasing up to 58.8% and net water secretion ($J(v)$) decreasing up to 87%. A strong correlation between AQP1 protein expression and water transport in IBDUs transfected with AQP1-siRNAs was consistent with the decrease in water transport by IBDUs resulting from AQP1 gene silencing by AQP1-siRNAs. This study is the first to demonstrate the feasibility of utilizing siRNAs to specifically reduce the expression of AQPs in epithelial cells and provides direct evidence of the contribution of AQP1 to water transport by biliary epithelia.

PMID: 12468529 [PubMed - indexed for MEDLINE]

Type IV collagenase (M(r) 72,000) expression in human prostate: benign and malignant tissue.

Stearns ME, Wang M.

Department of Pathology, Medical College of Pennsylvania, Philadelphia 19129.

The expression of type IV collagenase (M(r) 72,000) has been examined in tissues from patients with benign prostatic hyperplasia (6 patients) and varying Gleason grades of malignant prostate cancer (18 patients). Immunoperoxidase labeling indicated that expression of the type IV collagenase was weak or nonexistent in benign tissue but consistently strong in the glandular and ductal epithelial cells of prostate tumors diagnosed at Gleason grades 1-8. In moderate to advanced cancer (i.e., Gleason grades 2 to 8), invasive tumor foci in the stromal tissue produced relatively modest amounts of type IV collagenase. The normal stromal tissue (i.e., fibroblasts) uniformly failed to produce detectable levels of type IV collagenase in the 24 patients examined. Northern and quantitative slot blot hybridization assays demonstrated that collagenase type IV mRNA levels were low in benign tissue and high in malignant tumors. In contrast, the stromal cells did not express significant amounts of type IV collagenase mRNA. Enzyme-linked immunosorbent assays demonstrated that the amounts of type IV collagenase protein correlated directly with the mRNA levels in the tumor tissue. The studies suggest that type IV collagenase may be selectively overexpressed by malignant, preinvasive prostatic epithelial cells.

PMID: 7679051 [PubMed - indexed for MEDLINE]

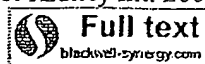
TNF-alpha and IL-8 are upregulated in the epidermis of normal human skin after UVB exposure: correlation with neutrophil accumulation and E-selectin expression.

Strickland I, Rhodes LE, Flanagan BF, Friedmann PS.

Department of Dermatology, University of Liverpool, United Kingdom.

The in vivo response to ultraviolet B (UVB) radiation in skin is characterized by the accumulation of both mononuclear and polymorphonuclear cells within the dermis and an induction of vascular endothelial adhesion molecules. Epidermal production of cytokines (IL-8 and TNF-alpha) has been strongly implicated in the development of UVB-induced inflammation. In the current study, we examined the time course of IL-8 and TNF-alpha mRNA and protein expression in the epidermis over a 24-h period after in vivo UVB irradiation. Also, the induction of adhesion molecule expression and the accumulation of neutrophils within the dermis were followed. We found constitutive expression of both cytokines (mRNA and protein) in the epidermis of unirradiated skin. IL-8 was rapidly upregulated after irradiation and mRNA and protein increased at 4 h, reaching a maximum between 8 and 24 h. TNF-alpha mRNA and protein was minimally increased by 8 h after UVB irradiation and reached a maximum by 24 h. No significant alteration in ICAM-1 or VCAM-1 expression was observed. E-selectin expression, which was absent from control samples, was increased from 4 h onward and also reached a maximum at 24 h, coinciding with peak neutrophil accumulation. A strong correlation ($r = 0.96$) was found between number of E-selectin-positive vessels and numbers of infiltrating neutrophils at this time. Moreover, because E-selectin expression was increased before any apparent increase in TNF-alpha protein (4 h), TNF-alpha does not appear to be involved in the early induction of the adhesion molecule, but cytokines such as TNF-alpha and IL-8 may act subsequently to augment the inflammatory response.

PMID: 9129230 [PubMed - indexed for MEDLINE]



Basic fibroblast growth factor expression is increased in human renal fibrogenesis and may mediate autocrine fibroblast proliferation.

Strutz F, Zeisberg M, Hemmerlein B, Sattler B, Hummel K, Becker V, Muller GA.

Department of Nephrology and Rheumatology, Georg-August-University Gottingen, Germany. fstrutz@gwdg.de

BACKGROUND: Interstitial fibroblasts play a critical role in renal fibrogenesis, and autocrine proliferation of these cells may account for continuous matrix synthesis. Basic fibroblast growth factor (FGF-2) is mitogenic for most cells and exerts intracrine, autocrine, and paracrine effects on epithelial and mesenchymal cells. The aims of the present studies were to localize and quantitate the expression of FGF-2 in normal and pathologic human kidneys and to study the in vitro effects of FGF-2 on proliferation, differentiation, and matrix production of isolated cortical kidney fibroblasts. **METHODS:** FGF-2 protein expression was localized by immunofluorescence double labelings in normal and fibrotic human kidneys. Subsequently, interstitial FGF-2 labeling was determined semiquantitatively in 8 normal kidneys and 39 kidneys with variable degrees of interstitial fibrosis and was correlated with the morphometrically determined interstitial cortical volume. In addition, FGF-2 expression was quantitated by immunoblot analysis in three normal and six fibrotic kidneys. FGF-2 mRNA was localized by in situ hybridizations. Seven primary cortical fibroblast lines were established, and expression of FGF-2 and FGF receptor-1 (FGFR-1) were examined. The effects of FGF-2 on cell proliferation were determined by bromodeoxyuridine incorporation and cell counts, those on differentiation into myofibroblasts by staining for alpha-smooth muscle actin, and those on matrix synthesis by enzyme-linked immunosorbent assay for collagen type I and fibronectin. Finally, proliferative activity in vivo was evaluated by expression of MIB-1 (Ki-67 antigen). **RESULTS:** In normal kidneys, FGF-2 expression was confined to glomerular, vascular, and a few tubular as well as interstitial fibroblast-like cells. The expression of FGF-2 protein was increased in human kidneys, with tubulointerstitial scarring correlating with the degree of interstitial fibrosis ($r = 0.84$, $P < 0.01$). Immunoblot analyses confirmed a significant increase in FGF-2 protein expression in kidneys with interstitial scarring. In situ hybridization studies demonstrated low-level detection of FGF-2 mRNA in normal kidneys. However, FGF-2 mRNA expression was robustly up-regulated in interstitial and tubular cells in end-stage kidneys, indicating that these cells are the source of excess FGF-2 protein. Primary cortical fibroblasts express FGF-2 and FGFR-1 in vitro. FGF-2 induced a robust growth response in these cells that could be blocked specifically by a neutralizing FGF-2 antibody. Interestingly, the addition of the neutralizing antibody alone did reduce basal proliferation up to 31.5%. In addition, FGF-2 induced expression of alpha-smooth muscle actin up to 1.6-fold, but no significant effect was observed on the synthesis of collagen type I and fibronectin. Finally, staining for MIB-1 revealed a good correlation of interstitial FGF-2 positivity

with interstitial and tubular proliferative activity ($r = 0.71$, $P < 0.01$ for interstitial proliferation, $N = 30$). CONCLUSIONS: Interstitial FGF-2 protein and mRNA expression correlate with interstitial scarring. FGF-2 is a strong mitogen for cortical kidney fibroblasts and may promote autocrine fibroblast growth. Expression of FGF-2 correlates with interstitial and tubular proliferation in vivo.

PMID: 10760088 [PubMed - indexed for MEDLINE]



Adiposity elevates plasma MCP-1 levels leading to the increased CD11b-positive monocytes in mice.

Takahashi K, Mizuarai S, Araki H, Mashiko S, Ishihara A, Kanatani A, Itadani H, Kotani H.

Banyu Tsukuba Research Institute in collaboration with Merck Research Laboratories, Tsukuba, Ibaraki 300-2611, Japan.

Obesity is currently considered as an epidemic in the western world, and it represents a major risk factor for life-threatening diseases such as heart attack, stroke, diabetes, and cancer. Taking advantage of DNA microarray technology, we tried to identify the molecules explaining the relationship between obesity and vascular disorders, comparing mRNA expression of about 12,000 genes in white adipose tissue between normal, high fat diet-induced obesity (DIO) and d-Trp34 neuropeptide Y-induced obesity in mice. Expression of monocyte chemoattractant protein-1 (MCP-1) mRNA displayed a 7.2-fold increase in obese mice as compared with normal mice, leading to substantially elevated MCP-1 protein levels in adipocytes. MCP-1 levels in plasma were also increased in DIO mice, and a strong correlation between plasma MCP-1 levels and body weight was identified. We also showed that elevated MCP-1 protein levels in plasma increased the CD11b-positive monocyte/macrophage population in DIO mice. Furthermore, infusion of MCP-1 into lean mice increased the CD11b-positive monocyte population without inducing changes in body weight. Given the importance of MCP-1 in activation of monocytes and subsequent atherosclerotic development, these results suggest a novel role of adiposity in the development of vascular disorders.

PMID: 13129912 [PubMed - indexed for MEDLINE]



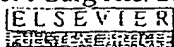
Augmented expression of neuronal nitric oxide synthase in the atria parasympathetically decreases heart rate during acute myocardial infarction in rats.

Takimoto Y, Aoyama T, Tanaka K, Keyamura R, Yui Y, Sasayama S.

Department of Cardiovascular Medicine, Graduate School of Medicine, Kyoto University, Kyoto, Japan.

BACKGROUND: Nitric oxide (NO) synthesized within sinoatrial cells recently has been shown to participate in the autonomic control of heart rate. We hypothesized that NO in the neuronal cells in the heart was increased and parasympathetically regulated heart rate after myocardial infarction (MI). **METHODS AND RESULTS:** We examined heart rate dynamics and neuronal NO synthase (nNOS) expression and activities in the atria of rats with MI 1, 3, 7, and 14 days after MI (n=7 to 22 for each group). Both the mRNA levels of nNOS in the atria determined by competitive reverse transcriptase-polymerase chain reaction and the protein levels determined by Western blotting were significantly increased compared with controls 1, 3, and 7 days after MI. nNOS activity in the atria 1 day after infarction was also increased in MI rats. nNOS immunoreactivity was observed in nerve fibers in the atria. After infusion of a specific inhibitor of nNOS and iNOS, 1-(2-trifluoromethylphenyl) imidazole (TRIM) (50 mg/kg IV), heart rate was significantly ($P<0.01$) increased in MI rats compared with controls 1, 3, and 7 days after MI. The iNOS-specific inhibitor, 1400W (10 mg/kg SC), did not significantly affect the heart rate in rats with MI. The effect of TRIM was abolished by pretreatment with L-arginine (25 mg/kg IV) or by parasympathetic blockade with atropine but not by propranolol. There was a strong correlation ($r=0.837$, $P<0.0001$) between the nNOS protein expression and heart rate change after TRIM infusion. **CONCLUSIONS:** These results indicate that increased nNOS parasympathetically decreased heart rate via the production of NO in rats with acute MI.

PMID: 11815433 [PubMed - indexed for MEDLINE]



Differential upregulation of cellular adhesion molecules at the sites of oxidative stress in experimental acute pancreatitis.

Telek G, Ducroc R, Scoazec JY, Pasquier C, Feldmann G, Roze C.

INSERM U 410, Universite Paris 7 Denis Diderot, 75870 Paris, France.

BACKGROUND: Severe acute pancreatitis (AP)(2) is associated with exaggerated leukocyte adherence and activation. Endothelial cellular adhesion molecules (CAMs) can be induced by cytokines, but also directly by oxygen free radicals (OFRs), mediated by nuclear factor kappa-B (NF-kappa B). We investigated the behavior of inducible CAMs in relation to pancreatic oxidative stress. Our novel modification of cerium capture histochemistry (reaction of OFRs with cerium produces laser reflective Ce perhydroxide precipitates) combined with reflectance confocal laser scanning microscopy (CLSM) allows the histological codemonstration of in vivo OFR production and immunolabeled CAMs, or NF-kappa B. **METHODS:** Taurocholate AP was induced in rats; sham operated and normal animals served as controls. To achieve in situ, in vivo reaction of cerium with OFRs, animals were perfused with CeCl(3) solution at different time points (1, 2, 8, 24 h) and then sacrificed. E-selectin, P-selectin, ICAM-1, VCAM, and NF-kappa B p65 were labeled by immunofluorescence (IF) on frozen sections of cerium perfused pancreata. IF and Ce perhydroxide reflectance were simultaneously detected by CLSM. Pancreatic gene expression of the same CAMs was quantified by competitive RT-PCR (MIMIC internal control). **RESULTS:** Control pancreata showed negligible reflectance and minimal CAM expression. Early (1, 2 h) AP samples were characterized by intense, heterogeneous acinar OFR production, strong P-selectin, and increasing ICAM expression, with nuclear translocation of p65, histologically all colocalizing with the areas of acinar oxidative stress. Adherent polymorphonuclear leukocytes (PMNs) displayed weak OFR formation. Later (8, 24 h), a slowly declining P-selectin, but persisting ICAM-1 expression, was paralleled by widespread adherence of PMNs producing surprisingly large amounts of OFRs. VCAM and E-selectin showed a mild increase at 24 h. CAM gene activation was in good correlation with the protein expression. **CONCLUSIONS:** The early acinar oxidative stress is colocalized with NF-kappa B activation, preferential P-selectin, and ICAM upregulation in this AP model. Subsequently, adherent, activated PMNs become the major source of OFRs, thereby contributing to tissue damage. Copyright 2001 Academic Press.

PMID: 11180997 [PubMed - indexed for MEDLINE]

Myotonic dystrophy: an unstable CTG repeat in a protein kinase gene.

Timchenko L, Monckton DG, Caskey CT.

Department of Molecular and Human Genetics, Baylor College of Medicine, Texas Medical Center, Houston 77030, USA.

Myotonic dystrophy (DM) is caused by the amplification of CTG repeats in the 3' untranslated region of a gene encoding a protein homologous to serine/threonine protein kinases. In DM patients the CTG repeats are extremely unstable, varying in length from patient to patient and generally increasing in length in successive generations. There is a strong correlation between the size of the repeats and the age of onset and severity of the disease. The molecular basis of the effect of the CTG expansion on the development of the DM phenotype continues to be investigated. The first working hypothesis of the molecular mechanism of DM was a reduction in steady-state myotonin-protein kinase (Mt-PK) mRNA and protein levels. However, although the consensus finding is that the Mt PK mRNA and protein levels are decreased in DM patients, it is still not clear if this reduction leads directly to the DM phenotype. In this short review we discuss the molecular aspects of CTG instability and the expression of the myotonin-protein kinase gene in normal and DM populations.

Publication Types:

- Review
- Review, Tutorial

PMID: 7620117 [PubMed - indexed for MEDLINE]

Induction of class 3 aldehyde dehydrogenase in the mouse hepatoma cell line Hepa-1 by various chemicals.

Torronen R, Korkalainen M, Karenlampi SO.

Department of Physiology, University of Kuopio, Finland.

The mouse hepatoma cell line Hepa-1 was shown to express an aldehyde dehydrogenase (ALDH) isozyme which was inducible by TCDD and carcinogenic polycyclic aromatic hydrocarbons. The induced activity could be detected with benzaldehyde as substrate and NADP as cofactor (B/NADP ALDH). As compared with rat liver and hepatoma cell lines, the response was moderate (maximally 5-fold). There was an apparent correlation between this specific form of ALDH and aryl hydrocarbon hydroxylase (AHH) in the Hepa-1 wild-type cell line--in terms of inducibility by several chemicals. However, the magnitude of the response was clearly smaller for ALDH than for AHH. Southern blot analysis showed that a homologous gene (class 3 ALDH) was present in the rat and mouse genome. The gene was also expressed in Hepa-1 and there was a good correlation between the increase of class 3 ALDH-specific mRNA and B/NADP ALDH enzyme activity after exposure of the Hepa-1 cells to TCDD. It is concluded that class 3 ALDH is inducible by certain chemicals in the mouse hepatoma cell line, although the respective enzyme is not inducible in mouse liver in vivo.

PMID: 1505055 [PubMed - indexed for MEDLINE]



Relationship between cyclin D1 and p21(Waf1/Cip1) during differentiation of human myeloid leukemia cell lines.

Ullmannova V, Stockbauer P, Hradcova M, Soucek J, Haskovec C.

Department of Molecular Genetics, Institute of Hematology and Blood Transfusion, U Nemocnice 1, 128 20 Prague 2, Czech Republic. ullman@uhkt.cz

Expression of cell cycle-regulating genes was studied in human myeloid leukemia cell lines ML-1, ML-2 and ML-3 during induction of differentiation in vitro. Myelomonocytic differentiation was induced by phorbol ester (12-o-Tetradecanoyl-phorbol-13-acetate, TPA), tumor necrosis factor alpha (TNFalpha) or interferon gamma (INFgamma), or their combination. Differentiation (with the exception of TNFalpha alone) was accompanied by inhibition of DNA synthesis and cell cycle arrest. Inhibition of proliferation was associated with a decrease in the expression of cdc25A and cdc25B, cdk6 and Ki-67 genes, and with increased p21(Waf1/Cip1) gene expression, as measured by comparative RT-PCR. Expression of the following genes was not changed after induction of differentiation: cyclin A1, cyclin D3, cyclin E1 and p27(Kip1). Surprisingly, cyclin D1 expression was upregulated after induction by TPA, TNFalpha with IFNgamma or BA. Cyclin D2 was upregulated only after induction by BA. The results of the expression of the tested genes obtained by comparative RT-PCR were confirmed by quantitative real-time (RQ) RT-PCR and Western blotting. Quantitative RT-PCR showed as much as a 288-fold increase of cyclin D1 specific mRNA after a 24h induction by TPA. The upregulation of cyclin D1 in differentiating cells seems to be compensated by the upregulation of p21(Waf1/Cip1). These results, besides others, point to a strong correlation between the expression of cyclin D1 and p21(Waf1/Cip1) on the one hand and differentiation on the other hand in human myeloid leukemic cells and reflect a rather complicated network regulating proliferation and differentiation of leukemic cells.

PMID: 12921950 [PubMed - indexed for MEDLINE]



Intestinal carbamoyl phosphate synthase I in human and rat. Expression during development shows species differences and mosaic expression in duodenum of both species.

Van Beers EH, Rings EH, Posthuma G, Dingemanse MA, Taminiau JA, Heymans HS, Einerhand AW, Buller HA, Dekker J.

Pediatric Gastroenterology and Nutrition, Department Pediatrics, Emma Children's Hospital, Academic Medical Center, Amsterdam, The Netherlands.

The clinical importance of carbamoyl phosphate synthase I (CPSI) relates to its capacity to metabolize ammonia, because CPSI deficiencies cause lethal serum ammonia levels. Although some metabolic parameters concerning liver and intestinal CPSI have been reported, the extent to which enterocytes contribute to ammonia conversion remains unclear without a detailed description of its developmental and spatial expression patterns. Therefore, we determined the patterns of enterocytic CPSI mRNA and protein expression in human and rat intestine during embryonic and postnatal development, using in situ hybridization and immunohistochemistry. CPSI protein appeared during human embryogenesis in liver at 31-35 e. d. (embryonic days) before intestine (59 e.d.), whereas in rat CPSI detection in intestine (at 16 e.d.) preceded liver (20 e.d.). During all stages of development there was a good correlation between the expression of CPSI protein and mRNA in the intestinal epithelium. Strikingly, duodenal enterocytes in both species exhibited mosaic CPSI protein expression despite uniform CPSI mRNA expression in the epithelium and the presence of functional mitochondria in all epithelial cells. Unlike rat, CPSI in human embryos was expressed in liver before intestine. Although CPSI was primarily regulated at the transcriptional level, CPSI protein appeared mosaic in the duodenum of both species, possibly due to post-transcriptional regulation.

PMID: 9446830 [PubMed - indexed for MEDLINE]

Malignant transformation of the human endometrium is associated with overexpression of lactoferrin messenger RNA and protein.

Walmer DK, Padin CJ, Wrona MA, Healy BE, Bentley RC, Tsao MS, Kohler ME, McLachlan JA, Gray KD.

Department of Obstetrics and Gynecology, Duke University Medical Center, Durham, North Carolina 27710.

In the mouse uterus, lactoferrin is a major estrogen-inducible uterine secretory protein, and its expression correlates directly with the period of peak epithelial cell proliferation. In this study, we examine the expression of lactoferrin mRNA and protein in human endometrium, endometrial hyperplasias, and adenocarcinomas using immunohistochemistry, Western immunoblotting, and Northern and in situ RNA hybridization techniques. Our results reveal that lactoferrin is expressed in normal cycling endometrium by a restricted number of glandular epithelial cells located deep in the zona basalis. Two thirds (8 of 12) of the endometrial adenocarcinomas examined overexpress lactoferrin. This tumor-associated increase in lactoferrin expression includes an elevation in the mRNA and protein of individual cells and an increase in the number of cells expressing the protein. In comparison, only 1 of the 10 endometrial hyperplasia specimens examined demonstrates an increase in lactoferrin. We also observe distinct cytoplasmic and nuclear immunostaining patterns under different fixation conditions in both normal and malignant epithelial cells, similar to those previously reported in the mouse reproductive tract. Serial sections of malignant specimens show a good correlation between the localization of lactoferrin mRNA and protein in individual epithelial cells by in situ RNA hybridization and immunohistochemistry. Although the degree of lactoferrin expression in the adenocarcinomas did not correlate with the tumor stage, grade, or depth of invasion in these 12 patients, there was a striking inverse correlation between the presence of progesterone receptors and lactoferrin in all 8 lactoferrin-positive adenocarcinomas. In summary, lactoferrin is expressed in a region of normal endometrium known as the zona basalis which is not shed with menstruation and is frequently overexpressed by progesterone receptor-negative cells in endometrial adenocarcinomas.

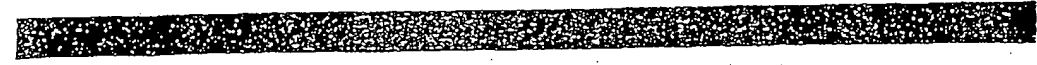
PMID: 7867003 [PubMed - indexed for MEDLINE]

TPL



Cancer Research

AN OFFICIAL JOURNAL OF THE AMERICAN ASSOCIATION FOR CANCER RESEARCH



March 1, 1995
Volume 55 • Number 5
PP. 975-1197
ISSN 0008-5472 • CNREA 8

LIBRARY OF THE

MAR 9 6 1995

1000 1000 1000



Cancer Research

AN OFFICIAL JOURNAL OF THE AMERICAN ASSOCIATION FOR CANCER RESEARCH

American Association for Cancer Research, Inc.

Publications Staff
Managing Editor
Margaret Foti
Assistant Managing Editor
Mary Anne Mennite
Manager, Editorial Services
Heide M. Puszyu
Staff Editors
Lisa A. Chippendale
Pamela M. Grubow
Michael J. Beveridge
Kathleen C. Assenmacher
Supervisor, Manuscript
Processing
Margaret A. Pickels
Assistant Supervisor,
Manuscript Processing
Theresa A. Griffith
Staff Assistant
Mary Ellen Pining
Editorial Assistants
Valerie L. Taylor
Andrea Conrad
Katherine V. Pawlowaki
Bethann Massarella
Charles W. Wells, Jr.
Administrative Staff
Executive Director
Margaret Foti
Director of Administration
Adam D. Blistein
Controller
Joan D. Brokenshire
Coordinator, Financial
Operations
George L. Moore
Meetings Coordinator
Jeffrey M. Ruben
Meeting Planner
Carol L. Kanoff
Public Information Coordinator
Jenny Anne Horst-Mertz
Executive Assistant for
Programs
Ruth E. Fortson
Administrative Assistant
Robin E. Felder
Systems Specialist
Lydia I. Rodriguez
Staff Assistant
Lori L. Holmes
Secretary
Malika L. Wright
Editorial Secretary
Diana F. Certo
Financial Clerk
Paul Perreault
Office Clerk
James J. Waters
Data Entry Clerk
Robert A. Simms II

Editor-in-Chief

Carlo M. Croce

Associate Editors

Stuart A. Aaronson
Jenny M. Adams
David S. Albens
Carmen J. Allegra
Frederick R. Appelbaum
James O. Armstrong
William M. Baird
Allan Balmain
J. Carl Barrett
Renato Baserga
William T. Beck
Joseph R. Bertino
Mina J. Bissell
Clara D. Bloomfield
Gianni Bonadonna
Ernest C. Borden
G. Tim Bowden
Edward Bresnick
Samuel Broder
Ronald N. Buick
Paul A. Bunn, Jr.
C. Patrick Burns
Fernando Cabanillas
Bruno Calabretta
Eli Canaan
Robert L. Capizzi
Webster K. Cavenee
Bruce D. Cheson
David Colcher
Robert L. Comis
Allan H. Conney
Neal G. Copeland
Joseph G. Cory
William M. Crist
Benoit de Crombrughe

Riccardo Dalla-Favera
Richard L. Davidson
Eugene R. DeSombre
T. Michael Dexter
Ralph E. Durand
Alan Eastman
Gertrude B. Elion
Leonard C. Erickson
Nelson Fausto
Eric R. Fearon
Isaiah J. Fidler
Robert A. Floyd
Judah Folkman
Kenneth A. Foon
Joseph F. Fraumeni, Jr.
Stephen H. Friend
Minoru Fukuda
Philip Furmanski
Eugene W. Gerner
Eli Glaser
David W. Golde
Michael M. Gottesman
J. W. Grisham
F. Peter Guentrich
Sen-jiro Hakomori
Philip C. Hanawalt
Curtis C. Harris
John C. Harshbarger
Stephen S. Hecht
Carl-Henrik Heldin
Brian E. Henderson
Richard B. Hochberg
Wauw Ki Hong
Tasuku Honjo
Kay Huebner

John T. Isaacs
Mark A. Israel
Elaine S. Jaffe
Rakesh K. Jain
Peter A. Jones
V. Craig Jordan
John H. Kenney
Young S. Kim
Kenneth W. Kinzler
Tadamitsu Kishimoto
Alfred G. Knudson, Jr.
Kurt W. Kohn
Lawrence N. Kolonel
Donald W. Kufe
John S. Lazo
Jay A. Levy
Frederick P. Li
Victor Ling
Lance A. Lione
Martin Lipkin
Marc E. Lippman
Gerald Litwack
Leroy F. Liu
Lawrence A. Loeb
Dan L. Longo
Reuben Lotan
David B. Ludlum
Tak W. Mak
Michael J. Mastrangelo
Lynn M. Matrisian
W. Gillies McKenna
Anna T. Meadows
John Mendelsohn
Christopher J. Michetja
John D. Minna

Beatrice Mintz
Malcolm S. Mitchell
Ruth J. Muschel
Yusuke Nakamura
Garth L. Nicolson
Kenneth Nilsson
Susumu Nishimura
Jeffrey A. Norton
Kenneth Olden
Gilbert S. Omenn
Richard J. O'Reilly
Robert F. Ozols
Michael A. Palladino, Jr.
Peter L. Pedersen
Anthony E. Pegg
Angel Pellicer
Bice Perussia
Gordon L. Phillips
Cecil B. Picken
Jacalyn H. Pierce
Vito Quaranta
Frank J. Rauscher III
Donald J. Reed
Ralph A. Reisfeld
Richard A. Rifkind
Leslie L. Robison
Igor B. Roninson
Howard J. Scher
Robert T. Schirack
J. Schlessinger
Manfred Schwab
Joseph V. Simone
Francis M. Sirotnak
Anna Marie Skalka

Michael B. Sporn
Martha R. Stampfer
Eric J. Stanbridge
Gary S. Stein
Bernard S. Strauss
Takashi Sugimura
Saraswati Sukumar
James A. Swenberg
Paul Talalay
Tadatsugu Taniguchi
Steven R. Tannenbaum
Masaki Terada
Kenneth D. Tew
Donald J. Tindall
George J. Todaro
Jeffrey M. Trent
Giorgio Trinchieri
Takashi Tsuruo
Axel Ullrich
Peter Vaupel
Giancarlo Vacciho
Daniel D. Von Hoff
Michael D. Waterfield
Lee W. Wattenberg
Ralph R. Weichselbaum
I. Bernard Weinstein
Bengt Westermark
Raymond L. White
Gordon F. Whitmore
Max S. Wicha
Walter Willert
H. Rodney Withers
Sheldon Wolff
Stuart H. Yuspa
Harald zur Hausen

Cover Editorial Board

Sidney Weinhouse,
Cover Editor

Hugh J. Czech
Clark W. Heath, Jr.

Edwin A. Mirand
Raymond W. Ruddon

Takashi Sugimura
John H. Weisburger

Cancer Research is sponsored by the American Association for Cancer Research, Inc. and receives major support from the American Cancer Society, Inc. Publication costs are also met by a grant from the Elsa U. Pardee Foundation. Accelerated mailing of journals to AACR members in Japan is supported by a generous grant from the Banyu Pharmaceutical Company.

Subscription Information

Cancer Research is published twice a month, one volume per year, by the American Association for Cancer Research, Inc. (AACR). Subscriptions include the *Proceedings of the American Association for Cancer Research*, issued in March of each year. Except for members of the AACR, all subscriptions are payable in advance to Cancer Research, P.O. Box 5000, Denville, NJ 07834 [Telephone: (800) 875-2997; FAX: (201) 627-5872], to which all business communications, remittances (in United States currency or its equivalent), and subscription orders should be sent. In Japan, send orders and inquiries to (sole agent): USACO Corporation, Tsutsumi Bldg., 15-12, Shimabashi 1-chome, Minato-ku, Tokyo 105, Japan; Tel. (03) 502-6471. Individuals who are not AACR members may subscribe to Volume 55 (1995) of *Cancer Research* at the rate of \$460 U.S./\$520 foreign. *Cancer Research* is only available to institutions as a combined subscription with *Clinical Cancer Research*. The combined 1995 institutional subscription price of \$495 U.S./\$575 foreign includes a subscription to *Clinical Cancer Research*. Canadian subscribers should add 7% GST. Changes of address notification should be sent 60 days in advance and include both old and new addresses. Member subscribers should send address changes to: AACR Member Services, Public Ledger Bldg., Suite E16, 150 South Independence Mall West, Philadelphia, PA 19106-3483. Nonmember subscribers should send changes of address to: Cancer Research, P.O. Box 3000, Denville, NJ 07834. Copies of the journal which are undeliverable because of address changes will be destroyed.

Malignant Transformation of the Human Endometrium Is Associated with Overexpression of Lactoferrin Messenger RNA and Protein

David K. Walmer,¹ Cheryl J. Padin, Mark A. Wrona, Bridget E. Healy, Rex C. Bentley, Ming-Sound Tsao, Matthew F. Kohler, John A. McLachlan, and Karen D. Gray

Department of Obstetrics and Gynecology, Duke University Medical Center, Durham, North Carolina 27710 [D. K. W., B. E. H., M. F. K.]; Department of Obstetrics and Gynecology, University of Michigan, Ann Arbor, Michigan 48109 [C. J. P.]; School of Medicine, University of Maryland, Baltimore, Maryland 21201 [M. A. W.]; Department of Pathology, Duke University Medical Center, Durham, North Carolina 27710 [R. C. B.]; Department of Pathology, Montreal General Hospital, Montreal, Quebec, Canada H3G1A4 [M.-S. T.]; Laboratory of Reproductive and Developmental Toxicology, National Institute of Environmental Health Sciences, Research Triangle Park, North Carolina 27709 [J. A. M.]; and Department of Obstetrics and Gynecology, Uniformed Services University of the Health Sciences, Bethesda, Maryland 20814-7799 [K. D. G.]

ABSTRACT

In the mouse uterus, lactoferrin is a major estrogen-inducible uterine secretory protein, and its expression correlates directly with the period of peak epithelial cell proliferation. In this study, we examine the expression of lactoferrin mRNA and protein in human endometrium, endometrial hyperplasias, and adenocarcinomas using immunohistochemistry, Western immunoblotting, and Northern and *in situ* RNA hybridization techniques. Our results reveal that lactoferrin is expressed in normal cycling endometrium by a restricted number of glandular epithelial cells located deep in the zona basalis. Two thirds (8 of 12) of the endometrial adenocarcinomas examined overexpress lactoferrin. This tumor-associated increase in lactoferrin expression includes an elevation in the mRNA and protein of individual cells and an increase in the number of cells expressing the protein. In comparison, only 1 of the 10 endometrial hyperplasia specimens examined demonstrates an increase in lactoferrin. We also observe distinct cytoplasmic and nuclear immunostaining patterns under different fixation conditions in both normal and malignant epithelial cells, similar to those previously reported in the mouse reproductive tract. Serial sections of malignant specimens show a good correlation between the localization of lactoferrin mRNA and protein in individual epithelial cells by *in situ* RNA hybridization and immunohistochemistry. Although the degree of lactoferrin expression in the adenocarcinomas did not correlate with the tumor stage, grade, or depth of invasion in these 12 patients, there was a striking inverse correlation between the presence of progesterone receptors and lactoferrin in all 8 lactoferrin-positive adenocarcinomas. In summary, lactoferrin is expressed in a region of normal endometrium known as the zona basalis which is not shed with menstruation and is frequently overexpressed by progesterone receptor-negative cells in endometrial adenocarcinomas.

INTRODUCTION

The uterus is a sex steroid-responsive organ that plays a major role in women's health. Hysterectomies were the most frequently performed major surgical procedures in a 20-year study interval (1965-1984; Ref. 1). Fifty-eight to 80% of these 12.5 million procedures were performed for estrogen-related disorders of proliferation. Chronic unopposed estrogen exposure, most commonly associated with type II ovulatory disorders, eventually leads to the development of complex endometrial hyperplasia and adenocarcinoma. Since the sex steroids, estrogen and progesterone, act on their target tissues by regulating the expression of a wide variety of signaling molecules, identifying these regulatory factors will provide critical information towards understanding normal reproduction and reproductive tract pathology. Our current knowledge of estrogen and progesterone action on the reproductive tract is based to a great extent on information collected from rodents (2). Although differences exist

between the reproductive physiology of rodents and humans, the mouse has been a useful model for studying steroid hormone action in the human female reproductive tract (3, 4). One potential regulatory molecule shown to be regulated by estrogen in the mouse reproductive tract is lactoferrin. Lactoferrin is a basic glycoprotein with an extraordinarily high affinity for iron that was originally discovered in milk. This protein is expressed in a wide variety of tissues, most notably in polymorphonuclear leukocytes and most mammalian exocrine glandular secretions. In the mammary gland (5) and the female reproductive tract of the mouse (6-8), lactoferrin is regulated by endocrine hormones. Prolactin stimulates lactoferrin synthesis in the breast; whereas in the uterus and vagina, the ovarian sex steroid, 17 β -estradiol, is the inducer. (6, 7, 9). To date, lactoferrin is one of the few genes that have been identified in the rodent that are directly regulated by estradiol. The lactoferrin gene contains an ERE² that is important for regulating its expression *in vivo* in the mouse reproductive tract. Being linked to estradiol, the expression of lactoferrin by the uterine epithelium parallels the onset of DNA synthesis. Although sequencing information suggests that the human lactoferrin gene also contains a functional imperfect ERE in the 5'-flanking promoter region (10, 11), there is very little data regarding lactoferrin expression in the human female reproductive tract.

The purpose of our study was to examine the expression of lactoferrin in the human endometrium under normal and pathological conditions by immunohistochemistry, immunoblotting, and Northern and *in situ* RNA hybridization techniques. In addition, we looked for correlations between lactoferrin expression and several parameters, such as the stage of the menstrual cycle, the distribution of estrogen and progesterone receptors, HER-2/*neu* expression, markers of cell proliferation, and the histopathological grade and extent of myometrial invasion in the adenocarcinomas. Our data demonstrates that lactoferrin is expressed in a very restricted number of glands in the basal region of normal human endometrium and is markedly overexpressed in a significant number of the uterine adenocarcinomas by PR-negative cells.

MATERIALS AND METHODS

Tissue Preparation and Histological Evaluation. Surgical pathology specimens were obtained from Duke University Medical Center (Durham, NC) and the Department of Pathology at Montreal General Hospital (Quebec, Montreal, Canada). Cycling endometrium was obtained from 22 women (ages 31-49), and atrophic endometrium was obtained from 7 postmenopausal women (ages 64-77). Hysterectomies from cycling women were performed for subserosal leiomyomas ($n = 6$), pelvic relaxation ($n = 8$), pelvic pain ($n = 4$), peritoneal endometriosis ($n = 2$), and cancer of either the cervix ($n = 1$) or the ovary ($n = 1$). In addition, 12 adenocarcinomas, 3 atypical complex hyperplasias, 3 complex hyperplasias without atypia, and 4 simple hyperplasias were analyzed. Each human uterus was bivalved shortly after

Received 8/15/94; accepted 12/30/94.

The costs of publication of this article were defrayed in part by the payment of page charges. This article must therefore be hereby marked advertisement in accordance with 18 U.S.C. Section 1734 solely to indicate this fact.

¹ To whom requests for reprints should be addressed, at Department of Obstetrics and Gynecology, Box 3145, Duke University Medical Center, Durham, NC 27710.

² The abbreviations used are: ERE, estrogen response element; PCNA, proliferating cell nuclear antigen; ER, estrogen receptor; PR, progesterone receptor.

hysterectomy, and endometrium was removed from the fundal region. A full thickness biopsy was placed into either 10% neutral-buffered formalin or Bouin's solution overnight at room temperature before dehydration, paraffin embedding, and sectioning at 4 μ m on silanized slides. Histological evaluations of hematoxylin and eosin-stained slides were performed blindly by one board-certified pathologist. Normal endometrial samples were dated by the criteria of Noyes *et al.* (12). Endometrial hyperplasias and carcinomas were classified according to the current recommendations of the International Society of Gynecological Pathologists under the auspices of WHO (13). Histological grading of tumors was performed according to Federation Internationale des Gynecologues et Obstetristes criteria (14). Each specimen was read a minimum of three times, and only specimens that were read consistently the same way were included in the study. Unstained sections of the same tissues were used for the cytochemical analysis of protein and mRNA expression using specific reagents. A few endometrial samples were frozen for subsequent protein and RNA extraction, which were evaluated by Western and Northern blotting, respectively. All human tissues were handled with the precautions and the guidelines required by Duke University and National Institute of Environmental Health Sciences.

Immunolocalization. Slides chosen for study were deparaffinized and rinsed in 20% glacial acetic acid at 4°C for 15 s to inhibit endogenous alkaline phosphatase. All subsequent incubations and washes were at room temperature. Sections were next equilibrated in PBS for 20 min and incubated for 20 min with 1.5% normal goat serum diluted in PBS to block nonspecific binding. Detection of lactoferrin was performed primarily with a rabbit anti-human lactoferrin polyclonal antiserum generated in our laboratory and affinity purified. Similar results were also seen with a nonaffinity-purified commercial antiserum (Biogenex, San Ramon, Ca). Following incubation at room temperature with primary antisera for 60 min, the sections were washed in PBS twice for 10 min each, and lactoferrin was localized using an alkaline phosphatase-biotin-sueplavidin detection system (Vectastain ABC-AP kit; Vector Laboratories, Burlingame, CA) or the Super Sensitive Detection System: Biogenex, San Ramon, CA). To identify nonspecific staining, preimmune rabbit serum was used in place of the primary antibody. The immunoreaction was quantitated by determining the percentage of glands and the percentage of cells staining for lactoferrin in the zona basalis and the zona functionalis, with a minimum of 300 cells counted in each region. PR antibody was provided by Geoffrey Greene (KD68), and a commercial source was also used (Biogenex, San Ramon, CA). Identical staining patterns were confirmed with both preparations. Other commercially obtained antisera include PCNA (Biogenex, San Ramon, CA), ER (ER1D5; AMAC, Westbrook, Ma), MIB-1 (AMAC), and HER-2/*neu* (Biogenex, San Ramon, CA). The primary antisera incubations were 2 h for the PR, 1 h for PCNA, MIB-1, and ER, and 30 min for HER-2/*neu*. Antisera dilutions were 1:100 for MIB-1 and 1:20 for HER-2/*neu*. Antigen retrieval (Biogenex, San Ramon, CA) was performed before adding the progesterone primary antisera.

Western Blot Analysis. Proteins were extracted from endometrial biopsies by homogenization on ice in 1% Triton-X and 20 mM Tris-HCl (pH 7.4) with protease inhibitors (10 μ g/ml leupeptin, 200 KU/ml aprotinin, and 20 μ g/ml phenylmethylsulfonyl fluoride) and clarified by centrifugation at 45,000 rpm for 30 min in a Beckman 70.1 Ti rotor; then the supernatant was analyzed for protein concentration by the BCA protein assay (Pierce, Rockford, IL). Aliquots of 200 μ g were separated by electrophoresis on an 8.5% SDS polyacrylamide gel, blotted onto nitrocellulose membranes, incubated with polyclonal rabbit antihuman lactoferrin antisera, and localized with an 125 I-labeled donkey anti-rabbit immunoglobulin, as described previously (7).

In Situ Hybridization. All slides were pretreated with 0.2 N HCl for 50 min at room temperature, digested with 1 μ g/ml proteinase-K (Sigma Chemical Co., St. Louis, MO) in 0.1 M Tris-HCl (pH 7.4)-0.05 M EDTA for 15 min at 37°C, and then treated with 0.1 M methanolamine-0.25% acetic anhydride for 5 min at room temperature and 0.1 M Tris-glycine (pH 7.4) for 30 min at room temperature. The sections were subsequently dehydrated with graded ethanol, air dried, and prehybridized at 50°C for 1 h in 2 \times SSC, 10 mM DTT, 5 \times Denhardt's solution, 100 μ g/ml of both salmon sperm DNA and yeast tRNA, and 50% formamide (15). The slides were then hybridized overnight at 50°C in the same medium with 10% dextran sulfate and 2 \times 10⁶ cpm/ μ l of the specific RNA probe. The lactoferrin oligonucleotide probe was amplified by PCR using primers that spanned nucleotides 718-1654 (10) and cloned into pGEM-4Z. 32 S-labeled sense and antisense RNA probes were made with the

Promega Riboprobe kit (Promega, Madison, WI), washed twice in 1 \times SSC for 10 min at room temperature, digested with RNase [2.8 μ g/ml RNase-A, 0.3 μ g/ml RNase-T1, 10 mM Tris-HCl (pH 7.4), and 15 mM NaCl], and washed again with 1 \times SSC twice for 20 min each time at 50°C, twice for 20 min in 0.1 \times SSC at 55°C, and once for 20 min at 60°C. The sections were then dehydrated and dipped in Kodak autoradiographic emulsion (NTB-2) for detection of specific mRNA expression. The slides were allowed to develop for 2 weeks. After this period, the slides were developed using Kodak D19 developer and Kodak Rapid Fixer.

Northern RNA Analysis. Total cellular RNA was purified from frozen tissue by the guanidine isothiocyanate-cesium chloride method, and poly(A)⁺-RNA was isolated by oligo(dT)-cellulose chromatography using methods described previously (15). For Northern blot analysis, poly(A)⁺-RNA was resolved by electrophoresis on 1.5% formaldehyde agarose gels, stained with ethidium bromide, and transferred to a nylon membrane. The membrane was probed with a 32 P-labeled lactoferrin cDNA derived from human uterus (nucleotides 718-1654; accession no. S52659) using PCR techniques, followed by cloning into pGEM-4Z (Promega, Madison, WI). In order to insure that the quality and quantity of RNA analyzed by Northern blotting was equivalent between control and treated groups, the blot was probed simultaneously for glyceraldehyde-3-phosphate dehydrogenase.

Statistical Analysis. Values are presented as means \pm SD. Differences between the zona basalis and functionalis were tested by the two-tailed Student's *t* test.

RESULTS

Immunohistochemical Analysis of Lactoferrin Protein

Normal Cycling Endometrium. Immunohistochemical studies of normal cycling human endometrium localize lactoferrin protein predominantly to the glandular epithelium deep in the zona basalis and not to the functionalis (Fig. 1A). The association of lactoferrin protein expression with the zona basalis is statistically significant ($P < 0.001$; Fig. 2). Two to 56% of the glands express lactoferrin at any given time during the menstrual cycle. Within positive glands, lactoferrin protein immunolocalization is heterogeneous in that positively staining epithelial cells are interspersed with cells negative for lactoferrin expression. No apparent differences in morphology, PCNA, ER, or PR expression are seen to account for the heterogeneous pattern of intra- and intergland lactoferrin expression in normal endometrium. Similar to our previous findings in mouse uterine epithelial cells, the positive-staining glandular cells of the human endometrium demonstrate two distinct immunostaining patterns for lactoferrin, cytoplasmic and nuclear (Fig. 1B), seen with both formalin and Bouin's fixation. In evaluating the temporal expression of lactoferrin, there is a trend towards more glands expressing lactoferrin during the secretory phase. Because of the large variance, the trend is not statistically significant. As expected, the polymorphonuclear leukocytes in the endometrium also stain intensely for lactoferrin protein, which is stored in their secondary granules (Fig. 3). These results demonstrate, for the first time, that lactoferrin protein is expressed in the human endometrium predominantly by polymorphonuclear leukocytes and epithelial cells of glands located deep in the zona basalis.

Proliferative Endometrial Disorders: Hyperplasias and Adenocarcinomas. Immunohistochemistry reveals that the expression of lactoferrin protein is increased in 66.6% (8 of 12) of the endometrial adenocarcinomas examined. In one-half of these cases (4 of 12), lactoferrin is intensely expressed by malignant epithelial cells throughout the entire tumors (Fig. 4). The other four adenocarcinomas demonstrate increased staining for lactoferrin in concentrated regions of the tumors. In all eight cases where lactoferrin expression is elevated, the cells expressing lactoferrin have one similarity with normal positive glands in that they demonstrate heterogeneous staining of interspersed positive and negative cells. However, the expression of lactoferrin by the malignant cells clearly differs from normal

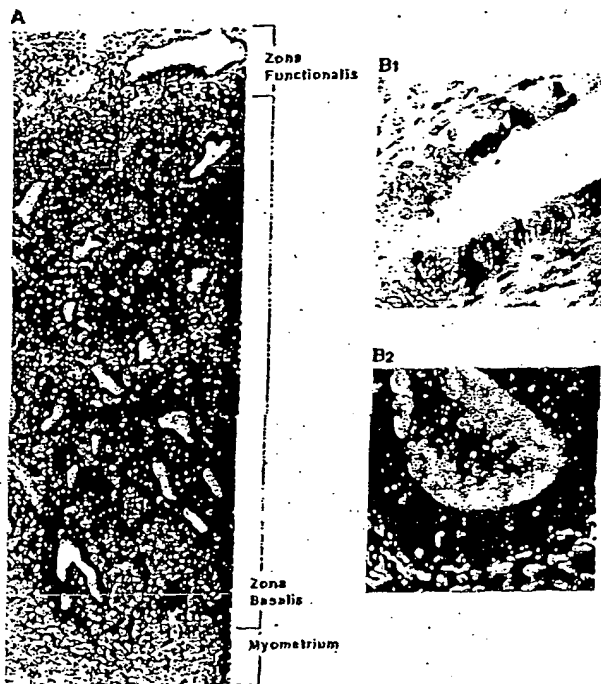


Fig. 1. Localization of lactoferrin protein in normal cycling endometrium by immunohistochemistry using a specific polyclonal antibody. Our analysis reveals that lactoferrin protein is present in a limited number of glands located in the zona basalis of the endometrium (A); $\times 10$. Also, note that lactoferrin is heterogeneous within positive glands, i.e., cells staining for lactoferrin are interspersed with negative-staining epithelial cells throughout the gland. Two immunohistochemical staining patterns are noted for lactoferrin in normal uterine epithelium. In one pattern, lactoferrin protein is immunolocalized primarily over the cytoplasm (B1), and in the other, the staining is seen over the nucleus (B2); $\times 40$.

positive glands in that the lactoferrin is not limited to the basal regions of the tumors, many more cells are positive, and the relative intensity of the staining over individuals cells is increased. Although increased lactoferrin expression is associated with malignant transformation, we do not find a correlation between lactoferrin protein presence and the stage, nuclear grade, Fédération Internationale des Gynécologues et Obstétristes grade, or the depth of myometrial invasion in the 12 tumors studied (Table 1). In sharp contrast to the common dysregulation of lactoferrin expression found in the malignant endometrium, only 1 of 10 endometrial hyperplasia specimens evaluated contained an increased number of cells staining for lactoferrin. The hyperplastic specimen overexpressing lactoferrin was read as complex without atypia.

In Situ and Northern Analyses of Lactoferrin mRNA Expression in Normal and Malignant Endometrium

To further our understanding of the location of lactoferrin protein synthesis in the human endometrium, we examined lactoferrin mRNA expression by *in situ* and Northern hybridization using specific ^{35}S -labeled probes for human lactoferrin. No detectable RNA hybridization is observed in the normal endometrium by *in situ* hybridization, even in the presence of immunodetectable protein, using equivalent hybridization conditions and development times as used for the adenocarcinomas. Consistent with the results obtained by *in situ* hybridization, long exposure times were required to demonstrate lactoferrin mRNA in normal endometrium by Northern blot using poly(A)⁺-mRNA. This indicates that lactoferrin mRNA is present in normal

tissue but in very low levels, consistent with the very limited pattern of protein expression in normal endometrium. Equivalent RNA loading and quality for each specimen was demonstrated by ethidium bromide staining of the RNA gels (data not shown) and by probing for the housekeeping gene glyceraldehyde-3-phosphate dehydrogenase that does not fluctuate significantly with the metabolic state of the tissue. A representative Northern blot is shown in Fig. 5. *In situ* hybridization with several adenocarcinomas reveals that there is a direct correlation between the localization of lactoferrin mRNA and the immunostaining of expressed lactoferrin protein (Fig. 4). Lactoferrin mRNA is not associated with polymorphonuclear leukocytes by *in situ* hybridization in either normal or malignant tissue.

Western Blot Analysis

To confirm the specificity of the antisera that we used for immunohistochemistry, we performed Western blot analysis on proteins extracted from both normal and malignant endometrium which were separated by 8.5% SDS-polyacrylamide gel electrophoresis (Fig. 6). Immunoblotting identified a single broad protein band with a molecular weight between 70,000–80,000 in both normal and neoplastic endometrial tissue homogenates, consistent with the reported molecular weight of human lactoferrin. Supporting the immunocytochemical analysis, a representative immunoblot clearly demonstrates that the proportion of protein that is lactoferrin is markedly increased in the adenocarcinomas in comparison to the normal endometrium. The molecular weight of lactoferrin in the adenocarcinomas appears to have a slightly higher molecular weight than the predominant form in normal tissue.

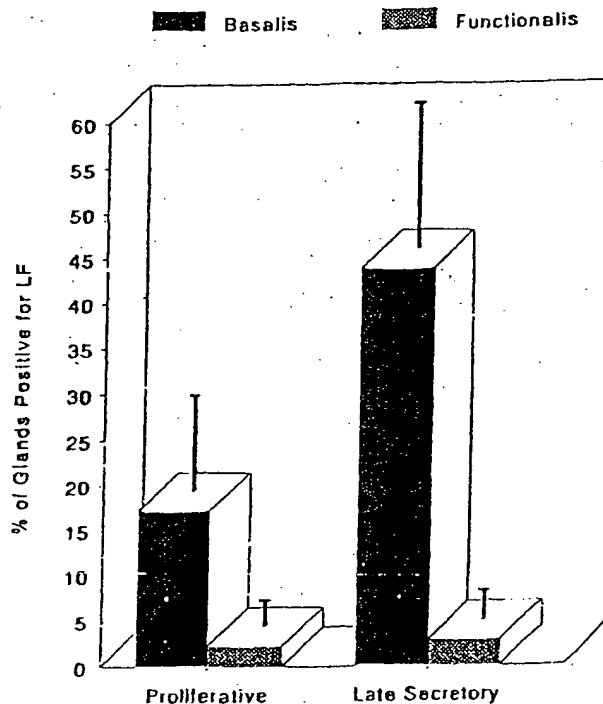


Fig. 2. Percentage of endometrial glands expressing lactoferrin protein by immunohistochemistry. Significantly more glands are positive in the region of the zona basalis than in the zona functionalis of the endometrium ($P < 0.001$). Zona basalis, ■; zona functionalis, □. Although there is a trend towards more of the basalis glands expressing lactoferrin in the secretory phase (right ■ compared with the left ■), this was not statistically significant.



Fig. 3. Polymorphonuclear leukocytes (arrows) are scattered throughout the endometrium and stain intensely for lactoferrin. Lactoferrin is a known component of the secondary granules in polymorphonuclear leukocytes. The presence of a segmented nucleus and lactoferrin protein is an excellent method for identifying this group of inflammatory cells. A, $\times 20$. B, $\times 50$.

Correlation of Lactoferrin Expression with the Expression of PCNA, Ki-67, HER-2/neu, ER, and PR

In an attempt to characterize the phenotype of endometrial cells which express lactoferrin, we performed immunohistochemistry on serial sections for the Ki-67 antigen, PCNA, HER-2/neu, lactoferrin, ER, and PR. In normal tissue, Ki-67 and PCNA expression are cell cycle-specific markers of cell proliferation (16, 17). Upon analysis of normal cycling endometrium, no relationship between lactoferrin protein expression and ER, PR, or Ki-67 expression was observed. Similarly, in most of the adenocarcinomas evaluated, no relationship was noted between lactoferrin and PCNA protein expression. However, in one adenocarcinoma (Fig. 7), there was a clear inverse relationship seen between lactoferrin and PCNA localization, which was present throughout the entire tumor. Most dramatic, however, was a striking inverse correlation seen between lactoferrin and PR expression in 8 of 8 PR-positive uterine adenocarcinomas (Fig. 7). Two tumors negative for PR also did not express lactoferrin. Although an inverse correlation was also suggested with HER-2/neu and PR, the inverse correlation was more precise with lactoferrin in these tumors.

DISCUSSION

In the mouse uterus, lactoferrin is an estrogen-induced uterine secretory protein that is present throughout the epithelium (7), and it

is expressed concomitantly with epithelial cell proliferation. In contrast to lactoferrin's ubiquitous expression in the estrogenized mouse uterine epithelium, lactoferrin protein is limited to glandular epithelial cells in the basal regions of normal human endometrium and usually to glands that were directly adjacent to the myometrium (i.e., the deepest glands of the zona basalis). This regional localization of lactoferrin expression is not surprising in that other biochemical parameters have been reported to show site specificity in primate endometrium. These parameters include the proliferative index and the expression of the secretory component of IgA (18). Similar to our observations in the endometrium, lactoferrin is also expressed regionally in the mammary gland. In bovine breast tissue, lactoferrin is localized primarily to the basal alveolar cells (19); whereas in human breast tissue, the ductal epithelium appears to be the primary source of secreted lactoferrin during lactation (20).

Examining the endometrium on different days of the menstrual cycle demonstrates a trend towards increased lactoferrin expression during the luteal phase. Although this data is not statistically significant, the cyclic variation may be biologically relevant. Kim *et al.* (21) recently reported that the basal endometrial epithelial cells are unique because they proliferate during the postovulatory luteal phase. Interestingly, in the mouse uterus, there is a direct correlation between lactoferrin expression and epithelial cell proliferation (6). Therefore, lactoferrin may have a similar role in the human and mouse endometrium. If lactoferrin expression is cyclic, the ERE in the 5'-flanking promoter region of the human lactoferrin gene may be activated during the luteal phase (10, 11).

Another similarity between human and mouse uterine lactoferrin expression is the observation of two immunohistochemical staining patterns. In one pattern, the antisera binds primarily over the cytoplasm, and in the other, the nucleus is the primary site of localization. Although this could represent a fixation artifact, we have now observed this pattern in two species and under different fixation conditions. It has been demonstrated that signaling peptides, i.e., platelet-derived growth factor (22), Int-2 (23), and probasin (24), can be selectively directed into the nucleus, cytoplasm, or secreted. It is believed that this differential processing may allow proteins to have intracrine, autocrine, and paracrine roles, depending on the physiological state of the cell. The two localization patterns observed suggest that lactoferrin might have signaling sequences that direct the final destination of the mature peptide.

In normal endometrium, lactoferrin mRNA is present but in very low levels. Prolonged exposure times are needed to visualize the mRNA band with Northern analysis. Although with *in situ* hybridization the lactoferrin mRNA signal is easily seen in adenocarcinomas, we failed to localize the lactoferrin mRNA in normal endometrium using an equivalent exposure time. These low levels of mRNA in normal endometrium suggest that the synthesis and degradation of lactoferrin mRNA is more tightly regulated in normal tissue than in the adenocarcinomas. Because of the low levels of message in normal tissue, we are unable at this time to definitively conclude that lactoferrin mRNA is synthesized by the same epithelial cells which express the protein.

In endometrial adenocarcinomas, malignant transformation of the endometrium is associated with the up-regulation of lactoferrin mRNA and protein biosynthesis. The up-regulation at the RNA level is demonstrated by an increase in steady-state RNA levels using both *in situ* hybridization and Northern analysis techniques. In these cancers, we also observe an increase in the number of lactoferrin-positive cells, which express both the protein and mRNA. In this study, 8 of the 12 adenocarcinomas evaluated overexpress lactoferrin, compared with only 1 of 10 hyperplastic specimens. The form of lactoferrin protein extracted from endometrial adenocarcinomas appears to have

LACTOFERRIN DYSREGULATION IN ENDOMETRIAL CANCER

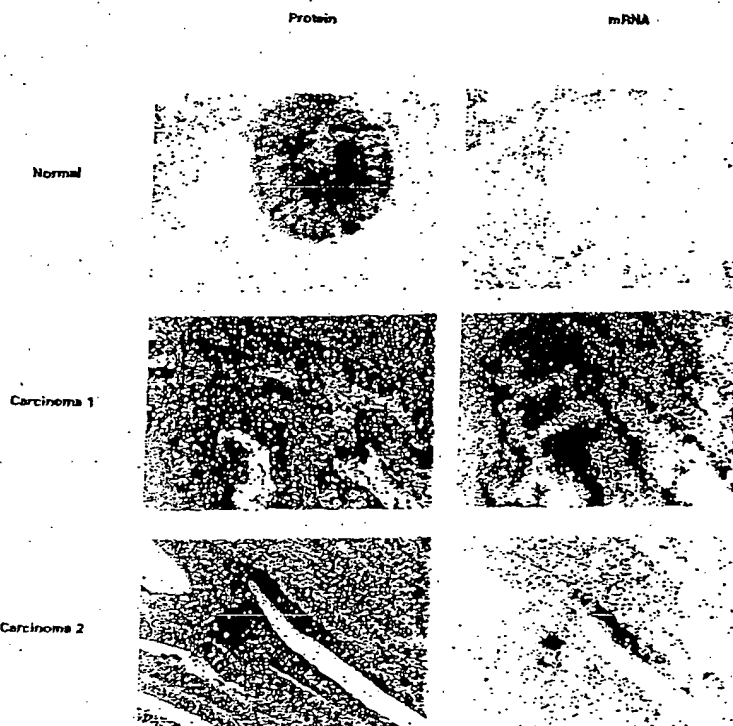


Fig. 4. Colocalization of lactoferrin protein (left panels) and mRNA (right panels) in a normal proliferative endometrium and endometrial adenocarcinomas by performing immunohistochemistry and *in situ* RNA hybridization on serial sections. Dual analysis of protein and mRNA expression reveals that glands in normal endometrium do not have detectable mRNA, as measured by *in situ* hybridization (top panels; X 40), whereas analysis of the adenocarcinomas clearly demonstrates a direct correlation between protein and RNA expression for lactoferrin (middle and bottom panels; X 10). Note that lactoferrin protein and mRNA is distributed in a heterogeneous pattern in the epithelial cells of the adenocarcinomas. As is shown in Fig. 1, a heterogeneous staining pattern for lactoferrin protein is also seen frequently in normal endometrium.

a slightly higher molecular weight than the protein present in normal tissue. This could be due to alterations in the processing of the lactoferrin mRNA, protein, or glycosylation by the malignant cells. Alternatively, there could be minor differences between lactoferrin protein which is present in neutrophils and the form synthesized by uterine epithelial cells. We suggest two hypotheses to explain lactoferrin overexpression in endometrial adenocarcinomas. In the first hypothesis, lactoferrin biosynthesis is deregulated by the same processes that lead to the malignant transformation of endometrium. If this hypothesis is true then lactoferrin may be a useful marker for endometrial adenocarcinoma investigation, and further research is needed to determine whether lactoferrin plays a contributing role in the malignant transformation. A second hypothesis is that lactoferrin-positive human endometrial adenocarcinomas evolve from the clonal expansion of cells residing in the regenerative zone (zona basalis) of normal endometrium. It is interesting to speculate that lactoferrin expression in endometrial cancer may be linked to estrogen action in

some way, since proliferative disorders of human endometrium are linked to chronic estrogen exposure over several years and sequencing data suggests that the promoter for the human lactoferrin gene does contain an ERE.

Although the function of lactoferrin is unknown, a variety of biological roles have been proposed for lactoferrin which could link this protein to a role in cancer, including the regulation of DNA synthesis (25-29), modulation of the immune response (25, 30, 31), and iron transport (32). Some forms of lactoferrin are reported to have RNase activity (33, 34). Secreted RNases are involved in development, reproductive function, neoplasia, angiogenesis, and immune suppression. (35, 36) If angiogenesis and immunosuppression are components of lactoferrin RNase activity, these properties could promote tumor growth.

In the endometrial adenocarcinomas, we observed a heterogeneous expression pattern for lactoferrin, PCNA, Her-2/neu, ER, and PR. With regard to prognosis, patient survival is reportedly worse when

Table 3 Correlation of lactoferrin and PR expression in human endometrial adenocarcinomas

An inverse correlation indicates that lactoferrin and progesterone were not expressed in the same regions of the tumor by immunohistochemical analysis. PR was detected with the antisera KD68, and lactoferrin was detected by a specific polyclonal antisera.

Type of cancer	Age	Stage	Therapy	FIGO ^a grade	Lymph nodes	Myometrial invasion %	Lactoferrin expressed	Inverse correlation with PR
Endometrioid	37	1	None	1	0/12	0	No	No
Endometrioid	61	1	Estrogen	1-3	ND	60	Yes	Yes
Endometrioid	67	1	Estrogen	2-3	ND	60	Yes	Yes
Endometrioid, squamous differentiation	39	1a	None	2	ND	0	Yes	Yes
Endometrioid	69	1b	None	1	ND	29	No	No
Endometrioid	57	1b	None	1	ND	36	Yes	Yes
Endometrioid	72	1b	None	2-3	0/15	5	Yes	Yes
Endometrioid	67	1c	Estrogen	1	ND	50	Yes	Yes
Endometrioid, squamous differentiation	62	2a	None	2	ND	80	No	No
Endometrioid	78	2a	None	2	0/17	5	Yes	Yes
Endometrioid, squamous differentiation	61	3c	None	3	1/27	50	No	No
Endometrioid	64	4b	None	2-3	ND	75	Yes	Yes

^a FIGO, Federation Internationale des Gynecologues et Obstetristes; ND, not done.

1 2 3 4

Fig. 5. Northern analysis of lactoferrin mRNA expression confirms that endometrial adenocarcinomas (Lanes 3 and 4) significantly overexpress the 2.5-kilobase transcript of human lactoferrin in comparison to normal endometrium (Lanes 1 and 2). The Northern hybridization data supports the *in situ* RNA results and confirms that lactoferrin RNA expression is dysregulated in uterine adenocarcinomas. Normal uterine tissues appear to contain low steady-state RNA levels of lactoferrin, reflecting a controlled pattern of protein expression. Equivalent RNA loading and quality for each specimen was demonstrated by ethidium bromide staining of the RNA gels (data not shown) and by probing for a housekeeping gene (glyceraldehyde-3-phosphate dehydrogenase) that does not fluctuate significantly with the metabolic state of the tissue.

endometrial adenocarcinomas lose sex steroid receptors (37, 38), have a higher proliferative index (39), and demonstrate DNA aneuploidy. During the tumor progression of endometrial adenocarcinomas, it appears that the loss of steroid hormone receptors occurs earlier than either the increase in proliferation rate or the development of DNA aneuploidy (40). In our study, we note a striking inverse correlation between the expression of lactoferrin and PR in the endometrial adenocarcinomas. An inverse relationship also has been described for HER-2/*neu* and PR in endometrial adenocarcinomas that correlates with patient prognosis. Furthermore, in cancers of the human endometrium, ovary and breast Her-2/*neu* expression has been associated with advanced disease and poor survival (41-43). HER-2/*neu* is an oncogene that shares sequence homology with the epidermal growth factor receptor and is speculated to contribute to aberrant growth. Of note is that lactoferrin biosynthesis in the mouse uterus is associated with the expression of the epidermal growth factor. Like HER-2/*neu*, the epidermal growth factor receptor is also frequently overexpressed in PR-negative cells of endometrial adenocarcinomas (44). The amplification of growth factor receptor expression in PR-negative endometrial adenocarcinomas may be associated with the acquisition of growth autonomy and hormone independence, which may contribute to the poorer prognosis of PR-negative endometrial carcinomas (45). Some endometrial adenocarcinomas, including recurrent tumors, can be treated successfully with progesterone therapy (46, 47). Although the significance of the inverse relationship between lactoferrin and PR expression is not known, we speculate that the PR-negative cells do not undergo the normal growth inhibition and secretory differentiation normally associated with progesterone action.

A survey of human tissues reveals that lactoferrin is expressed by most normal mammalian exocrine glands and may be a prognostic marker in tumors (20). Lactoferrin is found in normal ductule breast epithelium and in primary breast carcinomas. In breast tumors, there is an inverse correlation between lactoferrin and ERs (20). Notably, lactoferrin expression in breast cancer may fall into the same category

A. Immunoblot

B. Coomassie Blue Protein Staining

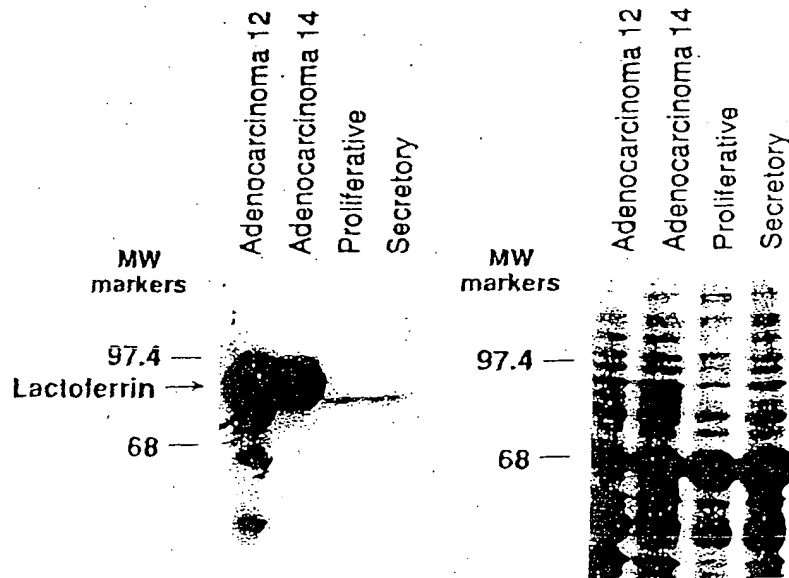


Fig. 6. Western blot analysis using an antiserum specific for human lactoferrin was performed on proteins extracted from normal and malignant endometrium and separated by SDS-polyacrylamide gel electrophoresis. A broad protein band with a molecular weight between 70,000 and 80,000 is detected in both normal and neoplastic endometrial tissue homogenates, consistent with the reported molecular weight of human lactoferrin (A). The most significant observation from the immunoblotting studies is that lactoferrin protein is markedly elevated in the adenocarcinomas, in comparison to normal endometrium, which supports the immunocytochemical analysis that demonstrates a greater number of cells positive for lactoferrin protein in the uterine tumors. B, the relative amount of protein loaded in each lane by Coomassie blue staining.

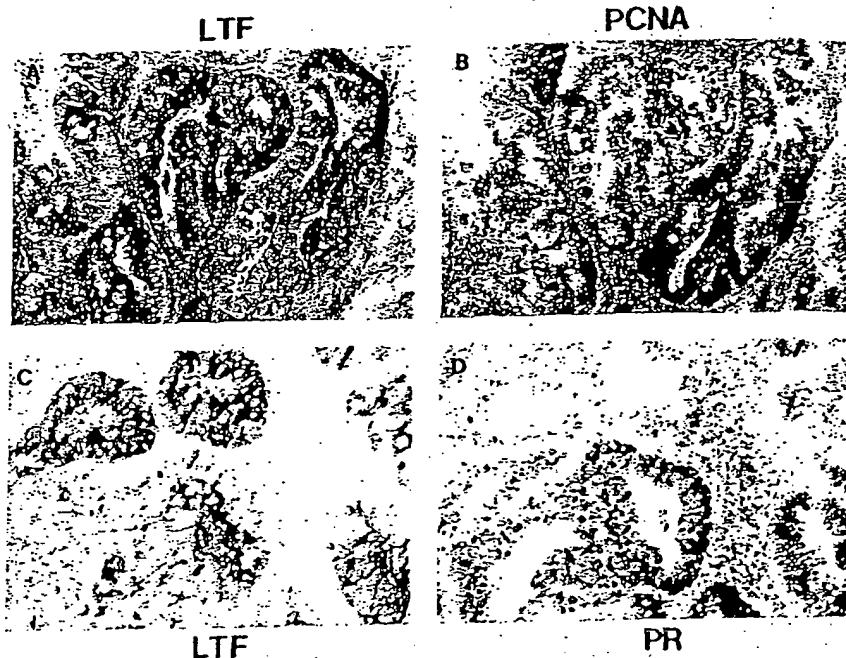


Fig. 7. Correlation of lactoferrin protein expression with the PCNA, a marker of proliferation, and PR as measured by immunohistochemistry performed on serial sections; $\times 20$. In most cases, no relationship between lactoferrin and PCNA expression is found in either normal or malignant endometrium (data not shown). However, in 1 of 12 adenocarcinomas, an inverse correlation is seen between lactoferrin (A) and PCNA (B) localization. This striking pattern was consistent throughout the entire tumor, suggesting the possibility of cell cycle regulation of lactoferrin expression in this adenocarcinoma. The bottom panels exhibit an inverse correlation between lactoferrin (C) and PR expression (D), which was seen in all eight endometrial adenocarcinomas which expressed PR.

as the other markers for ER-negative tumors, such as amplification of EGF receptor, HER-2/*neu*, and transforming growth factor α expression, which are associated with poor prognosis. In gastric carcinomas, lactoferrin expression is associated with transformation of specific cell types including intestinal-type carcinomas, adenomas, and incomplete intestinal metaplasias (28). Although this is complete speculation at this time, perhaps lactoferrin overexpression in the various malignancies may complement the actions of the growth factor pathway molecules and contribute to the autonomous growth of these tumors.

In conclusion, our studies reveal that lactoferrin is associated with a unique population of epithelial cells in the zona basalis and that lactoferrin overexpression may be associated with malignant transformation of the human endometrium. Further studies are needed to elucidate the role of lactoferrin in normal and pathological endometrial physiology.

ACKNOWLEDGMENTS

We gratefully acknowledge Dr. Geoffrey Greene from the Ben May Institute at the University of Chicago for providing the antisera to the PR (KD68) and the collaborative and collegial relationship between the intramural program at the National Institute of Environmental Health Sciences and the Department of Obstetrics and Gynecology at Duke University Medical Center that made this research possible.

REFERENCES

- Pokras, R., and Halmagel, V. Hysterectomies in the United States. In: National Health Survey, DHHS Publication PHS 88-1753, Series 13, #92, pp. 1-26, 1987.
- Pollard, J. Regulation of polypeptide growth factor synthesis and growth factor-related gene expression in the rat and mouse uterus before and after implantation. *J. Reprod. Fertil.*, 58: 721-731, 1990.
- Martin, L. Estrogens, anti-estrogens and the regulation of cell proliferation in the female reproductive tract in vivo. In: J. McLachlan (ed.), *Estrogens in the Environment*, pp. 105-121. New York: Elsevier North Holland, Inc., 1979.
- Martin, L., and Finn, C. A. Hormonal regulation of cell division in epithelial and connective tissues of the mouse uterus. *J. Endocrinol.*, 47: 363-371, 1968.
- Green, M. R., and Pastewka, J. V. Lactoferrin is a marker for prolactin response in mouse mammary explants. *Endocrinology*, 103: 1510-1513, 1978.
- Walmer, D. K., Wrona, M. A., Hughes, C. L., and Nelson, K. G. Lactoferrin expression in the mouse reproductive tract during the natural estrous cycle: correlation with circulating estradiol and progesterone. *Endocrinology*, 131: 1458-1466, 1992.
- Teng, C. T., Pentecost, B. T., Chen, Y. H., Newbold, R. R., Eddy, E. M., and McLachlan, J. A. Lactoferrin gene expression in the mouse uterus and mammary gland. *Endocrinology*, 124: 992-999, 1989.
- McMaster, M. T., Teng, C. T., Dey, S. K., and Andrews, G. K. Lactoferrin in the mouse uterus: analyses of the preimplantation period and regulation by ovarian steroids. *Mol. Endocrinol.*, 6: 101-111, 1992.
- Teng, C. T., Walker, M. P., Bhanacharyya, S. N., Klapper, D. G., DiAugustine, R. P., and McLachlan, J. A. Purification and properties of an oestrogen-stimulated mouse uterine glycoprotein (approx. 70 kDa). *Biochem. J.*, 240: 413-422, 1986.
- Rey, M. W., Woloshuk, S. L., deBoer, H. A., and Pieper, F. R. Complete nucleotide sequence of human mammary gland lactoferrin. *Nucleic Acids Res.*, 18: 5288, 1990.
- Teng, C. T., Liu, Y., Yang, N., Walmer, D. K., and Panella, T. Differential molecular mechanism of the estrogen action that regulates lactoferrin gene in human and mouse. *Mol. Endocrinol.*, 6: 1969-1981, 1992.
- Noyes, R. W., Hertig, A. T., and Rock, J. Dating the endometrial biopsy. *Fertil. Steril.*, 1: 3-25, 1950.
- Silverberg, S. G., and Kurman, R. J. Tumor classification. In: S. G. Silverberg and R. J. Kurman (eds.), *Tumors of the Uterine Corpus and Gestational Trophoblastic Disease*, pp. 13. Washington, DC: Armed Forces Institute of Pathology, 1992.
- Announcement, FIGO Stages: 1988 Revision. *Gynecol. Oncol.*, 35: 125-126, 1989.
- Sambrook, J., Fritsch, E. F., and Maniatis, T. *Molecular Cloning: A Laboratory Manual*. Cold Spring Harbor, NY: Cold Spring Harbor Laboratory, 1989.
- Galand, P., and Degraef, C. Cyclin/PCNA immunostaining as an alternative to tritiated thymidine pulse labelling for marking S phase cells in paraffin sections from animal and human tissues. *Cell Tissue Res.*, 22: 383-392, 1989.
- Kokeguchi, S., Hayase, R., and Sekiba, K. Proliferative activity in normal endometrium and endometrial carcinoma measured by immunohistochemistry using Ki-67 and anti-DNA polymerase α antibody, and by flow cytometry. *Acta Medica Okayama*, 46: 115-121, 1992.
- Suzuki, M., Ogawa, M., Tamada, T., Nagura, H., and Watanabe, K. Immunohistochemical localization of secretory component and IgA in the human endometrium in relation to menstrual cycle. *Acta Histochem. Cytochem.*, 17: 223-229, 1984.
- Hurley, W. L., and Reiman, J. J. Bovine lactoferrin in involuting mammary tissue. *Cell Biology Int.*, 17: 283-289, 1993.
- Campbell, T., Skilton, R. A., Coombes, R. C., Shousha, S., Graham, M. D., and Luqmani, Y. A. Isolation of a lactoferrin cDNA clone and its expression in human breast cancer. *Br. J. Cancer*, 65: 19-26, 1992.
- Kim, S., Goodman, A. L., Williams, R. F., Hodgen, G. D., Hsui, J. G., and Chwalisz, K. Progesterone induces cyclic renewal in the "basalis" layer of primate endometrium: a possible site of action in anti-progesterone-induced endometrial regression. The American Fertility Society Annual Meeting Program, O-063, S32-S35, 1994. (Abstract)
- Lee, B. A., Maher, D. W., Hannink, M., and Donoghue, D. J. Identification of a signal for nuclear targeting in platelet-derived growth-factor-related molecules. *Mol. Cell. Biol.*, 7: 3527-3537, 1987.

25. Acland, P., Dixon, M., Peters, G., and Dickson, C. Subcellular fate of the int-2 oncoprotein is determined by choice of initiation codon. *Nature (Lond.)*, 343: 662-665, 1990.
26. Spence, A., Sheppard, P., Davie, J., Mamo, Y., Nishi, N., McKeehan, W., Dodd, J., and Natusik, R. Regulation of a bifunctional mRNA results in synthesis of secreted and nuclear proteins. *Proc. Natl. Acad. Sci. USA*, 86: 7843-7847, 1989.
27. Gentile, P., and Broxmeyer, H. E. Interleukin-6 ablates the accessory cell-mediated suppressive effects of lactoferrin on human hematopoietic progenitor cell proliferation *in vitro*. *Ann. NY Acad. Sci.*, 628: 74-83, 1991.
28. Rejman, J. J., Oliver, S. P., Muenchen, R. A., and Turner, J. D. Proliferation of the MAC-T bovine mammary epithelial cell line in the presence of mammary secretion whey proteins. *Cell Biol. Int. Rep.*, 16: 993-1001, 1992.
29. Broxmeyer, H. E. Suppressor cytokines and regulation of myelopoiesis. Biology and possible clinical uses. *Am. J. Pediat. Hematol.-Oncol.*, 14: 22-30, 1992.
30. Tuccari, G., Barresi, G., Arena, F., and Inferera, C. Immunocytochemical detection of lactoferrin in human gastric carcinomas and adenomas. *Arch. Pathol. Lab. Med.*, 113: 912-915, 1989.
31. Lagmani, Y. A., Campbell, T. A., Bennett, C., Coombes, R. C., and Paterson, I. M. Expression of lactoferrin in human stomach. *Int. J. Cancer*, 49: 684-687, 1991.
32. Djcha, A., and Brock, J. H. Effect of transferrin, lactoferrin, and chelated iron on human T-lymphocytes. *Br. J. Haematol.*, 80: 235-241, 1992.
33. Broxmeyer, H. E., Mantel, C., Gentile, P., Srivastava, C., Miyazawa, K., Zucali, J. R., Rado, T. A., Levi, S., and Arosio, P. Actions of H-subunit ferritin and lactoferrin as suppressor molecules of myelopoiesis *in vitro* and *in vivo*. *Curr. Stud. Hematol. Blood Transfus.*, 178-181, 1991.
34. Sanchez, L., Calvo, M., and Brock, J. H. Biological role of lactoferrin. *Arch. Dis. Child.*, 67: 657-661, 1992.
35. Furmanski, P., and Li, Z. P. Multiple forms of lactoferrin in normal and leukemic human granulocytes. *Exp. Hematol.*, 18: 932-935, 1990.
36. Furmanski, P., Li, Z. P., Fortuna, M. B., Swamy, C. V., and Das, M. R. Multiple molecular forms of human lactoferrin: identification of a class of lactoferrins that possess ribonuclease activity and lack iron-binding capacity. *J. Exp. Med.*, 170: 415-429, 1989.
37. Felt, J. W., Snyder, D. J., Lobb, R. R., Alderman, E. M., Bethune, J. L., Riordan, J. F., and Valler, B. L. Isolation and characterization of angiogenin, an angiogenic protein from human carcinoma cells. *Biochemistry*, 24: 5480-5486, 1985.
38. D'Alessio, G., Di Donato, A., Parente, A., and Piccoli, R. Seminal RNase: a unique member of the ribonuclease superfamily. *Trends Biochem. Sci.*, 16: 104-106, 1991.
39. Mayer, T. K., and Mooney, R. A. Laboratory analyses for steroid hormone receptors, and their applications to clinical medicine. *Clin. Chim. Acta*, 172: 1-33, 1988.
40. Vilho, R., Alanko, A., Isomaa, V., and Kuoppila, A. The predictive value of steroid hormone receptor analysis in breast, endometrial and ovarian cancer. *Med. Oncol. Tumor Pharmacother.*, 3: 197-210, 1986.
41. Rosenberg, P., Wingren, S., Simonsen, E., Sial, O., Risberg, B., and Nordenskjold, B. Flow cytometric measurements of DNA index and S-phase on paraffin-embedded early stage endometrial cancer: an important prognostic indicator. *Gynecol. Oncol.*, 35: 50-54, 1989.
42. Ponninen, R., Mattila, J., Kuoppala, T., and Koivula, T. DNA ploidy, cell proliferation and steroid hormone receptors in endometrial hyperplasia and early adenocarcinoma. *J. Cancer Res. Clin. Oncol.*, 119: 426-429, 1993.
43. Slamon, D. J., Clark, G. M., Wong, S. G., Levin, W. J., Ullrich, A., and McGuire, W. L. Human breast cancer: correlation of relapse and survival with amplification of the HER-2/*neu* oncogene. *Science (Washington DC)*, 235: 177-182, 1987.
44. Slamon, D. J., Godolphin, W., Jones, L. A., et al. Studies of the HER-2/*neu* proto-oncogene in human breast and ovarian cancer. *Science (Washington DC)*, 244: 707-712, 1989.
45. Berchuck, A., Rodriguez, G., Kinney, R. B., Soper, J. T., Dodge, R. K., Clarke-Pearson, D. L., and Bast, R. C., Jr. Overexpression of HER-2/*neu* in endometrial cancer is associated with advanced stage disease. *Am. J. Obstet. Gynecol.*, 164: 15-21, 1991.
46. Bigsby, R. M., Li, A. X., Bomalaski, J., Siehman, F. B., Look, K. Y., and Sotton, G. P. Immunohistochemical study of HER-2/*neu*, epidermal growth factor receptor, and steroid receptor expression in normal and malignant endometrium. *Obstet. Gynecol.*, 79: 95-100, 1992.
47. Lindahl, B., Ferno, M., Gullberg, B., Norgren, A., and Willen, R. 5-year survival rate in endometrial carcinoma stage I-II related to steroid receptor concentration, degree of differentiation, age and myometrial invasion. *Anticancer Res.*, 12: 409-412, 1992.
48. Koborn, E. I. Gestagens and endometrial carcinoma. *Gynecol. Oncol.*, 4: 398-411, 1976.
49. Creasman, W. T. Clinical correlates of estrogen and progesterone binding protein in human endometrial carcinoma. *Obstet. Gynecol.*, 53: 363-376, 1980.

Comparison of *TP53* Mutations Identified by Oligonucleotide Microarray and Conventional DNA Sequence Analysis¹

Wen-Hsiang Wen, Leslie Bernstein, Jennifer Lescallett, Yasmin Beazer-Barclay, Jane Sullivan-Halley, Marga White, and Michael F. Press²

Department of Pathology [W.-H. W., M. F. P.], The Norris Comprehensive Cancer Center [L. B., J. S.-H., M. F. P.], and Department of Preventive Medicine [L. B., J. S.-H.], University of Southern California School of Medicine, Los Angeles, California 90033; Affymetrix, Inc., Santa Clara, California 95051 [J. L.]; and Gene Logic, Inc., Gaithersburg, Maryland 20878 [Y. B.-B.]

ABSTRACT

As the rate of gene discovery accelerates, more efficient methods are needed to analyze genes in human tissues. To assess the efficiency, sensitivity, and specificity of different methods, alterations of *TP53* were independently evaluated in 108 ovarian tumors by conventional DNA sequence analysis and oligonucleotide microarray (p53 GeneChip). All mutations identified by oligonucleotide microarray and all disagreements with conventional gel-based DNA sequence analysis were confirmed by re-analysis with manual and automated dideoxy DNA sequencing. A total of 77 ovarian cancers were identified as having *TP53* mutations by one of the two approaches, 71 by microarray and 63 by gel-based DNA sequence analysis. The same mutation was identified in 57 ovarian cancers, and the same wild type *TP53* sequence was observed in 31 ovarian cancers by both methods, for a concordance rate of 81%. Among the mutation analyses discordant by these methods for *TP53* sequence were 14 cases identified as mutated by microarray but not by conventional DNA sequence analysis and 6 cases identified as mutated by conventional DNA sequence analysis but not by microarray. Overall, the oligonucleotide microarray demonstrated a 94% accuracy rate, a 92% sensitivity, and an 100% specificity. Conventional DNA sequence analysis demonstrated an 87% accuracy rate, 82% sensitivity, and a 100% specificity. Patients with *TP53* mutations had significantly shorter overall survival than those with no mutation ($P = 0.02$). Women with mutations in loop2, loop3, or the loop-sheet-helix domain had shorter survival than women with other mutations or women with no mutations ($P = 0.01$). Although further refinement would be helpful to improve the detection of certain types of *TP53* alterations, oligonucleotide microarrays were shown to be a powerful and effective tool for *TP53* mutation detection.

INTRODUCTION

TP53 mutations are the most common genetic alterations in human malignancies. About 570 different *TP53* mutations have been identified by analysis of more than 8000 human cancers since 1989 (1). Most mutations were identified by conventional methods such as SSCP³ and DNA sequencing. Other methods, such as denaturing gradient gel electrophoresis, heteroduplex analysis, and cleavage methods (2), have also been used. In general, these traditional gel-based sequencing methods are relatively time-consuming, labor-intensive, sequential processes. Relatively few studies have analyzed the entire coding sequence from exons 2 through 11. Therefore, current estimates of *TP53* alterations and its mutational spectrum may be incomplete. A more accurate and rapid method would provide more complete information in future studies of *TP53*. Methods based on hybridization of test DNA or RNA with multiple, defined oligo-

nucleotides or cDNA probes attached to a solid glass or nylon matrix have been developed and are referred to as "oligonucleotide microarrays" or "DNA microarrays" or "gene chips." By analyzing different hybridization patterns or levels between control and test DNA or RNA, oligonucleotide microarrays have been used for the analysis of known genes (such as *TP53*, *BRCA1*, the ataxia-telangiectasia gene, the cystic fibrosis transmembrane conductance regulator gene, HIV reverse transcriptase and protease genes, and the cytochrome P450 gene), *de novo* DNA sequencing, comparative sequence analysis, and gene expression studies (3-5). However, relatively little is known about the sensitivity and specificity of microarray methods compared with gel-based DNA sequence analysis. In this study, we compared *TP53* mutations detected by conventional gel-based DNA sequence analysis with those identified by oligonucleotide microarray (p53 GeneChip) in 108 ovarian cancers. The relationship between *TP53* mutations and patient survival was also evaluated.

MATERIALS AND METHODS

Tumor Specimens. Clinical information and *TP53* alterations identified by SSCP and conventional sequence analysis from most of these cases has been reported separately (6). The 108 ovarian carcinomas studied here for *TP53* alterations included 77 serous carcinomas, 5 mucinous carcinomas, 12 endometrioid carcinomas, 5 clear cell carcinomas, 7 mixed epithelial carcinomas, and 2 undifferentiated ovarian adenocarcinomas.

DNA Extraction. Genomic DNA from 108 frozen ovarian epithelial carcinomas, available through the University of Southern California Tumor and Tissue Bank, was analyzed for *TP53* mutations. Frozen tissue sections stained with H&E were used to confirm that the tumor tissue selected for analysis was composed predominantly of tumor cells. DNA was extracted from 10 to 20 serial frozen tissue sections (10 μ m thick) of the tumor collected in Eppendorf tubes. The extraction solution consisted of 300 μ l of 10 mM Tris-HCl, 25 mM EDTA, 100 mM NaCl, 0.5% SDS, and Proteinase K (0.1 mg/ml) incubated overnight at 50°C. After complete digestion, DNA was purified by centrifugation after deproteinization with phenol:chloroform:isoamyl alcohol (50:49:1) treatment and precipitation with ethanol and sodium acetate (3 M; pH 5.2) overnight at -20°C. The DNA yield was determined by spectrophotometry and analyzed by SSCP. DNA sequence analysis (6), automated DNA sequence analysis (7, 8), and p53 GeneChip assay as described below.

SSCP. The PCR was used to amplify each of the exons contributing to the open reading frame of the *TP53* gene. Each of the oligonucleotide primer pairs was designed to span not only the exon of interest but also sufficient flanking intron sequence so that splice junction mutations would be included for analysis. The sequence for each primer pair is described elsewhere (6). Each exon of *TP53* was amplified by the PCR technique through 35 reaction cycles in a thermal cycler using 100 ng of genomic DNA, 4 mM deoxynucleotide triphosphates, 6 μ Ci of [³²P]dATP, 6 μ Ci [³²P]dCTP, and 25 pmol of the appropriate oligonucleotide primer pair. Conformational differences in the PCR products were resolved on nondenaturing mutation detection enhancement polyacrylamide gels with the addition of 5% glycerol at room temperature. All samples identified by SSCP as having altered mobility were further characterized by DNA sequencing for the exon putatively identified as mutated. In previous studies from our laboratory, SSCP has had an 85% sensitivity and a 98% specificity for *TP53* mutations (6).

Manual DNA Sequencing. DNA segments identified as having altered mobility by SSCP were evaluated by manual DNA sequence analysis. Ovarian

Received 6/23/99; accepted 3/17/00.

The costs of publication of this article were defrayed in part by the payment of page charges. This article must therefore be hereby marked advertisement in accordance with 18 U.S.C. Section 1734 solely to indicate this fact.

¹Supported in part by Grants CA48780 and CA50589 from the National Cancer Institute, Grant DAMD17-94-4234 from the United States Army Medical Research and Materiel Command and a California SEER Registry Special Study grant.

²To whom requests for reprints should be addressed, at USC Norris Comprehensive Cancer Center, Norris Topping Tower, Room 5409, 1441 Eastlake Avenue, University of Southern California School of Medicine, Los Angeles, CA 90033.

³The abbreviations used is: SSCP, single-strand conformational polymorphism.

carcinoma template DNA was reamplified with the appropriate PCR primer pair, and amplified PCR product was purified (PCR Purification kit; Qiagen, Inc.). Both the sense and antisense strands were analyzed by the dideoxynucleotide chain termination technique with PCR sense and antisense primers, which were end-labeled using polynucleotide kinase. The products of these sequencing reactions were then separated by electrophoresis on 6% denaturing polyacrylamide gels (National Diagnostics, Atlanta, GA).

Automated DNA Sequence Analysis of All SSCP-negative Samples. Ovarian carcinoma cases with no mobility shift identified by SSCP screening were subjected to complete DNA sequence analysis of each exon contributing to the *TP53* open reading frame (exons 2–11) by automated DNA sequence analysis, as described elsewhere (7), to identify those mutations that SSCP failed to identify.

p53 GeneChip Assay. Oligonucleotide microarrays are manufactured using light-directed combinatorial chemistry. In the context of the p53 GeneChip, the synthesis cycles were repeated until oligonucleotides of ~18 bases in length were constructed. Approximately 65,000 different oligonucleotide probes were synthesized in a 1.2 × 1.2-cm area (grid) consisting of 256 cells in each dimension. Each probe cell (50 μm × 50 μm) was arranged and constructed to accommodate 10⁷ copies of each oligonucleotide. These probes were designed to interrogate each base of exons 2–11 of the human *TP53* coding sequence (~1262 bases) and +2/-2 splice sites in a standard tiling format as well as a redundant tiling format for both sense and antisense strands (Fig. 1A). The first format, standard tiling, was the compilation of complementary probes designed to interrogate the normal sequence and every possible single-base mismatch, single-base deletion, and +2/-2 splice site junctures along the coding region of the *TP53* gene. More specifically, probes in the standard tiles had a common substitution position located at the twelfth base from the 3' end. Each probe set represents A, C, G, T, a 1-bp deletion, and an empty cell for background subtraction (Fig. 1B). Five probes per sense and antisense directions were arranged for each nucleotide position (Fig. 1C). The second format, redundant tiling, was designed to interrogate over 300 common mutations reported more than once in the *TP53* database (9), with the exception of deletions or insertions >1 bp. Each redundantly tiled mutation had 12 probes (6 sense and 6 antisense) designed to interrogate the mismatch. The substitution position was placed at different locations on the probe for maximum hybridization and discrimination of the mutant target. The hybridization pattern and intensity was then determined by laser scanner and analyzed by software based on the mixture detection algorithm. When a mutation occurred, the software called the mutation according to the codon in which the mutation existed. Probes from sense and antisense strands in both tiling formats were used to generate a confidence score for mutations. Mutations that occurred in codons with redundantly tiled nucleotides, in addition to the standard tiling, had the highest confidence score. These scores were higher because of the increased number of probes available to calculate the average intensity from each probe cell. Confidence scores (GeneChip score) ranged from 1 to 36. A score of 36 was the highest indicator that a mutation was present. Cases with scores <10 were regarded as wild-type *TP53*. Through experience prior to initiating this study, we found that samples that showed alternative tiling and on initial processing scored <10 were associated with only standard tiling when processed a second time. These samples proved to be false-positive samples in our pilot investigations with non-study samples. No false-positives produced an alternative tiling pattern when processed on an array a second time.

Tumor DNA from all 108 specimens was analyzed by p53 GeneChip Assay (Affymetrix). Each sample DNA was PCR amplified, fragmented with DNase, labeled with Fluorescein-N6-ddATP (DuPont NEN, Boston, MA) by way of a terminal transferase reaction and hybridized to a p53 GeneChip Array. Fluorescently labeled fragmented DNA samples were washed over the chip and allowed to bind to complementary oligonucleotide probes. Hybridized probe arrays were then read using the GeneArray Scanner (Hewlett-Packard, JHP G2500A). As a quality assurance step, a control oligonucleotide was added to each sample during hybridization to examine the signal intensity and proper alignment of the probe array after the scan. Prior to the collection of image data, the scanner confirmed the correct position and alignment of the chip by focusing on a series of defined positions.

To account for any variations that occurred during the assay, each sample batch was processed with human placental DNA as a wild-type control (Sigma

Chemical Co., St. Louis, MO). Any sequence mismatch present in sample DNA was identified by comparison to the control placental DNA (Fig. 1B).

Repeat DNA Sequencing. Automated and/or manual DNA sequencing was used to confirm each mutation identified by the p53 GeneChip assay. In addition, six samples that were wild type by p53 GeneChip but mutated by conventional gel-based assays were also reconfirmed as mutated with automated sequence analysis. Fourteen samples, initially wild type by the above "conventional" gel-based DNA sequence analyses but mutated by p53 GeneChip analysis, were also re-analyzed to confirm the presence of these mutations in either the manual sequence analysis or automated sequence analysis method or in both. Samples were sequenced on an ABI 377 sequencer using the ABI Prism dRhodamine Dye Terminator Cycle Sequencing kit. Each reaction was performed under the conditions outlined by the manufacturer (Perkin-Elmer-Applied Biosystems, Inc., Foster City, CA). Sequencing primers spanned exons 2–11 of the *TP53* gene. Samples were analyzed using the ABI Sequence Navigator Software (version 1.0.1). It was not considered necessary to use a fourth method to confirm the presence of mutations in these samples because re-analysis with either of the "conventional" methods, manual sequencing or automated sequencing, did eventually demonstrate the mutations.

Statistics. Statistical analyses were conducted using the SAS and Epilog software packages. The differences between *TP53* mutations identified by conventional sequence analysis and *TP53* mutations identified by p53 GeneChip were evaluated using Fisher's exact test. Differences in overall survival according to *TP53* status were assessed by log-rank test. Cox proportional hazards analyses were conducted to assess the joint effects of *TP53* alterations, age, grade, stage, and histological type of carcinoma on risk of ovarian cancer death.

RESULTS

***TP53* Mutations Identified by Conventional SSCP and DNA Sequence Analysis.** Among the 108 DNA samples of ovarian carcinoma analyzed, 54 cases were identified by gel shift with SSCP screening of PCR products, and 53 of these SSCP alterations were confirmed by manual gel-based DNA sequence analysis. All ovarian tumor DNAs that lacked SSCP alterations were subjected to complete automated DNA sequence analysis of exons 2–11 (7), and an additional 10 mutations were identified. The 63 cases with mutations, identified by these "conventional" DNA sequence methods, included 57 cases with single-bp substitution mutations, 3 with deletion mutations, and 3 with combined deletion and insertion mutations (Table 1). Among the 57 substitution mutations were 49 missense mutations, 4 nonsense mutations, and 4 splice junction mutations. In addition, 4 cases contained DNA polymorphisms. DNA from 41 cases showed no sequence alteration. Those cases with DNA polymorphisms and those cases with no sequence alterations were both considered to have wild-type *TP53* sequences (45 cases; 42%).

***TP53* Mutations Identified by Oligonucleotide Microarray.** Among the 108 ovarian carcinoma DNA samples, 71 (66%) had GeneChip scores for at least one position that was between 10 and 36 and were, therefore, identified as mutated. Thirty-seven (34%) cases were identified as having wild-type *TP53* gene with either a GeneChip score of <10 or a DNA polymorphism identified. The identified 71 ovarian tumors with mutations included 69 with single-bp substitution mutations and 2 with single-bp deletion mutations. Among the 69 ovarian tumors with substitution mutations were 56 with missense mutations, 7 with nonsense mutations, and 6 with splice junction mutations. Three ovarian tumors had two *TP53* mutations. All three cases had two single-bp substitution mutations for a total of 72 single-bp substitution mutations identified among cases in this cohort. One case with two mutations had both a missense and a splice junction mutation, and the other two cases each had two missense mutations identified. Because no effort was made to characterize more than one mutation using the "conventional" DNA sequence analysis

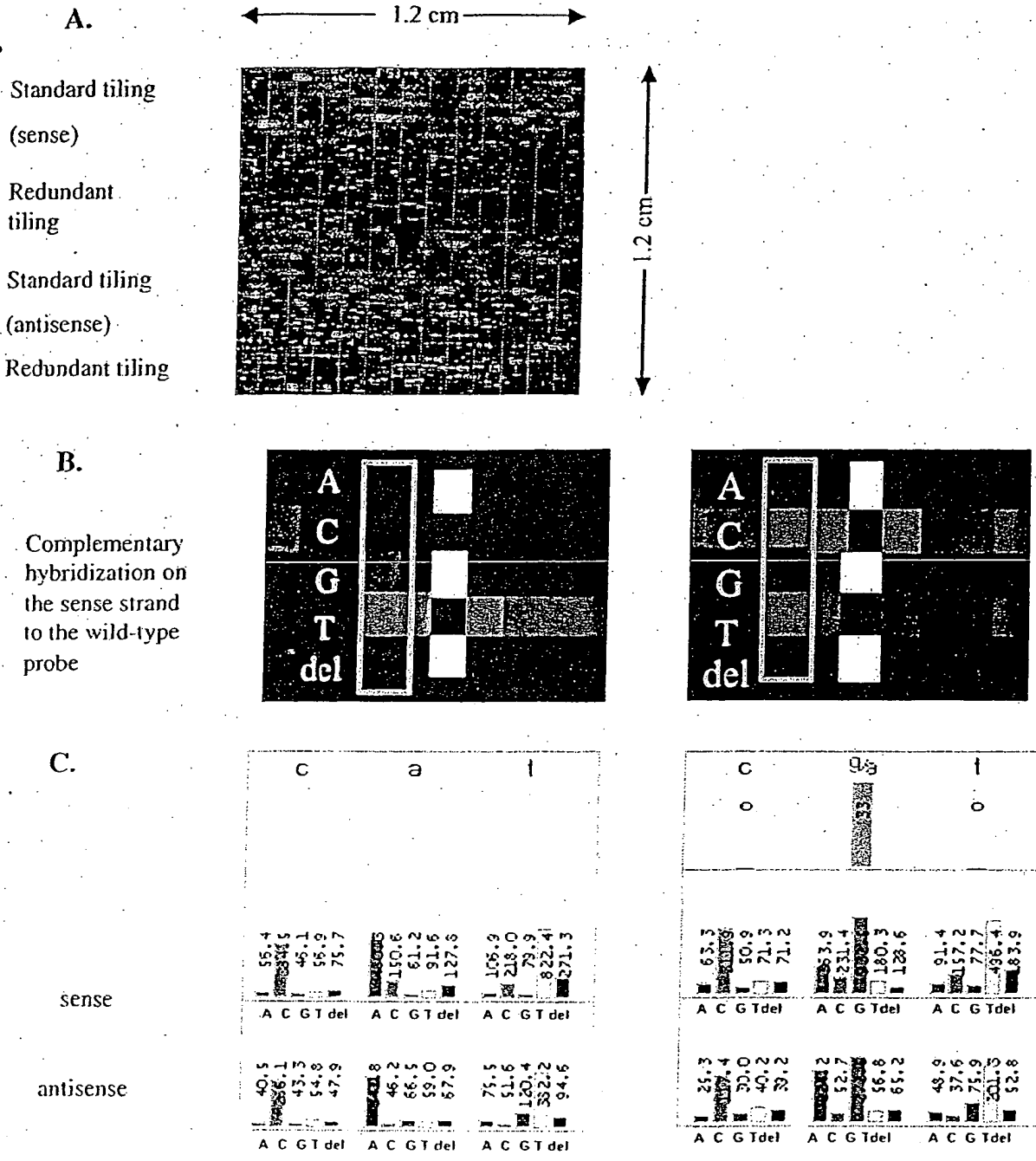


Fig. 1. Arrangement of p53 GeneChip (A) and examples of sequence analysis at a particular nucleotide (B and C). A, p53 GeneChip architecture. Approximately 65,000 different oligonucleotide probes were synthesized in a 1.2×1.2 -cm area. These probes interrogated each base and flanking intron sequences of exons 2-11 of the human TP53 gene in a standard tiling format as well as a redundant tiling format for both sense and antisense strands. B, examples of oligonucleotide probe hybridization in wild-type target (left) and mixture target (right). Hybridization signal intensity for each individual tile of each nucleotide position can be ordered from high signal intensity to low signal intensity as follows: white > green > blue > black. The highest fluorescent tile indicates hybridization with the complementary nucleotide sequence. In the first illustration (wild type, left picture), the fluorescent green signal identified within the indicated area represents the strongest hybridization of the normal A nucleotide to a "T" nucleotide at the queried position. In the second illustration (wild type/mutant mixture, right picture), the fluorescent green signal identified within the indicated area represents hybridization of mutated G nucleotide in test DNA to a "C" nucleotide at the queried position. The weaker blue hybridization signal of wild-type A to the "T" nucleotide in the oligonucleotide probe is also shown, demonstrating lower signal than observed with wild-type sample (left), which shows a green signal. The white signal at multiple tiles in that nucleotide position for both wild-type and mutant target represents the hybridization by control oligonucleotide, which is shown as a white straight dotted line on the grid in A. C, hybridization signal intensities for test DNA at three queried positions in sense and antisense directions. Each probe in a tile set is perfectly complementary to the reference sequence, except for a mismatch at the 12th nucleotide position. At this position, each of the four possible nucleotide substitutions A, C, G, and T and a single-bp deletion are represented in the probe set. Sense and antisense probe hybridization data and probe set relative hybridization intensities are shown in individual columns using five different colors for each nucleotide position analyzed. The relative hybridization intensities for each nucleotide at a queried position permit a nucleotide identification call to be made. The wild-type base A (left) and mixture (mutant/wild type) A/G (right) correspond to the images of B (left) and B (right).

Table 1 Classification of TP53 mutations identified by conventional DNA sequence analysis and DNA oligonucleotide microarray^a

Mutation type	Sequencing	Microarray	Total
Single-bp substitutions	57	69	71
Missense	49	56	58
Nonsense	4	7	7
Splice junction	4	6	6
Deletion and/or insertion	6	2	6
Single-bp deletion	2	2	2
Multiple bp deletion	1	0	1
Deletion and insertion	3	0	3
Total	63	71	77

^a Cases containing more than one TP53 mutation had the second mutation excluded from this comparison because no attempt was made to characterize more than one TP53 mutation by conventional DNA sequence analyses.

Table 2 Comparison of TP53 mutations identified by conventional DNA sequence analysis and oligonucleotide microarray analysis

	Mutations detected by sequencing	Wild-type by sequencing	Total no.
Mutations detected by microarray	57	14	71
Wild-type by microarray	6	31	37
Total no.	63	45	108

methods described above, only one of the two mutations identified in these three ovarian tumors by p53 GeneChip was included in the comparative evaluation of the methods (Table 1). In addition, among seven cases with a TP53 polymorphism, five also had a missense mutation. These cases were considered in the analysis as showing a single missense substitution.

Comparison of TP53 Mutations Identified by Oligonucleotide Microarray and Conventional DNA Sequence Analysis. A total of 77 ovarian cancers had TP53 mutations identified by at least one of the two approaches. The 77 tumors with identified mutations included 71 with single-bp substitution mutations, 3 with deletion mutations, and 3 with combined deletion/insertion mutations (Table 1). Among the 71 ovarian tumors with substitution mutations were 58 with missense mutations, 7 with nonsense mutations, and 6 with splice junction mutations.

Both methods identified a mutation in 57 ovarian cancers and no mutation in 31 ovarian cancers for a concordance rate of 81% (Table 2). As described previously, 71 ovarian tumors with mutations (71 of 108; 66%) were identified by DNA microarray and 63 (63 of 108; 58%) by conventional gel-based DNA sequence analysis. There were 6 cases identified by conventional DNA sequence analysis but not by DNA oligonucleotide microarray (Table 3) and 14 cases identified as mutated by DNA oligonucleotide microarray but not by conventional DNA sequence analysis (Table 4). These cases were all resequenced and confirmed as mutated by manual or automated DNA sequence analysis or both.

In this cohort of ovarian tumors, one case had an exon 4 (GTG→TTG) Val73Leu missense mutation, which was identified by conventional DNA sequence analysis but not by p53 GeneChip analysis (Table 3). The cohort contained two identical Lys132Arg missense mutations (AAG→AGG). One of these mutations was identified by both approaches; the other was detected initially only by the

oligonucleotide microarray approach (Table 4). A Cys141Trp (TGC→TGG) missense mutation, missed by conventional DNA sequence analysis, was identified by p53 GeneChip analysis (Table 4). A nonsense Gln167Stop (CAG→TAG) mutation was identified by p53 GeneChip analysis but not by conventional DNA sequence analysis (Table 4).

One of two mutations involving codon 195 was detected by conventional DNA sequence analysis but not by the p53 GeneChip. The other mutation at codon 195 was detected by p53 GeneChip but not by conventional DNA sequence analysis. The codon 195 mutation detected by conventional DNA sequence analysis but not by p53 GeneChip analysis was a deletion/insertion mutation involving codons 193–195 (9-bp deletion of CATCTTATC with a 6-bp insertion of GCCCCT, which encoded a deletion of His, Leu, and Ile and an insertion of Ala, Pro; Table 3). The codon 195 mutation detected by p53 GeneChip but not by conventional DNA sequence analysis was an Ile195Asn (ATC→AAC) missense mutation (Table 4). Neither of two Arg196Stop (CGA→TGA) mutations were detected by conventional DNA sequence analysis, but both were detected by p53 GeneChip. Missense substitutions at codons 220 and 237 were identified with oligonucleotide microarray analysis but not with conventional DNA sequence analysis (Table 4). On the other hand, a missense mutation at codon 267 (CGG→CCG; Arg267Pro) was detected by conventional DNA sequence analysis but not by p53 GeneChip analysis (Table 3).

Splice site mutations involving the substitution of an A for a G at the –2 position (intron 6 splice site acceptor) and a T for a G at the +2 position (intron 7 splice site donor) were detected by oligonucleotide microarray analysis but were not detected by conventional DNA sequence analysis (Table 4).

Deletion/insertion mutations at codon 219 and codons 247–251 and a deletion at codons 264–265 were identified by conventional DNA sequence analysis but not by p53 GeneChip analysis (Table 3). The deletion/insertion mutation at codon 219 involved the loss of CCC and insertion of GTGTTC (Pro219Val,Phe). The deletion/insertion mutation of codons 247–251 involved a loss of CATCTTATC and an insertion of GCCCCT, predicting the loss of amino acids His, Leu, and Ile and the insertion of Ala, Pro at this position.

Three of the seven mutations at codon 273 were detected by conventional DNA sequence analysis, whereas all seven were detected by p53 GeneChip. Six of the mutations were Arg273Cys mutations, and one was an Arg273Gly mutation. All four of the missed mutations were Arg273Cys mutations.

Overall, TP53 oligonucleotide microarray analysis identified 71 of the 77 mutations, whereas conventional DNA sequence analyses identified 63 of the 77 mutations. This difference in detection between these approaches was marginally statistically significant ($P = 0.091$, Fisher exact test). Sixty-nine of the 71 single-bp substitution mutations, including missense, nonsense, and splice junction mutations (Table 1), were detected by the TP53 oligonucleotide microarray analysis, whereas 57 were detected by conventional DNA sequence analyses. The TP53 oligonucleotide microarray detected significantly more single-bp substitution mutations than conventional DNA se-

Table 3 TP53 mutations detected by conventional DNA sequence analysis but not identified by DNA microarray analysis

Case no.	Genomic location	Codon	DNA sequence change	Predicted amino acid changes	Mutation type
715	Exon 4	73	GTG→TTG	Val→Leu	Missense
805	Exon 6	219	Deletion of CCC. Insertion of GTGTTC	Loss of Pro. Insertion of Val, Phe	Deletion/Insertion
2719	Exon 6	193–195	Deletion of CATCTTATC. Insertion of GCCCCT	Loss of His, Leu, Ile. Insertion of Ala, Pro	Deletion/Insertion
2001	Exon 7	247–251	Deletion of AACCGGAGGCCATC. Insertion of GGGC	Truncated protein	Frameshift/Nonsense
2332	Exon 8	267	CGG→CCG	Arg→Pro	Missense
696	Exon 8	264–265	Loss of ACT	Loss of Leu	Deletion

TP53 MUTATIONS ANALYZED BY DNA CHIP TECHNOLOGY

Table 4 TP53 mutations identified by DNA microarray but not by conventional DNA sequence analysis

Case no.	Genomic location	Codon	DNA sequence change	Amino acid change	Mutation type	TP53 geneChip score
1748	Exon 5	132	AAG→AGG	Lys→Arg	Missense	26
2348	Exon 5	141	TGC→TGG	Cys→Trp	Missense	16
1566	Exon 5	167	CAG→TAG	Gln→stop	Nonsense	11
2741	Exon 6	195	ATC→AAC	Ile→Asn	Missense	24
2729	Exon 6	196	CGA→TGA	Arg→stop	Nonsense	11
2733	Exon 6	196	CGA→TGA	Arg→stop	Nonsense	12
712	Exon 6	220	TAT→TGT	Tyr→Cys	Missense	31
690	Intron 6	Splice acceptor	-2: a→g	NA*	Splice junction	33
2347	Exon 7	237	ATG→ATA	Met→Ile	Missense	11
835	Intron 7	Splice donor	+2: t→g	NA	Splice junction	12
2735	Exon 8	273	CGT→TGT	Arg→Cys	Missense	12
993	Exon 8	273	CGT→TGT	Arg→Cys	Missense	12
2311	Exon 8	273	CGT→TGT	Arg→Cys	Missense	11
2327	Exon 8	273	CGT→TGT	Arg→Cys	Missense	11

* NA, not applicable.

quence analyses ($P = 0.0024$, Fisher exact test). However, TP53 oligonucleotide microarray detected only two of the six deletion and/or insertion mutations, whereas conventional DNA sequence analyses detected all six. This difference was marginally statistically significant ($P = 0.06$, Fisher exact test).

Of the 49 missense mutations identified by conventional DNA sequencing, DNA microarray analysis detected 47 (96%). Of the four splice junction mutations identified by conventional DNA sequence analysis, microarray technology detected all of them (100%). Of the seven cancers with a premature stop codon identified by conventional DNA sequencing, oligonucleotide microarray analysis detected six, including four nonsense mutations caused by single-bp substitutions and two frameshift mutations caused by single-bp deletions. Among the four cases that had multiple-bp deletions and/or insertions, microarray analysis missed all of them, whether or not the mutation led to a frameshift. In conclusion, microarray achieved a 94% accuracy (102 of 108), a 92% sensitivity (71 of 77), and a 100% (31 of 31) specificity in mutation detection. Conventional DNA sequence analysis demonstrated an 87% (94 of 108) accuracy rate, an 82% (63 of 77) sensitivity, and a 100% (31 of 31) specificity.

Relationship between TP53 Alterations and Survival. One hundred and four of the 108 patients with survival data available were analyzed for the relationship between TP53 mutation and overall

survival. The presence of TP53 mutations was associated with shorter survival ($P = 0.02$; Fig. 2A). Women with mutations in loop2, loop3, or the loop-sheet-helix domain had a significantly shorter survival than women who had other mutations in their ovarian cancers and women who had no mutations in their ovarian cancers ($P = 0.01$; Fig. 2B). Age (Trend test, $P = 0.03$), grade ($P = 0.02$), and stage ($P = 0.002$) were also associated with shortened overall survival. Mucinous histopathology was associated with a lack of TP53 mutations ($P = 0.023$) but not with survival. Serous (*versus* all others) tumors were not associated with overall survival ($P = 0.94$). Cox proportional hazards analysis, adjusting for the other factors such as size, stage, and grade, suggested that TP53 was an independent predictor of shortened overall survival after including these factors in the analysis. However, formal statistical significance was not demonstrated ($P = 0.09$), probably because of the limited sample size.

DISCUSSION

This study was designed to assess the sensitivity, specificity, and accuracy of DNA microarrays (p53 GeneChip) in identifying TP53 mutations relative to conventional gel-based DNA sequence analysis. Overall, the two methods showed a high level of concordance, with 88 of the 108 tumors (81%) showing the same result. With the inclusion

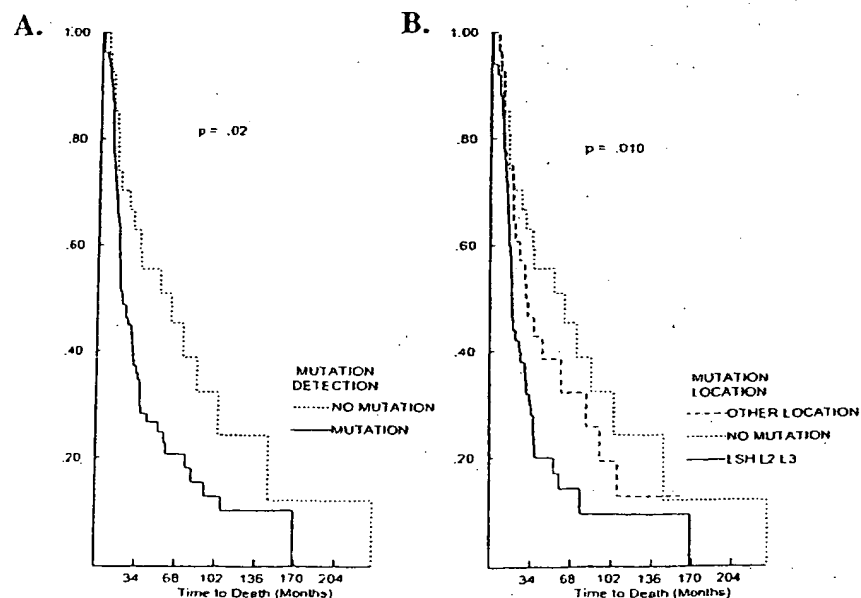


Fig. 2. Cumulative probability of survival for women with ovarian carcinomas showing differences in TP53 tumor suppressor gene status. A, women whose ovarian cancer had TP53 mutation (—) showed a significantly shorter overall survival ($P = 0.02$) than women whose ovarian cancer had wild-type TP53 (---). B, a significantly shorter survival ($P = 0.01$) was observed for women whose ovarian cancer had mutations located in the highly conserved loop-sheet-helix, loop2, or loop3 domains of TP53 (—), compared with women whose ovarian cancer had mutations located in any other site in TP53 (---) or in women whose ovarian cancer had wild-type TP53 (---).

of 14 mutations initially not identified with conventional sequence analysis, the DNA microarray achieved an accuracy of 94% (102 of 108), whereas conventional DNA sequence analysis, including the six mutations not identified with p53 GeneChip analysis, achieved an accuracy of 87% (94 of 108) relative to the final *TP53* status determined from assessment of both approaches together. In addition, three cases were identified with double mutations, two with double missense mutations, and one with a missense mutation and a splice junction mutation. Microarray analysis also detected polymorphisms in seven cases, five of which had coexistent missense mutations. These observations provided an estimate of the frequency of cases with multiple alterations in the *TP53* gene, which has probably been underestimated and underreported in the past (1, 10).

Although there was a high level of concordance between the microarray analysis and conventional DNA sequence analysis, six mutations identified by conventional DNA sequence analysis were not identified by microarray analysis. Four of these mutations (four of six; 67%) involved multiple-bp deletions and/or insertions, including two cases with in-frame deletions and insertions, one case with a frameshift mutation attributable to a 15-bp deletion and 4-bp insertion, and one case with an in-frame 3-bp deletion (Table 3). The two other cases not identified by microarray had missense mutations. The detection rate for nucleotide deletions and insertions was lower with microarray (two of six; 33%) than with conventional DNA sequence analysis (six of six; 100%).

The p53 GeneChip assay showed a higher detection rate for single-bp substitutions of any type including missense mutations, nonsense mutations, and splice junction mutations than did conventional DNA sequence analysis [56 of 58 (97%) versus 49 of 58 (84%); 7 of 7 (100%) versus 4 of 7 (57%); and 6/6 (100%) versus 4 of 6 (67%); Table 1], respectively. Overall, p53 GeneChip assay identified 97% (69 of 71) of single-base substitutions, whereas conventional DNA sequence analysis identified 80% (57 of 71). For single-bp deletion mutations, p53 GeneChip showed the same detection rate as sequence analysis (two of two; 100%). All 14 mutations missed by conventional DNA sequence analysis (Table 4) were of the single-bp substitution type, whereas four of the six (67%) mutations missed by p53 GeneChip assay were deletions >1 bp or complex frameshift mutations. Among the 14 mutations missed by first round of DNA sequencing, no minor bandshift was seen, even after rechecking the SSCP gel or gel-based sequencing data; therefore, misinterpretation of the original sequence was unlikely. Because a majority (9 of 14; 64%) of these cases had a GeneChip score between 11 and 12, it was possible that these DNA samples had less mutant target DNA hybridizing to the probe cell on the array, which was difficult to detect by SSCP and DNA sequencing.

On the other hand, mutations missed by the p53 GeneChip were mostly multiple-base deletion/insertion, which had clear nucleotide changes on DNA sequencing gels. The p53 microarray could be improved by introduction of oligonucleotides designed to identify all previously observed multiple-bp deletion or insertion mutations. Alternatively, p53 microarrays could be used for initial analysis of *TP53* mutations, with all apparently wild-type DNA samples subjected to conventional DNA sequence analysis.

Although a variety of oligonucleotide microarrays have emerged in the market during the past few years, few studies have compared the mutations or sequences identified by both the microarray and conventional sequence approaches (11, 12). In a previous study, exon 11 of *BRCA1* was characterized in 15 patients and 20 control samples. Fourteen of the 15 patient samples with previously known mutations were correctly diagnosed, with no false-positive results identified. The *BRCA1* chip achieved a sensitivity of 93% (14 of 15) and specificity of 100% (20 of 20). Eight single-nucleotide polymorphisms were also

detected. In the second report, the *BRCA1* DNA was used for sequence comparisons of *BRCA1* exon 11 in human, chimpanzee, gorilla, and orangutan DNA samples.

While our manuscript was in review, another paper reported a comparison of *TP53* mutations in 100 lung cancers determined by oligonucleotide microarray and gel-based DNA sequence analysis (13). Dideoxynucleotide sequence analysis of exons 5–9 detected 76% of mutations within this region of the gene. The p53 GeneChip assay detected 80% of the mutations within this same region (exons 5–9) of the gene and 81% of all mutations in exons 2–11 (13). Similar to our experience reported here, the p53 GeneChip detected 46 of 52 missense mutations (88%) but none of five frameshift mutations (13). Accordingly, the p53 GeneChip appears to perform best when analyzing single-base mismatch substitution mutations and single-bp deletion mutations. Conversely, in our hands it failed to identify deletions or insertions >1 bp. The prevalence of deletions and insertions in *TP53* is, however, relatively low, depending on the tumor type. The occurrence of deletions and/or insertions >1 bp is estimated to be 7% in the *TP53* database (9). This value correlated well with our results in these 108 ovarian carcinoma samples. On the other hand, the majority of *BRCA1* mutations are not single-bp substitutions but insertions and deletions. However, oligonucleotide microarray did achieve a high sensitivity and specificity in a relatively small number of cases. The sensitivity of the DNA microarray for mutation detection in *BRCA1* (14 of 15; 93%) was similar to the sensitivity achieved here for *TP53* (71 of 77; 92%).

Overall, *TP53* mutations in these ovarian cancers occurred predominantly in exons 5–8. Nineteen (25%) mutations were in exon 5, 11 (14%) mutations were in exon 6, 15 (20%) mutations were in exon 7, 24 (31%) mutations were in exon 8. Six (8%) mutations were located in introns at splice junctions, and only one mutation was identified in exon 4 (1%) and exon 9 (1%). Most of the studies analyzing the entire open reading frame of *TP53* (14–18) in ovarian cancer had a limited number of cases analyzed. Two of the five studies (17, 18) that analyzed more than 60 cases identified 15 and 18% of mutations outside exon 5–8, with a predominance of deletion/insertion mutations in these regions. However, we did not find a similar distribution in our study. Because we confirmed all SSCP-positive cases by manual sequencing and rescreened SSCP-negative cases by automated DNA sequencing, as well as reanalyzed all DNAs by a p53 GeneChip assay, it is unlikely that a significant number of mutations were missed. Therefore, our estimate of *TP53* mutations in ovarian cancer is considered to be representative. The difference in mutation spectrum among studies might be attributed to environmental mutagenic exposure and/or endogenous factors, such as genetic differences, that contribute to carcinogenesis.

The most frequently mutated codons in our study were codon 273 (seven mutations), codon 179 (four mutations), and codon 234 (four mutations). Two of these (codon 179 and codon 273) are also "hot-spots" of tobacco-associated lung cancers, but most of the mutations (10 of 12; 83%) in these two codons in ovarian cancer were transition mutations rather than transversion mutations as observed in lung cancer (19). On the other hand, mutations frequently related to benzo(a)pyrene exposure in lung cancer, such as mutations in codon 157 (GTC→TTC), codon 248 (CGG→CTG), or related to aflatoxin exposure in liver cancer, such as mutations in codon 249 (AGG→AGT), were not identified. The higher overall percentage of transition (60%) compared with transversion mutations (32%) in our study suggest that most ovarian cancers arise spontaneously rather than because of exogenous carcinogen exposure.

The significance of *TP53* alteration as a prognostic factor in ovarian cancers varies among different studies (reviewed in Ref. 6). The factors that cause variable results include insufficient samples, differ-

ence in screening methods, and incomplete analysis of the open reading frame. In our study, we tried to minimize these factors by using both conventional gel-based DNA sequencing and microarray analysis to analyze mutations in the entire open reading frame of *TP53* in 108 ovarian carcinomas: (a) the high percentage (77 of 108; 71%) of *TP53* mutations indicates that *TP53* function is abrogated mostly by mutation of the gene itself in ovarian cancer, although other nonmutational mechanisms, such as defects in *TP53* pathway that mediate its function or loss of mechanisms that activate *TP53* (20), could be involved in the pathogenesis of those cancers that have wild type *TP53*; (b) the DNA-binding structural motifs (loop-sheet-helix, loop2, and loop3) of *TP53* overlap almost exclusively with the conserved regions of the protein sequence, where the majority of mutations are found and affect its sequence-specific DNA binding activity (21). These "hot-spot" amino acids are highly conserved and are believed to represent regions of structural or functional importance (22). In our analysis, *TP53* mutation was shown to be a predictor of overall survival in ovarian cancer. Patients with mutations in loop2, loop3, or the loop-sheet-helix domain had shorter survival than patients with mutations in other locations or no mutation. This observation supports the current concept that these sequence-specific DNA binding domains are functionally important, and mutations in these areas could have more deleterious effects as opposed to other mutant and/or wild-type *TP53*. Further *in vivo* functional characterization, such as the biological activity of these mutants, would provide more information.

A few possible mechanisms of false-negative and false-positive mutations detected by DNA microarray have been described. These include microarray design, imperfect hybridization conditions, and molecular interactions on microarrays (23, 24). The addition of more probes, such as redundant tiling based on common mutations related to deletion/insertion mutations, as well as other mutations, is expected to improve the sensitivity of the microarray in overall detection. In addition, enzyme approaches, such as polymerase and ligase, have also been adapted for use with microarray (24). It has been suggested that deletion and insertion would lead to the formation of energetically favored duplexes containing bulged nucleotides with wild-type probes over duplexes containing single-bp mismatches (23). All of these possibilities suggest that microarray detection can be improved. Although sequencing the entire coding region is a sensitive technique for overall detection of mutations, it is more time consuming and labor intensive than analysis by DNA microarray technology. For example, screening of the entire coding region of *TP53* requires the amplification of 11 PCR products (exon 4 is split in two amplicons), 22 sequencing lanes, and the manual examination of over 1262 bases. The high costs and increased turnaround times impedes the usage of this technology on a regular basis. On the other hand, the time from purified DNA to data analysis was ~4.5 h for the p53 GeneChip. The average batch size/day was 12 samples, including a reference sample and negative control (blank). In conclusion, although there was a high concordance rate between the two methods, the p53 GeneChip assay detected more mutations, had greater overall accuracy for detection of sequence alterations, and was more effective in terms of time and cost.

ACKNOWLEDGMENTS

We thank Ivonne Villalobos, Norris Cancer Center, University of Southern California School of Medicine, for preparing the manuscript and Dr. Timothy

Triche for the assistance of the Children's Cancer Group Microarray Core Facility at Children's Hospital Los Angeles, USC/Norris Comprehensive Cancer Center.

REFERENCES

- Hainaut, P., Hernandez, T., Robinson, A., Rodriguez-Tome, P., Flores, T., Hollstein, M., Harris, C., and Montesano, R. IARC Database of p53 gene mutations in human tumors and cell lines: updated compilation, revised formats and new visualization tools. *Nucleic Acids Res.*, 26: 205-213, 1998.
- Cotton, R. Slowly but surely towards better scanning for mutations. *Trends Genet.*, 13: 43-46, 1997.
- Wallace, R. DNA on a chip: serving up the genome for diagnostics and research. *Mol. Med. Today*, 3: 384-389, 1997.
- Southern, E. M. DNA chips. Analysing sequence by hybridization to oligonucleotides on a large scale. *Trends Genet.*, 12: 110-115, 1996.
- Lipshutz, R., Fodor, S., Gingeras, T., and Lockhart, D. High density synthetic oligonucleotide arrays. *Nat. Genet. Suppl.*, 21: 20-24, 1999.
- Wen, W., Reles, A., Sullivan-Halley, J., Bernstein, L., Jones, L., El-Naggar, A., Felix, J., Runnebaum, I., and Press, M. p53 mutations and expression in ovarian cancer: correlation with overall survival. *Int. J. Gynecol. Pathol.*, 18: 29-41, 1999.
- Wang-Gohrke, S., Hees, S., Pochon, A., Wen, W., Reles, A., Press, M., Krienberg, R., and Runnebaum, I. Genomic semi-automated cycle sequencing as a sensitive screening technique for p53 mutations in frozen tumor samples. *Oncol. Rep.*, 5: 65-68, 1998.
- Runnebaum, I., Kohler, T., Stuckeler, E., Kieback, H., and Krienberg, R. p53 mutation is associated with high S-phase fraction in primary fallopian tube adenocarcinoma. *Br. J. Cancer*, 74: 1157-1160, 1996.
- Beroud, C., Verdier, F., and Soussi, T. p53 gene mutation: software and database. *Nucleic Acids Res.*, 24: 147-150, 1996.
- Beroud, C., and Soussi, T. p53 gene mutation: software and database. *Nucleic Acids Res.*, 26: 200-204, 1998.
- Hacia, J., Brody, L., Chee, M., Fodor, S., and Collins, F. Detection of heterogeneous mutations in BRCA1 using high density oligonucleotide arrays and two-color fluorescence analysis. *Nat. Genet.*, 14: 441-447, 1996.
- Hacia, J., Makalowski, W., Edgerton, K., Erdos, M., Robbins, C., Fodor, S., Brody, L., and Collins, F. Evolutionary sequence comparisons using high-density oligonucleotide arrays. *Nat. Genet.*, 18: 155-158, 1998.
- Ahrendt, S., Halachmi, S., Chow, J., Wu, L., Halachmi, N., Yang, S., Wehage, S., Jen, J., and Sidransky, D. Rapid p53 sequence analysis in primary lung cancer using an oligonucleotide probe array. *Proc. Natl. Acad. Sci. USA*, 96: 7382-7387, 1999.
- Kihana, T., Tsuda, H., Teshima, S., Okada, S., Matsuura, S., and Hirohashi, S. High incidence of p53 gene mutation in human ovarian cancer and its association with nuclear accumulation of p53 protein and tumor. *DNA aneuploidy. Jpn. J. Cancer Res.*, 83: 978-984, 1992.
- Kupryjanczyk, J., Thor, A., Beauchamp, R., Merriitt, V., Edgerton, S., Bell, D., and Yandell, D. p53 gene mutations and protein accumulation in human ovarian cancer. *Proc. Natl. Acad. Sci. USA*, 90: 4961-4965, 1993.
- Kupryjanczyk, J., Bell, D., Dimeo, D., Beauchamp, R., Thor, A., and Yandell, D. p53 gene analysis of ovarian borderline tumors and stage I carcinomas. *Hum. Pathol.*, 26: 387-392, 1995.
- Skilling, J., Sood, A., Niemann, T., Lager, D., and Buller, R. An abundance of p53 null mutations in ovarian carcinoma. *Oncogene*, 13: 117-123, 1996.
- Casey, G., Lopez, M., Ramos, J., Plummer, S., Arboleda, M., Shaughnessy, M., Karlan, B., and Slamon, D. DNA sequence analysis of exons 2 through 11 and immunohistochemical staining are required to detect all known p53 alterations in human malignancies. *Oncogene*, 13: 1971-1981, 1996.
- Bennett, W., Hussain, S., Vahakangas, K., Khan, M., Shields, P., and Hanis, C. Molecular epidemiology of human cancer risk: gene-environment interactions and p53 mutation spectrum in human lung cancer. *J. Pathol.*, 187: 8-18, 1999.
- Kubbutat, M., and Vousden, K. Keeping an old friend under control: regulation of p53 stability. *Mol. Med. Today*, 4: 250-256, 1998.
- Arrowsmith, C., and Morin, P. New insights into p53 function from structural studies. *Oncogene*, 12: 1379-1385, 1996.
- Walker, D., Bond, J., Tarone, R., Harris, C., Makalowski, W., Boguski, M., and Greenblatt, M. Evolutionary conservation and somatic mutation hotspot maps of p53: correlation with p53 protein structural and functional features. *Oncogene*, 18: 211-218, 1999.
- Hacia, J. Resequencing and mutational analysis using oligonucleotide microarrays. *Nat. Genet. Suppl.*, 21: 42-47, 1999.
- Southern, E., Mir, K., and Shechepinov, M. Molecular interactions on microarrays. *Nat. Genet. Suppl.*, 21: 5-9, 1999.

Down-regulation of prostate-specific antigen expression by finasteride through inhibition of complex formation between androgen receptor and steroid receptor-binding consensus in the promoter of the PSA gene in LNCaP cells.

Wang LG, Liu XM, Kreis W, Budman DR.

Department of Medicine, New York University, Manhasset 11030, USA.

As a specific competitive inhibitor of 5alpha-reductase, an intracellular enzyme that converts testosterone to dihydrotestosterone, finasteride is being extensively used for the treatment of benign prostatic hyperplasia and in experimental settings for prostate cancer. In this study, we showed that finasteride markedly inhibited prostate-specific antigen (PSA) secretion and expression. The promoter of the PSA gene contains several well-known cis-regulatory elements. Among them, steroid receptor-binding consensus (SRBC) has been identified as a functional androgen-responsive element. Our previous study showed that PSA was not only present in conditioned medium of the PSA-positive LNCaP cells but was also detectable in small amounts in PSA-negative cell lines, PC-3 and DU-145 (L. G. Wang et al., *Oncol. Rep.*, 3: 911-917, 1996). A strong correlation between binding of nuclear factors to SRBC and the level of PSA present in the conditioned medium and cell extracts was found in these three cell lines, whereas no such correlation with binding was obtained using Sp1 oligonucleotide as a probe. Binding of LNCaP cell nuclear proteins to SRBC was diminished when the cells were exposed to 25 microM finasteride, at which concentration 50% of both PSA mRNA and protein were inhibited. As a major component of DNA-protein complexes, the level of androgen receptor was dramatically decreased in the cells treated with finasteride. Our data indicate that inhibition of complex formation between SRBC and nuclear proteins due to the remarkable decrease in the level of androgen receptor plays a key role in the down-regulation of PSA gene expression by finasteride in LNCaP cells.

PMID: 9044850 [PubMed - indexed for MEDLINE]

Expression of calcyclin in human melanocytic lesions.

Weterman MA, van Muijen GN, Bloemers HP, Ruiter DJ.

Department of Biochemistry, University of Nijmegen, The Netherlands.

When comparing two subsequent stages of melanocytic tumor progression we identified calcyclin as a new potential progression marker, the expression of which was correlated with metastatic behavior of various human melanoma cell lines in nude mice. In this study, we describe a good correlation between RNA and protein levels in the xenografts of these cell lines and extended these experiments to a panel of 120 routinely processed human melanocytic cutaneous lesions. Northern blot analysis demonstrated that calcyclin RNA expression was elevated in melanoma metastases as compared to several types of nevocellular nevi. Calcyclin staining using a specific polyclonal antiserum showed a more complex pattern. A stronger staining in a higher percentage of positive cells was observed in thick primary melanoma (≥ 1.5 mm) as compared to thin primary melanoma (< 1.5 mm). Calcyclin expression was also present in a higher percentage of cells showing a stronger staining in melanomas with higher Clark levels ($> II$) corresponding to the vertical growth phase of primary melanomas. Protein expression in nevocellular nevi was confined to the dermal part and was highest in the lower parts of the dermis. Remarkably, dysplastic nevi (atypical moles), potential precursors of melanoma, did not show any expression at all, either in junctional or dermal parts. Confinement of the expression to the dermal part of nondysplastic nevi and primary melanomas may reflect interactions with the microenvironment of the reticular dermis that occurs with vertical growth.

PMID: 8261423 [PubMed - indexed for MEDLINE]

Severely decreased MARCKS expression correlates with ras reversion but not with mitogenic responsiveness.

Wojtaszek PA, Stumpo DJ, Blackshear PJ, Macara IG.

Department of Pathology, University of Vermont College of Medicine, Burlington 05405.

Phorbol ester-inducible phosphorylation of MARCKS, the '80-kDa' substrate of protein kinase C, was undetectable in several phenotypically dominant, non-transformed revertants independently derived from the ras-transformed cell line NIH3T3 DT-ras. Extremely low expression of MARCKS protein accounted for this apparent lack of phosphorylation. MARCKS-encoding mRNA levels were correspondingly decreased relative to normal and ras-transformed cells in all four ras revertant cell lines studied: C-11 and F-2, derived by 5-azacytidine treatment and selection with ouabain; CHP 9CJ, derived by ethylmethane sulfonate mutagenesis and selection with cis-hydroxy-L-proline; and 12-V3, derived by transfection with the human Krev-1 gene. However, re-expression of MARCKS after transfection of a cloned MARCKS cDNA into the C-11 ras revertant cells was not sufficient to induce retransformation. In fact, no significant difference in sensitivity to mitogenic stimulation by phorbol esters was observed among several cell lines expressing widely varying levels of MARCKS. This evidence argues against a direct role for MARCKS in mitogenic signaling. However, the strong correlation between attenuation of MARCKS expression and phenotypically dominant ras reversion suggests that a common negative regulatory mechanism might be responsible for both effects, presenting a potentially useful strategy for identifying factors involved in transducing the ras signal.

PMID: 8437859 [PubMed - indexed for MEDLINE]

[Expression of human telomerase reverse transcriptase in cervix cancer and its significance]

[Article in Chinese]

Xi L, Zhu T, Wu P, Xu Q, Huang L, Li KZ, Lu YP, Ma D.

Department of Obstetrics and Gynecology, Tongji Hospital, Tongji Medical College, Huazhong University of Science and Technology, Wuhan 430030, China.

OBJECTIVE: To investigate the expression of human telomerase reverse transcriptase (hTERT) mRNA and protein in cervix cancer, cervical intraepithelial neoplasia (CIN) and normal cervix. **METHODS:** Expression of hTERT mRNA and the other two subunits of telomerase, human telomerase RNA component (hTR), human telomerase-associated protein (hTP1) was determined by RT-PCR in 3 cervix cancer cell lines, 2 diploid cell lines, 38 cases of cervix cancer, 16 cases of CIN and 20 cases of normal cervix. Telomerase activity was also examined by telomeric repeat amplification protocol enzyme-linked immunosorbent assay (TRAP-ELISA). Expression of hTERT protein was detected in all the cell lines and 101 cases of paraffinized cervix tissue sections. **RESULTS:** hTERT mRNA expression was detected in all of the three cervix cancer cell lines, 81.6% of cervix cancer, 37.5% of CIN, 5.0% of normal cervix, while in neither of the two diploid cell lines. The other two subunits of telomerase were prevalently expressed in all of the cell lines and most cervix tissues. There was a strong correlation between hTERT mRNA expression and telomerase activity. Immunostaining also revealed that hTERT protein was expressed in all three cervix cancer cell lines, 65.5% of cervix cancer, 28.0% of CIN and 4.8% of normal cervix. **CONCLUSION:** Up-regulation of hTERT may play an important role in the development of CIN and cervix cancer, hTERT could be used as an early diagnostic biomarker for cervix cancer.

PMID: 16008894 [PubMed - in process]

266: Mol Cell Biol. 1999 Nov;19(11):7357-68.

Related Articles, Links

FREE full text article at
mcb.asm.org

FREE full text article
in PubMed Central

A sampling of the yeast proteome.

Futcher B, Latter GI, Monardo P, McLaughlin CS, Garrels JJ.

Cold Spring Harbor Laboratory, Cold Spring Harbor, New York 11724, USA.
futcher@cshl.org

In this study, we examined yeast proteins by two-dimensional (2D) gel electrophoresis and gathered quantitative information from about 1,400 spots. We found that there is an enormous range of protein abundance and, for identified spots, a good correlation between protein abundance, mRNA abundance, and codon bias. For each molecule of well-translated mRNA, there were about 4,000 molecules of protein. The relative abundance of proteins was measured in glucose and ethanol media. Protein turnover was examined and found to be insignificant for abundant proteins. Some phosphoproteins were identified. The behavior of proteins in differential centrifugation experiments was examined. Such experiments with 2D gels can give a global view of the yeast proteome.

PMID: 10523624 [PubMed - indexed for MEDLINE]

A Sampling of the Yeast Proteome

B. FUTCHER,^{1*} G. I. LATTER,¹ P. MONARDO,¹ C. S. McLAUGHLIN,² AND J. I. GARRELS³

Cold Spring Harbor Laboratory, Cold Spring Harbor, New York 11724¹; Department of Biological Chemistry, University of California, Irvine, California 92717²; and Proteome, Inc., Beverly, Massachusetts 01915³

Received 15 June 1999/Returned for modification 16 July 1999/Accepted 28 July 1999

In this study, we examined yeast proteins by two-dimensional (2D) gel electrophoresis and gathered quantitative information from about 1,400 spots. We found that there is an enormous range of protein abundance and, for identified spots, a good correlation between protein abundance, mRNA abundance, and codon bias. For each molecule of well-translated mRNA, there were about 4,000 molecules of protein. The relative abundance of proteins was measured in glucose and ethanol media. Protein turnover was examined and found to be insignificant for abundant proteins. Some phosphoproteins were identified. The behavior of proteins in differential centrifugation experiments was examined. Such experiments with 2D gels can give a global view of the yeast proteome.

The sequence of the yeast genome has been determined (9). More recently, the number of mRNA molecules for each expressed gene has been measured (27, 30). The next logical level of analysis is that of the expressed set of proteins. We have begun to analyze the yeast proteome by using two-dimensional (2D) gels.

2D gel electrophoresis separates proteins according to isoelectric point in one dimension and molecular weight in the other dimension (21), allowing resolution of thousands of proteins on a single gel. Although modern imaging and computing techniques can extract quantitative data for each of the spots in a 2D gel, there are only a few cases in which quantitative data have been gathered from 2D gels. 2D gel electrophoresis is almost unique in its ability to examine biological responses over thousands of proteins simultaneously and should therefore allow us a relatively comprehensive view of cellular metabolism.

We and others have worked toward assembling a yeast protein database consisting of a collection of identified spots in 2D gels and of data on each of these spots under various conditions (2, 7, 8, 10, 23, 25). These data could then be used in analyzing a protein or a metabolic process. *Saccharomyces cerevisiae* is a good organism for this approach since it has a well-understood physiology as well as a large number of mutants, and its genome has been sequenced. Given the sequence and the relative lack of introns in *S. cerevisiae*, it is easy to predict the sequence of the primary protein product of most genes. This aids tremendously in identifying these proteins on 2D gels.

There are three pillars on which such a database rests: (i) visualization of many protein spots simultaneously, (ii) quantification of the protein in each spot, and (iii) identification of the gene product for each spot. Our first efforts at visualization and identification for *S. cerevisiae* have been described elsewhere (7, 8). Here we describe quantitative data for these proteins under a variety of experimental conditions.

MATERIALS AND METHODS

Strains and media. *S. cerevisiae* W303 (*MATa ade2-1 his3-11,15 leu2-3,12 trp1-1 ura3-1 can1-100*) was used (26). -Met YNB (yeast nitrogen base) medium was 1.7 g of YNB (Difco) per liter, 5 g of ammonium sulfate per liter, and

adenine, uracil, and all amino acids except methionine; -Met -Cys YNB medium was the same but without methionine or cysteine. Medium was supplemented with 2% glucose (for most experiments) or with 2% ethanol (for ethanol experiments). Low-phosphate YEPD was described by Warner (28).

Isotopic labeling of yeast and preparation of cell extracts. Yeast strains were labeled and proteins were extracted as described by Garrels et al. (7, 8). Briefly, cells were grown to 5×10^6 cells per ml at 30°C; 1 ml of culture was transferred to a fresh tube, and 0.3 mCi of [³⁵S]methionine (e.g., Express protein labeling mix; New England Nuclear) was added to this 1-ml culture. The cells were incubated for a further 10 to 15 min and then transferred to a 1.5-ml microfuge tube, chilled on ice, and harvested by centrifugation. The supernatant was removed, and the cell pellet was resuspended in 100 µl of lysis buffer (20 mM Tris-HCl [pH 7.6], 10 mM NaF, 10 mM sodium pyrophosphate, 0.5 mM EDTA, 0.1% deoxycholate; just before use, phenylmethylsulfonyl fluoride was added to 1 mM, leupeptin was added to 1 µg/ml, pepstatin was added to 1 µg/ml, tosyl-sulfonyl phenylalanyl chloromethyl ketone was added to 10 µg/ml, and soybean trypsin inhibitor was added to 10 µg/ml).

The resuspended cells were transferred to a screw-cap 1.5-ml polypropylene tube containing 0.28 g of glass beads (0.5-mm diameter; Biospec Products) or 0.40 g of zirconia beads (0.5-mm diameter; Biospec Products). After the cap was secured, the tube was inserted into a MiniBeadbeater 8 (Biospec Products) and shaken at medium high speed at 4°C for 1 min. Breakage was typically 75%. Tubes were then spun in a microfuge for 10 s at 5,000 × g at 4°C.

With a very fine pipette tip, liquid was withdrawn from the beads and transferred to a prechilled 1.5-ml tube containing 7 µl of DNase I (0.5 mg/ml; Cooper product no. 6330)-RNase A (0.25 mg/ml; Cooper product no. 3679)-Mg (50 mM MgCl₂) mix. Typically 70 µl of liquid was recovered. The mixture was incubated on ice for 10 min to allow the RNase and DNase to work.

Next, 75 µl of 2× SDS (2× SDS is 0.6% sodium dodecyl sulfate [SDS], 2% mercaptoethanol, and 0.1 M Tris-HCl [pH 8]) was added. The tube was plunged into boiling water, incubated for 1 min, and then plunged into ice. After cooling, the tube was centrifuged at 4°C for 3 min at 14,000 × g. The supernatant was transferred to a fresh tube and frozen at -70°C. About 5 µl of this supernatant was used for each 2D gel.

2D polyacrylamide gels. 2D gels were made and run as described elsewhere (6-8).

Image analysis of the gels. The Quest II software system was used for quantitative image analysis (20, 22). Two techniques were used to collect quantitative data for analysis by Quest II software. First, before the advent of phosphorimagers, gels were dried and fluorographed. Each gel was exposed to film for three different times (typically 1 day, 2 weeks, and 6 weeks) to increase the dynamic range of the data. The films were scanned along with calibration strips to relate film optical density to disintegrations per minute in the gels and analyzed by the software to obtain a linear relationship between disintegrations per minute in the spots and optical densities of the film images. The quantitative data are expressed as parts per million of the total cellular protein. This value is calculated from the disintegrations per minute of the sample loaded onto the gel and by comparing the film density of each data spot with density of the film over the calibration strips of known radioactivity exposed to the same film. This yields the disintegrations per minute per millimeter for each spot on the gel and thence its parts-per-million value.

After the advent of phosphorimaging, gels bearing ³⁵S-labeled proteins were exposed to phosphorimager screens and scanned by a Fuji phosphorimager, typically for two exposures per gel. Calibration strips of known radioactivity were exposed simultaneously. Scan data from the phosphorimager was assimilated by Quest II software, and quantitative data were recorded for the spots on the gels.

* Corresponding author. Mailing address: Cold Spring Harbor Laboratory, Cold Spring Harbor, NY 11724. Phone: (516) 367-8828. Fax: (516) 367-8369. E-mail: fletcher@csll.org.

Measurements of protein turnover. Cells in exponential phase were pulse-labeled with [35 S]methionine, excess cold Met and Cys were added, and samples of equal volume were taken from the culture at intervals up to 90 min (in one experiment) or up to 160 min (in a second experiment). Incorporation of 35 S into protein was essentially 100% by the first sample (10 min). Extracts were made, and equal fractions of the samples were loaded on 2D gels (i.e., the different samples had different amounts of protein but equal amounts of 35 S). Spots were quantitated with a phosphorimaging and Quest software.

The software was queried for spots whose radioactivity decreased through the time course. The algorithm examined all data points for all spots, drew a best-fit line through the data points, and looked for spots where this line had a statistically significant negative slope. In one of the experiments, there was one such spot. To the eye, this was a minor, unidentified spot seen only in the first two samples (10 and 20 min). In the other experiment, the Quest software found no spots meeting the criteria. Therefore, we concluded that none of the identified spots (and all but one of the visible spots) represented proteins with long half-lives.

Centrifugal fractionation. Cells were labeled, harvested, and broken with glass beads by the standard method described above except that no detergent (i.e., no deoxycholate) was present in the lysis buffer. The crude lysate was cleared of unbroken cells and large debris by centrifugation at $300 \times g$ for 30 s. The supernatant of this centrifugation was then spun at $16,000 \times g$ for 10 min to give the pellet used for Fig. 6B. The supernatant of the $16,000 \times g$, 10-min spin was then spun at $100,000 \times g$ for 30 min to give the supernatant used for Fig. 6A.

Protein abundance calculations. A haploid yeast cell contains about 4×10^{-12} g of protein (1, 15). Assuming a mean protein mass of 50 kDa, there are about 50×10^6 molecules of protein per cell. There are about 1.8 methionines per 10 kDa of protein mass, which implies 4.5×10^6 molecules of methionine per cell (neglecting the small pool of free Met). We measured (i) the counts per minute in each spot on the 2D gels, (ii) the total number of counts on each gel (by integrating counts over the entire gel), and (iii) the total number of counts loaded on the gel (by scintillation counting of the original sample). Thus, we know what fraction of the total incorporated radioactivity is present in each spot. After correcting for the methionine (and cysteine [see below]) content of each protein, we calculated an absolute number of protein molecules based on the fraction of radioactivity in each spot and on 50×10^6 total molecules per cell.

The labeling mixture used contained about one-fifth as much radioactive cysteine as radioactive methionine. Therefore, the number of cysteine molecules per protein was also taken into account in calculating the number of molecules of protein, but Cys molecules were weighted one-fifth as heavily as Met molecules.

mRNA abundance calculations. For estimation of mRNA abundance, we used SAGE (serial analysis of gene expression) data (27) and Affymetrix chip hybridization data (29a, 30). The mRNA column in Table 1 shows mRNA abundance calculated from SAGE data alone. However, the SAGE data came from cells growing in YEFD medium, whereas our protein measurements were from cells growing in YNB medium. In addition, SAGE data for low-abundance mRNAs suffers from statistical variation. Therefore, we also used chip hybridization data (29a, 30) for mRNA from cells grown in YNB. These hybridization data also had disadvantages. First, the amounts of high-abundance mRNAs were systematically underestimated, probably because of saturation in the hybridizations, which used 10 μ g of cRNA. For example, the abundance of *ADH1* mRNA was 197 copies per cell by SAGE but only 32 copies per cell by hybridization, and the abundance of *ENO2* mRNA was 248 copies per cell by SAGE but only 41 by hybridization. When the amount of cRNA used in the hybridization was reduced to 1 μ g, the apparent amounts of mRNA were similar to the amounts determined by SAGE (29a, 29b). However, experiments using 1 μ g of cRNA have been done for only some genes (29a). Because amounts of mRNA were normalized to 15,000 per cell, and because the amounts of abundant mRNAs were underestimated, there is a 2.2-fold overestimate of the abundance of nonabundant mRNAs. We calculated this factor of 2.2 by adding together the number of mRNA molecules from a large number of genes expressed at a low level for both SAGE data and hybridization data. The sum for the same genes from hybridization data is 2.2-fold greater than that from SAGE data.

To take into account these difficulties, we compiled a list of "adjusted" mRNA abundance as follows. For all high-abundance mRNAs of our identified proteins, we used SAGE data. For all of these particular mRNAs, chip hybridization suggested that mRNA abundance was the same in YEFD and YNB media. For medium-abundance mRNAs, SAGE data were used, but when hybridization data showed a significant difference between YEFD and YNB, then the SAGE data were adjusted by the appropriate factor. Finally, for low-abundance mRNAs, we used data from chip hybridizations from YNB medium but divided by 2.2 to normalize to the SAGE results. These calculations were completed without reference to protein abundance.

CAI. The codon adaptation index (CAI) was taken from the yeast proteome database (YPD) (13), for which calculations were made according to Sharp and Li (24). Briefly, the index uses a reference set of highly expressed genes to assign a value to each codon, and then a score for a gene is calculated from the frequency of use of the various codons in that gene (24).

Statistical analysis. The JMP program was used with the aid of T. Tully. The JMP program showed that neither mRNA nor protein abundances were normally distributed; therefore, Spearman rank correlation coefficients (r_s) were

calculated. The mRNA (adjusted and unadjusted) and protein data were also transformed so that Pearson product-moment correlation coefficients (r_p) could be calculated. First, this was done by a Box-Cox transformation of log-transformed data. This transformation produced normal distributions, and an r_p of 0.76 was achieved. However, because the Box-Cox transformation is complex, we also did a simpler logarithmic transformation. This produced a normal distribution for the protein data. However, the distribution for the mRNA and adjusted mRNA data was close to, but not quite, normal. Nevertheless, we calculated the r_p and found that it was 0.76, identical to the coefficient from the Box-Cox transformed data. We therefore believe that this correlation coefficient is not misleading, despite the fact that the log(mRNA) distribution is not quite normal.

RESULTS

Visualization of 1,400 spots on three gel systems. Yeast proteins have isoelectric points ranging from 3.1 to 12.8, and masses ranging from less than 10 kDa to 470 kDa. It is difficult to examine all proteins on a single kind of gel, because a gel with the needed range in pI and mass would give poor resolution of the thousands of spots in the central region of the gel. Therefore, we have used three gel systems: (i) pH "4 to 8" with 10% polyacrylamide; (ii) pH "3 to 10" with 10% polyacrylamide; and (iii) nonequilibrium with 15% polyacrylamide (7, 8). Each gel system allows good resolution of a subset of yeast proteins.

Figure 1 shows a pH 4–8, 10% polyacrylamide gel. The pH at the basic end of the isoelectric focusing gel cannot be maintained throughout focusing, and so the proteins resolved on such gels have isoelectric points between pH 4 and pH 6.7. For these pH 4–8 gels, we see 600 to 900 spots on the best gels after multiple exposures.

The pH 3–10 gels (not shown) extend the pI range somewhat beyond pH 7.5, allowing detection of several hundred additional spots. Finally, we use nonequilibrium gels with 15% acrylamide in the second dimension. These allow visualization of about 100 very basic proteins and about 170 small proteins (less than 20 kDa). In total, using all three gel systems, about 1,400 spots can be seen. These represent about 1,200 different proteins, which is about one-quarter to one-third of the proteins expressed under these conditions (27, 30). Here, we focus on the proteins seen on the pH 4–8 gels.

Although nearly all expressed proteins are present on these gels, the number seen is limited by a problem we call coverage. Since there are thousands of proteins on each gel, many proteins comigrate or nearly comigrate. When two proteins are resolved, but are close together, and one protein spot is much more intense than the other, a problem arises in visualizing the weaker spot: at long exposures when the weak signal is strong enough for detection, the signal from the strong spot spreads and covers the signal from the weaker spot. Thus, weak spots can be seen only when they are well separated from strong spots.

For a given gel, the number of detectable spots initially rises with exposure time. However, beyond an optimal exposure, the number of distinguishable spots begins to decrease, because signals from strong spots cover signals from nearby weak spots. At long exposures, the whole autoradiogram turns black. Thus, there is an optimum exposure yielding the maximum number of spots, and at this exposure the weakest spots are not seen.

Largely because of the problem of coverage, the proteins seen are strongly biased toward abundant proteins. All identified proteins have a CAI of 0.18 or more, and we have identified no transcription factors or protein kinases, which are nonabundant proteins. Thus, this technology is useful for examining protein synthesis, amino acid metabolism, and glycolysis but not for examining transcription, DNA replication, or the cell cycle.

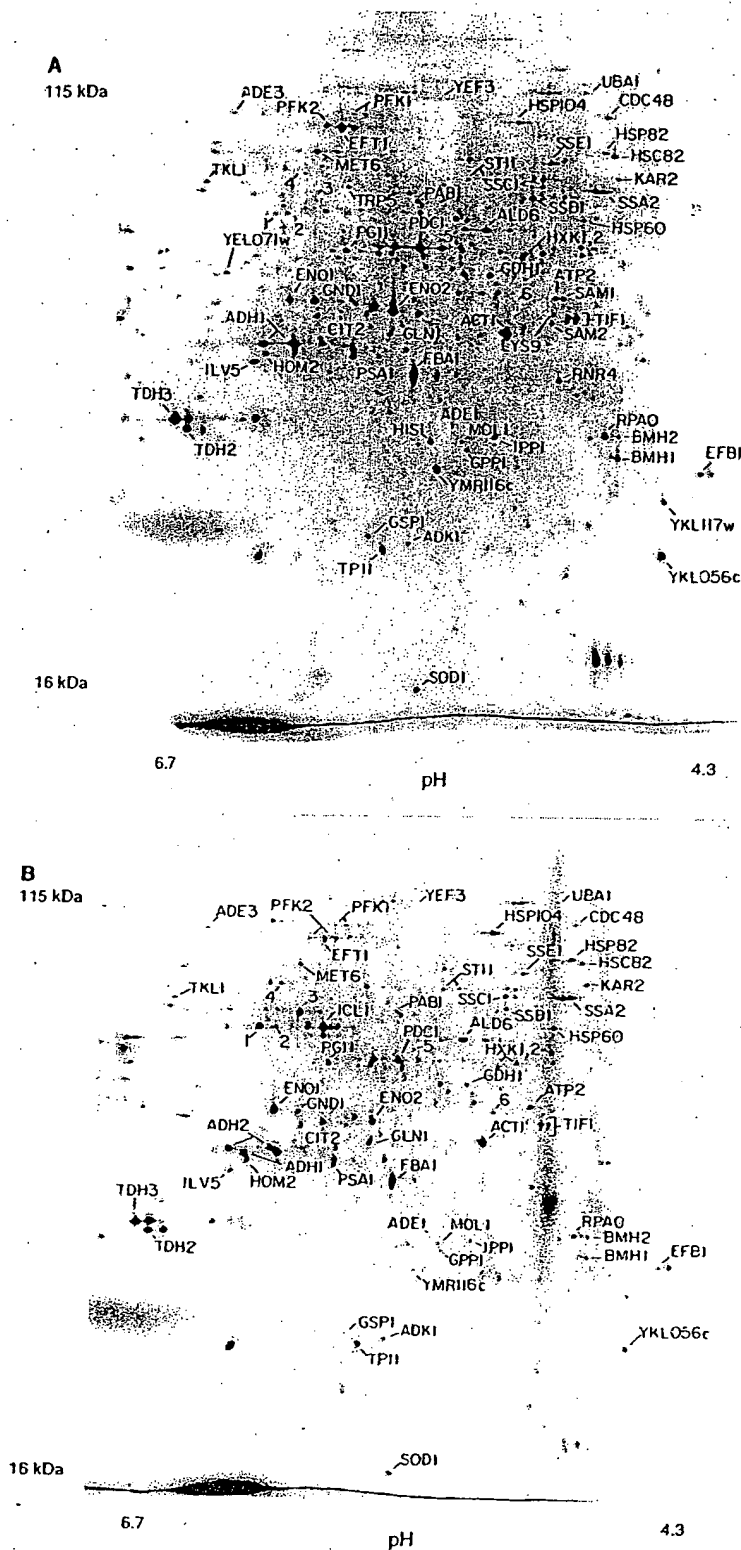


FIG. 1. 2D gels. The horizontal axis is the isoelectric focusing dimension, which stretches from pH 6.7 (left) to pH 4.3 (right). The vertical axis is the polyacrylamide gel dimension, which stretches from about 15 kDa (bottom) to at least 130 kDa (top). For panel A, extract was made from cells in log phase in glucose; for panel B, cells were grown in ethanol. The spots labeled 1 through 6 are unidentified proteins highly induced in ethanol.

Spot identification. The identification of various spots has been described elsewhere (7, 8). At present, 169 different spots representing 148 proteins have been identified. Many of these spots have been independently identified (2, 10, 23, 25). The main methods used in spot identification have been analysis of amino acid composition, gene overexpression, peptide sequencing, and mass spectrometry.

Pulse-chase experiments and protein turnover. Pulse-chase experiments were done to measure protein half-lives (Materials and Methods). Cells were labeled with [35 S]methionine for 10 min, and then an excess of unlabeled methionine was added. Samples were taken at 0, 10, 20, 30, 60, and 90 min after the beginning of the chase. Equal amounts of 35 S were loaded from each sample; 2D gels were run, and spots were quantitated. Surprisingly, almost every spot was nearly constant in amount of radioactivity over the entire time course (not shown). A few spots shifted from one position to another because of post-translational modifications (e.g., phosphorylation of Rpa0 and Efb1). Thus, the proteins being visualized are all or nearly all very stable proteins, with half-lives of more than 90 min. Gygi et al. (10) have come to a similar conclusion by using the N-end rule to predict protein half-lives. This result does not imply that all yeast proteins are stable. The proteins being visualized are abundant proteins; this is partly because they are stable proteins.

Protein quantitation. Because all of the proteins seen had effectively the same half-life, the abundance of each protein was directly proportional to the amount of radioactivity incorporated during labeling. Thus, after taking into account the total number of protein molecules per cell, the average content of methionine and cysteine, and the methionine and cysteine content of each identified protein, we could calculate the abundance of each identified protein (Tables 1 and 2; Materials and Methods). About 1,000 unidentified proteins were also quantified, assuming an average content of Met and Cys.

Many proteins give multiple spots (7, 8). The contribution from each spot was summed to give the total protein amount. However, many proteins probably have minor spots that we are not aware of, causing the amount of protein to be underestimated.

When the proteins on a pH 4–8 gel were ordered by abundance, the most abundant protein had 8,904 ppm, the 10th most abundant had 2,842 ppm, the 100th most abundant had 314 ppm, the 500th most abundant had 57 ppm, and the 1,000th most abundant (visualized at greater than optimum exposure) had 23 ppm. Thus, there is more than a 300-fold range in abundance among the visualized proteins. The most abundant 10 proteins account for about 25% of the total protein on the pH 4–8 gel, the most abundant 60 proteins account for 50%, and the most abundant 500 proteins account for 80%. Since it seems likely that the pH 4–8 gels give a representative sampling of all proteins, we estimate that half of the total cellular protein is accounted for by fewer than 100 different gene products, principally glycolytic enzymes and proteins involved in protein synthesis.

Correlation of protein abundance with mRNA abundance. Estimates of mRNA abundance for each gene have been made by SAGE (27) and by hybridization of cRNA to oligonucleotide arrays (30). These two methods give broadly similar results, yet each method has strengths and weaknesses (Materials and Methods). Table 1 lists the number of molecules of mRNA per cell for each gene studied. One measurement (mRNA) uses data from SAGE analysis alone (27); a second incorporates data from both SAGE and hybridization (30) (adjusted mRNA) (Table 1; Materials and Methods). We correlated protein abundance with mRNA abundance (Fig. 2). For ad-

justed mRNA versus protein, the Spearman rank correlation coefficient, r_s , was 0.74 ($P < 0.0001$), and the Pearson correlation coefficient, r_p , on log transformed data (Materials and Methods) was 0.76 ($P < 0.00001$). We obtained similar correlations for mRNA versus protein and also for other data transformations (Materials and Methods). Thus, several statistical methods show a strong and significant correlation between mRNA abundance and protein abundance. Of course, the correlation is far from perfect; for mRNAs of a given abundance, there is at least a 10-fold range of protein abundance (Fig. 2). Some of this scatter is probably due to posttranscriptional regulation, and some is due to errors in the mRNA or protein data. For example, the protein Yef3 runs poorly on our gels, giving multiple smeared spots. Its abundance has probably been underestimated, partly explaining the low protein/mRNA ratio of Yef3. It is the most extreme outlier in Fig. 2.

These data on mRNA (27, 30) and protein abundance (Table 1) suggest that for each mRNA molecule, there are on average 4,000 molecules of the cognate protein. For instance, for Act1 (actin) there are about 54 molecules of mRNA per cell and about 205,000 molecules of protein. Assuming an mRNA half-life of 30 min (12) and a cell doubling time of 120 min, this suggests that an individual molecule of mRNA might be translated roughly 1,000 times. These calculations are limited to mRNAs for abundant proteins, which are likely to be the mRNAs that are translated best.

A full complement of cell protein is synthesized in about 120 min under these conditions. Thus, 4,000 molecules of protein per molecule of mRNA implies that translation initiates on an mRNA about once every 2 s. This is a remarkably high rate; it implies that if an average mRNA bears 10 ribosomes engaged in translation, then each ribosome completes translation in 20 s; if an average protein has 450 residues; this in turn implies translation of over 20 amino acids per s, a rate considerably higher than estimated for mammals (3 to 8 amino acids per s) (18). These estimates depend on the amount of mRNA per cell (11, 27).

The large number of protein molecules that can be made from a single mRNA raises the issue of how abundance is controlled for less abundant proteins. Many nonabundant proteins may be unstable, and this would reduce the protein/mRNA ratio. In addition, many nonabundant proteins may be translated at suboptimal rates. We have found that mRNAs for nonabundant proteins usually have suboptimal contexts for translational initiation. For example, there are over 600 yeast genes which probably have short open reading frames in the mRNA upstream of the main open reading frame (17a). These may be devices for reducing the amount of protein made from a molecule of mRNA.

Correlation of codon bias with protein abundance. The mRNAs for highly expressed proteins preferentially use some codons rather than others specifying the same amino acid (14). This preference is called codon bias. The codons preferred are those for which the tRNAs are present in the greatest amounts. Use of these codons may make translation faster or more efficient and may decrease misincorporation. These effects are most important for the cell for abundant proteins, and so codon bias is most extreme for abundant proteins. The effect can be dramatic—highly biased mRNAs may use only 25 of the 61 codons.

We asked whether the correlation of codon bias with abundance continues for medium-abundance proteins. There are various mathematical expressions quantifying codon bias; here, we have used the CAI (24) (Materials and Methods) because it gives a result between 0 and 1. The r_s for CAI versus protein abundance is 0.80 ($P < 0.0001$), similar to the mRNA-protein

TABLE 1. Quantitative data^a

Function	Name	CAI	mRNA	Adjusted mRNA	Protein (Glu) (10 ³)	Protein (Eth) (10 ³)	E/G ratio
Carbohydrate metabolism	Adh1	0.810	197	197	1,230	972	0.79
	Adh2	0.504	0		0	963	>20
	Cit2	0.185	1	2.8	23	288	12
	Eno1	0.870	No <i>Nla</i>		410	974	2.4
	Eno2	0.892	248	248	650	215	0.33
	Fba1	0.868	179	179	640	608	0.95
	Hxk1,2	0.500	13	10.5	62	46	
	Id1	0.251	0		0	671	>20
	Pdb1	0.342	5	5	41	33	
	Pdc1	0.903	226	226	280	205	0.73
	Pfk1	0.465	5	5	75	53	0.71
	Pgi1	0.681	14	14	160	120	0.75
	Pyc1	0.260	1	0.7	37	34	
	Tal1	0.579	5	5	110	35	
	Tdh2	0.904	63	63	430	876	NR
	Tdh3	0.924	460	460	1,670	1,927	NR
	Tpi1	0.817	No <i>Nla</i>		No Met	No Met	
Protein synthesis	Efb1	0.762	33	16.5	358	362	
	Eft1,2	0.801	26	26	99	54	0.55
	Prt1	0.303	4	0.7	12	6	
	Rpa0	0.793	246	246	277	100	0.36
	Tif1,2	0.752	29	29	233	106	0.46
	Yef3	0.777	36	36	14	ND	
Heat shock	Hsc82	0.581	2	2.9	112	75	0.67
	Hsp60	0.381	9	2.3	35	82	2.3
	Hsp82	0.517	2	1.3	52	135	2.6
	Hsp104	0.304	7	7	70	161	2.3
	Kar2	0.439	5	10.1	43	102	2.4
	Ssa1	0.709	2	4.3	303	421	1.4
	Ssa2	0.802	10	5	213	324	1.5
	Ssb1,2	0.850	50	50	270	85	
	Ssc1	0.521	2	2.6	68	80	1.2
	Sse1	0.521	8	8	96	48	
	Sti1	0.247	1	1.1	25	44	1.7
Amino acid synthesis	Ade1	0.229	4	4	14	27	
	Ade3	0.276	2	1.7	12	9	
	Ade5,7	0.257	2	1.4	14	4	
	Arg4	0.229	1	8.1	41	41	
	Gdh1	0.585	10	27	148	55	
	Gln1	0.524	11	11	77	104	1.3
	His4	0.267	3	3	15	23	1.5
	Ilv5	0.801	6	6	152	109	0.7
	Lys9	0.332	4	4	32	17	0.52
	Met6	0.657	No <i>Nla</i>	22	190	80	0.42
	Pro2	0.248	3	3	30	12	
	Ser1	0.258	2	1.2	15	8	
	Trp5	0.319	5	5	28	12	
Miscellaneous	Act1	0.710	54	54	205	164	0.78
	Adk1	0.531	No <i>Nla</i>		47	43	
	Ald6	0.520	3	3	181	159	
	Atp2	0.424	1	4.1	76	109	1.4
	Bmh1	0.322	46	46	191	137	0.72
	Bmh2	0.384	1	1.4	134	147	
	Cdc48	0.306	2	2.4	32	26	
	Cdc60	0.299	2	0.86	6	2	
	Erg20	0.373	5	5	92	39	
	Gpp1	0.603	16	5	234	158	
	Gsp1	0.621	3	3	115	39	0.34
	Ipp1	0.620	4	4	254	147	0.58
	Lcb1	0.173	0.3	0.8	19	40	
	Mol1	0.423	0	0.45	20	16	
	Pab1	0.488	3	3	41	19	0.47
	Psa1	0.600	15	15	148	56	
	Rnr4	0.497	6	6	44	37	
	Sam1	0.494	5	5	59	21	
	Sam2	0.497	3	15	63	20	
	Sod1	0.376	36	36	631	618	
	Uba1	0.212	2	2	14	20	
	YKL056	0.731	62	62	253	112	0.44
	YLR109	0.549	21	21	930		
	YMR116	0.777	41	41	184	40	0.20

^a CAI, a measure of codon bias, is taken from the YPD. mRNA, number of mRNA molecules per cell from SAGE data (27); adjusted mRNA, number of mRNA molecules per cell based on both SAGE and chip hybridization (30) (see Materials and Methods); Protein (Glu), number of molecules of protein per cell in YNB-glucose; Protein (Eth), number of molecules of protein per cell in YNB-ethanol; E/G ratio, ratio of protein abundance in ethanol to glucose. The E/G ratio is not given if it was close to 1 or if it was not repeatable (NR) in multiple gels. Some gene products (e.g., Tif1 and Tif2 [Tif1,2]) were difficult to distinguish on either a protein or an mRNA basis; these are pooled. No *Nla*, there was no suitable *Nla*III site in the 3' region of the gene, and so there are no SAGE mRNA data; No Met, the mature gene product contains no methionines, and so there are no reliable protein data.

TABLE 2. Functions of proteins listed in Table 1

Name ^a	YPD title lines ^b
Adh1	Alcohol dehydrogenase I; cytoplasmic isozyme reducing acetaldehyde to ethanol, regenerating NAD ⁺
Adh2	Alcohol dehydrogenase II; oxidizes ethanol to acetaldehyde, glucose repressed
Cit2	Citrate synthase, peroxisomal (nonmitochondrial); converts acetyl-CoA and oxaloacetate to citrate plus CoA
Eno1	Enolase 1 (2-phosphoglycerate dehydratase); converts 2-phospho-D-glycerate to phosphoenolpyruvate in glycolysis
Eno2	Enolase 2 (2-phosphoglycerate dehydratase); converts 2-phospho-D-glycerate to phosphoenolpyruvate in glycolysis
Fba1	Fructose biphosphate aldolase II; sixth step in glycolysis
Hxk1	Hexokinase I; converts hexoses to hexose phosphates in glycolysis; repressed by glucose
Hxk2	Hexokinase II; converts hexoses to hexose phosphates in glycolysis and plays a regulatory role in glucose repression
Icl1	Isocitrate lyase, peroxisomal; carries out part of the glyoxylate cycle; required for gluconeogenesis
Pdb1	Pyruvate dehydrogenase complex, E1 beta subunit
Pdc1	Pyruvate decarboxylase isozyme 1
Pfk1	Phosphofructokinase alpha subunit, part of a complex with Pfk2p which carries out a key regulatory step in glycolysis
Pgi1	Glucose-6-phosphate isomerase, converts glucose-6-phosphate to fructose-6-phosphate
Pyc1	Pyruvate carboxylase 1; converts pyruvate to oxaloacetate for gluconeogenesis
Tal1	Transaldolase; component of nonoxidative part of pentose phosphate pathway
Tdh2	Glyceraldehyde-3-phosphate dehydrogenase 2; converts D-glyceraldehyde 3-phosphate to 1,3-dephosphoglycerate
Tdh3	Glyceraldehyde-3-phosphate dehydrogenase 3; converts D-glyceraldehyde 3-phosphate to 1,3-dephosphoglycerate
Tpi1	Triosephosphate isomerase; interconverts glyceraldehyde-3-phosphate and dihydroxyacetone phosphate
Efb1	Translation elongation factor EF-1β; GDF/GTP exchange factor for Tef1p/Tef2p
Eft1	Translation elongation factor EF-2; contains diphthamide which is not essential for activity; identical to Eft2p
Eft2	Translation elongation factor EF-2; contains diphthamide which is not essential for activity; identical to Eft1p
Eft1	Translation initiation factor eIF3 beta subunit (p90); has an RNA recognition domain
Rpa0 (RPPO)	Acidic ribosomal protein A0
Tif1	Translation initiation factor 4A (eIF4A) of the DEAD box family
Tif2	Translation initiation factor 4A (eIF4A) of the DEAD box family
Yef3	Translation elongation factor EF-3A; member of ATP-binding cassette superfamily
Hsc82	Chaperonin homologous to <i>E. coli</i> HtpG and mammalian HSP90
Hsp60	Mitochondrial chaperonin that cooperates with Hsp10p; homolog of <i>E. coli</i> GroEL
Hsp82	Heat-inducible chaperonin homologous to <i>E. coli</i> HtpG and mammalian HSP90
Hsp104	Heat shock protein required for induced thermotolerance and for resolubilizing aggregates of denatured proteins; important for [psi ⁺]-to-[psi ⁻] prion conversion
Kar2	Heat shock protein of the endoplasmic reticulum lumen required for protein translocation across the endoplasmic reticulum membrane and for nuclear fusion; member of the HSP70 family
Ssa1	Cytoplasmic chaperone; heat shock protein of the HSP70 family
Ssa2	Cytoplasmic chaperone; member of the HSP70 family
Ssb1	Heat shock protein of HSP70 family involved in the translational apparatus
Ssb2	Heat shock protein of HSP70 family, cytoplasmic
Ssc1	Mitochondrial protein that acts as an import motor with Tim44p and plays a chaperonin role in receiving and folding of protein chains during import; heat shock protein of HSP70 family
Sse1	Heat shock protein of the HSP70 family; multicopy suppressor of mutants with hyperactivated Ras/cyclic AMP pathway
Sti1	Stress-induced protein required for optimal growth at high and low temperature; has tetratricopeptide repeats
Adel1	Phosphoribosylamidoimidazole-succinocarboxamide synthase; catalyzes the seventh step in de novo purine biosynthesis pathway
Ade3	C, tetrahydrofolate synthase (trifunctional enzyme), cytoplasmic
Ade5,7	Phosphoribosylamine-glycine ligase plus phosphoribosylformylglycinamide cyclo-ligase; bifunctional protein
Arg4	Argininosuccinate lyase; catalyzes the final step in arginine biosynthesis
Gdh1	Glutamate dehydrogenase (NADP ⁺); combines ammonia and α-ketoglutarate to form glutamate
Gln1	Glutamine synthetase; combines ammonia to glutamate in ATP-driven reaction
His4	Phosphoribosyl-AMP cyclohydrolase/phosphoribosyl-ATP pyrophosphohydrolase/histidinol dehydrogenase; 2nd, 3rd, and 10th steps of his biosynthesis pathway
Ilv5	Ketol-acid reductoisomerase (acetohydroxy, acid reductoisomerase) (alpha-keto-β-hydroxylacyl) reductoisomerase; second step in Val and Ilv biosynthesis pathway
Lys9	Saccharopine dehydrogenase (NADP ⁺ , L-glutamate forming) (saccharopine reductase), seventh step in lysine biosynthesis pathway
Met6	Homocysteine methyltransferase; (5-methyltetrahydropteroyl triglutamate-homocysteine methyltransferase), methionine synthase, cobalamin independent
Pro2	γ-Glutamyl phosphate reductase (phosphoglutamate dehydrogenase), proline biosynthetic enzyme
Ser1	Phosphoserine transaminase; involved in synthesis of serine from 3-phosphoglycerate
Tip5	Tryptophan synthase, last (5th) step in tryptophan biosynthesis pathway
Act1	Actin; involved in cell polarization, endocytosis, and other cytoskeletal functions
Adk1	Adenylate kinase (GTP:AMP phosphotransferase), cytoplasmic
Ald6	Cytosolic acetaldehyde dehydrogenase
Atp2	Beta subunit of F1-ATP synthase; 3 copies are found in each F1 oligomer
Bmh1	Homolog of mammalian 14-3-3 protein; has strong similarity to Bmh2p
Bmh2	Homolog of mammalian 14-3-3 protein; has strong similarity to Bmh1p
Cdc48	Protein of the AAA family of ATPases; required for cell division and homotypic membrane fusion
Cdc60	Leucyl-tRNA synthetase, cytoplasmic
Erg20	Farnesyl pyrophosphate synthetase; may be rate-limiting step in sterol biosynthesis pathway
Gpp1 (Rhr2)	DL-Glycerol phosphate phosphatase
Gsp1	Ran, a GTP-binding protein of the Ras superfamily involved in trafficking through nuclear pores
Ipp1	Inorganic pyrophosphatase, cytoplasmic
Lcb1	Component of serine C-palmitoyltransferase; first step in biosynthesis of long-chain base component of sphingolipids
Mol1 (Thi4)	Thiamine-repressed protein essential for growth in the absence of thiamine
Pab1	Poly(A)-binding protein of cytoplasm and nucleus; part of the 3'-end RNA-processing complex (cleavage factor I); has 4 RNA recognition domains
Psa1	Mannose-1-phosphate guanylttransferase; GDP-mannose pyrophosphorylase
Rnr4	Ribonucleotide reductase small subunit
Sam1	S-Adenosylmethionine synthetase 1
Sam2	S-Adenosylmethionine synthetase 2
Sod1	Copper-zinc superoxide dismutase
Uba1	Ubiquitin-activating (E1) enzyme
YKL056	Resembles translationally controlled tumor protein of animal cells and higher plants
YLR109 (Ahp1)	Alkyl hydroperoxide reductase
YMR116 (Asc1)	Abundant protein with effects on translational efficiency and cell size, has two WD (WD-40) repeats

^a Accepted name from the *Saccharomyces* genome database and YPD. Names in parentheses represent recent changes.

^b Courtesy of Proteome, Inc., reprinted with permission.

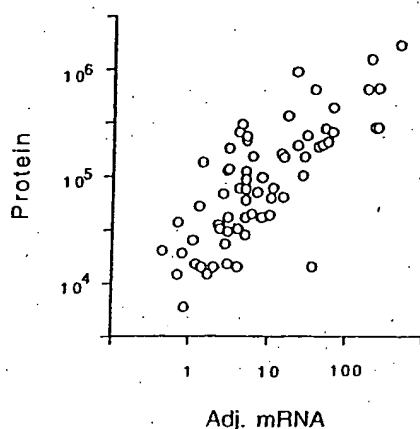


FIG. 2. Correlation of protein abundance with adjusted mRNA abundance. The number of molecules per cell of each protein is plotted against the number of molecules per cell of the cognate mRNA, with an r_p of 0.76. Note the logarithmic axes. Data for mRNA were taken from references 27 and 30 and combined as described in Materials and Methods.

correlation, confirming a strong correlation between CAI and protein abundance (Fig. 3). The relationship between CAI and protein abundance is log linear from about 1,000,000 to about 10,000 molecules per cell. We have no data for rarer proteins.

It is not clear whether CAI reflects maximum or average levels of protein expression. The proteins used for the CAI-protein correlation included some proteins which were not expressed at maximum levels under the condition of the experiment (Hsc82, Hsp104, Ssa1, Ade1, Arg4, His4, and others). When these proteins were removed from consideration and the correlation between CAI and the remaining (presumably constitutive) proteins was recalculated, the r_p was essentially unchanged (not shown).

The equation describing the graph in Fig. 3 is $\log(\text{protein molecules/cell}) = (2.3 \times \text{CAI}) + 3.7$. Thus, under certain conditions (a CAI of 0.3 or greater; a constitutively expressed gene), a very rough estimate of protein abundance can be made by raising 10 to the power of $[(2.3 \times \text{CAI}) + 3.7]$.

The distribution of CAI over the genome (Fig. 4) consists of a lower, bell-shaped distribution, possibly indicating a region where there is no selection for codon bias, and an upper, flat distribution, starting at a CAI of about 0.3, possibly indicating a region where there is selection for codon bias. Almost all of the proteins whose abundance we have measured are in the upper, flat portion of the distribution. In the lower, bell-shaped region, we do not know whether there is a correlation between CAI and protein abundance.

Changes in protein abundance in glucose and ethanol. A comparison of cells grown in glucose (Fig. 1A) with cells grown in ethanol (Fig. 1B) is shown in Table 1. As is well known, some proteins are induced tremendously during growth on ethanol. Two striking examples are the peroxisomal enzymes Icl1 (isocitrate lyase) and Cit2 (citrate synthase), which are induced in ethanol by more than 100- and 12-fold, respectively (Fig. 1; Table 1). These enzymes are key components of the glyoxylate shunt, which diverts some acetyl coenzyme A (acetyl-CoA) from the tricarboxylic acid cycle to gluconeogenesis. *S. cerevisiae* requires large amounts of carbohydrate for its cell wall; in ethanol medium, this carbohydrate comes from gluconeogenesis, which depends on the glyoxylate shunt and on the glycolytic pathway running in reverse. The need for

gluconeogenesis also explains why glycolytic enzymes are abundant even in ethanol medium. Thus, 2D gel analysis shows the prominence of the glycolytic and glyoxylate shunt enzymes in cells grown on ethanol, emphasizing that gluconeogenesis, presumably largely for production of the cell wall, is a major metabolic activity under these conditions.

During gluconeogenesis, substrate-product relationships are reversed for the glycolytic enzymes. One might expect that not all glycolytic enzymes would be well adapted to the reverse reaction. Indeed, 2D gels show that in ethanol, Adh2 (alcohol dehydrogenase 2) is strongly induced (16), while its isozyme Adh1 is not greatly affected. Adh1 and Adh2 each interconvert acetaldehyde and ethanol. Adh1 has a relatively high K_m for ethanol (17 mM), while Adh2 has a lower K_m (0.8 mM) (5). Thus, it is thought that Adh1 is specialized for glycolysis (acetaldehyde to ethanol), while Adh2 is specialized for respiration (ethanol to acetaldehyde) (5, 29). Similarly, Eno1 (enolase 1) is induced in ethanol, while its isozyme Eno2 (enolase 2) decreases in abundance (Table 1) (4, 19). Eno1 is inhibited by 2-phosphoglycerate (the glycolytic substrate), while Eno2 is inhibited by phosphoenolpyruvate (the gluconeogenic substrate) (4). Perhaps Eno1 has a lower K_m for phosphoenolpyruvate than does Eno2, though to our knowledge this has not been tested. Thus, the 2D gels distinguish isozymes specialized for growth on glucose (Adh1 and Eno2) from isozymes specialized for ethanol (Adh2 and Eno1).

Many heat shock proteins (e.g., Hsp60, Hsp82, Hsp104, and Kar2) were about twofold more abundant in ethanol medium than in glucose medium. This is consistent with the increased heat resistance of cells grown in ethanol (3).

Enzymes involved in protein synthesis (Efl1, Rpa0, and Tif1) were about twice as abundant in glucose medium as in ethanol medium. This may reflect the higher growth rate of the cells in glucose.

Phosphorylation of proteins. To examine protein phosphorylation, we labeled cells with ^{32}P and ran 2D gels to examine phosphoproteins. About 300 distinct spots, probably representing 150 to 200 proteins, could be seen on pH 4–8 gels (Fig. 5B). We then aligned autoradiograms of three gels, each with a different kind of labeled protein (^{32}P only [Fig. 5B], ^{32}P plus ^{35}S [Fig. 5A], and ^{35}S only [not shown, but see Fig. 1 for example]). In this way, we made provisional identification of

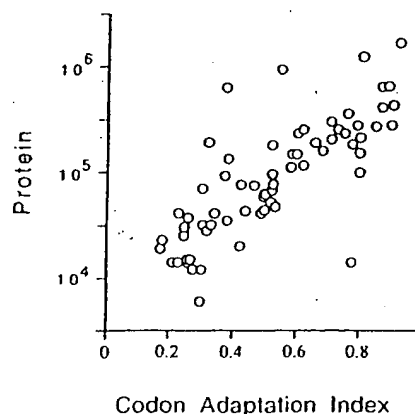


FIG. 3. Correlation of protein abundance with CAI. The number of molecules per cell of each protein is plotted against the CAI for that protein. Note the logarithmic scale on the protein axis. Data for the CAI are from the YPD database (13).

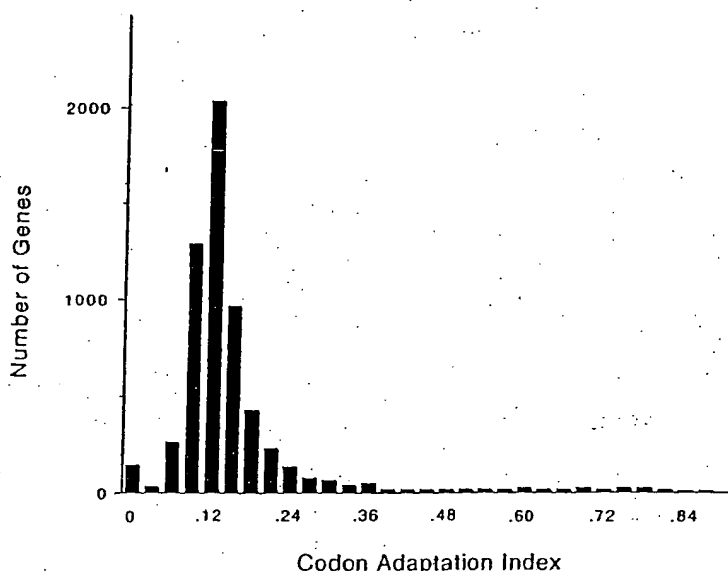


FIG. 4. Distribution of CAI over the whole genome, shown in intervals of 0.030 (i.e., there are 150 genes with a CAI between 0.000 and 0.030, inclusive; 31 genes with a CAI between 0.031 and 0.060; 269 genes with a CAI between 0.061 and 0.090; 1,296 genes with a CAI between 0.091 and 0.120; etc.). The distribution peaks with 2,028 genes with a CAI between 0.121 and 0.150.

some of the ^{32}P -labeled spots as particular ^{35}S -labeled spots. All such identifications are somewhat uncertain, since precise alignments are difficult, and of course multiple spots may exactly comigrate. Nevertheless, we believe that most of the provisional identifications are probably correct. Among the major ^{32}P -labeled proteins are the hexokinases Hxk1 and Hxk2, the acidic ribosome-associated protein Rpa0, the translation factors Yef3 and Efb1, and probably Hsp70 heat shock proteins of the Ssa and Ssb families. Rpa0 and Efb1 are quantitatively monophosphorylated.

Many yeast proteins resolve into multiple spots on these 2D gels (7). Yef3 has five or more spots, at least four of which comigrate with ^{32}P . Tpi1 has a major spot showing no ^{32}P labeling and a minor, more acidic spot which overlaps with some ^{32}P label. Tif1 has at least seven spots (7); two of these overlap with some ^{32}P label, but five do not (Fig. 5). Efb1 has at least three spots (7), and none of these overlap with ^{32}P , although there are three nearby, unidentified ^{32}P -labeled spots (a, c, and d in Fig. 5). Spots that seem to be extra forms of Met6, Pdc1, Eno2, and Fba1 can be seen in Fig. 6A, but there is little ^{32}P at these positions in Fig. 5. Thus, phosphorylation explains some but not all of the different protein isoforms seen.

The cell cycle is regulated in part by phosphorylation. We compared ^{32}P -labeled proteins from cells synchronized in G_1 with α -factor, in cells synchronized in G_1 by depletion of G_1 cyclins, and in cells synchronized in M phase with nocodazole. Only very minor differences were seen, and these were difficult to reproduce. The cell cycle proteins regulated by phosphorylation may not be abundant enough for this technique to be applied easily.

Centrifugal fractionation. We fractionated ^{35}S -labeled extracts by centrifugation (Materials and Methods). Figure 6A shows the proteins in the supernatant of a high-speed ($100,000 \times g$, 30 min) centrifugation, while Fig. 6B shows the proteins in the pellet of a low-speed ($16,000 \times g$, 10 min) centrifugation. Many proteins are tremendously enriched in one fraction or the other, while others are present in both.

Most glycolytic enzymes (e.g., Tdh2, Tdh3, Eno2, Pdc1, Adh1, and Fba1) are enriched in the supernatant fraction. The only exception is Pfk1 (not indicated), which is found in both pellet and supernatant fractions. Many proteins involved in protein synthesis (Eft1, Yef3, Prt1, Tif1, and Rpa0) are in the pellet, possibly because of the association of ribosomes with the endoplasmic reticulum. However, Efb1 is in the supernatant, as is a substantial portion of the Eft1. Perhaps surprisingly, several mitochondrial proteins (Atp2 [not shown] and Ily5) are largely in the supernatant. Perhaps glass bead breakage of cells releases mitochondrial proteins. The nuclear protein Gsp1 is in the pellet fraction. The enrichment produced by centrifugation makes it possible to see minor spots which are otherwise poorly resolved from surrounding proteins. Figure 6B shows that the previously identified Tif1 spot is surrounded by as many as six other spots that cofractionate. We observed six identical or very similar additional spots when we overexpressed Tif1 from a high-copy-number plasmid (not shown). Signal overlaps only one or two of these spots in ^{32}P -labeling experiments (Fig. 5), and so the different forms are not mainly due to different phosphorylation states.

DISCUSSION

Our experience with developing a 2D gel protein database for *S. cerevisiae* is summarized here. With current technology, we can see the most abundant 1,200 proteins, which is about one-third to one-quarter of the proteins expressed. The remaining proteins will be difficult to see and study with the methods that we have used, not because of a lack of sensitivity but because weak spots are covered by nearby strong spots.

Of the 1,200 proteins seen, we have identified 148, with a bias toward the most abundant proteins. Steady application of the methods already used would allow identification of most of the remaining proteins. Gene overexpression will be particularly useful, since it is not affected by the lower abundance of the remaining visible proteins.

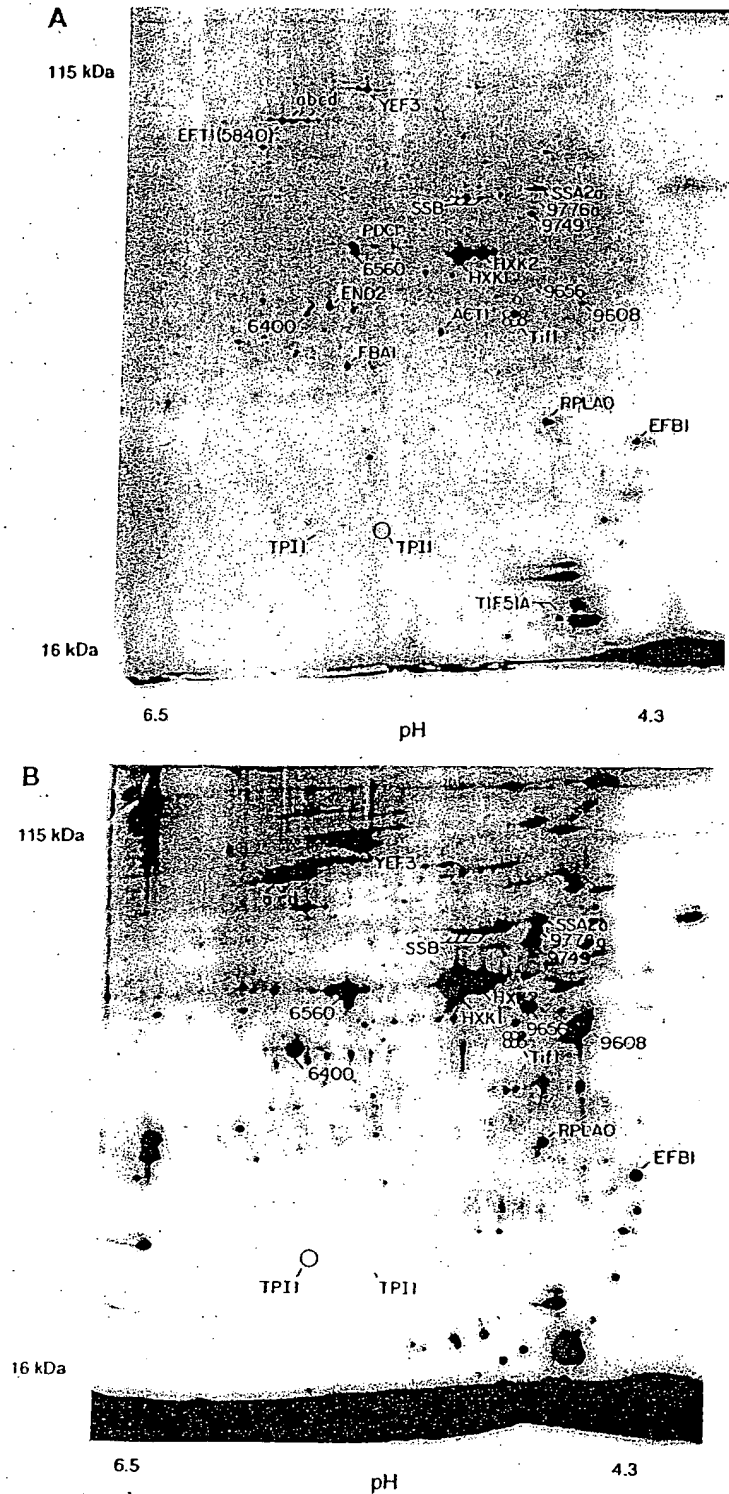


FIG. 5. Phosphorylated proteins. (A) Mixture of ^{32}P -labeled proteins and ^{35}S -labeled proteins. Two separate labeling reactions were done, one with ^{32}P and one with ^{35}S , and extracts were mixed and run on a 2D gel. Spots marked with numbers rather than gene names represent spots noted on ^{35}S gels but unidentified. Spots labeling with ^{32}P were identified by (i) increased labeling compared to the ^{35}S -only gel (not shown); (ii) the characteristic fuzziness of a ^{32}P -labeled spot; and (iii) the decay of signal intensity seen on exposures made 4 weeks later (not shown). A minor form of TPI1 and at least six minor forms of TIF1 have been noted in overexpression experiments (see also Fig. 6B); positions of the minor forms are indicated by circles. (B) ^{32}P -only labeling. The major form of TPI1, which is not labeled with ^{32}P , is indicated by a large circle; positions of seven forms of TIF1 are indicated by smaller circles.

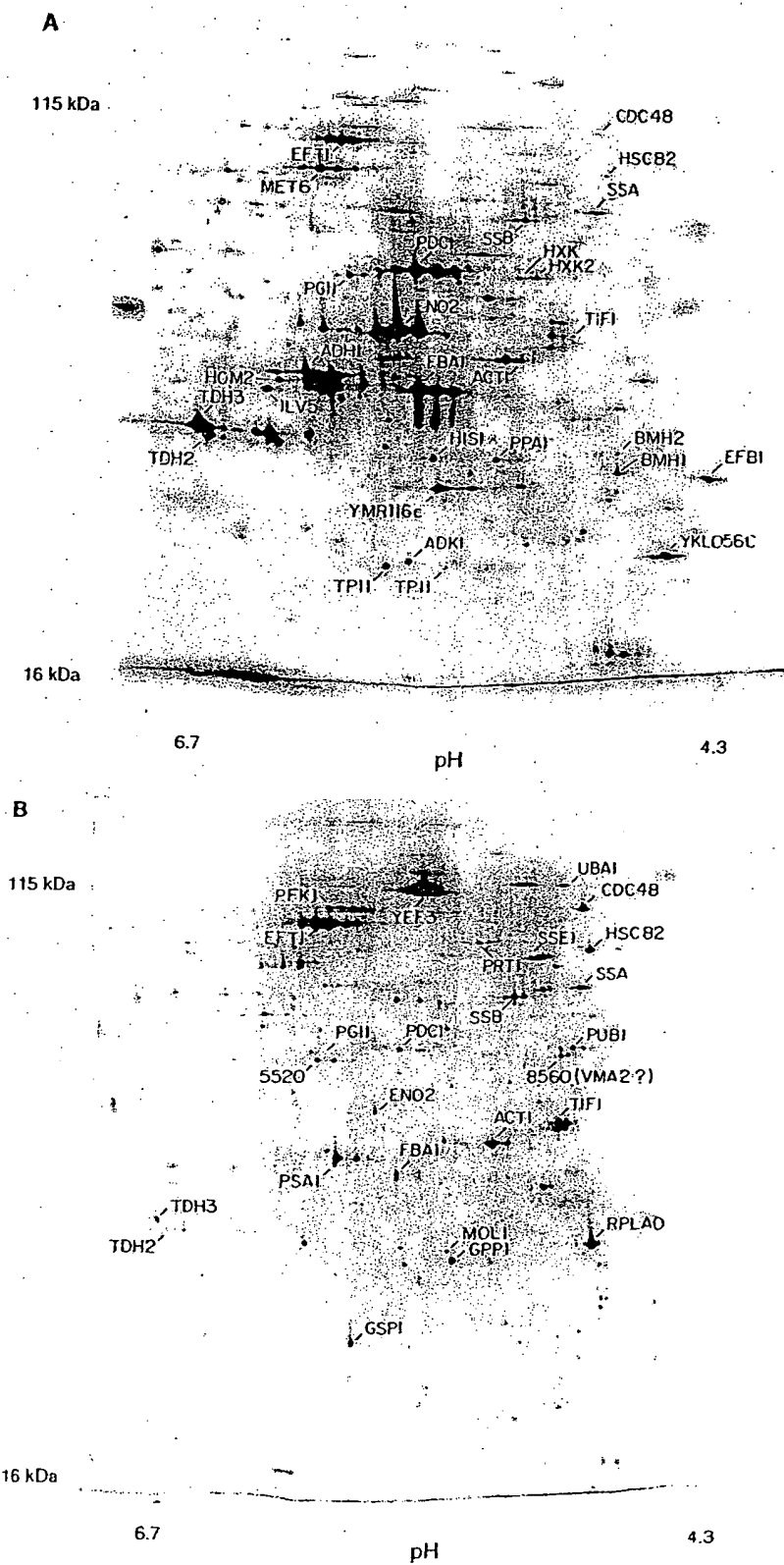


FIG. 6. Fractionation by centrifugation. (A) Proteins in the supernatant of a $100,000 \times g$, 30-min spin; proteins in the pellet of a $16,000 \times g$, 10-min spin. Supernatant fractions examined in multiple experiments done over a wide range of g forces looked similar to each other, as did the pellet fractions.

2D gels of the kind that we have used are not suitable for visualization of rare proteins. However it will be possible to study on a global basis metabolic processes involving relatively abundant proteins, such as protein synthesis, glycolysis, gluconeogenesis, amino acid synthesis, cell wall synthesis, nucleotide synthesis, lipid metabolism, and the heat shock response.

Gygi et al. (10) have recently completed a study similar to ours. Despite generating broadly similar data, Gygi et al. reached markedly different conclusions. We believe that both mRNA abundance and codon bias are useful predictors of protein abundance. However, Gygi et al. feel that mRNA abundance is a poor predictor of protein abundance and that "codon bias is not a predictor of either protein or mRNA levels" (10). These different conclusions are partly a matter of viewpoint. Gygi et al. focus on the fact that the correlations of mRNA and codon bias with protein abundance are far from perfect, while we focus on the fact that, considering the wide range of mRNA and protein abundance and the undoubted presence of other mechanisms affecting protein abundance, the correlations are quite good.

However, the different conclusions are also partly due to different methods of statistical analysis and to real differences in data. With respect to statistics, Gygi et al. used the Pearson product-moment correlation coefficient (r_p) to measure the covariance of mRNA and protein abundance. Depending on the subset of data included, their r_p values ranged from 0.1 to 0.94. Because of the low r_p values with some subsets of the data, Gygi et al. concluded that the correlation of mRNA to protein was poor. However, the r_p correlation is a parametric statistic and so requires variates following a bivariate normal distribution; that is, it would be valid only if both mRNA and protein abundances were normally distributed. In fact, both distributions are very far from normal (data not shown), and so a calculation of r_p is inappropriate. There was no statistical backing for the assertion that codon bias fails to predict protein abundance.

We have taken two statistical approaches. First, we have used the Spearman rank correlation coefficient (r_s). Since this statistic is nonparametric, there is no requirement for the data to be normally distributed. Using the r_s , we find that mRNA abundance is well correlated with protein abundance ($r_s = 0.74$), and the CAI is also well correlated with protein abundance ($r_s = 0.80$) (and also with mRNA abundance [data not shown]). For the data of Gygi et al. (10), we obtained similar results, though with their data the correlation is not as good; $r_s = 0.59$ for the mRNA-to-protein correlation, and $r_s = 0.59$ for the codon bias-to-protein correlation.

In a second approach, we transformed the mRNA and protein data to forms where they were normally distributed, to allow calculation of an r_p (Materials and Methods). Two transformations, Box-Cox and logarithmic, were used; both gave good correlations with our data [e.g., $r_p = 0.76$ for $\log(\text{adjusted RNA})$ to $\log(\text{protein})$]. We were not able to transform the data of Gygi et al. to a normal distribution.

Finally, there are also some differences in data between the two studies. These may be partly due to the different measurement techniques used: Gygi et al. measured protein abundance by cutting spots out of gels and measuring the radioactivity in each spot by scintillation counting, whereas we used phosphorimaging of intact gels coupled to image analysis. We compared our data to theirs for the proteins common between the studies (but excluding proteins whose mRNAs are known to differ between rich and minimal media, and excluding Tif1, which was anomalous in differing by 100-fold between the two data sets). The r_s between the two protein data sets was 0.88 ($P < 0.0001$). Although this is a strong correlation, the fact that

it is less than 1.0 suggests that there may have been errors in measuring protein abundance in one or both studies. After normalizing the two data sets to assume the same amount of protein per cell, we found a systematic tendency for the protein abundance data of Gygi et al. to be slightly higher than ours for the highest-abundance proteins and also for the lowest-abundance proteins but slightly lower than ours for the middle-abundance proteins. These systematic differences suggest some systematic errors in protein measurement. Although we do not know what the errors are, we suggest the following as a reasonable speculation. For the highest-abundance proteins, we may have underestimated the amount of protein because of a slightly nonlinear response of the phosphorimager screens. For the lowest-abundance proteins, Gygi et al. may have overestimated the amount of protein because of difficulties in accurately cutting very small spots out of the gel and because of difficulties in background subtraction for these small, weak spots. The difference in the middle abundance proteins may be a consequence of normalization, given the two errors above.

The low-abundance proteins in the data set of Gygi et al. have a poor correlation with mRNA abundance. We calculate that the r_s is 0.74 for the top 54 proteins of Gygi et al. but only 0.22 for the bottom 53 proteins, a statistically significant difference. However, with our data set, the r_s is 0.62 for the top 33 proteins and 0.56 (not significantly different) for the bottom 33 proteins (which are comparable in abundance to the bottom 53 proteins of Gygi et al.). Thus, our data set maintains a good correlation between mRNA and protein abundance even at low protein abundance. This is consistent with our speculation that protein quantification by phosphorimaging and image analysis may be more accurate for small, weak spots than is cutting out spots followed by scintillation counting. Our relatively good correlations even for nonabundant proteins may also reflect the fact that we used both SAGE data and RNA hybridization data, which is most helpful for the least abundant mRNAs. In summary, we feel that the poor correlation of protein to mRNA for the nonabundant proteins of Gygi et al. may reflect difficulty in accurately measuring these nonabundant proteins and mRNAs, rather than indicating a truly poor correlation *in vivo*. It is not surprising that observed correlations would be poorer with less-abundant proteins and mRNAs, simply because the accuracy of measurement would be worse.

How well can mRNA abundance predict protein abundance? With $r_p = 0.76$ for logarithmically transformed mRNA and protein data, the coefficient of determination, $(r_p)^2$, is 0.58. This means that more than half (in log space) of the variation in protein abundance is explained by variation in mRNA abundance. When converted back to arithmetic values, protein abundances vary over about 200-fold (Table 1), and $(r_p)^2 = 0.58$ for the log data means that of this 200-fold variation, about 20-fold is explained by variation in the abundance of mRNA and about 10-fold is unexplained (but could be due partly to measurement errors). For proteins much less abundant than those considered here, we imagine the *in vivo* correlation between mRNA and protein abundance will be worse, and other regulatory mechanisms such as protein turnover will be more important.

Some important conclusions can be drawn from this sampling of the proteome. First, there is an enormous range of protein abundance, from nearly 2,000,000 molecules per cell for some glycolytic enzymes to about 100 per cell for some cell cycle proteins (26a). Second, about half of all cellular protein is found in fewer than 100 different gene products, which are mostly involved in carbohydrate metabolism or protein synthe-

sis. Third, the correlation between protein abundance and CAI is log linear as far as we can see, which is from about 10,000 protein molecules per cell to about 1,000,000. This is somewhat surprising, because it implies that selective forces for codon bias are significant even at moderate expression levels. It also means that codon bias is a useful predictor of protein abundance even for moderately low bias proteins. Fourth, there is a good correlation between protein abundance and mRNA abundance for the proteins that we have studied. This validates the use of mRNA abundance as a rough predictor of protein abundance, at least for relatively abundant proteins. Fifth, for these abundant proteins, there are about 4,000 molecules of protein for each molecule of mRNA. This last conclusion raises questions as to how the levels of nonabundant proteins are regulated and suggests that protein instability, regulated translation, suboptimal rates of translation, and other mechanisms in addition to transcriptional control may be very important for these proteins.

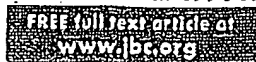
ACKNOWLEDGMENTS

We thank Neena Sarcen and Nick Bizios (CSHL 2D gel laboratory) for production of 2D gels, Tom Volpe for help with some experiments, Corine Driessens for help with calculations and statistics, and Herman Wijnen and Nick Edgington for comments on the manuscript. We especially thank Tim Tully for in-depth statistical analysis and for insightful discussions on statistical interpretations.

This work was supported by grant P41-RR02188 from the NIH Biomedical Research Technology Program, Division of Research Resources, to J.I.G., by Small Business Innovation Research grant R44 GM54110 to Proteome, Inc., by grant DAMD17-94-14050 from the Army Breast Cancer Program to B.F., and by NIH grant RO1 GM45410 to B.F.

REFERENCES

- Baroni, M. D., E. Martegani, P. Monti, and L. Alberghina. 1989. Cell size modulation by *CDC25* and *R452* genes in *Saccharomyces cerevisiae*. *Mol. Cell. Biol.* 9:2715-2723.
- Boucherie, H., F. Sagliocco, R. Joubert, I. Maillet, J. Labarre, and M. Perrot. 1996. Two-dimensional gel protein database of *Saccharomyces cerevisiae*. *Electrophoresis* 17:1683-1699.
- Elliott, B., and B. Futcher. 1993. Stress resistance of yeast cells is largely independent of cell cycle phase. *Yeast* 9:33-42.
- Entian, K. D., B. Meurer, H. Kohler, K. H. Mann, and D. Mecke. 1987. Studies on the regulation of enolases and compartmentation of cytosolic enzymes in *Saccharomyces cerevisiae*. *Biochim. Biophys. Acta* 923:214-221.
- Ganzhorn, A. J., D. W. Green, A. D. Hershey, R. M. Gould, and B. V. Plapp. 1987. Kinetic characterization of yeast alcohol dehydrogenases. Amino acid residue 294 and substrate specificity. *J. Biol. Chem.* 262:3754-3761.
- Garrels, J. I. 1989. The Quest system for quantitative analysis of two-dimensional gels. *J. Biol. Chem.* 264:5269-5282.
- Garrels, J. I., B. Futcher, R. Kobayashi, G. I. Latter, B. Schwender, T. Volpe, J. R. Warner, and C. S. McLaughlin. 1994. Protein identifications for a *Saccharomyces cerevisiae* protein database. *Electrophoresis* 15:1466-1486.
- Garrels, J. I., C. S. McLaughlin, J. R. Warner, B. Futcher, G. I. Latter, R. Kobayashi, B. Schwender, T. Volpe, D. S. Anderson, R. Mesquita-Fuentes, and W. E. Payne. 1997. Proteome studies of *S. cerevisiae*: identification and characterization of abundant proteins. *Electrophoresis* 18:1347-1360.
- Goffeau, A., B. G. Barrell, H. Bussey, R. W. Davis, B. Dujon, H. Feldmann, F. Galibert, J. D. Hoheisel, C. Jacq, M. Johnston, E. J. Louis, H. W. Mewes, Y. Murakami, P. Philippson, H. Tettelin, and S. G. Oliver. 1996. Life with 6000 genes. *Science* 274:563-567.
- Gygi, S. P., Y. Rochon, B. R. Franza, and R. Aebersold. 1999. Correlation between protein and mRNA abundance in yeast. *Mol. Cell. Biol.* 19:1720-1730.
- Hereford, L. M., and M. Rosbash. 1977. Number and distribution of polyadenylated RNA sequences in yeast. *Cell* 10:453-462.
- Herrick, D., R. Parker, and A. Jacobson. 1990. Identification and comparison of stable and unstable mRNAs in *Saccharomyces cerevisiae*. *Mol. Cell. Biol.* 10:2269-2284.
- Hodges, P. E., A. H. McKee, B. P. Davis, W. E. Payne, and J. I. Garrels. 1999. The Yeast Proteome Database (YPD): a model for the organization of genome-wide functional data. *Nucleic Acids Res.* 27:69-73.
- Ikemura, T. 1985. Codon usage and tRNA content in unicellular and multicellular organisms. *Mol. Biol. Evol.* 2:13-34.
- Johnston, G. C., F. R. Pringle, and L. H. Hartwell. 1977. Coordination of growth with cell division in the yeast *S. cerevisiae*. *Exp. Cell Res.* 105:79-98.
- Johnston, M., and M. Carlson. 1992. Regulation of carbon and phosphate utilization, p. 193-281. In E. Jones, J. Pringle, and J. Broach (ed.), *The molecular and cellular biology of the yeast Saccharomyces*. Cold Spring Harbor Laboratory Press, Cold Spring Harbor, N.Y.
- Kornblatt, M. J., and A. Klugerman. 1989. Characterization of the enolase isozymes of rabbit brain: kinetic differences between mammalian and yeast enolases. *Biochem. Cell. Biol.* 67:103-107.
- Latter, G., and B. Futcher. Unpublished data.
- Mathews, B., N. Sonenberg, and J. W. B. Hershey. 1996. Origins and targets of translational control, p. 1-29. In J. W. B. Hershey, M. B. Mathews, and N. Sonenberg (ed.), *Translational control*. Cold Spring Harbor Laboratory Press, Cold Spring Harbor, N.Y.
- McAlister, L., and M. J. Holland. 1982. Targeted deletion of a yeast enolase structural gene. Identification and isolation of yeast enolase isozymes. *J. Biol. Chem.* 257:7181-7188.
- Monardo, P. J., T. Boutell, J. I. Garrels, and G. I. Latter. 1994. A distributed system for two-dimensional gel analysis. *Comput. Appl. Biosci.* 10:137-143.
- O'Farrell, P. H. 1975. High resolution two-dimensional electrophoresis of proteins. *J. Biol. Chem.* 250:4007-4021.
- Patterson, S. D., and G. I. Latter. 1993. Evaluation of storage phosphor imaging for quantitative analysis of 2-D gels using the Quest II system. *BioTechniques* 15:1076-1083.
- Sagliocco, F., J. C. Guillemot, C. Monribot, J. Capdevielle, M. Perrot, E. Ferran, P. Ferrara, and H. Boucherie. 1996. Identification of proteins of the yeast protein map using genetically manipulated strains and peptide-mass fingerprinting. *Yeast* 12:1519-1533.
- Sharp, P. M., and W. H. Li. 1987. The Codon Adaptation Index—a measure of directional synonymous codon usage bias, and its potential applications. *Nucleic Acids Res.* 15:281-295.
- Shevchenko, A., O. N. Jensen, A. V. Podtelejnikov, F. Sagliocco, M. Wilm, O. Vorm, P. Mortensen, A. Shevchenko, H. Boucherie, and M. Mann. 1996. Linking genome and proteome by mass spectrometry: large-scale identification of yeast proteins from two dimensional gels. *Proc. Natl. Acad. Sci. USA* 93:14440-14445.
- Thomas, B. J., and R. Rothstein. 1989. Elevated recombination rates in transcriptionally active DNA. *Cell* 56:619-630.
- Tyers, M., and B. Futcher. Unpublished data.
- Velculescu, V. E., L. Zhang, W. Zhou, J. Vogelstein, M. A. Basrai, D. E. Bassett, Jr., P. Hieter, B. Vogelstein, and K. W. Kinzler. 1997. Characterization of the yeast transcriptome. *Cell* 88:243-251.
- Warner, J. 1991. Labeling of RNA and phosphoproteins in *S. cerevisiae*. *Methods Enzymol.* 194:423-428.
- Wills, C. 1976. Production of yeast alcohol dehydrogenase isoenzymes by selection. *Nature* 261:26-29.
- Wodicka, L. Personal communication.
- Wodicka, L. Unpublished data.
- Wodicka, L., H. Dong, M. Mittmann, M.-H. Ho, and D. J. Lockhart. 1997. Genome-wide expression monitoring in *Saccharomyces cerevisiae*. *Nat. Biotechnol.* 15:1359-1367.



Overexpression of a DEAD box protein (DDX1) in neuroblastoma and retinoblastoma cell lines.

Godbout R, Packer M, Bie W.

Department of Oncology, Cross Cancer Institute and University of Alberta, 11560 University Ave., Edmonton, Alberta T6G1Z2, Canada.

The DEAD box gene, DDX1, is a putative RNA helicase that is co-amplified with MYCN in a subset of retinoblastoma (RB) and neuroblastoma (NB) tumors and cell lines. Although gene amplification usually involves hundreds to thousands of kilobase pairs of DNA, a number of studies suggest that co-amplified genes are only overexpressed if they provide a selective advantage to the cells in which they are amplified. Here, we further characterize DDX1 by identifying its putative transcription and translation initiation sites. We analyze DDX1 protein levels in MYCN/DDX1-amplified NB and RB cell lines using polyclonal antibodies specific to DDX1 and show that there is a good correlation with DDX1 gene copy number, DDX1 transcript levels, and DDX1 protein levels in all cell lines studied. DDX1 protein is found in both the nucleus and cytoplasm of DDX1-amplified lines but is localized primarily to the nucleus of nonamplified cells. Our results indicate that DDX1 may be involved in either the formation or progression of a subset of NB and RB tumors and suggest that DDX1 normally plays a role in the metabolism of RNAs located in the nucleus of the cell.

PMID: 9694872 [PubMed - indexed for MEDLINE]

150: Virchows Arch. 2002 May;440(5):461-75. Epub 2002 Mar 23. [Related Articles](#), [Links](#)

 [SpringerLink](#)

Expression of somatostatin receptor types 1-5 in 81 cases of gastrointestinal and pancreatic endocrine tumors. A correlative immunohistochemical and reverse-transcriptase polymerase chain reaction analysis.

Papotti M, Bongiovanni M, Volante M, Allia E, Landolfi S, Helboe L, Schindler M, Cole SL, Bussolati G.

Department of Biomedical Sciences and Oncology, University of Turin, Via Santena 7, 10126 Turin, Italy. mauro.papotti@unito.it

Somatostatin receptors (SSTRs) have been extensively mapped in human tumors by means of autoradiography, reverse-transcriptase polymerase chain reaction (RT-PCR), in situ hybridization (ISH) and immunohistochemistry (IHC). We analyzed the SSTR type 1-5 expression by means of RT-PCR and/or IHC in a series of 81 functioning and non-functioning gastroenteropancreatic (GEP) endocrine tumors and related normal tissues. Moreover, we compared the results with clinical, pathological and hormonal features. Forty-six cases (13 intestinal and 33 pancreatic) were studied for SSTR 1-5 expression using RT-PCR, IHC with antibodies to SSTR types 2, 3, 5 and ISH for SSTR2 mRNA. The vast majority of tumors expressed SSTR types 1, 2, 3 and 5, while SSTR4 was detected in a small minority. Due to the good correlation between RT-PCR and IHC data on SSTR types 2, 3, and 5, thirty-five additional GEP endocrine tumors were studied with IHC alone. Pancreatic insulinomas had an heterogeneous SSTR expression, while 100% of somatostatinomas expressed SSTR5 and 100% gastrinomas and glucagonomas expressed SSTR2. Pre-operative biopsy material showed an overlapping immunoreactivity with that of surgical specimens, suggesting that the SSTR status can be detected in the diagnostic work-up. It is concluded that SSTRs 1-5 are heterogeneously expressed in GEP endocrine tumors and that IHC is a reliable tool to detect SSTR types 2, 3 and 5 in surgical and biopsy specimens.

PMID: 12021920 [PubMed - indexed for MEDLINE]



Expression of deoxycytidine kinase in leukaemic cells compared with solid tumour cell lines, liver metastases and normal liver.

van der Wilt CL, Kroep JR, Loves WJ, Rots MG, Van Groenigen CJ, Kaspers GJ, Peters GJ.

Department of Medical Oncology, VU University Medical Center, Amsterdam, The Netherlands.

Deoxycytidine kinase (dCK) is required for the phosphorylation of several deoxyribonucleoside analogues that are widely employed as chemotherapeutic agents. Examples include cytosine arabinoside (Ara-C) and 2-chlorodeoxyadenosine (CdA) in the treatment of acute myeloid leukaemia (AML) and gemcitabine to treat solid tumours. In this study, expression of dCK mRNA was measured by a competitive template reverse transcriptase polymerase chain reaction (CT RT-PCR) in seven cell lines of different histological origin, 16 childhood and adult AML samples, 10 human liver samples and 11 human liver metastases of colorectal cancer origin. The enzyme activity and protein expression levels of dCK in the cell lines were closely related to the mRNA expression levels ($r=0.75$, $P=0.026$ and $r=0.86$, $P=0.007$). In AML samples, dCK mRNA expression ranged from 1.16 to 35.25 ($\times 10^{-3}$) dCK/beta-actin. In the cell line panel, the range was 2.97-56.9 ($\times 10^{-3}$) dCK/beta-actin of dCK mRNA expression. The enzyme activity in liver metastases was correlated to dCK mRNA expression ($r=0.497$, $P=0.05$). In the liver samples, these were not correlated. dCK mRNA expression showed only a 36-fold range in liver while a 150-fold range was observed in the liver metastases. In addition, dCK activity and mean mRNA levels were 2.5-fold higher in the metastases than in the liver samples. Since dCK is associated with the sensitivity to deoxynucleoside analogues and because of the good correlation between the different dCK measurements in malignant cells and tumours, the CT-RT PCR assay will be useful in the selection of patients that can be treated with deoxycytidine analogues.

PMID: 12628850 [PubMed - indexed for MEDLINE]

Galanin in pituitary adenomas.

Grenback E, Bjellerup P, Wallerman E, Lundblad L, Anggard A, Ericson K, Aman K, Landry M, Schmidt WE, Holdfelt T, Hulting AL.

Department of Molecular Medicine, Endocrine and Diabetes Unit, Karolinska Hospital, S-17176 Stockholm, Sweden. Eva.Grenback@ks.se

Tumor galanin content was measured in extracts from human pituitary adenomas using a specific RIA method for monitoring human galanin. Twenty-two out of twenty-four tumors contained galanin with notably high levels in corticotroph adenomas, varying levels in clinically inactive tumors, and low levels in GH secreting adenomas. Tumor galanin and ACTH contents were closely correlated in all tumors. In four young patients with microadenomas and highly active Mb Cushing tumor galanin was inversely related to tumor volume. The molecular form of tumor galanin, studied with reverse-phase HPLC, was homogeneous with the majority of tumor galanin coeluting with standard human galanin. In the tumors analysed with in situ hybridization there was a good correlation between galanin peptide levels and galanin mRNA expression. In some tumors galanin mRNA and POMC levels coexisted, in others they were essentially in different cell populations. Levels of plasma galanin-LI were not related to tumor galanin concentration, and galanin levels were in the same range in sinus petrosus close to the pituitary venous drainage as in peripheral blood. Corticotrophin releasing hormone injections in two patients caused ACTH, but no detectable galanin release into sinus petrosus. Our results demonstrate that corticotroph, but not GH adenomas, express high levels of galanin, in addition to ACTH, and that in some tumors both polypeptides are synthesised in the same cell population. However, galanin levels in plasma were not influenced by the tumor galanin content.

PMID: 14700749 [PubMed - indexed for MEDLINE]

Full text article at
www.bloodjournal.org

BCL2 protein expression parallels its mRNA level in normal and malignant B cells.

Shen Y, Iqbal J, Huang JZ, Zhou G, Chan WC.

Department of Pathology and Microbiology, University of Nebraska Medical Center, Omaha, USA.

The regulation of B-cell lymphoma 2 (BCL2) protein expression in germinal center (GC) B cells has been controversial. Previous reports have indicated posttranscriptional regulation plays a dominant role. However, a number of recent studies contradicted these reports. Using real-time polymerase chain reaction (PCR) and Standardized Reverse Transcriptase-PCR (StaRT-PCR), we measured the level of mRNA expression in GC, mantle zone (MNZ), and marginal zone (MGZ) cells from laser capture microdissection. Both quantitative RT-PCR measurements of microdissected GC cells from tonsils showed that GC cells had low expression of BCL2 transcripts commensurate with the low protein expression level. These results are in agreement with microarray studies on fluorescence-activated cell sorter (FACS)-sorted cells and microdissected GC cells. We also examined BCL2 mRNA and protein expression on a series of 30 cases of diffuse large B-cell lymphoma (DLBCL) and found, in general, a good correlation. The results suggested that BCL2 protein expression is regulated at the transcriptional level in normal B cells and in the neoplastic cells in most B-cell lymphoproliferative disorders.

PMID: 15242877 [PubMed - indexed for MEDLINE]

Full text article at
www.bloodjournal.org

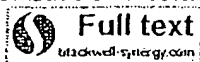
Cyclin D1-negative mantle cell lymphoma: a clinicopathologic study based on gene expression profiling.

Fu K, Weisenburger DD, Greiner TC, Dave S, Wright G, Rosenwald A, Chiorazzi M, Iqbal J, Gesk S, Siebert R, De Jong D, Jaffe ES, Wilson WH, Delabie J, Ott G, Dave BJ, Sanger WG, Smith LM, Rimsza L, Braziel RM, Muller-Hermelink HK, Campo E, Gascoyne RD, Staudt LM, Chan WC; Lymphoma/Leukemia Molecular Profiling Project.

Department of Pathology and Microbiology, University of Nebraska Medical Center, 983135 Nebraska Medical Center, Omaha, NE 68198-3135, USA. kfu@unmc.edu

Cyclin D1 overexpression is believed to be essential in the pathogenesis of mantle cell lymphoma (MCL). Hence, the existence of cyclin D1-negative MCL has been controversial and difficult to substantiate. Our previous gene expression profiling study identified several cases that lacked cyclin D1 expression, but had a gene expression signature typical of MCL. Herein, we report the clinical, pathologic, and genetic features of 6 cases of cyclin D1-negative MCL. All 6 cases exhibited the characteristic morphologic features and the unique gene expression signature of MCL but lacked the t(11;14)(q13; q32) by fluorescence in situ hybridization (FISH) analysis. The tumor cells also failed to express cyclin D1 protein, but instead expressed either cyclin D2 (2 cases) or cyclin D3 (4 cases). There was good correlation between cyclin D protein expression and the corresponding mRNA expression levels by gene expression analysis. Using interphase FISH, we did not detect chromosomal translocations or amplifications involving CCND2 and CCND3 loci in these cases. Patients with cyclin D1-negative MCL were similar clinically to those with cyclin D1-positive MCL. In conclusion, cases of cyclin D1-negative MCL do exist and are part of the spectrum of MCL. Up-regulation of cyclin D2 or D3 may substitute for cyclin D1 in the pathogenesis of MCL.

PMID: 16123218 [PubMed - indexed for MEDLINE]



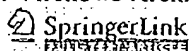
Neurokinin 1 receptor and relative abundance of the short and long isoforms in the human brain.

Caberlotto L, Hurd YL, Murdock P, Wahlin JP, Melotto S, Corsi M, Carletti R.

Department of Biology, Psychiatry CEDD, GlaxoSmithKline Medicine Research Centre, Verona, Italy. Laura.L.Caberlotto@gsk.com

Substance P exerts its various biochemical effects mainly via interactions through neurokinin-1 receptors (NK1). Recently, the NK1 receptor has attracted considerable interest for its possible role in a variety of psychiatric disorders including depression and anxiety. However, little is known regarding the anatomical distribution of NK1 in the human central nervous system (CNS). Riboprobe in situ hybridization, quantitative PCR and in vitro autoradiography were performed. Highest NK1 mRNA levels were localized in the locus coeruleus and ventral striatum, while moderate hybridization signals were observed in the cerebral cortex (most abundant in the visual cortex), hippocampus and different amygdaloid nuclei. Very low levels of the NK1 mRNA were detected in the cerebellum and thalamus. In view of the existence of a long and short isoform of the NK1 receptor, it was of interest to assess whether there was a differential distribution of the two splice variants in the human CNS and peripheral tissues. A quantitative TaqMan PCR analysis showed that the long NK1 isoform was the most prevalent throughout the human brain, while in peripheral tissues the truncated form was the most represented. ³H-Substance P autoradiography revealed a good correlation between receptor binding sites and NK1 mRNA expression throughout the brain, with the highest levels of binding in the locus coeruleus. These results provide the anatomical evidence that the NK1 receptors have a strong association with neuronal systems relevant to mood regulation and stress in the human brain, but do not suggest a region-specific role of the two isoforms in the CNS.

PMID: 12752772 [PubMed - indexed for MEDLINE]



Human chorionic gonadotrophin beta expression in malignant Barrett's oesophagus.

Couvelard A, Paraf F, Vidaud D, Dubois S, Vidaud M, Flejou JE, Degott C.

Service d'Anatomie Pathologique, Hopital Beaujon, 92118 Clichy cedex, France.
anne.couvelard@bjn.ap-hop-paris.fr

BACKGROUND: Human chorionic gonadotrophin beta (hCGbeta) is expressed in several non-trophoblastic tumours, and this is usually associated with aggressive behaviour. Little is known about hCGbeta expression in Barrett's adenocarcinoma. **MATERIALS AND METHODS:** We determined the hCGbeta profile in a large series of surgically resected Barrett's adenocarcinoma (a) at mRNA level using real-time quantitative reverse-transcription polymerase chain reaction analysis and (b) at protein level using immunohistochemistry with a polyclonal antibody and with a monoclonal antibody specific for free hCGbeta. We then sought links between the hCGbeta protein expression pattern and clinical and pathological parameters, including patient outcome as well as vascular endothelial growth factor (VEGF) expression. **RESULTS:** hCGbeta protein expression was observed in 43 of 76 (57%) Barrett's adenocarcinomas. We showed a strong correlation between hCGbeta protein abundance and CGB mRNA level. We observed a statistical link between hCGbeta protein expression and infiltrative tumour type ($P=0.023$), perineural neoplastic invasion ($P=0.007$) and VEGF protein expression ($P=0.016$). hCGbeta expression tended to be associated with a poor outcome (16% versus 36% survival 8 years after resection). **CONCLUSION:** Expression of hCGbeta correlates with specific infiltrative characteristics and is associated with higher VEGF expression. Both molecules may play a co-ordinated role in the development of Barrett's adenocarcinomas.

PMID: 15309632 [PubMed - indexed for MEDLINE]

Assessment of proliferative activity in colorectal carcinomas by quantitative reverse transcriptase-polymerase chain reaction (RT-PCR).

Duchrow M, Hasemeyer S, Broll R, Bruch HP, Windhovel U.

Surgical Research Laboratory, Surgical Clinic, Medical University of Lubeck, Ratzeburger Allee 160, D-23538 Lubeck, Germany.

The monoclonal antibody Ki-67 and the isospecific monoclonal antibody MIB-1 are routinely used in oncology to assess the proliferation index of tumor cells. A more objective and sensitive method is the determination of the of Ki-67 protein-specific mRNA by quantitative reverse transcriptase-polymerase chain reaction (RT-PCR). In 25 resected colorectal adenocarcinomas of different stages and grades we determined between 0.2 and 4.4 amol (10(-18) mol) Ki-67 protein-specific mRNA per microgram total RNA (median = 0.88 amol). The corresponding Ki-67 indices (expressing the percentage of Ki-67/MIB-1 positive tumor cells) ranged from 41 to 81% (median = 61%). We found a good correlation between Ki-67 index and mRNA expression ($r = 0.75$), a significant correlation between both data and tumor stage (primary tumor, regional nodes, metastasis [pTNM] staging classification) ($p < 0.001$), but not between both data and tumor grade. Both Ki-67 indices ($p = 0.05$) and mRNA levels ($p = 0.014$) correlated significantly to the patients' survival. These results demonstrate that the Ki-67-protein-specific quantitative RT-PCR is a useful method for the characterization of tumor cell proliferation.

PMID: 11486701 [PubMed - indexed for MEDLINE]

Comment in:

- [Equine Vet J. 2002 Jul;34\(4\):326-7.](#)

Molecular characterisation of carbohydrate digestion and absorption in equine small intestine.

Dyer J, Fernandez-Castano Merediz E, Salmon KS, Proudman CJ, Edwards GB, Shirazi-Beechey SP.

Department of Veterinary Preclinical Sciences, University of Liverpool, UK.

Dietary carbohydrates, when digested and absorbed in the small intestine of the horse, provide a substantial fraction of metabolisable energy. However, if levels in diets exceed the capacity of the equine small intestine to digest and absorb them, they reach the hindgut, cause alterations in microbial populations and the metabolite products and predispose the horse to gastrointestinal diseases. We set out to determine, at the molecular level, the mechanisms, properties and the site of expression of carbohydrate digestive and absorptive functions of the equine small intestinal brush-border membrane. We have demonstrated that the disaccharidases sucrase, lactase and maltase are expressed diversely along the length of the intestine and D-glucose is transported across the equine intestinal brush-border membrane by a high affinity, low capacity, Na⁺/glucose cotransporter type 1 isoform (SGLT1). The highest rate of transport is in duodenum > jejunum > ileum. We have cloned and sequenced the cDNA encoding equine SGLT1 and alignment with SGLT1 of other species indicates 85-89% homology at the nucleotide and 84-87% identity at the amino acid levels. We have shown that there is a good correlation between levels of functional SGLT1 protein and SGLT1 mRNA abundance along the length of the small intestine. This indicates that the major site of glucose absorption in horses maintained on conventional grass-based diets is in the proximal intestine, and the expression of equine intestinal SGLT1 along the proximal to distal axis of the intestine is regulated at the level of mRNA abundance. The data presented in this paper are the first to provide information on the capacity of the equine intestine to digest and absorb soluble carbohydrates and has implications for a better feed management, pharmaceutical intervention and for dietary supplementation in horses following intestinal resection.

PMID: 12117106 [PubMed - indexed for MEDLINE]

Comment in:

- [Blood. 2003 Aug 15;102\(4\):1550-1.](#)

FREE full text article at:
www.bloodjournal.org

Transcript profiling of human platelets using microarray and serial analysis of gene expression.

Gnatenko DV, Dunn JJ, McCorkle SR, Weissmann D, Perrotta PL, Bahou WF.

Department of Medicine, Program in Genetics, State University of New York, Stony Brook 11794-8151, USA.

Human platelets are anucleate blood cells that retain cytoplasmic mRNA and maintain functionally intact protein translational capabilities. We have adapted complementary techniques of microarray and serial analysis of gene expression (SAGE) for genetic profiling of highly purified human blood platelets. Microarray analysis using the Affymetrix HG-U95Av2 approximately 12 600-probe set maximally identified the expression of 2147 (range, 13%-17%) platelet-expressed transcripts, with approximately 22% collectively involved in metabolism and receptor/signaling, and an overrepresentation of genes with unassigned function (32%). In contrast, a modified SAGE protocol using the Type IIS restriction enzyme MmeI (generating 21-base pair [bp] or 22-bp tags) demonstrated that 89% of tags represented mitochondrial (mt) transcripts (enriched in 16S and 12S ribosomal RNAs), presumably related to persistent mt-transcription in the absence of nuclear-derived transcripts. The frequency of non-mt SAGE tags paralleled average difference values (relative expression) for the most "abundant" transcripts as determined by microarray analysis, establishing the concordance of both techniques for platelet profiling. Quantitative reverse transcription-polymerase chain reaction (PCR) confirmed the highest frequency of mt-derived transcripts, along with the mRNAs for neurogranin (NGN, a protein kinase C substrate) and the complement lysis inhibitor clusterin among the top 5 most abundant transcripts. For confirmatory characterization, immunoblots and flow cytometric analyses were performed, establishing abundant cell-surface expression of clusterin and intracellular expression of NGN. These observations demonstrate a strong correlation between high transcript abundance and protein expression, and they establish the validity of transcript analysis as a tool for identifying novel platelet proteins that may regulate normal and pathologic platelet (and/or megakaryocyte) functions.

PMID: 12433680 [PubMed - indexed for MEDLINE]

Transcript profiling of human platelets using microarray and serial analysis of gene expression

Dmitri V. Gnatenko, John J. Dunn, Sean R. McCorkle, David Weissmann, Peter L. Perrotta, and Wadie F. Bahou

Human platelets are anucleate blood cells that retain cytoplasmic mRNA and maintain functionally intact protein translational capabilities. We have adapted complementary techniques of microarray and serial analysis of gene expression (SAGE) for genetic profiling of highly purified human blood platelets. Microarray analysis using the Affymetrix HG-U95Av2 approximately 12 600-probe set maximally identified the expression of 2147 (range, 13%-17%) platelet-expressed transcripts, with approximately 22% collectively involved in metabolism and receptor/signaling, and an overrepresentation of genes with unassigned function (32%). In contrast, a modified SAGE protocol using the Type IIS restriction enzyme

MmeI (generating 21-base pair [bp] or 22-bp tags) demonstrated that 89% of tags represented mitochondrial (mt) transcripts (enriched in 16S and 12S ribosomal RNAs), presumably related to persistent mt-transcription in the absence of nuclear-derived transcripts. The frequency of non-mt SAGE tags paralleled average difference values (relative expression) for the most "abundant" transcripts as determined by microarray analysis, establishing the concordance of both techniques for platelet profiling. Quantitative reverse transcription-polymerase chain reaction (PCR) confirmed the highest frequency of mt-derived transcripts, along with the mRNAs for neurogranin (NGN, a protein kinase C substrate) and

the complement lysis inhibitor clusterin among the top 5 most abundant transcripts. For confirmatory characterization, immunoblots and flow cytometric analyses were performed, establishing abundant cell-surface expression of clusterin and intracellular expression of NGN. These observations demonstrate a strong correlation between high transcript abundance and protein expression, and they establish the validity of transcript analysis as a tool for identifying novel platelet proteins that may regulate normal and pathologic platelet (and/or megakaryocyte) functions. (Blood. 2003;101:2285-2293)

© 2003 by The American Society of Hematology

Introduction

Human blood platelets play critical roles in normal hemostatic processes and pathologic conditions such as thrombosis, vascular remodeling, inflammation, and wound repair. Generated as cytoplasmic buds from precursor bone marrow megakaryocytes, platelets are anucleate and lack nuclear DNA, although they retain megakaryocyte-derived mRNAs.^{1,2} Platelets contain rough endoplasmic reticulum and polyribosomes, and they retain the ability for protein biosynthesis from cytoplasmic mRNA.³ Quiescent platelets generally display minimal translational activity, although newly formed platelets such as those found in patients with immune thrombocytopenic purpura (ITP) synthesize various α -granule and membrane glycoproteins (GPs), including GPIb and GPIIb/IIIa ($\alpha_{IIb}\beta_3$). Furthermore, stimulation of quiescent platelets by agonists such as α -thrombin increases protein synthesis of various platelet proteins, including Bcl-3.⁴ Like nucleated cells, the rapid translation of preexisting mRNAs may be regulated by integrin ligation to extracellular matrices.⁵ In the case of platelets, the primary integrin involved in this process appears to be $\alpha_{IIb}\beta_3$ with cooperative signals mediated by the collagen receptor $\alpha_2\beta_1$.^{6,7}

Integrin-mediated platelet protein synthesis appears to be regulated at the level of translation initiation involving the eukaryotic initiation factor 4E (eIF4E). Instead of directly influencing eIF4E activity via posttranslational modifications (ie, phosphorylation), platelet eIF4E activity best correlates with its spatial redistribution to the mRNA-enriched cytoskeleton.⁸ Furthermore, because protein translation is partially inhibited by the immunosuppressant rapamycin, it suggests that adhesion- and/or aggregation-induced outside-in-signaling function to regulate protein synthesis through the mTOR (mammalian target of rapamycin) pathway.^{6,8,9}

Despite the biologic importance of platelets and their intact protein synthetic capabilities, remarkably little is known about platelet mRNAs. Younger platelets contain larger amounts of mRNA with a greater capacity for protein synthesis, as determined by using fluorescent nucleic acid dyes such as thiazole orange.¹⁰ This assay has been used as a quantitative determinant of younger or "reticulated" platelets (RPs). Indeed increased reticulated platelets are typically found in patients with conditions associated with rapid platelet turnover such as ITP; typically RP percentages in

From the Department of Medicine, Department of Pathology, and Program in Genetics, State University of New York, Stony Brook; Biology Department, Brookhaven National Laboratory, Upton, NY; and Department of Pathology, Robert Wood Johnson Medical Center, New Brunswick, NJ.

Submitted September 16, 2002; accepted November 3, 2002. Prepublished online as Blood First Edition Paper, November 14, 2002; DOI 10.1182/blood-2002-09-2797.

Supported by grants HL49141 and HL53665, by a Veteran's Administration REAP award (W.F.B.), and by National Institutes of Health Center grant MO1 10710-5 to the University Hospital General Clinical Research Center. W.B. is an Established Investigator of the American Heart Association. Studies at

Brookhaven National Laboratory were supported by a Laboratory Directed Research and Development award (J.J.D.) and by the Offices of Biological and Environmental Research, and of Basic Energy Sciences (Division of Energy Biosciences) of the US Department of Energy.

Reprints: Wadie F. Bahou, Division of Hematology, HSCT-15-040, State University of New York at Stony Brook, Stony Brook, NY 11794-8151; e-mail: wbahou@notes.cc.sunysb.edu.

The publication costs of this article were delayed in part by page charge payment. Therefore, and solely to indicate this fact, this article is hereby marked "advertisement" in accordance with 18 U.S.C. section 1734.

© 2003 by The American Society of Hematology

such patients approach 10% to 20% of all platelets, considerably higher than in healthy control subjects.¹¹ Interestingly, high RPs have been associated with enhanced thrombotic risk when identified in patients with thrombocytosis,¹⁰ suggesting that quantitatively increased mRNA levels may be associated with the prothrombotic phenotype. Whether this is related to globally altered gene expression profiles or to select changes more evident during situations of rapid platelet turnover remains unknown. Certainly, technical limitations of this assay limit its utility in defining prothrombotic genotypes,¹⁰⁻¹² and it cannot identify differentially expressed genes that may be causally implicated in disordered platelet phenotypes.

Toward the goal of defining the molecular anatomy of the platelet genome, we have adapted complementary techniques of microarray and serial analysis of gene expression (SAGE) for genetic profiling of highly purified human blood platelets. Microarray technology represents a "closed" profiling strategy limited by the target genes imprinted onto gene chips. In contrast, SAGE is an "open" architectural system that can be used to identify novel genes and to quantify differentially expressed mRNAs.¹³⁻¹⁵ The sequence of each tag along with its positional location uniquely identifies the gene from which it is derived, and differentially expressed genes can be identified in a quantitative manner because the tag frequency reflects the mRNA level at the time of cellular harvest and analysis. By using both technologies, we have identified a number of previously uncharacterized genes that appear to be expressed in human platelets, while simultaneously establishing the dominant frequency of mitochondrial-expressed genomes comprising the platelet mRNA pool. These observations provide a panoramic overview of the platelet transcriptome, while additionally providing insights into the molecular pathways regulating platelet (and/or megakaryocyte) function in normal and pathologic conditions.

Materials and methods

Reagents and supplies

Thermus aquaticus (Taq) polymerase was purchased from (Roche, Indianapolis, IN). T4 DNA ligase was purchased from Invitrogen (Carlsbad, CA), and restriction enzymes were from New England Biolabs (Beverly, MA), except for *MmeI*, which was obtained from the Center for Technology Transfer (Gdansk, Poland). All oligonucleotides were synthesized on an Applied Biosystems (Foster City, CA) 3-channel synthesizer and are listed in Table 1. Monoclonal antibodies used for flow cytometric analysis included the FITC (fluorescein isothiocyanate)-conjugated anti-CD41 (α_{IIb}β₃) immunoglobulin G1 (IgG1; Immunotech, Miami, FL); phycoerythrin (PE)-conjugated anti-glycophorin (IgG2; Becton Dickinson Pharmingen, San Diego, CA); and peridinin chlorophyll protein (PERCP)-conjugated anti-CD45 (IgG1; Becton Dickinson Pharmingen).

Platelet isolation, purification, and immunodetection

All human subjects provided informed consent for an IRB (Institutional Review Board)-approved protocol completed in conjunction with the General Clinical Research Center at Stony Brook University Hospital. Peripheral blood (20 mL) from healthy volunteers drawn into 2 mL of 4% sodium citrate (0.4% vol/vol final concentration) was used to isolate erythrocytes by differential centrifugation (1500g) or to isolate pure leukocytes by density-gradient centrifugation as previously described.¹⁶ Platelets collected from healthy volunteers by apheresis were used within 24 hours of collection. After addition of 2 mM EDTA (ethylenediaminetetraacetic acid), apheresis-derived platelets from a single donor were centrifuged at 140g for 15 minutes at 25°C. To minimize leukocyte contamination, only the upper 9/10 of the platelet-rich plasma (PRP) was

used for gel filtration over a BioGel A50M column (1000 mL total volume) equilibrated with HBMT (HEPES-buffered modified Tyrodes buffer: 10 mM HEPES (*N*-2-hydroxyethylpiperazine-*N'*-2-ethanesulfonic acid) pH 7.4, 150 mM NaCl, 2.5 mM KCl, 0.3 mM NaH₂PO₄, 12 mM NaHCO₃, 0.2% bovine serum albumen [BSA], 0.1% glucose, 2 mM EDTA). Gel-filtered platelets (GFPs) were subsequently filtered through a 5-μm nonwetting nylon filament filter (BioDesign, Carmel, NY) at 25°C and harvested by centrifugation at 1500g for 10 minutes at 25°C. Platelets were gently and thoroughly resuspended in 10 mL HBMT buffer and incubated with 120 μL murine monoclonal anti-CD45 antibody conjugated to magnetic microbeads (Miltenyi Biotec, Bergisch Gladbach, Germany) on a rotating platform for 45 minutes at 25°C. Magnetic separation columns were used to capture CD45⁺ cells (leukocyte fraction) by positive selection (MACS II; Miltenyi Biotec). Purified platelets were concentrated by centrifugation at 1500g and immediately used for total RNA isolation.

The efficiency of platelet purification was documented at each step by flow cytometry.¹⁷ Briefly, aliquots containing 2 × 10⁶ platelets were incubated with saturating concentrations of FITC-conjugated anti-CD41, PE-conjugated anti-glycophorin, and PERCP-conjugated anti-CD45 for 15 minutes in the dark at 25°C, washed with phosphate-buffered saline (PBS), and fixed in PBS/1% formalin. Samples were analyzed using a FACScan (fluorescence-activated cell sorter scan) flow cytometer (Becton Dickinson) using CELLQuest software designed to quantify the number of CD45⁺ and glycophorin-positive events in the sample (expressed as the number of events per 100 000 CD41⁺ events). For some experiments, fixed platelets were permeabilized with 0.1% Triton-X/PBS for 30 minutes at 25°C prior to the addition of primary antibodies, all as previously described.¹⁷

Platelet protein detection was completed by sodium dodecyl sulfate (SDS)-polyacrylamide gel electrophoresis (PAGE) and immunoblot analysis as previously described, using the species-specific horseradish peroxidase-conjugated secondary antibody and enhanced chemiluminescence.¹⁸ Antibodies included the anticlustarin monoclonal antibody (Quidel, Santa Clara, CA; 1:1000 primary and 1:10 000 secondary) and the antineurogranin rabbit polyclonal antibody (Chemicon International, Temecula, CA; 1:1000 primary and 1:10 000 secondary).

Molecular analyses and microarray profiling

Purified, individual cell fractions were resuspended in 10 mL Trizol reagent (Invitrogen), transferred into diethylpyrocarbonate (DEPC)-treated Corex (Springfield, MA) tubes, and serially purified and precipitated by using isopropanol essentially as previously described.¹⁸ Total cellular RNA was harvested by centrifugation at 12 500g for 20 minutes at 4°C, washed 2 times with 75% ethanol (10 mL/tube), and resuspended in 100 μL DEPC-treated water. Platelet mRNA quantitation was performed by using fluorescence-based real-time PCR (polymerase chain reaction) technology (TaqMan Real-Time PCR; Applied Biosystems, Foster City, CA). Oligonucleotide primer pairs were generated by using Primer3 software (www.genome.wi.mit.edu), designed to generate approximately 200-base pair (bp) PCR products at the same annealing temperature, and are outlined in Table 1. Purified platelet mRNA (4 μg) was used for first-strand cDNA synthesis using oligo(dT) and SuperScript II reverse transcriptase (Invitrogen). For real-time reverse transcription (RT)-PCR analysis, the RT reaction was equally divided among primer pairs and used in a 40-cycle PCR reaction for each target gene by using the following cycle: 94°C for 30 seconds, 55°C for 30 seconds, 72°C for 1 minute, and 71°C for 10 seconds (40 cycles total). mRNA levels were quantified by monitoring real-time fluorometric intensity of SYBR green I. Relative mRNA abundance was determined from triplicate assays performed in parallel for each primer pair and was calculated by using the comparative threshold cycle number (ΔCt method) as previously described.¹⁸

Gene expression profiles were completed by using the approximately 12 600-probe set HG-U95Av2 gene chip (Affymetrix, Santa Clara, CA). Total cellular RNA (5 μg) was used for cDNA synthesis by using SuperScript Choice system (Life Technologies, Rockville, MD) and an oligo(dT) primer containing the T7 polymerase recognition sequence (Primer S1; Table 1), followed by cDNA purification using GFX spin columns. In vitro transcription was completed in the presence of biotinylated ribonucleotides by using a BioArray HighYield RNA Transcript

Table 1. Oligonucleotide primers

Primer	Gene and primer direction	Sequence (5' - 3')	Nucleotide Position
S1	Oligo (dT)	5'-Bn-GGCCAGTGAATTTGTAATACGACTCCTATAGGAGGCGG-(dT) ₂₄ -3'	—
Cassette A	SAGE	5'-TTTGGATTTCCTGGTCGAGTACAACCTAGGCTTAATCCGACATG-3' 3'-*CCTAAACGACCACTCATGTTGATCCGAAATAGGCTp-5'	—
Cassette B	SAGE	5'-pTTTCATGCGGAGACGTCCGCCACTAGTGTGCAACTGACTA*-3' 3'-NNAAGTACCGCTCTGCAGGCGGTGATCAGCGTTGACTGAT-5'	—
S2	SAGE	5'-Bn-GGATTTCCTGGTCGAGTACA-3'	—
S3	SAGE	5'-Bn-TAGTCAGGTGCGACACTAGTGGC-3'	—
GP4	Glycoprotein IIb [F]	5'-AGGGCTTTGAGAGACTCATCTGTA-3'	2094-2117
GP5	Glycoprotein IIb [R]	5'-ACAATCTTGCTGTTGGATTCTG-3'	2301-2279
GP6	Glycoprotein IIIa [F]	5'-TATAAAGAGGCCAGCTCTACCTTC-3'	2335-2358
GP7	Glycoprotein IIIa [R]	5'-CACTTCCACATATGACATCTCC-3'	2532-2509
PAR18	PAR1 [F]	5'-AATGTCAGTTCTGATATGGAACA-3'	2585-2608
PAR19	PAR1 [R]	5'-CCCAATGTTCAAACTCTTTAGC-3'	2776-2753
SR8	16S rRNA [F]	5'-TGCAAGGTAGCATATCACTTGT-3'	2586-2609
SR9	16S rRNA [R]	5'-GTTTAGGACCTGTGGTTGTTAG-3'	2785-2762
NADH10	NADH2 [F]	5'-CTAGCCCCCATCTCAAAATCATATAC-3'	4875-4898
NADH11	NADH2 [R]	5'-AATGGTTATGTTAGGTTGTACGG-3'	5075-5052
THYM12	Thymosin β4 [F]	5'-AAGACAGAGACGCAAGAGAAAAAT-3'	135-158
THYM13	Thymosin β4 [R]	5'-GCAGCAGCTCATTAAACTTGTAT-3'	336-313
CLUS14	Clusterin [F]	5'-CCAACAGAAATTCATACGAGAAGG-3'	1006-1028
CLUS15	Clusterin [R]	5'-CGTTATATTCTCGGTCAACCTCT-3'	1222-1199
NRG16	Neurogranin [F]	5'-GCCCTTTAGTTAGTTCTGCACTC-3'	1351-1374
NRG17	Neurogranin [R]	5'-TTTCTTTAAGTCAGTGTGCTTG-3'	1567-1544
TCR18	T-cell receptor β-chain [F]	5'-CCCAACTATGTTTGGTATCGT-3'	131-153
TCR19	T-cell receptor β-chain [R]	5'-CTAGCACTGCAGATGTAGAAGCT-3'	332-310
CD4520	CD45 [F]	5'-GCTCAGAATGGCAAGTA-3'	3771-3788
CD4521	CD45 [R]	5'-CACACCATACACATACA-3'	4280-4261

[F] indicates forward (sense) strand; [R], reverse (antisense) strand; Bn, biotin; p, a phosphorylated 5' end (cassettes A and B); underlining, *Mnl*I sites in cassettes A and B; arrows, corresponding sequence for S2 and S3 within cassettes A and B, respectively; bold, the *Mme*I site; and N, A, C, T, or G, nucleotide position based on the following accession numbers: glycoprotein IIb (J02764), glycoprotein IIIa (M35999), PAR1 (M62424), 16S rRNA and NADH2 (NC_001807), thymosin β4 (M17733), clusterin (M25915), neurogranin (X99076), TCR β-chain (AF043182), CD45 (Y00638).

*Indicates an amino-modified 3' end in both cassettes; —, not applicable.

Labeling Kit (Enzo Diagnostics, Farmingdale, NY), and, after metal-induced fragmentation, 15 μg biotinylated cRNA was hybridized to the HG-U95Av2 oligonucleotide probe array for 16 hours at 45°C. After washing, the cRNA was detected with streptavidin-phycoerythrin (Molecular Probes, Eugene, OR) and analysis was completed by using a Hewlett-Packard Gene Array Scanner (Affymetrix). The average difference value (AD) for each probe set was quantified using MAS 4.01 software (Affymetrix), calculated as an average of fluorescence differences for perfectly matched versus single-nucleotide mismatched 25-mer oligonucleotides (16 to 20 oligonucleotide pairs per probe set). The software is designed to exclude "positive calls" in the presence of high average differences with associated high mismatch intensities.

SAGE profiles

Platelet SAGE libraries were generated essentially as previously described,¹² modified as outlined in Figure 1 for the use of *Mme*I as the tagging enzyme.¹⁹ This type IIS restriction enzyme cleaves 20 of 18 bp past its nonpalindromic (TCCRAC) recognition sequence, thereby generating longer tags (21- or 22-mer) than those obtained using *Bsm*FI as the standard tagging enzyme (13-14 bp tags). These longer *Mme*I-generated tags potentially provide for more definitive "tag-to-gene" identification and are particularly useful in characterizing expression patterns in the absence of complete genomic sequence data (comprehensive methods detailed in Dunn et al¹⁹). Briefly, poly(A) mRNA was isolated from 10 μg total platelet RNA using the oligo(dT) S1 primer conjugated to magnetic beads (Dyna Beads, Lake Success, NY), followed by cDNA synthesis using SuperScript II reverse transcriptase (Invitrogen). The cDNA was then digested

with the restriction enzyme *Nla*III (anchoring enzyme), ligated to cassette A using T4 DNA ligase, and, after the beads were extensively washed, the cDNA was digested with *Mme*I to release the tags from the beads. After purification, tags were ligated to degenerate cassette B linkers (specifically

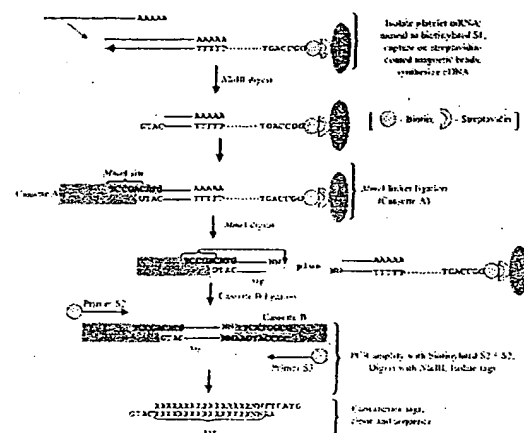


Figure 1. Schema outlining the modified SAGE protocol used in platelet analyses. The final tags are flanked by the *Nla*III (anchoring enzyme) CATG sequence, thereby providing tag-to-gene identification when exported to a relational database (refer to "Bioinformatic analyses" and Table 1 for details).

designed to anneal to the nonuniform *MmeI* overhangs), and PCR-amplified using biotinylated primers S2 and S3 for 30 cycles (95°C for 30 seconds; 58°C for 30 seconds; 72°C for 30 seconds) using Platinum Taq DNA polymerase (Gibco BRL). A fraction (20%) of the pooled PCR products were then subjected to one round of linear amplification using primer pair S2/S3, followed by a second round of 25 amplifications using primer S2 alone (95°C for 30 seconds, 58°C for 30 seconds, 72°C for 30 seconds). Primer S3 was subsequently added for one cycle (95°C for 2.5 minutes, 58°C for 30 seconds, 72°C for 5 minutes); the latter steps were collectively adapted to exclude heteroduplex formation.¹⁸ Unincorporated primers were removed by incubation with 200 U *Escherichia coli* exonuclease I for 60 minutes at 37°C. PCR products were then pooled and digested with *MolIII* to release tags, and biotinylated linker arms were cleared using streptavidin-coated immunoaffinity magnetic beads (DynaL Biotech). Tags were concatamerized using 5 U/μL T4 DNA ligase, and products more than 100 bp were isolated by size-fractionation in low-melting agarose gels. The DNA was purified by GFX spin columns, and the concatamers were cloned into the *SphI* site of pZero (Invitrogen). After transformation into *E. coli* TOP10 cells, recombinant clones were isolated and sequenced in 96-well microtiter plates using an ABI 377 sequencer and ABI Prism BigDye terminator chemistry (Perkin-Elmer Applied Biosystems, Branchburg, NJ).

Bioinformatic analyses

Functional grouping of genes determined to be present by Affymetrix MAS 4.01 software was performed using a dChip program linked to the National Center for Biotechnology LocusLink, which is an annotated reference database for genes and their postulated functions.²⁰ Of the approximately 12 600-probe sets represented on the Affymetrix HG-U95Av2 Gene chip, functional annotations exist for approximately 8100 with the remainder categorized as unknown. Microarray data were visualized and analyzed using BRB-ArrayTools software (Version 2.1), kindly developed and provided by Dr Richard Simon and Amy Peng (linus.nci.nih.gov/BRB-ArrayTools.html). A logarithmic (base 2) transformation was applied to the average difference values for individual data sets for determination of microarray concordancies. Discordancy was defined as a 2-log difference in the maximum log intensities between individual experiments.

SAGE tags were extracted by using in-house SAGE software uniquely modified to identify *MmeI* tags. The software ensures that only unambiguous 21- to 22-bp tag sequences are extracted for transcript profiling. Tags with ambiguities (Ns), lengths other than 21 or 22 bp, or with ambiguous orientations were extracted to separate files for manual editing or further examination. Finalized data were exported to a relational database for tag quantification and genetic identification.²⁰

Results

Platelet purification

To ensure that the RNA profiles accurately represented those of circulating blood platelets, a number of complementary methods were implemented to remove contaminating nucleated leukocytes. Purification methods incorporating gel filtration, a 5-μm leukocyte reduction filter, and magnetic CD45 immunodepletion allowed for the cumulative enrichment of highly purified platelets. The efficacy of this purification method was initially established by using peripheral blood platelet-rich plasma as the starting material. The final product contained no more than 3 to 5 leukocytes per 1×10^5 platelets as determined by parallel flow cytometric analysis, representing an approximate 450-fold reduction of nucleated leukocytes. These results correlated well with molecular evidence for leukocyte depletion as determined by RT-PCR using both CD45 and T-cell receptor β-chain (TCRβ) primers (see Figure 2). Because the total RNA yield from peripheral blood platelets was insufficient for microarray studies, we adapted the protocol to platelet apheresis donors with nearly identical final purity (Figure

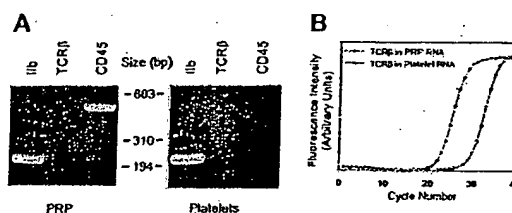


Figure 2. Determination of platelet purity. (A) Total cellular RNA (1.8 μg) from platelet-rich plasma (PRP) or purified platelets from a single apheresis donor were analyzed by RT-PCR (35 cycles) using oligonucleotide primers specific for glycoprotein IIb (GPIIb), T-cell receptor β-chain (TCRβ), or CD45; 10 μL of the 50 μL reactions were analyzed by ethidium-stained agarose gel electrophoresis. Minimal to no TCRβ gene product was visually evident only in PRP. Size markers corresponding to *HaeIII*-restricted ϕ X174 DNA are shown. (B) Real-time RT-PCR was completed by using 1.8 μg total RNA and TCRβ-specific oligonucleotide primers optimized for quantitative analysis by real-time PCR.¹⁸ On the basis of parallel determinations using RNA isolated from known amounts of purified leukocyte standards, the leukocyte-depletion protocol represents an approximate 2.5-log purification from the starting PRP. Results are representative of one complete set of experiments repeated on 2 separate occasions, and data points represent the mean from triplicate wells, with standard errors of the mean (SEM) less than 1% (not shown).

2). The platelet recovery was nearly 65% of the starting material, yielding approximately 2.3×10^{11} platelets from an initial apheresis pack containing approximately 3.6×10^{11} platelets. The bulk of the losses occurred during the initial centrifugation and filtration steps. The purification protocol was less effective at removing erythrocytes, although there were less than 50 glycoprotein-positive cells per 1×10^5 platelets after the final purification step. Nonetheless, these cells represent unlikely sources for contaminating cellular RNA (see "Cellular microarray analysis" below).

Cellular microarray analysis

The purified platelet RNA was sufficient for microarray studies and was used for cRNA generation and hybridization to the Affymetrix HG-U95Av2 GeneChip. The anatomic profile of platelet RNAs from 3 healthy male donors was determined by using Affymetrix software. Of the 12 599 probe sets imprinted onto the chip, a maximum of 2147 (17%) transcripts were computationally identified as "present" by the Affymetrix software, 152 (1.2%) were equivocal, and nearly 82% were absent. As a fraction of the total genes present on the chip, the percentage of platelet-expressed genes (15%-17%) was generally lower than that obtained from other human cell types in which 30% to 50% of genes are present as determined by Affymetrix software (J. Schwedes, personal communication, May 2002). The "limited number" of platelet-expressed transcripts presumably reflects the lack of ongoing gene transcription in the anucleate platelet. Because less than 1% of circulating red blood cells contain residual RNA, it is unlikely that any of these transcripts are erythrocyte derived, although this was formally addressed by isolating total cellular RNA from 20 mL of whole blood (corresponding to an ~3-log fold excess of erythrocytes than that identified in our final sample). The total cellular yield of RNA from this starting material was approximately 250 ng, suggesting that less than 1 ng erythrocyte-derived RNA was present in the purified platelet preparations. Despite this, however, both α- and β-globin transcripts—along with both the ferritin heavy and light chains—were identified as abundant transcripts (Table 2). Although the most parsimonious explanation would be residual contaminating reticulocytes, this is not supported by our erythrocyte contamination estimates, and their significance remains unresolved.

As a means of better dissecting the molecular anatomy of the platelet, expressed genes were grouped on the basis of assigned

Table 2. Top 50 human platelet-expressed genes

Accession no.	Gene symbol	AD values, range*	Gene transcript†	Leukocyte expression‡
M17733	TMSB4X	140 142-307 852	Thymosin β 4 mRNA, complete cds	+
X99076	NRGN	101 510-148 279	Neurogranin gene	+
M25079	HBB	40 839-229 556	β -globin mRNA, complete cds	+
M25915	CLU	84 720-140 246	Complement cytotoxicity inhibitor (clusterin) complete cds	-
J04755	FTHP1	82 980-148 621	Ferritin H processed pseudogene, complete cds	-
D78361	OAZ1	73 098-118 140	mRNA for ornithine decarboxylase antizyme	-
X04409	GNAS	77 761-94 781	mRNA for coupling protein G(s) α -subunit (alpha-S1)	-
M25897	PF4	62 811-126 908	Platelet factor 4 mRNA, complete cds	-
AB021288	B2M	61 689-108 921	β 2-microglobulin	+
X00351	ACTB	25 143-73 775	mRNA for β -actin	-
D21261	TAGLN2	76 687-101 931	mRNA for KIAA0120 gene	+
AL031670	FTLL1	69 865-99 966	Ferritin, light polypeptide 1	+
U59632	GPIIB	41 404-110 328	Platelet glycoprotein IIb chain mRNA	-
M21121	CCL5	47 308-106 399	T-cell-specific protein (RANTES) mRNA, complete cds	-
X13710	GPX1	41 318-96 878	Unspliced mRNA for glutathione peroxidase	-
J00153	HBA1	21 326-144 201	Alpha globin gene cluster on chromosome 16	+
M22919	MYL6	46 337-106 833	Nonmuscle/smooth muscle alkali myosin light chain gene	+
L20941	FTH1	52 787-74 763	Ferritin heavy chain mRNA, complete cds	-
J03040	SPARC	51 156-74 261	SPARC/osteonectin mRNA, complete cds	-
X56009	GNAS	45 543-72 096	GSA mRNA for α subunit of GsGTP binding protein	-
X58536	HLA	31 183-82 613	mRNA for major HLA class I locus C heavy chain	+
M54995	PPBP	46 571-67 169	Connective tissue activation peptide III mRNA	-
U34995	GAPD	35 095-70 250	Normal keratinocyte subtraction library mRNA, clone H22a	+
L40399	MLM3	32 107-73 364	Clone zap112 (mult. protein homolog 3) mRNA	-
X77548	NCOA4	31 452-61 036	cDNA for RFG (RET proto-oncogene RET/PTC3)	-
U90551	H2AFL	35 086-51 892	Histone 2A-like protein (H2AFL) mRNA	-
M11353	H3F3A	31 614-55 813	H3.3 histone class C mRNA	-
Z12962	RPL41	36 003-54 853	mRNA for homologue to yeast ribosomal protein L41	+
X06956	TUBA1	20 988-61 798	HALPHA 44 gene for α -tubulin	-
AB028950	TLN1	24 571-58 611	mRNA for KIAA 1027 protein	-
Y12711	PGRMC1	33 680-43 174	mRNA for putative progesterone binding protein	-
M16279	MIC2	30 894-48 166	Integrated membrane protein (MIC2) mRNA	-
D78577	YWHAH	24 785-50 437	Brain 14-3-3 protein β -chain	-
AF070585	TOP3B	20 027-67 945	Clone 24675, unknown cDNA	-
AA524802	Unknown	23 846-39 481	CDNA, IMAGE clone 954213	-
AB009010	UBC	28 745-38 389	mRNA for polyubiquitin Ubc	+
X57985	H2AFO	21 678-52 108	Genes for histones H2B.1 and H2A	-
X54304	MLCB	25 733-34 109	mRNA for myosin regulatory light chain	-
M14539	F13A1	23 691-48 474	Factor XIII subunit α -polypeptide mRNA, 3' end	-
A1540958	Unknown	24 872-41 118	cDNA, PEC 1.2_15_HOI.1 5' end/clone	-
AL050396	FLNA	13 634-55 235	cDNA DKFZp 586K1720	-
X56841	HLA-E	12 890-49 327	Nonclassical MHC class I antigen gene	-
M26252	PKM2	15 450-47 786	TCB (cytosolic thyroid hormone-binding protein)	-
M14630	PTMA	19 314-45 088	Prothymosin alpha mRNA	-
AF045229	RGS10	19 156-34 243	Regulator of G protein signaling 10 mRNA	-
AA477898	Unknown	16 863-44 756	cDNA, Z834108.1 5' end	-
X95404	FLI1	15 216-37 456	mRNA for nonmuscle type cofilin	-
M34480	ITGA2B	8 627-45 495	Platelet glycoprotein IIb (GPIIb) mRNA	-
Z83738	H2BFE	18 001-31 306	H1H2B/e gene	-
L19779	H2AFO	17 319-38 951	Histone H2A.2 mRNA, complete cds	-

*Gene expression quantifications were calculated as the average difference (AD) value (matched versus mismatched oligonucleotides) for each probe set using Affymetrix GeneChip software, version 4.01. The range of values from 3 distinct platelet microarrays is shown; the normalization value for all microarray analyses was 250.

†Transcripts are rank-ordered (highest to lowest) using BRB-ArrayTools software by log-intensities of AD values obtained from 3 different healthy donors; 33 of the top 40 transcripts were listed among the top 50 in all 3 microarray sets.

‡Leukocyte expression was determined by microarray analysis using purified peripheral blood leukocytes, followed by construction of rank-intensity plots for comparison to platelet top 50 transcripts. †† Top leukocyte-derived transcripts identified within the ranked top 50 platelet transcripts are depicted by a (+) present, or (-) absent. cds indicates coding sequence.

gene annotations, and this analysis was used to provide a panoramic definition of the platelet transcriptome. Of the genes that could be cataloged within assigned "clusters," those involved in metabolism (11%) and receptor/signaling (11%) represented the largest groups. Also evident in these analyses is the relatively large percentage of genes involved in functions unrelated to these key groups (ie, miscellaneous, 25%), and the overrepresentation of genes with unknown function (32%) as annotated by Affymetrix

and RefSeq databases.²¹ These results identify a vast array (nearly one half) of platelet genes (and gene products) that presumably have important, but poorly characterized functions, in platelet and/or megakaryocyte biology.

Although microarray analysis is not truly quantitative, rank-ordering using the mean log-intensities from 3 independent microarray analyses allowed for the categorization of the top platelet transcripts (Table 2). Computational analyses demonstrated that

only 10 of the top 100 genes were discordant among the 3 platelet microarrays, although 71 of 100 genes were discordant between platelet and leukocyte arrays. An inventory of the top 50 platelet genes is listed in Table 2, which also delineates those found to be highly expressed in peripheral blood leukocytes by parallel microarray experiments with this purified cellular fraction (data not shown). Further analysis of these cell subsets demonstrated that approximately 25% ($n = 547$) of the total platelet transcripts were platelet restricted. Furthermore, only 10 of the 50 most highly expressed genes were found to overlap, confirming the distinct cellular profiles of each transcriptome. Of the 12 overlap genes, 3 corresponded to globin or ferritin chains (again suggesting the presence of contaminating reticulocytes in both purified fractions), and another 4 were involved in actin cytoskeletal reorganization and human leukocyte antigen (HLA) expression, gene products that regulate critical functions in both cell types. Given the importance of cytoskeletal reorganization in downstream platelet activation events, it is not unexpected that components of the actin machinery system would demonstrate prominent transcript expression. Previous estimates suggest that 20% to 30% of the total platelet proteome is comprised of actin with other components such as actin-binding protein, myosin, and talin accounting for an additional 2% to 5% of the total protein.^{1,22} The mRNAs encoding the actin-related machinery are overrepresented in our microarray analysis, with 8 such transcripts found among the 50 highest platelet-expressed genes. Interestingly thymosin β 4 demonstrated the highest expression pattern. In unstimulated platelets, 30% to 40% of actin is polymerized as F-actin,²² whereas the balance of actin monomers (G-actin) are polymerization inhibited by sequestering proteins such as profilin (100 μ M) and thymosin β 4 (600 μ M).²³ The high thymosin β 4 transcript expression not only correlates with its known abundance in platelets but also supports the importance of actin inhibitory proteins in maintaining the nonstimulated state of circulating platelets.

Platelet SAGE analyses

Although these initial studies identified the distribution and relative expression patterns of the genes within the Affymetrix data set, they do not allow for analyses of genes that are unrepresented by these oligonucleotide chips. Unlike closed microarray profiling strategies, SAGE is an open architectural system that is ideally suited for novel gene and pathway identification. Accordingly, the platelet RNA used for microarray studies was used for platelet SAGE. A total of 2033 tags were initially cataloged, of which 1800 (89%) corresponded to mitochondrial-derived genes. These results were quite different from those obtained by microarray analyses, but the discrepancy can be resolved by the nonrepresentation of the mitochondrial genome on the gene chip. The mitochondrial genome is a compact approximately 16.6-kilobase (kb) sequence encoding 13 genes and 2 ribosomal subunits.²⁴ Primary mitochondrial transcripts are polycistronic and typically contain premature termination or unpredictable splice sites, resulting in multiple polyadenylated transcripts from individual genes.^{24,25} Indeed, the overall distribution of platelet-derived mitochondrial SAGE tags is quite similar to that found in muscle.²⁵ All 13 genes containing *Nla*III sites were detected, whereas neither of the non-*Nla*III-containing genes were identified (nicotinamide adenine dinucleotide [NADH] dehydrogenase subunit 4L and adenosine triphosphatase [ATPase] 8). Most of the tags were from the 16S and 12S ribosomal RNAs—which collectively accounted for 68% of the total mitochondrial tags—with the fewest tags represented by NADH dehydrogenase subunits 3, 5, 6, and cytochrome c oxidase 1

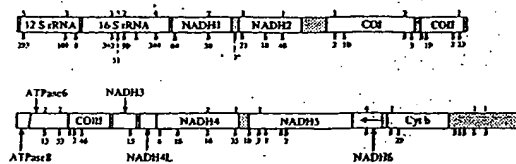


Figure 3. Schema of the mitochondrial genome with SAGE tag distributions (only tags with identical matches are displayed). The abundance of the SAGE tags ($n = 1800$) at individual *Nla*III sites (arrows) within the mitochondrial heavy strand is shown on the bottom, whereas those tags corresponding to the mitochondrial light strand are delineated above the arrows (the presence of an unaccompanied arrow implies no SAGE tags at that *Nla*III site). The gene products of mt-DNA (RefSeq accession no. NC_001807) are delineated by the open rectangles, whereas stippled boxes represent tRNA genes and control regions (the single tag represented by the [•] refers to mitochondrial transfer RNA-serine). Note that NADH6 is encoded by the light strand and that there are no *Nla*III sites within the ATPase8 gene segment. COI, cytochrome c oxidase subunit; Cyt b, cytochrome b.

(Figure 3). The NADH dehydrogenase subunit 6 RNA is the only mRNA encoded by the light (L) strand of mitochondrial DNA and was the least abundantly detected transcript.

The unusually high preponderance of mitochondrial-derived genes is not inconsistent with the known enrichment of these genomes in human platelets,^{1,24} and presumably reflects persistent transcription from the mitochondrial (mt) genome in the absence of nuclear-derived transcripts. This overrepresentation of mtDNA in platelets is considerably greater than that of its closest cell type (skeletal muscle), in which mt genomes represent approximately 20% to 25% of all SAGE tags.²⁵ Interestingly, the energy metabolism of platelets is not dissimilar from that of skeletal muscle, both cell types actively using glycolysis and large amounts of glycogen for ATP generation.²⁶ Like muscle, platelets are metabolically adapted to rapidly expend large amounts of energy required for aggregation, granule release, and clot retraction. Similar to the situation in all eukaryotic cells, platelet mitochondria represent the primary source of ATP, which is generated from oxidative phosphorylation reactions occurring within these organelles. Mitochondria are also responsible for most of the toxic reactive oxygen species generated as by-products of oxidative phosphorylation and are central regulators of the apoptotic process in other cellular types. The mtDNA encodes polypeptides found within 4 of the 5 multifunctional complexes that regulate oxidative phosphorylation within the platelet mitochondria.²⁷ Whether the continued generation of these polypeptides has a role in platelet energy metabolism and/or the apoptotic mechanisms regulating platelet survival remains speculative, although not inconsistent with our observations.

Comparative analysis of SAGE and microarray transcript abundance

Complete SAGE libraries require the sequencing of up to 30 000 tags for an exhaustive cataloging of individual mRNAs, especially those with limited copy numbers.^{13,28} Given the preponderance of mt-derived transcripts, comparable sampling would have required sequence analysis of nearly 300 000 SAGE tags, an inordinate number for comprehensive analysis of the platelet transcriptome. For platelets, alternative methodologies incorporating subtractive SAGE will be required for more comprehensive transcript profiling.²⁹ Our initial sampling of nonmitochondrial genes remains informative, however, and entirely consistent with the results of platelet microarray studies. As shown in Table 3, SAGE tags for the genes encoding thymosin β 4, β 2-microglobulin, neurogranin, and the platelet glycoprotein Ib polypeptide were among the most frequently identified platelet genes, similar to the rank-ordered results determined by microarray analysis. To formally confirm the

Table 3. SAGE-identified nonmitochondrial tags

Frequency	CATG + SAGE tags*	Accession no.†	Gene	Microarray‡
26	GTTGTGGTTAATCTGGT	NM_004048.1	β 2-microglobulin (B2M), mRNA	PPP
21	TTGGTGAAGGAAGAGT	NM_021109.1	Thymosin β 4; X chromosome (TMSB4X), mRNA	P
8	AGCTCCGCAGCCAGGTC	NM_002620.1	Platelet factor 4 variant 1 (PF4V1), mRNA	P
8	AGCTCCGCAGCCGGGTT	NM_002619.1	Platelet factor 4 (PF4), mRNA	P
7	TGTATAAAGACAACCTC	NM_002704.1	Proplatelet basic protein (β -thromboglobulin)	Pp
5	GGGCACAATGCGGTCCA	NM_000407.1	Glycoprotein Ib polypeptide, mRNA	P
3	AGGTAATAAAGGTAAT	NM_003512.1	H2A histone family, member L (H2AFL), mRNA	P
3	AGTGGCAAGTAATGGC	NM_021914.2	Cofilin 2 (muscle) (CFL2), mRNA	N/A
3	TGACTGTGCTGGGTTGG	NM_006176.1	Neurogranin (protein kinase C substrate, RC3) mRNA	P
3	TGGGGGTTTCCTTTACC	NM_002032.1	Ferritin, heavy polypeptide 1 (FTH1), mRNA	P
2	CCCTGTGACTACCTAT	NM_025158.1	Hypothetical protein FLJ22251 (FLJ22251), mRNA	N/A
2	CCTGTAACCCAGCTAC	NM_032779.1	Hypothetical protein FLJ14397 (FLJ14397), mRNA	N/A
2	CTGTAGTCCCAGCTAC	NM_017962.1	Hypothetical protein FLJ20825 (FLJ20825), mRNA	N/A

*Unique tags identified more than once.

†Refers to the RefSeq accession no.²¹ Note that this number does not necessarily correspond to the accession no. provided by Affymetrix software annotations (Table 1).

‡Presence (P) or absence (A) is based on results from 3 distinct platelet microarray experiments. Capitalized "P" designates a gene that is in the top 50 on all 3 microarray experiments, whereas small "p" designates those transcripts not in the top 50. Two of the genes (β 2-microglobulin and β -thromboglobulin) are represented by 3 and 2 probe sets, respectively, on the HG-U95Av2 gene chip; for β 2-M, all 3 probe sets were in the top 50 genes, whereas for thymosin β 4 1 of 2 was in the top 50 for all experiments (the other probe set was in the top 75 for all experiments). N/A indicates oligonucleotide not present on Affymetrix HG-U95Av2 gene chip.

results independently obtained by SAGE and microarray analysis, quantitative RT-PCR was completed by using oligonucleotide primers specific for 2 abundant mitochondrial transcripts, 16S rRNA and NADH2 thymosin β 4 (high-abundance by microarray and SAGE), 2 incompletely characterized high-abundance transcripts (neurogranin and clusterin; see "Protein immunoanalysis of platelet clusterin and neurogranin"), a low-abundant transcript (T-cell receptor β -polypeptide), and the genes encoding proteins with well-established quantitative determinations (ie, glycoprotein $\alpha_{IIb}\beta_3$ [\sim 50 000 receptors/platelet]; protease-activated receptor-1 (PAR1) [\sim 1800 receptors/platelet]).¹ As shown in Figure 4, these analyses reveal excellent concordance between SAGE and microarray studies, demonstrating the predominant frequency of the mitochondrial-derived 16S rRNA/NADH2 transcripts, with incrementally lower expression of other transcripts as initially demonstrated by microarray (16S > NADH2 > thymosin β 4 > neurogranin > clusterin > $\alpha_{IIb}\beta_3$ > PAR1 > TCR β).

Given the small number of nonmitochondrial SAGE tags available for analysis ($n = 233$), limited conclusions can be drawn using traditional (nonsubtraction) platelet SAGE libraries as pre-

sented here. Overall, a total of 126 unique tags were identified, the majority of which (94) were represented only once. Of the total unique tags, nearly one half represented novel genes not present on the Affymetrix U95Av2 GeneChip. Of the genes with unique tags identified more than once, there was excellent concordance with microarray expression analysis, with nearly all of the SAGE tags in Table 3 corresponding to platelet top 75 microarray transcripts. The platelet factor (PF) 4 variant represents a single aberration because this was rank-ordered approximately 350 by microarray, although its SAGE tag frequency was identical to that of the predominant PF4 transcript. The lack of extensive nonmitochondrial SAGE sampling precludes any further extrapolations from this apparent aberration. Of note, a subset of these tags had long poly(A) tracts; although they all corresponded to genes identified in the RefSeq database.²¹ We cannot exclude the possibility of a SAGE artifact for this small subset of tags (\sim 2%, representing 46 of 2033 tags), although the authenticity of the vast majority of tags (\sim 98%) clearly validates the methodology. These tags are most likely explained by the unique biology of the platelet (ie, mRNA decay in the absence of de novo transcription) or to mRNA degradation occurring during the extensive purification methods. In summary, even with a remarkably limited sampling, the power of this approach in gene identification of relatively abundant and less abundant transcripts is evident. It is clear, however, given the unique molecular anatomy of the platelet (ie, abundance of mitochondrial transcripts), that SAGE adaptations will be required for more comprehensive genetic profiling.²⁹

Protein immunoanalysis of platelet clusterin and neurogranin

Although most of the "most abundant" transcripts would conform to a priori predictions for platelet-expressed mRNAs, a number of transcripts were identified that had been poorly characterized in human platelets. To further establish the authenticity of highly expressed transcripts such as clusterin and neurogranin, confirmatory protein analyses were completed. As shown in Figure 5, both proteins were clearly detected in purified platelet lysates; furthermore, their cellular platelet distributions conformed to those predicted based on previously proposed functions. Note for example that clusterin—functionally characterized as a complement lysis inhibitor able to block the terminal complement reaction—is primarily expressed on the extracellular platelet membrane.³⁰

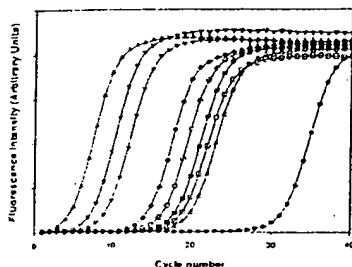
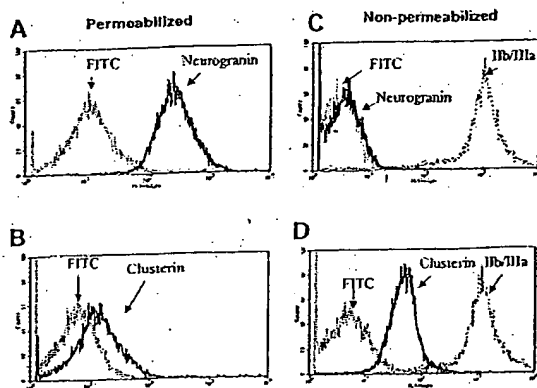


Figure 4. Quantitative real-time RT-PCR analysis of platelet transcripts. Real-time RT-PCR was completed by using purified platelet RNA and oligonucleotide primer pairs specifically designed using Primer3 software to generate similarly-sized (\sim 200-bp) PCR products, optimized to the same annealing temperature. In graph, (□) represents 16S, (■) represents 16S, (△) represents PAR1, (▲) represents 16S rRNA, (▽) represents NADH2, (▼) represents thymosin, (○) represents clusterin, (◆) represents neurogranin, and (●) represents TCR β . Curves are representative of one complete set of experiments (repeated twice), and line plots reflect average determinations from 3 wells performed in parallel with SEM less than 1% for all data points.



Given the importance of complement activation in platelet destruction, the prominent expression of cell-surface clusterin might suggest a role for this protein in normal and pathologic events regulating platelet survival. Interestingly, a clusterin-deficient knockout mouse has been generated that demonstrates enhanced cardiac dysfunction in a model of autoimmune myocarditis.³¹ Although these mice apparently have normal baseline hemograms (B. Aronow, personal communication, October 2002), it remains unestablished if they would be predisposed to immune-type thrombocytopenia in systemic models of autoimmunity.

Similarly, the gene encoding an intracellular effector protein that may have key roles in downstream platelet activation events has now been demonstrated to have abundant transcript expression in human platelets. Neurogranin is a highly expressed platelet transcript with its gene product demonstrating a primarily intracellular pattern of distribution. Neurogranin is generally described as a brain-specific, Ca^{2+} -sensitive calmodulin-binding phosphoprotein that is preferentially expressed in neuronal cell bodies and dendrites.^{32,33} It is a specific protein kinase C (PKC) substrate that can also be modified by nitric oxide and other oxidants to form intramolecular disulfide bonds. Both its phosphorylation and oxidation state attenuate its binding affinity for calmodulin.³³ In stimulated platelets, PKC generation is linked to various activation pathways such as calcium-regulated kinases, mitogen-activated protein (MAP) kinases, and receptor tyrosine kinases.¹ Thus, these observations suggest that platelet neurogranin may function as a previously unidentified component of a PKC-dependent activation pathway coupled to one (or more) of these effector proteins.

Discussion

These data provide documentation for a unique platelet mRNA profile that may provide a tool for analyzing platelet molecular networks. Nonetheless, the molecular analysis of the platelet transcriptome may be confounded by the constant decay of mRNAs in the absence of new gene transcription, a situation that may, for example, limit the identification of low-abundance transcripts. Similarly, because the circulating platelet pool contains

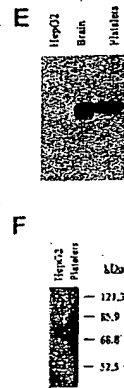


Figure 5. Immunoblot analysis of platelet neurogranin and clusterin. (A-D) Gel-filtered platelets were either fixed in 3.7% formaldehyde (nonpermeabilized) or fixed with permeabilization in the presence of 0.1% Triton-X, followed by flow cytometric analysis using anti-clusterin, anti- α -tubulin, or anti-neurogranin antibodies and the FITC-conjugated species-specific secondary antibody (in C, the FITC-conjugated anti-rabbit and anti-mouse controls are essentially superimposed). (E-F) Ten micrograms of solubilized HepG2 cells (hepatocyte cell line), human brain, or purified platelet lysates were analyzed by SDS-PAGE,¹⁷ and immunoblot analysis were completed by using 1:1000 dilutions of either anti-neurogranin (18% SDS-PAGE) or anti-clusterin (8% SDS-PAGE) antibodies. The anti-clusterin antibody recognized 2 platelet immunoreactive species under shorter exposure. Although the relative neurogranin and clusterin protein abundances are suboptimally quantified by these analyses, platelet clusterin appears to demonstrate considerable expression when compared with that previously identified in hepatocytes.³¹

a mixed population of variably aged platelets, a "static" mRNA profile represents an average of this heterogeneous blood pool. Despite these potential limitations, the combination of genomic and proteomic technologies are likely to provide powerful tools for the global analysis of platelet function. Current strategies for cataloging "whole cellular proteomes" are generally accomplished by using 2 developing methodologies: (1) high resolution 2-dimensional polyacrylamide gel electrophoresis (2-DE) with mass spectrometric sequence identification,³⁴ and (2) microcapillary liquid chromatography with tandem mass spectrometry (μ LC-MC/MC).³⁵ Further modifications of both procedures have been devised for direct comparative studies between 2 cellular proteomes. The introduction of 2-DE differential gel electrophoresis has now made it possible to detect and quantify differences between experimental sample pairs resolved on the same 2-dimensional gel.³⁶ Likewise, the application of isotope-coded affinity tags to μ LC-MC/MC represent a novel means of quantitative analyses between cellular proteomes.³⁷ The success of both approaches relies on the availability of comprehensive genomic databases and mathematical algorithms for optimal protein identification. Indeed, mathematical modeling studies have demonstrated the need to delineate both protein and mRNA expression levels for optimal definition of intracellular networks.³⁸ Our data present an initial framework for delineating platelet function by defining the molecular anatomy of human platelets, information that is likely to provide important clues into the dynamic protein interactions regulating normal and pathologic platelet functions. Furthermore, because the platelet transcriptome mirrors the mRNAs derived from precursor megakaryocytes, these analyses may provide insights into the biochemical and molecular events regulating megakaryocytopoiesis and/or proplatelet formation.

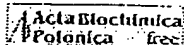
Acknowledgments

We thank Dr Maurcen Krause, Jean Wainer, and Lesley Scudder for assistance with some of the experiments; John Schwedes (University DNA microarray facility) with the microarray analysis; and Ms Shirley Murray for manuscript preparation.

References

- Steinberg P, Hill R. Platelets and megakaryocytes. In: Le R, et al, eds. *Wintrobe's Clinical Hematology*. Baltimore, MD: Williams & Wilkins; 1999.
- Newman P, Gorski J, White G, Gidwitz S, Cretney C, Aster R. Enzymatic amplification of platelet-specific messenger RNA using the polymerase chain reaction. *J Clin Invest*. 1988;82:739-743.
- Kieffer N, Guichard J, Forcet J, Vainchenker W, Breton-Gorius J. Biosynthesis of major platelet proteins in human blood platelets. *Eur J Biochem*. 1987;164:189-195.
- Weyrich A, Dixon D, Pober R, et al. Signal-dependent translation of a regulatory protein, Bcl-2, in activated human platelets. *Proc Natl Acad Sci U S A*. 1998;95:5556-5561.
- Benecke BJ, Ben Zeev A, Penman S. The control of mRNA production, translation and turnover in

- suspended and reattached anchorage-dependent fibroblasts. *Cell*. 1978;14:931-939.
6. Pabla R, Weyrich AS, Dixon DA, et al. Integrin-dependent control of translation: engagement of integrin α IIb β 3 regulates synthesis of proteins in activated human platelets. *J Cell Biol*. 1999;144:175-184.
 7. Chicurel ME, Singer RH, Meyer CJ, Ingber DE. Integrin binding and mechanical tension induce movement of mRNA and ribosomes to focal adhesions. *Nature*. 1998;392:730-733.
 8. Lindemann S, Tolley N, Eyre J, Kraiss L, Mahoney T, Weyrich A. Integrins regulate the intracellular distribution of eukaryotic initiation factor 4E in platelets. *J Biol Chem*. 2001;276:33947-33951.
 9. Brown EJ, Schreiber SL. A signaling pathway to translational control. *Cell*. 1996;86:517-520.
 10. Rinder H, Schuster J, Rinder C, Wang C, Schwesidler H, Smith B. Correlation of thrombosis with increased platelet turnover in thrombocytosis. *Blood*. 1998;91:1288-1294.
 11. Richards E, Baglin T. Quantitation of reticulated platelets: methodology and clinical application. *Br J Haematol*. 1995;91:445-451.
 12. Robinson M, Mackie I, Khair K, et al. Flow cytometric analysis of reticulated platelets: evidence for a large proportion of non-specific labelling of dense granules by fluorescent dyes. *Br J Haematol*. 1998;100:351-357.
 13. Velculescu V, Zhang L, Vogelstein B, Kinzler K. Serial analysis of gene expression. *Science*. 1995;270:484-487.
 14. Zhang L, Zhou W, Velculescu V, et al. Gene expression profiles in normal and cancer cells. *Science*. 1997;276:1268-1272.
 15. Morin PJ, Sparks AB, Korinek V, et al. Activation of beta-catenin-Tcf signaling in colon cancer by mutations in beta-catenin or APC. *Science*. 1997;275:1787-1790.
 16. Bahou W, Campbell A, Wicha M. cDNA cloning and molecular characterization of MSE55: a novel human serum constituent protein that displays bone marrow stromal endothelial cell-specific expression. *J Biol Chem*. 1992;267:13986-13992.
 17. Bahou W, Collier B, Potter C, Norton K, Kulok J, Goligorsky M. The thrombin receptor extracellular domain contains sites crucial for peptide ligand-induced activation. *J Clin Invest*. 1993;91:1405-1413.
 18. Heid C, Stevens J, Livak K, Williams P. Real-time quantitative PCR. *Genome Res*. 1996;6:986-994.
 19. Dunn J, McCorkle S, Praissman L, et al. Genome signature tags (GSTs): a system for profiling genomic DNA. *Nucleic Acid Res*. 2001;29:137-140.
 20. Kroll T, Wolf S. Ranking: a closer look on globalization methods for normalization of gene expression arrays. *Nucleic Acids Res*. 2002;30:e50.
 21. Pruitt KD, Maglott DR. RefSeq and LocusLink: NCBI gene-centered resources. *Nucleic Acids Res*. 2001;29:137-140.
 22. Fox JE, Boyles JK, Reynolds CC, Phillips DR. Actin filament content and organization in unstimulated platelets. *J Cell Biol*. 1984;98:1985-1991.
 23. Safer D, Etzinger M, Nachmias VT. Thymosin beta 4 and Fx, an actin-sequestering peptide, are indistinguishable. *J Biol Chem*. 1991;266:4029-4032.
 24. Wallace DC. Mouse models for mitochondrial disease. *Am J Med Genet*. 2001;106:71-93.
 25. Welle S, Bhatt K, Thornton C. Inventory of high-abundance mRNAs in skeletal muscle of normal men. *Genome Res*. 1999;9:506-513.
 26. Karpaluk S, Charnatz A, Langer RM. Glycogenesis and glycogenolysis in human platelets. Incorporation of glucose, pyruvate, and citrate into platelet glycogen; glycogen synthetase and fructose-1,6-diphosphatase activity. *J Clin Invest*. 1970;49:140-149.
 27. Raha S, Robinson BH. Mitochondria, oxygen free radicals, and apoptosis. *Am J Med Genet*. 2001;106:62-70.
 28. Yu J, Zhang L, Hwang P, Rago C, Kinzler K, Vogelstein B. Identification and classification of p53-regulated genes. *Proc Natl Acad Sci U S A*. 1999;96:14517-14522.
 29. Wang E, Miller L, Ohnmacht G, Liu E, Marincola F. High-fidelity mRNA amplification for gene profiling. *Nat Biotechnol*. 2000;18:157-159.
 30. Kirschbaum L, Sharpe JA, Murphy B, et al. Molecular cloning and characterization of the novel, human complement-associated protein, SP-40,40: a link between the complement and reproductive systems. *EMBO J*. 1989;8:711-718.
 31. McLaughlin L, Zhu G, Mistry M, et al. Apolipoprotein J/clusterin limits the severity of murine autoimmune myocarditis. *J Clin Invest*. 2000;105:1105-1113.
 32. Martinez DA, Perez JL, Bernal J, Coloma A. Structure, organization, and chromosomal mapping of the human neurogranin gene (NRGN). *Genomics*. 1997;41:243-249.
 33. Wu J, Li J, Huang K, Huang F. Attenuation of PKC and PKA signal transduction in the neurogranin knockout mouse. *J Biol Chem*. 2002;277:19498-19505.
 34. Gygi S, Rochon Y, Franza B, Aebersold R. Correlation between protein and mRNA abundance in yeast. *Mol Cell Biol*. 1999;19:1720-1730.
 35. Link A, Eng J, Schieltz DM, et al. Direct analysis of protein complexes using mass spectrometry. *Nat Biotechnol*. 1999;17:676-682.
 36. Unlü M, Morgan M, Minden J. Difference gel electrophoresis: a single gel method for detecting changes in protein extracts. *Electrophoresis*. 1997;18:2071-2077.
 37. Gygi S, Rist B, Gerber SA, Turecek F, Gelb MH, Aebersold R. Quantitative analysis of complex protein mixtures using isotope-coded affinity tags. *Nat Biotechnol*. 1999;17:994-999.
 38. Hatzimanikatis V, Lee K. Dynamical analysis of gene networks requires both mRNA and protein expression information. *Metab Eng*. 1999;1:275-281.



Expression level of Ubc9 protein in rat tissues.

Golcbiowski F, Szulc A, Sakowicz M, Szutowicz A, Pawelczyk T.

Department of Molecular Medicine, Medical University of Gdansk, 80-211 Gdansk, Poland.

Ubc9 is a homologue of the E2 ubiquitin conjugating enzyme and participates in the covalent linking of SUMO-1 molecule to the target protein. In this report we describe a simple and efficient method for obtaining pure human recombinant Ubc9 protein. The purified Ubc9 retained its native structure and was fully active in an in vitro sumoylation assay with the promyelocytic leukaemia (PML) peptide as a substrate. In order to better understand the physiology of Ubc9 protein we examined its levels in several rat tissues. Immunoblot analyses performed on tissue extracts revealed quantitative and qualitative differences in the expression pattern of Ubc9. The Ubc9 protein was present at a high level in spleen and lung. Moderate level of Ubc9 was detected in kidney and liver. Low amount of Ubc9 was observed in brain, whereas the 18 kDa band of Ubc9 was barely visible or absent in heart and skeletal muscle. In heart and muscle extracts the Ubc9 antibodies recognized a 38 kDa protein band. This band was not visible in extracts of other rat tissues. A comparison of the relative levels of Ubc9 mRNA and protein indicated that the overall expression level of Ubc9 was the highest in spleen and lung. In spleen, lung, kidney, brain, liver and heart there was a good correlation between the 18 kDa protein and Ubc9 mRNA levels. In skeletal muscle the Ubc9 mRNA level was unproportionally high comparing to the level of the 18 kDa protein. The presented data indicate that in the rat the expression of the Ubc9 protein appears to have some degree of tissue specificity.

PMID: 14739995 [PubMed - indexed for MEDLINE]

Protein abundance and mRNA levels of the adipocyte-type fatty acid binding protein correlate in non-invasive and invasive bladder transitional cell carcinomas.

Gromova I, Gromov P, Wolf H, Celis JE.

Department of Medical Biochemistry and Danish Centre for Human Genome Research,
The University of Aarhus, Aarhus C, Denmark.

The adipocyte type fatty acid-binding protein (A-FABP) is a small molecular weight fatty acid-binding protein whose expression correlates both with the grade of atypia and the stage of bladder transitional cell carcinomas (TCCs). To determine if the protein abundance correlates with the mRNA levels in non-invasive and invasive lesions, we have analysed fresh TCCs (grade II, Ta; grade III, T2-4) by two-dimensional polyacrylamide gel electrophoresis (2D-PAGE) and measured the mRNA levels using the reverse transcription linked polymerase chain reaction (RT-PCR). Overall, the results showed a good correlation between protein abundance and mRNA levels, indicating that the lack of expression of the protein observed in some lesions reflects low levels of transcription of the A-FABP gene rather than translational regulation. In addition, our studies showed that the loss of A-FABP protein observed in some tumors is not compensated by an increase in the skin fatty acid-binding protein PA-FABP, as is the case in the A-FABP knockout mice.

PMID: 9664136 [PubMed - indexed for MEDLINE]

Expression of the pS2 gene in breast tissues assessed by pS2-mRNA analysis and pS2-protein radioimmunoassay.

Hahnel E, Robbins P, Harvey J, Sterrett G, Hahnel R.

Department of Pathology, University of Western Australia, Queen Elizabeth II Medical Centre, Nedlands.

The expression of the pS2 gene in breast tissues was assessed by measuring pS2-protein using a radioimmunoassay, and by determining pS2-mRNA using Northern blotting. There was a good correlation between the two measurements, indicating that expression of the pS2 gene in breast tissues may be assessed by either method. Since radioimmunoassay is technically easier and more efficient than Northern blotting, radioimmunoassay will be the method of choice in routine applications.

PMID: 1463873 [PubMed - indexed for MEDLINE]

Breast Cancer Research and Treatment

Marc E. Lippman, MD, editor-in-chief

LEH SCHMIDT, LIBRARIAN
University of Wisconsin

DEC 17 1992

1305 Linden Drive
Madison, WI 53706

Kluwer Academic Publishers

Breast Cancer Research and Treatment

Marc E. Lippman, M.D. ¹ (Editor-in-Chief), Gary C. Chamness, Ph.D. ² / Robert L. Dickson, Ph.D. ¹ (Editors),
C. Kent Osborne, M.D. ² / Gary M. Clark, Ph.D. ² (Associate Editors)

¹ Vincent T. Lombardi Cancer Research Center, Georgetown University, Washington DC, USA

² University of Texas Health Science Center at San Antonio, San Antonio, TX, USA

Editorial office address:

Karen S. Cullen, BREA Editorial Office, Kluwer Academic Publishers, 101 Philip Drive, Assinippi Park,
Norwell, MA 02061, USA; Tel: 617-871-6300; Fax: 617-871-6528; E-mail: Karen@world.std.com.

EDITORIAL ADVISORY BOARD

George Blumenschein (Arlington,
Texas)

Gianni Bonadonna (Milan, Italy)

Paul P. Carbone (Madison,
Wisconsin)

Dean P. Edwards (Denver,
Colorado)

Evert Engelsman (Amsterdam, The
Netherlands)

Bernard Fisher (Pittsburgh,
Pennsylvania)

Edwin Fisher (Pittsburgh,
Pennsylvania)

Jan-Åke Gustafsson (Stockholm,
Sweden)

Kathryn Horwitz (Denver,
Colorado)

Elwood V. Jensen (Hamburg,
Germany)

V. Craig Jordan (Madison, Wisconsin)

Roger King (London, United Kingdom)

Heinrich Maass (Hamburg, Germany)

Kenneth S. McCarty, Jr. (Durham,
North Carolina)

Daniel Medina (Houston, Texas)

Henri Rochefort (Montpellier, France)

Richard Santen (Hershey,
Pennsylvania)

Jeffrey Schlom (Bethesda, Maryland)

Haruo Sugano (Tokyo, Japan)

Jeffrey M. Trent (Tucson, Arizona)

ISSN 0167-6806

All Rights Reserved

© 1992 by Kluwer Academic Publishers

No part of the material protected by this copyright notice may be reproduced or utilised in any form or by any means, electronic or mechanical, including photocopying, recording or by any information storage and retrieval system, without written permission from the copyright owner.

Printed in The Netherlands

Brief communication

Expression of the pS2 gene in breast tissues assessed by pS2-mRNA analysis and pS2-protein radioimmunoassay

Erika Hähnel, Peter Robbins, Jennet Harvey, Gregory Sterrett and Roland Hähnel
Department of Pathology, University of Western Australia, Queen Elizabeth II Medical Centre, Nedlands, 6009, Western Australia

Key words: breast tissue, pS2-mRNA, pS2 protein, radioimmunoassay

Summary

The expression of the pS2 gene in breast tissues was assessed by measuring pS2-protein using a radioimmunoassay, and by determining pS2-mRNA using Northern blotting. There was a good correlation between the two measurements, indicating that expression of the pS2 gene in breast tissues may be assessed by either method. Since radioimmunoassay is technically easier and more efficient than Northern blotting, radioimmunoassay will be the method of choice in routine applications.

Introduction

Expression of the pS2 gene is controlled by estrogen. This was first described in the MCF-7 breast cancer cell line [1]. pS2 expression has since been reported to be useful as a prognostic indicator [2, 3], although this was not confirmed in another series [4].

pS2 expression may be assessed in tissue homogenates by analysis of pS2-mRNA [5], by radioimmunoassay of the pS2-protein [2], or by immunocytochemical detection of the pS2 protein in tissue sections [5]. It was the aim of this study to establish the correlation between pS2-mRNA and pS2-protein by radioimmunoassay in a series of tissues obtained from mastectomy specimens performed for carcinoma of the breast. Primary breast carcinoma tissue, metastatic carcinoma within axillary nodes, and macroscopically benign breast tissue were examined.

Materials and methods

Breast tissues

Tissue specimens from mastectomies performed for carcinoma of the breast were examined. 32 primary breast carcinomas, 10 axillary lymph nodes containing metastatic breast carcinoma, and 20 samples of uninvolved breast tissue were analyzed for pS2 expression.

The primary breast carcinomas were histologically classified using a conventional subclassification. The presence or absence of primary tumour was assessed. The presence of metastatic carcinoma within lymph nodes studied was verified by histological examination of the node remnant after sampling.

'Uninvolved' breast tissue was sampled from sites well removed from the primary breast tumour (usually in another quadrant of the breast), and was selected only if the tissue appeared macroscopically unremarkable. Tissue sampling occurred imme-

diately upon arrival of the mastectomy specimen in the laboratory, with minimal delays between removal and sampling.

Tissues for pS2 analysis were snap frozen in liquid nitrogen and stored at -70°C until processed.

Extraction of RNA and determination of pS2-mRNA

Details of the procedure have been described in our previous paper [6]. Briefly, the deep-frozen tissue was homogenized in a micro-dismembrator. The homogeneous powder was extracted with guanidiniumisothiocyanate/phenol/chloroform/isoamylalcohol, and RNA was precipitated with isopropanol. The washed RNA pellet was dissolved in SDS and glyoxylated, and the RNA preparation loaded onto agarose gel. After electrophoresis the gel was capillary blotted onto Zeta-probe membranes. Membranes were hybridized overnight with cDNA probes pS2 and 36B4, which were labeled with [$\alpha^{32}\text{P}$] dCTP by nick translations. Washed membranes were exposed to Kodak X-omat AR film. Relative intensities of the mRNA bands were assessed visually as not detectable, very weak, weak, medium, strong, and very strong, taking the intensities of the ubiquitous 36B4 bands into account.

Radioimmunoassay of pS2-protein

Deep frozen specimens were pulverized with a microdismembrator. The tissue powder was suspended in 10 volumes of pH 7.5 phosphate buffer. The homogenate was centrifuged in a refrigerated centrifuge at 4°C for 60 minutes at $2600\times g$. The supernatant was removed with a Pasteur pipette, carefully avoiding the fat layer on the top. The protein concentration in the supernatant was estimated by use of the Coomassie dye-binding method [7]. An aliquot of the supernatant was diluted to a protein concentration between 1 and 2 mg/ml before assay of the pS2-protein. In one case the protein concentration of the supernatant was well below 1 mg/ml.

The estimation of the pS2-protein was performed using a solid phase, two-site radioimmunoassay. The kits were bought from CIS Biointernational, Gif-sur-Yvette, France (ELSA-PS2). In this method the molecules of pS2 are sandwiched between two monoclonal antibodies; the first one is coated on the ELSA solid phase, the second one is radiolabeled with 125-iodine. The radioactivity bound to the ELSA is proportional to the concentration of pS2-protein. Details of the procedure are supplied with the kit [8].

Results and discussion

32 primary breast carcinomas, metastatic breast carcinoma in 10 lymph nodes, and 20 samples of benign breast tissue from mastectomies were investigated. Two of the carcinomas were of the infiltrating lobular type, two were ductal carcinomas *in situ*, one was a multicentric invasive ductal carcinoma, all others were invasive ductal carcinomas.

Examples of pS2 Northern blots have been shown in our previous paper [6] which demonstrate that undegraded pS2-mRNA can be isolated by the method used.

The results of the pS2-protein and pS2-mRNA assays are shown on Fig. 1. There was a good correlation between the two types of results. When pS2-mRNA could not be detected by Northern blot, pS2-protein results were usually below 1 ng/mg protein (22 of 30), or between 1 and 3.7 ng/mg (6 of 30). Two were exceptions (7.7 and 14.6); one of them could have been due to the very low protein content in the cytosol which would lead to a large pS2 value and an associated error. There was no explanation for the other high result. Very weak pS2-mRNA signals on Northern blots corresponded to pS2-protein values between 1.1 and 19.2 with an average of 6.6 ng/mg protein (median 5.7). The mean and median pS2-protein concentration in the tissue with weak pS2-mRNA signals were 14.3 and 10.7 ng/mg protein, respectively. The average pS2-protein concentration increased to 32.7 (median 31.5) ng/mg protein for tissues assessed as medium pS2-mRNA intensity, and to 43.3 (median 53.8) ng/mg protein for tissues with strong or very strong

pS2-mRNA signals. These values should be used as an approximate guide only, since the number of samples in the various groups was fairly small. One-way analysis of variance confirmed that the means of the pS2-protein values in the groups made up according to their pS2-mRNA signal intensity, were significantly different ($p < 10^{-6}$).

If the pS2 gene is expressed, its expression is on average greater in breast carcinomas than in uninvolved breast tissue. If one takes pS2-protein values above 4 ng/mg protein as cut-off, the average pS2-protein in 14 breast cancers was 34.3 (median 35.2), while it was only 18.1 (median 13.8) in 12 uninvolved breast tissue samples. If the cut-off is taken at 10 ng/mg protein, average pS2-protein in breast carcinoma is also about twice the level of uninvolved tissue. There were not enough lymph node metastases which expressed the pS2 gene to allow a comparison with carcinoma or uninvolved breast tissue.

Recent preliminary results of pS2 by radioimmunoassay [9] are similar to ours for breast cancer but considerably lower than our results for normal breast tissue.

The values of the pS2-protein measured obviously depend on the protein used for calibration. We used the pS2-protein standards supplied with the CIS kit, which according to the supplier gave values from 0 to 740 ng/mg protein in a series of 205 breast cancer cytosols. Previously, a different standard had been used for presumably the same series of breast carcinomas [2], and a conversion factor to current standards is given as 2.8 [8].

It was noticed that the correlation between pS2-protein and pS2-mRNA was better in breast carcinoma specimens than in uninvolved breast tissue. This is unexplained, though it could be due to the variable content of cell or tissue types in adjoining parts of a specimen, a variation more likely to occur in our sampling of non-malignant breast tissue compared to sampling of carcinomas. A similar variability in breast carcinoma specimens will probably have a smaller influence on the pS2 results, since the malignant cells – if they do express the pS2 gene – contain more pS2-protein than normal breast.

CORRELATION OF pS2 - mRNA AND pS2 - PROTEIN

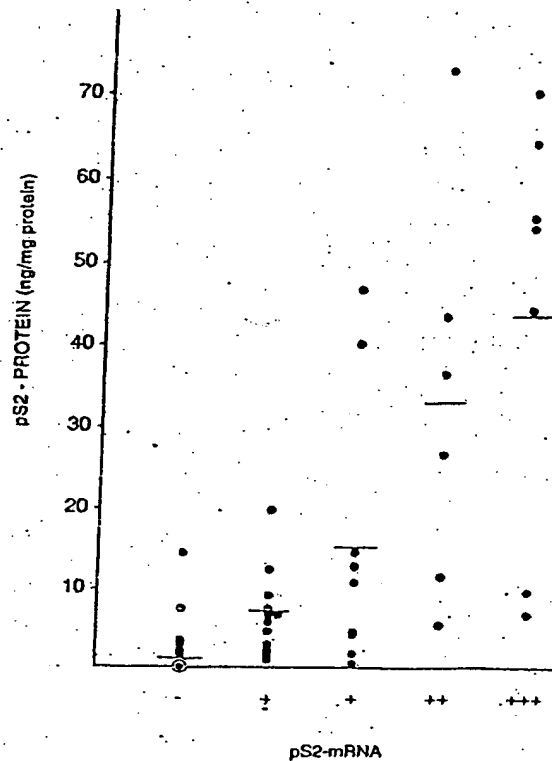


Fig. 1. Correlation between pS2-protein by radioimmunoassay and pS2-mRNA by Northern blot. ⊗ = 22 results below 1. The horizontal lines indicate the mean values.

Acknowledgements

This investigation was supported in part by a grant from the Sir Charles Gairdner Hospital Research Foundation. The authors wish to thank Professor P. Chambon, Strasbourg, France, for the gift of pS2 and 36B4 cDNAs. A preliminary account of our results was presented at the First Joint Conference of the American Association for Cancer Research and the European Association for Cancer Research, held at Santa Margherita, Italy, 6–9 November, 1991.

References

1. Masiakowski P, Breathnach R, Bloch J, Gannon F, Krust A, Cham-

- bon P: Cloning of cDNA sequences of hormone-regulated genes from the MCF-7 human breast cancer cell lines. *Nucleic Acids Res* 10: 7895-7903, 1982
2. Fockens JA, Rio MC, Seguin P, Van Putten WLJ, Fauque J, Nap M, Klijn JGM, Chambon P: Predication of relapse and survival in breast cancer patients by pS2 protein status. *Cancer Res* 50: 3832-3837, 1990
3. Fockens JA, Van Putten WLJ, Ponengen H, Rodenburg CJ, Reubi JC, Berns PMJJ, Henzen-Logmans SC, Van Der Burg MEL, Alexjeva-Figusch J, Klijn JGM: Prognostic value of pS2 protein and receptors for epidermal growth factor, insulin-like growth factor, and somatostatin in patients with breast and ovarian cancer. *J Steroid Biochem Molec Biol* 37: 815-821, 1990
4. Henry JA, Piggou NH, Mallick UK, Nicholson S, Farndon JR, Westley BR, May FEB: pNR-2/pS2 immunohistochemical staining in breast cancer: Correlation with prognostic factors and endocrine response. *Br J Cancer* 63: 615-622, 1991
5. Rio MC, Bellocq JP, Gairard B, Rasmussen UB, Krust A, Koehl C, Calderoli H, Schiff V, Renaud R, Chambon P: Specific expression of the pS2 gene in subclasses of breast cancer in comparison with expression of the estrogen and progesterone receptors and the oncogene ERBB2. *Proc Natl Acad Sci USA* 84: 9243-9247, 1987
6. Hähnel E, Joyce R, Sterrett GF, Harvey JM, Hähnel R: Detection of estradiol-induced messenger RNA (pS2) in uninvolved breast tissue from mastectomies for breast cancer. *Breast Cancer Res Treat* 20: 167-176, 1991
7. Bradford M: A rapid and sensitive method for the quantitation of microgram quantities of protein utilizing the principle of protein-dye binding. *Anal Biochem* 72: 248-254, 1976
8. CIS ELSA-pS2: Immunoradiometric assay of pS2 protein. Package insert, December, 1990
9. Kouyoumdjian JC, Boissier B, Rymer JC, Bagnard G, Rotten D, Levailant JP, Constancis B, Philippon C, Flourey C, Thirion B: Determination of several prognostic parameters in human normal breast, benign mastopathies, and adenocarcinomas. *J Tumour Marker Oncol* 6: 111, 1991

Expression of the multidrug resistance-associated protein (MRP) mRNA and protein in normal peripheral blood and bone marrow haemopoietic cells.

Legrand O, Perrot JY, Tang R, Simonin G, Gurbuxani S, Zittoun R, Marie JP.

Laboratoire de Cinetique et de Cultures Cellulaires, Hotel Dieu, Paris, France.

We studied the expression of multidrug resistance-associated protein (MRP) in normal haemopoietic cells from peripheral blood and bone marrow. The MRP mRNA levels were estimated by RT/PCR and in situ hybridization (ISH) assay, and the protein levels by flow cytometry. 21 samples of peripheral blood and 21 samples of bone marrow (11 normal bone marrow donors, 10 patients in complete remission after chemotherapy for large cell lymphoma or acute myeloid leukaemia) were analysed. In peripheral blood the mean MRP mRNA level in CD3+ cells was statistically higher than in the other cells (3-fold by the methods used). The levels of MRP in CD3+ varied from one individual to another (4.5-34.8 units by RT/PCR and 5-23 grains/cell by ISH); however, this was proportional to the variation in all the cell lineages of same individual ($r = 0.84$). In bone marrow the mean MRP levels of the various cell lineages (including CD34+) were similar to the basal level in HL60 cells. Individual expression levels were again variable; however, there was no difference between untreated normal bone marrow and post chemotherapy normal bone marrow. MRP protein expression was determined by flow cytometry with the monoclonal antibody MRPM6. The CD4+ lymphocytes exhibited a higher MRP protein expression than the other cell lineages, including CD8+ cells. There was a good correlation between the three methods used (RT/PCR and ISH, $P = 0.0001$, $r = 0.87$; RT/PCR and flow cytometry, $P = 0.0001$, $r = 0.85$; ISH and flow cytometry, $P = 0.002$, $r = 0.67$).

PMID: 8757504 [PubMed - indexed for MEDLINE]



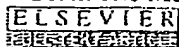
Vascular endothelial growth factor enhances cardiac allograft arteriosclerosis.

Lemstrom KB, Krebs R, Nykanen AI, Tikkanen JM, Sihvola RK, Aaltola EM, Hayry PJ, Wood J, Alitalo K, Yla-Herttuala S, Koskinen PK.

Cardiopulmonary Research Group, Transplantation Laboratory, University of Helsinki and Helsinki University Central Hospital, Helsinki, Finland. Karl.Lemstrom@helsinki.fi

BACKGROUND: Cardiac allograft arteriosclerosis is a complex process of alloimmune response, chronic inflammation, and smooth muscle cell proliferation that includes cross talk between cytokines and growth factors. **METHODS AND RESULTS:** Our results in rat cardiac allografts established alloimmune response as an alternative stimulus capable of inducing vascular endothelial growth factor (VEGF) mRNA and protein expression in cardiomyocytes and graft-infiltrating mononuclear inflammatory cells, which suggests that these cells may function as a source of VEGF to the cells of coronary arteries. Linear regression analysis of these allografts with different stages of arteriosclerotic lesions revealed a strong correlation between intragraft VEGF protein expression and the development of intimal thickening, whereas blockade of signaling downstream of VEGF receptor significantly reduced arteriosclerotic lesions. In addition, in cholesterol-fed rabbits, intracoronary perfusion of cardiac allografts with a clinical-grade adenoviral vector that encoded mouse VEGF(164) enhanced the formation of arteriosclerotic lesions, possibly secondary to increased intragraft influx of macrophages and neovascularization in the intimal lesions. **CONCLUSIONS:** Our findings suggest a positive regulatory role between VEGF and coronary arteriosclerotic lesion formation in the allograft cytokine microenvironment.

PMID: 12034660 [PubMed - indexed for MEDLINE]



[3H]MK-801 binding and the mRNA for the NMDAR1 subunit of the NMDA receptor are differentially distributed in human and rat forebrain.

Meoni P, Mugnaini M, Bunnemann BH, Trist DG, Bowery NG.

Department of Pharmacology, Medical School, University of Birmingham, UK.
meonip@novel15.bham.ac.uk

The distributions of [3H]MK-801 binding and the NMDA NR1 subunit mRNA were studied using receptor autoradiography and in-situ hybridization in rat and human brain whole-hemisphere coronal sections. Receptor protein detected by radioligand autoradiography and the mRNA for the key subunit of the receptor presented similar distributions in the forebrain, with a few areas showing an imbalance between the levels of mRNA and receptor protein. Human frontal cortex showed a relative abundance of NMDAR1 mRNA as compared to [3H]MK-801 binding. The same area in rat brain did not show any difference in the two distributions. In comparison, the rat claustrum presented a relative excess of NMDAR1 mRNA which was not detected in human sections. Human caudate nucleus exhibited relatively high levels of [3H]MK-801 binding that were unmatched in rat caudate. The hippocampi of either species presented similar levels of [3H]MK-801 binding and NMDAR1 mRNA, but when the two signals were measured in specific subfields of the hippocampal formation, the differential distribution of the two signals reflected the anatomy of hippocampal connections assuming a preferential dendritic distribution for MK-801 binding. Interestingly, rat and human hippocampi also showed some important species-dependent difference in the relative distribution of the receptor protein and mRNA. The data presented show an overall good correlation between the mRNA for the key subunit of the NMDA receptor and the functional receptor detected with radioligand binding and highlight the presence of local differences in their ratio. This may reflect different splicing of the mRNA for the NMDAR1 subunit in specific brain areas of rat and human. The species-dependent differences in the relative distribution of the mRNA for the key subunit of the NMDA receptor and that of a marker of functional receptors also highlights important differences in the NMDA function in rat and human brain.

PMID: 9526033 [PubMed - indexed for MEDLINE]

Differential expression of the short and long forms of the gamma 2 subunit of the GABAA/benzodiazepine receptors.

Miralles CP, Gutierrez A, Khan ZU, Vitorica J, De Blas AL.

Division of Molecular Biology and Biochemistry, School of Biological Sciences,
University of Missouri-Kansas City 64110-2499.

The distribution of the mRNAs encoding the gamma 2S and gamma 2L subunits of the GABAA receptor in the rat brain has been revealed by in situ hybridization, northern blot and dot blot analysis using specific antisense oligonucleotides. In addition, the quantitative distribution of the gamma 2S and gamma 2L subunit peptides participating in the fully assembled GABAA receptors/benzodiazepine receptors has been mapped by immunoprecipitation with specific anti-gamma 2S and anti-gamma 2L antibodies. Several neuronal types and brain regions are enriched in gamma 2L such as neurons of the layer II of striate cortex and cerebellar Purkinje cells as well as the inferior colliculus, superior colliculus, deep cerebellar nuclei, medulla and pons. Other neuronal types and regions are enriched in gamma 2S such as the mitral cells of the olfactory bulb, pyramidal neurons of the pyriform cortex, layer VI of the neocortex, granule cells of the dentate gyrus and pyramidal cells of the hippocampus. Other cortical areas and cerebellar granule cells express both gamma 2S and gamma 2L in comparable amounts. There is a good correlation between the relative expression of gamma 2S and gamma 2L mRNAs and the relative presence of these protein subunits in fully assembled and mature receptors in the studied brain regions. The differential distribution of gamma 2S and gamma 2L might result in differential ethanol sensitivity of the neurons expressing these GABAA receptor subunits.

PMID: 7968350 [PubMed - indexed for MEDLINE]

The alpha(v)beta6 integrin receptor for Foot-and-mouth disease virus is expressed constitutively on the epithelial cells targeted in cattle.

Monaghan P, Gold S, Simpson J, Zhang Z, Weinreb PH, Violette SM, Alexandersen S, Jackson T.

Institute for Animal Health, Pirbright Laboratory, Ash Road, Pirbright, Surrey GU24 0NF, UK.

Field strains of Foot-and-mouth disease virus (FMDV) use a number of alpha(v)-integrins as receptors to initiate infection on cultured cells, and integrins are believed to be the receptors used to target epithelial cells in animals. In this study, immunofluorescence confocal microscopy and real-time RT-PCR were used to investigate expression of two of the integrin receptors of FMDV, alpha(v)beta6 and alpha(v)beta3, within various epithelia targeted by this virus in cattle. These studies show that alpha(v)beta6 is expressed constitutively on the surfaces of epithelial cells at sites where infectious lesions occur during a natural infection, but not at sites where lesions are not normally formed. Expression of alpha(v)beta6 protein at these sites showed a good correlation with the relative abundance of beta6 mRNA. In contrast, alpha(v)beta3 protein was only detected at low levels on the vasculature and not on the epithelial cells of any of the tissues investigated. Together, these data suggest that in cattle, alpha(v)beta6, rather than alpha(v)beta3, serves as the major receptor that determines the tropism of FMDV for the epithelia normally targeted by this virus.

PMID: 16186231 [PubMed - in process]

Comment in:

- J Invest Dermatol. 1994 Nov;103(5):742-4.

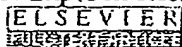
T-cell receptor V beta-family usage in primary cutaneous and primary nodal T-cell non-Hodgkin's lymphomas.

Preesman AH, Hu HZ, Tilanus MG, de Geus B, Schuurman HJ, Reitsma R, van Wichen DE, van Vloten WA, de Weger RA.

Department of Pathology, University Hospital Utrecht, The Netherlands.

To evaluate whether the expression of T-cell receptor (TCR) V beta families in eight cases of malignant T-cell lymphomas took place in a preferential manner, we analyzed four cases of mycosis fungoides (MF), the most common form of primary cutaneous T-cell non-Hodgkin's lymphomas (NHL), and four cases of primary nodal T-cell NHL. The usage of V beta families in T-cell populations was investigated on mRNA that was transcribed to cDNA using a C beta primer and reverse transcriptase. Subsequently, the specific usage of the families was analyzed by polymerase chain reaction (PCR) using combinations of the selected C beta-oligonucleotide primer and one of the family-specific V beta primers. Peripheral blood lymphocytes from four healthy volunteers and 1 "reactive" lymph node served as a control and expressed all 20 V beta families tested for. In T-cell lines, with restricted V beta expression, and in three patients with advanced MF, only one or two V beta families were expressed at the mRNA level. In an early MF lesion this monoclonal expression was absent: several V beta families were expressed with a weak intensity. This may indicate either a polyclonal origin of MF, or that too few monoclonal neoplastic cells were present in the tissue specimen. In the four nodal T-cell NHL, only one family could be clearly distinguished, whereas some of the other V beta families showed only a weak expression. These latter families represent the reactive T-cell component in the nodal T-cell NHL. Both in nodal T-cell NHL and in MF there was no preferential expression of a particular V beta family. There was a good correlation between PCR data and the expression of V beta-family protein products observed by immunohistochemistry on tissue sections of the T-cell lymphomas. All T-cell lines, three cases of MF, and three cases of nodal T-cell NHL showed a rearrangement of the TCR beta chain on DNA level.

PMID: 1331246 [PubMed - indexed for MEDLINE]



Expression and distribution of laminin alpha1 and alpha2 chains in embryonic and adult mouse tissues: an immunochemical approach.

Sasaki T, Giltay R, Talts U, Timpl R, Talts JF.

Max-Planck-Institute for Biochemistry, Martinsried, D-82152, Germany.

Protein levels, mRNA expression, and localization of laminin alpha1 and alpha2 chains in development and in adult mice were examined. Recombinant fragments were used to obtain high-titer-specific polyclonal antibodies for establishing quantitative radioimmuno-inhibition assays. This often demonstrated an abundance of alpha2 chain, but also distinct amounts of alpha1 chain for adult tissues. The highest amounts of alpha1 were found in placenta, kidney, testis, and liver and exceeded those of alpha2. All other tissue extracts showed a higher content of alpha2, which was particularly high in heart and muscle when compared to alpha1. Content of gamma1 chain, shared by most laminins, was also analyzed. This demonstrated gamma1 chain levels being equal to or moderately exceeding the sum of alpha1 and alpha2 chains, indicating that these isoforms represent the major known laminin isoforms in most adult mouse tissues so far examined. Moreover, we found good correlation between radioimmuno-inhibition data and mRNA levels of adult tissues as measured by quantitative real-time reverse transcriptase-PCR. Embryonic tissues were also analyzed by radioimmuno-inhibition assays. This demonstrated for day 11 embryos comparable amounts of alpha1 and gamma1 and a more than 25-fold lower content of alpha2. This content increased to about 10% of alpha1 in day 13 embryos. The day 18 embryo showed in heart, kidney, and liver, but not yet in brain and lung; alpha1/alpha2 chain ratios comparable to those in adult tissues. Immunostaining demonstrated alpha1 in Reichert's membrane (day 7.5), while alpha2 could not be detected before day 11.5. These data were compared with immunohistochemical localization results on several more embryonic and adult tissue sections. Our results regarding localization are consistent with those of earlier work with some notable exceptions. This was in part due to epitope masking for monoclonal antibodies commonly used in previous studies in esophagus, intestine, stomach, liver, kidney, and spleen.

PMID: 11969289 [PubMed - indexed for MEDLINE]

FREE full text article at
www.jbc.org

Discordant regulation of granzyme H and granzyme B expression in human lymphocytes.

Sedelies KA, Sayers TJ, Edwards KM, Chen W, Pellicci DG, Godfrey DI, Trapani JA.

Cancer Immunology Laboratory, Peter MacCallum Cancer Centre, Locked Bag 1, A'Beckett Street, East Melbourne, 8006, Australia.

We analyzed the expression of granzyme H in human blood leukocytes, using a novel monoclonal antibody raised against recombinant granzyme H. 33-kDa granzyme H was easily detected in unfractionated peripheral blood mononuclear cells, due to its high constitutive expression in CD3(-)CD56(+) natural killer (NK) cells, whereas granzyme B was less abundant. The NK lymphoma cell lines, YT and Lopez, also expressed high granzyme H levels. Unstimulated CD4(+) and particularly CD8(+) T cells expressed far lower levels of granzyme H than NK cells, and various agents that classically induce T cell activation, proliferation, and enhanced granzyme B expression failed to induce granzyme H expression in T cells. Also, granzyme H was not detected in NK T cells, monocytes, or neutrophils. There was a good correlation between mRNA and protein expression in cells that synthesize both granzymes B and H, suggesting that gzmH gene transcription is regulated similarly to gzmB. Overall, our data indicate that although the gzmB and gzmH genes are tightly linked, expression of the proteins is quite discordant in T and NK cells. The finding that granzyme H is frequently more abundant than granzyme B in NK cells is consistent with a role for granzyme H in complementing the pro-apoptotic function of granzyme B in human NK cells.

PMID: 15069086 [PubMed - indexed for MEDLINE]

Quantitative determinations of the steady state transcript levels of hexokinase isozymes and glucose transporter isoforms in normal rat tissues and the malignant tumor cell line AH130.

Shinohara Y, Yamamoto K, Inoo K, Yamazaki N, Terada H.

Faculty of Pharmaceutical Sciences, University of Tokushima, Japan.
yasuo@ph.tokushima-u.ac.jp

The steady state transcript levels of the four hexokinase (HK) isozymes and four glucose transporter (GLUT) isoforms were determined quantitatively by Northern analysis of RNA samples from rat tissues using synthetic fragments of the RNAs encoding the HK isozymes and GLUT isoforms. Results showed that the levels of HK isozyme transcripts were low in rat tissues, the level of that most highly expressed, the type I isozyme (HKI), in the brain being 0.025% of the total poly(A)+ RNA. A good correlation was found between the reported HK activities and the total amounts of transcripts encoding all HK isozymes in various tissues, showing that the HK activities in tissues can be estimated from the total amount of transcripts encoding HK isozymes. The proposed associated expressions of HK isozymes and GLUT isoforms in particular tissues were confirmed at their transcript levels. The steady state transcript levels of type II HK and the type I GLUT isoform in the malignant tumor cell line AH130 were also determined quantitatively.

PMID: 9459591 [PubMed - indexed for MEDLINE]



Rat kidney glutamyl aminopeptidase (aminopeptidase A): molecular identity and cellular localization.

Song L, Ye M, Troyanovskaya M, Wilk E, Wilk S, Healy DP.

Department of Pharmacology, Mount Sinai School of Medicine, City University of New York, New York 10029.

Glutamyl aminopeptidase [aminopeptidase A (EAP), EC 3.4.11.7] is an ectoenzyme that selectively hydrolyzes acidic amino acid residues from the amino terminus of oligopeptides. EAP activity is highest within the kidney and small intestine. The murine pre-B cell BP-1/6C3 and the human kidney glycoprotein gp160 differentiation antigens have been reported to have biochemical properties indistinguishable from EAP. It is not known, however, if rat kidney EAP is a homologue of these antigens or molecularly distinct. Using the reverse transcription-polymerase chain reaction method with oligonucleotide primers based on the BP-1/6C3 nucleotide sequence, we isolated a 450-bp partial cDNA from rat kidney poly(A)⁺ RNA. The partial cDNA encoded a predicted protein that was 92% and 86% identical to the murine BP-1/6C3 and human gp160 antigens, respectively; the amino acid sequence within the zinc-binding domain was completely conserved. Purification of EAP from rat kidney and microsequence analysis of a tryptic digest peptide fragment (18-mer) indicated that the fragment was highly similar to a region within the BP-1/6C3 and gp160 proteins. Northern blot hybridization and immunoblot analyses were also consistent with labeling of products the same size as reported for the BP-1/6C3 and gp160 antigens. There was a good correlation between the cellular distribution of EAP mRNA and EAP immunoreactivity, with proximal tubules and glomerular mesangial cells having the highest densities. These results indicate that rat kidney EAP is a species homologue of the murine BP-1/6C3 and human gp160 antigens. Furthermore, on the basis of its cellular localization, rat kidney EAP is likely to be involved in degradation of oligopeptides within the glomerulus and the glomerular filtrate. Since cells that express EAP also express receptors for angiotensin II, an intrarenal vasoactive hormone that is a substrate for EAP, these results further suggest that EAP may play a role in modulating the activity of intrarenal angiotensin II.

PMID: 7943354 [PubMed - indexed for MEDLINE]

- 111: Skin Pharmacol Appl Skin Physiol. 2003 May-Jun;16(3):143-50. Related Articles, Links



Transcriptional activity of potent glucocorticoids: relevance of glucocorticoid receptor isoforms and drug metabolites.

Spika I, Hammer S, Kleuser B, Korting HC, Schafer-Korting M.

Institut für Pharmazie, Abteilung für Pharmakologie und Toxikologie, Freie Universität Berlin, Berlin, Germany.

As compared to standard glucocorticoids (GC), prednicarbate (PC) is favorable in the treatment of eczema due to its high benefit/risk ratio. The remarkable anti-inflammatory effects of PC are in strong contrast to its reported low glucocorticoid receptor (GR) binding affinity. In transfected COS-7 cells we related the transcriptional potencies of PC, its metabolites and conventional GC to their receptor binding properties. Moreover, the expression pattern of the human GR isoform hGRalpha and its mutual dominant negative inhibitor hGRbeta in skin cells have been investigated as well as the influence of hGRbeta on receptor binding and transactivation. hGRalpha mRNA and protein was largely overexpressed in skin cells. hGRbeta showed no influence on hGRalpha binding and transactivation. Concentration response curves indicated the greater transactivation potency of betamethasone 17-valerate followed by dexamethasone and prednisolone 17-ethylcarbonate. Native PC appeared almost as potent as dexamethasone. With both a strong correlation was observed between transactivation and GR binding. Copyright 2003 S. Karger AG, Basel

PMID: 12677094 [PubMed - indexed for MEDLINE]

Cell proliferation in human soft tissue tumors correlates with platelet-derived growth factor B chain expression: an immunohistochemical and in situ hybridization study.

Wang J, Coltrera MD, Gown AM.

Department of Pathology, University of Washington, Seattle 98195.

The authors tested the hypothesis that the B chain of the platelet-derived growth factor (PDGF), a known connective tissue mitogen and growth factor, could be expressed by human soft tissue tumors, and that its expression could play a role in the control of cell proliferation in these tumors. Using a set of 56 soft tissue tumors, including benign tumors and all three grades of sarcomas, PDGF-B chain protein was localized using immunohistochemistry and PDGF-B mRNA was localized using in situ hybridization. The hypothesis that PDGF-B expression was related to cell proliferation was tested by simultaneously demonstrating the expression of the proliferating cell nuclear antigen in sequential tissue sections of the same tumors. Sixty and 82% of tumors had demonstrable PDGF-B mRNA and protein, respectively, with a strong correlation between their degrees of expression ($P = 0.0001$). Among the sarcomas, a strong correlation between PDGF-B expression and increasing malignant tumor grade ($P = 0.006$), and between PDGF-B expression and increasing proliferating cell nuclear antigen index ($P = 0.01$) was found. All tumors were also demonstrated to express the beta receptor of PDGF via immunohistochemistry. These studies suggest that PDGF-B expression may be an important mediator of cell proliferation control, via an autocrine mechanism, in human soft tissue tumors and may correlate with clinical outcome in the sarcomas.

PMID: 7903911 [PubMed - indexed for MEDLINE]

Expression of cytokines and growth factors in human glomerulonephritides.

Waldherr R, Noronha IL, Niemir Z, Kruger C, Stein H, Stumm G.

Department of Pathology, University of Heidelberg, Germany.

Numerous experimental studies point to the potential role of cytokines and growth factors in the pathogenesis of renal disease. However, from the various autocrine and paracrine mediators identified in vitro and in animal models, so far only a few have been demonstrated in selected human glomerulopathies. We examined two types of glomerulonephritis (GN): extracapillary GN with anti-neutrophil cytoplasmic autoantibodies (ANCA), an example of an acute form of GN, and mesangial IgA GN, usually a chronic form of GN, with immunocytochemistry, in situ hybridization and the polymerase chain reaction. Normal renal tissue from tumour nephrectomies served as a control. In ANCA-positive GN with active renal lesions (crescents, glomerular and vascular necrosis), infiltrating mononuclear cells in glomeruli and in the interstitium expressed interleukin (IL)-1 beta, tumour necrosis factor (TNF)-alpha, IL-2, interferon (IFN)-gamma, platelet-derived growth factor (PDGF) and transforming growth factor (TGF)-beta. Cytokine expression was also observed in activated resident cells, including endothelial cells, capsular epithelial cells, smooth muscle cells of vessel walls, fibroblasts and some tubular epithelial cells. In addition, we noted an increase in the cytokine and growth factor receptors TNF-R, IL-1R type II, IL-2R, IFN-gamma R and PDGF beta-R. In contrast, in mesangial IgA-GN, IL-1 beta, TNF-alpha, IFN-gamma and IL-2 were usually absent in glomeruli. Mesangial expansion in this disorder was accompanied by an increased expression of PDGF, PDGF beta-R, TGF-beta and IL-6 in mesangial areas. In both conditions a good correlation was observed between cytokine expression at the mRNA (in situ hybridization) and protein level (immunocytochemistry). (ABSTRACT TRUNCATED AT 250 WORDS)

Publication Types:

- [Review](#)
- [Review, Tutorial](#)

PMID: 8398664 [PubMed - indexed for MEDLINE]



Estrogen regulation of the cytochrome P450 3A subfamily in humans.

Williams ET, Leyk M, Wrighton SA, Davies PJ, Loose DS, Shipley GL, Strobel HW.

Department of Biochemistry, Medical School, University of Texas Health Science Center at Houston, 6431 Fannin, MSB 6.200, Houston, TX 77030, USA.

This study examines the possible role of estrogen in regulating the expression of the human CYP3A subfamily: CYP3A4, CYP3A5, CYP3A7, and CYP3A43. To accomplish this goal, mRNA was quantified from human livers and endometrial samples, and total CYP3A protein levels were evaluated by Western immunoblot analysis of the liver samples. The human endometrial samples were from premenopausal and postmenopausal women. The premenopausal endometrium was either in the proliferative or secretory phase, whereas for the postmenopausal endometrium samples, the women had been treated with either a placebo or estropipate, an estrogen substitute. After analyses, CYP3A4 mRNA was shown to have lower hepatic expression in females than in males. In the endometrium, CYP3A4 and CYP3A43 are down-regulated by estrogen, whereas CYP3A5 is expressed at higher levels during the secretory phase. CYP3A7 was not detected in the endometrium. In addition, the CYP3A subfamily showed increased mRNA expression in the liver as age increased. The expression levels of total CYP3A protein and total CYP3A mRNA showed good correlation. Despite apparent regulation of CYP3A4 mRNA expression by estrogen, the effects of estrogen may be overshadowed by additional regulators of gene expression.

PMID: 15282264 [PubMed - indexed for MEDLINE]

Expression of superoxide dismutases, catalase, and glutathione peroxidase in glioma cells.

Zhong W, Yan T, Lim R, Oberley LW.

Radiation Research Laboratory, Department of Radiology, The University of Iowa, Iowa City 52242, USA.

Four primary antioxidant enzymes were measured in both human and rat glioma cells. Both manganese-containing superoxide dismutase (MnSOD) and copper-zinc-containing superoxide dismutase (CuZnSOD) activities varied greatly among the different glioma cell lines. MnSOD was generally higher in human glioma cells than in rat glioma cells and relatively higher than in other tumor types. High levels of MnSOD in human glioma cells were due to the high levels of expression of MnSOD mRNA and protein. Heterogeneous expression of MnSOD was present in individual glioma cell lines and may be due to subpopulations or cells at different differentiation stages. Less difference in CuZnSOD, catalase, or glutathione peroxidase was found between human and rat glioma cells. The human glioma cell lines showed large differences in sensitivity to the glutathione modulating drugs 1,3-bis (2-chloroethyl)-1-nitrosourea (BCNU) and buthionine sulfoximine (BSO). A good correlation was found between sensitivity to BCNU and the activities of catalase in these cell lines. Only one cell line was sensitive to BSO and this line had low CuZnSOD activity.

PMID: 10641728 [PubMed - indexed for MEDLINE]



Somatostatin receptors in primary human breast cancer: quantitative analysis of mRNA for subtypes 1--5 and correlation with receptor protein expression and tumor pathology.

Kumar U, Grigorakis SI, Watt HL, Sasi R, Snell L, Watson P, Chaudhari S.

Fraser Laboratories For Diabetes Research, Department of Medicine, McGill University, Royal Victoria Hospital, 687 Pine Avenue West, H3A 1A1 Montreal, Quebec, Canada. ujendra.kumar@muhc.mcgill.ca

Somatostatin receptors (SSTRs) have been identified in most hormone-producing tumors as well as in breast cancer. In the present study, we determined SSTR1-5 expression in primary ductal NOS breast tumors through semi-quantitative RT-PCR and immunocytochemistry. The results from the analysis of 98 samples were correlated with several key histological markers and receptor expression. All five SSTR subtypes are variably expressed at the mRNA level in breast tumors with 91% of samples showing SSTR1, 98% SSTR2, 96% SSTR3, 76% SSTR4, and 54% SSTR5. SSTR1-5 are localized to both tumor cells and the surrounding peritumoral regions as detected by immunocytochemistry. Levels of SSTR mRNA, when corrected for beta-actin levels, were highest for SSTR3 followed by SSTR1, SSTR2, SSTR5, and SSTR4. Furthermore, there was good correlation between mRNA and protein expression with 84% for SSTR1, 79% for SSTR2, 89% for SSTR3, 68% for SSTR4, 68% for SSTR5, and 78% for all five receptors. SSTR1, 2 and 4 were correlated with ER levels whereas SSTR2 showed an additional correlation with PR levels. These correlations were independent of patient age and histological grade. Moreover, using immunocytochemistry, blood vessels exhibited receptor-specific localization for SSTR2 and SSTR5. Our results indicate significant correlations between mRNA and protein expression along with receptor-specific distribution of SSTR subtypes in tumors and receptor-specific expression in vascular structures may be considered as a novel diagnosis for breast tumors with receptor subtype agonists.

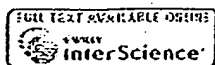
Publication Types:

- Evaluation Studies

PMID: 15986128 [PubMed - indexed for MEDLINE]

Erratum in:

- Int J Cancer 2002 Feb 20;97(6):878.



Immunohistochemical analysis of NY-ESO-1 antigen expression in normal and malignant human tissues.

Jungbluth AA, Chen YT, Stockert E, Busam KJ, Kolb D, Iversen K, Coplan K, Williamson B, Altorki N, Old LJ.

Ludwig Institute for Cancer Research, Memorial Sloan-Kettering Cancer Center, New York, NY, USA. jungblua@mskcc.org

NY-ESO-1, a member of the CT (cancer/testis) family of antigens, is expressed in normal testis and in a range of human tumor types. Knowledge of NY-ESO-1 expression has depended on RT-PCR detection of mRNA and there is a need for detecting NY-ESO-1 at the protein level. In the present study, a method for the immunochemical detection of NY-ESO-1 in paraffin-embedded tissues has been developed and used to define the expression pattern of NY-ESO-1 in normal tissues and in a panel of human tumors. No normal tissue other than testis showed NY-ESO-1 reactivity, and expression in testis was restricted to germ cells particularly spermatogonia. In human tumors, the frequency of NY-ESO-1 antigen expression corresponds with past analysis of NY-ESO-1 mRNA expression e.g., 20-30% of lung cancers, bladder cancers and melanoma, and no expression in colon and renal cancer. Co-typing of NY-ESO-1 antigen and mRNA expression in a large panel of lung cancers showed a good correlation. There is great variability in NY-ESO-1 expression in individual tumors, ranging from an infrequent homogeneous pattern of staining to highly heterogeneous antigen expression. Copyright 2001 Wiley-Liss, Inc.

PMID: 11351307 [PubMed - indexed for MEDLINE]

187: Am J Physiol Cell Physiol. 2001 Oct;281(4):C1396-402.

Related Articles, Links



Modulation of glucagon receptor expression and response in transfected human embryonic kidney cells.

Ikegami T, Cypess AM, Bouscarel B.

Department of Medicine, George Washington University Medical Center, Washington, District of Columbia 20037, USA.

The modulation of glucagon receptor (GR) expression and biological response was investigated in human embryonic kidney cell (HEK-293) clones permanently expressing the GR with different densities. The GR mRNA expression level in these clones was upregulated by cellular cAMP accumulation and presented a good correlation with both the protein expression level and the maximum number of glucagon binding sites. However, the determination of glucagon-induced cAMP accumulation in these cell lines revealed that the enhancement of receptor expression did not lead to a proportional increase in cAMP formation. Under these conditions, the maximum cAMP production induced by NaF and forskolin was not significantly different among selected clones, regardless of the receptor expression level. High receptor-expressing clones showed the greatest susceptibility for agonist-induced desensitization compared with clones with lower GR expression levels. The results of the present study suggest that the GR can recruit non-GR-specific desensitization mechanism(s). Furthermore, the partial inhibition or alteration of the overall cAMP synthesis pathway at the receptor level may be a necessary adaptive step for a cell in response to a massive increase in membrane receptor expression level.

PMID: 11546678 [PubMed - indexed for MEDLINE]



Modulation of the glutamatergic receptors.(AMPA and NMDA) and of glutamate vesicular transporter 2 in the rat facial nucleus after axotomy.

Eleore L, Vassias I, Vidal PP, de Waele C.

LNRS (CNRS-Paris V), ESA 7060, Centre Universitaire des Saints-Peres, 45 rue des Saints-Peres, 75270 Paris Cedex 06, France.

Facial nerve axotomy is a good model for studying neuronal plasticity and regeneration in the peripheral nervous system. We investigated in the rat the effect of axotomy on the different subunits of excitatory glutamatergic AMPA (GLuR1-4), NMDA (NR1, NR2A-D) receptors, post-synaptic density 95, vesicular glutamate transporter 2, beta catenin and cadherin. mRNA levels and/or protein production were analyzed 1, 3, 8, 30 and 60 days after facial nerve axotomy by in situ hybridization and immunohistofluorescence. mRNAs coding for the GLuR2-4, NR1, NR2A, B, D subunits of glutamatergic receptors and for post-synaptic density 95, were less abundant after axotomy. The decrease began as early as 1 or 3 days after axotomy; the mRNAs levels were lowest 8 days post-lesion, and returned to normal or near normal 60 days after the lesion. The NR2C subunit mRNAs were not detected in either lesioned or intact facial nuclei.

Immunohistochemistry using specific antibodies against GLuR2-3 subunits and against NR1 confirmed this down-regulation. There was also a large decrease in vesicular glutamate transporter 2 immunostaining in the axotomized facial nuclei at early stages following facial nerve section. In contrast, no decrease of NR2A subunit and of post-synaptic density 95 could be detected at any time following the lesion. beta Catenin and cadherin immunoreactivity pattern changed around the cell body of facial motoneuron by day 3 after axotomy, and then, tends to recover at day post-lesion 60 days. Therefore, our results suggest a high correlation between restoration of nerve/muscle synaptic contact, synaptic structure and function in facial nuclei. To investigate the mechanisms involved in the change of expression of these proteins following axotomy, the facial nerve was perfused with tetrodotoxin for 8 days. The blockade of action potential significantly decreased GLuR2-3, NR1 and NR2A mRNAs in the ipsilateral facial nuclei. Thus, axotomy-induced changes in mRNA abundance seemed to depend partly on disruption of activity.

PMID: 16182453 [PubMed - in process]

FREE full text article at
bjophth.bmjjournals.com

Intravitreal invading cells contribute to vitreal cytokine milieu in proliferative vitreoretinopathy.

El-Ghrably IA, Dua HS, Orr GM, Fischer D, Tighe PJ.

Larry A Donoso Laboratory for Eye Research, Department of Ophthalmology, University of Nottingham, UK.

AIM: To examine the contribution of infiltrating cells in the local production of cytokines within the vitreous of patients with proliferative vitreoretinopathy (PVR). **METHODS:** The presence of mRNA coding for IL-6, IL-8, IL-1beta, IL-1alpha, TNFalpha, IFNgamma, IL-12, and HPRT was investigated in 25 vitreous samples from patients with PVR, 11 vitreous samples from patients with retinal detachment (RD) not complicated by PVR, and 10 vitreous samples from patients with macular hole (MH). A quantitative reverse transcriptase polymerase chain reaction (RT-PCR) using an internal competitor was used to investigate these samples. From these samples, 15 PVR, 8 RD, and 8 MH were analysed for the protein levels of the same cytokines using enzyme linked immunosorbent assay (ELISA). Spearman correlation was used to test any association between mRNA and cytokine protein levels as an indicator of the contribution these cells make to the intravitreal cytokine milieu. **RESULTS:** A strong correlation was found between mRNA and their respective cytokine levels (protein products) for IL-6, IL-8, IL-1beta, IL-1alpha, TNFalpha, IFNgamma (Spearman $r = 0.83, 0.73, 0.67, 0.91, 0.73,$ and 0.73 respectively), but not for IL-12. The median levels of IL-6, IL-8, IL-1beta, and IFNgamma mRNA and their respective cytokines were significantly higher ($p < 0.05$) in patients with PVR than in those with macular hole. There was no statistically significant difference in the median levels of IL-1alpha mRNA between PVR and MH but the cytokine IL-1alpha was detected at a significantly higher level in PVR compared with MH patients. Between PVR and RD patients, there was no statistically significant difference in mRNA levels for all the investigated cytokines ($p > 0.05$) except for IL-6 where there was a statistical significance ($p = 0.038$). In contrast, the median levels of IL-6, IL-8, and IL-1beta cytokines were significantly higher ($p < 0.05$) in patients with PVR than in those with RD, whereas for IL-1alpha and IFNgamma no significant statistical difference was detected between PVR and RD patients ($p > 0.05$). When results of RD and MH patients were compared, a statistical difference was only detected in mRNA levels of IFNgamma ($p = 0.008$). However, no difference was detected for IFNgamma (protein product) or for any of the other cytokines between RD and MH patients. **CONCLUSION:** Levels of both protein and mRNA encoding IL-6, IL-8, IL-1beta, and IFNgamma is significantly increased in vitreous samples from patients with PVR. The strong correlation between ELISA detectable cytokines (protein products) and their respective mRNA levels suggest that intravitreal, invasive cells are the major source of these cytokines, with the exception of IL-12. Cells invading the vitreous do not appear to locally produce IL-12 mRNA. This would appear to implicate cells peripheral to the

vitreal mass as the major source of this cytokine.

PMID: 11264138 [PubMed - indexed for MEDLINE]



Pre-translational regulation of cytochrome P450 genes is responsible for disease-specific changes of individual P450 enzymes among patients with cirrhosis.

George J. Liddle C, Murray M, Byth K, Farrell GC.

Department of Gastroenterology and Hepatology, University of Sydney at Westmead Hospital, NSW, Australia.

We have recently reported that disease-specific differential alterations in the hepatic expression of xenobiotic-metabolizing cytochrome P450 (CYP P450) enzymes occur in patients with advanced liver disease. In order to determine whether the observed changes in CYP proteins are modulated at pre- or post-translational levels, we have now examined the hepatic levels of mRNA for CYPs 1A2, 2C9, 2E1 and 3A4 by solution hybridization in the same livers of 20 controls (surgical waste from histologically normal livers), 32 cases of hepatocellular and 18 of cholestatic severe chronic liver disease. CYP1A2 mRNA and CYP1A immunoreactive protein were both reduced in livers with hepatocellular and cholestatic types of cirrhosis. In contrast, CYP3A4 mRNA and protein were reduced only in livers from patients with hepatocellular diseases. For 1A2 and 3A4 there were significant correlations between mRNA species and the respective protein contents ($r_{S1A2} = 0.74$, $r_{S3A4} = 0.64$, $P < 0.0001$). CYP2C9 mRNA was reduced in patients with both cholestatic and hepatocellular types of liver disease, but 2C protein was reduced only in patients with cholestatic dysfunction. The correlation between CYP2C9 mRNA and protein, was also significant ($r_s = 0.36$, $P < 0.005$) but mRNA levels accounted for only 13% of the variability in protein rankings. This is probably a consequence of other CYP2C proteins apart from 2C9 being detected by the anti-2C antibody. CYP2E1 mRNA and protein were reduced in patients with cholestatic liver disease, but in hepatocellular disease the expression of only CYP2E1 mRNA was decreased. CYP2E1 mRNA was significantly correlated with CYP2E1 protein but accounted for only 18% of the variability in protein rankings ($r_s = 0.43$, $P < 0.0005$). Taken collectively these data indicate that the disease-specific alterations of xenobiotic-metabolizing CYP enzymes among patients with cirrhosis is due, at least in part, to pre-translational mechanisms. The lack of a strong correlation between CYP2E1 mRNA and protein suggests that this gene, like its rat orthologue, may be subject to pre-translational as well as translational and/or post-translational regulation.

PMID: 7741759 [PubMed - indexed for MEDLINE]

FREE full text article at
clincancerres.aacrjournals.org

Thymidine kinase, thymidylate synthase, and dihydropyrimidine dehydrogenase profiles of cell lines of the National Cancer Institute's Anticancer Drug Screen.

Grem JL, Danenberg KD, Behan K, Parr A, Young L, Danenberg PV, Nguyen D, Drake J, Monks A, Allegra CJ.

Developmental Therapeutics Department, Medicine Branch, Division of Clinical Sciences, National Cancer Institute at the National Naval Medical Center, Bethesda, Maryland 20889, USA.

PURPOSE: To determine the expression of three targets of 5-fluorouracil (5-FU) and 5-fluoro-2'-deoxyuridine (FdUrd) in human tumor cell lines and to compare these with the 50% growth inhibition concentrations (GI(50)) from the National Cancer Institute database. **EXPERIMENTAL DESIGN:** Thymidine kinase (TK) activity was assessed by conversion of [(3)H]thymidine to [(3)H]TMP. Thymidylate synthase (TS) protein expression was determined by Western analysis. TS and dihydropyrimidine dehydrogenase (DPD) mRNA expression were measured by quantitative reverse transcription-PCR. **RESULTS:** The median (range) for the targets were as follows: 5-FU GI(50), 20.8 microM (0.8-536); FdUrd GI(50), 0.75 microM (0.25-237); TK, 0.93 nmol/min/mg (0.16-5.7); in arbitrary units: TS protein, 0.41 (0.05-2.95); TS mRNA, 1.05 (0.12-6.41); and DPD mRNA, 1.09 (0.00-24.4). A moderately strong correlation was noted between 5-FU and FdUrd GI(50)s ($r = 0.60$), whereas a weak-moderate correlation was seen between TS mRNA and protein expression ($r = 0.45$). Neither TS expression nor TK activity correlated with 5-FU or FdUrd GI(50)s, whereas lines with lower DPD expression tended to be more sensitive to 5-FU. Cell lines with faster doubling times and wild-type p53 were significantly more sensitive to 5-FU and FDURD. **CONCLUSIONS:** The lack of correlation may in part be attributable to the influence of downstream factors such as p53, the observation that the more sensitive cell lines with faster doubling times also had higher TS levels, and the standard procedure of the screen that uses a relatively short (48-h) drug exposure.

PMID: 11309351 [PubMed - indexed for MEDLINE]

349: Arch Biochem Biophys. 1997 Jan 15;337(2):275-83.

ELSEVIER

Related Articles, Links

Human hepatic microsomal epoxide hydrolase: comparative analysis of polymorphic expression.

Hassett C, Lin J, Carty CL, Laurenzana EM, Omiecinski CJ.

Department of Environmental Health, University of Washington, Seattle 98105-6099, USA.

Interindividual variation in the expression of human microsomal epoxide hydrolase (mEH) may be an important risk factor for chemically induced toxicities, including cancer and teratogenesis. In this study, phenotypic variability and mEH genetic polymorphisms were examined in a bank of 40 transplant-quality human liver samples. Immunochemically determined protein content, enzymatic activities, polymorphic amino acids, as well as mEH RNA levels were evaluated in parallel. Enzymatic activity was assessed using (+/-)-benzo[a]pyrene-4,5-epoxide at 2 substrate concentrations. The relative hydrolyzing activities obtained using saturating substrate levels were highly correlated ($r = 0.85$) with results derived from limiting substrate concentrations and exhibit approximately an 8-fold range in activity levels across the panel of 40 liver samples. mEH enzyme activity also demonstrated strong correlation ($r > \text{or} = 0.74$) with an 8.4-fold variation determined for mEH protein content within the same samples. However, these protein/activity measurements were poorly correlated ($r < \text{or} = 0.23$) with mEH RNA levels, which exhibited a 49-fold variation. Two common polymorphic amino acid loci in the mEH protein did not exclusively account for variation in enzymatic activity, although this conclusion is confounded by heterozygosity in the samples. These data demonstrate the extent of hepatic mEH functional variability in well-preserved human tissues and suggest that polymorphism of mEH protein expression is regulated in part by posttranscriptional controls, which may include nonstructural regulatory regions of the mEH transcript.

PMID: 9016823 [PubMed - indexed for MEDLINE]

High-level mRNA quantification of proliferation marker pKi-67 is correlated with favorable prognosis in colorectal carcinoma.

Ihmann T, Liu J, Schwabe W, Hausler P, Behnke D, Bruch HP, Broll R, Windhovel U, Duchrow M.

St. Elisabeth Klinik, Klinik für Anesthesiologie, Schmerztherapie und Intensivmedizin, Saarlouis, Germany.

PURPOSE: The present study retrospectively examines the expression of pKi-67 mRNA and protein in colorectal carcinoma and their correlation to the outcome of patients. **METHODS:** Immunohistochemistry and quantitative RT-PCR were used to analyze the expression of pKi-67 in 43 archival specimens of patients with curatively resected primary colorectal carcinoma, who were not treated with neo-adjuvant therapy. **RESULTS:** We determined a median pKi-67 (MIB-1) labeling index of 31.3% (range 10.3-66.4%), and a mean mRNA level of 0.1769 (DeltaC(T): range 0.01-0.69); indices and levels did not correlate. High pKi-67 mRNA DeltaC(T) values were associated with a significantly favorable prognosis, while pKi-67 labeling indices were not correlated to prognostic outcome. A multivariate analysis of clinical and biological factors indicated that tumor stage (UICC) and pKi-67 mRNA expression level were independent prognostic factors. **CONCLUSION:** Quantitatively determined pKi-67 mRNA can be a good and new prognostic indicator for primary resected colorectal carcinoma.

Publication Types:

- Evaluation Studies

PMID: 15449182 [PubMed - indexed for MEDLINE]

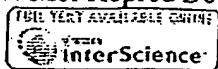
Cellular location and age-dependent changes of the regulatory subunits of cAMP-dependent protein kinase in rat testis.

Landmark BF, Oyen O, Skalhegg BS, Fauske B, Jahnsen T, Hansson V.

Institute of Medical Biochemistry, University of Oslo, Norway.

This study was undertaken to examine the expression and cellular location of the various cAMP-dependent protein kinase (PKA) subunits in different testicular cell types, using cDNA probes, isoenzyme-specific antibodies and activity measurements. Amounts of mRNA and protein were examined in cultured Sertoli cells, cultured peritubular cells, germ cells (pachytene spermatocytes, round spermatids), Leydig cell tumours as well as whole testes from rats of various ages. In Sertoli cells, there was a good correlation between the amount of mRNA and the respective immunoreactive proteins. In other types of cell, such as germ cells and Leydig tumour cells, this was not always the case. Large amounts of RII beta mRNA were found in Leydig tumour cells, whereas the amount of immunoreactive protein was low. Furthermore, large amounts of small-sized, germ cell-specific mRNAs for RI alpha (1.7 kb) and RII alpha (2.2 kb) were also found in the developing rat testis after 30 to 40 days of age, but the large amounts of mRNA were only partially reflected at the protein level. Pachytene spermatocytes and round spermatids were practically devoid of both RII alpha and RII beta protein. During spermatid differentiation, there was a decrease in RI alpha and an increase in RII alpha protein. Cell specific distribution of the various PKA subunits in testicular cell types is described. In some types of cell, discrepancies between mRNA and protein were demonstrated, which clearly suggest cell specific differences in translational efficiencies for some of these mRNAs, particularly the small-sized mRNAs for RI alpha and RII alpha in meiotic and post-meiotic germ cells.

PMID: 8107013 [PubMed - indexed for MEDLINE]



c-fos and estrogen receptor gene expression pattern in the rat uterine epithelium during the estrous cycle.

Mendoza-Rodriguez CA, Merchant-Larios H, Segura-Valdez ML, Moreno-Mendoza N, Cruz ME, Arteaga-Lopez P, Camacho-Arroyo I, Dominguez R, Cerbon M.

Facultad de Quimica, Universidad Nacional Autonoma de Mexico, Ciudad Universitaria, Coyoacan 04510, Mexico, D.F., Mexico.

Different studies in ovariectomized estrogen treated animals support the idea that c-fos plays a role in the proliferation of uterine epithelial cells. However, these studies invite us to reassess the role played by c-fos in epithelial cell types of the endometrium during the estrous cycle. The present study was undertaken to determine the c-fos and estrogen receptor (ER) gene expression pattern in the rat uterine epithelium during the estrous cycle in which natural and cyclic changes of steroid hormones occur, and correlate these changes with the proliferation status of this cellular types. Proliferation was assessed during the estrous cycle using bromodeoxyuridine incorporation to DNA. ERalpha and beta proteins were assessed by immunohistochemistry. The regulation of c-fos gene expression in the uterus of intact animals during the estrous cycle was evaluated using both in situ hybridization and immunohistochemistry. Estradiol (E(2)) and progesterone (P(4)) plasma levels were assessed by radioimmunoassay. The results indicated that luminal (LE) and glandular epithelia (GE) presented maximal proliferation during the metestrus (M) and the diestrus (D) days. However, during the proestrus (P) day only LE presented proliferation, and during the estrus (E) day only the stromal cells proliferated. A marked immunostaining for ERalpha was detected in both LE and GE cells during the early phases of the cycle but diminished on the P and the E day. In contrast, ERbeta was undetectable in both epithelia during all stages of the cycle. The highest c-fos mRNA level was detected in both epithelia on the M day, followed by a significant reduction during the other days of the cycle. The highest protein content was observed on the M and D days, and the minimal value was detected on the E day. The c-Fos protein level in LE was increased during M and D days, presenting a high correlation with the cellular proliferation pattern of this cell type. In conclusion, the overall results indicate that c-Fos protein presented a good correlation with uterine epithelial cell proliferation of LE. In the case of GE, the same tendency was observed, although no significant correlation was found. Both in LE and GE, c-fos mRNA did not strictly correlate with its protein levels. c-fos seems to have a postranscriptional regulation in uterine epithelial cells during the rat's estrous cycle. Copyright 2003 Wiley-Liss, Inc.

PMID: 12589649 [PubMed - indexed for MEDLINE]

401: Biochem Biophys Res Commun. 1995 Sep 25;214(3):1009-14.

[Related Articles, Links](#)

ELSEVIER
JOURNAL

Differential expression of heat shock protein 70 in well healing and chronic human wound tissue.

Oberringer M, Baum HP, Jung V, Welter C, Frank J, Kuhlmann M, Mutschler W, Hanselmann RG.

Department of Traumatology, University of Saarland, Germany.

Heat shock protein 70 (hsp 70) is an important member of the heat shock protein family, which is induced by different forms of stress. We attempted to find out if hsp 70 is also involved in wound healing, which likewise resembles a stress situation for cells too. Therefore we collected tissue samples from well healing and chronic human wound tissue. We used Northern- and Western-blot analysis to study the expression of hsp 70. At the protein level we found a strong correlation between well healing wounds and high expression of hsp 70, whereas chronic wounds showed no or weak expression. Interestingly hsp 70 mRNA did not show this significant correlation, displaying a variant expression pattern in the same kind of wound tissue, possibly due to unknown posttranscriptional regulating step, which has to be investigated in further studies. To localize hsp 70 mRNA and protein was used insitu hybridization and immunohistochemistry. Both displayed an overexpression in endothelial cells of capillary vessels.

Cell localization and regulation of expression of cytochrome P450 1A1 and 2B1 in rat lung after induction with 3-methylcholanthrene using mRNA hybridization and immunohistochemistry.

Pairon JC, Trabelsi N, Buard A, Fleury-Feith J, Bachelet CM, Poron E, Beaune P, Brochard P, Laurent P.

INSERM Unite 139, Hopital Henri Mondor, Creteil, France.

In order to characterize the response of various pulmonary cell types to polycyclic aromatic hydrocarbons, the expression of cytochrome P450 (CYP) 1A1 and 2B1 mRNA in the lung of rats, with or without induction by 3-methylcholanthrene (3MC), was analyzed by in situ hybridization using appropriate 35S-labeled riboprobes. The expression of the corresponding proteins was investigated immunohistochemically. Following induction with 3MC, the kinetics of mRNA expression differed considerably between Clara cells and type II pneumocytes and venous endothelial cells. In Clara cells, mRNA expression was detected as early as 1 h after induction, peaked between 2 and 4 h, and was completely undetectable at 14 h. In contrast, venous endothelial cells and type II pneumocytes exhibited permanent mRNA expression of CYP 1A1 in 3MC-pretreated rats. These kinetic results explain the striking absence of correlation between mRNA and protein expression observed in Clara cells 24 h after the end of the induction protocol, as these cells exhibited intense protein expression with no mRNA. In contrast, a good correlation was observed for mRNA and protein expression of CYP 2B1, with similar expressions for Clara cells and type II pneumocytes, but no expression in endothelial cells. This study clearly distinguished the regulation of CYP 1A1 expression in the rat lung from that described in the liver. The differences observed in the various lung cell types, whatever the post-transcriptional mechanisms involved, emphasize that studies must be performed at the cellular level in order to understand the specific response to xenobiotics, not only of this organ as a whole but also of its various anatomic structures.

PMID: 7917307 [PubMed - indexed for MEDLINE]



VASCULAR ENDOTHELIAL GROWTH FACTOR EXPRESSION CORRELATES WITH MATRIX METALLOPROTEINASES MT1-MMP, MMP-2 AND MMP-9 IN HUMAN GLIOBLASTOMAS

Carine MUNAUT¹, Agnès NOËL¹, Olivier HOUGRAND², Jean-Michel FORDART¹, Jacques BONIVER² and Manuel DEPREZ^{2*}

¹Laboratory of Tumour and Development Biology, University of Liège, Liège, Belgium

²Laboratory of Neuropathology, University of Liège, Liège, Belgium

Vascular endothelial growth factor (VEGF) is the major endothelial mitogen in central nervous system neoplasms and it is expressed in 64–95% of glioblastomas (GBMs). Tumour cells are the main source of VEGF in GBMs whereas VEGF receptors (VEGFR-1, its soluble form sVEGFR-1, VEGFR-2 and neuropilin-1) are expressed predominantly by endothelial cells. Infiltrating tumour cells and newly-formed capillaries progress through the extracellular matrix by local proteolysis involving matrix metalloproteinases (MMPs). Recent studies have shown that VEGF expression and bioavailability can be modulated by MMPs. We reported previously that the expression of MT1-MMP in human breast cancer cells was associated with an enhanced VEGF expression. We used quantitative RT-PCR, Western blot, gelatin zymography and immunohistochemistry to study the expression of VEGF, VEGFR-1, VEGFR-2, sVEGFR-1, neuropilin-1, MT1-MMP, MMP-2, MMP-9 and TIMP-2 in 20 human GBMs and 5 normal brains. The expression of these MMPs was markedly increased in most GBMs with excellent correlation between mRNA and protein levels; activated forms of MMP-2 and MMP-9 were present in 8/18 and 7/18 of GBMs. A majority of GBMs (17/20) also expressed high levels of VEGF, as previously reported, with strong correlation between VEGF and MT1-MMP gene expression levels, and double immunostaining showed that VEGF and MT1-MMP peptides co-localize in tumour and endothelial cells. Our results suggest that the interplay between metalloproteinases and VEGF previously described in experimental tumours may also be operative in human GBMs. Because of its dual ability to activate MMP-2 and to up-regulate VEGF, MT1-MMP might be of central importance in the growth of GBMs and represent an interesting target for anti-cancer treatments.

© 2003 Wiley-Liss, Inc.

Key words: VEGF; MMPs; glioblastomas; brain; tumor

Angiogenesis is critical for the development of normal tissue and solid tumours. This process includes the degradation of the extracellular matrix (ECM) and the proliferation, migration and differentiation of endothelial cells, and is finely regulated by inhibitory and promoting factors.^{1,2} Among positive factors, vascular endothelial growth factor (VEGF) has been proposed as the major endothelial mitogen in central nervous system (CNS) neoplasms.³ Strong VEGF expression has been detected by immunohistochemistry in 64–95% of glioblastomas (GBMs).^{4–6} GBMs are the most common malignant primitive tumours of the CNS in adults.⁷ Microvascular proliferation is characteristic of these tumours and is an essential WHO diagnostic criteria.⁷ Tumour cells are the main source of VEGF in GBMs whereas VEGF receptors are predominantly expressed by endothelial cells.^{8,9} These receptors differ both in terms of affinity and transduction signaling.^{10–12} VEGFR-1 (flt-1) and VEGFR-2 (flk/KDR) belong to the Class II tyrosine-kinase receptor family. VEGFR-1 has a soluble isoform (sVEGFR-1) that modulates VEGF availability.^{8,13} Neuropilin-1 (NRP1) is a co-receptor for VEGF that increases by 10-fold the affinity of the VEGF₁₆₅ isoform for VEGFR-2.¹⁴ NRP1 is thought to modulate VEGF-mediated tumour angiogenesis in human malignant astrocytomas.¹⁰ The coordinated up-regulation of VEGF and its receptors appears as a critical event in the control of angiogenesis.^{8,12}

Infiltrating tumour cells and newly-formed capillaries progress through the ECM by local proteolysis involving matrix metalloproteinases (MMPs).^{15,16} MMPs are proteolytic enzymes that are synthesized as inactive zymogens. Their activation requires the removal of a propeptide by proteinase cleavage and can be inhibited by various tissue inhibitors of MMPs (TIMPs). Most MMPs are secreted as soluble enzymes but a subset of them are inserted in the cell membrane by a transmembrane domain or by a glycosylphosphatidylinositol anchor and are classified as membrane-type MMPs (MT-MMPs).^{17,18} In cultured tumour cells, MT-MMPs tend to accumulate on the cytoplasmic membrane of invadopodia where they selectively mediate local pericellular proteolysis. GBMs express high levels of MT1-MMP, MMP-2 and MMP-9.^{19,20} Among these MMPs, MT1-MMP might play a central role in the remodeling of the ECM as this membrane-bound protease is able to activate MMP-2 and MMP-13.^{21,22} Moreover, MT1-MMP has been shown to promote cell migration in various carcinoma cell lines by its ability to cleave laminin-5, a major constituent of basement membrane,^{23,24} and through the processing of CD44H (the major receptor for hyaluronan)²⁵ and of $\alpha_5\beta_1$ integrin.²⁶

MT1-MMP is involved in both developmental and tumour angiogenesis.²⁷ MT1-MMP overexpression in human melanoma cells has been associated with enhanced *in vitro* invasion and increased *in vivo* tumour growth and vascularization.²⁸ We have shown previously that in MCF-7 breast cancer cells, VEGF transcription is upregulated when MT1-MMP is overexpressed.²⁹ Up-regulation of VEGF by MT1-MMP has also been reported in a model of human glioma xenograft by Deryugina *et al.*³⁰ These experimental data suggest a link between MT1-MMP and the VEGF network. We have tested for the presence of such a link in human glioblastomas. We compared the expression of VEGF and its receptors (VEGFR-1, sVEGFR-1, VEGFR-2, NRP1) with

Grant sponsor: Communauté Française de Belgique (Actions de Recherches Concertées); Grant sponsor: Commission of European Communities; Grant sponsor: Fonds de la Recherche Scientifique Médicale; Grant sponsor: Fonds National de la Recherche Scientifique (FNRS, Belgium); Grant sponsor: Fédération Belge Contre le Cancer; Grant sponsor: Fonds Spéciaux de la Recherche (University of Liège); Grant sponsor: Centre Anticancéreux près l'Université de Liège; Grant sponsor: FB Assurances; Grant sponsor: Fondation Léon Frédéricq (University of Liège); Grant sponsor: D.G.T.R.E. from the "Région Wallonne"; Grant sponsor: Fonds d'Investissements de la Recherche Scientifique (CHU, Liège, Belgium); Grant sponsor: Federal Office for Scientific, Technical and Cultural Affairs (Brussels, Belgium).

*Correspondence to: Laboratory of Neuropathology, Tower of Pathology B23/1, B-4000 Sart Tilman (Liège), Belgium. Fax: +32-4-3662919. E-mail: Manuel.Deprez@ulg.ac.be

Received 23 October 2002; Revised 12 March 2003; Accepted 27 April 2003

DOI 10.1002/ijc.11313
Published online 26 June 2003 in Wiley InterScience (www.interscience.wiley.com).

This material may be protected by Copyright law (Title 17 U.S. Code)

MT1-MMP, MMP-2, MMP-9 and TIMP-2 in a series of 20 GBMs and 5 normal brains. Using quantitative RT-PCR, gelatin zymography, Western blot and immunohistochemistry, we showed a strong correlation between the expression of VEGF, MT1-MMP, MMP-2 and MMP-9 in GBMs. These results are in accordance with previous *in vitro* studies and add to the evidence of an interplay between VEGF and MMPs in the progression of human GBMs.

MATERIAL AND METHODS

Patients

We studied 20 GBMs diagnosed at the Laboratory of Neuropathology-CHU Liège between 1997 and 2001. The series included 17 primary GBMs (*i.e.*, no previous history of lower grade diffuse astrocytoma) and 3 secondary GBMs (*i.e.*, previous history of lower grade diffuse astrocytoma). Clinical information on these 20 cases have been reported previously as part of a larger series.³¹ The gender ratio was 1/1, and the age at time of diagnosis ranged from 41–79 years (mean 56 years). Normal brain cortex and white matter were obtained from 5 patients with intractable epilepsy treated by partial temporal lobectomy. Histological examination of these specimens showed severe hippocampal sclerosis; frozen tissue was sampled from microscopically normal inferior temporal gyri. Our study was approved by the Ethical Committee of the Faculty of Medicine of the University of Liège.

RNA extraction and cDNA synthesis

Total RNA was extracted from cryosections with RNeasy Mini Kit (QIAGEN GmbH, Hilden, Germany) according to the manufacturer's protocol. Total RNA (1 µg) was reverse transcribed with a ThermoScript reverse transcriptase (ThermoScript RT-PCR System, Invitrogen, Carlsbad, CA) and random hexamers as primers.

Primers

Primers pairs used in our study are described in Table 1. Primers for the VEGF gene were chosen to distinguish between VEGF₁₈₉, VEGF₁₆₅, VEGF₁₄₅ and VEGF₁₂₁ mRNA isoforms. Intron-spanning primers and probes for the TaqMan system (primers for VEGFR-1 (Flt-1), sVEGFR-1, VEGFR-2 (KDR/Flk-1) and NRPI) were designed to meet specific criteria by using Primer Express software (Perkin Elmer, Foster City, CA). All primers were synthesized by Eurogentec (Liège, Belgium). The 5'- and 3'-end nucleotides of the probe were labeled with a reporter (FAM = 6-carboxy-fluorescein) and a quencher dye (TAMRA = 6-carboxy-tetramethylrhodamine). We conducted BLASTn (National Center for Biotechnology Information, Bethesda) searches against dbEST and the non redundant set of GenBank, EMBL, and DDBJ database sequences to confirm the total gene specificity of the nucleotide sequences chosen for the primers. The specificity of the amplified PCR products was confirmed either by restriction digest or by sequencing. The 18S ribosomal RNA was measured using the Pre-Developed TaqMan Assay Reagents Endogenous control kit from Applied Biosystems (Foster City, CA).

TABLE 1—SEQUENCE OF PRIMERS AND TaqMan PROBES USED FOR RT-PCR STUDIES

Gene and accession number	Position	Sequence	Size	Cycles
MMP-2 FP	1740F	5'-AGATCTTCTTCTCAAGGACCGTT-3'	225 bp	33
MMP-2-RP NM_004530	1964R	5'-GGCTGGTCAGTGGCTTGGGGTA-3'		
MMP-9-FP	1592F	5'-GCGGAGATTGGGAACCACTGTA-3'	208 bp	37
MMP-9-RP J05070	1800R	5'-GACGCGCTGTGTACACCCACA-3'		
MMP-14-FP	1288F	5'-GGATACCCAATGCCCATTTGGCCA-3'	221 bp	32
MMP-14-RP NM_004995	1508R	5'-CCATTGGGCATCCAGAAGAGAGC-3'		
TIMP1-FP	78F	5'-CATCCTGTTGTGCTGTGGCTGAT-3'	168 bp	33
TIMP1-RP M12670	245R	5'-GTCATCTTGATCTCATAACGCTGG-3'		
TIMP-2-FP	78F	5'-CTCGCTGGACGTTGGAGGAAAGAA-3'	155 bp	30
TIMP-2-RP NM_003255	245R	5'-AGCCCATCTGGTACCTGTGGTTCA-3'		
VEGF-FP	1208F	5'-CCTGGTGGACATCTTCCAGGAGTA-3'	479 bp 407 bp 347 bp 275 bp	33
VEGF-RP AH001553	1687R	5'-CTCACCGCCTCGGCTTGTCACA-3'		
28S rRNA-RP	12403F	5'-GTTACCCCACTAATAGGGAACGTGA-3'	212 bp	19
28S rRNA-RP U13369	12614R	5'-GATTCTGACTTAGAGGCGTTTCAGT-3'		
VEGFR1-FP	2438F	5'-TCCCTTATGATGCCAGCAAGT-3'	79 bp	40
VEGFR1-RP	2516R	5'-CCAAAAGCCCTCTTCCAA-3'		
VEGFR1 Probe AF063657	2469	5'-CCGGGAGAGACTTAAACTGGGCAAATCA-3'		
sVEGFR1-FP	2209F	5'-ACAATCAGAGGTGAGCACTGCAA-3'	180 bp	40
sVEGFR1-RP	2388R	5'-TCCGAGCCTGAAAGTTAGCAA-3'		
sVEGFR1 Probe U01134	2257	5'-TCCAAATTTAAAGCACAAAGGAATGATTGTACCAC-3'		
VEGFR2-FP	791F	5'-CTTCGAAGCATCAGCATAAGAACT-3'	156 bp	40
VEGFR2-RP	946R	5'-TGGTCATCAGCCCACTGGAT-3'		
VEGFR2 Probe AF063658	820	5'-AACCGAGACCTAAAACCCAGTCTGGGAGT-3'		
NRPI-FP	1831F	5'-CACAGTGGAAACAGGTGATGACTTC-3'	112 bp	40
NRPI-RP	1942R	5'-AACCATATGTTGGAACTCTGATTGT-3'		
NRPI Probe XM_034725	1883	5'-CCACAGAAAAGCCCAACGGTCATAGACA-3'		

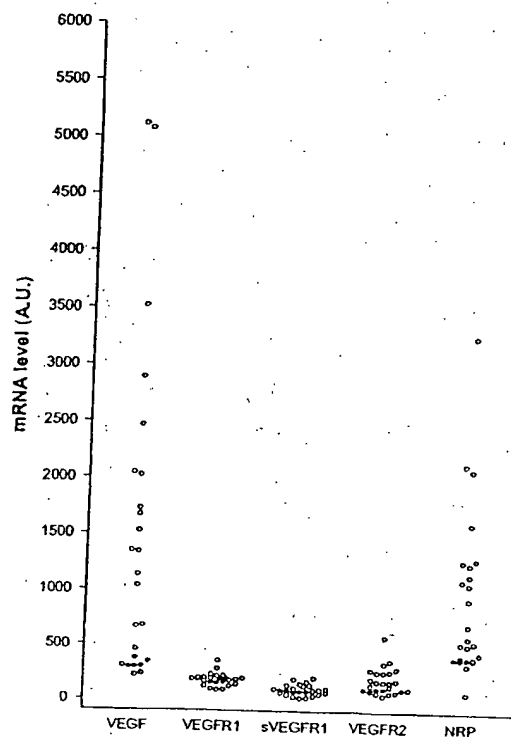


FIGURE 1 – VEGF and VEGF receptors mRNA quantification: scatter of the distribution. Normal brain (black spots) and GBMs (white spots) mRNA levels are expressed as normalized values (as described in Material and Methods: A.U. = arbitrary units). Each point represents the mean of 3 separate experiments.

End point quantitative PCR for MT1-MMP, MMP-2, MMP-9, TIMP-2 mRNA and VEGF mRNA isoforms

MT1-MMP, MMP-2, MMP-9, TIMP-2 and VEGF mRNA isoforms (VEGF₁₈₉, VEGF₁₆₅, VEGF₁₄₅ and VEGF₁₂₁) were measured in 10 ng aliquots of cDNA using Taq polymerase (Takara, Shiga, Japan) and 5 pmol of each primers (Table I). The thermal cycling conditions included 2 min at 95°C for denaturation and then amplification 15 sec at 94°C, 20 sec at 66°C and 20 sec at 72°C (30 sec for VEGF isoforms) with a final incubation 2 min at 72°C. PCR products were resolved on 2% Nusieve 3:1 agarose gels (BioWhittaker, Rockland, MD) and analyzed using a Fluor-S Multimager (Bio-Rad, Hercules, CA) after ethidium bromide staining. Specific mRNA levels were expressed as the ratio of specific transcripts/28S transcripts. Experiments were repeated at least 3 times in duplicate.

Real-time quantitative PCR for VEGFR-1, sVEGFR-1, VEGFR-2 and NRP1 mRNA

Real-time quantitative RT-PCR analyses for VEGFR-1, sVEGFR-1, VEGFR-2, NRP1 mRNAs and 18S rRNA were carried out using the ABI PRISM 7700 Sequence Detection System instrument and software (PE Applied Biosystems). The sequences of the PCR primer pairs and fluorogenic probes that were used for each gene are shown in Table I. A standard curve was generated by 5-fold serial dilution of placenta cDNA to cover the range of 50,000–80 ng and was run in duplicate during every experiment. For each experimental sample, the amount of target gene was determined from this standard curve. The relative expression level of the target gene was normalized against 18S rRNA to compen-

sate for variation in the quality of RNA and the amount of input cDNA (as described by the manufacturer PE Applied Biosystems in User Bulletin 2). PCR was carried out with the TaqMan Universal PCR Master Mix (Applied Biosystems) using 5 µl of diluted cDNA (equivalent to 10 ng total RNA), 200 nM of the probe, and 400 nM primers in a 25 µl final reaction mixture. After a 2 min incubation at 50°C to allow for UNG cleavage, AmpliTaq Gold was activated by an incubation for 10 min at 95°C. Each of the 40 PCR cycles consisted of 15 sec of denaturation at 95°C and hybridization of probe and primers for 1 min at 60°C.

To confirm amplification specificity, the PCR products were also examined by subsequent 2% agarose gel electrophoresis. Experiments were repeated at least 3 times in duplicate.

Immunohistochemistry for VEGF and MT1-MMP

Sections (4 µm thick) were cut from formalin-fixed, paraffin embedded tumour tissue. They were hydrated through graded alcohols and incubated in H₂O₂ (0.3% 15 min). Sections were autoclaved for 11 min at 126°C in citrate buffer pH6 for antigen retrieval (Dako, Glostrup, Denmark). For double immunostaining sections were incubated in primary monoclonal Ab anti-MT1-MMP (Ab-4) 1:100 (Oncogene Research Products, San Diego, CA) followed by peroxidase-conjugated EnVision (Dako). Immunoreactivity was visualized with 3,3'-diaminobenzidine (DAB+, Dako). Sections were then incubated with polyclonal Ab anti-VEGF 1:150 (Santa Cruz, Santa Cruz, CA) for 1 hr at room temperature, followed by alkaline phosphatase-conjugated EnVision (Dako). Immunoreactivity for VEGF was visualized with Fast Red chromogenic substrate (Dako). Single immunostaining was also carried out on serial sections using each primary antibody alone with the corresponding enzyme-chromogene combination. Negative controls were obtained by omitting the primary antibodies.

Gelatin zymography assay

MMP-2 and MMP-9 activities were quantified by gelatin zymography on 2 normal brains and 18 GBMs. Ten cryosections (10 µm) were homogenized in buffer (0.1 M Tris-HCl pH 8.1, 0.4% Triton X-100) and centrifuged for 20 min at 5,000g. The pellets were discarded. 25 µg of total protein from homogenate supernatants were mixed with non reducing sample buffer (62.5 mM Tris-HCl, pH 6.8; 2% SDS; 10% glycerol; 0.1% bromophenol blue) and electrophoresed directly on 10% SDS-polyacrylamide gels (SDS-PAGE) containing 0.1% gelatin (w/v).³² After electrophoresis, gels were washed for 1 hr at room temperature in a 2% (v/v) Triton X-100 solution to remove SDS, transferred to a buffer (50 mM Tris-HCl, pH 7.6, containing 10 mM CaCl₂) and incubated for 18 hr at 37°C. Gels were stained for 30 min with 0.1% (w/v) Coomassie brilliant blue G250 in 45% (v/v) methanol/10% (v/v) acetic acid and destained in 10% (v/v) acetic acid/20% (v/v) methanol. Gels were analyzed with Quantity One software (version 4.2.2, Bio-Rad Laboratories, Hercules, CA) after densitometric scanning of the gels using a Fluor-S Multimager (BioRad).

Western blot

MT1-MMP protein levels were analyzed in 2 normal brains and 15 GBMs. Brain extracts (25 µg) were mixed with 1/2 sample buffer [0.25 M Tris (pH 6.8), 10% SDS (w/v), 4% sucrose (v/v), 5% β-mercaptoethanol (v/v) and 0.125% bromophenol blue (w/v)] and boiled for 5 min. They were separated on 10% SDS-PAGE gels and transferred to a PVDF filter (NEN, Boston, MA). After blocking with 5% milk (w/v), 0.1% tween 20 (w/v) in PBS for 2 hr at room temperature, membranes were exposed to the primary antibody (10 µg/ml, clone 113-5B7, Ab-4, Oncogene Research Products, San Diego, CA) at 4°C overnight followed by incubation with a horseradish peroxidase-conjugated rabbit anti-mouse antibody (1.3 µg/ml, Dako, Glostrup, Denmark). Signals were detected with an enhanced chemoluminescence (ECL) kit (NEN, Boston, MA). The relative intensities of the immunoreactive bands were analyzed with Quantity One software (version 4.2.2, Bio-Rad).

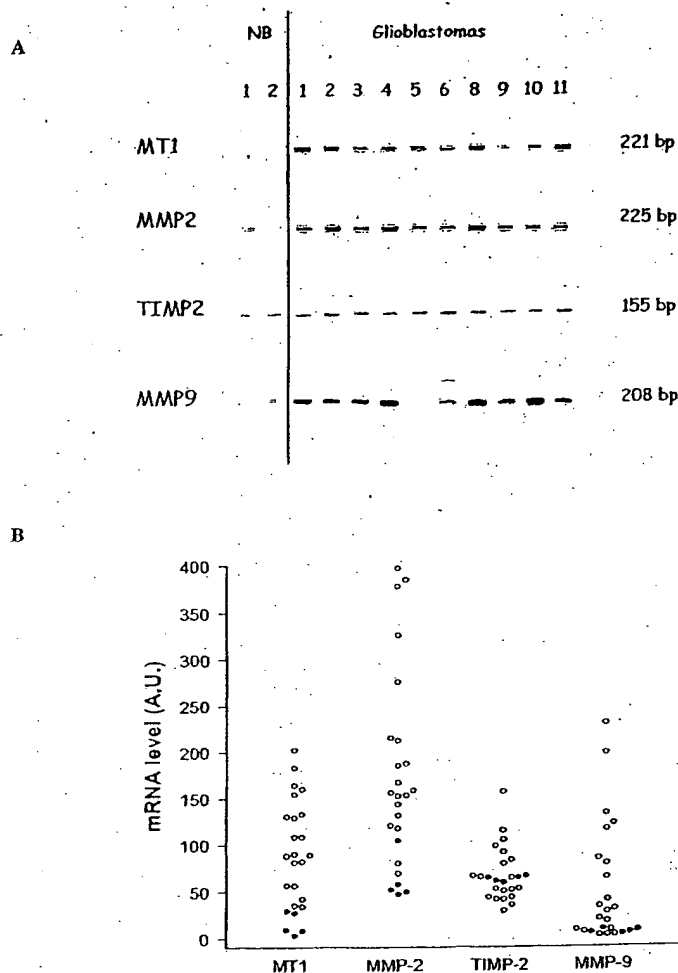


FIGURE 2—MMPs and TIMP-2 mRNA quantification. (a) Representative 2% agarose gels of RT-PCR products for MT1-MMP, MMP-2, TIMP-2 and MMP-9 in 2 normal brains (NB) and 10 GBMs. (b) Scatter plots (as described in Fig. 1). Experiment was repeated at least 3 times in duplicate.

Laboratories) after densitometric scanning of the X-ray films using a Fluor-S Multimager (Bio-Rad).

Statistics

VEGF, VEGFRs, MMPs and TIMP-2 expression values in GBMs were correlated using Spearman's test. Correlation was considered significant for 2-tailed p -value < 0.05 . Statistical analysis was carried out using the Prism 3.0 software (GraphPad, San Diego, CA).

RESULTS

Expression of VEGF and VEGF receptors

VEGF mRNA was present in normal brains (295–375, arbitrary units; mean = 322) and in all GBM samples (217–5,112; mean = 1,774) as reported previously (Fig. 1).³¹ In most GBMs, VEGF mRNA levels were raised 2–15-fold above normal brain values. The most abundant isoform in all cases was VEGF₁₆₅, followed by VEGF₁₂₁, VEGF₁₈₉ and VEGF₁₄₅ (data not shown). VEGFR-1 expression was found at similar levels in GBMs (89–357; mean = 182) and normal controls (154–198; mean = 181). There was no correlation between VEGFR-1 and VEGF mRNA levels ($p = 0.35$) in GBMs. VEGFR-2 was expressed in all GBMs (48–582;

mean = 210) and in 8/20 cases at least twice normal values (87–111; mean = 103). VEGF and VEGFR-2 expressions were correlated significantly ($p = 0.0035$) in GBMs. NRP1 expression varied broadly between GBMs (75–3,260; mean = 1,061) contrasting with a constant baseline expression in normal controls (383–397; mean = 390). In tumours, NRP1 correlated with VEGFR-2 ($p = 0.0119$) but not with VEGF ($p = 0.084$), nor VEGFR-1 ($p = 0.066$). sVEGFR-1 was expressed at low levels both in normal brains (84–92; mean = 87) and GBMs (25–208; mean = 101). sVEGFR-1, however, was found to correlate with VEGFR-1 ($p = 0.0289$), VEGFR-2 ($p = 0.0029$), and NRP1 ($p = 0.0027$) but not with VEGF ($p = 0.053$).

Expression of MMPs and TIMP-2

MT1-MMP, MMP-2 and MMP-9 were expressed in both normal brains and GBMs but at much higher levels in the latter (Fig. 2a). MT1-MMP mRNA levels were constantly higher in GBMs (34–202; mean = 106) than in normal controls (3–29; mean = 15). MMP-2 and MMP-9 mRNA levels were higher than controls in 18/20 and 14/20 cases respectively (Fig. 2b) and correlated with each other ($p = 0.0187$). MT1-MMP mRNA levels correlated with MMP-2 ($p = 0.0008$) and MMP-9 ($p = 0.005$). TIMP-2 had a non-discriminative distribution in relation to the controls. TIMP-2

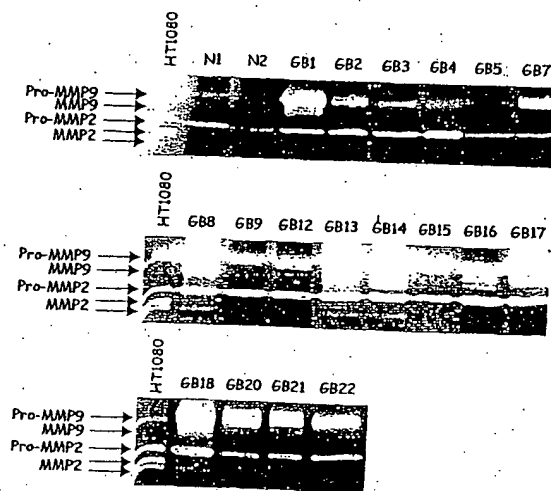


FIGURE 3 - Zymographic analysis of MMP-2 and MMP-9 in tissue extracts either from normal brain (N) or GBMs (GB). Medium conditioned by human HT1080 cells was included as positive control. Positions of pro-MMP-9, MMP-9, pro-MMP-2 and MMP-2 are indicated by arrows.

TABLE II - ZYMOGRAMS AND WESTERN BLOT QUANTIFICATION OF MMPs IN NORMAL BRAIN AND GBMs¹

	Gelatin zymography				Western blot
	proMMP-9	MMP-9	proMMP-2	MMP-2	MT1-MMP
N1	0.41	0.00	1.52	0.00	0.44
N2	0.28	0.00	0.83	0.00	0.47
GB1	9.00	1.25	2.45	0.35	1.58
GB2	4.28	0.00	2.88	0.09	0.47
GB3	1.67	0.00	2.86	0.00	0
GB4	1.40	0.00	4.33	0.03	0
GB5	0.47	0.00	1.15	0.00	ND
GB7	5.29	0.00	1.12	0.00	0
GB8	5.75	3.78	4.63	0.65	0.55
GB9	5.02	0.00	4.09	0.00	0.45
GB12	5.08	0.00	4.79	0.20	3.18
GB13	6.86	4.58	4.93	0.48	1.55
GB14	5.59	6.75	5.53	0.76	0.94
GB15	8.00	0.00	5.13	0.00	ND
GB16	5.55	1.10	5.66	0.00	2.50
GB17	6.61	2.04	6.00	0.00	0
GB18	14.79	4.34	8.20	0.40	1.97
GB20	18.85	0.00	2.12	0.00	0
GB21	16.52	0.00	2.37	0.00	ND
GB22	20.66	0.00	5.11	0.00	0.86

¹Extracts expressed as arbitrary units. N, normal brain; GB, glioblastoma; ND, not determined.

was correlated with MT1-MMP ($p = 0.0019$) and MMP-2 ($p = 0.0002$) but not with MMP-9 ($p = 0.1408$).

Correlation between MT1-MMP protein and activated MMP-2 and -MMP-9

By gelatin zymography, pro-MMP-2 and pro-MMP-9 were detected in the 18 GBMs and 2 controls examined (Fig. 3, Table II). In most GBMs, levels of these inactive forms were higher than in normal brains and were correlated with their respective mRNA levels (MMP-2: $p < 0.0001$; MMP-9: $p = 0.01$). Activated forms of MMP-2 and MMP-9 were not found in normal brain. By contrast, they were present in 8/18 (MMP-2) and 7/18 (MMP-9) GBMs. MT1-MMP protein levels were quantified by Western blot in 15 GBMs and 2 normal brains (Fig. 4, Table II). They were signifi-

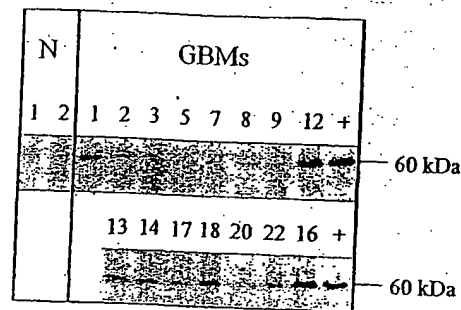


FIGURE 4 - Western blot analysis using the ab4 antibody (clone 113-5B7) raised against the catalytic domain of MT1-MMP. Protein extracts from MT1-MMP transfected A2058 cells (clone SL5,²⁸) were used as a positive control (+). MT1-MMP protein is detected in normal brain (N) and GBMs.

TABLE III - CORRELATION BETWEEN VEGF, VEGF RECEPTORS, MMPs AND TIMP-2 EXPRESSED AS p VALUES DERIVED FROM SPEARMAN'S TEST

	MT1-MMP	MMP-2	MMP-9	TIMP-2
VEGF	0.0250	0.0245	0.0053	0.0094
VEGFR-1	0.0073	0.0710	<0.0001	0.4542
VEGFR-2	<0.0001	0.0168	0.0004	0.0153
NRP1	0.0053	0.1334	0.2457	0.5480
sVEGFR-1	0.0313	0.0469	0.0194	0.2563

cantly correlated with zymogram-derived activated MMP-2 levels ($p = 0.0226$) but not with activated MMP-9 levels ($p = 0.06$). Interestingly, MT1-MMP protein and mRNA levels were correlated significantly ($p = 0.089$), arguing for a predominantly transcriptional regulation in GBMs.

Correlation between VEGF network and MMPs

mRNA levels of VEGF and VEGF receptors were compared to MT1-MMP, MMP-2, MMP-9 and TIMP-2 (Table III). There was a significant correlation between VEGF expression and MT1-MMP, MMP-2 and MMP-9. A similar correlation was also observed between VEGFR-2 and MMPs. Interestingly, TIMP-2 expression was correlated with VEGF and VEGFR-2 but not with other VEGF receptors.

Immunohistochemistry for VEGF and MT1-MMP

VEGF immunoreactivity was shown in both tumour and endothelial cells, as previously reported (Fig. 5a,b).³¹ By single immunostaining, MT1-MMP was detected in glioblastoma cells as a diffuse cytoplasmic staining (Fig. 5c,d). MT1-MMP positivity was also seen in endothelial cells and perivascular cells (Fig. 5c). By double immunostaining, we observed the co-localization of VEGF and MT1-MMP in the cytoplasm of numerous tumour cells (Fig. 5e,f).

DISCUSSION

GBMs are highly malignant tumours with poor prognosis. They show major microvascular proliferation and express high levels of VEGF.⁴⁻⁹ VEGF is a strong mitogen for endothelial cells thereby promoting angiogenesis. Previous reports^{32,34} have suggested that VEGF also stimulates tumour cell invasion, migration and survival in malignant epithelial cells through an autocrine loop by which overexpression of MMPs induces VEGF secretion and leads to subsequent amplification of cell proliferation and protection against apoptosis. We and others reported previously that in human melanoma and breast carcinoma cells, MT1-MMP upregulates VEGF expression whereas TIMP-2 reduces it.^{28,29,35} Therefore the

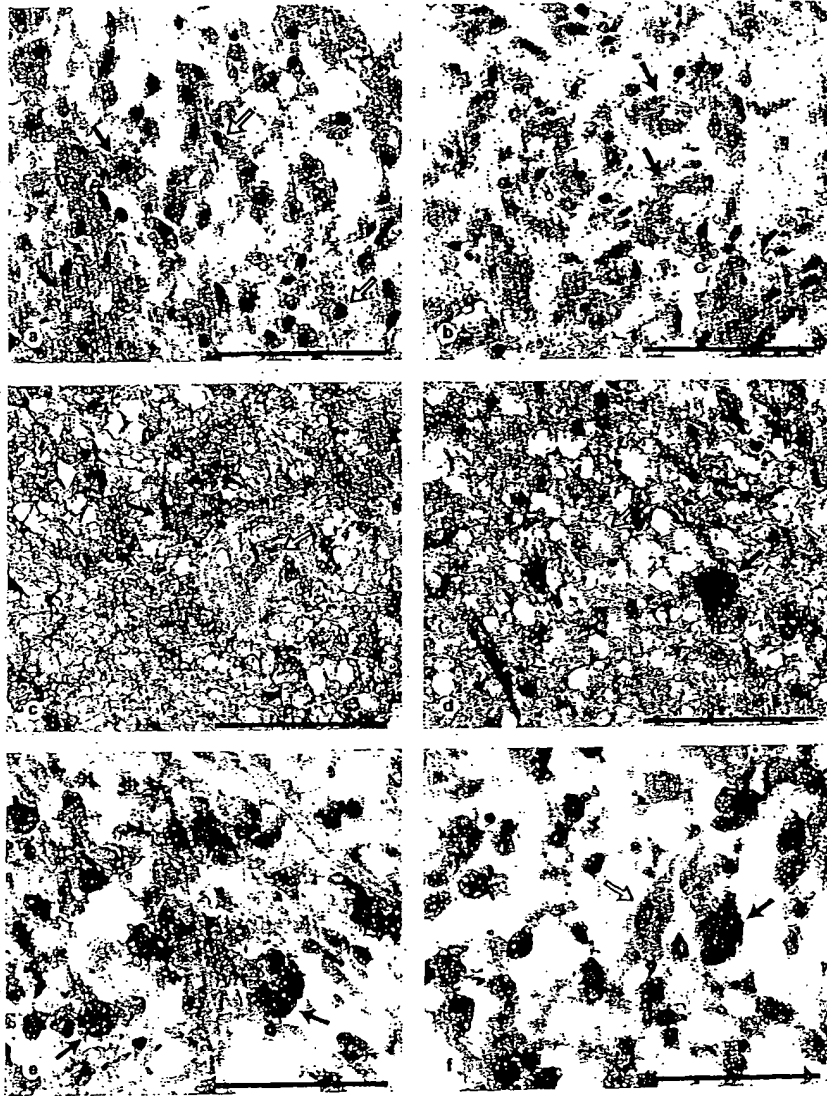


FIGURE 5 - Immunohistochemistry (scale bar = 50 μ m). (a,b) VEGF positive tumour and endothelial cells (plain arrows) show granular red staining of the cytoplasm. Negative cells (empty arrow) are seen in their close vicinity. (c) MT1-MMP positive cells show a strong brown cytoplasmic staining. They include tumours cells (plain arrow) and endothelial cells (empty arrow). (d) MT1-MMP positive tumour cells (plain arrow) are mixed with negative cells (empty arrow). (e,f) Double staining with VEGF (red) and MT1-MMP1 (brown). Double positive tumour cells (plain arrows) contrast with negative or single weakly positive cell (empty arrow).

pericellular proteolysis mediated by MT1-MMP in GBMs could also induce an autocrine loop resulting in enhanced VEGF expression. In turn, VEGF could act as a paracrine factor on endothelial cells to stimulate angiogenesis or possibly as an autocrine factor promoting glioblastoma cells survival-migration and invasion as demonstrated recently in the various tumour cell culture models.

We compared the expression of VEGF and its receptors with MT1-MMP, MMP-2 and MMP-9 in 20 GBMs and 5 normal brains. The expression of these MMPs was markedly increased in most GBMs with excellent correlation between mRNA and protein levels. MT1-MMP expression has been shown previously to correlate with glioma aggressiveness and its transfection in different tumour cell lines triggers an angiogenic phenotype and promotes tumour growth.^{20,28-30,36-38} A majority of GBMs (17/20) also expressed high levels of VEGF, as previously reported, with a strong correlation between VEGF and MT1-MMP gene expression levels. Double immunostaining studies showed co-expression of VEGF and MT1-MMP by the same tumour cells. These data suggest that the transcrip-

tional control of VEGF by MT1-MMP could be operative not only *in vitro* but also *in vivo* in human GBMs.

MT1-MMP could also promote the growth of GBMs by its ability to activate MMP-2 in the presence of low concentration of TIMP-2.⁴⁰ Pro-MMP-2 activation occurs after the formation of a ternary complex that contains pro-MMP-2 linked to cell surface MT1-MMP via a TIMP-2 bridge. In accordance with this hypothesis, we found that MMP-2 activation occurred in 8/18 of our GBMs^{20,41} among which 7/7 tested for MT1-MMP showed high contents of this protease.

Activated MMP-9 was also found in 7/18 of our GBMs. This is an interesting finding as active MMP-9 is able to mobilize VEGF from its ECM reservoir.³⁹ Therefore, MMPs could promote VEGF-mediated angiogenesis in GBMs by both transcriptional (MT1-MMP) and post translational (MMP-9) mechanisms.

VEGF binding to VEGFR-2 triggers the proliferation and migration of endothelial cells whereas its binding to VEGFR-1 has

opposite effects on glioblastoma cell lines.^{12,42} In our study, VEGF mRNA levels were correlated with VEGFR-2 but not VEGFR-1, NRP1 and sVEGFR-1. Collectively our data suggest that GBMs display a specific and complex pattern of VEGF receptors, transducing VEGF signaling toward cell proliferation and migration.

In conclusion, our study adds to the evidence for an interplay between metalloproteinases and VEGF in human GBMs as previously documented in experimental tumours. Because of its dual ability to activate MMP-2 and to up-regulate VEGF, MT1-MMP might be of central importance in the growth of human glioblastomas and represent an interesting target for anti-cancer treatments.

ACKNOWLEDGEMENTS

The authors wish to express their gratitude to the neurosurgeons of the CHU-Liège (Prof. A. Stevenaert), and CHR-Liège (Prof. J.

Born) and Dr. A. Michotte (VUB-Brussels) for their contribution to the collection of cases, to Dr. L. de Leval for her assistance in immunohistochemistry, and to M.R. Pignon for her excellent technical assistance. This work was supported by grants from the Communauté Française de Belgique (Actions de Recherches Concertées), the Commission of European Communities, the Fonds de la Recherche Scientifique Médicale, the Fonds National de la Recherche Scientifique (FNRS, Belgium), the Fédération Belge Contre le Cancer, the Fonds spéciaux de la Recherche (University of Liège), the Centre Anticancéreux près l'Université de Liège, the FB Assurances, the Fondation Léon Frédéricq (University of Liège), the D.G.T.R.E. from the "Région Wallonne", the Fonds d'Investissements de la Recherche Scientifique (CHU, Liège, Belgium), the Interuniversity Attraction Poles (I.U.A.P.) from the Federal Office for Scientific, Technical and Cultural Affairs (O.S.T.C., Brussels, Belgium).

REFERENCES

- Folkman J, Klagsbrun M. Angiogenic factors. *Science* 1987;235:442-7.
- Carmeliet P, Jain RK. Angiogenesis in cancer and other diseases. *Nature* 2000;407:249-57.
- Plate KH, Breier G, Weich HA, Risau W. Vascular endothelial growth factor is a potential tumour angiogenesis factor in human gliomas in vivo. *Nature* 1992;359:845-8.
- Oehning RD, Miletic M, Valter MM, Pietsch T, Neumann J, Fimmers R, Schlegel U. Vascular endothelial growth factor (VEGF) in astrocytic gliomas—a prognostic factor? *J Neurooncol* 1999;45:117-25.
- Pietsch T, Valter MM, Wolf HK, von Deimling A, Huang HJ, Cavenee WK, Wiestler OD. Expression and distribution of vascular endothelial growth factor protein in human brain tumors. *Acta Neuropathol (Berl)* 1997;93:109-17.
- Nishikawa R, Cheng SY, Nagashima R, Huang HJ, Cavenee WK, Matsutani M. Expression of vascular endothelial growth factor in human brain tumors. *Acta Neuropathol (Berl)* 1998;96:453-62.
- Kleihues P, Cavenee WK. Pathology and genetics of tumours of the nervous system. Lyon: IARC Press, 2000. 29-39.
- Plate KH, Breier G, Weich HA, Mennel HD, Risau W. Vascular endothelial growth factor and glioma angiogenesis: coordinate induction of VEGF receptors, distribution of VEGF protein and possible in vivo regulatory mechanisms. *Int J Cancer* 1994;59:520-9.
- Machein MR, Plate KH. VEGF in brain tumors. *J Neurooncol* 2000;50:109-20.
- Ding H, Wu X, Roncari L, Lau N, Shannon P, Nagy A, Guha A. Expression and regulation of neuropilin-1 in human astrocytomas. *Int J Cancer* 2000;88:584-92.
- Kunkel P, Ulbricht U, Bohlen P, Brockmann MA, Fillbrandt R, Stavrou D, Westphal M, Lamszus K. Inhibition of glioma angiogenesis and growth in vivo by systemic treatment with a monoclonal antibody against vascular endothelial growth factor receptor-2. *Cancer Res* 2001;61:6624-8.
- Herold-Mende C, Steiner HH, Andl T, Riede D, Buttler A, Reisser C, Fussenig NE, Mueller MM. Expression and functional significance of vascular endothelial growth factor receptors in human tumor cells. *Lab Invest* 1999;79:1573-82.
- Hiratsuka S, Minowa O, Kuno J, Noda T, Shibuya M. Flt-1 lacking the tyrosine kinase domain is sufficient for normal development and angiogenesis in mice. *Proc Natl Acad Sci USA* 1998;95:9349-54.
- Soker S, Takashima S, Miao HQ, Neufeld G, Klagsbrun M. Neuropilin-1 is expressed by endothelial and tumor cells as an isoform-specific receptor for vascular endothelial growth factor. *Cell* 1998;92:735-45.
- Egeblad M, Werb Z. New functions for the matrix metalloproteinases in cancer progression. *Nat Rev Cancer* 2002;2:161-74.
- Pepper MS. Role of the matrix metalloproteinase and plasminogen activator-plasmin systems in angiogenesis. *Arterioscler Thromb Vasc Biol* 2001;21:1104-17.
- Sternlicht MD, Werb Z. How matrix metalloproteinases regulate cell behavior. *Annu Rev Cell Dev Biol* 2001;17:463-516.
- Sounni NE, Janssen M, Foidart JM, Noel A. Membrane Type-1 Matrix Metalloproteinase and TIMP2 in tumor angiogenesis. *Matrix Biol* 2003;22:55-61.
- Belien AT, Paganetti PA, Schwab ME. Membrane-type 1 matrix metalloproteinase (MT1-MMP) enables invasive migration of glioma cells in central nervous system white matter. *J Cell Biol* 1999;144:373-84.
- Lampert K, Machein U, Machein MR, Conca W, Peter HH, Volk B. Expression of matrix metalloproteinases and their tissue inhibitors in human brain tumors. *Am J Pathol* 1998;153:429-37.
- Sato H, Takino T, Okada Y, Cao J, Shinagawa A, Yamamoto E, Seiki M. A matrix metalloproteinase expressed on the surface of invasive tumour cells. *Nature* 1994;370:61-5.
- Knauper V, Will H, Lopez-Otin C, Smith B, Atkinson SJ, Stanton H, Hembry RM, Murphy G. Cellular mechanisms for human procollagenase-3 (MMP-13) activation. Evidence that MT1-MMP (MMP-14) and gelatinase a (MMP-2) are able to generate active enzyme. *J Biol Chem* 1996;271:17124-31.
- Koshikawa N, Giannelli G, Cirulli V, Miyazaki K, Quaranta V. Role of cell surface metalloproteinase MT1-MMP in epithelial cell migration over laminin-5. *J Cell Biol* 2000;148:615-24.
- Gilles C, Polette M, Coraux C, Tournier JM, Meneguzzi G, Munaut C, Volders L, Rousselle P, Birembaut P, Foidart JM. Contribution of MT1-MMP and of human laminin-5 gamma2 chain degradation to mammary epithelial cell migration. *J Cell Sci* 2001;114:2967-76.
- Kajita M, Itoh Y, Chiba T, Mori H, Okada A, Kinoh H, Seiki M. Membrane-type 1 matrix metalloproteinase cleaves CD44 and promotes cell migration. *J Cell Biol* 2001;153:893-904.
- Deryugina EI, Ratnikov B, Monosov E, Postnova TI, DiScipio R, Smith JW, Strongin AY. MT1-MMP initiates activation of pro-MMP-2 and integrin α 3 promotes maturation of MMP-2 in breast carcinoma cells. *Exp Cell Res* 2001;263:209-23.
- Zhou Z, Apte SS, Soininen R, Cao R, Baaklini GY, Rauser RW, Wang J, Cao Y, Tryggvason K. Impaired endochondral ossification and angiogenesis in mice deficient in membrane-type matrix metalloproteinase 1. *Proc Natl Acad Sci USA* 2000;97:4052-7.
- Sounni NE, Baramova EN, Munaut C, Maquoi E, Frankenne F, Foidart JM, Noel A. Expression of membrane type 1 matrix metalloproteinase (MT1-MMP) in A2058 melanoma cells is associated with MMP-2 activation and increased tumor growth and vascularization. *Int J Cancer* 2002;98:23-8.
- Sounni NE, Devy L, Hajitou A, Frankenne F, Munaut C, Gilles C, Deroanne C, Thompson EW, Foidart JM, Noel A. MT1-MMP expression promotes tumor growth and angiogenesis through an upregulation of vascular endothelial growth factor expression. *FASEB J* 2002;16:555-64.
- Deryugina EI, Soroceanu L, Strongin AY. Upregulation of vascular endothelial growth factor by membrane-type 1 matrix metalloproteinase stimulates human glioma xenograft growth and angiogenesis. *Cancer Res* 2002;62:580-8.
- Munaut C, Boniver J, Foidart JM, Deprez M. Macrophage migration inhibitory factor (MIF) expression in human glioblastomas correlates with VEGF expression. *Neuropathol Appl Neurobiol* 2002;28:452-60.
- Munaut C, Noel A, Weidle UH, Krell HW, Foidart JM. Modulation of the expression of interstitial and type-IV collagenases in coculture of HT1080 fibrosarcoma cells and fibroblasts. *Invasion Metastasis* 1995;15:169-78.
- Bachelder RE, Crago A, Chung J, Wendt MA, Shaw LM, Robinson G, Mercurio AM. Vascular endothelial growth factor is an autocrine survival factor for neuropilin-expressing breast carcinoma cells. *Cancer Res* 2001;61:5736-40.
- Chung J, Bachelder RE, Lipscomb EA, Shaw LM, Mercurio AM. Integrin (α 6 β 4) regulation of eIF-4E activity and VEGF translation: a survival mechanism for carcinoma cells. *J Cell Biol* 2002;158:165-74.
- Hajitou A, Sounni NE, Devy L, Grignani-Debrus C, Lewalle JM, Li H, Deroanne CF, Lu H, Colige A, Nusgens BV, Frankenne F, Maron A.

- et al. Downregulation of vascular endothelial growth factor by tissue inhibitor of metalloproteinase-2: effect on in vivo mammary tumor growth and angiogenesis. *Cancer Res* 2001;61:3450-7.
36. Forsyth PA, Laing TD, Gibson AW, Rewcastle NB, Brasher P, Sutherland G, Johnston RN, Edwards DR. High levels of gelatinase-B and active gelatinase-A in metastatic glioblastoma. *J Neurooncol* 1998;36:21-9.
37. Nakada M, Nakamura H, Ikeda E, Fujimoto N, Yamashita J, Sato H, Seiki M, Okada Y. Expression and tissue localization of membrane-type 1, 2, and 3 matrix metalloproteinases in human astrocytic tumors. *Am J Pathol* 1999;154:417-28.
38. Kachra Z, Beaulieu E, Delbecchi L, Mousseau N, Berthelet F, Moudjian R, Del Maestro R, Beliveau R. Expression of matrix metalloproteinases and their inhibitors in human brain tumors. *Clin Exp Metastasis* 1999;17:555-66.
39. Bergers G, Brekken R, McMahon G, Vu TH, Itoh T, Tamaki K, Tanzawa K, Thorpe P, Itohara S, Werb Z, Hanahan D. Matrix metalloproteinase-9 triggers the angiogenic switch during carcinogenesis. *Nat Cell Biol* 2000;2:737-44.
40. Strongin AY, Collier I, Bannikov G, Mariner BL, Grant GA, Goldberg GL. Mechanism of cell surface activation of 72-kDa type IV collagenase. Isolation of the activated form of the membrane metalloprotease. *J Biol Chem* 1995;270:5331-8.
41. Nakada M, Kita D, Futami K, Yamashita J, Fujimoto N, Sato H, Okada Y. Roles of membrane type 1 matrix metalloproteinase and tissue inhibitor of metalloproteinases 2 in invasion and dissemination of human malignant glioma. *J Neurosurg* 2001;94:464-73.
42. Millauer B, Witzmann-Voos S, Schnurch H, Martinez R, Moller NP, Risau W, Ullrich A. High affinity VEGF binding and developmental expression suggest Flk-1 as a major regulator of vasculogenesis and angiogenesis. *Cell* 1993;72:835-46.

INTERNATIONAL

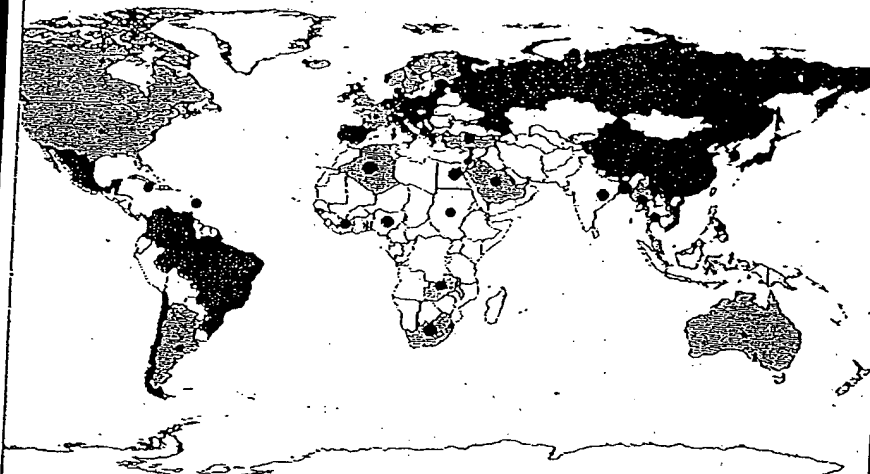
Journal of Cancer

HEALTH SCIENCES LIBRARY
UNIVERSITY OF WISCONSIN

SEP 10 2003

1305 Linden Drive
Madison, WI 53706

Helicobacter pylori and gastric cancer: facing the enigmas



Map Source: ESRI Data & Maps

Prevalence of *H. pylori*
(%)

- 1st quartile (19-39.9)
- 2nd quartile (39.9-67.5)
- 3rd quartile (67.5-81.2)
- 4th quartile (81.2-96.3)

Gastric cancer incidence *

- (100 000)
- ≤ 5
- ▨ 5-10
- ▩ 10-15
- 15-20
- > 20

* Age and sex-standardized



International Union Against Cancer

COUNCIL

J. SEFFRIN, President (USA)
L.J. DENIS, Treasurer (Belgium)
J. BAIJY, Chair, Finance Committee (USA)

G. BRIEN (Australia)
R.C. BURTON (Australia)
M. DAUBE (Australia)
K.A. DINSHAW (India)
L. ELOVAJIO (Finland)
M.K. GOSPODAROWICZ (Canada)
R.T. HUDSON (Ireland)
T. KITAGAWA (Japan)
A. PUNDALIK KURKURE (India)
R.E. LENHARD (USA)
A. LLOMBART-BOSCH (Italy)

M. LUWIA (Indonesia)
C. MALLINSON (UK)
I.H. MARCHESI (Brazil)
H.F. MICKELSON (USA)
K. NILSSON (Sweden)
S. OMAR (Egypt)
T. PHILIP (France)
E. ROBINSON, Past President (Israel)
Y. SALOOJEE (South Africa)
H. SANCHE-GARNIER (France)

R.J. SCHWEITZER (USA)
O. SOREIDE (Norway)
K. TAJIMA (Japan)
W. WEBER (Switzerland)
S. WILKINSON (UK)
D. ZACKS (USA)
D. ZARIDZE (Russia)
Y. HUI ZHANG (China)
M. Ziv (Israel)
M. ZUR HAUSEN (Germany)

UICC, URL: <http://www.uicc.org>
UICC, E-mail: info@uicc.org

The International Union Against Cancer (UICC) is devoted exclusively to all aspects of the world-wide fight against cancer. Its objectives are to advance scientific and medical knowledge in research, diagnosis, treatment and prevention of cancer, and to promote all other aspects of the campaign against cancer throughout the world. Particular emphasis is placed on professional and public education.

Founded in 1933, the UICC is a non-governmental, independent association of more than 290 member organizations in over 80 countries. Members are voluntary cancer leagues and societies, cancer research and/or treatment centers, and in some countries ministries of health.

The UICC is non-profit, non-political, and non-sectarian. Its headquarters are in Geneva, Switzerland. It creates and carries out programs around the world in collaboration with hundreds of volunteer experts. Supported by membership dues, national subscriptions, grants and donations, its annual budget is about US \$4 million.

The UICC is governed by its members which meet in General Assembly every 4 years. Its elected Council and Executive Committee are responsible for Program structure and implementation.

The UICC organizes an International Cancer Congress every 4 years as well as annual symposia, workshops, and training courses. It publishes the *International Journal of Cancer* (30 issues per year), *UICC News* (quarterly), the *International Calendar of Meetings on Cancer* (bi-annually), and a number of technical reports, textbooks and manuals.

SUBSCRIPTION INFORMATION

© 2003 Wiley-Liss, Inc., a Wiley Company. All rights reserved. No part of this publication may be reproduced in any form or by any means, except as permitted under section 107 or 108 of the 1976 United States Copyright Act, without either the prior written permission of the publisher, or authorization through the Copyright Clearance Center, 222 Rosewood Drive, Danvers, MA 01923, telephone: (978) 750-8400, fax: (978) 750-4470. Requests to the publisher for permission should be addressed to the Permissions Department, c/o John Wiley & Sons, Inc., 111 River St., Hoboken, NJ 07030. Fax: (201) 748-6008; Tel.: (201) 748-6011; <http://www.wiley.com/go/permissions>.

International Journal of Cancer (Print ISSN 0020-7136; Online ISSN 1097-0215) is published 30 times a year, semi-monthly with extra issues in January, March, May, July, September, and November, by Wiley-Liss, Inc., through Wiley Subscription Services, Inc., a Wiley Company. Send subscription inquiries in care of John Wiley & Sons, Inc., Attn: Journals Admin Dept UK, 111 River St., Hoboken, NJ 07030, (201) 748-6645.

Advertising inquiries should be addressed to Advertising Department, c/o John Wiley & Sons, Inc., 111 River St., Hoboken, NJ 07030. Telephone: (201) 748-6921.

Offprint sales and inquiries should be directed to the Customer Service Department, in care of John Wiley & Sons, 111 River St., Hoboken, NJ 07030. Telephone: (201) 748-8776.

Subscription price: Volumes 103-107, 2003 (30 issues). Print only: \$2,495 worldwide. Electronic only: \$2,495 worldwide. A combination price of \$2,620 worldwide includes the subscription in both electronic and print formats. All subscriptions containing a print element, shipped outside the U.S., will be sent by air. Payment must be made in U.S. dollars drawn on U.S. bank. Periodicals postage paid at Hoboken, NJ and at additional mailing offices. Postmaster: send address changes to INTERNATIONAL JOURNAL OF CANCER, Subscription Distribution, c/o John Wiley & Sons, Inc., 111 River St., Hoboken, NJ 07030.

Change of address: Please forward to the subscriptions address listed above 6 weeks prior to move; enclose present mailing label with change of address. Claims for missing issues: Claims for undelivered copies will be accepted only after the following issue has been received. Please enclose a mailing label or cite your subscriber reference number. Missing copies will be supplied when losses have been sustained in transit and where reserve stock permits. Send claims in care of John Wiley & Sons, Inc., Attn: Journals Admin Dept UK, 111 River St., Hoboken, NJ 07030.

Indexed by: EMBASE/Excerpta Medica • Current Contents/Life Sciences • Science Citation Index • Scisearch • BIOSIS Data Base • Index Medicus • Cambridge Scientific Abstracts • Chemical Abstracts • Reference Update • Smoking and Health Database.

This journal is printed on acid-free paper.

INTERNATIONAL JOURNAL OF CANCER

2003 Wiley-Liss, Inc.

The *International Journal of Cancer* is published for the International Union Against Cancer by Wiley-Liss, Inc., a division of John Wiley & Sons, Inc. Five volumes are issued annually, each consisting of six numbers.

Abstracting and other journals may reprint the summaries of articles without requesting authorization. Authors alone are responsible for views expressed in signed articles. The mention of specific companies or of certain manufacturers' products does not imply that they are endorsed or recommended by the International Union Against Cancer.

References: When quoting from the *International Journal of Cancer*, please use the official abbreviation:
Int. J. Cancer

Thyroid

VOLUME 7

NUMBER 5

OCTOBER 1997

CLINICAL RESEARCH

- Levothyroxine Suppressive Therapy is Partially Effective in Treating Patients with Benign, Solid Thyroid Nodules and Multinodular Goiters.
NICOLAU LIMA, MEYER KNOBEL, HUMBERTO CAVALIERE,
CLAUDIA SZTEJNSZNAJD, EDUARDO TOMIMORI, and
GERALDO MEDEIROS-NETO 691
- Is Percutaneous Ethanol Injection a Useful Alternative for the Treatment of the Cold Benign Thyroid Nodule? Five Years' Experience.
NADIA CARACCIO, ORLANDO GOLETTI, PIERO VINCENZO LIPPOLIS,
ARTURO CASOLARO, ENRICO CAVINA, PAOLO MICCOLI, and FABIO MONZANI 699
- Value of Combined Technetium-99m Hydroxy Methylene Diphosphonate and Thallium-201 Imaging in Detecting Bone Metastases from Thyroid Carcinoma.
MD. SAYEEDUL ALAM, RYO TAKEUCHI, KANJI KASAGI, TAKASHI MISAKI,
SHINICHI MIYAMOTO, YASUHIRO IIDA, AKINARI HIDAKA, and JUNJI KONISHI 705
- Human Thyroid Carcinoma Cell Lines and Normal Thyrocytes: Expression and Regulation of Matrix Metalloproteinase-1 and Tissue Matrix Metalloproteinase Inhibitor-1 Messenger-RNA and Protein.
G. AUST, A. HOFMANN, S. LAUE, A. ROST, T. KÖHLER, and W.A. SCHERBAUM 713
- MUC1 Mucin Gene, Transcripts, and Protein in Adenomas and Papillary Carcinomas of the Thyroid.
IVAN BIÈCHE, EMMANUEL RUFFET, ALAIN ZWEIBAUM, FRANÇOISE VILDÉ,
ROSETTE LIDEREAU, and BRIGITTE FRANC 725
- Incidence and Clinical Characteristics of Thyroid Carcinoma After Iodine Prophylaxis in an Endemic Goiter Country.
C. BACHER-STIER, G. RICCABONA, M. TÖTSCH, G. KEMMLER, W. OBERAIGNER,
and R. MONCAYO 733
- Opposite Changes in Serum Soluble CD8 in Patients at the Active Stages of Graves' and Hashimoto's Diseases.
MIKIO WATANABE, NOBUYUKI AMINO, KAZUNORI HOCHITO,
KIYOSHI WATANABE, KANJI KUMA, and YOSHINORI IWATANI 743
- Urinary Iodine Excretion During Normal Pregnancy in Healthy Women Living in the Southwest of France: Correlation with Maternal Thyroid Parameters.
PHILIPPE CARON, MADELEINE HOFF, SAMUEL BAZZI, ALAIN DUFOR,
GÉRARD FAURE, IMAD GHANDOUR, PATRICK LAUZU, YVAN LUCAS,
DOMINIQUE MARAVAL, FRÉDÉRIC MIGNOT, PASCAL RÉSSIGEAC,
FRANÇOISE VERTONGEN, and VÉRONIQUE GRANGÉ 749

(continued)

Human Thyroid Carcinoma Cell Lines and Normal Thyrocytes: Expression and Regulation of Matrix Metalloproteinase-1 and Tissue Matrix Metalloproteinase Inhibitor-1 Messenger-RNA and Protein

G. AUST,¹ A. HOFMANN,² S. LAUE,² A. ROST,³ T. KÖHLER,³ and W.A. SCHERBAUM⁴

ABSTRACT

Matrix metalloproteinase-1 (MMP-1) and tissue matrix metalloproteinase inhibitor 1 (TIMP-1) play an important role in remodeling the extracellular matrix in normal and pathological processes. The effect of phorbol-myristate acetate (PMA), interleukin-1 (IL-1), and tumor necrosis factor- α (TNF- α) on MMP-1 and TIMP-1 expression was studied on highly purified thyrocytes and undifferentiated 8505 C, C 643, HTh 74, SW 1736 thyroid carcinoma cells compared with thyroid-derived fibroblasts. Messenger RNA (mRNA) levels were monitored by competitive semiquantitative reverse transcriptase polymerase chain reaction (RT-PCR) after 24 hours. Culture supernatants were assayed for free and/or complexed MMP-1 and TIMP-1 after 48 hours using enzyme-linked immunosorbent assay (ELISA) systems (detection limit: <2 ng/mL). MMP-1 and TIMP-1 mRNA were present in all cell types, although thyrocytes showed MMP-1 mRNA levels near the detection limit. 8505 C expressed MMP-1 mRNA levels of up to 10^6 times those of the other cells analyzed. PMA and IL-1 increased MMP-1 mRNA in most cell types. TIMP-1 mRNA increased after treatment with PMA in all cells except 8505 C, whereas only slight effects were shown after IL-1 stimulation. MMP-1 protein was undetectable in normal thyrocyte cultures, but was secreted spontaneously by all cell lines ([ng/mL]; C 643: 15 ± 7 ; HTh 74: 81 ± 1 ; SW 1736: 13 ± 2 ; 8505C: 2097 ± 320). There was a strong correlation between levels of MMP-1 mRNA and protein ($r = 0.99$, $p < .0001$). PMA and IL-1 increased MMP-1 secretion in all cell types after 48 hours. Fibroblasts ([ng/mL] 517 ± 55) and the cell lines (C 643: 142 ± 48 ; HTh 74: 115 ± 13 ; SW 1736: 202 ± 14 ; 8505 C: 120 ± 19) secreted TIMP-1 in unstimulated cultures, whereas only a trace amount was detected in thyrocyte cultures, even after PMA treatment. IL-1 upregulated TIMP-1 secretion after 48 hours in SW 1736, HTh 74, and C 643 cells. Our data suggest that in contrast to normal thyrocytes, dedifferentiated thyroid carcinoma cell lines are potential producers of MMP-1 as well as TIMP-1. High MMP-1 or MMP-1/TIMP-1 expression may play a role in tissue invasion of undifferentiated thyroid cancer cells.

INTRODUCTION

MATRIX METALLOPROTEINASES, (MMPs) constitute a family of structurally related proteolytic enzymes responsible for the proteolytic degradation of extracellular matrix (ECM) components. They are important participants in normal tissue remodeling and contribute to the phenotype of several pathological conditions that are associated with progressive ECM degradation. MMPs are highly regulated at different levels (1). At the transcriptional level, MMP expression can be directly induced or

suppressed on external stimulation, ie, with cytokines, phorbol 12-myristate 13-acetate (PMA), lipopolysaccharide (LPS), or retinoic acid (2,3). After secretion at post-transcriptional level, latent MMP proenzymes are regulated by proteolytic activation and interaction with tissue inhibitors of matrix metalloproteinase (TIMPs), their specific inhibitors. Any imbalance between the proteolytic MMPs activities and the TIMPs that could be influenced and caused by cytokines could potentially lead to pathological conditions (4).

MMP-1, although known as an interstitial collagenase,

¹Institut of Anatomy, ²Department of Internal Medicine III, and ³Institute of Clinical Chemistry and Pathobiochemistry, University of Leipzig, Germany. ⁴Department of Endocrinology, University of Duesseldorf.

is the only enzyme active at neutral pH that can degrade extracellular fibers comprised of collagen types I, II, and III. With this initial step, MMP-1 provides the cleavage products to other collagenase types (5). The major specific inhibitor of MMP-1 is TIMP-1, a 28.5-kd glycoprotein, which forms 1:1 stoichiometric complexes with the protease (6). Cytokines and growth factors have been shown to regulate the expression of both MMP-1 and TIMP-1 (1,7,8).

Although the participation of MMP-1 as the initial collagenase in tissue breakdown during tumor development is well documented (9–11), only one study has described the expression (12) but no study has as yet investigated the regulation of this enzyme in different thyroid tumors. Few studies have been published investigating the role of other MMPs in normal and pathological thyroid tissue by *in situ* hybridization and immunohistochemistry (13–16). Furthermore, tissue remodeling includes both the action of MMPs and their inhibitors; thus, these enzymes could be involved in autoimmune and other nonautoimmune thyroid diseases during morphological changes (17,18). It is still unknown whether or not thyrocytes are able to express MMPs and TIMPs. Although type IV collagenases (MMP-2 and MMP-9) were detected in various human epithelial cells of different tissue origin (19,20), only one study described the secretion of MMP-1 by epithelial cells (21).

Highly purified normal thyrocytes and four thyroid carcinoma cell lines were included in this study to investigate the involvement of these cells in MMP-1 and TIMP-1 production during thyroid tissue remodeling processes and in malignant thyroid neoplasms. MMP-1 and TIMP-1 expression were studied at both the mRNA and protein level by semiquantitative RT-PCR and ELISA measurement, respectively.

In unstimulated carcinoma cell lines both MMP-1 and TIMP-1 mRNA were expressed, partly at a high level, followed by the spontaneous secretion of the proteins. The various conditions for the stimulation of the different cell lines by cytokines and PMA were defined. In contrast to the cell lines, normal thyrocytes did not secrete MMP-1 and only trace amount of TIMP-1, even after stimulation with PMA.

MATERIALS AND METHODS

Preparation of tissues, thyroid-derived cells, and cell lines

Thyrocytes were prepared from surgical thyroid specimens from 3 patients (1 Graves' disease, 2 nontoxic goiter; mean age 54.3 ± 5.0 years). Fibroblasts were separated from thyroid tissue of 5 other patients (3 Graves' disease, 2 nontoxic goiter; mean age 43.6 ± 6.4 years). Graves' disease and nontoxic goiter were diagnosed on the strength of clinical, biochemical, and immunologic features as well as thyroid scintiscans.

Thyroid tissue was trimmed of fat and connective tissue immediately after surgery. Thyroid-derived cells were enriched after gradual enzymatic digestion of tissue and cultured over a period of 16 hours as described. Thyrocytes were obtained from the adherent fraction by incubating

the cell monolayer with phosphate buffered saline (PBS) without $\text{Ca}^{2+}/\text{Mg}^{2+}$ for 45 minutes (22). Residual fibroblasts were removed after subsequent incubation of the cells with the fibroblast-specific mab FibAS01 (22) and goat-anti-mouse IgG-DYNABEADS® M450 (DYNAL, Hamburg, Germany) according to the manufacturer's protocol.

Thyroid-derived fibroblasts were obtained after culturing small pieces of thyroid tissue in Dulbecco's Modified Eagle's Medium (DMEM) with 10% fetal calf serum (FCS) and harvested in the 5th to 7th passage. The purity of the thyrocytes and fibroblasts was determined by using indirect immunofluorescence technique on a FACS-Scan (Becton Dickinson GmbH, Heidelberg, Germany) as described (22).

The following human anaplastic thyroid carcinoma cell lines were cultured in DMEM with 10% FCS: C 643 (23); SW 1736 (23); and HTh 74 (24). The cell line 8505 C (25) was purchased from the German Collection of Microorganisms and Animal Cell Cultures (DSM ACC219). This cell line was established from a primary thyroid tumor characterized histologically as a undifferentiated carcinoma that was partially composed of poorly differentiated papillary cells (25). This is a feature of a subgroup of anaplastic carcinoma (26). The majority of these coexistent better differentiated carcinoma foci in anaplastic carcinoma were papillary (26).

In vitro cultures

Using 24-well plates, 1×10^5 cells were cultured for 24 hours. The medium was aspirated and replaced with 500 μL OPTI-MEM (GIBCO BRL, Grand Island, NY) without FCS to eliminate possible stimulation of MMP-1 and TIMP-1 production by FCS. The medium contained the desired concentration of human IL-1 α (10 U/mL; Pepro Tech EC Ltd., London, UK), TNF- α (100 U/mL; Pepro Tech EC Ltd.), interferon- γ (IFN- γ) (500 U/mL; Pepro Tech EC Ltd.), or 10 ng/mL PMA (SIGMA).

Triplicate cultures of each stimulator were analyzed after 3, 6, and 24 hours at the mRNA and after 24 and 48 hours at the protein level. The supernatants were removed and stored at -80°C for further use. First, a collagenolytic assay based on the digestion of type I collagen was performed. This method showed direct evidence of free pro-MMP-1 enzyme in the cell culture supernatants of unstimulated and IL-1 α stimulated 8505 C, HTh 74, and C634 cells (data not shown). However, the method does not allow quantitation of MMP-1 enzyme activity. Thus, the cell culture supernatants were assayed for MMP-1, TIMP-1, and MMP1/TIMP-1 complex by ELISA (Amersham Life Sciences, Braunschweig, Germany). The MMP-1 assay (sensitivity: 1.7 ng/mL) detected only total human MMP-1, ie, free MMP-1 and MMP-1 complexed with inhibitors such as TIMP-1. It did not detect MMP-1 bound by the nonspecific protease inhibitor α_2 -macroglobulin. The MMP-1/TIMP-1 assay (sensitivity: 1.5 ng/mL) detected MMP-1/TIMP-1 complex, ie, activated MMP-1 that has been subsequently complexed with the specific MMP-1 inhibitor TIMP-1. It did not detect free active MMP-1, free TIMP-1, or pro-MMP-1. There was no cross-reactivity with active MMP-1 bound by the nonspecific protease inhibitor α_2 -macroglobulin. The TIMP-1 assay (sensitivity:

1.25 ng/mL) detected total human TIMP-1, ie, free TIMP-1 and that complexed with MMPs. The assay did fully cross-react with TIMP-1 in complexes with other MMP. It did not cross-react with TIMP-2.

RNA extraction and cDNA synthesis

For gene expression studies, 5 mL RNazol™ B (Biotex Laboratories Inc., Houston, TX) was added to the cell culture wells. The content of three wells of any cell type was pooled and then stored frozen for further mRNA analysis in liquid nitrogen. Total cellular RNA (cDNA) was isolated from the probes according to the manufacturer's protocol. RNA was fractionated on a denaturing 1.0% agarose gel and stained with ethidium bromide to confirm that spectrophotometric measurements were accurate and that the RNA had not been degraded. Five micrograms total RNA was reverse-transcribed to cDNA using the First-strand cDNA synthesis kit of Pharmacia (Uppsala, Sweden) in a total reaction volume of 15 μ L.

mRNA analysis by competitive RT-PCR

To correct for variations across different cDNA preparations, all samples were first adjusted to contain equal input glyceraldehyde-3-phosphate dehydrogenase (GAPDH) cDNA concentrations. Semi-quantitative GAPDH RT-PCR was used with a heterologous synthetic competitor fragment. The generation of the specific PCR products from the competitor and the cDNA with the GAPDH primers were published earlier (22,27).

We then estimated the MMP-1 and TIMP-1 cDNA in these adjusted samples. The primers were selected using the DNAsis computer program (Hitachi Software Engineering Co, Yokohama, Japan). The primer pairs span one or more introns to allow unambiguous discrimination between cDNA and unwanted contaminating genomic DNA. In quantitating MMP-1 and TIMP-1 cDNA, a rapid one-step method was introduced to synthesize an internal homologous competitor (plan diagram of procedure: Fig. 1, exemplary for MMP-1 [28]). A hybrid primer was synthesized (MMP-1hy) that consisted of two segments (seg₁, seg₂). It

had a length of 40 nucleotides, in which 20 nucleotides (seg₁) at the 3' end corresponded to the opposite strand of the target sequence a predetermined distance from primer MMP-1f, and 20 nucleotides at the 5' end (seg₂ = MMP-1r) that corresponded to the target sequence upstream from the segment seg₁. Amplification with the primers MMP-1f and MMP-1hy from the cDNA resulted in a 478-base pair (bp) (polymerase chain reaction (PCR) product. It was freed from excess primers and deoxynucleoside-triphosphates (dNTPs) using the Qiaquick Gel Extraction Kit (Qiagen GmbH, Hilden, Germany) and quantified. A known number of copies of the competitor was introduced in the GAPDH-adjusted samples and amplified with the primers MMP-1f and MMP-1r. With this approach, two products were generated, one derived from the cDNA (560 bp) and another, 82 bp smaller in size derived from the internal competitor (Fig. 1). PCR products were resolved by gel electrophoresis (1.5% agarose gel). The relative amounts of sample cDNA and competitor were quantified by measuring the intensity of ethidium fluorescence with a CCD image sensor and analyzing the data with the EASY program (Herolab, Wiesloch, Germany). The initial amounts of sample cDNA and competitor were assumed to be equal in those reactions where the ratio of the two products was judged to be equal. This was expressed in arbitrary units (AU) (22,29). One AU was defined as the lowest concentration of competitor yielding a detectable amplification product when added to PCR alone. For example, if equivalence between sample cDNA and competitor was reached using a 100-fold concentrated competitor the relative sample cDNA concentration was 100 AU. Thyrocytes and the cell lines were analyzed for the expression of thyroid-specific and cytokine receptor mRNAs in a simple RT-PCR. The sequences of the TPO and cytokine receptor primer pairs have been published by Watson et al. (30) and Tada et al. (31) and gave the following product sizes: TPO: 506 bp; IL-1R type I (p80): 300 bp; IL-1R type II (p68): 392 bp; TNF- α R (p75): 324 bp; TNF- α R (p55): 587 bp and IFN- γ R: 899 bp. The thyroglobulin (Tg) and thyroid stimulating hormone receptor (TSH-R) primer pairs were selected according to the published sequences using the DNAsis program (Table 1).

Each 25- μ L amplification reaction contained 2.5 μ L 10 \times concentrated PCR buffer (15 mM MgCl₂, Boehringer Mannheim, Germany), 0.3 U Taq DNA polymerase (Boehringer Mannheim, Germany), 100 μ M dNTPs (Perkin Elmer, Weiterstadt, Germany), 0.1 μ M of each primer (IMB, Jena, Germany), and 1 μ L cDNA and competitor in adjusted dilution. Furthermore, restriction mapping (restriction enzymes: Boehringer Mannheim GmbH, Germany) was carried out to confirm the originality of the PCR product (Fig. 1, Table 1).

Statistics

Protein levels of thyrocyte or fibroblast cultures from the different patients and of the thyroid carcinoma cell lines obtained from three separate experiments were presented as mean \pm SEM values. Statistical comparisons between unstimulated and stimulated cell cultures were performed by the alternate (Welch) t-test. The correlation between basal mRNA levels and the unstimulated protein secretion in all cell types was calculated according to the Spearman method.

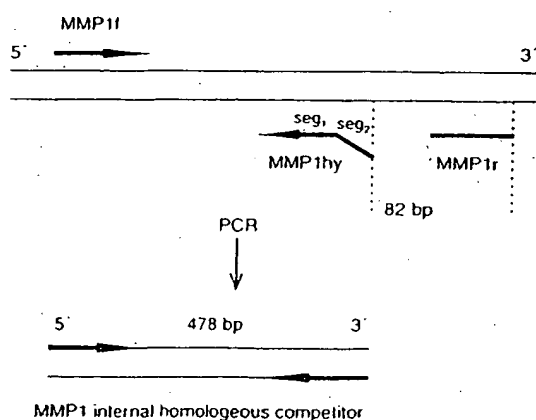


FIG. 1. General scheme for generating homologous competitors used for quantitative PCR.

TABLE 1. PRIMERS, LENGTH OF AMPLIFIED TEMPLATES, RESTRICTION MAPPING AND ASSAY CONDITIONS FOR RT-PCR

		Primer	Length of -3' cDNA (bp)	Length of competitor (bp)	Annealing temperature	Number of cycles
Tg	forward	GCAGATCTTACTGAGTGGCT	416		60	35
	reverse	TGTCAGCACAGTGGCAATAC				
TSH-R exons 1-4	forward	ACTTGCTGCAGCTGGTGCT	354		65	35
	reverse	TGAGGGCATCAGGCTCTATG				
TSH-R exons 4-10	forward	GAAATTCGGAATACCAGGAACCTTA ACT	896		53	35
	reverse	AACTCATCGGACTTGGGGGTACA				
MMP-1	forward	TGGGAGCAAACACATCTGAC	560	478	64	33
	reverse	ATCACTTCTCCCGAATCGT				
	hybrid	ATCACTTCTCCCGAATCGT CCATATATGGCTTGGATGCC				
TIMP-1	forward	CTTAGGGGATGCCGCTGACA	351	274	64	30
	reverse	GGCAGGCAGGCAAGGTGACG				
	hybrid	GGCAGGCAGGCAAGGTGACG GGATGGATAAACAGGGAAC				

Tg indicates thyroglobulin; TSH-R, thyroid stimulating hormone receptor; MMP-1, matrix metalloproteinase-1; TIMP-1, tissue inhibitor of metalloproteinase-1; bp, base pair.

RESULTS

Thyroid specific and cytokine receptor mRNA expression

Isolated thyrocytes as well as 8505 C cells expressed Tg and thyroperoxidase (TPO) mRNA, whereas transcripts of the TSH-R (exons 1-4, 354 bp, exons 4-10, 896 bp) were present only in the thyrocytes. The three anaplastic thyroid carcinoma cell lines SW 1736, C 634, and HTh 74 were completely negative for the Tg, TPO, and TSH-R mRNAs (Fig. 2). All cell lines and thyrocytes expressed IL-1R (type I and type II), TNF- α (p75 and p55) and IFN- γ mRNA (Fig. 2).

Basal MMP-1 and TIMP-1 mRNA and protein expression

In most stimulation experiments, mRNA levels did not increase until 24 hours of incubation. The 24-hour mRNA levels are shown in Figures 3 and 4. The 3- and 6-hour levels are demonstrated in those experiments where the mRNA levels reached their peak before 24 hours of stimulation. If not otherwise indicated, the MMP-1 levels were measured using the ELISA system, which recognizes free/complexed MMP-1.

MMP-1 and TIMP-1 mRNA were found during unstimulated culture in all investigated cell types, although the mRNA levels varied over a great range. 8505 C showed a basal MMP-1 mRNA level 20 times as high as those of the HTh 74 cells, 6×10^4 times as high as C 643, and 2×10^6 times as high as SW 1736 cells. In thyrocytes, MMP-1 mRNA levels were found near the detection limit (Figs. 3 and 4).

Generally, when analyzing the noted cell types, the measured basal MMP-1 or TIMP-1 mRNA levels correlated well with the basal protein expression (MMP-1: $r = 0.99$, $p < .0001$; TIMP-1: $r = 0.98$, $p < .002$). Corresponding to the high MMP-1 mRNA level, 8505 C cells secreted extremely high levels of MMP-1. No MMP-1 or TIMP-1 was

detected in unstimulated thyrocyte cultures at any time-point examined. All other cell types showed a spontaneous MMP-1 and TIMP-1 secretion (Figs. 5 and 6). Thyroid-derived fibroblasts produced basal TIMP-1 levels of up to 4 times higher in the four carcinoma cell lines, which secreted nearly the same amounts of basal TIMP-1 protein. Nevertheless, TIMP-1 secretion of fibroblasts was found at lower levels than expected after TIMP-1 mRNA measurement in 4 of 5 analyzed patients. The results of the fibroblast cultures from patient five showing a higher TIMP-1 expression than those from the 4 other patients (basal 24 hour: 50 ± 2 ; PMA 24 hour: 90 ± 6 ng/mL TIMP-1) was omitted in Figure 6.

Comparing the basal amount of free/complexed and TIMP-1 complexed MMP-1 after 24 hours of stimulation, a significant level of MMP-1 was not complexed with TIMP-1 in 8505 C cultures, whereas in fibroblast cultures most of the MMP-1 activity was inhibited by TIMP-1. The anaplastic carcinoma cell line HTh 74 did not show such a great discrepancy between free/complexed and TIMP-1 complexed MMP-1 level as 8505 C cells (Fig. 7).

Effects of IL-1 α on MMP-1 and TIMP-1 mRNA and protein expression

Experiments were performed to determine whether human thyroid epithelial cells and thyroid carcinoma cell lines could produce or increase basal MMP-1 and TIMP-1 secretion after exposure to various stimuli. The results from these stimulation experiments are summarized in Figures 3 through 5. Generally, there was a delay in protein secretion level in comparison to the mRNA expression level. At the protein level, the cytokine-mediated stimulating or inhibiting effect is more distinct after 48 hours compared with 24 hours, even when the mRNA level had already decreased after 6 hours.

IL-1 upregulated MMP-1 mRNA in SW 1736 cells up to 100 times and, in thyroid-derived fibroblasts, up to 12 times after 24 hours of incubation (Fig. 3). This increased mRNA level was accompanied by a significantly enhanced

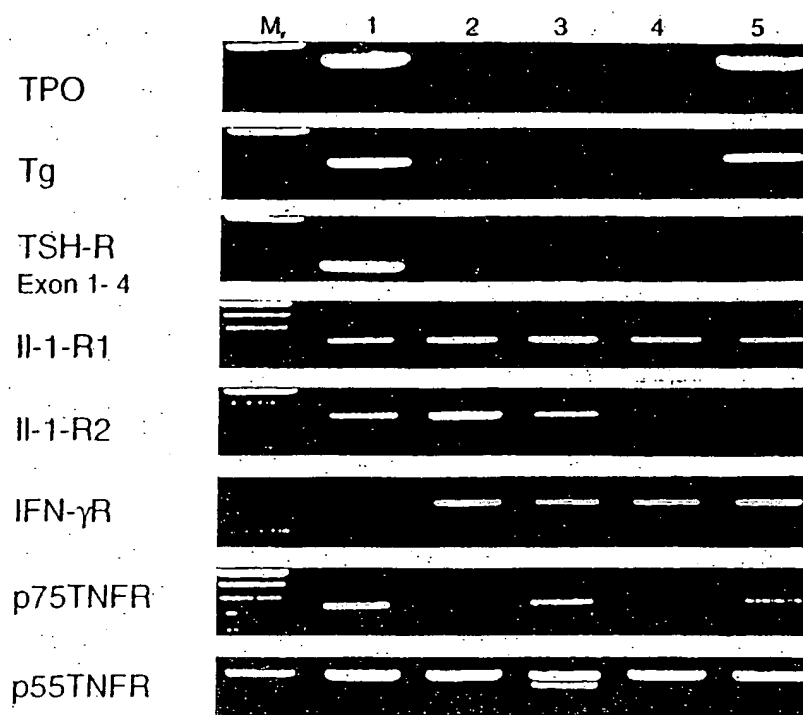


FIG. 2. Amplification of thyroid specific and interleukin-receptor mRNA in thyrocytes (1), SW 1736 (2), C 643 (3), HTH 74 (4) and 8505 C (5) cells using RT-PCR; M_r = 100-bp ladder (GIBCO).

MMP-1 secretion after 48 hours. Furthermore, IL-1 α increased MMP-1 mRNA expression in thyrocytes up to seven times after 6 hours, but no MMP-1 protein could be detected in thyrocyte cultures. IL-1 had no stimulatory effect on MMP-1 mRNA expression in C 643, HTh 74, and 8505 C cells after 24 hours, although a significant increase of MMP-1 secretion was found in HTh-74 and SW 1736 cells after 48 hours of incubation (Fig. 5). This discrepancy may be explained by a possible increase in MMP-1 mRNA level after 24 hours of stimulation. The same effect could also be observed in the IL-1 stimulated TIMP-1 at the mRNA as well as the protein level: the only slight effect of IL-1 on TIMP-1 mRNA expression in carcinoma cell lines after 24 hours was accompanied by a significant increase of TIMP-1 secretion in 8505 C and HTh 74 cells after 48 hours (Figs. 4 and 6).

Effects of TNF- α on both MMP-1/TIMP-1 mRNA and protein expression

In contrast to IL-1, TNF- α did not stimulate the MMP-1 and TIMP-1 mRNA and protein levels in all carcinoma cell lines and thyrocytes. Only thyroid-derived fibroblasts responded with a slight upregulation of MMP-1 and TIMP-1 mRNA expression after TNF- α stimulation, which was not accompanied by an increase of MMP-1 and TIMP-1 secretion.

Effects of PMA, and IFN- γ on MMP-1 and TIMP-1 mRNA and protein expression

PMA was included in our study as a positive control because it is known to upregulate or induce both MMP-1 and TIMP-1 secretion in various cell types (1,32). Indeed, PMA was able to induce or enhance MMP-1 mRNA levels in all cell types investigated, although the detected levels varied to a large extent (Fig. 3). This result is in good correlation with the significantly increased MMP-1 protein levels that were already detectable after 24 hours of stimulation (Fig. 5). PMA upregulated TIMP-1 mRNA levels by up to 20 times in C 643, and up to 2 times in SW 1736 and HTh 74 cells, fibroblasts and thyrocytes, but it did not change the TIMP-1 mRNA content in 8505 cells (Fig. 4). At the protein level, we found a significant stimulation of TIMP-1 secretion in C 643 and HTh 74 cells, as well as in thyroid-derived fibroblasts (Fig. 6).

In contrast to PMA, IFN- γ was without effect on stimulation or downregulation of MMP-1 and TIMP-1 mRNA or protein in any of the cell types investigated (Figs 5 and 6).

The main inhibitor of MMP-1 is TIMP-1, which forms 1:1 stoichiometric complexes with MMP-1, although some other inhibitors can also bind MMP-1. On the other hand, TIMP-1 can bind other MMP types.

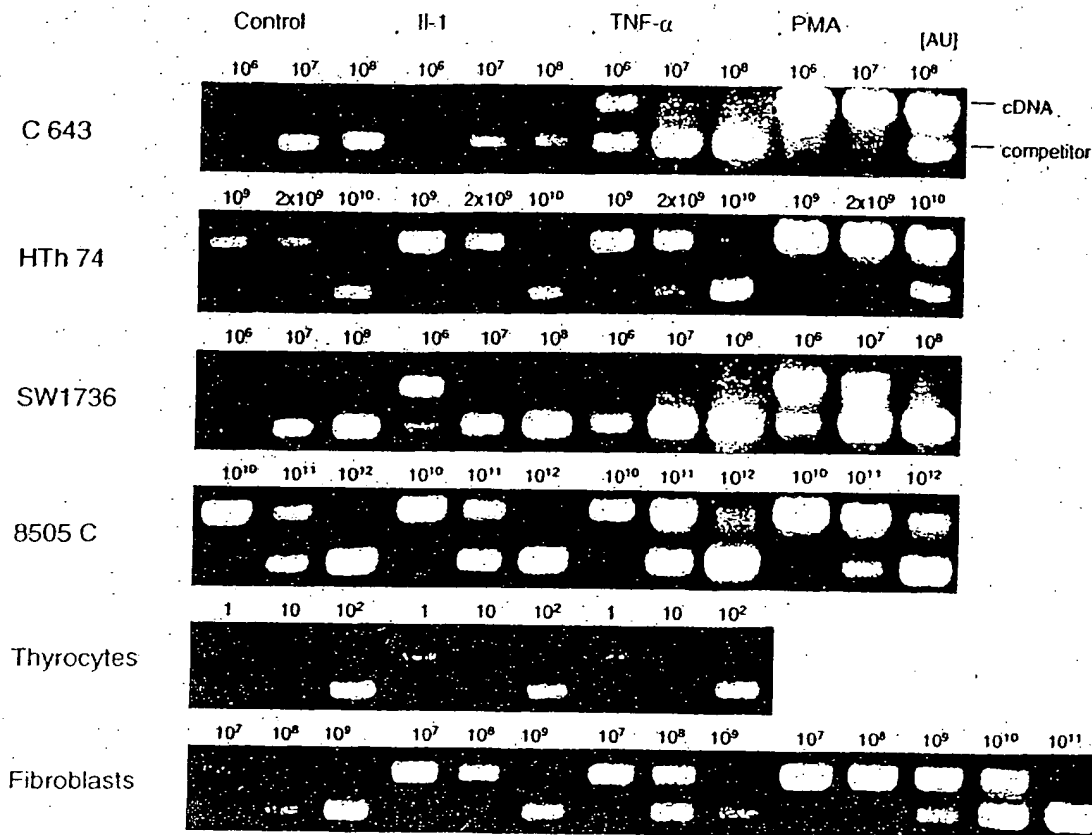


FIG. 3. Representative samples of competitive amplified MMP-1 mRNA of thyrocytes, thyroid-derived fibroblasts and thyroid carcinoma cell lines without stimulation (control) and after stimulation with 10 U/mL IL-1 α and 100 U/mL TNF- α and 10 ng/mL PMA after 24 hours. Serial dilutions of known amounts of the competitor fragment were coamplified with identical aliquots of cDNA. The 560-bp (cDNA) and 478-bp (competitor) PCR products were visualized by agarose gel electrophoresis and ethidiumbromide staining. The relative concentration of the added competitor was given in arbitrary units (AU) in the figure. One AU was defined as the lowest concentration of the competitor yielding a detectable amplification for MMP-1 mRNA. The ratio of competitor to cDNA fragments was determined by measuring the intensity of ethidium fluorescence with a CCD image sensor and analysis of data. Measured cDNA concentration can be expressed in AU.

DISCUSSION

Our findings demonstrate for the first time that thyroid carcinoma cell lines are able to express MMP-1 and TIMP-1 mRNA and protein at significant levels *in vitro*. The observation of spontaneous release of MMP-1 and TIMP-1 corresponds well with earlier studies covering the secretion of these proteins by several carcinoma cell lines (33,34).

However, in contrast to its clear physiological function in extracellular matrix breakdown, the role of MMP-1 in tumor growth and metastases is still controversial (9-11,35). Recently, Murray et al. (10) demonstrated that MMP-1 is associated with poor prognosis in colorectal cancer, and has a prognostic value independent of the Dukes stage. Therefore, MMP-1 could be a target for therapeutic intervention in such tumors. Furthermore, the hypothesis of whether or not cancer cells themselves are able to

produce MMP, or whether cancer cells stimulate the surrounding stromal cells to secrete MMP *in vivo*, is disputed. MMP-1 mRNA and protein were detected by both *in situ* hybridization and immunohistochemistry in stromal as well as tumor cells of head, neck, gastric, colorectal, and mammary carcinomas (9,10,36,37). In contrast, Kameyama (12) demonstrated by *in situ* hybridization that the MMP-1 mRNA was not expressed in the cancer cells but in the surrounding fibrous capsules of strongly differentiated papillary thyroid carcinoma tissue. Highly differentiated follicular carcinomas and follicular adenomas were depleted for MMP-1 transcripts. Undifferentiated follicular, papillary, and aggressive anaplastic carcinomas that showed poor prognosis and strong tumor invasive and metastatic potential and that can be compared in their morphological, genetic and growth features with undifferentiated thyroid carcinoma cell lines were not included this

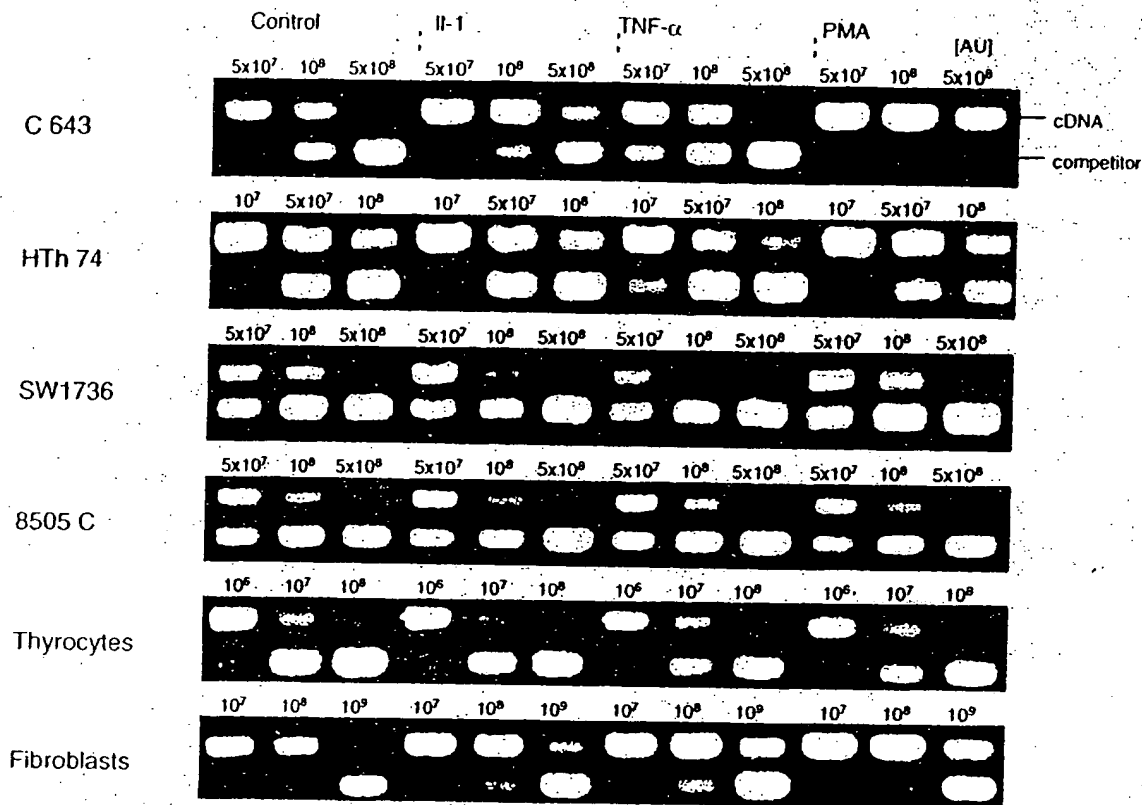


FIG. 4. Competitive TIMP-1 mRNA RT-PCR yielding a 351-bp (cDNA) and a 274-bp (competitor) PCR product. For further details see Figure 3.

study. However, the missing expression of MMP-1 by normal thyrocytes and the spontaneous secretion of this protein by highly malignant thyroid carcinoma cell lines, as demonstrated in our study, indicate the involvement of MMP-1 secretion of transformed thyrocytes in aggressive thyroid tumors.

Although all cell lines analyzed in our study spontaneously secreted MMP-1, we observed marked differences in the basal secretion capacity. The highest MMP-1 levels were determined in cultures of 8505 C cells. Only 8505 C cells expressed TPO and Tg mRNA that may be put down to residual differentiated components in the cell line (see *Materials*). However, none of the analyzed cell lines expressed TSH-R mRNA. The cell population doubling times were less than 40 hours. All cell lines had accumulations of multiple genetic events. These facts indicate the undifferentiated pathology of the studied lines. It is well known that anaplastic carcinoma cell lines well retain the malignant characteristics of their parental tumors (38–40).

Furthermore, we found a distorted proportion between MMP-1 and TIMP-1 mRNA/protein for carcinoma cell lines but not for normal thyroid-derived fibroblasts. The most disadvantageous constellation between MMP-1 and TIMP-1 was found in 8505 C cells. Similar to other studies (41), these results suggest the influence of an altered MMP/TIMP relation on tumor progression. However, it

should be mentioned that most studies, including the present one, do not take into consideration that a number of inhibitors distinct from TIMP-1 may regulate MMP-1 activity. Taking into account that the balance of active enzyme and TIMP-1 concentration strongly influence the extent of local matrix degradation, a number of studies showed unexpectedly high levels of TIMP-1 in malignant neoplasms (9,42,43). There is a great discussion as to whether the overall expression of MMP-1 and TIMP-1 or the amount of noncomplexed MMP-1 could be critical in aggressive tumor development. This fact underlines the nature of tissue breakdown, reflecting the complicated network of selective and coordinated production of individual proteinases and inhibitors under normal and pathophysiological conditions. Thus, the invasive and metastatic potential of thyroid tumors depends on the local net level of active MMPs.

The synthesis of MMP-1 and TIMP-1 is influenced by a variety of biochemical stimuli. The recent findings on MMP-1 and TIMP-1 gene promoters are useful in understanding the complex mechanisms implied in the regulation of MMP synthesis modulated by cytokines and tumor promoters (34,44,45). The promoter regions contain tumor promoter responsive elements (TRE) and binding motifs for the transcription factor PEA-3, which are recognized by proto-oncogenic transcription factors, such as the

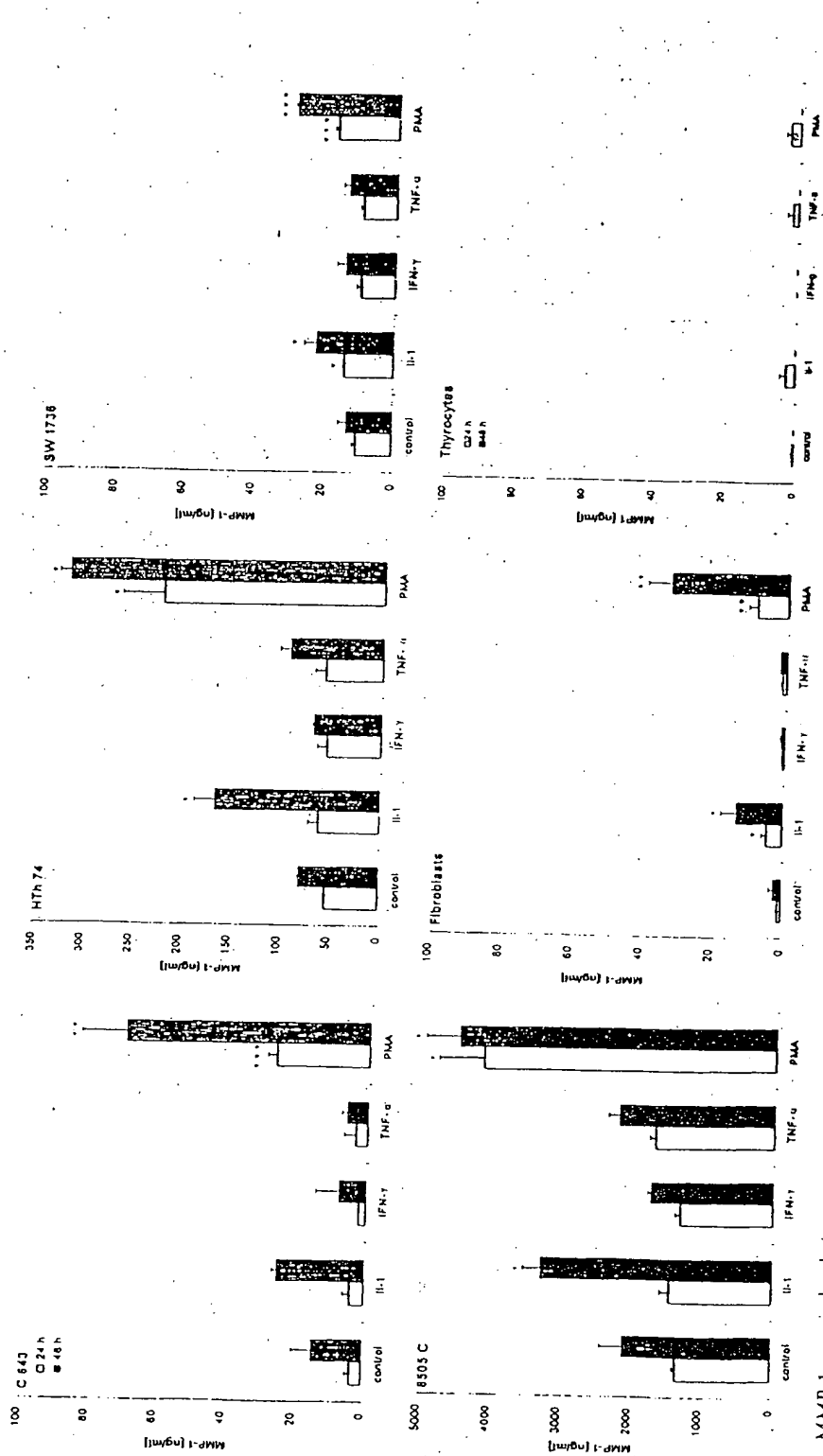


FIG. 5. MMP-1 protein levels (mean \pm SEM) in supernatants of unstimulated and stimulated cultures of thyrocytes ($n = 3$), thyroid-derived fibroblasts ($n = 4$) and the thyroid carcinoma cell lines 8505 C, SW 1736, C 643, HTh 74 ($n = 3$) detected by MMP-1 ELISA, which recognizes total MMP-1, i.e., free MMP-1 and that complexed with inhibitors such as TIMP-1, but not α_2 -macroglobulin. Cells were stimulated with 10 U/mL IL-1 α , 100 U/mL TNF- α , 500 U/mL IFN- γ , or 10 ng/mL PMA for 24 and 48 hours. For fibroblasts, each point represents the mean \pm SEM of four different donors, each experiment performed in triplicate. For cell lines, each point represents the mean \pm SEM of three separate experiments each performed in triplicate. Significant differences between the basal and stimulated MMP-1 levels are indicated by asterisks (* $p < .05$; ** $p < .01$; *** $p < .005$). Please note the differences in scale between 8505 C, HTh 74, and the other cell types.

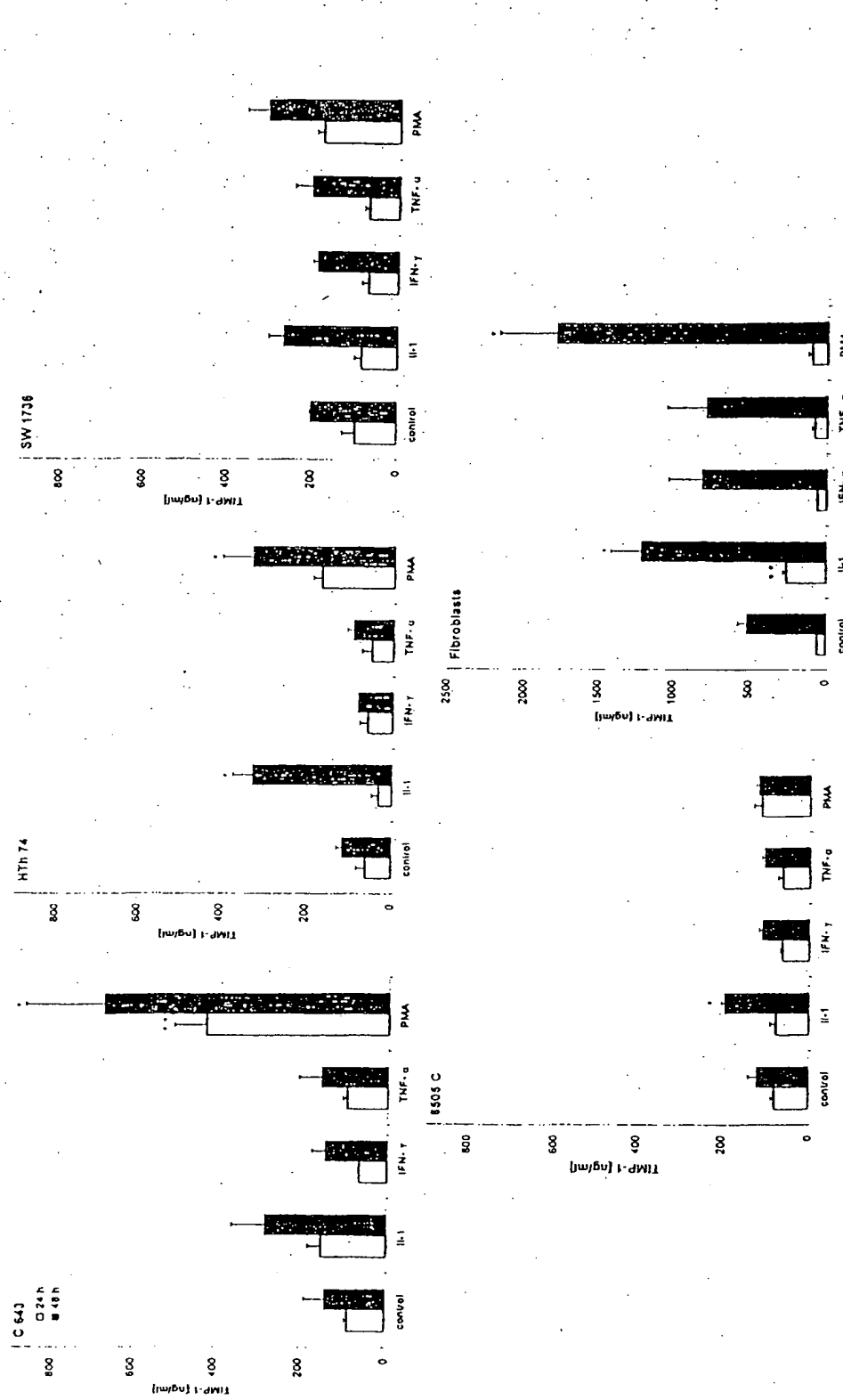


FIG. 6. ELISA detection of free and MMP-complexed TIMP-1 (mean \pm SEM). Asterisks indicate significant differences between the basal and stimulated TIMP-1 levels (* p < .05; ** p < .01; *** p < .005). For further details see Figure 5. Please note the differences in scale between fibroblasts and the other cell types.

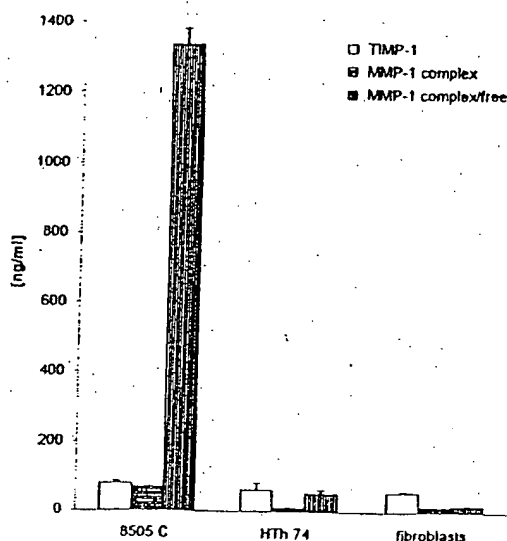


FIG. 7. Comparison between (i) free/complex and (ii) TIMP-1 complexed MMP-1 levels, and (iii) TIMP-1 levels in supernatants of unstimulated 8505 C and HTh 74 cells, and thyroid-derived fibroblasts after 24 hours using a (i) MMP-1 ELISA that recognizes total MMP-1 (see Figure 5). The (ii) MMP-1/TIMP-1 assay recognizes MMP-1/TIMP-1 complexes, ie, activated MMP-1 that has subsequently been complexed with the specific MMP inhibitor TIMP-1. The (iii) TIMP-1 ELISA recognizes total TIMP-1, ie, free TIMP-1 and that complexed with MMPs.

fos and *jun* family (45–47). IL-1, TNF- α , and PMA up-regulate proto-oncogenes like *fos* and *jun*, resulting in the stimulation of MMP-1 and TIMP-1 (45,48). The action of the cytokines is mediated by their specific receptors. In our study, IL-1R (type I and type II), TNF- α R (p75 and p55) and IFN- γ R mRNAs were demonstrated in all investigated cell types. PMA and IL-1 were shown to elevate MMP-1 and TIMP-1 in nearly all cell types investigated, thus confirming the results of several studies on other epithelial cells (reviewed in refs. 1,7,49). In the majority of experiments, we found a concordant expression of MMP-1 and TIMP-1 after stimulation, possibly achieved by the coordinated actions of the nuclear transcription factors, although MMP-1 and TIMP-1 expression can also be independently or even reciprocally regulated (1). The effect of TNF- α was not as distinct as in the case of PMA and IL-1, although several investigators found a pronounced effect of TNF- α particularly on TIMP-1 secretion (4,34). In contrast to studies performed with other cell types (863,864,819), IFN- γ did not influence MMP-1 and TIMP-1 expression in thyroid carcinoma cell lines. In summary, the involvement of the intrathyroidal physiological and pathological cytokine microenvironment in the regulation of MMP-1 and TIMP-1 induction activation and inhibition is strongly suggested.

Furthermore, the data demonstrate that regular human thyrocytes did not produce MMP-1, even after powerful stimulation with PMA. Investigating other mammalian epithelial cells, only one study revealed the production of

MMP-1 by rabbit corneal cells (21). It is yet not clear whether the MMP-1 mRNA detected in thyrocytes is due to a low level of constitutive transcription of the MMP-1 gene (illegitimate transcription), an existing pool of stable MMP-1 mRNA, or *in vitro* induction of MMP-1 mRNA. But it seems more likely that residual fibroblasts contained in the purified thyrocyte preparation (<0.2%) are responsible for the slightly positive RT-PCR results. Another explanation could be that thyrocytes are indeed MMP-1 producers, but the ELISA detection system used was not sensitive enough to measure extremely low MMP-1 secretion levels. Furthermore, the discrepancy between elevated TIMP-1 mRNA levels of thyrocytes and the extremely low TIMP-1 protein secretion by these cells is difficult to explain. Post-transcriptional regulatory events may be responsible for this confounding result.

Taken together, the present study suggests that the intrathyroidal cytokine microenvironment is involved in the regulation of MMP-1 and its inhibitor TIMP-1 in the thyroid, and that both proteins may be secreted by dedifferentiated thyroid carcinoma cells and involved in aggressive thyroid tumors *in vivo*.

REFERENCES

1. Ries C, Petrides PE 1995 Cytokine regulation of matrix metalloproteinase activity and its regulatory dysfunction in disease. *Biol Chem Hoppe Seyler* 376:345–355.
2. Pierce RA, Sandefur S, Doyle GA, Welgus HG 1996 Monocytic cell type-specific transcriptional induction of collagenase. *J Clin Invest* 97:1890–1899.
3. Pan L, Eckhoff C, Brinckerhoff CE 1995 Suppression of collagenase gene expression by all-trans and 9-cis retinoic acid is ligand dependent and requires both RARs and RXRs. *J Cell Biochem* 57:575–589.
4. Shingu M, Nagai Y, Isayama T, Naono T, Nobunaga M 1993 The effects of cytokines on metalloproteinase inhibitors (TIMP) and collagenase production by human chondrocytes and timp production by synovial cells and endothelial cells. *Clin Exp Immunol* 94:145–149.
5. Goldberg GI, Wilhelm SM, Kronberger A, Bauer EA, Grant GA, Eisen AZ 1986 Human fibroblast collagenase. Complete primary structure and homology to an oncogene transformation-induced rat protein. *J Biol Chem* 261:6600–6605.
6. Docherty AJ, Lyons A, Smith BJ, Wright EM, Stephens PE, Harris TJ, Murphy G, Reynolds JJ 1985 Sequence of human tissue inhibitor of metalloproteinases and its identity to erythroid-potentiating activity. *Nature* 318:66–69.
7. Mauviel A 1993 Cytokine regulation of metalloproteinase gene expression. *J Cell Biochem* 53:288–295.
8. Murphy G 1995 Matrix metalloproteinases and their inhibitors. *Acta Orthop Scand Suppl* 266:55–60.
9. Nomura H, Fujimoto N, Seiki M, Mai M, Okada Y 1996 Enhanced production of matrix metalloproteinases and activation of matrix metalloproteinase 2 (gelatinase A) in human gastric carcinomas. *Int J Cancer* 69:9–16.
10. Murray GI, Duncan ME, O'Neil P, Melvin WT, Fothergill JE 1996 Matrix metalloproteinase-1 is associated with poor prognosis in colorectal cancer. *Nat Med* 2:461–462.
11. Onisto M, Garbisa S, Caenazzo C, Freda MP, Di Francesco C, Nitti D, Liotta LA, Stetler-Stevenson WG 1993 Reverse transcription-polymerase chain reaction phenotyping of met-

- allopeptinases and inhibitors involved in tumor matrix invasion. *Diagn Mol Pathol* 2:74-80.
12. Kameyama K 1996 Expression of MMP-1 in the capsule of thyroid cancer—Relationship with invasiveness. *Pathol Res Pract* 192:20-26.
 13. Campo E, Merino MJ, Liotta L, Neumann R, Stetler-Stevenson W 1992 Distribution of the 72-kd type IV collagenase in nonneoplastic and neoplastic thyroid tissue. *Hum Pathol* 23:1395-1401.
 14. Demeure MJ, Damsky CH, Elfman F, Goretzki PE, Wong MG, Clark O 1992 Invasion by cultured human follicular thyroid cancer correlates with increased beta 1 integrins and production of proteases. *World J Surg* 16:770-776.
 15. Nakano T, Kusunoki T, Funasaka K, Murata K, Nishida S, Tomura T 1995 Study of type I and IV collagenase activity in human thyroid diseases. *Nippon Jibiinkoka Gakkai Kaiho* 98:937-941.
 16. Zedenius J, Stahle-Backdahl M, Enberg U, Grimelius L, Larsson C, Wallin G, Backdahl M 1996 Stromal fibroblasts adjacent to invasive thyroid tumors: expression of gelatinase A but not stromelysin 3 mRNA. *World J Surg* 20:101-106.
 17. Arai M, Niioka M, Maruyama K, Wada N, Fujimoto N, Nomiya T, Tanaka S, Okazaki I 1996 Changes in serum levels of metalloproteinases and their inhibitors by treatment of chronic hepatitis C with interferon. *Dig Dis Sci* 41:995-1000.
 18. Nikkari ST, O'Brien KD, Ferguson M, Hatsukami T, Welgus HG, Alpers CE, Clowes AW 1995 Interstitial collagenase (MMP-1) expression in human carotid atherosclerosis. *Circulation* 92:1393-1398.
 19. Knowlden J, Martin J, Davies M, Williams JD 1995 Metalloproteinase generation by human glomerular epithelial cells. *Kidney Int* 47:1682-1689.
 20. Buisson AC, Zahm JM, Polette M, Pierrot D, Bellon G, Puchelle E, Birembaut P, Tournier JM 1996 Gelatinase B is involved in the in vitro wound repair of human respiratory epithelium. *J Cell Physiol* 166:413-426.
 21. Tao Y, Bazan HE, Bazan NG 1995 Platelet-activating factor induces the expression of metalloproteinases-1 and -9, but not -2 or -3, in the corneal epithelium. *Invest Ophthalmol Vis Sci* 36:345-354.
 22. Aust G, Heuer M, Laue S, Lehmann I, Hofmann A, Heldin N-E, Scherbaum WA 1996 Expression of TNA-alpha mRNA and protein in pathological thyroid tissue and carcinoma cell lines. *Clin Exp Immunol* 105:148-154.
 23. Mark J, Ekedahl C, Dahlfors R, Westermark B 1987 Cytogenetical observations in five human anaplastic thyroid carcinomas. *Hereditas* 107:163-174.
 24. Heldin NE, Cvejic D, Smeds S, Westermark B 1991 Coexpression of functionally active receptors for thyrotropin and platelet-derived growth factor in human thyroid carcinoma cells. *Endocrinology* 129:2187-2193.
 25. Ito T, Seyama T, Hayashi Y, Hayashi T, Dohi K, Mizuno T, Iwamoto KS, Tsuyama N, Nakamura N, Akiyama M 1994 Establishment of two human thyroid carcinoma cell lines (8305C, 8505C) bearing p53 gene mutations. *International Journal of Oncology* 4:583-586.
 26. Wallin G, Backdahl M, Tallroth-Ekman E, Lundell G, Auer G, Lowhagen T 1989 Co-existent anaplastic and well differentiated thyroid carcinomas: a nuclear DNA study. *Eur J Surg Oncol* 15:43-48.
 27. Heuer M, Aust G, Ode-Hakim S, Scherbaum WA 1996 Different cytokine mRNA profiles in Graves' disease, Hashimoto's thyroiditis and non-autoimmune thyroid disorders determined by quantitative reverse transcriptase chain reaction (RT-PCR). *Thyroid* 6:97-106.
 28. Celi FS, Zenilman ME, Shuldiner AR 1993 A rapid and versatile method to synthesize internal standards for competitive PCR. *Nucleic Acids Res* 21:1047.
 29. Platzer C, Ode-Hakim S, Reinke P, Docke WD, Ewert R, Volk HD 1994 Quantitative PCR analysis of cytokine transcription patterns in peripheral mononuclear cells after anti-CD3 rejection therapy using two novel multispecific competitor fragments. *Transplantation* 58:264-268.
 30. Watson PF, Pickerill AP, Davies R, Weetman AP 1994 Analysis of cytokine gene expression in Graves' disease and multinodular goiter. *J Clin Endocrinol Metab* 79:355-360.
 31. Tada M, Diserens AC, Desbaillets I, de Tribolet N 1994 Analysis of cytokine receptor messenger RNA expression in human glioblastoma cells and normal astrocytes by reverse-transcription polymerase chain reaction. *J Neurosurg* 80:1063-1073.
 32. Nakano A, Tani E, Miyazaki K, Yamamoto Y, Furuyama J 1995 Matrix metalloproteinases and tissue inhibitors of metalloproteinases in human gliomas. *J Neurosurg* 83:298-307.
 33. Whitelock JM, O'Grady RL, Gibbins JR 1991 Interstitial collagenase (matrix metalloproteinase 1) associated with the plasma membrane of both neoplastic and nonneoplastic cells. *Invasion Metastasis* 11:139-148.
 34. Mackay AR, Ballin M, Pelina MD, Farina AR, Nason AM, Hartzler JL, Thorgeirsson UP 1992 Effect of phorbol ester and cytokines on matrix metalloproteinase and tissue inhibitor of metalloproteinase expression in tumor and normal cell lines. *Invasion Metastasis* 12:168-184.
 35. Urbanski SJ, Edwards DR, Maitland A, Leco KJ, Watson A, Kossakowska AE 1992 Expression of metalloproteinases and their inhibitors in primary pulmonary carcinomas. *Br J Cancer* 66:1188-1194.
 36. Polette M, Clavel C, Muller D, Abecassis J, Binnering I, Birembaut P 1991 Detection of mRNAs encoding collagenase 1 and stromelysin 2 in carcinomas of the head and neck by in situ hybridization. *Invasion Metastasis* 11:76-83.
 37. Clavel C, Polette M, Doco M, Binnering I, Birembaut P 1992 Immunolocalization of matrix metallo-proteinases and their tissue inhibitor in human mammary pathology. *Bull Cancer (Paris)* 79:261-270.
 38. Boghaert ER, Aini K, Taylor K, Greenberg VL, Fowler C, Zimmer SG 1996 Quantitative and qualitative differences in growth, invasion and lung colonization of an anaplastic and a papillary human thyroid cancer cell line in vitro and in vivo. *Clin Exp Metastasis* 14:440-450.
 39. Asakawa H, Kobayashi T, Komoike Y, Yamagawa T, Takahashi M, Wakasugi E, Maruyama H, Tamaki Y, Matsuzawa Y, Monden M 1996 Establishment of anaplastic thyroid carcinoma cell lines useful for analysis of chemosensitivity and carcinogenesis. *J Clin Endocrinol Metab* 81:3547-3552.
 40. Viglietto G, Maglione D, Rambaldi M, Ceruni J, Romano A, Trapasso F, Fedele M, Ippolito P, Chiappetta G, Bortti G, et al 1995 Upregulation of vascular endothelial growth factor (VEGF) and downregulation of placenta growth factor (PIGF) associated with malignancy in human thyroid tumors and cell lines. *Oncogene* 11:1569-1579.
 41. Nuovo GJ, MacConnell PB, Simsir A, Valea F, French DL 1995 Correlation of the in situ detection of polymerase chain reaction-amplified metalloproteinase complementary DNAs and their inhibitors with prognosis in cervical carcinoma. *Cancer Res* 55:267-275.
 42. Naruo S, Kanayama H, Takigawa H, Kagawa S, Yamashita K, Hayakawa T 1994 Serum levels of a tissue inhibitor of

- metalloproteinases-1 (TIMP-1) in bladder cancer patients. *Int J Urol* 1:228-231.
43. Kossakowska AE, Urbanski SJ, Watson A, Hayden LJ, Edwards DR 1993 Patterns of expression of metalloproteinases and their inhibitors in human malignant lymphomas. *Oncol Res* 5:19-28.
44. Edwards DR, Rocheleau H, Sharma RR, Wills AJ, Cowie A, Hassell JA, Heath JK 1992 Involvement of AP1 and PEA3 binding sites in the regulation of murine tissue inhibitor of metalloproteinases-1 (TIMP-1) transcription. *Biochim Biophys Acta* 1171:41-55.
45. Schonthal A, Herrlich P, Rahmsdorf HJ, Ponta H 1988 Requirement for fos gene expression in the transcriptional activation of collagenase by other oncogenes and phorbol esters. *Cell* 54:325-334.
46. Gutman A, Wasylyk B 1990 The collagenase gene promoter contains a TPA and oncogene; responsive unit encompassing the PEA3 and AP-1 binding sites. *EMBO J* 9:2241-2246.
47. Wasylyk C, Gutman A, Nicholson R, Wasylyk B 1991 The c-Ets oncoprotein activates the stromelysin promoter through the same elements as several non-nuclear oncoproteins. *EMBO J* 10:1127-1134.
48. Brenner DA, O'Hara M, Angel P, Chojkier M, Karin M 1989 Prolonged activation of jun and collagenase genes by tumour necrosis factor-alpha. *Nature* 337:661-663.
49. Opdenakker G, Van Damme J 1992 Cytokines and proteases in invasive processes: molecular similarities between inflammation and cancer. *Cytokine* 4:251-258.

Address reprint requests to:
Dr. Gabriela Aust
Institute of Anatomy
University of Leipzig
Liebigstr. 13
Leipzig, D-04103, Germany

REGULAR ARTICLE

This material may be protected by Copyright law (Title 17 U.S. Code)

A transcriptomic and proteomic analysis of the effect of CpG-ODN on human THP-1 monocytic leukemia cells

Cheng-Chin Kuo¹, Chu-Wei Kuo², Chi-Ming Liang³ and Shu-Mei Liang¹

¹ Institute of BioAgricultural Sciences, Academia Sinica

² Graduate Institutes of Life Sciences, National Defense Medical Center

³ Institute of Biological Chemistry, Academia Sinica, Taipei, Taiwan, Republic of China

The CpG motif of bacterial DNA (CpG-DNA) is a potent immunostimulating agent whose mechanism of action is not yet clear. Here, we used both DNA microarray and proteomic approaches to investigate the effects of oligodeoxynucleotides containing the CpG motif (CpG-ODN) on gene transcription and protein expression profiles of CpG-ODN responsive THP-1 cells. Microarray analysis revealed that 2 h stimulation with CpG-ODN up-regulated 50 genes and down-regulated five genes. These genes were identified as being associated with inflammation, antimicrobial defense, transcriptional regulation, signal transduction, tumor progression, cell differentiation, proteolysis and metabolism. Longer stimulation (8 h) with CpG-ODN enhanced transcriptional expression of 58 genes. Among these 58 genes, none except one, namely WNT1 inducible signaling pathway protein 2, was the same as those induced after 2 h stimulation. Proteomic analysis by two-dimensional gel electrophoresis, followed by mass spectrometry identified several proteins up-regulated by CpG-ODN. These proteins included heat shock proteins, modulators of inflammation, metabolic proteins and energy pathway proteins. Comparison of microarray and proteomic expression profiles showed poor correlation. Use of more reliable and sensitive analyses, such as reverse transcriptase polymerase chain reaction, Western blotting and functional assays, on several genes and proteins, nonetheless, confirmed that there is indeed good correlation between mRNA and protein expression after CpG-ODN treatment. This study also revealed that several anti-apoptotic and neuroprotective related proteins, not previously reported, are activated by CpG-DNA. These findings have extended our knowledge on the activation of cells by CpG-DNA and may contribute to further understanding of mechanisms that link innate immunity with acquired immune response(s).

Received: May 13, 2004
Revised: November 13, 2004
Accepted: November 15, 2004

Keywords:

ADP-ribosylation factor 3 / CpG-ODN / Heat shock protein / Microarray

Correspondence: Dr. Shu-Mei Liang, Institute of BioAgricultural Sciences, Academia Sinica, Taipei 115, Taiwan, Republic of China
E-mail: smyang@gate.sinica.edu.tw
Fax: +886-2-26515120

Abbreviations: ARF3, ADP-ribosylation factor 3; FPRL1, formyl peptide receptor-like 1; HEK293, human embryonic kidney 293 cells; HSP, heat shock protein; IL, interleukin; JNK, c-Jun NH₂-terminal kinase; LPS, lipopolysaccharide; LxR, nuclear receptor subfamily 1; MyD88, myeloid differentiation factor 88; PKC, protein kinase C gamma; PGK, phosphoglycerate kinase; TLR9, toll-like receptor 9; WISP-2, WNT1 inducible signaling pathway protein

1 Introduction

Mammals protect themselves against pathogen infection primarily via innate and adaptive immunity [1]. The innate immune system relies on a set of pattern recognition receptors (e.g., Toll-like receptors) to recognize foreign molecular structures such as lipopolysaccharide (LPS) and bacterial DNA [2, 3]. Innate immune cells recognize these molecular structures and initiate not only innate but also adaptive immunity by producing immunomodulatory cytokines and activating T and B immune cells [1]. Bacterial DNA can directly activate B cells to

proliferate and secrete immunoglobulins in a T cell-independent manner [4–6]. It also induces B cells and monocytes to activate transcription factor NF- κ B and secrete cytokines, including interleukin (IL) 12, tumor necrosis factor α (TNF- α), and interferon α/β [7–10]. The immunostimulatory activity of bacterial DNA has been assigned to unmethylated CpG motifs (GACGTT for murine, GTCGTT for human) [11]. Recent evidence shows that synthetic oligodeoxynucleotides containing a CpG motif (CpG-ODN), like bacterial DNA with the CpG moiety (CpG-DNA), induce potent Th1-like immune responses that are protective against several infectious agents and immune disorders in animal models [12, 13]. Biologically active CpG-ODN, like bacteria DNA, activates macrophages and immature dendritic cells to increase expression of MHC class II and costimulatory molecules, thereby transcribing cytokine mRNAs, and producing pro-inflammatory cytokines including TNF α , IL-1, IL-6 and IL-12 [9, 14–16]. CpG-ODN can therefore serve as an adjuvant and immunomodulator in vaccines against a wide variety of targets, including infectious agents, cancer antigens and allergens [17].

It has been suggested that unmethylated CpG-DNA-mediated immune activation functions through a toll-like receptor 9 (TLR9) signaling pathway [18]. Endocytosis and sequentially endosomal maturation as well as binding of heat shock protein (HSP) 90 to CpG-DNA are essential for induction of TLR9 signal transduction [19, 20]. It has also been shown that recognition of CpG-DNA causes TLR to form a dimer, which recruits the adaptor molecule, myeloid differentiation factor 88 (MyD88), through interaction between their C-terminal Toll/IL-1R domains. This recruitment of MyD88 to the Toll/IL-1R domain of TLR9 initiates a signaling pathway that sequentially involves IL-1R-associated kinase 1 and TNF- α receptor-associated factor 6 [18, 21, 22]. Studies using gene-deficient mice and RAW264.7 cells transiently transfected with dominant-negative forms of these molecules have indicated that the MyD88-mediated signaling pathway is essential for CpG-DNA-induced activation of NF- κ B and c-Jun NH₂-terminal kinase (JNK), as well as subsequent production of cytokines in monocytic cells [18, 21, 22]. The precise mechanism of action of CpG-DNA and CpG-ODN, nonetheless, is still not thoroughly understood. To further elucidate the molecular events after binding of CpG-ODN to TLR9, in this study, we treated CpG-ODN responsive THP-1 cells with CpG-ODN and evaluated changes by using DNA microarray and proteomic approaches. We have discovered up-regulation of more than 50 distinguished genes/proteins and identified induction of several anti-apoptotic and neuroprotecting genes by CpG-ODN treatment.

2 Materials and methods

2.1 Reagents

Phosphorothioate-modified CpG-ODN and GpC-ODN were synthesized by MDBio (Taipei, Taiwan). Human specific ODN sequences are: CpG-ODN, 5'-TCG TCG TTT TGT CGT

TTT GTC GTT-3'; GpC-ODN, 5'-TGC TGC TTT TGT GCT TTT GTG CTT-3'. The mouse specific CpG-ODN sequence is 5'-TCC ATG ACG TTC CTG ATG CT-3'. CHCA was from Sigma (St. Louis, MO, USA).

2.2 Cell culture

Cell lines were obtained from the American Type Culture Collection (Rockville, MD). Mouse RAW264.7 macrophage and human embryonic kidney 293 cells (HEK293) were cultured in DMEM supplemented with 10% heat inactivated fetal bovine serum, 100 U/mL penicillin, 100 μ g/mL streptomycin sulfate, 200 mmol/L L-glutamine, and 50 μ M β -mercaptoethanol in a humidified atmosphere of 5% CO₂ at 37°C. The medium was changed every 2 days for all experiments. Human THP-1 monocytic leukemia cells, which have been shown to express TLR9 and respond to CpG-DNA stimulation [23, 24], were cultured in RPMI1640 with the same supplements as for RAW264.7 cell cultures.

2.3 Human cDNA microarray

Total RNAs extracted from cultured THP-1 cells were isolated with TRIzol (Invitrogen, Leek, The Netherlands) and submitted to Genasia Biotechnology (Taipei, Taiwan) for further processing. In brief, 4 μ g of total RNA from CpG-ODN stimulated, or normal THP-1 cells was labeled with a fluorescence marker (U-vision, (Taipei, Taiwan)). Different colored fluorescence dyes (Cy5 and Cy3) were used to distinguish total RNA from normal and ODN stimulated cells. The labeled RNA was used for hybridization with the Human 1 cDNA microchip from Agilent Technologies (Palo Alto, CA, USA). The chips were scanned and the expression pattern was analyzed using genechip software. Genes showing up-regulation or down-regulation of RNA levels were analyzed and identified on a genomic database as suggested by the manufacturer of the microchip.

2.4 Protein preparation

THP-1 cells were seeded in a 175 cm² tissue culture flask at a density of 10⁶ cells per milliliter in culture medium. The cells were stimulated with or without 1.5 μ M CpG-ODN at defined times and harvested by centrifugation at 4°C, 1000 \times g for 15 min. Cell pellets were washed twice with ice-cold PBS, resuspended and sonicated in extraction buffer containing 25 mM Tris-HCl (pH 7.5), 2 mM β -mercaptoethanol and protease inhibitor cocktail. After centrifugation at 10 000 \times g for 20 min, ammonium sulfate was added to the supernatant until the final concentration reached 50% saturation w/v. The solution was stirred at 4°C for 30 min and centrifuged at 10 000 \times g for 30 min at 4°C. The supernatant fraction was then transferred into a fresh tube, and the precipitated protein pellet solubilized in extraction buffer. To remove salts and other contaminants, the extracts were treated with a pre-cooled (–20°C) solution of 10% TCA in acetone with 0.07% β -mercaptoethanol. Proteins were allowed to precipitate overnight at –20°C.

After centrifugation, the pellet was washed with ice-cold acetone, containing 0.07% β -mercaptoethanol. The supernatant was discarded and the pellet dried in a SpeedVac system (Model AES1010; Savant, Holbrook, NY, USA).

2.5 2-DE

2-DE was performed using an IPGphor IEF and a Hofer DALT vertical unit (Amersham Biosciences, Piscataway, NJ, USA). One milligram of dried protein sample was dissolved in 350 μ L of rehydration buffer solution, containing 7 M urea, 2 M thiourea, 4% w/v CHAPS, 5 mM tributyl phosphine, and 2% IPG and loaded onto an immobilized pH 3–10 linear gradient strip (18 cm), followed by rehydration for 16 h. IEF was then performed in the following manner: 100 V for 30 min, 250 V for 30 min, 500 V for 30 min, 1000 V for 30 min, 4000 V for 30 min, 6000 V for 55 000 Vh. At the end of IEF, the IPG strips were equilibrated for 15 min in buffer containing 6 M urea, 2% w/v SDS, 30% v/v glycerol, and 50 mM Tris, pH 6.8, then reduced with 65 mM dithioerythritol (DTE) and subsequently alkylated with 135 mM iodoacetamide for another 15 min. After equilibration, the IPG strips were immediately placed on top of a 12% SDS-PAGE (1.5 mm, 20 \times 24 cm). The second dimension gels were then overlaid with molten 0.8% agarose solution in SDS electrophoresis buffer. Electrophoresis was performed at 16°C, starting at 10 mA per gel for 1 h, followed by 45 mA per gel until the dye front reached the bottom of the gels.

2.6 Staining and image acquisition

Immediately after electrophoresis, gels were stained with SYPRO Ruby (Molecular Probes, Eugene, OR, USA). In brief, gels were fixed for 30 min in 10% methanol, 7% acetic acid, and then stained overnight in SYPRO Ruby stain. The staining solution was removed and gels were washed in 10% methanol and 7% acetic acid for 3 h. After staining, image acquisition was carried out on a Typhoon 9200 (Amersham Biosciences). To identify a protein, spot detection, quantification and matching of 2-D results were analyzed using ImageMaster software (Amersham Biosciences). The M_r of the proteins were calibrated according to the LMW-SDS Marker Kit (Amersham Biosciences), and their pI values were estimated from the position of the protein spots on the 2-D gel and confirmed with the information supplied by the manufacturer. Since most of the pI values for the truncated proteins had not been reported previously, the pI values of the truncated proteins were estimated from the position of the observed spots. To omit the variation due to the use of separate gels, after background subtraction, the intensity levels of protein spots on each gel were normalized as a proportion of one reference spot, and protein quantities were calculated by integrating the density over the spot area. Protein spots that showed reproducible modulation exceeding ~80% after CpG-ODN treatment in three experiments were further analyzed by MS.

2.7 In-gel digestion with trypsin and extraction of peptides

Protein spots were excised from stained gels and cut into pieces. In brief, gel spots were dehydrated with ACN for 10 min and dried in a vacuum centrifuge. Gel pieces were reswelled with 55 mM DTE in 25 mM ammonium bicarbonate (pH 8.5) at 37°C for 1 h. The solution was then exchanged with alkylation solution, which contained 100 mM iodoacetamide in 25 mM ammonium bicarbonate (pH 8.5), at room temperature for 1 h. After alkylation, the gel pieces were washed twice with 50% ACN in 25 mM ammonium bicarbonate (pH 8.5) for 15 min. The wash solution was discarded and the pieces of gel were dehydrated with ACN for 10 min and dried in a vacuum centrifuge. Tryptic digestion was initiated by reswelling the gel in 25 mM ammonium bicarbonate solution with 25 ng of trypsin (Promega, Madison, WI, USA). After incubation at 37°C for 16 h, tryptic peptides were extracted twice with 50% ACN containing 5% formic acid for 15 min with moderate sonication. The extracted solutions were pooled and evaporated to dryness in a vacuum centrifuge. The dried peptide mixture was dissolved in 0.1% formic acid and used for MS.

2.8 MALDI-Q-TOF MS and protein identification

Tryptic peptides analyses were performed using a Micromass Q-TOF Ultima MALDI (Micromass, Wythenshawe, U.K.) equipped with a 337 nm nitrogen laser and operated in reflection positive ion mode. Peptide mixtures (1 μ L) were premixed with 1 μ L of the matrix (5 mg CHCA in 50% ACN with 0.1% TFA) then spotted onto the MALDI target plate. Mass spectra were acquired for the mass range of 900–3500 Da and the individual spectra from MALDI MS or MS/MS were processed using the Micromass MassLynx 4.0 software. The generated peak list files were used to query the Swiss-Prot database using the MASCOT program (<http://www.matrixscience.com>) with the following parameters: peptide mass tolerance, 50 ppm; MS/MS ion mass tolerance, 0.25 Da; allowance of missed cleavage, 1; and consideration for variable modifications such as oxidation of methionine and carboxyamidomethylation of cysteines. Only significant hits as defined by MASCOT probability analysis were considered initially. In addition, when the PMF matches were between 5 and 9, at least one peptide sequence was manually checked by MALDI MS/MS analysis.

2.9 RT-PCR analysis

cDNA from THP-1 cells was produced with Superscript II reverse transcriptase (Invitrogen) using a oligo(dT)₁₅ primer for 1 h at 42°C. PCR of cDNA was performed using specific primers for the gene of interest and control β -actin. All PCR products were electrophoresed on a 1.5% agarose gel, and DNA bands were visualized by staining the gel with ethidium bromide.

Table 3. Continued

Gene name and description (changed fold ≥ 2)	Genebank number
Channel and transport	
Gamma-aminobutyric [61] A receptor	NM_004961
ATP synthase subunit F6	M37104
Transient receptor potential channel 1	Z73903
Choroideremia (Rab escort protein 1)	X57637
Signal transduction	
Protein kinase C, gamma	Z15114
Regulator of G-protein signaling 5	A1674877
Nck, Ash and phospholipase C binding protein (NAP4)	AB005216
Highly similar to adeylate kinase gene	AB016886
Enzyme and protease	
Phenylalanine hydroxylase	AA203389
Carboxypeptidase A1	X67318
Xylulokinase	AK001205
Pancreatic lipase	J05125
Ubiquitin specific protease 12	AF022789
Transmembrane protease, serine2	U75329
Aspartate beta-hydroxylase	U03109
Phosphoribosyl pyrophosphate amidotransferase	D13757
Tumor progression and cell differentiation	
CDC23	AF053977
WISP-2	AF100780
Microseminoprotein, beta	M34376
Dishevelled 3	NM_004423
Structure protein	
Trichohyalin	L09190
Kertain	AF061809
Other	
Human transferrin pseudogene	M22376
TIMP-2	U44383
Collagen-like protein	U67921
Human genomic DNA, chromosome 21q, section 60/105	AP001716
Human genomic DNA, chromosome 21q, section 64/105	AP001720
KIAA0136	D50926
KIAA0379	AB002377
KIAA0489	AB007958
KIAA1114	AL049732
KIAA1451	AB040884
KIAA0756	AB018299
Zinc finger protein 267	AF220492
Hypothetical protein FLJ10633	AK001495
Hypothetical protein EU01IMAGE 1955967	AK026108
Myb1 homolog like 1	AK001893
Antizyme inhibitor	D88674
Disintegrin-like and metalloprotease (reprolysin type) with Thrombospondin type 1 motif, 3	AB002364
ADP-ribosylation factor 3 (ARF-3)	M74491
Testis specific protein, Y-linked	M98525
Unnamed protein	AK026042

Table 4. List of antimicrobial and anti-inflammatory genes modulated by CpG-ODN treatment of THP-1 cells

Gene name	Genebank number	Expression fold	
		2 h	8 h
Connexin 59 gene	L29277	2.12 \pm 0.05	1.74 \pm 0.08
IL-18 receptor accessory protein	X58806	2.32 \pm 0.21	1.19 \pm 0.13
Integrin, alpha 1	X68742	2.01 \pm 0.03	1.05 \pm 0.10
Nuclear body protein Sp140	U63420	2.22 \pm 0.11	1.39 \pm 0.04
Pro-Pol-dUTPase polyprotein	AC004748	2.33 \pm 0.18	0.95 \pm 0.03
Thioredoxin	NM_003329	2.20 \pm 0.08	1.07 \pm 0.01
FPRL1	AF081535	0.95 \pm 0.06	2.13 \pm 0.11
IL-10 receptor	U08988	1.22 \pm 0.18	2.21 \pm 0.07
LxR	NM_005693	0.90 \pm 0.03	2.37 \pm 0.31
Vitamin D receptor	J03258	1.37 \pm 0.23	2.39 \pm 0.11

Expression fold is designated as the ratio of CpG-ODN treated over control

ulation but were down-regulated thereafter, while anti-inflammatory associated genes such as FPRL1, IL10 receptor, vitamin D receptor and LxR were up-regulated after 8 h stimulation (Tables 1, 3 and 4).

3.2 Verification of the microarray results with RT-PCR or Western blotting

To verify the results from the microarray analysis, we also performed RT-PCR on the up-regulated genes (Fig. 1). Consistent with results obtained in the microarray gene expression analysis, RT-PCR studies showed that the mRNA levels of some selected genes, including ubiquitin specific protease 12, regulator of G-protein signaling 5, NAP4 and ASH2L, were increased in response to CpG-ODN (Fig. 1, Table 3). In addition, the protein expression level of ARF-3

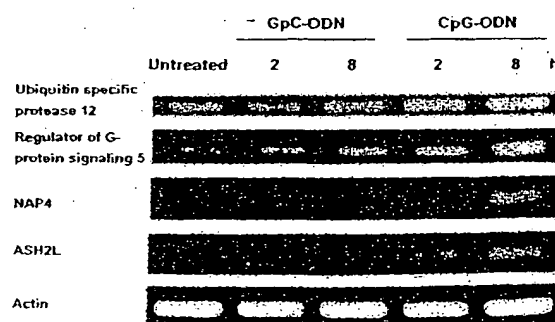


Figure 1. Induction of various genes by CpG-ODN. THP1 cells were stimulated with medium alone, 1.5 μ M CpG-ODN (as the negative control) or CpG-ODN for the indicated times. RT-PCR was then performed to analyze gene expression levels. β -actin was used as an internal control. The experiment was repeated three times with similar results.

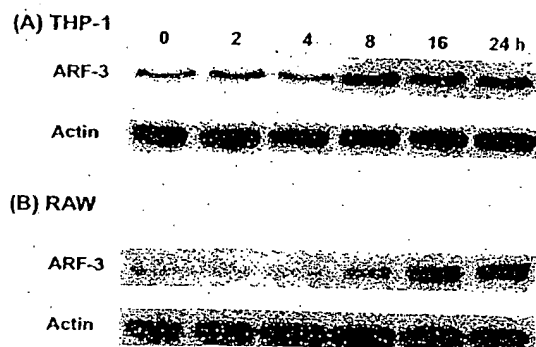


Figure 2. CpG-ODN induced ARF-3 protein expression in human THP-1 or mouse RAW264.7 cells. THP-1 (A) or mouse RAW264.7 (B) cells were incubated with 1.5 μM CpG-ODN for the indicated time points. The protein expression level of ARF-3 was determined by Western blotting of cell extracts using anti-ARF-3 antibody. The experiment was repeated three times with similar results.

was shown to increase in Western blotting analysis in cell lysates from THP-1 cells treated with CpG-ODN for 8–24 h (Fig. 2A). Similar studies showed that the ARF-3 protein was also induced by mouse specific CpG-ODN in other TLR9 expression cell lines such as the mouse macrophage RAW264.7 cell line (Fig. 2B).

3.3 Proteins regulated in CpG-ODN stimulated THP-1 cells

To further assess whether there was any correlation between regulation of gene expression and expression of cellular proteins, a proteomic approach was adopted to identify protein expression profiles. THP-1 cells were treated with CpG-ODN for defined times (from 8 to 40 h), and their cytoplasmic proteins were extracted for 2-DE analysis. Although the use of high concentrations of urea might give us a broader view of all the proteins affected by CpG-ODN, preliminary results from 2-D gels showed that the resolution of the protein mixtures were not satisfactory. To improve and get the best resolution from 2-DE, total proteins were roughly separated into supernatant and precipitated fractions using 50% saturated ammonium sulfate solution. To remove salts and other contaminants, both protein fractions were precipitated with TCA solution and then subjected to 2-DE. By protein spot determination analysis, about 500 and 450 well-resolved spots were observed on each pH 3.0–10.0 gel for precipitated or supernatant fractions, respectively. Comparative analysis of 2-DE between treatments and control showed that the intensities of the protein spots from the ammonium sulfate precipitated fraction did not change, while several protein spots were up-regulated by at least ~80% in the supernatant fraction of 8 h CpG-ODN stimulated THP-1 cells (Fig. 3).

The protein spots were individually excised from gels for further identification. After trypsin digestion, several protein spots were identified without ambiguity by MS MALDI-

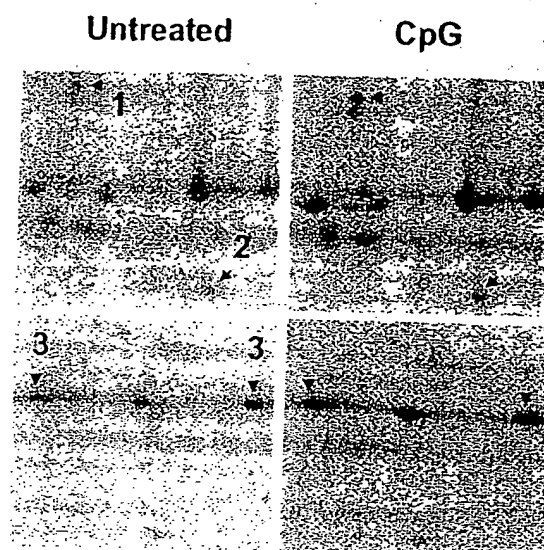


Figure 3. The effect of CpG-ODN on the 2-DE profile of THP-1 cells. THP-1 cells were treated with or without 1.5 μM CpG-ODN for 8 h. Total proteins were extracted and roughly separated into two fractions by 50% saturation with ammonium sulfate. The supernatant fraction was then separated by 2-DE. Protein spots were visualized by SYPRO Ruby staining. Comparison of CpG-ODN treated THP-1 cells to untreated cells showed that these proteins changed in intensity by over 80%. Protein spots were identified by trypsin digestion and MS. Localization of protein spots 1 (enol-coenzyme A hydratase), 2 (proteasome α) and 3 (cyclophilin A; two isoforms) are shown. The experiment was repeated three times with similar results.

TOF. These proteins included HSP60, HSP90, cyclophilin A, enol-coenzyme A hydratase, eukaryotic translation elongation factor, proteasome α and β chain and ATP synthase beta chain (Table 5). Similar experiments on cells treated for a longer period of time with CpG-ODN stimulation (25 h) revealed that 27 protein spots were changed in intensity by at least ~80%. These protein spots contained members of HSPs (HSP27, hsc70, grp78 and grp94), metabolic enzymes (phosphoglycerate kinase (PGK) and pyruvate kinase (PYK)), macrophage capping protein and cyclophilin A (Table 6). Among these proteins, macrophage capping protein, PGK, PYK, cyclophilin A and HSP27 (Figs. 4 and 5A) were found to be up-regulated. Interestingly, we found that a truncated form of grp78 with an expected mass of 25 kDa and pI of 5.3 was up-regulated while grp78 itself was down-regulated. A similar situation was also found for grp94 and hsc70 and their truncated derivatives (Table 7 and Fig. 5). In addition, we also observed six down-regulated protein spots on 2-D gels in samples after 25 h CpG-ODN treatment. Among these six proteins, we have successfully identified three as 40s ribosomal protein SA, grp78 and hsc70, respectively (Table 6), while the other three, due to their relative low abundance, have not been identified yet.

Table 5. List of proteins modulated by 8 h CpG-ODN treatment

Protein name	Accession no.	M_r (theor.)	pI (theor.)	Matched no.	Coverage%	Score	Expression fold
ATP synthase beta-chain	gi114549	56 525	5.26	16	58	171	2.33 ± 0.06
Cyclophilin A	P05092	17 870	7.82	5	35	62	2.85 ± 0.13
Enoyl-Coenzyme A hydratase	gi4503447 ^{a)}	35 971	6.61	11	44	62	2.52 ± 0.05
Eukaryotic translation elongation factor	gi4503481	50 087	6.25	6	25	68	3.41 ± 0.21
HSP60	P10809 ^{b)}	57 963	5.24	13	27	76	2.78 ± 0.03
HSP90-beta	P08238	83 133	4.97	10	18	65	2.36 ± 0.10
Proteasome α chain	gi4506181	25 882	6.92	11	59	80	2.52 ± 0.11
Proteasome β chain	gi4506193	26 472	8.27	9	46	84	3.85 ± 0.17

Expression fold is designated as the ratio of CpG-ODN treated over control

a) NCBI accession number

b) Swiss-Prot accession number

Table 6. List of proteins modulated by 16 and 25 h CpG-ODN treatment

Protein name	Swiss-Prot no.	M_r (theor.)	pI (theor.)	Matched no.	Coverage%	Score	Expression fold	
							16 h	25 h
Cyclophilin A	P05092	17 870	7.82	5	35	62	2.53 ± 0.02	2.48 ± 0.15
78 kDa glucose regulated protein (grp78)	P11021	72 288	5.07	13	30	148	0.61 ± 0.04	0.29 ± 0.06
HSP27	P04792	22 768	5.98	12	59	124	1.00 ± 0.01	2.61 ± 0.12
Heat shock cognate 70 kDa protein (hsc70)	P11142	70 854	5.37	16	34	114	0.64 ± 0.01	0.31 ± 0.03
Macrophage capping protein	P40121	38 494	5.88	9	30	58	1.31 ± 0.01	2.58 ± 0.03
Phosphoglycerate kinase	P00558	44 284	7.052	11	33	71	2.32 ± 0.11	4.23 ± 0.19
Pyruvate kinase	P14618	57 710	7.95	17	32	114	1.65 ± 0.07	2.70 ± 0.12
40s ribosomal protein SA (RSP40)	P08865	32 833	4.79	5	23	61	0.33 ± 0.02	0.35 ± 0.05

Table 7. List of truncated proteins detected in THP-1 cells after 25 h CpG-ODN treatment

Protein name	Swiss-Prot no.	M_r (obs.)	pI (obs.)	Matched no.	Coverage%	Score	Expression fold
94 kDa glucose-regulated protein (grp94)	P14625	~59 700	~5.00	12	14	104	New ^{a)}
Truncated form of grp78	P11021	~25 000	~5.30	12	22	75	New
Truncated form of hsc70	P11142	~22 000	~5.80	12	20	96	New
Truncated form of hsc70	P11142	~19 000	~6.10	11	18	113	New

a) New designated proteins detected in the CpG-ODN treated gel but not in the corresponding control gel

3.4 Comparison of microarray and proteomic results

Table 8 shows the expression of six genes and their corresponding proteins that were modulated by 8 h treatment of THP-1 cells with CpG-ODN. Besides enoyl-coenzyme A hydratase, there was poor correlation between the expression

of genes and their corresponding proteins (Table 8), suggesting that more in-depth studies were needed. To further evaluate whether changes observed in protein expression correlated with changes in mRNA levels, we randomly chose two proteins (PGK and PYK) that were induced after 16 h CpG-ODN treatment and determined their mRNA levels by

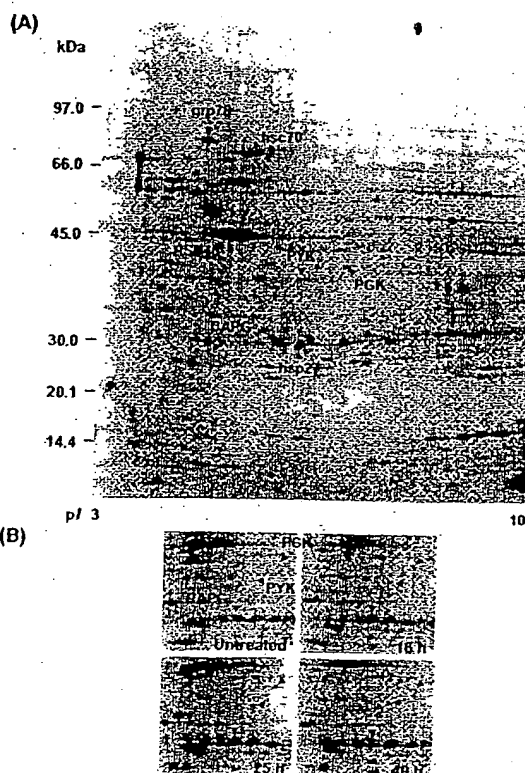


Figure 4. 2-D gel electrophoretic analysis of CpG-ODN-treated THP-1 cells. (A) Total cell protein from unstimulated THP-1 cells was subjected to 2-DE. (B) THP-1 cells were treated with or without 1.5 μ M CpG-ODN for defined times. Cellular proteins were extracted and separated by 2-DE. Several up-regulated proteins are shown in the SYPRO Ruby staining gel. Comparison of CpG-ODN treated THP-1 cells to untreated cells showed that these proteins changed in intensity by over 80%. The experiment was repeated three times with similar results.

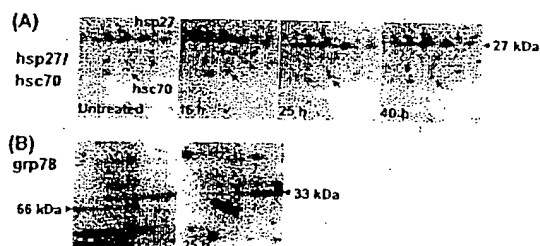


Figure 5. 2-D gel electrophoretic analysis of CpG-ODN-treated THP-1 cells. THP-1 cells were treated with or without 1.5 μ M CpG-ODN for defined times. Cellular proteins were extracted and separated by 2-DE. Protein spots were detected by SYPRO Ruby staining. (A) Expression of HSP27 was induced by increasing the period of CpG-ODN stimulation. A truncated form of hsc70 was detected on the gel. (B) The native form of grp78 was detected in untreated cells, while the truncated form of grp78 was observed after 25 h stimulation. The experiment was repeated three times with similar results.

Table 8. Comparison of gene and protein expression levels in THP-1 cells after 8 h CpG-ODN treatment

Protein name	Gene expression fold from microarray	Protein expression fold from 2-D gel
Enoyl-Coenzyme A hydratase	1.72 \pm 0.31	2.52 \pm 0.05
Eukaryotic translation elongation factor	0.95 \pm 0.01	3.41 \pm 0.21
HSP60	0.94 \pm 0.07	2.78 \pm 0.03
HSP90-beta	1.58 \pm 0.11	2.36 \pm 0.10
Proteasome α chain	0.98 \pm 0.03	2.52 \pm 0.11
Proteasome β chain	1.09 \pm 0.11	3.85 \pm 0.17

RT-PCR. Our results showed that mRNA levels of PYK increased after 16 h CpG-ODN treatment, while mRNA levels of PGK were dramatically increased after 24 h stimulation (Fig. 6). In addition, we also performed enzyme activity analysis and found that the activity of PGK and PYK were

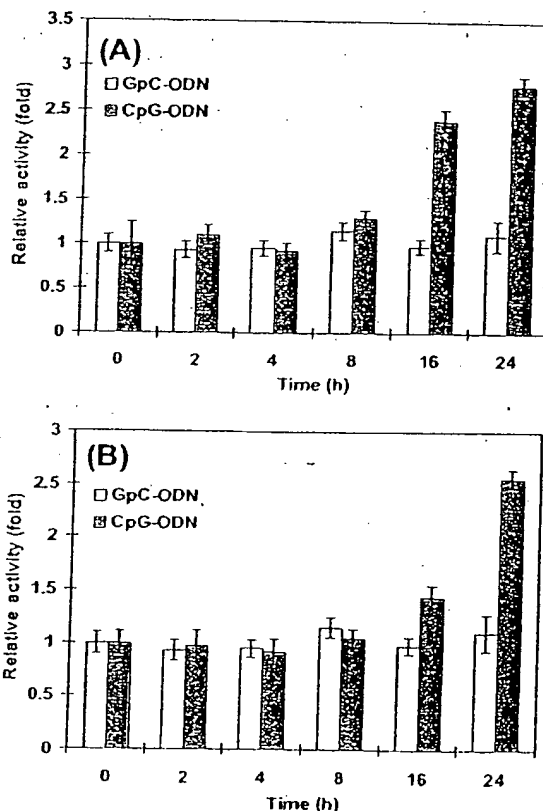


Figure 6. Activities of PYK and PGK induced by CpG-ODN. THP1 cells were stimulated with medium alone, 1.5 μ M GpC-ODN (as the negative control) or CpG-ODN for the indicated times. Cell lysates were extracted and assayed for (A) PYK and (B) PGK activities. Data represent mean \pm SEM. ($n = 3$).

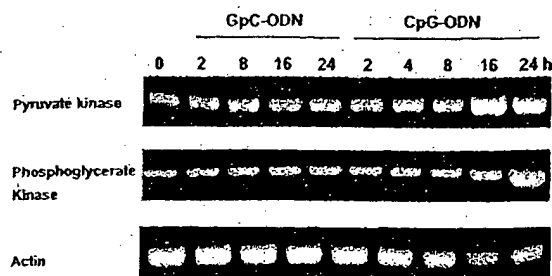


Figure 7. Induction of PYK and PGK transcripts by CpG-ODN. THP1 cells were stimulated with medium alone, 1.5 μ M GpC-ODN or CpG-ODN for the indicated times. RT-PCR was then performed to analyze gene expression. β -actin was used as an internal control. The experiment was repeated three times with similar results.

indeed increased by a factor ~ 2.5 after CpG-ODN stimulation (Fig. 7). To confirm that mRNA induced by CpG-ODN would also be accompanied by an increase in protein expression even though it was not detected in 2-D gel analysis, we used more sensitive and specific Western blotting analysis. As shown in Table 3 and Fig. 2, ARF-3 was identified in the microarray gene profile but not in the proteomic expression profile. Nevertheless, we observed enhanced protein expression of ARF-3 after CpG-ODN stimulation by Western blotting. Moreover, to investigate whether the up-regulation of ARF-3 by CpG-ODN is mediated through the TLR9 pathway, TLR9-deficient HEK293 cells were transiently cotransfected with hTLR9 and luciferase-reporter gene driven by a NF- κ B-dependent promoter. Our data showed that NF- κ B activity of untransfected HEK293 cells were not responsive to CpG-ODN stimulation, while in transfected HEK293 cells expressing hTLR9, NF- κ B luciferase activity was up-regulated 12-fold after 8 h CpG-ODN stimulation. The activation of NF- κ B induced by CpG-ODN was blocked by pretreatment of the transfected cells with an ARF-3 inhibitor, such as brefeldin A (Fig. 8), suggesting CpG-ODN induces ARF-3 and activates NF- κ B after the interaction of CpG-ODN with TLR9.

4 Discussion

In this study both microarray and proteomic approaches were used to evaluate the effect of CpG-ODN on gene/protein expression profiles of THP-1 cells at several time points. Comparison of the gene expression profiles showed that stimulation of the cells with CpG-ODN for different periods of time resulted in different profiles (Tables 1–4). The differences in mRNA expression between the cells with short and long stimulation could be attributable to the low reproducibility. However, to avoid experimental variations, we not only used the same batch of microarrays from the same manufacturer but also applied the samples of short and long term stimulation at the same time. In this way, we found that the

changes in expression fold of mRNA after CpG-ODN treatment were quite reproducible as shown by their mean \pm SEM (Table 4). A more likely explanation for the difference in the expression level of mRNA after different periods of stimulation with CpG-ODN is that the transient increase or decrease in these mRNA by CpG-ODN plays a significant role in modulating biological functions. For example, we found that the IL-18 receptor accessory protein from THP-1 cells was up-regulated after 2 h of CpG-ODN stimulation. The IL-18/IL18R system is known to activate Th1-mediated immune responses that play a critical role in host defense against infection [26]. Together with IL-18/IL18 R, several genes for antimicrobial defense were also increased, including thioredoxin, Pro-Pol-dUTPase polyprotein and Sp140. After 8 h of CpG-ODN stimulation, however, none of these genes was activated any more (Table 4). Since sustained or excessive production of these antimicrobial molecules might lead to inflammation and cellular damage [27], a plausible explanation is that THP-1 cells fight against the invasion of pathogens by up-regulating antimicrobial defense-associated genes at an early stage of stimulation and then shut them down to avoid over-activation. Whether this explanation is true remains to be verified.

It is noteworthy that our data also identified the up-regulation of several anti-inflammatory associated genes after 8 h of CpG-ODN stimulation. These genes included FPRL1, IL-10 receptor, vitamin D receptor, and LxR (Table 3). FPR and FPRL1 have been defined as chemotactic factors involved in host defense against bacterial infection and in the clearance of damaged cells. Additional studies have indicated that FPRL1 interacts with a menagerie of structurally diverse pro- and anti-inflammatory ligands associated with diseases, including amyloidosis, Alzheimer's diseases, prion disease and HIV [28, 29]. Therefore, FPRL1 may play an important role in regulating and/or balancing the production of pro- and anti-inflammatory molecules in CpG stimulated THP-1 cells. Additionally, a recent study has demonstrated that LxRs and their ligands act as negative regulators of macrophage inflammatory gene expression and inhibit the expression of inflammatory mediators such as inducible nitric oxide synthase, cyclooxygenase and IL-6 in response to bacterial infection or LPS stimulation [30]. Of interest, we found that a transcription factor gene connexin 59, a regulator of IL-6 expression, was up-regulated after 2 h of CpG-ODN stimulation. It is thus likely that CpG-ODN stimulation of THP-1 cells for 2 h may induce the expression of the pro-inflammatory cytokine IL-6 through the up-regulation of the connexin 59 gene, while 8 h of CpG-ODN treatment may counterbalance the initial inflammatory response by inducing LxR to inhibit IL-6 production.

Signal transduction molecules play an important role in cellular activation. Intracellular signal transduction systems employing various intermolecular interactions through docking elements, including SH2 and SH3 domains, have been reported [31–33]. Here we found that THP-1 cells treated with CpG-ODN for 2 h up-regulated gene expression

of Grb2-like protein (which contains an SH3 domain), while 8 h of stimulation induced Nck, Ash and phospholipase C binding protein (NAP4 which contains an SH2 domain). It is thus possible that Grb2-like protein and NAP4 may play important roles in CpG-ODN mediated signaling pathways. Furthermore, recent studies have also revealed that binding of CpG-DNA to TLR9 results in activation of JNK [34]. Since JNK is activated by Nck adaptor protein and Nck interacting kinase [35, 36], it is possible that CpG-ODN may activate JNK via up-regulation of NAP4. Although a recent publication described the gene expression profiles of a cultured mouse macrophage cell line after CpG-DNA stimulation [34], their microarray results were only conducted at one time-point (6 h stimulation). Moreover, they did not report the measurement of protein expression profiles in response to CpG-ODN stimulation.

Comparison of the gene and protein expression profiles showed that there was discordance between mRNA and protein levels (Table 8). Similar discordance between the expression pattern of genes and proteins was also reported in other system using different stimuli [37–41]. The discordance between mRNA and protein levels could be due to screening capability such as detection sensitivity, choice of cut-off point, quantitativity of microarray and 2-D gels, as well as time discrepancy between gene and protein expression [39, 40, 42, 43]. Alternatively, it could also be explained by post-transcriptional events, such as alternative splicing or PTM [39, 40, 42, 43]. Another possible explanation is that most of the spots observed in the 2-D gels are isoforms of some proteins. The intensity of each spots does not necessarily represent total amount of a certain protein and thus does not correlate with its mRNA level. Our finding that microarray results correlated better with Western blotting results (e.g., ARF-3 in Fig. 2), an approach more suitable than 2-D gels for determining the total amount rather than isoforms of a given protein, seems to suggest that formation of isoforms should be carefully taken into consideration when one tries to correlate mRNA and protein expression data.

Using a proteomics approach, we found that CpG-ODN treatment up-regulated the expression of many proteins including HSPs, metabolic enzymes, structural proteins, as well as macrophage capping protein, cyclophilin and proteasome α and β chain *etc.* HSPs are the most abundant and ubiquitous soluble intracellular proteins. They are up-regulated by various stressors including temperature, glucose deprivation, microbial infection and cancer [44]. They function as molecular chaperones to prevent protein aggregation and contribute to the folding of nascent and altered proteins. In addition, they are able to regulate immune responses, including production of inflammatory cytokines and chemokines and activation or maturation of immune cells [45, 46]. Beside HSPs, cyclophilin as well as proteasome α and β chain have also been reported to be involved in the immune response [39, 47]; proteasome β chain is consistently up-regulated in human neutrophils following LPS exposure [39]. Our finding that the protein levels of HSPs, cyclophilin, and

proteasome α and β chain were increased after CpG-ODN treatment suggests that these molecules might play a role in the immunostimulating effect of CpG-ODN. To what extent these proteins contribute to the immune responses of the cells to CpG-ODN is currently under study. Proteomic analysis also showed that truncated forms of grp78, grp94 and hsc70 were induced, a phenomenon similar to calreticulin observed by Richards and his coworkers [48]. The expression of full length hsc70 and grp78 were decreased, while the levels of their truncated derivatives was increased after CpG-ODN treatment. These results suggest that the degradation of these proteins has been enhanced. We also found that proteasome α and β chains as well as ubiquitin specific protease 12 were increased by CpG-ODN. Whether these enzymes or other enzymes were responsible for the generation of truncated hsc70 and grp78 remains to be elucidated.

Cells rely on multiple signaling pathways to determine their fates of survival, proliferation or apoptosis [49]. In fact, apoptosis plays an important role in regulating pathogen infection. To be able to grow and replicate in the target cells, pathogens may have to block apoptosis. Results from several laboratories have made it clear that HSP70 and HSP27 protect cells not only from heat, but also from most apoptotic stimuli [48, 50] by binding to Akt and subsequently mediating anti-apoptotic activity through activation of Akt [51–53]. Since our data revealed that CpG-ODN induced the expression of HSP90 and HSP27, it is possible that CpG-ODN might prevent apoptosis by up-regulation of HSPs.

Interestingly, our microarray data also showed that CpG-ODN mediated the induction of a set of genes associated with tumor progression and cell proliferation. Among these, one gene, WISP-2, was up-regulated by CpG-ODN after both 2 and 8 h stimulation. WISP genes were first identified as downstream targets of the Wnt-1 β -catenin signaling pathway. They belong to the CCN family of growth factors that have been receiving increasing attention lately due to some of the family members having been reported to be involved in angiogenesis and tumorigenesis [54]. It would be interesting to evaluate whether CpG-ODN plays a role in angiogenesis and tumorigenesis by regulating WISP-2. In addition, we found that some genes associated with neurodegeneration or neuroprotection, such as FPRL1, NMDAR (NMDA) receptor, PKC and dishevelled 3 were up-regulated. To our knowledge, this is the first report to suggest an association between these genes and CpG-ODN stimulation. As mentioned above, FPRL1 plays a crucial role in proinflammatory aspects of systemic amyloidosis and neurodegenerative disease such as Alzheimer's disease and prion disease [28]. NMDAR, PKC and dishevelled are involved in modulating amyloid precursor protein metabolism, which is central to the pathogenesis of Alzheimer's disease [55–57]. Most notably, recent studies have shown that the TLR4-dependent pathway is involved in neurodegeneration of the central nervous system [58]. Whether CpG-ODN moieties of pathogens play any role in neurodegenerative diseases such as Alzheimer's remains to be elucidated.

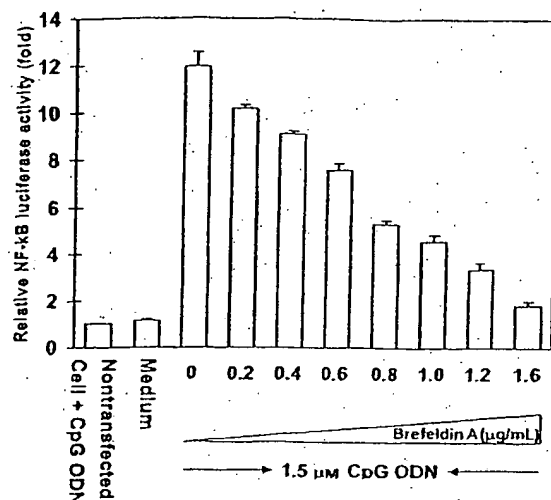


Figure 8. ARF-3 participates in the CpG-ODN-TLR9-NF-κB pathway. HEK293 cells were cotransfected with p5xNF-κB and human TLR9. After overnight transfection, the cells were incubated with or without 1.5 μM CpG-ODN for 8 h in the presence or absence of increasing concentrations of the ARF-3 inhibitor brefeldin A. After incubation, cells were lysed and NF-κB luciferase activity was measured. Data represent mean ± SEM. ($n = 3$).

Exposure of cells to LPS or microbial infection has been known to induce several genes encoding metabolic enzyme [34, 39]. Our microarray data also revealed that a large number of genes encoding proteins involved in energy synthesis and fatty acid oxidation, such as enoyl-coenzyme A hydratase, propionyl coenzyme A carboxylase and cytochrome p450 were activated by CpG-ODN treatment. In addition, we found that other proteins such as ARF-3 were up-regulated (Table 3, Fig. 8). ARFs are 20 kDa GTPases of the ras superfamily that are critical to vesicular trafficking, including exocytic protein transport and endocytosis [59, 60]. This study demonstrates for the first time that ARF-3 is involved in the activation of NF-κB induced by CpG-ODN (as shown in Fig. 8).

CpG-DNA/ODN has been shown to elicit primarily responses via the TLR9/MyD88 dependent pathway [18, 21, 22]. Chromosome location analysis showed that instead of localizing on one or two chromosome, the genes/proteins modulated by CpG-ODN stimulation are scattered on all chromosomes except chromosomes 23 and 24. These results seem to suggest that CpG-ODN either affects multiple chromosomes simultaneously or subsequently via cascades of cellular messengers. More studies are needed to elucidate its mechanism of actions.

5 Concluding remarks

In summary, by using microarray and proteomic approaches to evaluate the effect of CpG-ODN at different time points, we have found that genes/proteins regulated by CpG-ODN

are related to inflammatory responses, antimicrobial defense, transcriptional regulation, intracellular signal transduction, tumor progression, cell differentiation, proteolysis, anti-apoptosis as well as neurodegeneration and neuroprotection. Our results may help delineate the CpG-ODN mediated pathway and contribute to further understanding of mechanisms that link innate immunity with acquired immune response(s).

We thank Mr. Yen-Chieh Huang and Ms. V. R. Kavitha for technical assistance in RT-PCR analysis. We also thank the Core Facilities for Proteomics Research at the Academia Sinica, Taiwan for mass spectrometry analyses. This work was supported by the National Science Council (Grant NSC 91-3112-P001-002-Y) and Academia Sinica (Grant AS 91BC3PP), Republic of China.

6 References

- [1] Akira, S., Hemmi, H., *Immunol. Lett.* 2003, **85**, 85–95.
- [2] Janeway, C. A. Jr., Medzhitov, R., *Semin. Immunol.* 1998, **10**, 349–350.
- [3] Wagner, H., *Curr. Opin. Microbiol.* 2002, **5**, 62–69.
- [4] Halpern, M. D., Kurlander, R. J., Pisetsky, D. S., *Cell. Immunol.* 1996, **167**, 72–78.
- [5] Messina, J. P., Gilkeson, G. S., Pisetsky, D. S., *J. Immunol.* 1991, **147**, 1759–1764.
- [6] Yi, A. K., Krieg, A. M., *J. Immunol.* 1998, **160**, 1240–1245.
- [7] Tokunaga, T., Yamamoto, H., Shimada, S., Abe, H. et al., *J. Natl. Cancer Inst.* 1984, **72**, 955–962.
- [8] Yamamoto, S., Kuramoto, E., Shimada, S., Tokunaga, T., *Jpn. J. Cancer Res.* 1988, **79**, 866–873.
- [9] Stacey, K. J., Sweet, M. J., Hume, D. A., *J. Immunol.* 1996, **157**, 2116–2122.
- [10] Yi, A. K., Tuetken, R., Redford, T., Waldschmidt, M. et al., *J. Immunol.* 1998, **160**, 4755–4761.
- [11] Krieg, A. M., Yi, A. K., Matson, S., Waldschmidt, T. J. et al., *Nature* 1995, **374**, 546–549.
- [12] Kline, J. N., Waldschmidt, T. J., Businga, T. R., Lemish, J. E. et al., *J. Immunol.* 1998, **160**, 2555–2559.
- [13] Shirota, H., Sano, K., Hirasawa, N., Terui, T. et al., *J. Immunol.* 2001, **167**, 66–74.
- [14] Lipford, G. B., Sparwasser, T., Bauer, M., Zimmermann, S. et al., *Eur. J. Immunol.* 1997, **27**, 3420–3426.
- [15] Sparwasser, T., Miethke, T., Lipford, G., Borschert, K. et al., *Nature* 1997, **386**, 336–337.
- [16] Sparwasser, T., Miethke, T., Lipford, G., Erdmann, A. et al., *Eur. J. Immunol.* 1997, **27**, 1671–1679.
- [17] Takeda, K., Akira, S., *Genes Cells* 2001, **6**, 733–742.
- [18] Hemmi, H., Takeuchi, O., Kawai, T., Kaisho, T. et al., *Nature* 2000, **408**, 740–745.
- [19] Hacker, H., Mischak, H., Miethke, T., Liptay, S. et al., *EMBO J.* 1998, **17**, 6230–6240.
- [20] Bandholtz, L., Guo, Y., Palmberg, C., Mattsson, K. et al., *Cell. Mol. Life Sci.* 2003, **60**, 422–429.

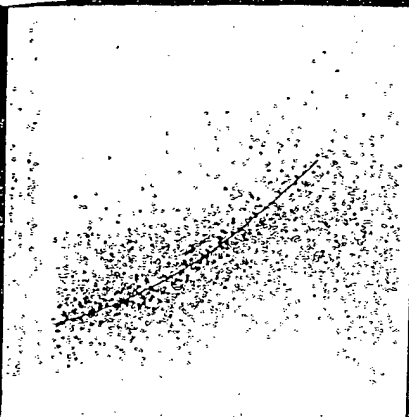
- [21] Bauer, S., Kirschning, C. J., Hacker, H., Redecke, V. et al., *Proc. Natl. Acad. Sci. USA* 2001, 98, 9237–9242.
- [22] Hacker, H., Vabulas, R. M., Takeuchi, O., Hoshino, K. et al., *J. Exp. Med.* 2000, 192, 595–600.
- [23] Takeshita, F., Leifer, C. A., Gursel, I., Ishii, K. J. et al., *J. Immunol.* 2001, 167, 3555–3558.
- [24] Akhtar, M., Watson, J. L., Nazli, A., McKay, D. M., *FASEB J.* 2003, 17, 1319–1321.
- [25] Lee, C. Y., *Methods Enzymol.* 1982, 90 Pt E, 121–126.
- [26] Kawakami, K., *J. Immunother.* 2002, 25 Suppl. 1, S12–19.
- [27] Nakanishi, K., Yoshimoto, T., Tsutsui, H., Okamura, H., *Annu. Rev. Immunol.* 2001, 19, 423–474.
- [28] Le, Y., Oppenheim, J. J., Wang, J. M., *Cytokine Growth Factor Rev.* 2001, 12, 91–105.
- [29] Le, Y., Murphy, P. M., Wang, J. M., *Trends Immunol.* 2002, 23, 541–548.
- [30] Joseph, S. B., Castrillo, A., Laffitte, B. A., Mangelsdorf, D. J., Tontonoz, P., *Nat. Med.* 2003, 9, 213–219.
- [31] Cohen, G. B., Ren, R., Baltimore, D., *Cell* 1995, 80, 237–248.
- [32] Pawson, T., *Nature* 1995, 373, 573–580.
- [33] Birge, R. B., Knudsen, B. S., Besser, D., Hanafusa, H., *Genes Cells* 1996, 1, 595–613.
- [34] Gao, J. J., Diesl, V., Wittmann, T., Morrison, D. C. et al., *J. Leukocyte Biol.* 2002, 72, 1234–1245.
- [35] Minden, A., Lin, A., Claret, F. X., Abo, A., Karin, M., *Cell* 1995, 81, 1147–1157.
- [36] Becker, E., Huynh-Do, U., Holland, S., Pawson, T. et al., *Mol. Cell Biol.* 2000, 20, 1537–1545.
- [37] Anderson, L., Seilhamer, J., *Electrophoresis* 1997, 18, 533–537.
- [38] Gygi, S. P., Rochon, Y., Franz, B. R., Aebersold, R., *Mol. Cell Biol.* 1999, 19, 1720–1730.
- [39] Fessler, M. B., Malcolm, K. C., Duncan, M. W., Worthen, G. S., *J. Biol. Chem.* 2002, 277, 31291–31302.
- [40] Kim, C. H., Kim do, K., Choi, S. J., Choi, K. H. et al., *Proteomics* 2003, 3, 2454–2471.
- [41] Scheurer, S. B., Raybak, J. N., Rosli, C., Neri, D., Elia, G., *Proteomics* 2004, 4, 1737–1760.
- [42] Corthals, G. L., Wasinger, V. C., Hochstrasser, D. F., Sanchez, J. C., *Electrophoresis* 2000, 21, 1104–1115.
- [43] Hegde, P. S., White, I. R., Debouck, C., *Curr. Opin. Biotechnol.* 2003, 14, 647–651.
- [44] Robert, J., *Dev. Comp. Immunol.* 2003, 27, 449–464.
- [45] Basu, S., Srivastava, P. K., *Cell Stress Chaperones* 2000, 5, 443–451.
- [46] Berwin, B., Nicchitta, C. V., *Traffic* 2001, 2, 690–697.
- [47] Fluckiger, S., Fijten, H., Whitley, P., Blaser, K., Cramer, R., *Eur. J. Immunol.* 2002, 32, 10–17.
- [48] Richards, J., Le Naour, F., Hanash, S., Beretta, L., *Ann. N. Y. Acad. Sci.* 2002, 975, 91–100.
- [49] Underhill, D. M., Ozinsky, A., *Annu. Rev. Immunol.* 2002, 20, 825–852.
- [50] Somersan, S., Larsson, M., Fonteneau, J. F., Basu, S. et al., *J. Immunol.* 2001, 167, 4844–4852.
- [51] Rane, M. J., Pan, Y., Singh, S., Powell, D. W. et al., *J. Biol. Chem.* 2003, 278, 27828–27835.
- [52] Solit, D. B., Basso, A. D., Olshen, A. B., Scher, H. I., Rosen, N., *Cancer Res.* 2003, 63, 2139–2144.
- [53] Sato, S., Fujita, N., Tsuruo, T., *Proc. Natl. Acad. Sci. USA* 2000, 97, 10832–10837.
- [54] Pennica, D., Swanson, T. A., Welsh, J. W., Roy, M. A. et al., *Proc. Natl. Acad. Sci. USA* 1998, 95, 14717–14722.
- [55] Lipton, S. A., *Cell Death Differ.* 1999, 6, 943–951.
- [56] Du, J., Zhou, S., Coggeshall, R. E., Carlton, S. M., *Neuroscience* 2003, 118, 547–562.
- [57] Mudher, A., Chapman, S., Richardson, J., Asuni, A. et al., *J. Neurosci.* 2001, 21, 4987–4995.
- [58] Lehnardt, S., Massillon, L., Follett, P., Jensen, F. E. et al., *Proc. Natl. Acad. Sci. USA* 2003.
- [59] Lenhard, J. M., Kahn, R. A., Stahl, P. D., *J. Biol. Chem.* 1992, 267, 13047–13052.
- [60] Morinaga, N., Adamik, R., Moss, J., Vaughan, M., *J. Biol. Chem.* 1999, 274, 17417–17423.
- [61] Balog, R. P., de Souza, Y. E., Tang, H. M., DeMasellis, G. M. et al., *Anal. Biochem.* 2002, 309, 301–310.

PROTEOMICS

www.proteomics-journal.de

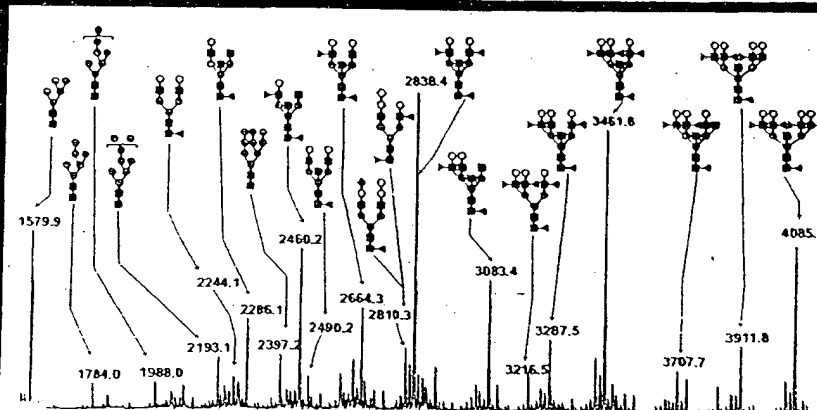
Q
7P93847

4'05



IPC '03

Proceedings of the 3rd International
Proteomics Conference (IPC '03)
held conjointly with the
1st Taiwan Proteomics Conference and the
2nd AOHUPO Congress
Taipei, Taiwan, 14–17 May 2004



EBLING LIBRARY
UNIVERSITY OF WISCONSIN

MAR 28 2005

750 Highland Avenue
Madison, WI 53705

Editor:
Richard J. Simpson



Now
18 issues
per year

WILEY-VCH

ISSN 1615-9853 • PROTC 5 (4) 831–1184 (2005) • Vol. 5 • No. 4 • March 2005

CONTENTS

Volume 5- Issue 4
March 2005
Proteomics 5 (4) 831-1184 (2005)

SPECIAL


IPC '03

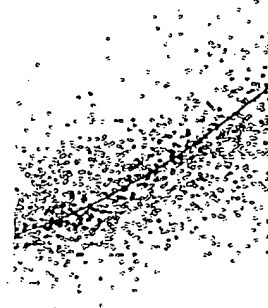
Proceedings of the 3rd International Proteomics
Conference held conjointly with the
1st Taiwan Proteomics Conference and the
2nd AOHUPO Congress
Taipei, Taiwan, 14-17 May 2004

Editor: Richard J. Simpson

- 831 EDITORIAL
IPC '03
Richard J. Simpson

Technology

- 840 SHORT COMMUNICATION
A new application of microwave technology to proteomics
*Hsueh-Fen Juan, Shing-Chuan Chang, Hsuan-Cheng Huang
and Shui-Tein Chen*
- 843 The development of an algorithm for the mass spectral interpretation
of phosphoproteins
Yupeng Zhao and Yen-Han Lin
 Supporting information see www.proteomics-journal.de
- 846 Tryptic transpeptidation products observed in proteome analysis
by liquid chromatography-tandem mass spectrometry
*Heike Schaefer, Daniel C. Chamrad, Katrin Marcus, Kai A. Reidegeld,
Martin Blüggel and Helmut E. Meyer*



Cover Illustration

has kindly been provided by
Takao Kawakami,
Clinical Proteome Center,
Tokyo Medical University,
Tokyo, Japan. This issue, p. 861

1019-6439
Received on: 07-23-98
International Journal of
Oncology.
1998

International Journal of Oncology



ISSN 1019-6439

An international journal devoted to Oncology Research and Cancer Treatment

VOLUME 13, NUMBER 2, AUGUST 1998

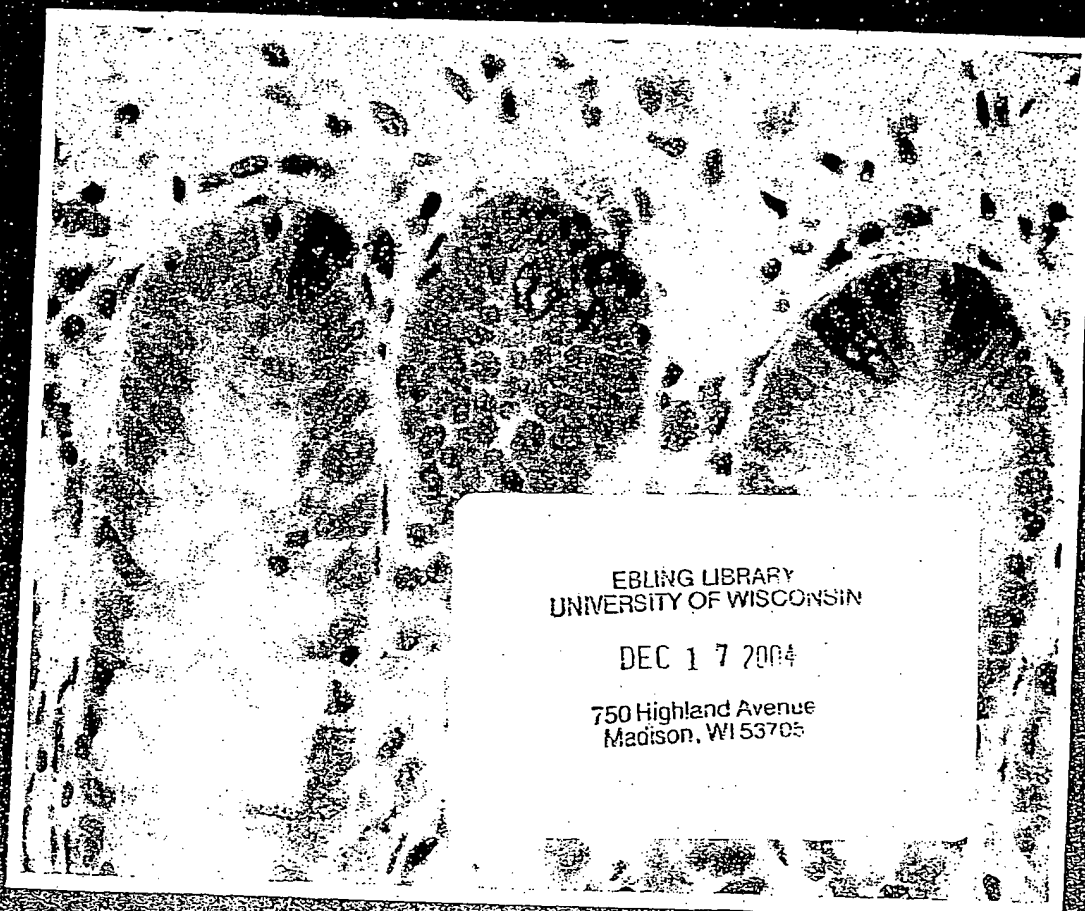


7. Rosin MP, Cairns P, Epstein JI, Schoenberg MP and Sidransky D: Partial allelotype of carcinoma *in situ* of the human bladder. *Cancer Res* 55: 5213-5216, 1995.
8. Birchmeier W and Birchmeier C: Epithelial-mesenchymal transitions in development and tumour progression. In: *Epithelial-Mesenchymal Interactions in Cancer*. Goldberg ID and Rosen EM (eds). Birkhäuser, Basel, pp1-15, 1995.
9. Sidransky D, von Eschenbach A, Tsai YC, Jones P, Summerhayes I, Marshall F, Paul M, Green P, Hamilton SR, Frost P, *et al*: Identification of p53 gene mutations in bladder cancers and urine samples. *Science* 252: 706-709, 1991.
10. Lopez-Beltran A, Croghan GA, Croghan I, Huben RP, Mettlin C and Gaeta JF: Prognostic factors in survival of bladder cancer. *Cancer* 70: 799-807, 1992.
11. Kern WH: The grade and pathologic stage of bladder cancer. *Cancer* 53: 1185-1189, 1984.
12. Jordan AM, Weingarten J and Murphy WM: Transitional cell neoplasms of the urinary bladder. Can biologic potential be predicted from histologic grading? *Cancer* 60: 2766-2774, 1987.
13. Wilkins MR, Sanchez JC, Gooley AA, Appel RD, Humphrey-Smith I, Hochstrasser DF and Williams KL: Progress with proteome projects: why all proteins expressed by a genome should be identified and how to do it. *Biotechnol Genet Eng Rev* 13: 19-50, 1996.
14. Ostergaard M, Rasmussen HH, Nielsen HV, Vorum H, Ørntoft TF, Wolf H and Celis JE: Proteome profiling of bladder squamous cell carcinomas: identification of markers that define their degree of differentiation. *Cancer Res* 57: 4111-4117, 1997.
15. Anderson L and Seilhamer J: A comparison of selected mRNA and protein abundances in human liver. *Electrophoresis* 18: 533-537, 1997.
16. Celis JE, Ratz G, Basse B, Lauridsen JB and Celis A: High resolution two-dimensional gel electrophoresis of proteins: isoelectric focusing and non-equilibrium pH gradient electrophoresis (NEPHGE). In: *Cell Biology: A Laboratory Handbook*. III. Celis JE (ed). Academic Press, pp222-230, 1994.
17. Chomczynski P and Sacchi N: Single-step method of RNA isolation by acid guanidinium thiocyanate-phenol-chloroform extraction. *Anal Biochem* 162: 156-159, 1987.
18. Hotamisligil GS, Johnson RS, Distel RJ, Ellis R, Papaioannou VE and Spiegelman BM: Uncoupling of obesity from insulin resistance through a targeted mutation in aP2, the adipocyte fatty acid binding protein. *Science* 274: 1377-1379, 1996.
19. Madsen P, Rasmussen HH, Leffers H, Honore B and Celis JE: Molecular cloning and expression of a novel keratinocyte protein psoriasis-associated fatty acid-binding protein (PA-FABP) that is highly up-regulated in psoriatic skin and that shares similarity to fatty acid-binding proteins. *J Invest Dermatol* 99: 299-305, 1992.
20. Veerkamp JH, Paulussen RJ, Peeters RA, Maatman RG, van Moerkerk HT and van Kuppevelt TH: Detection, tissue distribution and (sub)cellular localization of fatty acid-binding protein types. *Mol Cell Biochem* 98: 11-18, 1990.
21. Glatz JF, Vork MM, Cistola DP and van der Vusse GJ: Cytoplasmic fatty acid binding protein: significance for intracellular transport of fatty acids and putative role on signal transduction pathways. *Prostaglandins Leukot Essent Fatty Acids* 48: 33-41, 1993.
22. Spitsberg VL, Matitashvili E and Gorewit RC: Association and coexpression of fatty-acid-binding protein and glycoprotein CD36 in the bovine mammary gland. *Eur J Biochem* 230: 872-878, 1995.
23. Yang Y, Spitzer E, Kenney N, Zschiesche W, Li M, Kromminga A, Muller T, Spener F, Lezius A, Veerkamp JH, *et al*: Members of the fatty acid binding protein family are differentiation factors for the mammary gland. *J Cell Biol* 127: 1097-1109, 1994.
24. Glatz JF, Borchers T, Spener F and van der Vusse GJ: Fatty acids in cell signalling: modulation by lipid binding proteins. *Prostaglandins Leukot Essent Fatty Acids* 52: 121-127, 1995.
25. Hunt CR, Ro JH, Dobson DE, Min HY and Spiegelman BM: Adipocyte P2 gene: developmental expression and homology of 5'-flanking sequences among fat cell-specific genes. *Proc Natl Acad Sci USA* 83: 3786-3790, 1986.

Q
7IN84115

INTERNATIONAL

Journal of Cancer



EBLING LIBRARY
UNIVERSITY OF WISCONSIN

DEC 17 2004

750 Highland Avenue
Madison, WI 53705



Publication of the International Union Against Cancer
Published for the University of Wisconsin

Articles published online in Wiley InterScience
25 August 2004 - 8 October 2004
www.interscience.wiley.com

ISSN: 0020-7179

International Union Against Cancer

COUNCIL

J. SEFFRIN, President (USA)
L.J. DENIS, Treasurer (Belgium)
J. BAITY, Chair, Finance Committee (USA)

G. BRIEN (Australia)
R.C. BURTON (Australia)
M. DAUBE (Australia)
K.A. DINSHAW (India)
L. ELOVAINO (Finland)
M.K. GOSPODAROWICZ (Canada)
R.T. HUDSON (Ireland)
T. KITAGAWA (Japan)
A. PUNDALIK KURKURE (India)
R.E. LENHARD (USA)
A. LLOMBART-BOSCH (Italy)

M. LUWIA (Indonesia)
C. MALLINSON (UK)
L.H. MARCHESI (Brazil)
H.F. MICKELSON (USA)
K. NILSSON (Sweden)
S. OMAR (Egypt)
T. PHILIP (France)
E. ROBINSON, Past President (Israel)
Y. SALOOJEE (South Africa)
H. SANCHO-GARNIER (France)

R.J. SCHWEITZER (USA)
O. SOREIDE (Norway)
K. TAJIMA (Japan)
W. WEBER (Switzerland)
S. WILKINSON (UK)
D. ZACKS (USA)
D. ZARIDZE (Russia)
Y. HUI ZHANG (China)
M. ZIV (Israel)
H. ZUR HAUSEN (Germany)

UICC, URL: <http://www.uicc.org>
UICC, E-mail: info@uicc.org

The International Union Against Cancer (UICC) is devoted exclusively to all aspects of the world-wide fight against cancer. Its objectives are to advance scientific and medical knowledge in research, diagnosis, treatment and prevention of cancer, and to promote all other aspects of the campaign against cancer throughout the world. Particular emphasis is placed on professional and public education.

Founded in 1933, the UICC is a non-governmental, independent association of more than 290 member organizations in over 80 countries. Members are voluntary cancer leagues and societies, cancer research and/or treatment centers, and in some countries ministries of health.

The UICC is non-profit, non-political, and non-sectarian. Its headquarters are in Geneva, Switzerland. It creates and carries out programs around the world in collaboration with hundreds of volunteer experts. Supported by membership dues, national subscriptions, grants and donations, its annual budget is about US \$4 million.

The UICC is governed by its members which meet in General Assembly every 4 years. Its elected Council and Executive Committee are responsible for Program structure and implementation.

The UICC organizes an International Cancer Congress every 4 years as well as annual symposia, workshops, and training courses. It publishes the *International Journal of Cancer* (30 issues per year), *UICC News* (quarterly), the *International Calendar of Meetings on Cancer* (bi-annually), and a number of technical reports, textbooks and manuals.

SUBSCRIPTION INFORMATION

© 2005 Wiley-Liss, Inc., a Wiley Company. All rights reserved. No part of this publication may be reproduced in any form or by any means, except as permitted under section 107 or 108 of the 1976 United States Copyright Act, without either the prior written permission of the publisher, or authorization through the Copyright Clearance Center, 222 Rosewood Drive, Danvers, MA 01923, telephone: (978) 750-8400, fax: (978) 750-4470. Requests to the publisher for permission should be addressed to the Permissions Department, c/o John Wiley & Sons, Inc., 111 River St., Hoboken, NJ 07030. Fax: (201) 748-6008; Tel.: (201) 748-6011; <http://www.wiley.com/go/permissions>.

International Journal of Cancer (Print ISSN 0020-7136; Online ISSN 1097-0215) is published 30 times a year, semi-monthly with extra issues in January, March, May, July, September, and November, by Wiley-Liss, Inc., through Wiley Subscription Services, Inc., a Wiley Company. Send subscription inquiries in care of John Wiley & Sons, Inc., Attn: Journals Admin Dept UK, 111 River St., Hoboken, NJ 07030, (201) 748-6645.

Advertising inquiries should be addressed to Advertising Department, c/o John Wiley & Sons, Inc., 111 River St., Hoboken, NJ 07030. Telephone: (201) 748-6921.

Offprint sales and inquiries should be directed to the Customer Service Department, in care of John Wiley & Sons, 111 River St., Hoboken, NJ 07030. Telephone: (201) 748-8776.

Subscription price: Volumes 113-117, 2005 (30 issues). Print only: \$2,905 worldwide. Electronic only: \$2,905 worldwide. A combination price of \$3,195 worldwide includes the subscription in both electronic and print formats. A special personal rate is available to individuals for \$295 worldwide. All subscriptions containing a print element, shipped outside the U.S., will be sent by air. Payment must be made in U.S. dollars drawn on U.S. bank.

Periodicals postage paid at Hoboken, NJ and at additional mailing offices. Postmaster: send address changes to INTERNATIONAL JOURNAL OF CANCER, Subscription Distribution, c/o John Wiley & Sons, Inc., 111 River St., Hoboken, NJ 07030. Change of address: Please forward to the subscriptions address listed above 6 weeks prior to move; enclose present mailing label with change of address. Claims for missing issues: Claims for undelivered copies will be accepted only after the following issue has been received. Please enclose a mailing label or cite your subscriber reference number. Missing copies will be supplied when losses have been sustained in transit and where reserve stock permits. Send claims in care of John Wiley & Sons, Inc., Attn: Journals Admin Dept UK, 111 River St., Hoboken, NJ 07030.

Indexed by: EMBASE/Excerpta Medica • Current Contents/Life Sciences • Science Citation Index • Scisearch • BIOSIS Data Base • Index Medicus • Cambridge Scientific Abstracts • Chemical Abstracts • Reference Update • Smoking and Health Database.

This journal is printed on acid-free paper.

INTERNATIONAL JOURNAL OF CANCER

2005 Wiley-Liss, Inc.

The *International Journal of Cancer* is published for the International Union Against Cancer by Wiley-Liss, Inc., a division of John Wiley & Sons, Inc. Five volumes are issued annually, each consisting of six numbers.

Abstracting and other journals may reprint the summaries of articles without requesting authorization. Authors alone are responsible for views expressed in signed articles. The mention of specific companies or of certain manufacturers' products does not imply that they are endorsed or recommended by the International Union Against Cancer.

References: When quoting from the *International Journal of Cancer*, please use the official abbreviation:
Int. J. Cancer

Localization of Tissue Inhibitor of Metalloproteinases 1 (TIMP-1) in Human Colorectal Adenoma and Adenocarcinoma

Mads N. Holten-Andersen^{1,2*}, Ulla Hansen³, Nils Br  nner², Hans J  rgen Nielsen⁴, Martin Olemann¹ and Boye Schnack Nielsen¹

¹The Finsen Laboratory, Rigshospitalet, Denmark

²The Institute for Pharmacology and Pathobiology, The Royal Veterinary and Agricultural University, Denmark

³Department of Pathology, University Hospital Hvidovre, Denmark

⁴Department of Surgical Gastroenterology, University Hospital Hvidovre, Denmark

Tissue inhibitor of matrix metalloproteinases 1 (TIMP-1) inhibits the proteolytic activity of matrix metalloproteinases and hereby prevents cancer invasion. However, TIMP-1 also possesses other functions such as inhibition of apoptosis, induction of malignant transformation and stimulation of cell-growth. We have previously demonstrated that TIMP-1 is elevated in blood from colorectal cancer patients and that high TIMP-1 levels predict poor prognosis. To clarify the role of TIMP-1 in colorectal tumorigenesis, the expression pattern of TIMP-1 in benign and malignant colorectal tumors was studied. In all of 24 cases of colorectal adenocarcinoma TIMP-1 mRNA was detected by *in situ* hybridization. In all cases TIMP-1 expression was found in fibroblast-like cells located at the invasive front but was seen only sporadically in normal mucosa. No TIMP-1 mRNA was seen in any of the cases in benign or malignant epithelial cells, in vascular cells or smooth muscle cells. Comparison of sections processed for TIMP-1 *in situ* hybridization with sections immunohistochemically stained with antibodies against TIMP-1 showed good correlation between TIMP-1 mRNA and immunoreactivity. Combining TIMP-1 *in situ* hybridization with immunohistochemical staining for α -smooth muscle actin or CD68 showed TIMP-1 mRNA in myofibroblasts but not in macrophages. TIMP-1 mRNA was detected in 2 of 7 adenomatous polyps in the adenoma area: in both cases associated with focal stromal inflammation at the epithelial-stromal interface. In conclusion, TIMP-1 expression is a rare event in benign human colon tissue but is highly expressed by myofibroblasts in association with invading colon cancer cells.

Key words: TIMP-1; MMP; *in situ* hybridization; immunohistochemistry; myofibroblast

A prerequisite for cancer cell invasion and metastasis is the breakdown of tissue barriers mediated by proteolytic enzymes such as the matrix metalloproteinases (MMP).^{1,2} Under normal physiologic conditions, the tissue degrading activities of the MMPs are kept at bay by the presence of the naturally occurring inhibitors: tissue inhibitors of metalloproteinases (TIMP). TIMP-1, a 28 kDa glucoprotein demonstrated to be present in most bodily tissues and fluids, binds and inhibits MMPs in a 1:1 stoichiometric manner.^{3,4} Overexpression of TIMP-1 in various cancer models has shown a suppressive role in the malignant progression.⁵ However, as opposed to this anti-invasive role of TIMP-1, several recent studies have demonstrated quite different functions of this MMP-inhibitor including stimulation of cell growth, malignant transformation and inhibition of apoptosis, suggesting a possible tumor-promoting role of TIMP-1 in very early stages of tumorigenesis.^{6–10} Thus, it has been speculated that TIMP-1 may actually play a dual role in cancer progression and metastasis.¹¹

Several studies have demonstrated that tumor tissue levels of MMP mRNA and protein are significantly increased in various malignant diseases and that such MMP elevations are correlated with cancer cell invasion, metastasis and short patient survival.^{12,13} In addition, many reports have described similar overexpression of TIMP-1 mRNA and protein in several cancer types.^{14–20} Moreover, we and others have demonstrated that measurement of increased plasma levels of TIMP-1 by immunoassay serves as a strong marker for short survival and recurrence of disease in patients with colorectal cancer.^{21–23} Similarly, a strong correlation

between high protein levels and poor prognosis is known for the type-1 plasminogen activator inhibitor (PAI-1).^{24,25} Considering the protease inhibiting function of these inhibitors, these findings seemed controversial; however, alternative functions have been reported both for TIMP-1 as mentioned above as well as for PAI-1.²⁶

In order to better understand the role of TIMP-1 in colorectal cancer, histochemical analyses may provide some indications. A number of studies of the localization of TIMP-1 in colorectal cancer have been published; however, the results of these reports are somewhat contradictory. Newell and colleagues²⁷ reported that TIMP-1 mRNA was expressed both in invasive adenocarcinoma, carcinoma *in situ* and adenoma and that the expression was observed in both the stromal as well as the epithelial compartment of the tissues studied. In contrast, Zeng and colleagues^{12,20} reported that TIMP-1 mRNA was expressed only in the stromal compartment of colorectal adenocarcinomas in spindle-shaped cells surrounding the invasive cancer cells. The results of immunohistochemical studies of TIMP-1 in colon are also conflicting: Hewitt and colleagues¹⁹ reported that TIMP-1 was expressed in the connective tissue and basement membrane in both normal mucosa, adenomas and adenocarcinomas with only little staining of the neoplastic epithelium. On the other hand, Tomita and colleagues²⁸ reported that TIMP-1 was expressed in both stromal and epithelial cells in colonic polyps and adenomas, as well as in adenocarcinomas, in which the neoplastic cells were strongly immunoreactive.

In order to resolve these inconsistencies, we undertook our study and by *in situ* hybridization and immunohistochemistry demonstrated that TIMP-1 is expressed in myofibroblasts in the stroma at the invasive front of colorectal adenocarcinomas. Because TIMP-1 was virtually absent from normal colorectal epithelium, we evaluated the possibility of using TIMP-1 as a diagnostic tool to differentiate colorectal adenomas from Dukes' stage A colorectal adenocarcinomas.

Material and methods

Tissue samples

All tissue material included was obtained from University Hospital of Hvidovre (Copenhagen, Denmark) in accordance with a permission given by the local scientific ethical committee (KF 01-078/93). Fourteen archival samples (formalin fixed and paraffin embedded) collected from 1989 to 1993 included Dukes' stage A colorectal adenocarcinomas ($n = 8$) and colorectal adenomatous polyps ($n = 6$, 3 were pedunculated (1 with mild and 2 with

Grant sponsor: The Danish Cancer Society; Grant sponsor: European commission; Grant number: QL61-CT-2000-011131; Grant sponsor: Weimann Foundation.

*Correspondence to: Mads N Holten-Andersen, The Institute for Pharmacology and Pathobiology, The Royal Veterinary and Agricultural University, Denmark.

Received 16 February 2004; Accepted after revision 7 June 2004
DOI 10.1002/ijc.20566

Published online 13 September 2004 in Wiley InterScience (www.interscience.wiley.com).



moderate dysplasia) and 3 were sessile (1 with moderate and 2 with focally severe dysplasia). Samples from 16 colorectal adenocarcinomas (1 Dukes' stage A, 6 Dukes' stage B, 8 Dukes' stage C and 1 Dukes' stage D), 1 villous adenoma and 1 malignant colon lymphoma were prospectively collected during 1999–2000. These prospectively collected tissue specimens were dissected so that samples contained both normal mucosa and tumor tissue and were obtained within 30 min following surgical bowel resection. The specimens were immediately fixed in 4% neutral buffered formalin for 20–24 hr and then paraffin embedded. The 14 archival samples had also been formalin fixed and paraffin embedded.

Generation of nonoverlapping TIMP-1 cDNA fragments by PCR

The full length TIMP-1 cDNA (GenBank NM_003254) cloned in pSP64 vector²⁹ was used as template to generate 2 nonoverlapping PCR fragments for *in vitro* transcription, and named f104 (bp 56–378) and f106 (bp 398–680). First, the whole insert (~780 bp) was cut out by digestion with *Hind*III and *Bam*HI and purified after agarose gel electrophoresis using the Qiaex II gel extraction kit (Qiagen, Crawley, United Kingdom). To generate nonoverlapping antisense probes and the corresponding sense probe, 2 PCR fragments were generated using upstream primers flanked by a linker sequence containing an *Eco*RI restriction enzyme site (underlined nucleotides) and a T3 polymerase binding sequence (boldface) 5'-(**ggaattc**cattacacctactaaaggaga)-3', and downstream primers flanked by a linker sequence containing a *Bam*HI restriction enzyme site and a T7 polymerase binding sequence 5'-(**ggatccta**atagcactcactataggag)-3'. The TIMP-1 specific upstream primers were 5'-accacatggcccttg-3' for f104 and 5'-(linker)-gcaggatggactctgcac-3' for f106, and the downstream primers were 5'-(linker)-actctcgtcgtcggttg-3' for f104 and 5'-(linker)-tatctggagccgcaggag-3' for f106. PCR using the 2 f104 primers or the 2 f106 primers was done as previously described.³⁰

The PCR products were purified by column chromatography using S-200HR microspin columns (Amersham Pharmacia Biotech, Inc., Piscataway, NJ), and their size tested by agarose gel electrophoresis. Both migrated as ~300 bp fragments in accordance with the predicted size (322 and 282 bp, respectively). An ABI PRISM 310 genetic analyzer was employed for DNA sequencing analysis and was performed according to the manufacturer's instructions (Perkin Elmer, Applied Biosystems, Foster City, CA) using the primers specified above. The DNA sequences obtained were confirmed by comparison with the specific TIMP-1 cDNA nucleic acid sequence (GenBank NM_003254).

Plasmids containing human MMP-2 cDNA (pCol7201, bp 647–1284) and human MMP-9 cDNA (pCol9202, bp 1751–2326) have been described elsewhere.³¹

In vitro transcription

Antisense and sense riboprobes were labeled with ³⁵S UTP (NEN, Boston, MA) by *in vitro* transcription using T7 and T3 RNA polymerases (Roche, Basel, Switzerland). The DNA template was digested with DNase (Promega, Madison, WI). Nonincorporated ³⁵S UTP and DNA was removed by column chromatography using S-200HR microspin columns (Amersham Pharmacia Biotech, Inc., Piscataway, NJ). The ³⁵S activity was adjusted for every probe by dilution to 500,000 cpm/μl.

In situ hybridization

In situ hybridization was performed essentially as described previously.³² In brief, 3 μm paraffin sections were deparaffinized in xylene, hydrated with graded ethanol and boiled in a microwave oven for 10–12 min in 10 mM citrate buffer, pH 5.0. After additional 20 min at room temperature, the sections were dehydrated with graded ethanol and the ³⁵S labeled probes (2 × 10⁶ cpm in 20 μl hybridization mixture³¹ per slide) incubated overnight at 55°C in a humidified chamber. Sections were washed in Hellen-dahl chambers with SSC buffers containing 0.1% SDS and 10 mM DTT at 150 rpm at 55°C using a Bühler incubation shaker (Johanna Otto GmbH, Hechingen, Germany) for 10 min in 2×SSC,

10 min in 0.5×SSC, and 10 min in 0.2×SSC. Sections were then RNase A treated for 10 min to remove nonspecifically bound riboprobe. Subsequent wash was performed in 0.2×SSC as specified above. Sections were dehydrated and soaked into an autoradiographic emulsion (Ilford), exposed for 5–7 days if not otherwise stated and finally developed. Sections were counterstained with haematoxylin and eosin.

Immunoperoxidase staining

Immunohistochemistry was performed essentially as described previously.³² Five micrometer paraffin sections were deparaffinized with xylene and hydrated through ethanol/water dilutions. Tissue pretreatment was performed with protease-K (5 μg/ml) digestion for 20 min. Sections were blocked for endogenous peroxidase activity by treatment with 1% hydrogen peroxide for 15 min. The sections were washed in 50 mM Tris 150 mM NaCl, pH 7.6, containing 0.5% Triton X-100 (TBS-T). Incubation with antibodies was done overnight at 4°C. Sheep polyclonal antibodies (pAb) against TIMP-1 and nonimmune goat IgG were used at a final concentration of 4.0 μg/ml. Two monoclonal antibodies (MAb) against TIMP-1,³³ NM4 (clone rTIX6A, NeoMarkers, Fremont, CA) and CalB2 (clone 147-6D11, CalBiochem, Oncogene Res. Products, Cambridge, MA), and a MAb against trinitrophenyl (TNP)³⁴ were all incubated at 1.0 μg/ml (all 3 MABs are IgG1). CalB2 MAB recognizes both free TIMP-1 and TIMP-1 in complex with MMPs.³³ NM4 MAB only recognizes free TIMP-1.³³ According to the manufacturer's descriptions, both MABs are raised using recombinant human TIMP-1. The sheep polyclonal antibodies were raised by immunization with TIMP-1 purified from human dermal fibroblasts. The IgG was obtained by triple precipitation using ammonium-sulfate and characterized by immunodiffusion and rocket immunoelectrophoresis.³⁵ In addition, we have shown that the pAb recognize both free and MMP-complexed TIMP-1.³⁶ Furthermore, the specificity of the antibodies was analyzed by Western blotting analysis against recombinant human TIMP-1 expressed in NSO mouse myeloma cells. Here, the antibody preparation recognizes a band of approximately 28 kDa in accordance with the molecular weight of TIMP-1. To certify that the pAb recognize TIMP-1 in colon tumors, the antibodies were immobilized on a sepharose column. Total protein extracted from 3 colon adenocarcinomas was passed through the column 5 times and the bound and subsequently eluted protein analyzed in a Western blot using a TIMP-1 monoclonal antibody (MAC15). A single band of approximately 28 kDa was revealed in accordance with the molecular weight of TIMP-1 (results not shown). In immunohistochemistry, the sheep pAb were detected with biotinylated rabbit-anti-goat IgG, which cross-react with sheep IgG (1:100, code E466, DakoCytomation) followed by horseradish peroxidase in complex with streptavidin (code K377, DakoCytomation). The MABs were detected with the Envision-mouse reagent (EnVision reagent, K4003, DakoCytomation), followed by tyramine amplification, using biotinyl tyramine substrate as specified by the manufacturer (Nen, Boston, MA). Sections were developed with NovaRed substrate as specified by the manufacturer (Vector Laboratories, Burlingame, CA) for 15 min. Finally, sections were counterstained in Mayers haematoxylin, dehydrated in ethanol and mounted.

Combined *in situ* hybridization and immunohistochemistry

Double labeling by combining *in situ* hybridization and immunohistochemistry on paraffin sections has been described previously.³² In brief, using MAB against α-sm-actin (clone 1A4) diluted 1:1000, against cytokeratin (clone AE1/AE3) diluted 1:1000, or against CD68 (clone PGM1) diluted 1:200, sections were incubated for 2 hours at room temperature and then detected with anti-mouse-IgG/horse radish peroxidase-conjugated polymers (Envision-mouse reagent, DakoCytomation, Glostrup, Denmark). Sections were developed with diaminobenzidine (DAB) for 7–10 min, and immediately dehydrated for *in situ* hybridization, which was performed as described above using the antisense probes of f104. Sections were counterstained with haematoxylin.

Results

Analysis of TIMP-1 probes and antibodies for *in situ* hybridization and immunohistochemistry

Histopathological diagnosis of prospectively collected specimens from 18 colorectal lesions revealed 16 colorectal adenocarcinomas, 1 villous adenoma and 1 malignant lymphoma. ³⁵S-labeled antisense and sense RNA probes were generated by *in vitro* transcription from 2 nonoverlapping DNA sequences of the human TIMP-1 cDNA and tested by *in situ* hybridization on adjacent sections from 5 of the colorectal adenocarcinomas. The 2 antisense probes showed an identical hybridization pattern in all the 5 cases, located in the stromal compartment surrounding the invading cancer cells, while no specific signal was seen with the 2 sense probes (Fig. 1). To test whether the TIMP-1 mRNA was accompanied by TIMP-1 protein expression, immunohistochemistry was performed on 8 of the adenocarcinomas (including the 5 mentioned above) and the malignant lymphoma using sheep anti-human TIMP-1 polyclonal antibodies on sections adjacent to TIMP-1 *in situ* hybridized sections. The TIMP-1 mRNA and immunoreactivity was observed in the same cells in all of the 9 cases tested (Fig. 2A), including the malignant lymphoma. The anti-TIMP-1 polyclonal antibodies did not react with other cell populations in all of 8 adenocarcinomas and the malignant lymphoma apart from some normal and malignant epithelial cells that were weakly stained on the luminal apical surface. Two MABs against TIMP-1 (CalB2 and NM4) required strong signal amplification but showed a staining pattern similar to that of the polyclonal antibody preparation (Fig. 2B), with the only exception that neither of the 2 MABs stained the luminal apical surface of the normal and malignant epithelium. No signal was obtained with nonimmune goat serum or a MAB (of same subclass as CalB2 and NM4) directed against the synthetic hapten trinitrophenyl (TNP).

TIMP-1 mRNA expression patterns in colon cancer

Expression of TIMP-1 mRNA was then analyzed in the remaining 9 colorectal lesions by *in situ* hybridization. TIMP-1 mRNA

expression was in all the cases of colon adenocarcinoma (including those mentioned above) highly expressed in stromal fibroblast-like cells located at the invasive front (Fig. 3a,d). TIMP-1 mRNA signal was also observed in fibroblast-like cells located in the tumor stroma towards the colonic lumen in 8 of 10 cases where this tissue structure was present (data not shown). No or little TIMP-1 mRNA was detected in the central part of the carcinomas. In 5 of the 16 colorectal adenocarcinomas, we observed TIMP-1 mRNA signal in some fibroblast-like cells located around the muscle layer of some arteries located in the submucosa distant from the cancer area. The normal colonic mucosa, including the lamina propria that was present in all samples tested, was generally negative (Fig. 3b,e). Only a relatively weak TIMP-1 mRNA signal was detected in stromal fibroblast-like cells surrounding one or a very few normal crypts (Fig. 3c,f) in 3 out of 6 cases tested with extended exposure time (10 days vs. usually 5 days). In the villous adenoma, we saw only a few TIMP-1 mRNA positive cells associated with focal inflammation (data not shown). In the malignant lymphoma of the colon, TIMP-1 mRNA expressing fibroblast-like cells were, different from the adenocarcinomas, located in a diffuse pattern throughout the whole tumor. No TIMP-1 mRNA signal was observed in any of the 18 cases in the cancer cells, smooth muscle cells or vascular cells.

Characterization of TIMP-1 mRNA expressing cells

To test whether the TIMP-1 mRNA positive fibroblast-like cells could be (myo)fibroblasts and/or macrophages, sections from 4 colorectal adenocarcinomas and the malignant lymphoma were first immunohistochemically stained with antibodies directed against α -sm-actin [for detection of myofibroblast/smooth muscle cells (SMC)] or CD68 (for detection of macrophages) and subsequently incubated with a TIMP-1 mRNA antisense probe. In normal colon tissue, α -sm-actin is expressed by vascular smooth muscle cells, smooth muscle cells of lamina muscularis mucosae and tunica muscularis as well as pericryptal myofibroblasts.³⁷ In colon tumors, α -sm-actin is expressed by tumor-associated fibroblast-like cells located throughout the tumor stroma, which are defined as myofibroblasts. No TIMP-1 mRNA was detected in any α -sm-actin positive smooth muscle cells, including those of the vessels, the lamina muscularis mucosae and the tunica muscularis. In addition, no TIMP-1 mRNA was detected in the α -sm-actin positive pericryptal myofibroblasts of the lamina propria in any of the 5 lesions. TIMP-1 mRNA signal was in contrast seen in α -sm-actin-positive tumor associated myofibroblasts located at the invasive front of the colon cancers. In 3 of the adenocarcinomas, more than 80% of TIMP-1 mRNA-positive cells located close to the invading cancer cells were α -sm-actin-positive (Fig. 4). TIMP-1 mRNA positive fibroblast-like cells located more distant from the invasive cancer cells, towards the submucosa, expressed little or no α -sm-actin. In 1 adenocarcinoma and in the malignant lymphoma approximately 50% of the TIMP-1 mRNA positive cells expressed α -sm-actin. Thus, the TIMP-1 mRNA expressing cells constitute a subpopulation of tumor-associated myofibroblasts located at the invasive front of the tumor. No TIMP-1 mRNA signal could be identified in any of the CD68-positive cells (Fig. 4).

Expression of TIMP-1 and MMP-2 and 9 in colon cancer

MMP-2 and MMP-9 are 2 type IV collagenases expressed in the invasive cancer tissue of colorectal adenocarcinomas. Thus MMP-2 has been reported to be expressed by fibroblast-like cells in the cancer stroma,^{12,31} and MMP-9 by macrophages at the leading edge of the invasive cancer.³⁵ To directly compare the expression patterns of MMP-2 and MMP-9 with that of TIMP-1, adjacent sections from 5 colorectal adenocarcinomas were hybridized with probes for TIMP-1, MMP-2 and MMP-9 mRNAs. We found that the expression of TIMP-1 mRNA was localized characteristically at the invasive front of the growing tumor, whereas the expression of MMP-2 mRNA was most intense in the central areas, showing decreased expression towards the invasive front (Fig. 5a). MMP-9 mRNA expressing cells were found at the

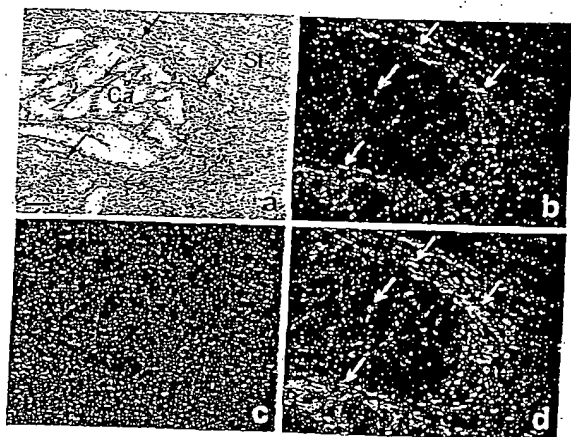


FIGURE 1—*In situ* hybridization with 2 nonoverlapping TIMP-1 specific probes in human colon cancer. Three adjacent sections from a colon adenocarcinoma were incubated with 2 nonoverlapping ³⁵S-labeled antisense probes for TIMP-1 mRNA (f106 (a,b) and f104 (d)) and a corresponding TIMP-1 sense probe, f106 (c). The *in situ* hybridization signal is identified as black silver grains and demonstrated in brightfield (a) and as a white pattern in darkfield illumination (b-d). The 2 antisense probes show the same hybridization pattern and the hybridization signal is seen in the same cells (arrows in a, b and d), whereas no specific signal is seen with the sense probe (c). Note that the TIMP-1 mRNA signal is located in the tumor stroma (indicated by St) surrounding the invasive cancer cells (Ca) that are devoid of TIMP-1 *in situ* hybridization signal. (a)-(d): Bar = 100 μ m.

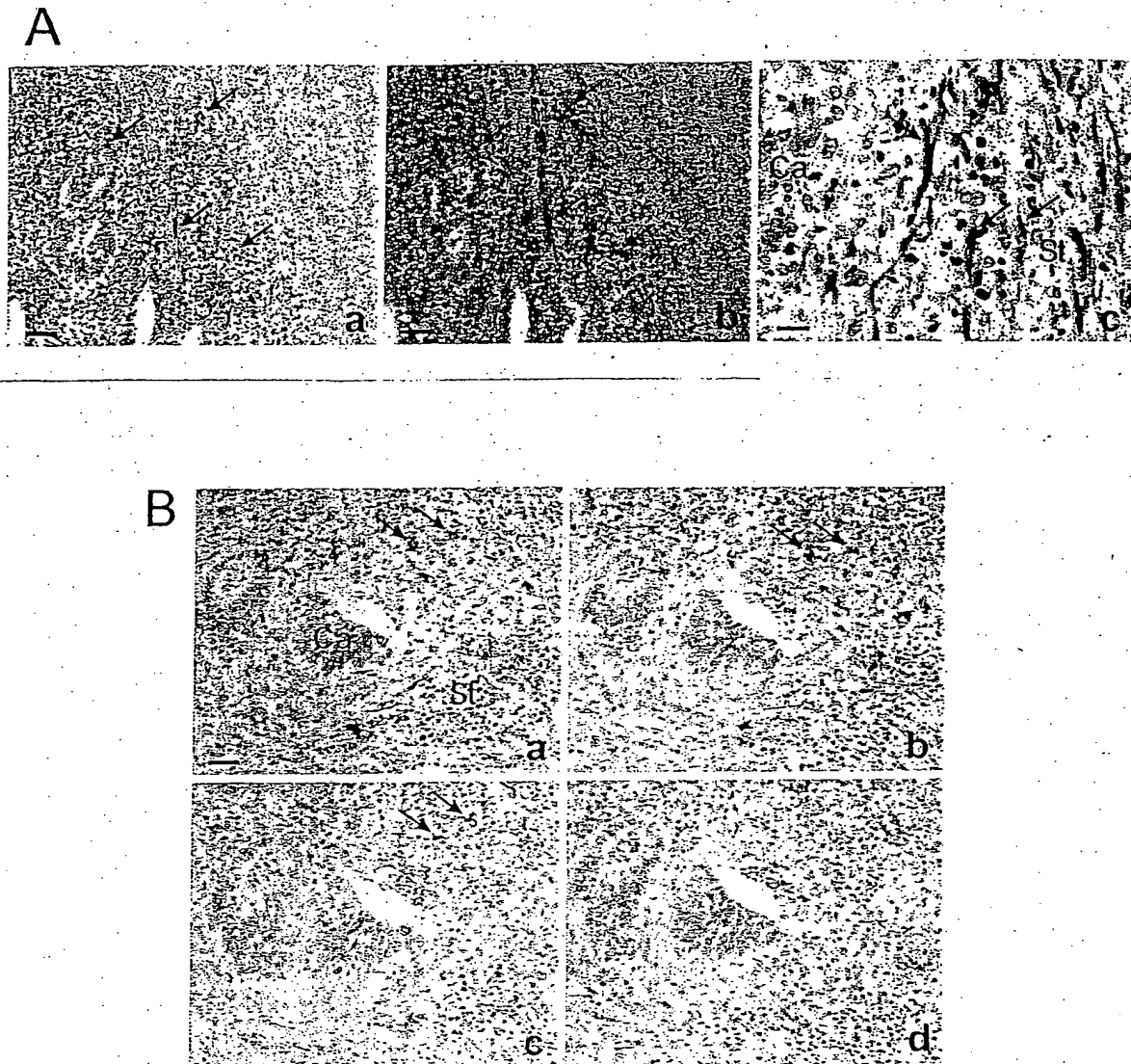


FIGURE 2—*In situ* hybridization and immunohistochemistry for TIMP-1 in human colon adenocarcinoma were incubated with polyclonal antibodies against TIMP-1 (a,c) and a TIMP-1 mRNA antisense probe (b). The TIMP-1 immunoreactivity (red-brown color, arrows in a and c) and the TIMP-1 mRNA (silver grains, arrows in b) are identified in the same cells (arrows in a,b). Immunoperoxidase staining with the TIMP-1 pAb reveals the TIMP-1-positive cells as fibroblast-like cells (arrows in c) located in the stroma (St). No TIMP-1 immunoreactivity is seen in cancer cells (Ca). a,b: bars = 50 μ m; c: bars = 13 μ m. (B) Four consecutive adjacent sections were incubated with CalB2 MAb anti-TIMP-1 (a), NM4 MAb (b), sheep anti TIMP-1 pAb (c) or mouse anti TIMP-1 pAb (d). The 3 MABs were detected with Envision reagent followed by TS amplification and the sheep pAb with biotinylated rabbit anti-goat followed by HRP-conjugated streptavidin (see Material and methods). The 3 TIMP-1 antibodies react with the same cells (arrows). No immunoreactivity is seen when the sections are incubated with anti-TNP.

invasive front like those expressing TIMP-1 mRNA but with a distinctly different distribution. Foci with high expression of TIMP-1 mRNA were not accompanied with increased expression of MMP-9 mRNA and vice-versa (Fig. 5b). Thus, TIMP-1 mRNA expression is not coregulated with MMP-2 or MMP-9 mRNA expression.

TIMP-1 in adenomas and Dukes' stage A carcinomas

TIMP-1 antigen can readily be measured in blood and we have previously reported that levels of TIMP-1 in blood are significantly

elevated in colorectal cancer patients compared to healthy donors and that high plasma TIMP-1 levels are associated with short survival of colorectal cancer patients.^{21,36} TIMP-1 has therefore been suggested to be a novel marker for detection of early stage colorectal cancer and for prognostic stratification of colorectal cancer patients.^{21,39} These findings, together with the characteristic expression pattern of TIMP-1 at the invasive front of virtually all the colon cancers and the absence or minute TIMP-1 expression in normal and benign colon mucosa, prompted the evaluation of TIMP-1 expression as a marker for early invasive colon cancer.

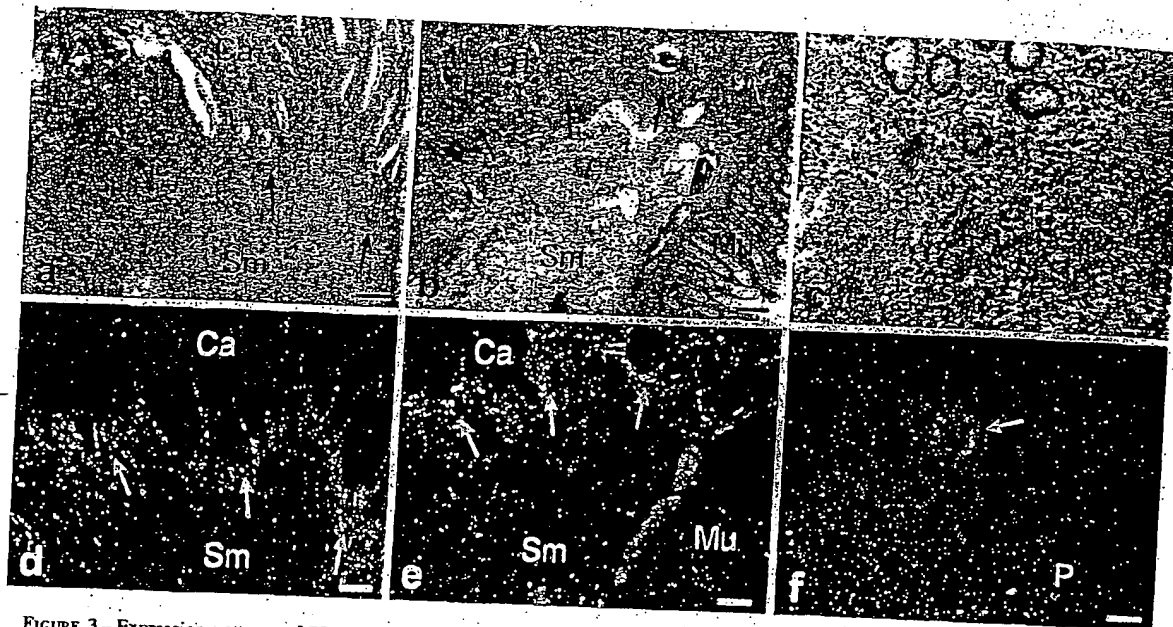


FIGURE 3 - Expression patterns of TIMP-1 mRNA in human colon cancer. Sections were incubated with an antisense probe for TIMP-1 mRNA. The TIMP-1 mRNA signal is demonstrated in brightfield (a-c) and darkfield (d-f). The TIMP-1 mRNA is highly expressed in a subpopulation of stromal fibroblast-like cells at the invasive front of the cancer (a,d), whereas a low hybridization signal is seen within central parts of the cancer area (Ca) and in the submucosa (Sm). The normal mucosa (indicated by Mu in b and e) is negative. A low *in situ* hybridization signal was detected in a few stromal cells surrounding a few normal-looking glands (c,f), see also text. Exposure time: a,b, d,e, 5 days; d,f, 10 days. (a,b,d,f) bars = 200 μ m; (c,f) bars = 25 μ m.

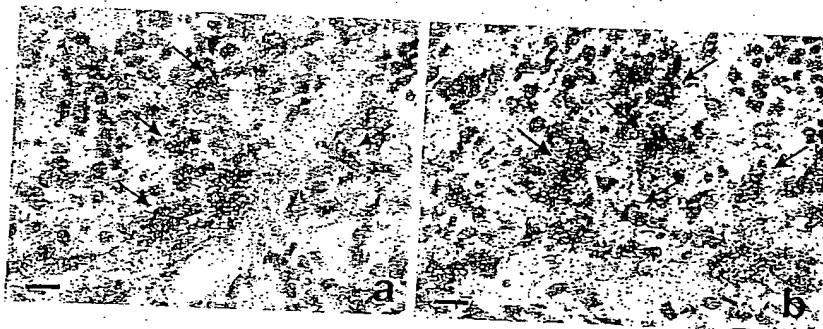


FIGURE 4 - Double labeling for TIMP-1 mRNA and α -sm-actin or CD68 in human colon cancer. Sections were first processed for immunohistochemistry incubating antibodies against α -sm-actin (a) or CD68 (b) and subsequently by *in situ* hybridization using the f104 TIMP-1 specific antisense probe. TIMP-1 mRNA signal is colocalized with α -sm-actin immunoreactivity in fibroblast-like cells that are considered as myofibroblasts (black arrows in a), whereas no CD68 immunoreactivity is seen in the TIMP-1 mRNA positive cells (black arrows in b) in an area with several CD68-positive macrophages (red arrows in b). Note that some of the α -sm-actin-positive myofibroblasts have little or no TIMP-1 mRNA signal (red arrows in a). Bars = 13 μ m.

Therefore, we compared TIMP-1 mRNA expression in an additional 6 colorectal adenomatous polyps with the expression in an additional 8 Dukes' stage A colorectal adenocarcinomas. TIMP-1 mRNA signal was detected in 2 of the 6 adenomas, whereas all 8 Dukes' stage A carcinomas showed TIMP-1 mRNA signal at the invasive front (Fig. 6). In 1 positive adenoma (pedunculated type), TIMP-1 mRNA expression was confined to a single focus in fibroblast-like cells associated with focal stromal inflammation (Fig. 6). However, histological analysis of additional sections from this sample clearly revealed disruption of the dysplastic epithelium in the same area. In the other TIMP-1 mRNA positive adenoma (sessile type), a few TIMP-1 mRNA expressing fibroblasts were located around small arteries not directly associated with the tumor area (data not shown).

Taken together, all of the 9 Dukes' stage A carcinomas analyzed showed TIMP-1 mRNA expression in myofibroblasts located at the invasive front of the tumors, whereas expression was detected in only 3 of 7 adenomas, and in these was seen in fibroblast-like cells associated with focal inflammation at the epithelial-stromal interface in 2 of the cases and with arteries in the submucosa in 1 case.

Discussion

Our study was undertaken to clarify the expression and cellular localization of the MMP inhibitor TIMP-1 in human colon adenocarcinomas. Our studies were founded on the use of 2 specific antisense RNA probes derived from 2 nonoverlapping TIMP-1

References

- Liotta LA, Steeg PS, Stetler-Stevenson WG. Cancer metastasis and angiogenesis: an imbalance of positive and negative regulation. *Cell* 1991;64:327-36.
- Stetler-Stevenson WG, Yu AE. Proteases in invasion: matrix metalloproteinases. *Semin Cancer Biol* 2001;11:143-52.
- Murphy G, Koklitis P, Carne AF. Dissociation of tissue inhibitor of metalloproteinases (TIMP) from enzyme complexes yields fully active inhibitor. *Biochem J* 1989;261:1031-4.
- Welgus HG, Stricklin GP. Human skin fibroblast collagenase inhibitor. Comparative studies in human connective tissues, serum, and amniotic fluid. *J Biol Chem* 1983;258:12259-64.
- Khokha R, Waterhouse P. The role of tissue inhibitor of metalloproteinase-1 in specific aspects of cancer progression and reproduction. *J Neurooncol* 1994;18:123-7.
- Docherty AJ, Lyons A, Smith BJ, Wright EM, Stephens PE, Harris TJ, Murphy G, Reynolds JJ. Sequence of human tissue inhibitor of metalloproteinases and its identity to erythroid-potentiating activity. *Nature* 1985;318:66-9.
- Guedez L, Courtemanche L, Stetler-Stevenson M. Tissue inhibitor of metalloproteinase (TIMP)-1 induces differentiation and an antiapoptotic phenotype in germinal center B cells. *Blood* 1998;92:1342-9.
- Hewitt RE, Brown KE, Corcoran M, Stetler-Stevenson WG. Increased expression of tissue inhibitor of metalloproteinases type 1 (TIMP-1) in a more tumorigenic colon cancer cell line. *J Pathol* 2000;192:455-9.
- Guedez L, Stetler-Stevenson WG, Wolff L, Wang J, Fukushima P, Mansoor A, Stetler-Stevenson M. In vitro suppression of programmed cell death of B cells by tissue inhibitor of metalloproteinases-1. *J Clin Invest* 1998;102:2002-10.
- Li G, Fridman R, Kim HR. Tissue inhibitor of metalloproteinase-1 inhibits apoptosis of human breast epithelial cells. *Cancer Res* 1999;59:6267-75.
- Jiang Y, Goldberg ID, Shi YE. Complex roles of tissue inhibitors of metalloproteinases in cancer. *Oncogene* 2002;21:2245-52.
- Zeng ZS, Guillem JG. Distinct pattern of matrix metalloproteinase 9 and tissue inhibitor of metalloproteinase 1 mRNA expression in human colorectal cancer and liver metastases. *Br J Cancer* 1995;72:575-82.
- Gomez DE, Alonso DF, Yoshiji H, Thorgeirsson UP. Tissue inhibitors of metalloproteinases: structure, regulation and biological functions. *Eur J Cell Biol* 1997;74:111-22.
- Guillem JG, Levy MF, Hsieh LL, Johnson MD, LoGerfo P, Forde KA, Weinstein IB. Increased levels of p16, c-myc, and ornithine decarboxylase RNAs in human colon cancer. *Mol Carcinog* 1990;3:68-74.
- Lu XQ, Levy M, Weinstein IB, Santella RM. Immunological quantitation of levels of tissue inhibitor of metalloproteinase-1 in human colon cancer. *Cancer Res* 1991;51:6231-5.
- Mimori K, Mori M, Shiraishi T, Fujie T, Baba K, Haraguchi M, Abe R, Ueo H, Akiyoshi T. Clinical significance of tissue inhibitor of metalloproteinase expression in gastric carcinoma. *Br J Cancer* 1997;76:531-6.
- Fong KM. TIMP1 and adverse prognosis in non-small cell lung cancer. *Clinical Cancer Research* 1996;2:1369-72.
- Ree AH, Flores VA, Berg JP, Maclandino GM, Nesland JM, Fodstad O. High levels of messenger RNAs for tissue inhibitors of metalloproteinases (TIMP-1 and TIMP-2) in primary breast carcinomas are associated with development of distant metastases. *Clin Cancer Res* 1997;3:1623-8.
- Hewitt RE, Leach JH, Powe DG, Clark IM, Cawston TE, Turner DR. Distribution of collagenase and tissue inhibitor of metalloproteinases (TIMP) in colorectal tumours. *Int J Cancer* 1991;49:666-72.
- Zeng ZS, Cohen AM, Zhang ZF, Stetler-Stevenson W, Guillem JG. Elevated tissue inhibitor of metalloproteinase 1 RNA in colorectal cancer stroma correlates with lymph node and distant metastases. *Clin Cancer Res* 1995;1:899-906.
- Holten-Andersen MN, Stephens RW, Nielsen HJ, Murphy G, Christensen JJ, Stetler-Stevenson W, Brunner N. High preoperative plasma tissue inhibitor of metalloproteinase-1 levels are associated with short survival of patients with colorectal cancer. *Clin Cancer Res* 2000;6:4292-9.
- Oberg A, Hoyhtya M, Tavelin B, Stenling R, Lindmark G. Limited value of preoperative serum analyses of matrix metalloproteinases (MMP-2, MMP-9) and tissue inhibitors of matrix metalloproteinases (TIMP-1, TIMP-2) in colorectal cancer. *Anticancer Res* 2000;20:1085-91.
- Pellegrini P, Contasta I, Berghella AM, Gargano E, Mammarella C, Adorno D. Simultaneous measurement of soluble carcinoembryonic antigen and the tissue inhibitor of metalloproteinase TIMP1 serum levels for use as markers of pre-invasive to invasive colorectal cancer. *Cancer Immunol Immunother* 2000;49:388-94.
- Grondahl-Hansen J, Christensen JJ, Rosenquist C, Brunner N, Mouridsen HT, Dano K, Blichert-Toft M. High levels of urokinase-type plasminogen activator and its inhibitor PAI-1 in cytosolic extracts of breast carcinomas are associated with poor prognosis. *Cancer Res* 1993;53:2513-21.
- Nielsen HJ, Pappot H, Christensen JJ, Brunner N, Thodacius-Ussing O, Moesgaard F, Dano K, Grondahl-Hansen J. Association between plasma concentrations of plasminogen activator inhibitor-1 and survival in patients with colorectal cancer. *BMJ* 1998;316:829-30.
- Wind T, Hansen M, Jensen JK, Andreasen PA. The molecular basis for anti-proteolytic and non-proteolytic functions of plasminogen activator inhibitor type-1: roles of the reactive centre loop, the shutter region, the flexible joint region and the small serpin fragment. *Biol Chem* 2002;383:21-36.
- Newell KJ, Witty JP, Rodgers WH, Matrisian LM. Expression and localization of matrix-degrading metalloproteinases during colorectal tumorigenesis. *Mol Carcinog* 1994;10:199-206.
- Tomita T, Iwata K. Matrix metalloproteinases and tissue inhibitors of metalloproteinases in colonic adenomas-adenocarcinomas. *Dis Colon Rectum* 1996;39:1255-64.
- O'Shea M, Willenbrock F, Williamson RA, Cockeitt ML, Freedman RB, Reynolds JJ, Docherty AJ, Murphy G. Site-directed mutations that alter the inhibitory activity of the tissue inhibitor of metalloproteinases-1: importance of the N-terminal region between cysteine 3 and cysteine 13. *Biochemistry* 1992;31:10146-52.
- Engelholm LH, Nielsen BS, Netzel-Arnett S, Solberg H, Chen XD, Lopez Garcia JM, Lopez-Otin C, Young MF, Birkedal-Hansen H, Dano K, Lund LR, Behrendt N, et al. The urokinase plasminogen activator receptor-associated protein/endo180 is coexpressed with its interaction partners urokinase plasminogen activator receptor and matrix metalloproteinase-13 during osteogenesis. *Lab Invest* 2001;81:1403-14.
- Pyke C, Ralfkiaer E, Huhtala P, Hurskainen T, Dano K, Tryggvason K. Localization of messenger RNA for Mr 72,000 and 92,000 type IV collagenases in human skin cancers by in situ hybridization. *Cancer Res* 1992;52:1336-41.
- Nielsen BS, Rank F, Lopez JM, Balbin M, Vizoso F, Lund LR, Dano K, Lopez-Otin C. Collagenase-3 expression in breast myofibroblasts as a molecular marker of transition of ductal carcinoma in situ lesions to invasive ductal carcinomas. *Cancer Res* 2001;61:7091-100.
- Holten-Andersen MN, Brunner N, Maimonis P, Jensen V, Murphy G, Piironen T. Characterization of monoclonal antibodies to tissue inhibitor of metalloproteinases-1. *Journal of clinical ligand assay* 2002;25:87-90.
- Shulman M, Wilde CD, Kohler G. A better cell line for making hybridomas secreting specific antibodies. *Nature* 1978;276:269-70.
- Hembry RM, Murphy G, Reynolds JJ. Immunolocalization of tissue inhibitor of metalloproteinases (TIMP) in human cells. Characterization and use of a specific antiserum. *J Cell Sci* 1985;73:105-19.
- Holten-Andersen MN, Murphy G, Nielsen HJ, Pedersen AN, Christensen JJ, Hoyer-Hansen G, Brunner N, Stephens RW. Quantitation of TIMP-1 in plasma of healthy blood donors and patients with advanced cancer. *Br J Cancer* 1999;80:495-503.
- Sappino AP, Dietrich PY, Skalli O, Widgren S, Gabbiani G. Colonic pericycral fibroblasts. Differentiation pattern in embryogenesis and phenotypic modulation in epithelial proliferative lesions. *Virchows Arch A Pathol Anat Histopathol* 1989;415:551-7.
- Nielsen BS, Timshel S, Kjeldsen L, Sehested M, Pyke C, Borregaard N, Dano K. 92 kDa type IV collagenase (MMP-9) is expressed in neutrophils and macrophages but not in malignant epithelial cells in human colon cancer. *Int J Cancer* 1996;65:57-62.
- Holten-Andersen MN, Christensen JJ, Nielsen HJ, Stephens RW, Jensen V, Nielsen OH, Sorensen S, Overgaard J, Lilja H, Harris A, Murphy G, Brunner N. Total levels of tissue inhibitor of metalloproteinases 1 in plasma yield high diagnostic sensitivity and specificity in patients with colon cancer. *Clin Cancer Res* 2002;8:156-64.
- Kay C, Lane N, Pascal RR. Colonic pericycral fibroblast sheath: replication, migration, and cytodifferentiation of a mesenchymal cell system in adult tissue. II. Fine structural aspects of normal rabbit and human colon. *Gastroenterology* 1968;54:852-65.
- Adegbayegba PA, Miffin RC, DiMari JF, Saada JJ, Powell DW. Immunohistochemical study of myofibroblasts in normal colonic mucosa, hyperplastic polyps, and adenomatous colorectal polyps. *Arch Pathol Lab Med* 2002;126:829-36.
- Poulsom R, Pignatelli M, Stetler-Stevenson WG, Liotta LA, Wright PA, Jeffery RE, Longcroft JM, Rogers L, Stamp GW. Stromal expression of 72 kDa type IV collagenase (MMP-2) and TIMP-2 mRNAs in colorectal neoplasia. *Am J Pathol* 1992;141:389-96.
- Rouyer N, Wolf C, Chenard MP, Rio MC, Chambou P, Bellocq JP, Basset P. Stromelysin-3 gene expression in human cancer: an overview. *Invasion Metastasis* 1994;14:269-75.

44. Okada A, Bellocq JP, Rouyer N, Chenard MP, Rio MC, Chambon P, Basset P. Membrane-type matrix metalloproteinase (MT-MMP) gene is expressed in stromal cells of human colon, breast, and head and neck carcinomas. *Proc Natl Acad Sci U S A* 1995;92:2730-4.
45. Nielsen BS, Sehested M, Duun S, Rank F, Timshel S, Rygaard J, Johnsen M, Dano K. Urokinase plasminogen activator is localized in stromal cells in ductal breast cancer. *Lab Invest* 2001;81:1485-501.
46. Offersen BV, Nielsen BS, Hoyer-Hansen G, Rank F, Hamilton-Dutoit S, Overgaard J, Andreasen PA. The myofibroblast is the predominant plasminogen activator inhibitor-1 expressing cell type in human breast carcinomas. *Am J Pathol* 2003;163:1887-99.
47. Duffy MJ, Reilly D, O'Sullivan C, O'Higgins N, Fennelly JJ, Andreasen P. Urokinase-plasminogen activator, a new and independent prognostic marker in breast cancer. *Cancer Res* 1990;50:6827-9.
48. Grondahl HJ, Christensen JJ, Rosenquist C, Brunner N, Mouridsen HT, Dano K, Blichert TM. High levels of urokinase-type plasminogen activator and its inhibitor PAI-1 in cytosolic extracts of breast carcinomas are associated with poor prognosis. *Cancer Res* 1993;53:2513-21.
49. Illemann M, Hansen U, Nielsen HJ, Andreasen PA, Hoyer-Hansen G, Lund LR, Dano K, Nielsen BS. Leading edge myofibroblasts in human colon cancer express PAI-1. *Am J Clin Pathol* 2004;122:256-65.
50. Saarialho-Kere UK, Vaalamo M, Puolakkainen P, Airola K, Parks WC, Karjalainen-Lindsberg ML. Enhanced expression of matrilysin, collagenase, and stromelysin-1 in gastrointestinal ulcers. *Am J Pathol* 1996;148:519-526.
51. McKaig BC, McWilliams D, Watson SA, Mahida YR. Expression and regulation of tissue inhibitor of metalloproteinase-1 and matrix metalloproteinases by intestinal myofibroblasts in inflammatory bowel disease. *Am J Pathol* 2003;162:1355-1360.

**This Page is Inserted by IFW Indexing and Scanning
Operations and is not part of the Official Record**

BEST AVAILABLE IMAGES

Defective images within this document are accurate representations of the original documents submitted by the applicant.

Defects in the images include but are not limited to the items checked:

☐ **BLACK BORDERS**

☐ **IMAGE CUT OFF AT TOP, BOTTOM OR SIDES**

☐ **FADED TEXT OR DRAWING**

☐ **BLURRED OR ILLEGIBLE TEXT OR DRAWING**

☐ **SKEWED/SLANTED IMAGES**

☐ **COLOR OR BLACK AND WHITE PHOTOGRAPHS**

☐ **GRAY SCALE DOCUMENTS**

☐ **LINES OR MARKS ON ORIGINAL DOCUMENT**

☒ **REFERENCE(S) OR EXHIBIT(S) SUBMITTED ARE POOR QUALITY**

☐ **OTHER:** _____

IMAGES ARE BEST AVAILABLE COPY.

As rescanning these documents will not correct the image problems checked, please do not report these problems to the IFW Image Problem Mailbox.